ENGINEERING SIGNAL SENSORS BASED ON REPROGRAMMED CRISPR TECHNOLOGIES

EDITED BY: Yuchen Liu, Yingxin Ma, Tao Xu, Yonghao Zhan and Zhicong Chen

PUBLISHED IN: Frontiers in Molecular Biosciences

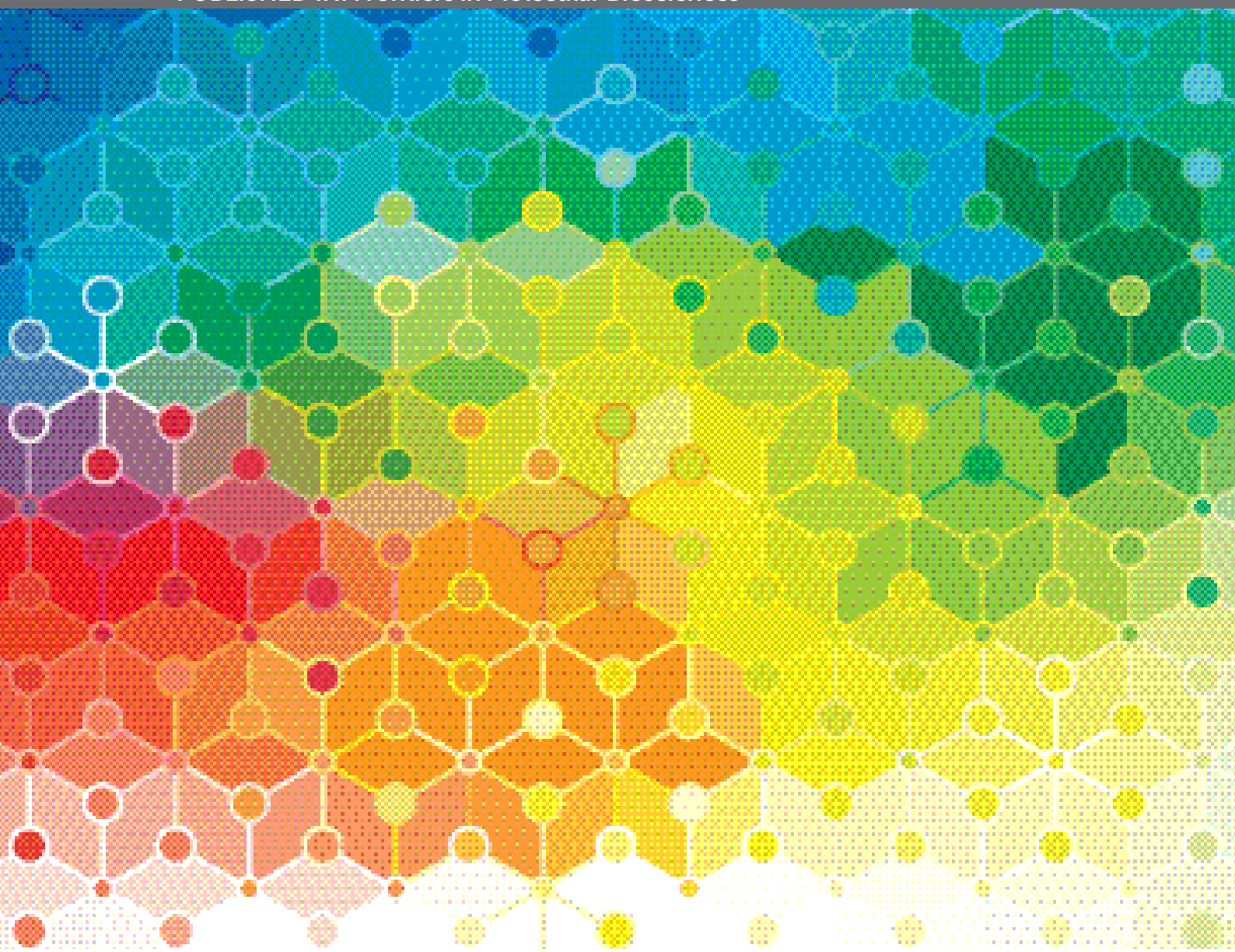

frontiers Research Topics

ISSN 1664-8714
ISBN 978-2-88971-553-4
DOI 10.3389/978-2-88971-553-4

About Frontiers

Frontiers is more than just an open-access publisher of scholarly articles: it is a pioneering approach to the world of academia, radically improving the way scholarly research is managed. The grand vision of Frontiers is a world where all people have an equal opportunity to seek, share and generate knowledge. Frontiers provides immediate and permanent online open access to all its publications, but this alone is not enough to realize our grand goals.

Frontiers Journal Series

The Frontiers Journal Series is a multi-tier and interdisciplinary set of open-access, online journals, promising a paradigm shift from the current review, selection and dissemination processes in academic publishing. All Frontiers journals are driven by researchers for researchers; therefore, they constitute a service to the scholarly community. At the same time, the Frontiers Journal Series operates on a revolutionary invention, the tiered publishing system, initially addressing specific communities of scholars, and gradually climbing up to broader public understanding, thus serving the interests of the lay society, too.

Dedication to Quality

Each Frontiers article is a landmark of the highest quality, thanks to genuinely collaborative interactions between authors and review editors, who include some of the world's best academicians. Research must be certified by peers before entering a stream of knowledge that may eventually reach the public - and shape society; therefore, Frontiers only applies the most rigorous and unbiased reviews.
Frontiers revolutionizes research publishing by freely delivering the most outstanding research, evaluated with no bias from both the academic and social point of view. By applying the most advanced information technologies, Frontiers is catapulting scholarly publishing into a new generation.

What are Frontiers Research Topics?

Frontiers Research Topics are very popular trademarks of the Frontiers Journals Series: they are collections of at least ten articles, all centered on a particular subject. With their unique mix of varied contributions from Original Research to Review Articles, Frontiers Research Topics unify the most influential researchers, the latest key findings and historical advances in a hot research area! Find out more on how to host your own Frontiers Research Topic or contribute to one as an author by contacting the Frontiers Editorial Office: frontiersin.org/about/contact

ENGINEERING SIGNAL SENSORS BASED ON REPROGRAMMED CRISPR TECHNOLOGIES

Topic Editors:
Yuchen Liu, Shenzhen University, China
Yingxin Ma, Chinese Academy of Sciences (CAS), China
Tao Xu, Anhui Medical University, China
Yonghao Zhan, Zhengzhou University, China
Zhicong Chen, Boston University, United States

Citation: Liu, Y., Ma, Y., Xu, T., Zhan, Y., Chen, Z., eds. (2021). Engineering Signal Sensors Based on Reprogrammed CRISPR Technologies.
Lausanne: Frontiers Media SA. doi: 10.3389/978-2-88971-553-4

Table of Contents

frontiers in Molecular Biosciences

EDITORIAL
published: 09 September 2021
doi: 10.3389/fmolb.2021.742961

Editorial: Engineering Signal Sensors Based on Reprogrammed CRISPR Technologies

Yuchen Liu[1]*, *Tao Xu*[2]* and *Yonghao Zhan*[3]*

[1]Institute of Translational Medicine, Shenzhen Second People's Hospital, First Affiliated Hospital of Shenzhen University, Shenzhen, China, [2]School of Pharmacy, Anhui Medical University, Hefei, China, [3]Department of Urology, The First Affiliated Hospital of Zhengzhou University, Zhengzhou, China

Keywords: CRISPR, SgRNA, signal sensor, disease diagnosis, disease treatment

Editorial on the Research Topic

Engineering Signal Sensors Based on Reprogrammed CRISPR Technologies

In the past few years, gene editing and regulation technologies based on the CRISPR-Cas system have developed rapidly. Using CRISPR technology, we can not only knock out genes and edit DNA sequences, but also regulate DNA transcriptions, and even target RNAs. The expression of CRISPR-Cas system in cells includes both constitutive and inducible manners. The signal-inducible CRISPR-Cas system has the characteristics of temporal and spatial specific expression, so it can be used in medical research. This Research Topic aims to develop the reprogrammed CRISPR systems for sensing and targeting specific disease signals. It includes original research articles from communities involved with gene engineering, synthetic biology, RNA biology and tumor biology.

Firstly, as a gene editing and regulation tool, CRISPR-Cas can be used for cleaving DNA targets or regulating DNA transcription. By targeting specific disease markers, the CRISPR system can be used to study the functions and mechanisms of key molecules, and also directly inhibit the occurrence and development of diseases. Chen et al. used CRISPR-Cas9 system to knockout the HBV integrated fragments in PLC/PRF/5 cells that can potentially express HBsAg, which suggested the prospect of controlling hepatitis B virus replication and treating hepatitis Lan et al. revealed the possibility of using the CRISPR-dCas9 transcriptional suppression system to treat intervertebral disk degeneration (IDD) through Parkin targeted inhibition. Ye et al. used CRISPR-dCas9 to knockdown the expression of SNHG9, a lncRNA which promotes cell proliferation, migration, and invasion of human hepatocellular carcinoma cells by increasing GSTP1 methylation. By targeting the oncogenic lncRNA PANDAR, Jia et al. observed proliferation inhibition and apoptosis induction in oral squamous cell carcinoma using CRISPR-dCas9. Cao et al. also observed anticancer effects in bladder cancer by using a similar CRISPR-dCas9 system and indicated that lncRNA SNGH3 serves as a oncogene and could be employed as a prospective diagnostic marker for clinical use. Zhao et al. developed the CRISPR-dCas9-KRAB, a much more stronger transcriptional inhibitor, to regualte lncRNA gadd7 which protects spermatocyte viability. Zheng and Chen found that downregulation of CacyBP by CRISPR/dCas9-KRAB prevents bladder cancer progression and suggested that CacyBP is an important oncogene contributing to malignant behavior. Chen and Zheng reported that lncRNA LINC00944 promotes tumorigenesis but suppresses Akt phosphorylation in renal cell carcinoma by knockdown of LINC00944 using CRISPR-dCas9-KRAB. Yang et al. constructed the CRISPR-dCas9-VPR, a transcriptional activator, to up-regulate lncRNA ERIC exrepssion which inhibits cell proliferation and invasion and promotes apoptosis in human bladder cancer. Yang et al. used both CRISPR-dCas9-VPR and CRISPR-dCas9-KRAB systems to study the biological functions of

OPEN ACCESS

Edited and reviewed by:
William C. Cho,
QEH, Hong Kong, SAR China

Correspondence:
Yuchen Liu
liuyuchenmdcg@163.com
Tao Xu
xutao@ahmu.edu.cn
Yonghao Zhan
yonghao_zhan@163.com

Specialty section:
This article was submitted to Molecular Diagnostics and Therapeutics, a section of the journal Frontiers in Molecular Biosciences

Received: *17 July 2021*
Accepted: *31 August 2021*
Published: *09 September 2021*

Citation:
Liu Y, Xu T and Zhan Y (2021) Editorial: Engineering Signal Sensors Based on Reprogrammed CRISPR Technologies. Front. Mol. Biosci. 8:742961. doi: 10.3389/fmolb.2021.742961

ITGB5, TIMP1, and TMEM176B, and found that the three genes synergistically affect the proliferation, invasion and migration capabilities of prostate cancer cells. More interestingly, Gan et al. demonstrated that TRIM58 is inactivated by promoter methylation in clear cell renal cell carcinoma, and TRIM58 DNA demethylation mediated by CRISPR-dCas9-TET1 can inhibit cancer cell proliferation and migration by reactivating TRIM58 expression.

Secondly, nucleases represented by CRISPR-Cas13 can also be used to cleave or edit cellular RNAs. Since the abnormal expression and activity of the transcriptome are more closely related to diseases, this will be a new direction. Che et al. designed the CRISPR-Cas13a to target the enhancer RNA-SMAD7, and knockdown of SMAD7e inhibits bladder cancer development both *in vitro* and *in vivo*. Zhang et al. also used CRISPR-Cas13 to inhibit the expression of another lncRNA GACAT3, and they found that knockdown of GACAT3 inhibited cell proliferation and motility, and induced apoptosis by increasing p21, Bax, and E-Cadherin expression in bladder cancer. Zhuang et al. used CRISPR-Cas13d, another enzyme similar to CRISPR-Cas13a, to cleave lncRNA MIR497HG and this induces bladder cancer progression through promoting the crosstalk between Hippo/Yap and TGF-β/Smad signaling. Li et al. constructed CRISPR-CasRx to cleave lncRNA LINC00341 which inhibits tumor cell growth both *in vitro* and *in vivo*. More interestingly, Cao et al. designed a dm^{6}ACRISPR demethylation system, dCas13b-ALKBH5, to accurately and specifically demethylate 3′UTR of PLOD2 mRNA, which has a high level of m^{6}A methylation in renal cell carcinoma. Their results suggested that PLOD2 mRNA demethylated by dCas13b-ALKBH5 might provide a new light on the treatment for renal cell carcinoma.

Thirdly, some intelligent CRISPR systems that regulated by internal and external signals have been designed to treat diseases. Wu et al. presented a blue light-inducible CRISPR-Cas9 system for inhibiting progression of melanoma cells. This light-inducible system may provide a novel strategy for skin cancer treatment. Huang et al. also constructed a light-inducible split-dCas9 system for inhibiting the progression of bladder cancer cells by activating p53 and E-cadherin expression. Zhuang et al. inserted the hTERT aptazyme into 3′UTR of the Cas13d system, and used the reprogrammed system to sense hTERT signals. This may provide a highly effective approach for cancer gene therapy. Yang et al. used CRISPReader technology to construct an endogenous molecular system for sensing the oncogenic transcription factor Ets-1. This system can specifically kill multiple types of cancer cells based on the recognition of Ets-1, and has a wide range of potential applications.

In addition to the works mentioned above, Yao et al. also proposed a special study. They found that synthetic artificial lncRNA shows a higher efficiency in malignant phenotype inhibition compared to the CRISPR/Cas system. This is indeed very interesting, because the guide RNA of the CRISPR-Cas system is very similar to lncRNA in structure and function. Maybe we can build a better gene editing and regulation system based on the artificial lncRNA.

Overall, this Research Topic fully demonstrates the feasibility of the CRISPR-Cas system to treat diseases by sensing or targeting DNA, RNA and protein targets. In the future, the clinical application progress of the CRISPR system will be more worthy of attention.

AUTHOR CONTRIBUTIONS

YL wrote the manuscript. TX and YZ approved it for publication.

ACKNOWLEDGMENTS

We thank all the contributors of this Research Topic.

Conflict of Interest: The authors declare that the research was conducted in the absence of any commercial or financial relationships that could be construed as a potential conflict of interest.

Publisher's Note: All claims expressed in this article are solely those of the authors and do not necessarily represent those of their affiliated organizations, or those of the publisher, the editors and the reviewers. Any product that may be evaluated in this article, or claim that may be made by its manufacturer, is not guaranteed or endorsed by the publisher.

frontiers in Molecular Biosciences

ORIGINAL RESEARCH
published: 17 November 2020
doi: 10.3389/fmolb.2020.607740

CRISPR-Cas13a Targeting the Enhancer RNA-SMAD7e Inhibits Bladder Cancer Development Both *in vitro* and *in vivo*

Wenan Che[1†], Shanting Ye[2†], Aoxiang Cai[1†], Xiaojuan Cui[1] and Yuandong Sun[1]*

[1] Hunan Key Laboratory of Economic Crops Genetic Improvement and Integrated Utilization, School of Life Sciences, Hunan University of Science and Technology, Xiangtan, China, [2] Shenzhen Second People's Hospital, The First Affiliated Hospital of Shenzhen University, Shenzhen, China

OPEN ACCESS

Edited by:
Yonghao Zhan,
Zhengzhou University, China

Reviewed by:
Xinbo Huang,
Peking University, China
Ziqi He,
Wuhan University, China

***Correspondence:**
Yuandong Sun
syd@hnust.edu.cn

[†] These authors have contributed equally to this work

Specialty section:
This article was submitted to Molecular Diagnostics and Therapeutics, a section of the journal Frontiers in Molecular Biosciences

Received: 18 September 2020
Accepted: 22 October 2020
Published: 17 November 2020

Citation:
Che W, Ye S, Cai A, Cui X and Sun Y (2020) CRISPR-Cas13a Targeting the Enhancer RNA-SMAD7e Inhibits Bladder Cancer Development Both in vitro and in vivo. Front. Mol. Biosci. 7:607740. doi: 10.3389/fmolb.2020.607740

Enhancers are cis-acting elements that can promote the expression of target genes and respond to estrogen to induce the transcription of eRNAs, which are closely associated with cancer development. Further study on eRNAs may lead to a better understanding of the significance of transcriptional regulation and the progression of malignant tumors. SMAD7 enhancer RNA (SMAD7e) is an estrogen-responsive eRNA. However, the relationship between SMAD7e and bladder cancer remains unclear. SMAD7e was significantly upregulated in bladder cancer tissues and estrogen-stimulated cells. Knockdown of SMAD7e by CRISPR-Cas13a suppressed cell proliferation and migration, and induced cell apoptosis and inhibited cell invasion. Estrogen caused overexpression of SMAD7e and played a facilitating role in bladder cancer cells. Furthermore, knockdown of SMAD7e by CRISPR-Cas13a prevented the cancer-promoting effects of estrogen on bladder cancer both *in vitro* and *in vivo*. The present study suggested the crucial role of SMAD7e in bladder cancer. Estrogen might promote the development of bladder cancer by inducing SMAD7e production. These findings may provide a potential target for CRISPR-mediated gene therapy for bladder cancer in the future.

Keywords: CRISPR-Cas13a, SMAD7e, bladder cancer, estrogen, enhancer RNA (eRNA)

INTRODUCTION

Estrogen is reported to be associated with the development of many cancers (Horie, 2010). To the best of our knowledge, bladder cancer mainly occurs in males, while female patients have lower survival rates (Hartge et al., 1990; Madeb and Messing, 2004; Xu et al., 2013; Murakawa et al., 2016). The sex difference in morbidity suggests the importance of estrogen for bladder cancer development. However, the molecular mechanisms of estrogen in bladder cancer remain unclear. Although there are many treatments for patients with bladder cancer, such as chemotherapy, radiation, and surgery, the 5-year survival rate is

low (Racioppi et al., 2012; Sofra et al., 2013; Rose and Milowsky, 2016). Therefore, there is a need to develop a more effective and safer method for treating bladder cancer.

Recently, several studies suggested that natural enhancers were occupied by RNA polymerase II (RNAP II) and transcribed into non-coding (nc) RNAs termed enhancer RNAs (eRNAs) (De Santa et al., 2010; Kim et al., 2010). The eRNA-producing enhancer regions have been exploited and eRNAs may play a crucial role in gene transcriptional regulation (Lam et al., 2013). Studies have confirmed that the abnormal expressions of eRNAs are closely related to diseases (He et al., 2013; IIott et al., 2014; Yao et al., 2015; Bal et al., 2017; Gras et al., 2017). SMAD7 is proved to be an intracellular protein with a well-known ability to antagonize transforming growth factor-β1 (TGF-β1) signaling through multiple mechanisms (Nakao et al., 1997). Recent studies have shown that SMAD7 plays a role in breast cancer development and progression (Rahman et al., 2017). SMAD7 facilitated the proliferation of cancer cells originating from colorectal, pancreatic, prostate, and lung (Brionesorta et al., 2011). Previous studies found that the corresponding enhancer of SMAD7 could be transcribed into functional transcripts – SMAD7e with estrogenic stimulation (Hah et al., 2013; Li et al., 2013). However, the roles of SMAD7e in bladder cancer are completely unclear. It would therefore be interesting to determine if the SMAD7e mediates the effect of estrogen on bladder cancer.

In this study, we examined the clinical significance of SMAD7e in 38 bladder cancer samples. The effects of SMAD7e knockdown on the proliferation, migration, apoptosis, and invasion of bladder cancer cells were determined. Moreover, we determined the promoting effect of estrogen on bladder cancer and the potential molecular mechanisms of estrogen in bladder cancer. In addition, we demonstrated that SMAD7e knockdown mediated by CRISPR-Cas13a reduced the cancer-promoting ability of estrogen on bladder cancer cells both *in vitro* and *in vivo*. This work suggested CRISPR-Cas13a as an effective tool to target one specific enhancer RNA- SMAD7e in bladder cancer and revealed its advantage in anticancer research.

RESULTS

SMAD7e Was Overexpressed in Bladder Cancer Tissues and Positively Correlated With Clinicopathological Features

We measured the relative expression levels of SMAD7e in a total of 38 patients with bladder cancer by real-time qPCR. Compared with normal counterparts, the SMAD7e expression was obviously overexpressed in 29 cancer tissues (**Figures 1A,B**). We further analyzed the relationship between SMAD7e expression and clinical features of patients. As shown in **Table 1**, there was a positive correlation between the SMAD7e expression level and the clinical features including histological grade and TNM stage of bladder cancer. However, sex and age had no relationship with the SMAD7e expression level. Therefore, SMAD7e may function as a oncogenic factor in bladder cancer.

Estrogen Induced the Production of SMAD7e, Facilitated Cell Proliferation, Increased Cell Migration, Suppressed Cell Apoptosis, and Promoted Cell Invasion in Bladder Cancer

We measured SMAD7e expression levels after estrogen stimulation for 1 h in 5637 cells and T24 cells, using RT qPCR. These results indicated that SMAD7e expression was significantly increased in bladder cancer cells when stimulated by estrogen (**Figure 2A**). To determine the impact of estrogen on bladder cancer cells, the cell proliferations of 5637 and T24 were determined by CCK8 and Edu assays. Estrogen-promoted cell growth was observed in 5637 cells and T24 cells (**Figures 2B,C**). We further determined that estrogen promoted cell migration in bladder cancer using wound healing assays (**Figure 2D**). Furthermore, estrogen suppressed cell apoptosis in bladder cancer. The relative activity of caspase-3 was determined using a caspase 3 ELISA (**Figure 2E**). Estrogen promoted cell invasion in bladder cancer (**Figure 2F**). These results demonstrated that estrogen played a cancer-promoting role in bladder cancer.

Knockdown of SMAD7e by CRISPR-Cas13a Suppressed Proliferation, Inhibited Migration, Promoted Apoptosis, and Decreased Invasion in Bladder Cancer Cells

CRISPR-Cas13a was used to measure the effect of SMAD7e knockdown on biological behaviors of bladder cancer cells. After Cas13a-SMAD7e or Cas13a-NC transfection for 24 h, the relative expression levels of SMAD7e were significantly reduced (**Figure 3A**). We used CCK8 and Edu assays to compare the cell proliferations between the SMAD7e knockdown group and the negative control group. The results showed that knockdown of SMAD7e suppressed cell growth in 5637 and T24 cells (**Figures 3B,C**). The cell migration was significantly inhibited, as shown by wound healing assays in 5637 and T24 cells (**Figure 4A**). We also used caspase 3 ELISA assays to compare the cell apoptosis rates of the two groups. The results indicated that knockdown of SMAD7e increased cell apoptosis (**Figure 4C**). Furthermore, knockdown of SMAD7e decreased cell invasion, as demonstrated using Transwell® assays (**Figure 4E**). Therefore, knockdown of SMAD7e inhibited the tumorigenicity of bladder cancer cells.

Knockdown of SMAD7e Attenuated the Carcinogenesis Effect of Estrogen in Bladder Cancer Cells

We hypothesized SMAD7e played a key role in the carcinogenic effects of estrogen in bladder cancer. Bladder cancer cells were transfected with Cas13a-SMAD7e or Cas13a-NC vectors and treated with estrogen. Compared with the negative control, cell proliferation was obviously decreased (**Figures 3B,D**); the cell migration ratio was reduced (**Figure 4B**); the cell apoptosis was increased (**Figure 4D**);

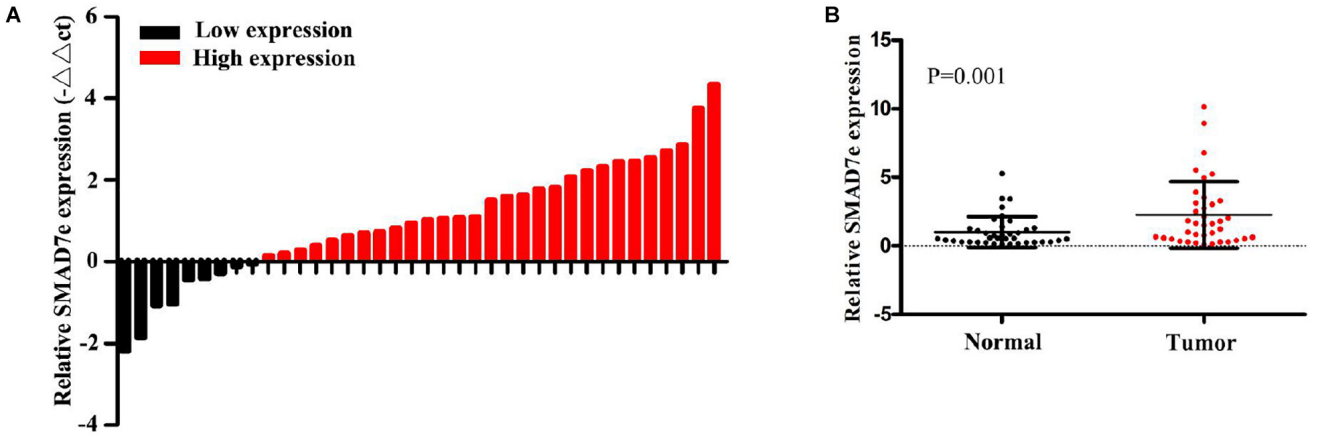

FIGURE 1 | The expression of SMAD7e in bladder cancer. **(A)** SMAD7e was up-regulated in bladder cancer. The relative expression levels of SMAD7e were detected by qPCR in 38 bladder cancer patients. **(B)** The relative expression level of SMAD7e was significantly increased in bladder cancer tissues compared to paired normal tissues. Data are shown as the mean ± SD.

and the invasive ability of the cells was also prominently weakened (**Figure 4F**) in the SMAD7e knockdown group treated with estrogen.

To verify the effects of SMAD7e on the carcinogenic effects of estrogen *in vivo*, xenograft models were established by injecting stable knockdown SMAD7e T24 cells and vector transfected T24 cells into subcutaneous tissues of nude mice. All nude mice developed xenogeneic tumors at the injection site (**Figure 5A**). Tumor growth of SMAD7e silenced cells was slower than that of the SMAD7e knockdown group treated with estrogen (**Figure 5B**). As shown in **Figures 5C,D**, downregulation of SMAD7e significantly decreased the xenograft tumor volume and tumor weight compared to the SMAD7e knockdown group treated with estrogen. In conclusion, knockdown of SMAD7 attenuated the effects of estrogen on bladder cancer.

TABLE 1 | Correlation between SMAD7e expression and clinicopathological characteristics of bladder cancer patients.

Characteristics	Total	SMAD7e expression		*P* value
		Low	High	
Gender				
Female	7	3 (28.6%)	4 (71.4%)	0.186
Male	31	6 (32.3%)	25 (67.7%)	
Age				
≤60	10	4 (30.0%)	6 (70.0%)	0.157
>60	28	5 (17.9%)	23 (82.1%)	
Histological grade				
Low	14	7 (60.0%)	7 (40.0%)	0.004**
High	24	2 (21.7%)	22 (78.3%)	
TNM stage				
0/I	6	4 (83.3%)	2 (16.7%)	0.007**
II/III/IV	32	5 (18.8%)	27 (81.2%)	

***p < 0.01 was considered significant.*

DISCUSSION

Previous studies on gene-related cancers have focused on coding genes, because they directly affect cell function. However, accumulating evidences has indicated that ncRNAs play a non-redundant role in regulating gene transcription and protein generation, including the eRNAs (Murakawa et al., 2016). Compared to other mRNAs and lncRNAs, eRNAs can promote the development of various cancers by regulating the expression of multiple genes, and should be ideal anticancer targets.

It has been reported that human breast cancer cell E2 binding to estrogen receptor α leads to increased transcription of eRNAs on enhancers, along with the upregulation of E2-associated coding genes (Wang et al., 2011). The corresponding enhancers of SMAD7 can respond to estrogen stimuli to transcribe SMAD7 eRNA. The eRNAs appear rapidly after induction, and the half-life is very short. The mean transcription unit length of eRNAs from the estrogen receptor binding site is ∼3–5 kb, and therefore eRNAs may interact with enhancers.

The production of eRNAs is positively correlated with the expression of the target genes. Increased evidence suggests that eRNAs may affect cell biological behaviors, such as cell migration, invasion, proliferation, and apoptosis by upregulating the expression of target genes. Some studies further indicates that CREB-binding protein (CBP) can directly bind to eRNAs (Castello et al., 2012). CBP controls gene expression patterns in organisms by regulating histone acetylation, reducing histone affinity for DNA, and facilitating chromatin loosening to promote transcription. Although some studies have shown that eRNAs play a role in gene regulation, further studies are needed to reveal their biological functions.

SMAD7e is an estrogen-associated eRNA that enhances gene transcription. Our study was the first to demonstrate the overexpression of SMAD7e in bladder cancer tissues. Further research demonstrated that the expression level of SMAD7e was closely associated with the histological grade and the TNM

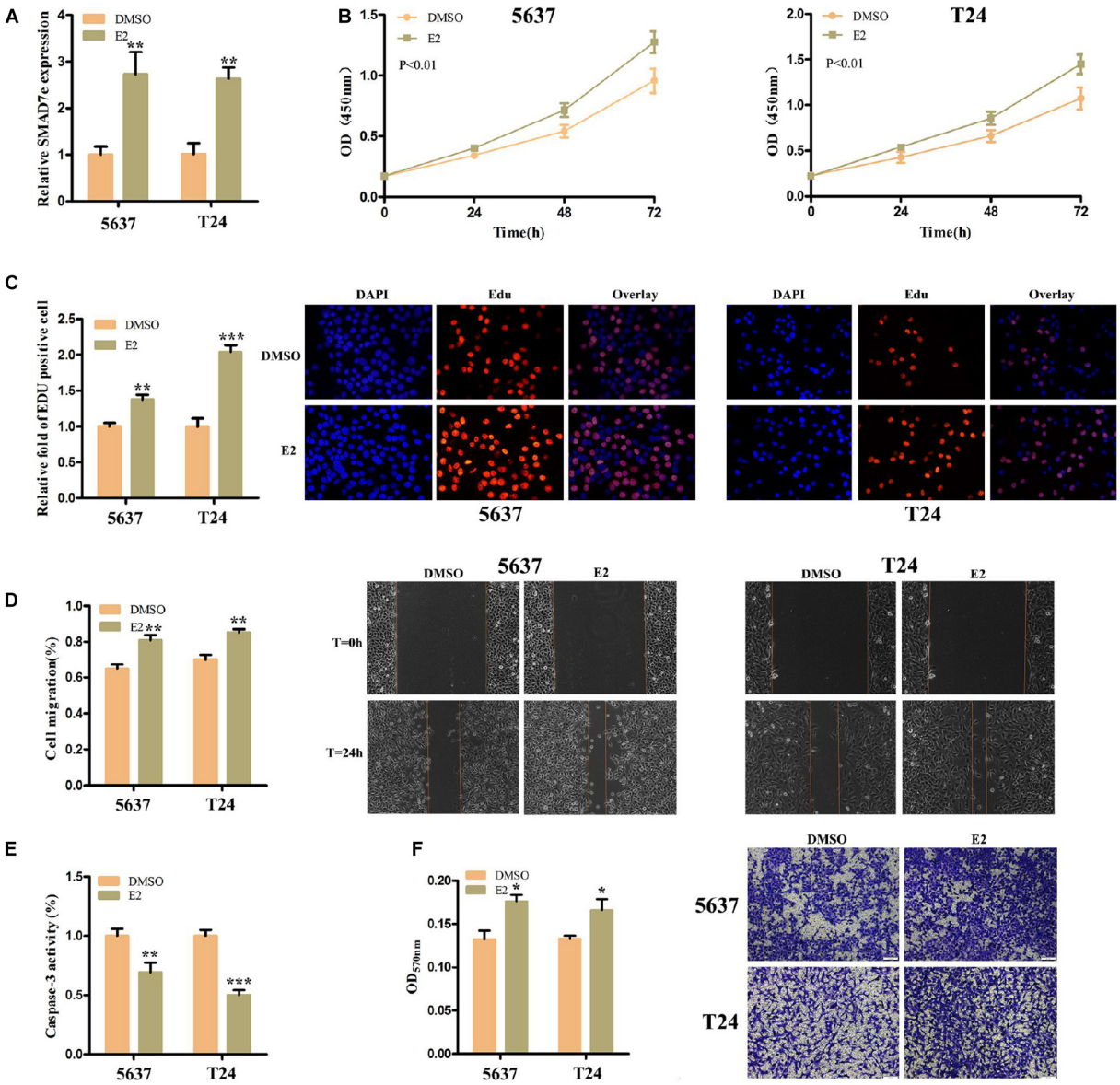

FIGURE 2 | The effect of E2 on bladder cancer cells. **(A)** After stimulation with estrogen for 1 h, the relative expression levels of SMAD7e were significantly increased in bladder cancer cells. **(B,C)** Estrogen facilitated cell proliferation as revealed by CCK8 and Edu assays in 5637 and T24 cells. **(D)** Estrogen promoted cell migration as revealed by wound healing assays in 5637 and T24 cells. **(E)** Estrogen reduced bladder cancer cell apoptosis. **(F)** Estrogen increased cell invasion as detected by Transwell® assays. E2 represents estrogen. Data are shown as the mean ± SD (*$p < 0.05$, **$p < 0.01$, ***$p < 0.001$).

stage. Our results suggested that SMAD7e may contribute to the initiation and progression of bladder cancer. In addition, we demonstrated that estrogen could induced the synthesis of SMAD7e and promoted the malignant biological behaviors of bladder cancer cells. Therefore, SMAD7e is a potential anticancer target in human bladder cancer.

To further verify the function of SMAD7e in bladder cancer, we knocked down SMAD7e by CRISPR-Cas13a (Abudayyeh et al., 2017). Since there lacks an effective tool to target this specific type of non-coding RNA, we therefore used the newly developed biological method- CRISPR-Cas13a to resolve the targeting problem. Some recent studies (Zhao et al., 2018; Qi et al., 2019; Chen et al., 2020) also used CRISPR-Cas13a to inhibit different cancers by suppressing oncogenic mRNAs. Our results showed that downregulation of SMAD7e suppressed proliferation and migration, promoted apoptosis, and decreased invasion in bladder cancer. Therefore, it was suggested that SMAD7e had a cancer-promoting effect in bladder cancer. We also hypothesize that there might be a unique relationship between SMAD7e and the tumor-promoting action of estrogen, whereby estrogen causes the induction of SMAD7e. Lastly, we observed the cell malignant abilities after estrogen treatment

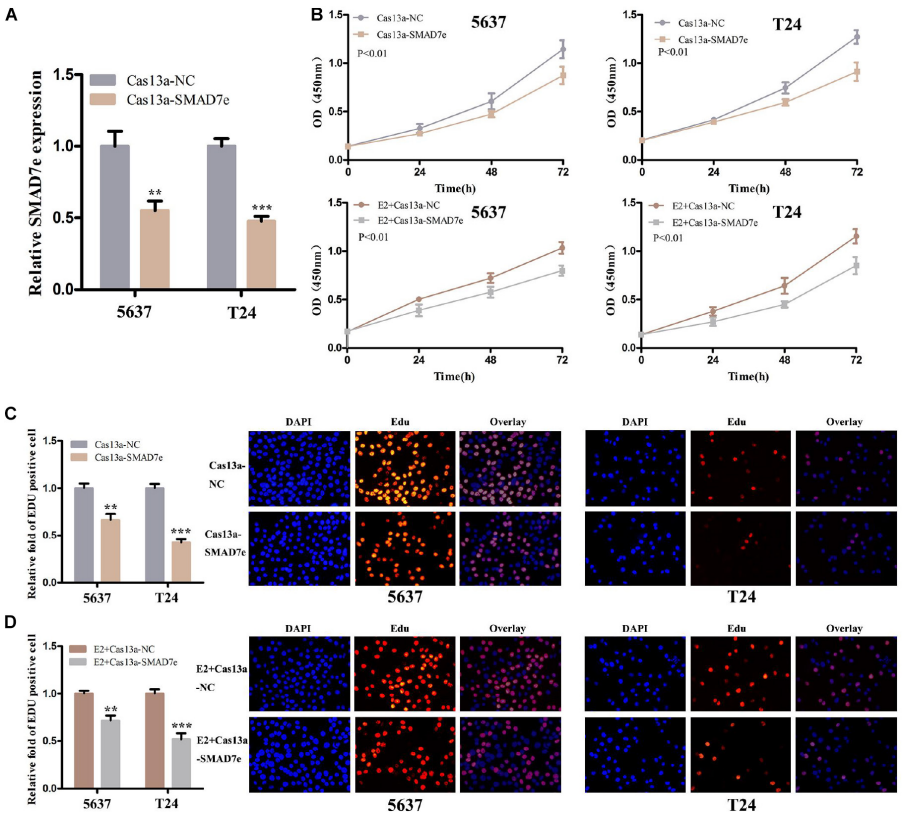

FIGURE 3 | The effect of Cas13a-SMAD7e on the proliferation of E2-treated bladder cancer cells. **(A)** SMAD7e expression levels were dramatically downregulated by Cas13a-SMAD7e. **(B)** Cell proliferation was detected by CCK8 assays in T24 and 5637 cells after transfection for 24 h. Knockdown of SMAD7e by Cas13a inhibited cell growth and reduced the proliferative effects of estrogen as determined by CCK8 assays in 5637 and T24 cells. **(C)** Edu assays were used to measure cell proliferation. Downregulation of SMAD7e inhibited cell growth of bladder cancer cells. **(D)** SMAD7e knockdown reduced the pro-proliferative effects of estrogen in 5637 and T24 cells. E2 represents estrogen. Data are shown as the mean ± SD (**$p < 0.01$, ***$p < 0.001$).

was impaired after Cas13a-SMAD7e transfection both *in vitro* and *in vivo*. These results demonstrated that SMAD7e might contribute to the carcinogenic effects of estrogen on bladder cancer, and that Cas13a-SMAD7e should be a powerful molecular approach to inhibit bladder cancer development.

MATERIALS AND METHODS

Patients and Tissue Specimens

Thirty-eight bladder urothelial carcinoma patients who received radical cystectomy were included in this study. The samples were stored in liquid nitrogen immediately after resection. These methods were based on approved guidelines. Formal written approvals from these patients were also received. The study was approved by the Research Ethics Committee of our institute.

Cell Culture and Treatments

Human bladder cancer cell lines (5637, T24) were obtained from the America Type Culture Collection (ATCC, Manassas, VA, United States). The 5637 cells were grown in RPMI-1640 medium (Gibco BRL, Gaithersburg, MD, United States) supplemented with 10% charcoal-stripped fetal bovine serum (FBS; Gibco BRL) and 1% antibiotics (100 U/mL penicillin and 100 μg/mL streptomycin sulfates) in a 5% CO_2 humidified incubator at 37°C. The T24 cells were cultured in DMEM medium (Gibco BRL), supplemented with 10% charcoal-stripped FBS (Gibco BRL) and 1% antibiotics (100 U/mL penicillin and 100 μg/mL streptomycin sulfates) in a 5% CO_2 humidified incubator at 37°C. Cells were treated with 10 nM DMSO (Sigma-Aldrich, St. Louis, MO, United States) or 10 nM estrogen (Sigma-Aldrich) for 1 h to induce SMAD7e.

CRISPR-Cas13a Vector Transfections

CRISPR-Cas13a targeting SMAD7e (Cas13a-SMAD7) and negative control (Cas13a-NC) were purchased from Syngen Tech Co., Beijing, China. Bladder cancer cells 5637 and T24 were seeded in 6-well plates and were transfected with 2.5 μg Cas13a-SMAD7e or Cas13a-NC when 80–90% confluent.

RNA Extraction and Real-Time qPCR Analysis

The total RNA of the tissue samples were extracted using the TRIzol reagent (Invitrogen, Carlsbad, CA, United States) according to manufacturer's instructions. The cDNA was

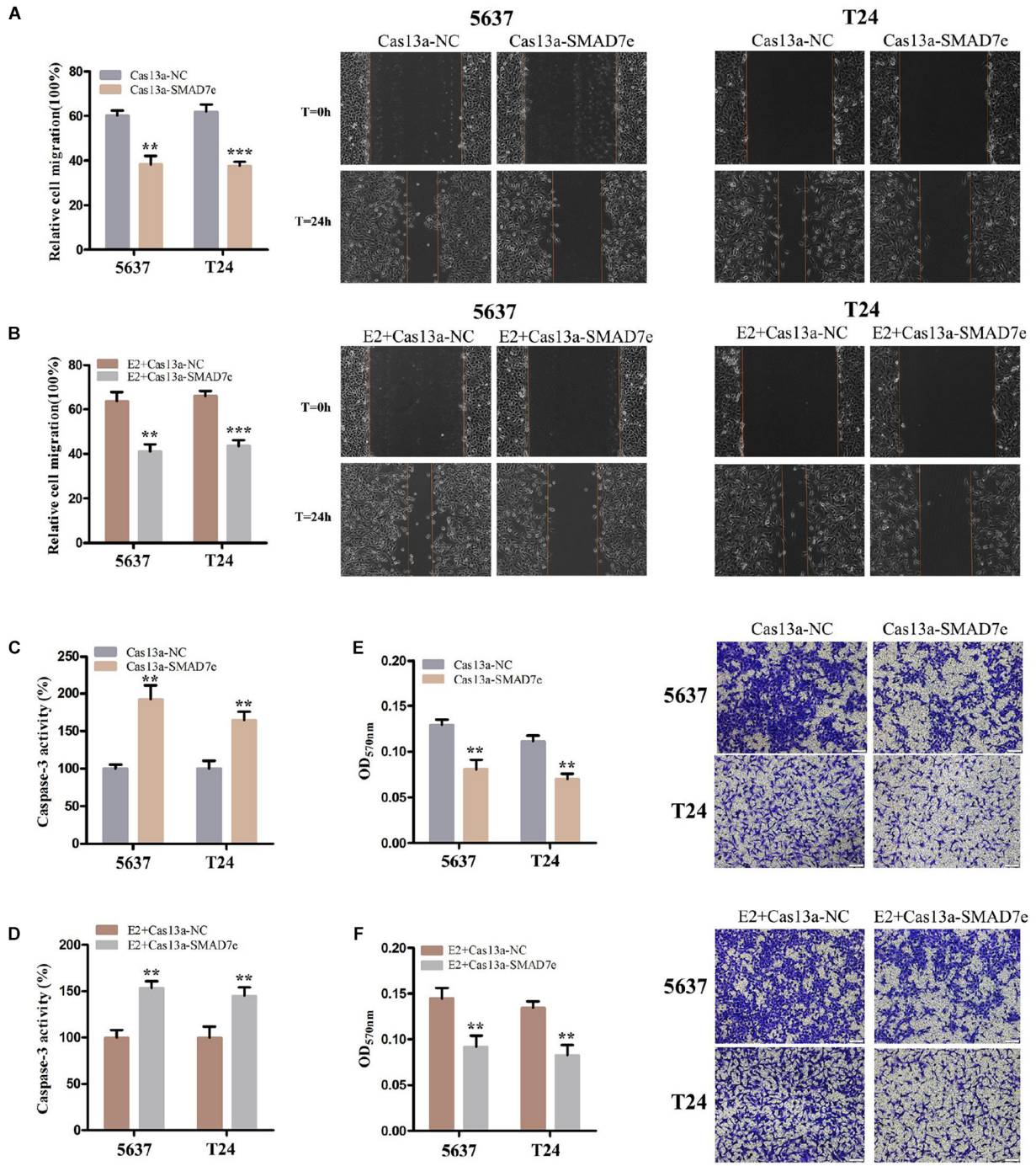

FIGURE 4 | The effect of Cas13a-SMAD7e on the migration of E2-treated bladder cancer cells. **(A,B)** Cell migration was detected by wound healing assays. SMAD7e knockdown inhibited migration of bladder cancer cells induced by estrogen. **(C,D)** The effects of knockdown of SMAD7e and SMAD7e knockdown with estrogen treatment were measured by caspase 3 ELISA assays. **(E,F)** Knockdown of SMAD7e and downregulation of SMAD7e attenuated estrogen-induced invasion of bladder cancer cells. E2 represents estrogen. Data are shown as the mean ± SD (**$p < 0.01$, ***$p < 0.00$).

synthesized using a Revertra Ace qPCR RT Kit (Toyobo, Osaka, Japan) according to the instructions. qPCR was carried out using real time PCR Master Mix (Toyobo) according to the instructions under conditions of 40 cycles of 15 s at 95°C, 15 s at 60°C, and 45 s at 75°C using the ABI PRISM 7500 Fluorescent Quantitative PCR System (Applied Biosystems, Foster City, CA, United States). The $2^{-\Delta\Delta Ct}$ method was chosen to calculate the relative expression levels.

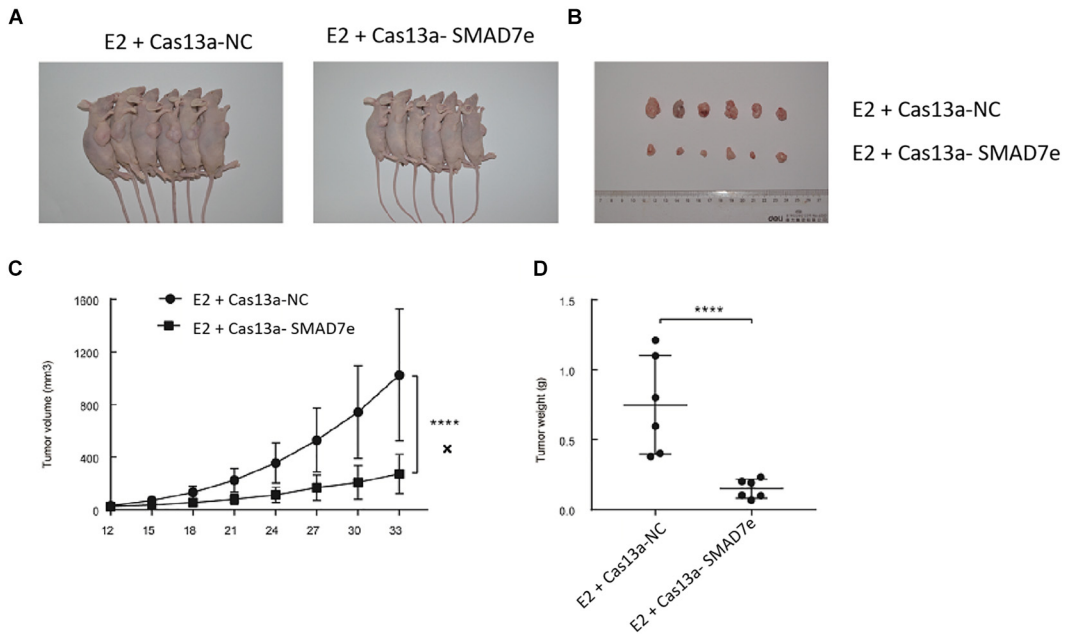

FIGURE 5 | The effect of Cas13a-SMAD7e on the *in vivo* growth of E2-treated bladder cancer cells. **(A)** Representative images of xenograft models. **(B)** Xenograft tumors from respective groups were shown after injection with SMAD7e stable knockdown T24 cells and vector transfected T24 cells. **(C)** Tumor growth curves were measured every 3 days. **(D)** Average weight of excised tumors. ****$p < 0.0001$.

Cell Proliferation Assays

Cell proliferation was determined using a Cell Counting Kit-8 (CCK-8) (TransGen, Beijing, China) and 5-ethynyl-20-deoxyuridine (Edu) assay kit (Ribobio, Guangzhou, China) China according to the instructions. For CCK-8 assays, cells were incubated in a 96-well plate for 24 h and then transiently transfected with CRISPR-Cas13a. The absorbance was detected at 0, 24, 48, and 72 h after transfection by a microplate reader (Bio-Rad, Hercules, CA, United States). Each test was carried out at least three times.

Cell Migration Assays

Cell migration was detected using the wound healing assay. Bladder cancer 5637 and T24 cells were cultured and transfected with either Cas13a-SMAD7e or Cas13a-NC for 24 h. For the wound healing assay, a sterile 200 μL pipette tip was used to create clear lines and photographs were immediately taken. The cells were cultured in medium supplemented with 1% FBS. The migration distance was observed after 24 h of wound formation and measured by the HMIAS-2000 software program. Experiments were repeated at least three times.

Cell Apoptosis Assays

Cell apoptosis was determined using enzyme-linked immunosorbent assays (ELISAs). Bladder cancer 5637 and T24 cells were transfected with Cas13a vector in petri plates. After 24 h, the caspase 3 ELISA assay kit (Hcusabio, Wuhan, China) was used to detect the activity of caspase 3 according to the manufacturer's protocol. OD values were measured at 450 nm by using a microplate reader (Bio-Rad). Each test was carried out at least three times.

Cell Invasion Assays

Cell invasion was detected using Transwell® assays. For the assay, about 1.5×10^5 5637 cells and 5×10^4T24 cells supplemented with 200 μL serum-free medium were plated into the upper chambers (24-well insert, pore size 8 μm: Corning, Sunnyvale, CA, United States) containing Matrigel® (1:8, 50 μL/well: BD Bioscience, San Jose, CA, United States). The lower chamber was filled with 500 μL of complete medium with 10% FBS and 1% antibiotics. Cells were cultured for 24 h and then cells under the surface of the lower chamber were washed with 1 × phosphate-buffered saline, fixed with methanol for 20 min, stained with 0.1% Crystal Violet for 25 min, and washed three times. Cells were observed using an inverted microscope and imaged. Each chamber with the invaded cells was than soaked in 1 mL 33% acetic acid for 10 min to wash out the Crystal Violet and 100 μL of 33% acetic acid was added into each well of the 96-well plates. The absorbance was determined at a wavelength of 570 nm using a microplate reader (Bio-Rad). Experiments were repeated at least three times.

Xenograft Tumor Model

Male BALB/c nude mice (4–6 weeks old), weighting 18–20 g, were purchased from Shanghai Experimental Animal Center (Shanghai, China). All mice were kept in a strict pathogen-free conditions. The Ethics Committee for Animal Experiments of University approved the animal

experiments. To establish the xenograft model, a total of 4×10^6 tumor cells were subcutaneously injected into the right flank of the nude mice. Every 3 days, we measured the tumor length and width with caliper. At the end point, the mice were euthanized, and tumor tissues were weighted.

Statistical Analysis

Each experiment was performed in triplicate. The data are presented as the mean ± standard deviation (SD), and all statistical analyses were conducted using SPSS 17 software (IBM, Chicago, IL, United States). The SMAD7e expression differences between bladder cancer tissues and matched normal tissues were analyzed using paired samples *t*-tests. CCK-8 assay data were analyzed by analysis of variance. Other data were analyzed by the independent samples *t*-test. $P < 0.05$ was regarded as statistically significant.

DATA AVAILABILITY STATEMENT

The original contributions presented in the study are included in the article/supplementary material, further inquiries can be directed to the corresponding author.

ETHICS STATEMENT

The animal study was reviewed and approved by Research Ethics Committee of Hunan University of Science and Technology.

AUTHOR CONTRIBUTIONS

AC, SY, WC, and XC performed the experiments and conducted the data analyses. YS supervised the project and wrote the manuscript. All authors contributed to the article and approved the submitted version.

FUNDING

This work was supported by the Scientific Research Project of National Natural Science Foundation of China (31873038), Hunan Province Education Department (17A072), Hunan Province Science and Technology Department (2019NK4218), and State Key Laboratory of Developmental Biology of Freshwater Fish (2017KF009).

REFERENCES

Abudayyeh, O. O., Gootenberg, J. S., Essletzbichler, P., Han, S., Joung, J., Belanto, J. J., et al. (2017). RNA targeting with CRISPR-Cas13. *Nature* 550, 280–284.

Bal, E., Park, H. S., Belaid-Choucair, Z., Kayserili, H., Naville, M., Madrange, M., et al. (2017). Mutations in ACTRT1 and its enhancer RNA elements lead to aberrant activation of Hedgehog signaling in inherited and sporadic basal cell carcinomas. *Nat. Med.* 23:1226. doi: 10.1038/nm.4368

Brionesorta, M. A., Tecalcocruz, A. C., Sosagarrocho, M., Caligaris, C., and Macíassilva, M. (2011). Inhibitory Smad7: emerging roles in health and disease. *Curr. Mol. Pharmacol.* 4, 141–153. doi: 10.2174/1874467211104020141

Castello, A., Fischer, B., Eichelbaum, K., Horos, R., Beckmann, B. M., Strein, C., et al. (2012). Insights into RNA biology from an atlas of mammalian mRNA-binding proteins. *Cell* 149, 1393–1406. doi: 10.1016/j.cell.2012.04.031

Chen, Y., Jiang, H., Wang, T., He, D., Tian, R., Cui, Z., et al. (2020). In vitro and in vivo growth inhibition of human cervical cancer cells via human papillomavirus E6/E7 mRNAs' cleavage by CRISPR/Cas13a system. *Antiviral Res.* 178:104794. doi: 10.1016/j.antiviral.2020.104794

De Santa, F., Barozzi, I., Mietton, F., Ghisletti, S., Polletti, S., Tusi, B. K., et al. (2010). A large fraction of extragenic RNA pol II transcription sites overlap enhancers. *PLoS Biol.* 8:e1000384. doi: 10.1371/journal.pbio.1000384

Gras, S. L., Keime, C., Anthony, A., Lotz, C., Longprez, L. D., Brouillet, E., et al. (2017). Altered enhancer transcription underlies Huntington's disease striatal transcriptional signature. *Sci. Rep.* 7:42875.

Hah, N., Murakami, S., Nagari, A., Danko, C. G., and Kraus, W. L. (2013). Enhancer transcripts mark active estrogen receptor binding sites. *Genome Res.* 23, 1210–1223. doi: 10.1101/gr.152306.112

Hartge, P., Harvey, E. B., Linehan, W. M., Silverman, D. T., Sullivan, J. W., Hoover, R. N., et al. (1990). Unexplained excess risk of bladder cancer in men. *J. Natl. Cancer Inst.* 82, 1636–1640. doi: 10.1093/jnci/82.20.1636

He, H., Li, W., Wu, D., Nagy, R., Liyanarachchi, S., Akagi, K., et al. (2013). Ultra-rare mutation in long-range enhancer predisposes to thyroid carcinoma with high penetrance. *PLoS One* 8:e61920. doi: 10.1371/journal.pone.0061920

Horie, S. (2010). Editorial comment to Inverse expression of estrogen receptor-beta and nuclear factor-kappaB in urinary bladder carcinogenesis. *Int. J. Urol.* 17, 810–810. doi: 10.1111/j.1442-2042.2010.02627.x

IIott, N. E., Heward, J. A., Roux, B., Tsitsiou, E., Fenwick, P. S., Lenzi, L., et al. (2014). Long non-coding RNAs and enhancer RNAs regulate the lipopolysaccharide-induced inflammatory response in human monocytes. *Nat. Commun.* 5:3979.

Kim, T. K., Hemberg, M., Gray, J. M., Costa, A. M., Bear, D. M., Wu, J., et al. (2010). Widespread transcription at neuronal activity-regulated enhancers. *Nature* 465, 182–187. doi: 10.1038/nature09033

Lam, M. T., Cho, H., Lesch, H. P., Gosselin, D., Heinz, S., Tanakaoishi, Y., et al. (2013). Rev-Erbs repress macrophage gene expression by inhibiting enhancer-directed transcription. *Nature* 498:511. doi: 10.1038/nature12209

Li, W., Notani, D., Ma, Q., Tanasa, B., Nunez, E., Chen, A. Y., et al. (2013). Functional roles of enhancer RNAs for oestrogen-dependent transcriptional activation. *Nature* 498, 516–520. doi: 10.1038/nature12210

Madeb, R., and Messing, E. M. (2004). Gender, racial and age differences in bladder cancer incidence and mortality. *Urol. Oncol.* 22, 86–92. doi: 10.1016/s1078-1439(03)00139-x

Murakawa, Y., Yoshihara, M., Kawaji, H., Nishikawa, M., Zayed, H., Suzuki, H., et al. (2016). Enhanced identification of transcriptional enhancers provides mechanistic insights into diseases. *Trends Genet.* 32, 76–88. doi: 10.1016/j.tig.2015.11.004

Nakao, A., Afrakhte, M., Morén, A., Nakayama, T., Christian, J. L., Heuchel, R., et al. (1997). Identification of Smad7, a TGFbeta-inducible antagonist of TGF-beta signalling. *Nature* 389, 631–635. doi: 10.1038/39369

Qi, F., Tan, B., Ma, F., Zhu, B., Zhang, L., Liu, X., et al. (2019). Synthetic light-switchable system based on CRISPR Cas13a regulates the expression of LncRNA MALAT1 and Affects the malignant phenotype of bladder cancer cells. *Int. J. Biol. Sci.* 15, 1630–1636. doi: 10.7150/ijbs.33772

Racioppi, M., D'Agostino, D., Totaro, A., Pinto, F., Sacco, E., D'Addessi, A., et al. (2012). Value of current chemotherapy and surgery in advanced and metastatic bladder cancer. *Urol. Int.* 88, 249–258. doi: 10.1159/000335556

Rahman, S., Zorca, C. E., Traboulsi, T., Noutahi, E., Krause, M. R., Mader, S., et al. (2017). Single-cell profiling reveals that eRNA accumulation at enhancer-promoter loops is not required to sustain transcription. *Nucleic Acids Res.* 45, 3017–3030. doi: 10.1093/nar/gkw1220

Rose, T. L., and Milowsky, M. I. (2016). Improving systemic chemotherapy for bladder cancer. *Curr. Oncol. Rep.* 18, 1–12.

Sofra, M., Fei, P. C., Fabrizi, L., Marcelli, M. E., Claroni, C., Gallucci, M., et al. (2013). Immunomodulatory effects of total intravenous and balanced inhalation anesthesia in patients with bladder cancer undergoing elective

radical cystectomy: preliminary results. *J. Exp. Clin. Canc Res.* 32:6. doi: 10.1186/1756-9966-32-6

Wang, D., Garciabassets, I., Benner, C., Li, W., Su, X., Zhou, Y., et al. (2011). Reprogramming transcription via distinct classes of enhancers functionally Defined by eRNA. *Nature* 474:390. doi: 10.1038/nature10006

Xu, Y., Zhang, N. Z., Chen, J., and Yuan, H. Q. (2013). Biomarkers in urothelial carcinoma of the bladder: the potential crosstalk between transforming growth factor-β1 and estrogen receptor β/androgen receptor pathways. *Med. Hypotheses* 80, 716–718. doi: 10.1016/j.mehy.2013.02.018

Yao, P., Lin, P., Gokoolparsadh, A., Assareh, A., Thang, M. W. C., and Voineagu, I. (2015). Coexpression networks identify brain region–specific enhancer RNAs in the human brain. *Nat. Neurosci.* 18:1168. doi: 10.1038/nn.4063

Zhao, X., Liu, L., Lang, J., Cheng, K., Wang, Y., Li, X., et al. (2018). A CRISPR-Cas13a system for efficient and specific therapeutic targeting of mutant KRAS for pancreatic cancer treatment. *Cancer Lett.* 431, 171–181. doi: 10.1016/j.canlet.2018.05.042

Conflict of Interest: The authors declare that the research was conducted in the absence of any commercial or financial relationships that could be construed as a potential conflict of interest.

frontiers in Molecular Biosciences

ORIGINAL RESEARCH
published: 19 November 2020
doi: 10.3389/fmolb.2020.606593

A Blue Light-Inducible CRISPR-Cas9 System for Inhibiting Progression of Melanoma Cells

Xia Wu[1,2], Haiyan Huang[2], Bo Yu[2]* and Jianzhong Zhang[1]**

[1] Department of Dermatology, Peking University People's Hospital, Beijing, China, [2] Department of Dermatology, Skin Research Institute of Peking University Shenzhen Hospital, Peking University Shenzhen Hospital, Shenzhen, China

Melanoma is an aggressive skin tumor that shows a high mortality rate and level of metastasis. BRAF gene mutation (BRAF V600E) is directly related to the occurrence of melanoma. In this study, a light-inducible gene expression system was designed to control the Cas9 transcription, which could then cleave the BRAF V600E. To prove the potential utility of this system in melanoma, the physiological function of melanoma cells was tested. It illustrated that the light-induced CRISPR-Cas9 system could inhibit the progression of G361 and A375 cells. Thus, this system may provide a novel therapeutic strategy of melanoma intervention.

Keywords: melanoma, light-inducible system, CRISPR/Cas9, gene switch, BRAF V600E

OPEN ACCESS

Edited by:
Yuchen Liu,
Shenzhen University, China

Reviewed by:
Fan Lin,
Shantou University, China
Jialin Meng,
The First Affiliated Hospital of Anhui Medical University, China

****Correspondence:***
Bo Yu
yubomd@163.com
Jianzhong Zhang
rmzjz@126.com

Specialty section:
This article was submitted to Molecular Diagnostics and Therapeutics, a section of the journal Frontiers in Molecular Biosciences

Received: *15 September 2020*
Accepted: *30 October 2020*
Published: *19 November 2020*

Citation:
Wu X, Huang H, Yu B and Zhang J (2020) A Blue Light-Inducible CRISPR-Cas9 System for Inhibiting Progression of Melanoma Cells. Front. Mol. Biosci. 7:606593. doi: 10.3389/fmolb.2020.606593

INTRODUCTION

Melanoma is one of the most malignant skin tumors. Despite its low prevalence rate, its incidence increases every year (Hernandez-Davies et al., 2015; Chang et al., 2020; Strub et al., 2020). For more than 40 years, there have been few available treatments, and none of the clinical trials conducted during this period have been successful (Schadendorf et al., 2018). *BRAF V600E* was found as the most common mutant position and had a strong connection with the morbidity and prognosis of melanoma (Young et al., 2012; Greaves et al., 2013). Over the past years, molecule-targeted drugs – such as BRAF and MEK inhibitors have been used in clinical practice (Luke et al., 2017; Dummer et al., 2018a,b; Chavda and Bhatt, 2020). Though effective initially, drug resistance often occurs after treatment for 2–18 months (Chang et al., 2020). As the resistance developed, the tumor cells almost always become more invasive to further dissemination and metastasis (Cohen-Solal et al., 2018). To understand the underlying mechanism of this resistance, previous researchers found the reactivation of the BRAF/MEK/ERKs pathway accounted for 80% of the resistant tumors (Rizos et al., 2014). In addition, the PI3-K/AKT pathway that is closely interacted with the BRAF/MEK/ERKs could be another cause of drug resistance when reactivated (Davies, 2012; Rizos et al., 2014).

CRISPR-Cas9 was used to edit the genome in various fields (Carey and Gagnon, 2020; Crunkhorn, 2020; Moghadam et al., 2020). Emerging evidence suggests that genome editing of BRAF V600E is possible and effectively induces the apoptosis of melanoma cells (Yang et al., 2017). Our group has tried to design sgRNAs targeting BRAF V600E and edited it with the combined effect of Cas9. According to the results of Sanger sequencing and cell function tests, the edited BRAF V600E caused the apoptosis of melanoma cells. Although CRISPR-Cas9 is efficient, how to precisely control its function requires further investigation (Akcakaya et al., 2018; Lino et al., 2018; Huang et al., 2020). Thus, developing a more accurate regulatory system is in urgent need. As an

epidermal tumor, melanoma is easily accessible to light, which is widely used in various disciplines as a gene regulatory tool, especially in synthetic biology (Yazawa et al., 2009; Kennedy et al., 2010; Rana and Dolmetsch, 2010; Lin et al., 2016). According to a previous study, a blue light-switchable transgene system (GAVPO) was presented and tested in mammalian cells and in mice (He et al., 2020). We considered applying this system to the treatment of melanoma.

Here, we described a light-inducible gene expression system based on CRISPR-Cas9 and the optimized light-switchable device (GAVPO) interaction. The GAVPO system consists of three parts: GAL4 (65), Vivid protein and p65 (Wang et al., 2012). The GAL4(65), which contains GAL4 residues 1–65, virtually eliminates binding to its consensus cognate DNA sequence, the upstream activating sequence of Gal (UASG). Vivid (VVD) protein, the smallest light-oxygen-voltage (LOV) domain–containing protein, forms a rapidly exchanging dimer upon blue-light activation. The transcriptional activator p65 was ligated to the C-terminal of GAL4 (65)-VVD fusion protein to produce the GAVP system. Then, the double mutations of C71V and N56K in the VVD domain decreased the background gene expression to a minimal level [optimized GAVP (GAVPO)], which was named the light-on system (Light On). When exposed to blue light, GAVPO binds to the UASG and activates downstream gene expression. In this study, we made a codon optimization of the original GAVPO sequence and combined the light-on system with CRISPR and applied it to melanoma, which was a controllable and efficient anti-tumor method. When the GAVPO-CRISPR system was transferred into melanoma cells, under the effect of blue light, the proliferation, invasion and migration of melanoma cells were inhibited, and the apoptosis rate was selectively increased. As a simple method, the light-induced tumor-killing module has worked effectively, and it was expected to become a novel anti-cancer method.

RESULTS

CRISPR-Cas9 System Cleaved the BRAF V600E

The function and specificity of our sgRNA were tested by gRNA Activity Assay Test Kit (Beijing Syngentech Co., Ltd.). The mKate gene in pHS-ACR-ZQ191 and pHS-ACR-ZQ190 was terminated prematurely by a terminator. In order to test the activity of our gRNA, the target mutant BRAF was inserted after the terminator. After the action of Cas9 and sgRNA, the double-strand DNA at the target site was cleaved to form a double-strand break (DSB), and the mKate was activated through cell homologous recombination. HEK293 cells were transfected with pHS-ACR-ZQ170 and pHS-AVC-ZQ190 as a negative control group (NC group) and transfected with pHS-ACR-ZQ170 and pHS-AVC-ZQ191 as the treatment group. The gRNA activity assay demonstrated that the CRISPR-Cas9 system specifically cleaved the mutant BRAF V600E (**Supplementary Figure S1**), but had no effect on the wild type.

The Cas9-sgRNA (BRAF V600E) plasmid was transferred to A375 and G361 cells, and the cell genome was extracted and amplified by Polymerase Chain Reaction (PCR). The amplified DNA fragments were cloned by TA cloning technology. Twenty-one single positive clones were picked randomly and the plasmids were extracted for sequencing. According to the results, we found that BRAF V600E was successfully cut out and three examples were shown (**Figure 1**).

The Blue Light-Inducible BRAF V600E Gene Cleavage System Was Designed and Constructed

As shown in **Figure 2**, we have constructed two vectors to form a blue light-induced BRAF V600E cleavage system. The GAVPO element driven by CMV promoter was a fusion protein composed of GAL4(65), VVD and p65. The Cas9 gene was promoted by 5 × UAS and sgRNA targeting BRAF V600E was promoted by a U6 promoter. The DNA-binding property of Gal4(65)-VVD-p65 fusion protein would be light-switchable. As the light induced dimerization of the fusion protein, it could bind to the UAS and activate Cas9 transcription. Therefore, blue light could flexibly regulate the work of Cas9-sgRNA systems. In this study, we call this system the "GAVPO-CRISPR."

Cell Proliferation Was Inhibited by the GAVPO-CRISPR System in Melanoma Cells

To examine the effects of the GAVPO-CRISPR system on melanoma cell growth under the illumination condition (0.84 W/m^2; 1 s:30 s), the cell counting kit-8 (CCK8) assay was performed. The results showed that the GAVPO-CRISPR system suppressed cell growth in A375 (**Figure 3C**) and G361 (**Figure 3D**) significantly ($P < 0.01$) after 72-h exposure to the blue light, compared to the negative controls. The colony-formation assay investigated further into the effect of GAVPO-CRISPR on the proliferation of melanoma cells (**Figures 3A,B**), and its results supported the CCK-8 experiment. After a 2-week cell culture, the picture of the cells stained with crystal violet solution directly reflects the inhibitory effect of light-induced GAVPO-CRISPR system on the growth of melanoma cells.

Cell Migration Was Suppressed by the GAVPO-CRISPR System in Melanoma Cells

To investigate the effects of the GAVPO-CRISPR system on melanoma cell migration under the blue light (0.84 W/m^2; 1 s:30 s), the wound healing assay was performed. Blue light and dark conditions were given when scratches were formed, and the healing of scratches was observed after 48 h. The results showed that GAVPO-CRISPR could inhibit the migration of A375 and G361 cells under blue light illumination (**Figures 4A,B**).

Cell Invasion Was Restrained by the GAVPO-CRISPR System in Melanoma Cells

Transwell assay was performed to assess the effect on cell invasion of GAVPO-CRISPR treated melanoma cells. After 24 h

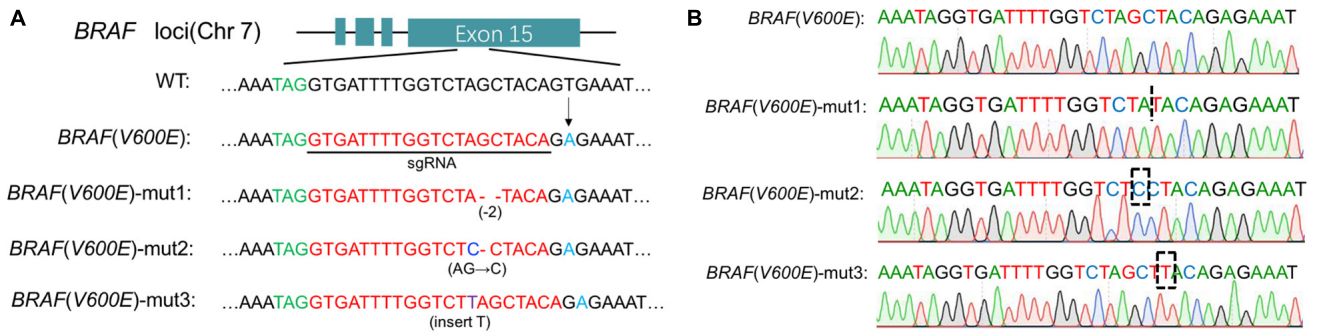

FIGURE 1 | Cas9 edited BRAF V600E. **(A)** Specific sgRNA was designed for BRAF locus. Under the action of Cas9/sgRNA, the BRAF V600E sequence was cut in melanoma cells. Here three examples are cited. **(B)** Detailed sequencing maps.

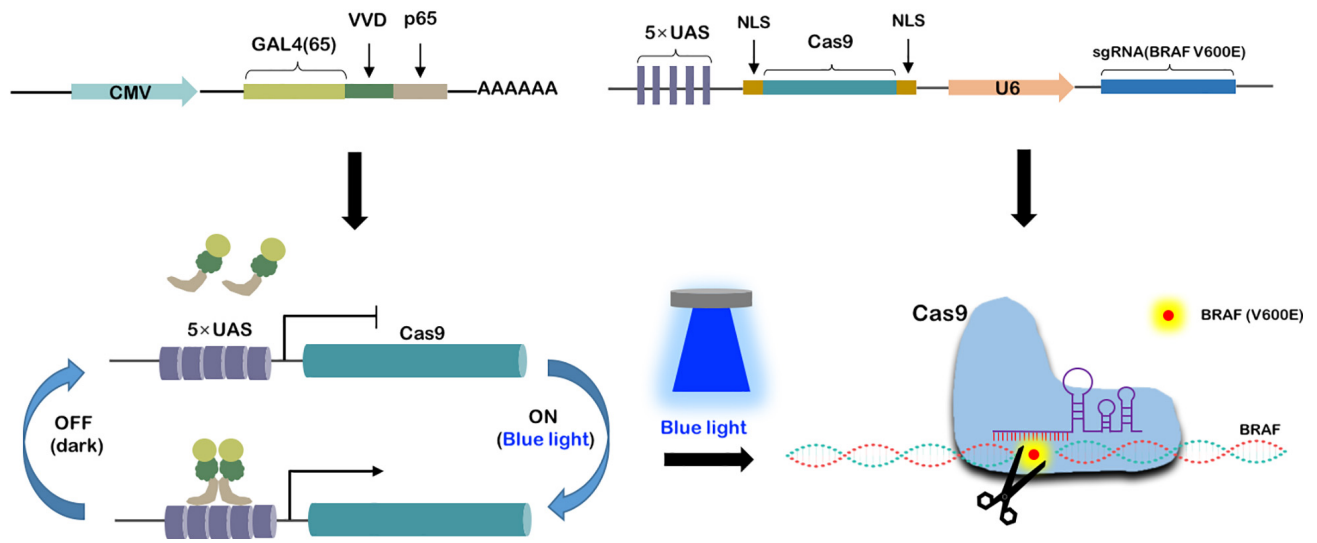

FIGURE 2 | Construction of blue light-induced BRAF V600E cleavage system. Synthesis of a blue light-induced BRAF V600E cleavage system based on two plasmids. One is CMV promoted GAL4(65), VVD and p65 fusion protein. The other is 5× UAS promoted Cas9 and U6 promoted sgRNA. Under blue light condition, the fusion proteins get dimerized and activated the 5× UAS promoter, leading to gRNA-Cas9 expression and BRAF V600E specific editing.

of dark and blue light (0.84 W/m^2; 1 s:30 s) conditions, the cell invasion rate was obviously suppressed in the GAVPO-CRISPR group compared to the groups under dark conditions and the control group under blue light (**Figures 5A,B**). These results demonstrated that the light-controlled system could restrain cell invasion in melanoma cells.

Cell Apoptosis Was Promoted by the GAVPO-CRISPR System in Melanoma Cells

Flow cytometry assay was performed to detect the effects on cell apoptosis of GAVPO-CRISPR treated melanoma cells. Before the flow cytometry, cells were cultured in dark and blue light (0.84 W/m^2; 1 s:30 s) condition for 48 h. As shown in **Figures 6A,B**, compared to the negative controls, the apoptosis of A375 and G361 in the GAVPO-CRISPR group was significantly increased. (***$P < 0.001$). These results demonstrated that the light-controlled system could promote cell apoptosis in melanoma cells.

DISCUSSION

Melanoma is a highly malignant skin cancer that is commonly treated with surgical resection and chemotherapy. Early stage patients benefit from the surgery, yet the prognosis of the late-stage patients is poor. Tumorigenesis is a result of accumulated multi-gene mutation, in which BRAF gene mutation (mainly BRAF V600E) is significantly higher than other pathogenic genes in melanoma. It is therefore one of the research hotspots in melanoma therapy.

In the field of gene therapy, CRISPR is a convenient and effective technology. Using CRISPR to edit the mutation sites of genes can effectively disrupt the function of pathogenic genes

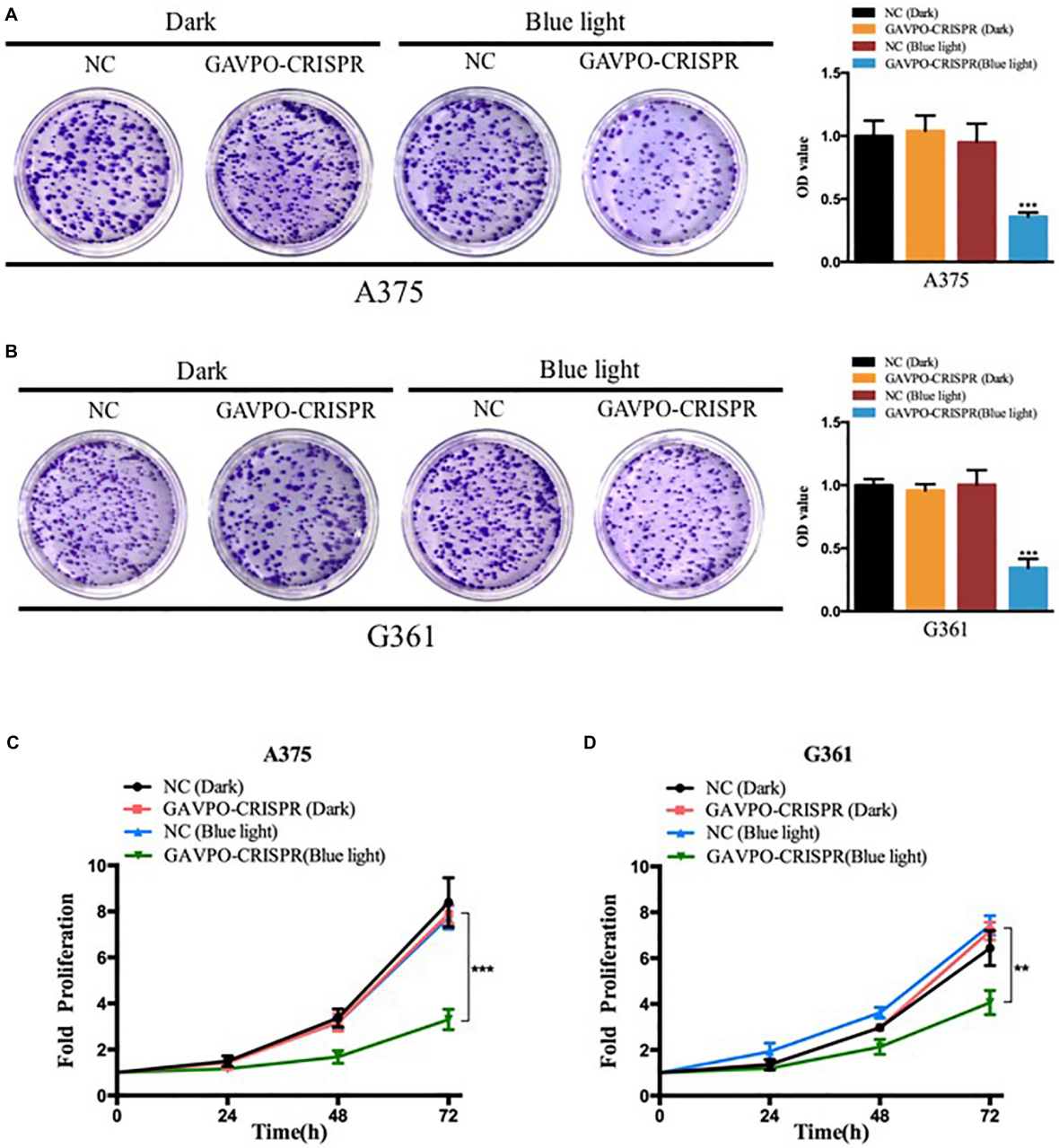

FIGURE 3 | Light-induced GAVPO-CRISPR system inhibited melanoma cell growth. **(A,B)** Colony-formation assay implicating the effect of light-induced GAVPO-CRISPR system under blue-light or dark conditions on cell proliferation in A375 **(A)** and G361 **(B)** cells, compared to the negative control. **(C,D)** CCK-8 assay representing the effect of light-induced GAVPO-CRISPR system under blue-light or dark conditions on cell proliferation in A375 **(C)** and G361 **(D)** cells, compared to the negative control. Data are presented as the means ± SD from at least three biological replicates. (*$P < 0.05$, **$P < 0.01$, ***$P < 0.001$).

(Yang et al., 2017; György et al., 2019; Wang D. et al., 2019; Zhao H. et al., 2020). In this study, we used CRISPR-Cas9 technology to edit the BRAF V600E gene and found a good inhibitory effect on tumor cells. Since melanoma is often found on the skin surface with a limited range of size. It is meaningful to control CRISPR in time and space dimensions.

As a simple and easy-to-obtain light source, blue light is often used for anti-inflammation and sterilization on the skin, without side effects on the human body (Lotan et al., 2019; Zhao J. et al., 2020). In this study, we used blue light as the controller of the CRISPR-Cas9 system. In the absence of blue light, the CRISPR system stopped working. When irradiated by blue light, CRISPR-Cas9 was activated to edit the gene. By controlling blue light exposure, the CRISPR-Cas9 tool can be flexibly regulated in the time and space dimensions, making it an ideal tool for anti-BRAF V600E.

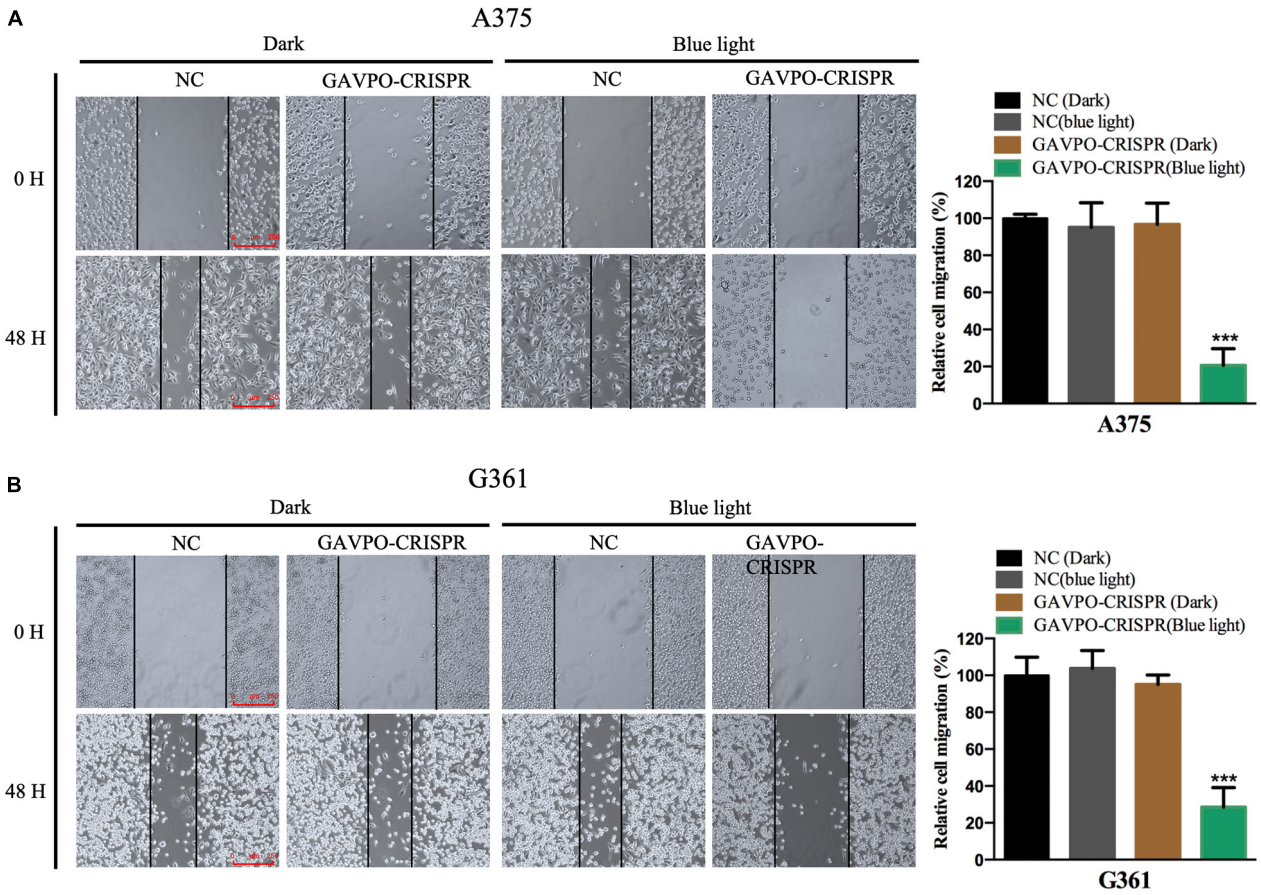

FIGURE 4 | Light-induced GAVPO-CRISPR system inhibited melanoma cell migration. **(A)** Wound healing assay implicating the effect of light-induced GAVPO-CRISPR system under blue-light or dark conditions on cell migration in A375 cells, compared to the negative control. **(B)** Wound healing assay representing the effect of light-induced GAVPO-CRISPR system under blue-light or dark conditions on cell migration in G361 cells, compared to the negative control. Data are presented as the means ± SD from at least three biological replicates. (*$P < 0.05$, **$P < 0.01$, ***$P < 0.001$).

In this study, we cultured cells under dark and 460 nm blue light conditions, respectively, and verified their functions through a series of cell functional experiments. The results showed that blue light could effectively activate the function of GAVPO-CRISPR and inhibit the proliferation of tumor cells.

In this study, melanoma mutant gene BRAF V600E was edited by the CRISPR gene-editing tool, resulting in an obvious killing effect on tumor cells. Then, combined with the characteristics of melanoma, the blue light on the surface of the skin can be used to control the work of CRISPR manually. This study expands the application scenario of the CRISPR tool and exerts its anti-tumor effect by effectively combining it with a photogenetic tool. In clinical gene therapy, we can further optimize the system, such as using smaller Cas protein (like CasX) to play the role of gene editing, and using vectors such as adeno-associated virus (AAV) to deliver them to organisms for cancer biotherapy. In fact, researchers have made many successful attempts in the treatment of diseases with light control devices. The research of AAV has entered the clinical treatment stage, the combination of AAV and light control devices is feasible (Wang E. et al., 2019; Yang et al., 2020; Yu et al., 2020).

In summary, we have synthesized a gene circuit that combined photogenetic tools and CRISPR gene editing techniques to specifically suppress the melanoma cells. Our study explores a new approach for the potential treatment of melanoma, and the synthetic gene circuit has the potential for clinical application.

MATERIALS AND METHODS

Plasmids Construction

To construct the vector expressing the Cas9 and sgRNA targeting BRAF V600E, the three sgRNAs were designed and synthesized by Syngentech Co., Ltd. (Beijing, China). To generate a plasmid that expresses sgRNA targeting mutant BRAF in melanoma cells, a plasmid (pHS-ACR-ZQ170) containing a U6 promoter driven sgRNA that targeted the mutant BRAF gene and a Cas9 protein driven by phEF1a promoter was constructed. In order to test the function and specificity of the sgRNA, two plasmids containing a wild-type BRAF sequence (pHS-ACR-ZQ190) and BRAF V600E (pHS-ACR-ZQ191) were constructed. Both plasmids contained a prematurely terminated mKate gene (a new type of dark red

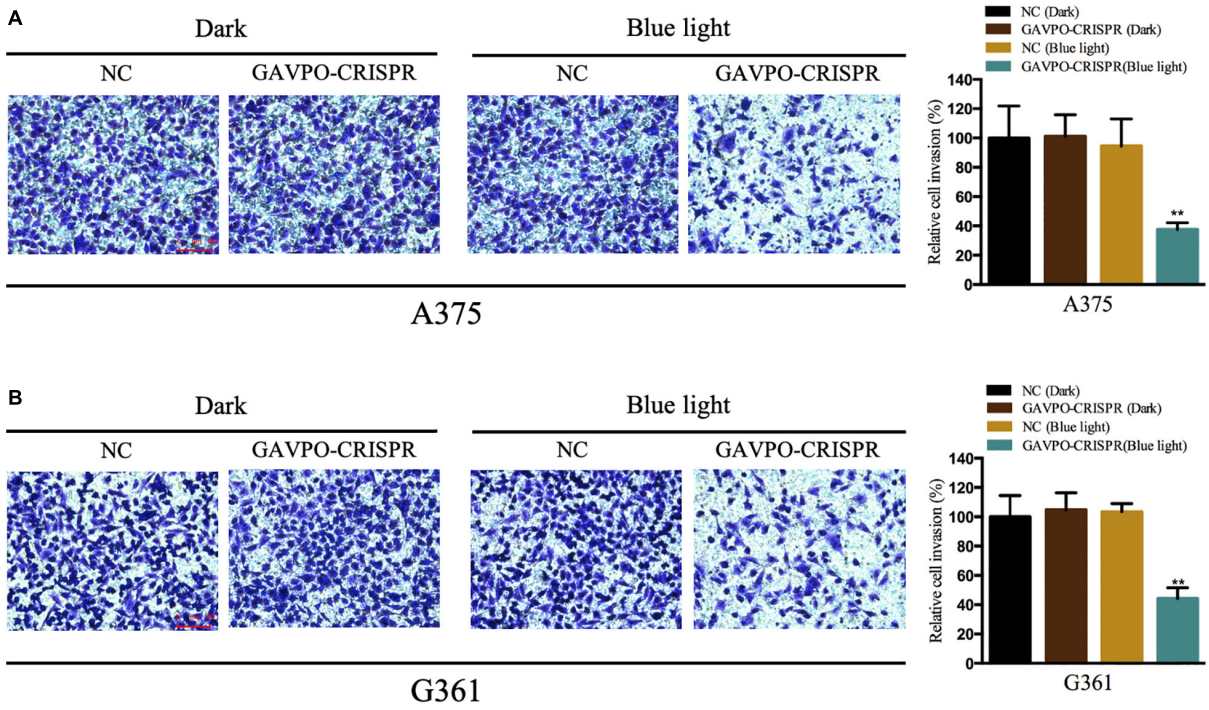

FIGURE 5 | Light-induced GAVPO-CRISPR system restricted melanoma cell invasion. **(A)** Transwell assay implicating the effect of light-induced GAVPO-CRISPR system under blue-light or dark conditions on cell invasion in A375 cells, compared to the negative control. **(B)** Transwell assay representing the effect of light-induced GAVPO-CRISPR system under blue-light or dark conditions on cell invasion in G361 cells, compared to the negative control. Data are presented as the means ± SD from at least three biological replicates. (*$P < 0.05$, **$P < 0.01$, ***$P < 0.001$).

fluorescent protein originated from TagRFP) driven by phEF1a promoter. After the single-strand annealing test, an effective sgRNA was picked out and used.

To construction the vector that expresses the GAL4(65)-VVD-p65, the sequence of GAL4(65)-VVD-p65 was inserted into pHS-AVC-LW477 between the restriction sites *Eco*RI and *Bam*HI. To create vectors expressing 5× UAS-Cas9-U6-sgRNA (BRAF V600E), we used the UAS sequence to replace CMV promoter, respectively and place the sequence of Cas9 in the middle of sgRNA and UAS in the pHS-ACR-LW352 vector. Finally, the ultimate two vectors (GAL4(65)-VVD-p65 and UAS-Cas9-sgRNA) were packaged by lentivirus. Relative sequences were presented in **Supplementary Table S1** and **Supplementary Figure S1**.

Cell Lines and Cell Culture

The melanoma cell lines (A375 and G361) were purchased from the Institute of Cell Research, Chinese Academy of Sciences, Shanghai, China. The A375 and G361 cells were maintained in 1640 medium (Invitrogen, Carlsbad, CA, United States) with 10% fetal bovine serum (FBS) and 1% antibiotics (100 ug/ml streptomycin and 100 U/ml penicillin) at 37°C in the atmosphere of 5% CO_2.

Cell Transfection and Illumination

The constructed vectors from *Escherichia coli* bacteria were extracted by E.Z.N.A Fastfiler Endo-free Plasmid Maxiprep kits (Omega, Norcross, GA, United States). The cell was transfected with vectors using Lipofectamine 3000 Transfection Reagent (Invitrogen, Carlsbad, CA, United States) according to the manufacturer's protocol. After transfection in dark about 12 h, cells were illuminated by a blue light LED lamp (460 nm, 0.84 W m^{-2}). The lentivirus vectors were packaged and concentrated by Syngentech Co., Ltd. (Beijing, China). After puromycin screening, cells were illuminated by blue light. The blue light can be controlled by a timer adjusting the illuminate dose.

DNA Extraction, Original TA Cloning and Gene Sequencing

The DNA Maxi Kit (Omega, Norcross, GA, United States) was used to extract cell DNA after transfection according to the manufacturer's protocol. The primers were used to amplify the sequence containing BRAFV600E by PCR, then the PCR fragments were sited into the pMDTM19-T vector using pMDTM19-T Vector Cloning Kit (Takara, Dalian, China). The primers used were:

BRAFV600E-forward: GCTGTGGATCACACCTGCCTTAAA
BRAFV600E-reverse: TCGCCCAGGAGTGCCAAGAGA

The cloning vectors were sequenced by Syngentech Co., Ltd. (Beijing, China).

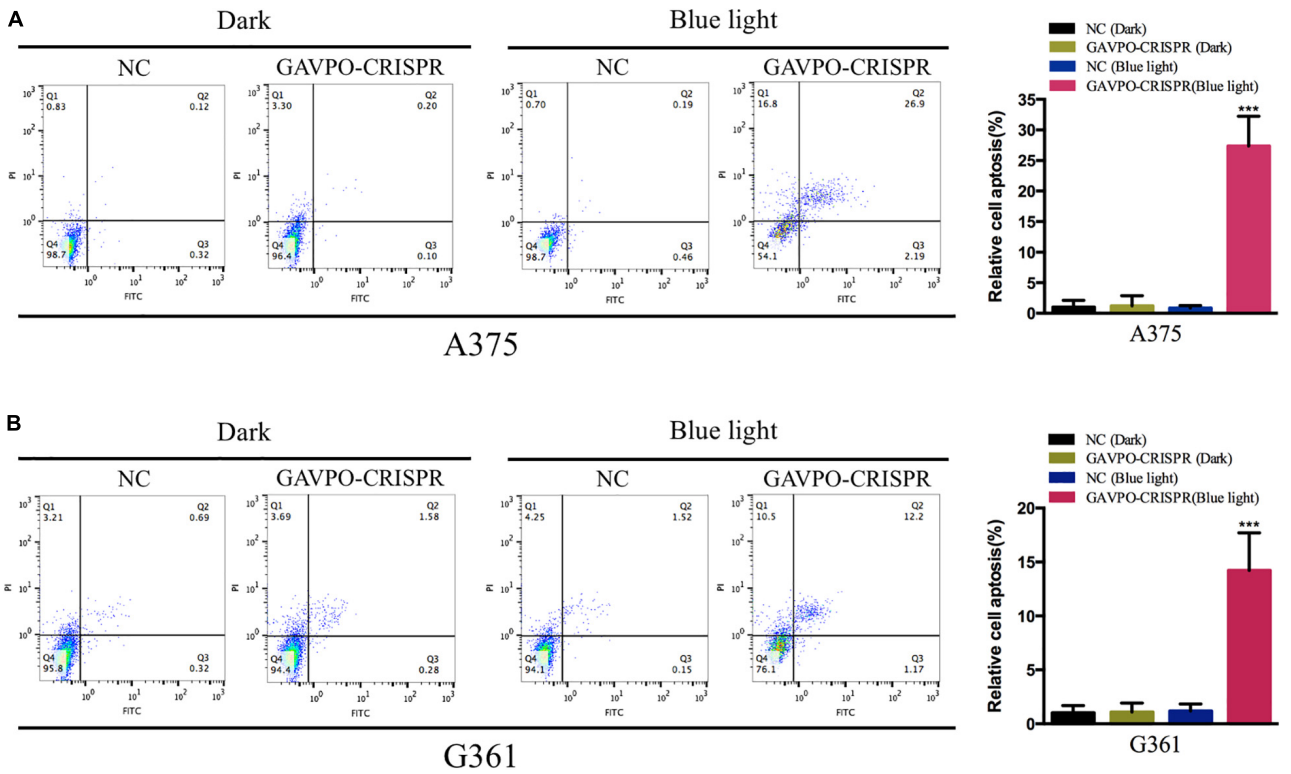

FIGURE 6 | Light-induced GAVPO-CRISPR system promoted melanoma cell apoptosis. **(A)** Flow cytometry results representing the effect of light-induced GAVPO-CRISPR system under blue-light or dark conditions on cell apoptosis in A375 cells, compared to the negative control. **(B)** Flow cytometry results representing the effect of light-induced GAVPO-CRISPR system under blue-light or dark conditions on cell apoptosis in G361 cells, compared to the negative control. Data are presented as the means ± SD from at least three biological replicates. (*$P < 0.05$, **$P < 0.01$, ***$P < 0.001$).

Wound Healing Assay

The wound healing assay was used to assess the migration ability of G361 and A375 *in vitro*. Before a blue light illumination, lentivirus infected cells were seeded in the 6-well plate to get more than 90% confluence and serum-starved for 24 h. Then illumination started, wounds were scratched by passing the sterile 200 μl pipette tip across the monolayer cells at the same time. We considered the time of wound infliction as 0 h, and wound closure was determined at 24 h. The width of the wound was monitored with the help of a digital camera system and the areas covered by migrated cells (%) were quantified.

Cell Proliferation Assay

The effects of dark and blue light illumination to melanoma cells were measured by CCK-8 assay. After dark and illumination treating, about 3×10^3 cells per well were seeded in a 96-well plate and pre-incubated for 12 h. At the time of 0, 24, 48, and 72 h, 10 μl of Cell Counting Kit solution (TransGen, Beijing, China) was added to each well. The absorbance at 450 nm was calculated by the CCK-8 reader machine (Bio-Rad, Hercules, CA, United States) after an hour's incubation. The experiments were performed at least three times. For the colony-formation assay, the transfected G361 and A375 cells were cultured in 6 cm culture dishes at a density of 2000 cells per well and incubated for 15 days and exposed to blue light. Finally, the cells were stained with 0.1% crystal violet and imaged. The stained cells were washed with 33% glacial acetic acid. The absorbance in each well was measured at 550 nm using a microplate reader.

Cell Invasion Assay

The effects of dark and blue light illumination on cell invasion were measured by Transwell assay. G361 and A375 cells were seeded in 24-well plates. About 5×10^5 cells were seeded in triplicate onto a 24-well plate with chambers (Corning, NY, United States) coated with Matrigel. The lower chamber contained 10% FBS medium and the upper one contained a serum-free medium. With the incubation of 24 h, we counted the percentage of cells passing the membranes under a microscope.

Flow Cytometry Assay

G361 and A375 cells were seeded in six-well plates. Then transfected cells were collected after incubation under light/dark for 24 h and harvested using trypsin without EDTA. According to the manufacturer's protocols, the FITC Annexin V Apoptosis Detection Kit (TransGen, Beijing, China) could double stain cells with FITC Annexin and PI. The ratio of early apoptotic cells in melanoma cells was determined by the flow cytometry (EPICS, XL-4, Beckman, CA, United States). The experiments were done at least three times.

Statistical Analyses

All data from at least three independent experiments were presented as mean ± standard deviation (SD). Statistical data was analyzed by SPSS 20.0 software (SPSS Inc., Chicago, IL, United States). $P < 0.05$ was considered statistically significant.

DATA AVAILABILITY STATEMENT

All datasets presented in this study are included in the article/**Supplementary Material**.

AUTHOR CONTRIBUTIONS

XW and HH performed the experiments and data analysis. XW prepared all the figures and wrote the manuscript. JZ and BY designed and supervised the project. All authors read and approved the final manuscript.

FUNDING

This work was supported by Shenzhen Sanming Project (no. SZSM201812059) and Shenzhen Key Medical Discipline Construction Fund (No. SZXK040).

SUPPLEMENTARY MATERIAL

The Supplementary Material for this article can be found online at: https://www.frontiersin.org/articles/10.3389/fmolb.2020.606593/full#supplementary-material

REFERENCES

Akcakaya, P., Bobbin, M. L., Guo, J. A., Malagon-Lopez, J., Clement, K., Garcia, S. P., et al. (2018). In vivo CRISPR editing with no detectable genome-wide off-target mutations. *Nature* 561, 416–419. doi: 10.1038/s41586-018-0500-9

Carey, C. M., and Gagnon, J. A. (2020). CRISPR rube goldberg machines for visualizing cell lineage. *Nat. Neurosci.* 2020:1161.

Chang, X., Zhang, T., Wang, Q., Rathore, M. G., Reddy, K., Chen, H., et al. (2020). HI-511 overcomes melanoma drug resistance via targeting AURKB and BRAF V600E. *Theranostics* 10, 9721–9740. doi: 10.7150/thno.44342

Chavda, J., and Bhatt, H. (2020). Systemic review on B-Raf(V600E) mutation as potential therapeutic target for the treatment of cancer. *Eur. J. Med. Chem.* 206:112675. doi: 10.1016/j.ejmech.2020.112675

Cohen-Solal, K. A., Kaufman, H. L., and Lasfar, A. (2018). Transcription factors as critical players in melanoma invasiveness, drug resistance, and opportunities for therapeutic drug development. *Pigment Cell Melanoma. Res.* 31, 241–252. doi: 10.1111/pcmr.12666

Crunkhorn, S. (2020). CRISPR-engineered fat cells prevent obesity. *Nat. Rev. Drug. Discov.* 19:672. doi: 10.1038/d41573-020-00155-4

Davies, M. A. (2012). The role of the PI3K-AKT pathway in melanoma. *Cancer J.* 18, 142–147. doi: 10.1097/ppo.0b013e31824d448c

Dummer, R., Ascierto, P. A., Gogas, H. J., Arance, A., Mandala, M., Liszkay, G., et al. (2018a). Encorafenib plus binimetinib versus vemurafenib or encorafenib in patients with BRAF-mutant melanoma (COLUMBUS): a multicentre, open-label, randomised phase 3 trial. *Lancet Oncol.* 19, 603–615. doi: 10.1016/s1470-2045(18)30142-6

Dummer, R., Ascierto, P. A., Gogas, H. J., Arance, A., Mandala, M., Liszkay, G., et al. (2018b). Overall survival in patients with BRAF-mutant melanoma receiving encorafenib plus binimetinib versus vemurafenib or encorafenib (COLUMBUS): a multicentre, open-label, randomised, phase 3 trial. *Lancet Oncol.* 19, 1315–1327. doi: 10.1016/s1470-2045(18)30497-2

Greaves, W. O., Verma, S., Patel, K. P., Davies, M. A., Barkoh, B. A., Galbincea, J. M., et al. (2013). Frequency and spectrum of BRAF mutations in a retrospective, single-institution study of 1112 cases of melanoma. *J. Mol. Diagn.* 15, 220–226. doi: 10.1016/j.jmoldx.2012.10.002

György, B., Nist-Lund, C., Pan, B., Asai, Y., Karavitaki, K. D., Kleinstiver, B. P., et al. (2019). Allele-specific gene editing prevents deafness in a model of dominant progressive hearing loss. *Nat. Med.* 25, 1123–1130. doi: 10.1038/s41591-019-0500-9

He, M., Wang, Y., Chen, X., Zhao, Y., Lou, K., Wang, Y., et al. (2020). Spatiotemporally controllable diphtheria toxin expression using a light-switchable transgene system combining multifunctional nanoparticle delivery system for targeted melanoma therapy. *J. Control. Release* 319, 1–14. doi: 10.1016/j.jconrel.2019.12.015

Hernandez-Davies, J. E., Tran, T. Q., Reid, M. A., Rosales, K. R., Lowman, X. H., Pan, M., et al. (2015). Vemurafenib resistance reprograms melanoma cells towards glutamine dependence. *J. Transl. Med.* 13:210.

Huang, X., Chen, Z., and Liu, Y. (2020). RNAi-mediated control of CRISPR functions. *Theranostics* 10, 6661–6673. doi: 10.7150/thno.44880

Kennedy, M. J., Hughes, R. M., Peteya, L. A., Schwartz, J. W., Ehlers, M. D., and Tucker, C. L. (2010). Rapid blue-light-mediated induction of protein interactions in living cells. *Nat. Methods* 7, 973–975. doi: 10.1038/nmeth.1524

Lin, F., Dong, L., Wang, W., Liu, Y., Huang, W., and Cai, Z. (2016). An efficient light-inducible P53 expression system for inhibiting proliferation of bladder cancer cell. *Int. J. Biol. Sci.* 12, 1273–1278. doi: 10.7150/ijbs.16162

Lino, C. A., Harper, J. C., Carney, J. P., and Timlin, J. A. (2018). Delivering CRISPR: a review of the challenges and approaches. *Drug Deliv.* 25, 1234–1257. doi: 10.1080/10717544.2018.1474964

Lotan, Y., Bivalacqua, T. J., Downs, T., Huang, W., Jones, J., Kamat, A. M., et al. (2019). Blue light flexible cystoscopy with hexaminolevulinate in non-muscle-invasive bladder cancer: review of the clinical evidence and consensus statement on optimal use in the USA - update 2018. *Nat. Rev. Urol.* 16, 377–386. doi: 10.1038/s41585-019-0184-4

Luke, J. J., Flaherty, K. T., Ribas, A., and Long, G. V. (2017). Targeted agents and immunotherapies: optimizing outcomes in melanoma. *Nat. Rev. Clin. Oncol.* 14, 463–482. doi: 10.1038/nrclinonc.2017.43

Moghadam, F., LeGraw, R., Velazquez, J. J., Yeo, N. C., Xu, C., Park, J., et al. (2020). Synthetic immunomodulation with a CRISPR super-repressor in vivo. *Nat. Cell. Biol.* 22, 1143–1154. doi: 10.1038/s41556-020-0563-3

Rana, A., and Dolmetsch, R. E. (2010). Using light to control signaling cascades in live neurons. *Curr. Opin. Neurobiol.* 20, 617–622. doi: 10.1016/j.conb.2010.08.018

Rizos, H., Menzies, A. M., Pupo, G. M., Carlino, M. S., Fung, C., Hyman, J., et al. (2014). BRAF inhibitor resistance mechanisms in metastatic melanoma: spectrum, and clinical impact. *Clin. Cancer. Res.* 20, 1965–1977. doi: 10.1158/1078-0432.ccr-13-3122

Schadendorf, D., van Akkooi, A. C. J., Berking, C., Griewank, K. G., Gutzmer, R., Hauschild, A., et al. (2018). Melanoma. *Lancet* 392, 971–984.

Strub, T., Ballotti, R., and Bertolotto, C. (2020). The "ART" of epigenetics in melanoma: from histone "alterations, to resistance and therapies". *Theranostics* 10, 1777–1797. doi: 10.7150/thno.36218

Wang, E., Lu, S. X., Pastore, A., Chen, X., Imig, J., Chun-Wei Lee, S., et al. (2019). Targeting an RNA-binding protein network in acute myeloid leukemia. *Cancer Cell* 35, e369–e384.

Wang, D., Tai, P. W. L., and Gao, G. (2019). Adeno-associated virus vector as a platform. (for)gene therapy delivery. *Nat. Rev. Drug. Discov.* 18, 358–378. doi: 10.1038/s41573-019-0012-9

Wang, X., Chen, X., and Yang, Y. (2012). Spatiotemporal control of gene expression by a light-switchable transgene system. *Nat. Methods* 9, 266–269. doi: 10.1038/nmeth.1892

Yang, M., Wei, H., Wang, Y., Deng, J., Tang, Y., Zhou, L., et al. (2017). Targeted disruption of V600E-mutant BRAF gene by CRISPR-Cpf1. *Mol. Ther. Nucleic Acids* 8, 450–458. doi: 10.1016/j.omtn.2017.05.009

Yang, Y., Zeng, B., Guo, J., Li, Y., Yang, Y., and Yuan, Q. (2020). Two-dimensional device with light-controlled capability for treatment of cancer-relevant infection diseases. *Anal. Chem.* 92, 10162–10168. doi: 10.1021/acs.analchem.0c02216

Yazawa, M., Sadaghiani, A. M., Hsueh, B., and Dolmetsch, R. E. (2009). Induction of protein-protein interactions in live cells using light. *Nat. Biotechnol.* 27, 941–945. doi: 10.1038/nbt.1569

Young, K., Minchom, A., and Larkin, J. (2012). BRIM-1, -2 and -3 trials: improved survival with vemurafenib in metastatic melanoma patients with a BRAF(V600E) mutation. *Future Oncol.* 8, 499–507. doi: 10.2217/fon.12.43

Yu, Y., Wu, X., Guan, N., Shao, J., Li, H., Chen, Y., et al. (2020). Engineering a far-red light-activated split-cas9 system for remote-controlled genome editing of internal organs and tumors. *Sci. Adv.* 6:eabb1777. doi: 10.1126/sciadv.abb1777

Zhao, H., Li, Y., He, L., Pu, W., Yu, W., Li, Y., et al. (2020). In vivo AAV-CRISPR/Cas9-mediated gene editing ameliorates atherosclerosis in familial hypercholesterolemia. *Circulation* 141, 67–79. doi: 10.1161/circulationaha.119.042476

Zhao, J., Li, B., Ma, J., Jin, W., and Ma, X. (2020). Photoactivatable RNA N(6)-methyladenosine editing with CRISPR-Cas13. *Small* 16:e1907301.

Conflict of Interest: The authors declare that the research was conducted in the absence of any commercial or financial relationships that could be construed as a potential conflict of interest.

frontiers in Molecular Biosciences

ORIGINAL RESEARCH
published: 09 December 2020
doi: 10.3389/fmolb.2020.617600

Synthetic Artificial Long Non-coding RNA Shows Higher Efficiency in Specific Malignant Phenotype Inhibition Compared to the CRISPR/Cas Systems

Lin Yao[1,2,3†], Quan Zhang[1,2,3†], Aolin Li[1,2,3†], Binglei Ma[1,2,3], Zhenan Zhang[1,2,3], Jun Liu[1,2,3], Lei Liang[1,2,3], Shiyu Zhu[1,2,3], Ying Gan[1,2,3] and Qian Zhang[1,2,3*]*

[1] Department of Urology, Peking University First Hospital, Beijing, China, [2] Institute of Urology, Peking University, Beijing, China, [3] National Research Center for Genitourinary Oncology, Beijing, China

OPEN ACCESS

Edited by:
Yuchen Liu,
Shenzhen University, China

Reviewed by:
Congcong Cao,
Peking University Shenzhen Hospital, China
Lisa Liu,
Temple University, United States

***Correspondence:**
Ying Gan
ganying1989@126.com
Qian Zhang
zhangqianbjmu@126.com

† These authors have contributed equally to this work

Specialty section:
This article was submitted to Molecular Diagnostics and Therapeutics, a section of the journal Frontiers in Molecular Biosciences

Received: 15 October 2020
Accepted: 09 November 2020
Published: 09 December 2020

Citation:
Yao L, Zhang Q, Li A, Ma B, Zhang Z, Liu J, Liang L, Zhu S, Gan Y and Zhang Q (2020) Synthetic Artificial Long Non-coding RNA Shows Higher Efficiency in Specific Malignant Phenotype Inhibition Compared to the CRISPR/Cas Systems. Front. Mol. Biosci. 7:617600. doi: 10.3389/fmolb.2020.617600

Objective: Both oncogenic transcription factors (TFs) and microRNAs (miRNAs) play an important regulator in human cancer by transcriptional and post-transcriptional regulation, respectively. These phenomena raise questions about the ability of artificial device to regulate miRNAs and TFs simultaneously. In this study, we aimed to construct an artificial long non-coding RNA, "alncRNA," which imitated CRISPR/Cas systems and to illuminate its therapeutic effects in bladder cancer cell lines. At the same time, we also compared the efficiency of alncRNA and CRISPR/Cas systems in regulating gene expression.

Study Design and Methods: Based on engineering principles of synthetic biology, we combined tandem arrayed cDNA sequences of aptamer for TFs with tandem arrayed cDNA copies of binding sites for the miRNAs to construct alncRNA. In order to prove the utility of this platform, we chose β -catenin, NF-κB, miR-940, and miR-495 as the functional targets and used the bladder cancer cell lines 5637 and T24 as the test models. Real-time Quantitative PCR (qPCR), dual-luciferase assay and relative phenotypic experiments were applied to severally test the expression of relative gene and therapeutic effects of our devices.

Result: Dual-luciferase assay indicated alncRNA could inhibit transcriptional activity of TFs. What's more, the result of qPCR showed that expression levels of the relative TFs target genes and miRNAs were reduced by corresponding alncRNA and the inhibitory effect was better than CRIPSR dCas9-KRAB. By functional experiments, decreased cell proliferation, increased apoptosis, and motility inhibition were observed in alncRNA-infected bladder cells.

Conclusion: In summary, our synthetic devices indeed function as anti-tumor regulator, which synchronously accomplish transcriptional and post-transcriptional regulation

in bladder cancer cell and show higher efficiency in specific malignant phenotype inhibition compared to the CRISPR/Cas systems. Most importantly, Anti-cancer effects were induced by the synthetic alncRNA in the bladder cancer lines. Our devices, therefore, provides a novel strategy for cancer therapy and could be a useful "weapon" for cancer cell.

Keywords: bladder cancer, synthetic biology, aptamer, miRNA, transcription factors

INTRODUCTION

Bladder cancer (BCa) is a malignant tumor that occurs on the mucous membrane of the bladder. It is the most common malignant tumor in the urinary system and one of the ten most common tumors in the whole body (Kluth et al., 2015; Kamat et al., 2016; Siegel et al., 2017). At present, the treatment for BCa is mainly of surgical treatment, but the post-operative recurrence and metastasis of tumor are still important factors that threaten the life of patients (Racioppi et al., 2012). In addition, chemotherapy or radiotherapy can reduce some of the symptoms of BCa patients, they all have certain curative effect on BCa, but the adverse reactions are large, and these treatment methods cannot actually prolong the survival of patients (Marta et al., 2012; Sofra et al., 2013). There are several novel anti-tumor drugs have been developed and clinically testing their effectiveness, however, these drugs can only be used in the adjuvant treatment of BCa (Wong et al., 2017). It is therefore necessary to develop new treatment methods for BCa. The molecular targeted therapy of tumor is a novel and effective way to improve the therapeutic effect of BCa.

Research on molecular biology confirms that the occurrence and development of malignant tumor is a multi-factor and multi-step process, and the development of BCa is more so (Hanahan and Weinberg, 2011). miRNAs are non-coding RNAs of approximately 19–23 nucleotides lengths, and like other small RNAs, miRNAs have been considered as the byproducts of transcription in the past (Djebali et al., 2012). With the deepening of the research on miRNAs, miRNAs had been found to have an effect on the biological physiological and pathological changes (Rupaimoole and Slack, 2017). As a type of endogenous small single-stranded non-coding RNA, miRNAs regulate the translation and stability of mRNAs through complementary binding with the 3′UTR of mRNAs and play a role in post-transcriptional regulation (Bracken et al., 2016). Although the number of miRNAs is relatively small, more than 1/3 of the cell transcriptional groups are regulated by miRNAs. In addition, the dysregulation of miRNAs expression is an important mechanism to promote the occurrence and development of tumors, and so is the human BCa. Previous work has shown that miR-495 can target phosphatase and tensin homolog and promote the proliferation and invasion of BCa cells through its interaction with phosphatase and tensin homolog (Tan et al., 2017). miR-940 plays a role in promoting the progression of human BCa by activating the c-myc protein, and its upregulation has been proved to serve as an effective biomarker that predicts the poor prognosis for BCa (Wang et al., 2018). Thus, regulating the dysregulation of miRNAs and reprogramming the signaling pathway in BCa cells will effectively control the malignant phenotype of BCa cells and achieve the purpose of treating BCa.

Transcription factors (TFs) are presented in the nucleus and play a central role in the expression of gene within the cells (Haberle and Stark, 2018). In tumor cells, TFs affect the formation, evolution and metastasis of the tumor by regulating the expression of oncogenes, tumor suppressor genes and cell cycle related molecules. To date, some cancer-related TFs such as β-catenin (Lee et al., 2006) and NF-κB (Culler et al., 2010) have been proved to be significantly abnormal and highly expressed in BCa, which is highly correlated with the malignancy of the tumor. Therefore, it would be a further important attempt to inhibit tumorigenesis if these cancer-related TFs can be restrained from continuing to function in the tumor cells.

In this study, we constructed a working "artificial long non-coding RNA" (alncRNA) based on synthetic biology principles and tested its effectiveness in the BCa cell lines. The alncRNA we constructed is mainly composed of miRNAs binding sites and cancer-related TFs specifically binding sites. This alncRNA can simultaneously absorb and downregulate cancer-related miRNAs and protein with the BCa cells and achieved multiple targets and inhibiting tumor cells at the same time.

MATERIALS AND METHODS

Cell Lines and Cell Culture

The human bladder cancer cell lines (T24, 5637, and SW780) and the human normal bladder epithelial cell line (SV-HUC1) are all bought from the American Type Culture Collection (ATCC, Manassas, VA, United States). In our study, we used two types of mediums, Dulbecco's modified Eagle's medium (DMEM, Gibco, Thermo Fisher Scientific, Waltham, MA, United States) and F12K medium (Gibco). The bladder cancer cell lines T24, 5637, and SW780 were grown in the DMEM, supplemented with 10% fetal bovine serum (Gibco). The SV-HUC1 cell line was grown in the F12K medium which was supplemented with 10% fetal bovine serum. All the cells were cultured at 37°C and 5% CO_2.

Construction of the Artificial Long Non-coding RNA and Cell Transfection

We linked the binding sites of miR-940 and miR-495 to construct the module 1 of the alncRNA. In addition, the aptamers for β-catenin and NF-κB were bulged by us to construct the

module 2. All the nucleic acid sequences required in our study were gained by chemical synthesis.

Dual-Luciferase Reporter Assay

The dual-luciferase reporter assay was performed to evaluate the transcriptional activity of β-catenin in our study. We constructed the dual-luciferase reporter vectors of β-catenin, respectively.

RNA Extraction and Real-Time Quantitative PCR Assay

Total RNAs from cancer tissues or cells after transfection were extracted using the TRIzol reagent (Invitrogen, Grand Island, NY, United States) according to the manufacturer's instructions. PrimeScript RT Reagent Kit with gDNA Eraser (Takara, Japan) was used to transform RNA to cDNA. The mRNA expression levels were measured by using SYBR® Premix Ex Taq™ (TaKaRa, Japan) according to the user's manuals on the Roche lightcycler 480 Real-Time PCR System. GAPDH was utilized as the control to normalize the data. The primer sequences were listed in **Table 1**. The comparative ΔCt method was used to analyze the results by calculating the relative amount. All experiments were carried out at least three repetitions.

Cell Proliferation Assay

In our study, we used CCK-8 assay (TransGen, Beijing, China) and Edu incorporation assay (Ribobio, Guangzhou, China) to determine cell proliferation. The operation steps of both experiments were mainly carried out according to the instructions of the manufacturer and adjusted through the operation steps of previous studies. Additionally, we have repeated these experiments for three times.

TABLE 1 | Relative primers used in this research.

Name	Sequences
GAPDH-F	CGCTCTCTGCTCCTCCTGTTC
GAPDH-R	ATCCGTTGACTCCGACCTTCAC
β-catenin-F	CTGCTCTAGTAATAAGCCGGCT
(β-catenin-R	CAGGTGACCACATTTATATCAT
NF-(κB-F	AGAGGCGTGTATAAGGGGCT
NF-(κB-R	TTACTGTCATAGATGGCGTCTG
c-MYC-F	GGCTCCTGGCAAAAGGTCA
c-MYC-R	CTGCGTAGTTGTGCTGATGT
Cyclin D1-F	GCTGCGAAGTGGAAACCAT
Cyclin D1-R	CCTCCTTCTGCACACATTTGAA
BCL-XL-F	GAGCTGGTGGTTGACTTTCTC
BCL-XL-R	TCCATCTCCGATTCAGTCCCT
TRAF1-F	TCCTGTGGAAGATCACCAATGT
TRAF1-R	GCAGGCACAACTTGTAGCC
Vimentin-F	GACGCCATCAACACCGAGTT
Vimentin-R	CTTTGTCGTTGGTTAGCTGGT
Slug-F	CGAACTGGACACACATACAGTG
Slug-R	CTGAGGATCTCTGGTTGTGGT
E-cadherin-F	CGAGAGCTACACGTTCACGG
E-cadherin-R	GGGTGTCGAGGGAAAAATAGG

Cell Apoptosis Assay

Flow cytometry assay and caspase-3 assay were used to determine the apoptosis level in our study. Aliquots of 1 × 106 cells were counted to measure the activity of caspase-3 by using caspase-3 ELISA assay kit (Biovision, Milpitas, CA, United States). The OD values were measured at 405 nm by using a microplate reader. As for flow cytometry assay, the flow cytometry assay kit (TransGen, Beijing, China) was used to evaluate the cell apoptosis level and the specific operation steps were performed according to the instructions of the manufacturer. Additionally, we have repeated these experiments for three times.

Cell Motility Assay

The level of cell motility was measured by wound-healing assay. A sterile 200 μL pipette tip was used to create the wound field when cells grown reached approximately 85–90% confluence. A digital camera system was used to monitor the migration of cells. After the wound was created for 24 h, the migration distance (μm) of cells was measured by the software program (HMIAS-2000). We have repeated these experiments for three times. Additionally, the specific experimental procedure is mainly referred to the previous literature.

Statistical Analysis

All the experiments were repeated five times. All the digital data were represented in the form of mean ± standard deviation (SD). SPSS 17.0 software (IBM Corp, Armonk, NY, United States) was used to perform the statistical analyses in our study. Statistical significance was tested by Chi square test, ANOVA and Student's *t*-test. $P < 0.05$ was considered to be statistically significant.

RESULTS

The Design and Construction of Artificial Long-Non-coding RNA for Suppressing BCa

The alncRNA we constructed that functions as a tumor suppressor is mainly composed of two modules, one of which is the module for downregulating the TFs that are related to the cancer, and the other is a module for down-regulation of miRNAs. The nucleic acid aptamers are small oligonucleotide sequences or short polypeptides screened and they can bind to the corresponding protein ligands with high affinity and strong specificity (Kwak et al., 2009). After the aptamers specifically binds to the protein ligands, the function of the protein will be inhibited (Culler et al., 2010; Liu et al., 2013). Inspired by the interaction between the aptamer and the protein ligand, we, respectively, connected two different aptamers to form the first module. In addition, some RNA elements can bind and regulate miRNAs based on the principle of base pairing. According to this principle, we designed the corresponding miRNA sponges and put them together in series to form the second modules.

In our study, we connected two aptamers for β-catenin (Tetsu and McCormick, 1999) and NF-κB in series to construct the first modules of the alncRNA we designed. In addition, after analyzing

the sequences of miRNA-495 and miRNA-940, we designed the miRNA sponges sequence of these two miRNAs according to the principle of competing endogenous RNAs (ceRNAs). We connected five miRNA sponges for miRNA-495 and five miRNA sponges for miRNA-940 in series to construct the second modules of the alncRNA. Finally, we effectively combine the two modules to form the complete alncRNA. In order for the alncRNA to be stably present in the cells without degradation, we attached the tail of MALAT1 at the 3′ end of the alncRNA (Zhan et al., 2018; **Figure 1**).

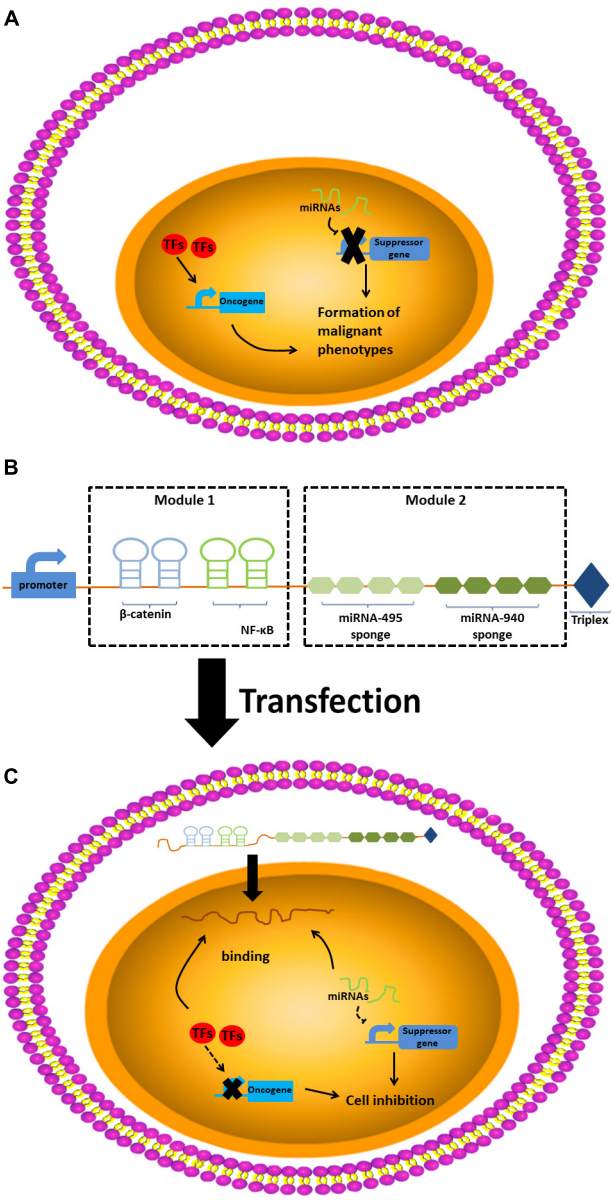

FIGURE 1 | The design and construction of artificial long-non-coding RNA. **(A)** The design of artificial long-non-coding RNA. **(B)** The construction of artificial long-non-coding RNA. **(C)** The work pattern of artificial long-non-coding RNA.

The alncRNA Inhibited the Oncogenic Factors β-Catenin in the BCa Cells

β-catenin and NF-κB are important oncogenic transcription factors, and their abnormal upregulation has been found in the tumor cells, especially BCa cells (Liu et al., 2016). In our study, to investigate the expression levels of them in the BCa, we used qRT-PCR assay to measure their expression levels in the BCa cell lines T24, 5637, and SW780. Meanwhile, we used the normal bladder epithelial cell line (SV-HUC1) as the control group to verify the abnormal overexpression of theβ-catenin and NF-κB in the BCa cells. The results were as expected, the expression levels of β-catenin and NF-κB were significantly higher than those of the control group (**Figure 2A**).

We set the aptamers of β-catenin and NF-κB in the alncRNA and intended to use them to absorbed these oncogenic factors. In this way, the alncRNA we designed would serve as an anti-cancer factor which may effectively inhibit the function of β-catenin and NF-κB and inhibit the development of BCa. In order to validate that the alncRNA can indeed absorb β-catenin and NF-κB to as the anti-cancer factors, we used the dual-luciferase reporters assay to verify this effect. The responsive promoter sequences of β-catenin and NF-κB were specifically set into the dual-luciferase vectors, respectively, and we used these reporters to sense the transcriptional activity of β-catenin and NF-κB within the cells (**Figures 2B,C**).

Firstly, we transfected the two dual-luciferase reporters into the cell lines in our study to observe the feasibility of these two reporters. Results as expected, the transcriptional activity of β-catenin in the BCa cell lines (T24, 5637, and SW780) was decreased obviously after transfected with the alncRNA compared to negative control alncRNA (**Figure 2B**). Next, we explore whether the alncRNA we constructed can inhibit the transcriptional activity of NF-κB within the cells. Surprisingly, the alncRNA can obviously inhibit the transcriptional activity of NF-κB in the BCa cells, but when it comes to the control group, there was no significant change in the transcriptional activity ofβ-catenin (**Figure 2C**). It may be that in the normal cells, the expression level of β-catenin is low, and they mainly located in the cytoplasm rather than the nucleus, so the reporters is not sensitive to them in the normal cells. In conclusion, we have proved that the alncRNA we constructed can effectively down-regulate the transcriptional activity ofβ-catenin in the BCa cells.

The alncRNA Inhibited the Oncogenic micoRNAs

In our study, we selected two oncogenic micoRNAs (miRNA-495 and miRNA-940) as the mainly targets of the module 2. To investigate the expression levels of miRNA-495 and miRNA-940 in the BCa cells, we also used the qRT-PCR assay to measure the relative expression of them in the T24, 5637, and SW780. Meanwhile, we used the SV-HUC1 as the control group. As expected, the expression levels of miRNA-495 and miRNA-940 in the BCa cell lines were higher than the normal baldder epithelial cell line (**Figures 3A,B**). After the transfection of the alncRNA, the expression level of the miRNA-495 and miRNA-940 in the cell lines were reduced to varying degrees

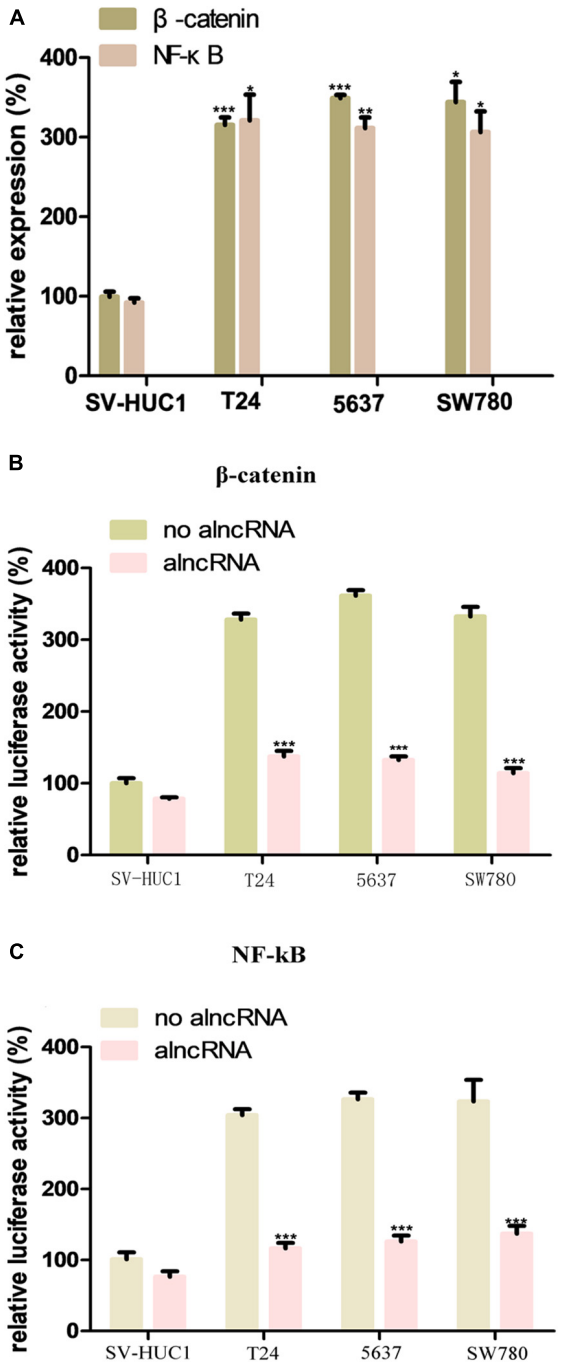

FIGURE 2 | The oncogenic factors β-catenin and NF-κB is repressed by alncRNA in the BCa cells. **(A)** QRT-PCR analyses the expression levels of β-catenin and NF-κB in the normal bladder epithelial cell line (SV-HUC1) and BCa cell lines T24, 5637 and SW780. **(B)** The relative luciferase activity of β-catenin in the normal bladder epithelial cell line and BCa cell lines. **(C)** The relative luciferase activity of NF-κB in the normal bladder epithelial cell line and BCa cell lines. $^{*}p < 0.05$, $^{**}p < 0.01$, and $^{***}p < 0.001$.

(**Figures 3A,B**). Therefore, we believed that the alncRNA we constructed was indeed effective in downregulating the target micoRNAs (miRNA-495 and miRNA-940).

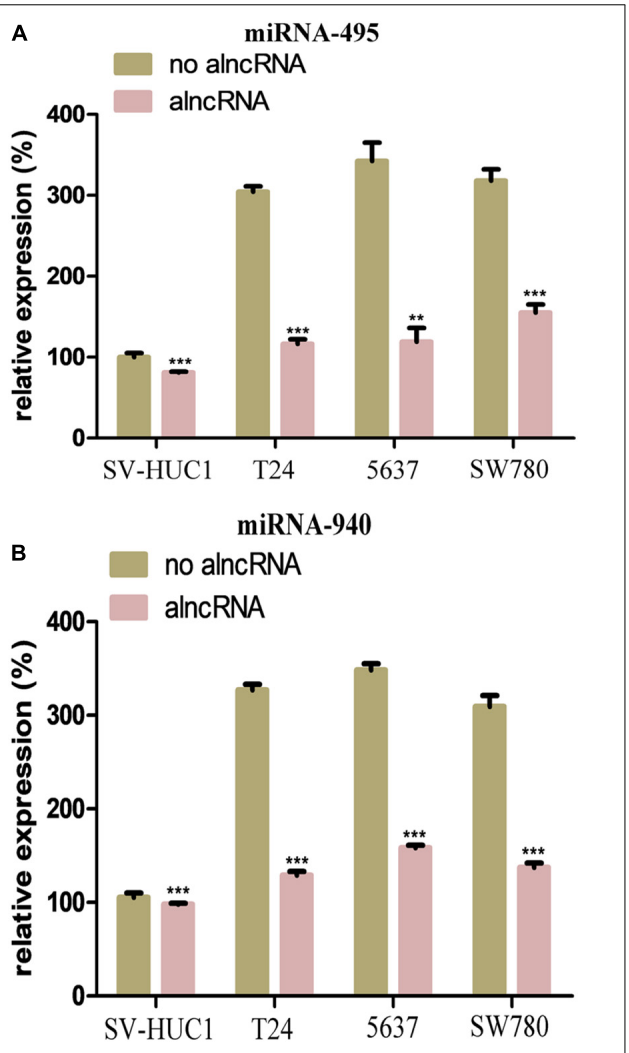

FIGURE 3 | The alncRNA inhibited the oncogenic micoRNAs in the BCa cells. **(A)** QRT-PCR analyses the expression levels of miRNA-495 in the normal bladder epithelial cell line (SV-HUC1) and BCa cell lines T24, 5637 and SW780. **(B)** QRT-PCR analyses the expression levels of miRNA-940 in the normal bladder epithelial cell line (SV-HUC1) and BCa cell lines T24, 5637, and SW780. $^{**}p < 0.01$ and $^{***}p < 0.001$.

The Inhibitory Effect of alncRNA Was Better Than CRISPR dCas9-KRAB

CRISPR/Cas9 genome engineering has revolutionized all aspects of biological research, including cancers, with epigenome engineering transforming gene regulation studies. Here, we would like to compare the inhibitory effect of alncRNA with CRISPR/Cas9. First, fusions of nuclease-inactive dCas9 to the Krüppel-associated box (KRAB) repressor (dCas9-KRAB) can silence target gene expression. So, we targeted dCas9-KRAB to the promoter of β-catenin, NF-κB, miRNA-495, and miRNA-940 (**Figure 4A**). Then we observed the expression levels of β-catenin, NF-κB, miRNA-495, and miRNA-940 were significantly decreased after transfected with the dCas9-KRAB. Unexpectedly, the results showed that the alncRNA showed a

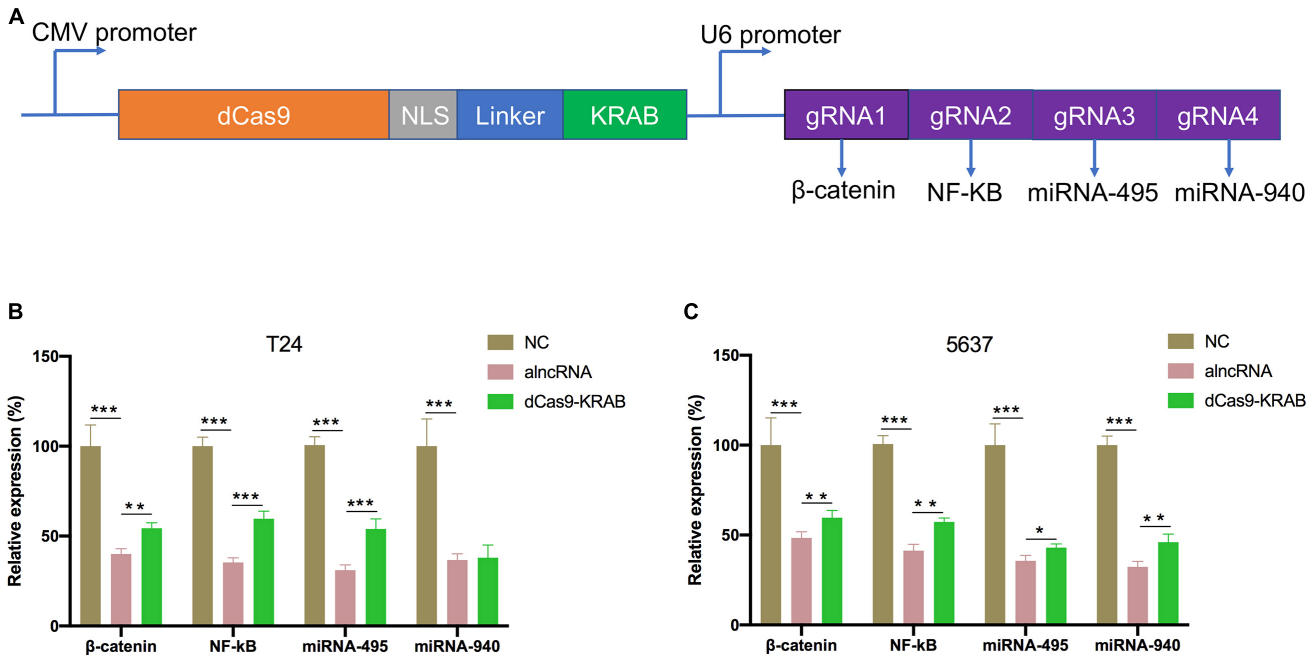

FIGURE 4 | The inhibitory effect of alncRNA was better than CRISPR dCas9-KRAB. **(A)** The construction of dCas9-KRAB and the targets of sgRNA. **(B)** QRT-PCR analyses the expression levels of β-catenin, NF-κB, miRNA-495 and miRNA-940 in the normal bladder epithelial cell line (SV-HUC1) and BCa cell line (T24) after transfected with the alncRNA and dCas9-KRAB. **(C)** QRT-PCR analyses the expression levels of β-catenin, NF-κB, miRNA-495, and miRNA-940 in the normal bladder epithelial cell line (SV-HUC1) and BCa cell line (5637) after transfected with the alncRNA and dCas9-KRAB. *$p < 0.05$, **$p < 0.01$, and ***$p < 0.001$.

better inhibitory effect than dCas9-KRAB in T24 and 5637 BCa cell lines (**Figures 4B,C**).

The alncRNA Effectively Inhibited the Downstream Oncogenic Signals

Next, we further investigated the action mechanism of the alncRNA to clarify its anti-cancer effect. We examined the relative expression of the downstream oncogenic signals of the target TFs and miRNAs in the BCa cell lines T24, 5637, and SW780. As we know from the previous qRT-PCR results, the alncRNA we constructed could significantly reduce the expression of the target oncogenic TFs and miRNAs. C-myc and cyclin D1 are the most important functional signaling molecules in the regulatory pathway ofβ-catenin and miRNA-940, while Bcl-XL and TRAF1 are the final signaling factors that are upregulated by miRNA-495 when they play a role in promoting the development of BCa. In theory, when we down-regulate these oncogenic TFs and miRNAs which are targeted by the alncRNA we constructed, these final effector factors will be inhibited. In this way, the alncRNA we constructed may effectively inhibit the malignant phenotype of the BCa cells and finally achieve the effect of treating BCa.

We mainly used qRT-PCR assay to determine whether the alncRNA could successfully down-regulate these important oncogenic signaling molecules (c-myc, cyclin D1, Bcl-XL, and TRAF1). As shown in the **Figure 5**, we found that the alncRNA can actually down-regulate the expression of c-myc, cyclin D1, Bcl-XL, and TRAF1in the BCa cell lines.

The alncRNA Induced the Cell Apoptosis of BCa Cell Lines

Prior to this, we have shown that the alncRNA can be used to interfere with the oncogenic signaling pathways. At present, we investigated the effect of the alncRNA on inducing cell apoptosis. In our work, we used caspase-3 ELISA assay and flow cytometry assay to evaluate the level of apoptosis induced by the alncRNA. First, apoptosis levels of BCa cell lines (T24, 5637, and SW780) were measured with caspase-3 ELISA assay (**Figure 6A**) and flow cytometry assay (**Figures 6B–G**). Next, after the stable expression of alncRNA in the BCa cells (T24, 5637 and SW780), we evaluated the apoptosis levels of these cells with caspase-3 ELISA assay (**Figure 6A**) and flow cytometry assay (**Figures 6B–G**). According to these experimental results, we concluded that the alncRNA we constructed could effectively induce cell apoptosis of BCa cells. Previous study has reported that β-catenin inhibited apoptosis by inhibiting the action of cleaved-PARP –apoptotic protein and caspase-3 protein (Jeon et al., 2011; Yang et al., 2015). Therefore, the alncRNA we constructed can promote apoptosis of the BCa cells by influencing the relevant pathways of β-catenin.

The alncRNA We Constructed Inhibited Cell Proliferation in BCa Cells

Next, we investigated whether the alncRNA can effectively inhibit cell proliferation in BCa cell lines (T24 and 5637). C-myc and cyclin D1 are well-known cell cycle regulator factors, which may serve as oncogenic factors and promote the cell proliferation of

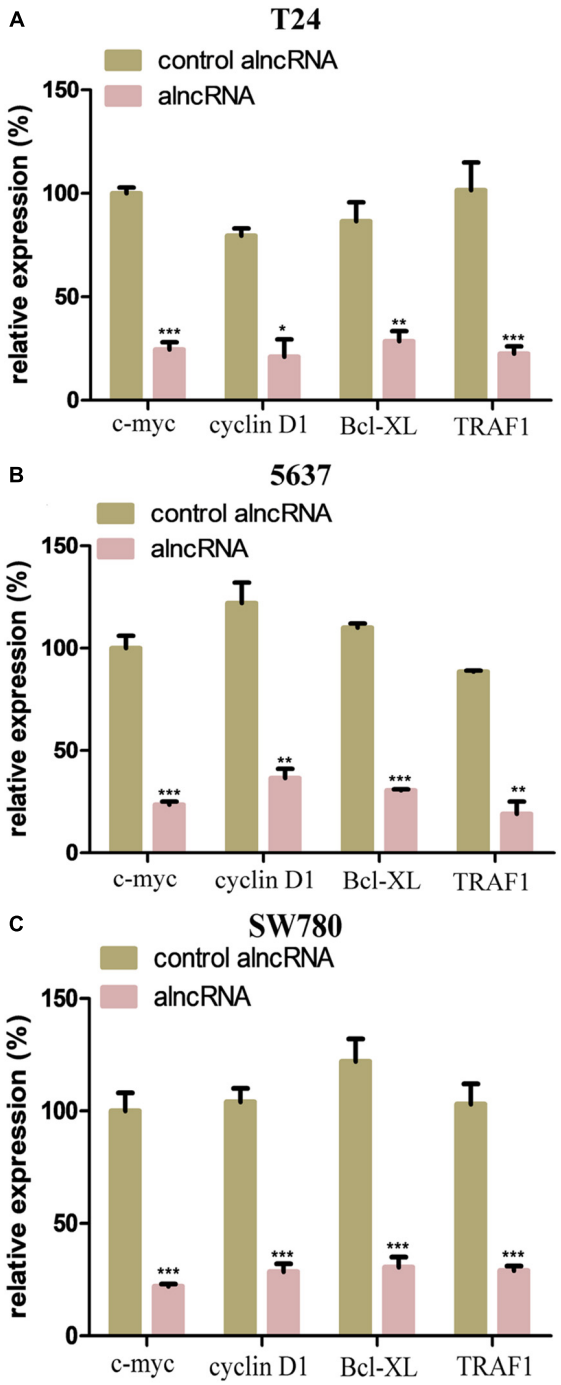

FIGURE 5 | The alncRNA effectively inhibited the downstream oncogenic signals. **(A)** QRT-PCR analyses the expression levels of the downstream oncogenic signals in BCa cell line (T24). **(B)** QRT-PCR analyses the expression levels of the downstream oncogenic signals in BCa cell line (5637). **(C)** QRT-PCR analyses the expression levels of the downstream oncogenic signals in BCa cell line (SW780). $^{*}p < 0.05$, $^{**}p < 0.01$, and $^{***}p < 0.001$.

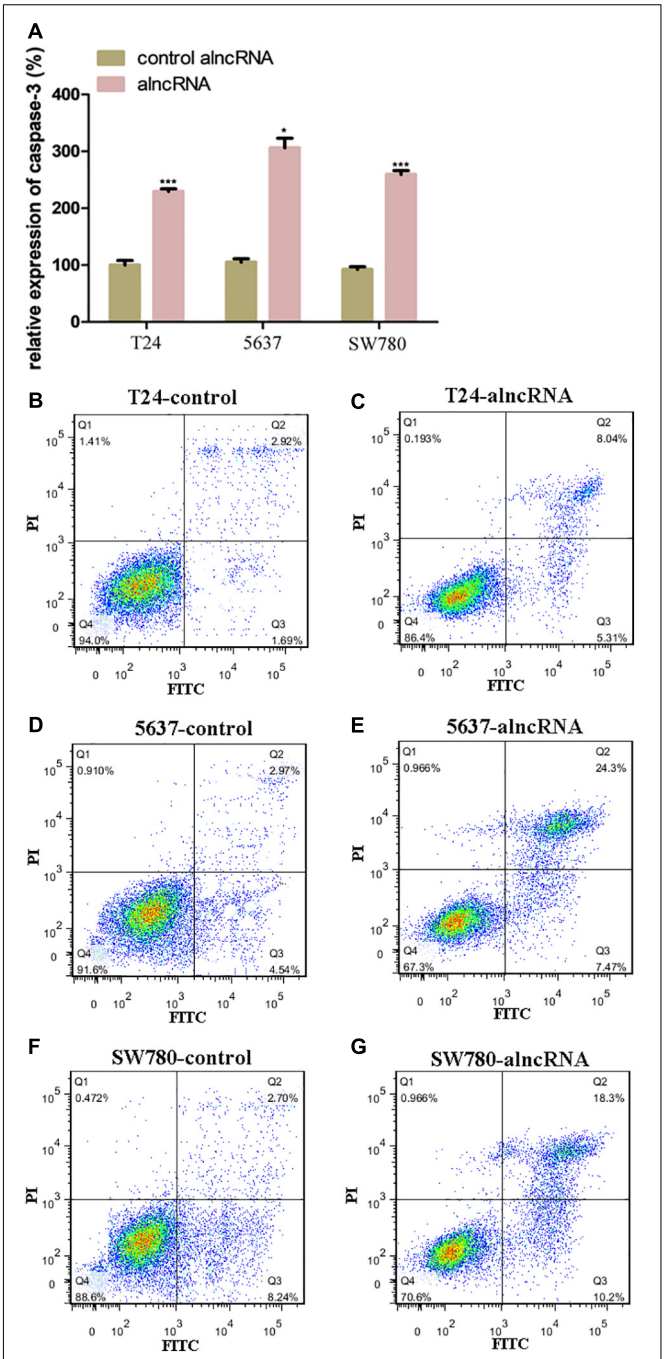

FIGURE 6 | The alncRNA induced the cell apoptosis of BCa cell lines. **(A)** The relative expression of caspases-3 in BCa cell lines with or without alncRNA. **(B,C)** The alncRNA induced apoptosis in BCa cell line (T24) by flow cytometry analysis following Annexin V and 7-AAD staining. **(D,E)** The alncRNA induced apoptosis in BCa cell line (5637) by flow cytometry analysis following Annexin V and 7-AAD staining. **(F,G)** The alncRNA induced apoptosis in BCa cell line (SW780) by flow cytometry analysis following Annexin V and 7-AAD staining. $^{*}p < 0.05$ and $^{***}p < 0.001$.

BCa cells. In our study, we planned to use this alncRNA to inhibit the signaling pathways associated with C-myc and cyclin D1 and tried to suppress tumor proliferation in this way. In the previous experimental results, we have demonstrated that the alncRNA we constructed indeed down-regulate the expression of C-myc and cyclin D1. Now, we planned to verify that this approach does

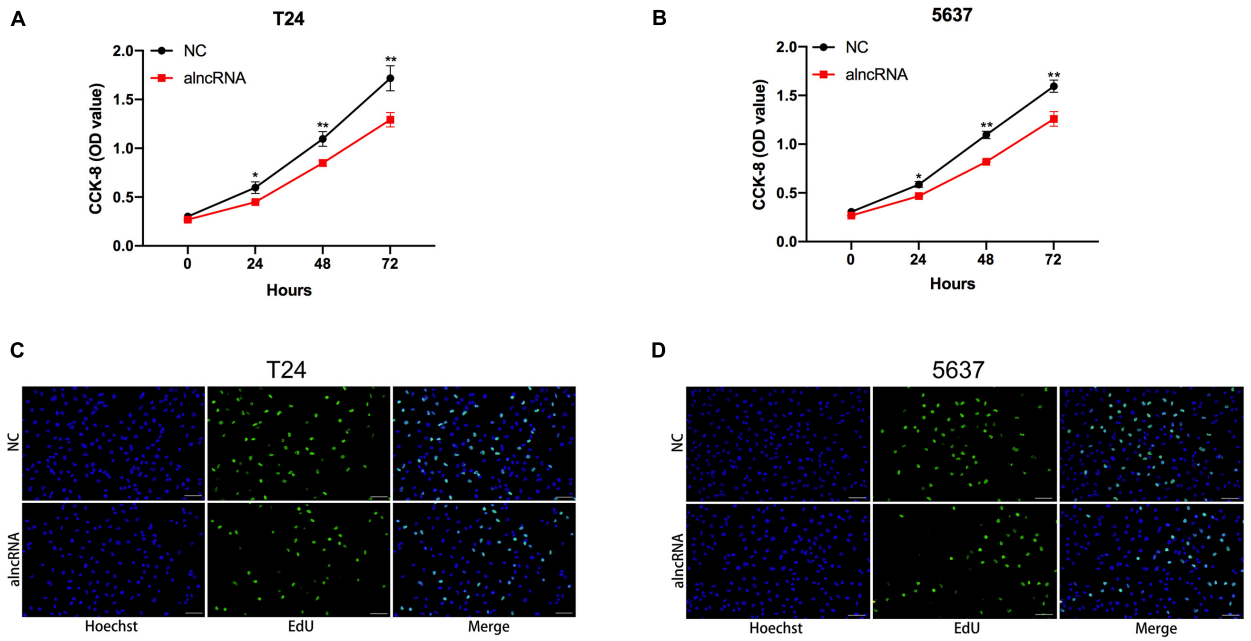

FIGURE 7 | The alncRNA inhibited cell proliferation in BCa cells **(A)** The growth curves of T24 cells infected with or without alncRNA were determined using CCK-8 assay. **(B)** The growth curves of 5637 cells infected with or without alncRNA were determined using CCK-8 assay. **(C)** The proliferation of T24 cells infected with or without alncRNA were also determined using the EDU incorporation assay. **(D)** The proliferation of 5637 cells infected with or without alncRNA were also determined using the EDU incorporation assay. $^{*}p < 0.05$ and $^{**}p < 0.01$.

inhibit cell proliferation in BCa cells (T24, 5637, and SW780). CCK-8 assay (**Figures 7A,B**) and edu assay (**Figures 7C,D**) were used to determine the cell proliferation levels of BCa cell lines T24 and 5637 in our study. First, we determined the levels of cell proliferation in BCa cell lines T24 and 5637. And then, after the stable expression of the alncRNA in the BCa cell lines, the cell proliferation of these cell lines will be measured again by using CCK-8 assay and edu assay. By comparison, we concluded that this alncRNA we constructed can effectively inhibit cell proliferation.

The alncRNA We Constructed Inhibited Cell Migration in BCa Cells

Last, we tried to elucidate whether the alncRNA acted as a cell migration suppressor in BCa cells. Within the BCa cells, the targeted miRNAs miRNA-495 and miRNA-940, as well as β-catenin, were reported to induce cancer cell migration and invasion by inducing epithelial-mesenchymal transition (EMT) (Sun et al., 2016; Chen et al., 2017; Zhong et al., 2017; Wang et al., 2018). We supposed that this alncRNA can inhibit the cell migration of the BCa cells by inhibiting EMT. To validate our hypothesis, we investigated the relationship between the expression levels of mesenchymal markers (vimentin, slug) and epithelial marker (E-cadherin) and the cell migration levels of BCa cell (T24, 5637, and SW780) under the function of the alncRNA. qRT-PCR was used to measure the expression levels of E-cadherin, vimentin and slug, while wound healing assay was used to evaluate the cell migration activity in our study. We found that when the alncRNA was present, the expression of vimentin and slug were decreased obviously, while the expression of E-cadherin was increase obviously (**Figures 8A,B**). In addition, we also found that the cell migration of BCa cells was significantly reduced when the alncRNA was present (**Figures 8C,D**).

DISCUSSION

Nucleic acid aptamer is a small series of nucleotide sequences or short polypeptides to be screened *in vitro*, and it can bind to the corresponding ligands with high affinity and strong specificity. In our study, we concatenate the apatamers of β-catenin and NF-κB together to form the module1 of the alncRNA. The relationship between the aptamer and the protein ligand was taken advantage of by us to make the alncRNA we constructed specifically bindβ-catenin and NF-κB, respectively, and inhibit their oncogenic role within the BCa cells.

As one of the important regulatory factors, micoRNAs can reverse the expression of the target genes by inhibiting the translation of the target genes or degrading the mRNAs of the target genes. However, in the course of the actual regulatory process, some non-coding RNAs also have the binding site of miRNAs, which act as the miRNA sponge within the cells. These non-coding RNA can prevent miRNAs from inhibiting the target genes, thus increasing the expression level of the target genes. According to this principle, we designed module 2 of alncRNA.

In our study, we effectively combined the sequences of the oncogenic transcription factors aptamers and the sequences of the oncogenic miRNAs to construct an anti-cancer alncRNA

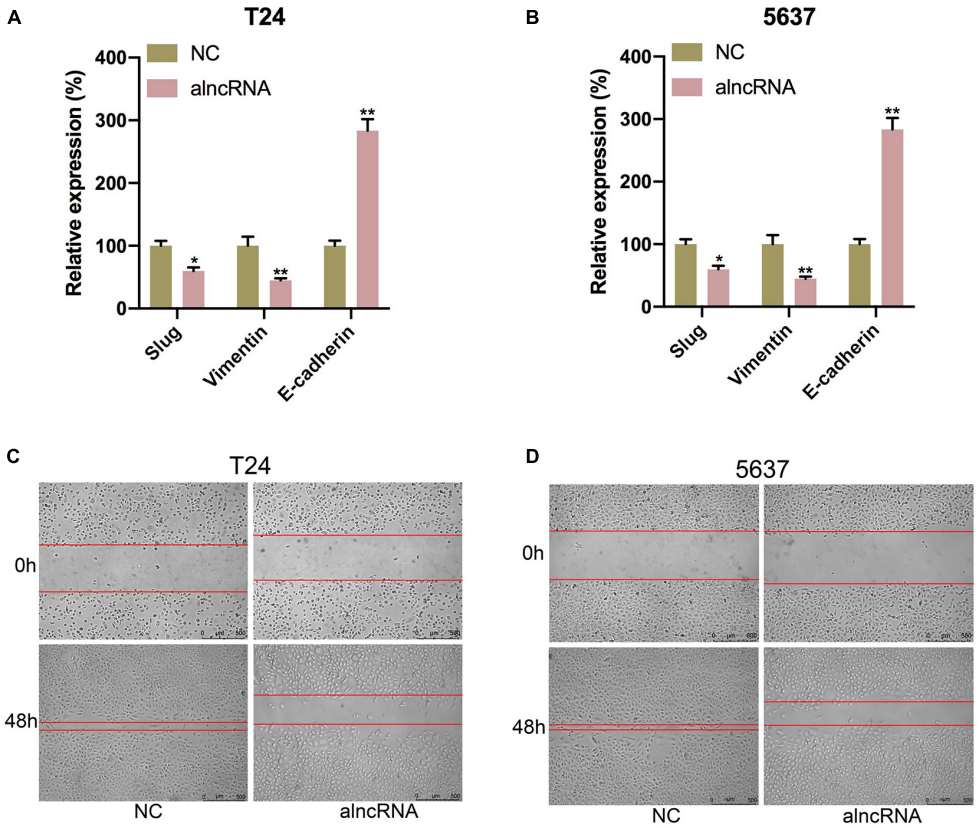

FIGURE 8 | The alncRNA we constructed inhibited cell migration in BCa cells. **(A)** The relative expression of E-cadherin, vimentin and slug in T24 cell with or without alncRNA. **(B)** The relative expression of E-cadherin, vimentin and slug in 5637 cell with or without alncRNA. **(C)** The relative rate of cell migration was calculated in T24 cell infected with or without alncRNAs using the wound-healing assay. **(D)** The relative rate of cell migration was calculated in 5637 cell infected with or without alncRNAs using the wound-healing assay. $^{*}p < 0.05$ and $^{**}p < 0.01$.

molecule. The alncRNA we constructed inhibited the malignant phenotype of the BCa cells by binding to the oncogenic factors specifically. Our study also demonstrated that the malignant phenotype of the BCa cells can indeed be effectively inhibited by constructing the form of alncRNA molecules. At the same time, the inhibitory effect of alncRNA was better than CRISPR dCas9-KRAB. This strategy of inhibiting the progression of BCa may also provide novel ideas for the treatment of other malignant tumors.

However, there are still some deficiencies in our works. Firstly, our work primarily focused on the level of eukaryotic cells rather than demonstrating the effectiveness of the alncRNA *in vivo*. After all, we have not been able to demonstrate the validity of the alncRNA *in vivo*, which is not convincing enough for the suitability of this strategy for the clinical treatment. Secondly, we mainly use transfection to get the alncRNA into the cancer cells in our work. This approach, however, cannot make the alncRNA stable in cells over the long term. Therefore, the use of other more effective approach that enable the alncRNA to be stably retained in the cells will be our focus in the future.

In summary, we successfully constructed the alncRNA which can down-regulate the oncogenic factors in the BCa cells.

DATA AVAILABILITY STATEMENT

The raw data supporting the conclusions of this article will be made available by the authors, without undue reservation, to any qualified researcher.

AUTHOR CONTRIBUTIONS

LY, QuZ, and AL designed the project and wrote the manuscript. LY, QuZ, AL, BM, ZZ, JL, LL, and SZ performed experiments and data analysis. QiZ and YG supervised the project and provided financial support for the project. All authors contributed to the article and approved the submitted version.

FUNDING

This work was supported by grants from the National Natural Science Foundation of China to QiZ (Nos. 81572510 and 81872088), a grant from Peking University Medicine Fund of Fostering Young Scholars' Scientific & Technological Innovation to YG (No. BMU2020PYB028), and a grant from the Scientific Research Seed Fund of Peking University First Hospital to YG (No. 2018SF026).

REFERENCES

Bracken, C. P., Scott, H. S., and Goodall, G. J. (2016). A network-biology perspective of microRNA function and dysfunction in cancer. *Nat. Rev. Genet.* 17, 719–732. doi: 10.1038/nrg.2016.134

Chen, H., Wang, X., Bai, J., and He, A. (2017). Expression, regulation and function of miR-495 in healthy and tumor tissues. *Oncol. Lett.* 13, 2021–2026. doi: 10.3892/ol.2017.5727

Culler, S. J., Hoff, K. G., and Smolke, C. D. (2010). Reprogramming cellular behavior with RNA controllers responsive to endogenous proteins. *Science* 330, 1251–1255. doi: 10.1126/science.1192128

Djebali, S., Davis, C. A., Merkel, A., Dobin, A., Lassmann, T., Mortazavi, A., et al. (2012). of transcription in human cells. *Nature* 489, 101–108. doi: 10.1038/nature11233

Haberle, V., and Stark, A. (2018). Eukaryotic core promoters and the functional basis of transcription initiation. *Nat. Rev. Mol. Cell Biol.* 19, 621–637. doi: 10.1038/s41580-018-0028-8

Hanahan, D., and Weinberg, R. A. (2011). Hallmarks of cancer: the next generation. *Cell* 144, 646–674. doi: 10.1016/j.cell.2011.02.013

Jeon, H. G., Yoon, C. Y., Yu, J. H., Park, M. J., Lee, J. E., Jeong, S. J., et al. (2011). Induction of caspase mediated apoptosis and down-regulation of nuclear factor-kappaB and Akt signaling are involved in the synergistic antitumor effect of gemcitabine and the histone deacetylase inhibitor trichostatin A in human bladder cancer cells. *J. Urol.* 186, 2084–2093. doi: 10.1016/j.juro.2011.06.053

Kamat, A. M., Hahn, N. M., Efstathiou, J. A., Lerner, S. P., Malmstrom, P. U., Choi, W., et al. (2016). Bladder cancer. *Lancet* 388, 2796–2810. doi: 10.1016/s0140-6736(16)30512-30518

Kluth, L. A., Black, P. C., Bochner, B. H., Catto, J., Lerner, S. P., Stenzl, A., et al. (2015). Prognostic and prediction tools in bladder cancer: a comprehensive review of the literature. *Eur. Urol.* 68, 238–253. doi: 10.1016/j.eururo.2015.01.032

Kwak, H., Hwang, I., Kim, J. H., Kim, M. Y., Yang, J. S., and Jeong, S. (2009). Modulation of transcription by the peroxisome proliferator-activated receptor delta–binding RNA aptamer in colon cancer cells. *Mol. Cancer Ther.* 8, 2664–2673. doi: 10.1158/1535-7163.mct-09-0214

Lee, H. K., Choi, Y. S., Park, Y. A., and Jeong, S. (2006). Modulation of oncogenic transcription and alternative splicing by beta-catenin and an RNA aptamer in colon cancer cells. *Cancer Res.* 66, 10560–10566. doi: 10.1158/0008-5472.can-06-2526

Liu, Y., Huang, W., Zhou, D., Han, Y., Duan, Y., Zhang, X., et al. (2013). Synthesizing oncogenic signal-processing systems that function as both "signal counters" and "signal blockers" in cancer cells. *Mol. Biosyst.* 9, 1909–1918. doi: 10.1039/c3mb70093c

Liu, Y., Zhan, Y., Chen, Z., He, A., Li, J., Wu, H., et al. (2016). Directing cellular information flow via CRISPR signal conductors. *Nat. Methods* 13, 938–944. doi: 10.1038/nmeth.3994

Marta, G. N., Hanna, S. A., Gadia, R., Correa, S. F., Silva, J. L., and Carvalho Hde, A. (2012). The role of radiotherapy in urinary bladder cancer: current status. *Int. Braz. J. Urol.* 38, 144–153. doi: 10.1590/s1677-55382012000200002

Racioppi, M., D'Agostino, D., Totaro, A., Pinto, F., Sacco, E., D'Addessi, A., et al. (2012). Value of current chemotherapy and surgery in advanced and metastatic bladder cancer. *Urol. Int.* 88, 249–258. doi: 10.1159/000335556

Rupaimoole, R., and Slack, F. J. (2017). MicroRNA therapeutics: towards a new era for the management of cancer and other diseases. *Nat. Rev. Drug Discov.* 16, 203–222. doi: 10.1038/nrd.2016.246

Siegel, R. L., Miller, K. D., and Jemal, A. (2017). Cancer statistics, 2017. *CA Cancer J. Clin.* 67, 7–30. doi: 10.3322/caac.21387

Sofra, M., Fei, P. C., Fabrizi, L., Marcelli, M. E., Claroni, C., Gallucci, M., et al. (2013). Immunomodulatory effects of total intravenous and balanced inhalation anesthesia in patients with bladder cancer undergoing elective radical cystectomy: preliminary results. *J. Exp. Clin. Cancer Res.* 32:6. doi: 10.1186/1756-9966-32-36

Sun, Y., Guan, Z., Liang, L., Cheng, Y., Zhou, J., Li, J., et al. (2016). NF-kappaB signaling plays irreplaceable roles in cisplatin-induced bladder cancer chemoresistance and tumor progression. *Int. J. Oncol.* 48, 225–234. doi: 10.3892/ijo.2015.3256

Tan, M., Mu, X., Liu, Z., Tao, L., Wang, J., Ge, J., et al. (2017). microRNA-495 promotes bladder cancer cell growth and invasion by targeting phosphatase and tensin homolog. *Biochem. Biophys. Res. Commun.* 483, 867–873. doi: 10.1016/j.bbrc.2017.01.019

Tetsu, O., and McCormick, F. (1999). Beta-catenin regulates expression of cyclin D1 in colon carcinoma cells. *Nature* 398, 422–426. doi: 10.1038/18884

Wang, R., Wu, Y., Huang, W., and Chen, W. (2018). MicroRNA-940 targets INPP4A or GSK3beta and activates the Wnt/beta-Catenin pathway to regulate the malignant behavior of bladder cancer cells. *Oncol. Res.* 26, 145–155. doi: 10.3727/096504017X14902261600566

Wong, Y. N. S., Joshi, K., Pule, M., Peggs, K. S., Swanton, C., Quezada, S. A., et al. (2017). Evolving adoptive cellular therapies in urological malignancies. *Lancet Oncol.* 18, e341–e353. doi: 10.1016/s1470-2045(17)30327-30323

Yang, T., Shi, R., Chang, L., Tang, K., Chen, K., Yu, G., et al. (2015). Huachansu suppresses human bladder cancer cell growth through the Fas/Fasl and TNF-alpha/TNFR1 pathway in vitro and in vivo. *J. Exp. Clin. Cancer Res.* 34:21. doi: 10.1186/s13046-015-0134-139

Zhan, H., Xie, H., Zhou, Q., Liu, Y., and Huang, W. (2018). Synthesizing a genetic sensor based on CRISPR-Cas9 for specifically killing of P53-deficient cancer cells. *ACS Synth. Biol.* 7, 1798–1807. doi: 10.1021/acssynbio.8b00202

Zhong, W., Chen, S., Qin, Y., Zhang, H., Wang, H., Meng, J., et al. (2017). Doxycycline inhibits breast cancer EMT and metastasis through PAR-1/NF-kappaB/miR-17/E-cadherin pathway. *Oncotarget* 8, 104855–104866. doi: 10.18632/oncotarget.20418

Conflict of Interest: The authors declare that the research was conducted in the absence of any commercial or financial relationships that could be construed as a potential conflict of interest.

frontiers in Molecular Biosciences

ORIGINAL RESEARCH
published: 09 December 2020
doi: 10.3389/fmolb.2020.616768

Silencing of lncRNA MIR497HG via CRISPR/Cas13d Induces Bladder Cancer Progression Through Promoting the Crosstalk Between Hippo/Yap and TGF-β/Smad Signaling

Changshui Zhuang[1†], Ying Liu[2†], Shengqiang Fu[3†], Chaobo Yuan[4], Jingwen Luo[5], Xueting Huang[6], Weifeng Yang[1], Wuwei Xie[7] and Chengle Zhuang[7]**

[1] Department of Urology, Union Shenzhen Hospital, Huazhong University of Science and Technology, Shenzhen, China, [2] Shenzhen People's Hospital, The First Affiliated Hospital of Southern University of Science and Technology, The Second Clinical Medical College of Jinan University, Shenzhen, China, [3] Department of Urology, The First Affiliated Hospital of Nanchang University, Nanchang, China, [4] Emergency Department, Union Shenzhen Hospital, Huazhong University of Science and Technology, Shenzhen, China, [6] Shenzhen Yantian District People's Hospital, Shenzhen, China, [5] Department of Thoracic Surgery, Union Shenzhen Hospital, Huazhong University of Science and Technology, Shenzhen, China, [7] Department of Urology, Peking University Shenzhen Hospital, Shenzhen, China

A subset of long non-coding RNAs (lncRNAs), categorized as miRNA-host gene lncRNAs (lnc-miRHGs), is processed to produce miRNAs and involved in cancer progression. This work aimed to investigate the influences and the molecular mechanisms of lnc-miRHGs MIR497HG in bladder cancer (BCa). The miR-497 and miR-195 were derived from MIR497HG. We identified that lnc-miRHG MIR497HG and two harbored miRNAs, miR-497 and miR-195, were downregulated in BCa by analyzing The Cancer Genome Atlas and our dataset. Silencing of MIR497HG by CRISPR/Cas13d in BCa cell line 5637 promoted cell growth, migration, and invasion *in vitro*. Conversely, overexpression of MIR497HG suppressed cell progression in BCa cell line T24. MiR-497/miR-195 mimics rescued significantly the oncogenic roles of knockdown of MIR497HG by CRISPR/Cas13d in BCa. Mechanistically, miR-497 and miR-195 co-ordinately suppressed multiple key components in Hippo/Yap and transforming growth factor β signaling and particularly attenuated the interaction between Yap and Smad3. In addition, E2F4 was proven to be critical for silencing MIR497HG transcription in BCa cells. In short, we propose for the first time to reveal the function and mechanisms of MIR497HG in BCa. Blocking the pathological process may be a potential strategy for the treatment of BCa.

Keywords: bladder cancer, MIR497HG, CRISPR/Cas13d, Yap, TGF-β

OPEN ACCESS

Edited by:
Yuchen Liu,
Shenzhen University, China

Reviewed by:
Yuhan Chen,
Southern Medical University, China
Mengjiao Wu,
Huazhong University of Science and Technology, China

****Correspondence:***
Chengle Zhuang
clzhuang@pku.edu.cn
Wuwei Xie
253663153@qq.com

† These authors have contributed equally to this work

Specialty section:
This article was submitted to Molecular Diagnostics and Therapeutics, a section of the journal Frontiers in Molecular Biosciences

Received: *13 October 2020*
Accepted: *05 November 2020*
Published: *09 December 2020*

Citation:
Zhuang C, Liu Y, Fu S, Yuan C, Luo J, Huang X, Yang W, Xie W and Zhuang C (2020) Silencing of lncRNA MIR497HG via CRISPR/Cas13d Induces Bladder Cancer Progression Through Promoting the Crosstalk Between Hippo/Yap and TGF-β/Smad Signaling. Front. Mol. Biosci. 7:616768. doi: 10.3389/fmolb.2020.616768

INTRODUCTION

Bladder cancer (BCa) is one of the most prevalent epithelial malignancies worldwide (Sanli et al., 2017). Most of the diagnosed patients have non–muscle-invasive BCa (MIBC) confined to the mucosa or lamina propria, and approximately 25% have MIBC that invades the detrusor muscle (Burger et al., 2013; Robertson et al., 2018). MIBC is more aggressive and have a worse prognosis (Felsenstein and Theodorescu, 2018; Robertson et al., 2018). Existing therapies for MIBC have not changed mortality rates over the past years (Felsenstein and Theodorescu, 2018). Genome and transcriptome profiling studies have revealed considerable differences in the molecular and genetic features of BCa cells, such as mutations, copy number, and gene epigenetic alterations, determining tumor heterogeneity and therapeutic resistance (Guo G. et al., 2013; Robertson et al., 2018; Kamoun et al., 2020). However, non-genetic or epigenetic mechanisms in BCa remain elusive.

Non-coding RNAs (ncRNAs), particularly long non-coding RNAs (lncRNAs, >200 nt) and microRNAs (miRNAs, 20–22 nt), are critical for epigenetic regulation (Spitale et al., 2011; Ameres and Zamore, 2013). Recent studies have reported that certain lncRNAs are referred to as miRNA-host gene and acquire functionality by serving as the precursor to microRNAs capable of regulatory role (Rodriguez et al., 2004; Cai and Cullen, 2007; Dhir et al., 2015). For example, MIR100HG-derived miR-100 and miR-125b induce chemotherapy resistance via augmenting Wnt pathway (Lu et al., 2017). MiR-675 derives from lncRNA-H19 and inhibits cell proliferation in response to cellular stress or oncogenic signals (Keniry et al., 2012). MiR-17∼92 cluster miRNAs encoded by MIR17HG downregulate transforming growth factor β (TGF-β) and STAT3 signaling in Feingold syndrome mouse models (Mirzamohammadi et al., 2018). LncRNA MIR497HG and derived miR-497∼195 cluster are downregulated in BCa (Itesako et al., 2014; Eissa et al., 2019). Furthermore, the expression of miR-195 and miR-497 is inhibited, and they function as tumor suppressors in various types of human cancer including breast cancer (Li et al., 2011), lung cancer (Chae et al., 2019), colorectal cancer (Guo S. T. et al., 2013), and hepatocellular carcinoma (Furuta et al., 2013). However, the impact of these lncRNAs or derived miRNAs in BCa progression is largely unknown.

The function of MIR497HG was verified via forward and reverse validation in BCa. To inhibit the expression of MIR497HG, we design siRNAs targeting MIR497HG while the expression of MIR497HG was not changed after transfection of siRNAs in our work. Other method to restrain MIR497HG expression is carried out in this study. New discovered type VI CRISPR system is used to suppress the expression of MIR497HG. A single protein effector (Cas13) can cleave a specific RNA with a single RNA (crRNA) in this system (Smargon et al., 2017). There are four subtypes (A–D) in type VI systems (Wang et al., 2019). Type VI-D CRISPR effectors, known as RfxCas13d, were recently discovered and used for RNA depletion with high efficiency and specificity in mammalian cells, including cancer (Abudayyeh et al., 2017; Granados-Riveron and Aquino-Jarquin, 2018).

Many signaling pathways such as JAK-STAT, nuclear factor κB, mTOR, and mitogen-activated protein kinase have been reported to affect the survival of BCa (Abbosh et al., 2015). Evolutionarily conserved Hippo pathway has been shown to paly critical roles during BCa progression and tumorigenesis (Xia et al., 2018). The Hippo pathway regulates cell proliferation and migration via the downstream effector Yes-associated protein (Yap; Mo et al., 2014). Yap is highly expressed and acts as oncogenes in BCa (Liu et al., 2013; Ciamporcero et al., 2016). TGF-β serine/threonine kinase complex binds to TGF-β receptors and further activates different downstream substrates and regulatory proteins, mainly the SMAD, inducing transcriptions of different target genes involved in cell proliferation and differentiation (Massagué, 2012). Besides, activation of the TGF-β/Smad signaling pathway often co-ordinates with Hippo/Yap pathway in human cancer, including BCa (Dong et al., 2019).

Here we report that MIR497HG plays antitumorigenic roles in BCa. We found that miR-497, miR-195, and their host gene MIR497HG were low expressed in BCa tissues and cell lines. MiR-497 and miR-195 synergistically targeted Yap and SMAD3 and their downstream genes and decreased the formation of a Yap-SMAD complex (Luo, 2017). We also identified that E2F4 is a critical transcriptional suppressor of MIR497HG. Our findings uncover an ncRNAs-mediated epigenetic mechanism to block the crosstalk between Hippo/Yap and TGFβ/Smad signaling. It may contribute to search for effective personalized targeted therapies to treat BCa.

MATERIALS AND METHODS

Cell Culture

SV-HUC-1 (normal human immortalized urothelial cell line) and the human BCa cell lines T24, 5637, RT4, UM-UC-3, SW780, and TCCSUP were purchased from the American Type Culture Collection (ATCC, Manassas, VA, United States). T24, 5637, and SW780 were cultured in RPMI-1640 medium. UM-UC-3 and TCCSUP were cultured in DMEM. RT4 was maintained in McCoy's 5a, and SV-HUC-1 was cultured in F-12K medium. Ten percent fetal bovine serum (Biological Industries, Beit Haemek, Israel) and 1% penicillin/streptomycin (GIBCO, Gaithersburg, MD, United States) were added to obtain complete growth medium.

BCa Specimens

All BCa samples were collected from the Peking University Shenzhen Hospital and Shenzhen University Nanshan Hospital. All patients signed written informed consent, and this study was approved by the Ethics Committee of Shenzhen University Nanshan Hospital. The pathological status of the specimens was provided by the board-certified pathologist.

Western Blot

Protein extracts were prepared in RIPA lysis buffer (#P0013B; Beyotime), supplemented with phenylmethylsulfonyl fluoride (PMSF; protease inhibitor and phosphatase inhibitor cocktail).

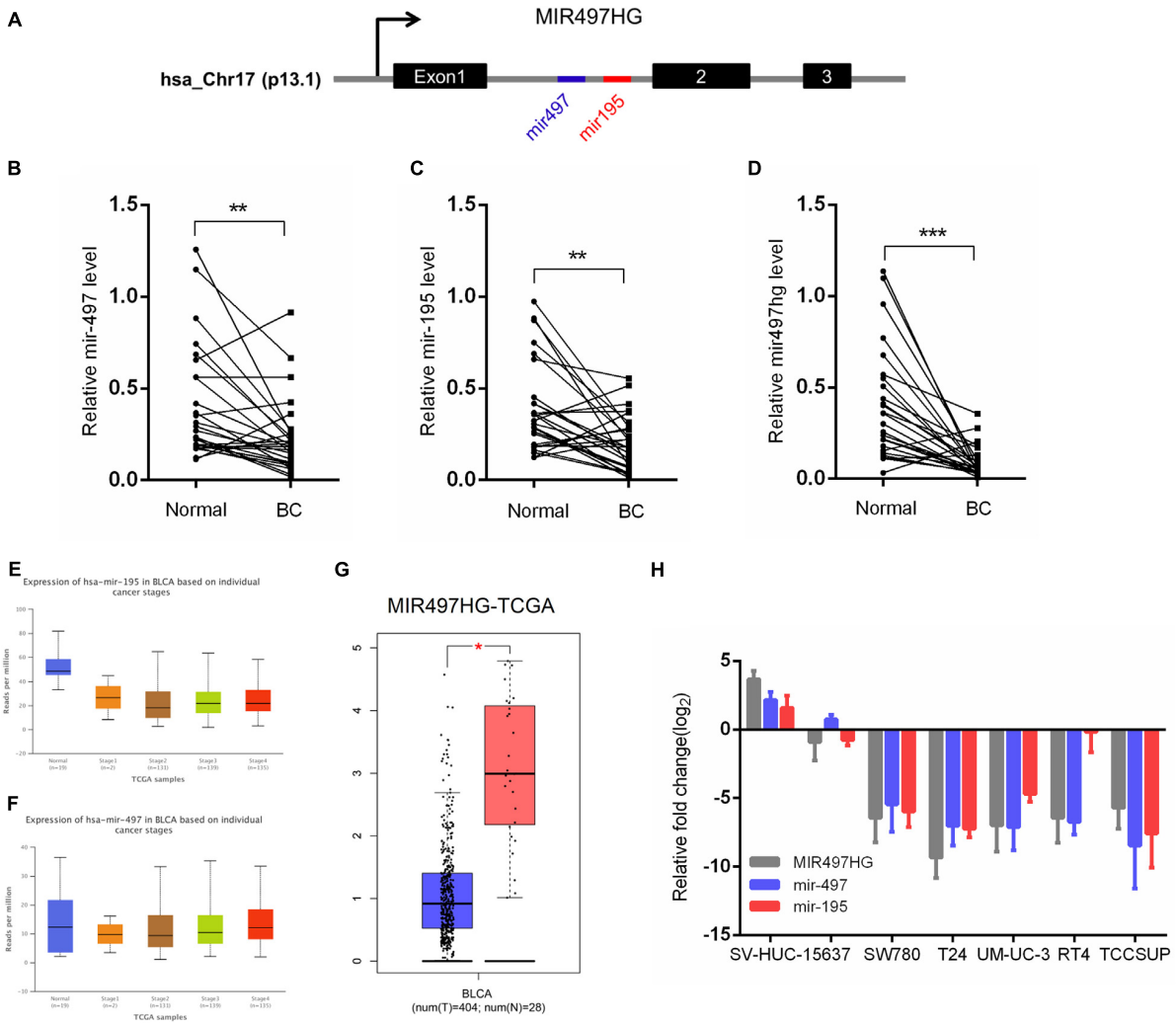

FIGURE 1 | MIR497HG and embedded miR-497 and miR-195 were downregulated in bladder cancer. **(A)** Genomic representation of MIR497HG, host gene of the miR-497/195 cluster, was shown on human chromosome 17. **(B–D)** The expression of MIR497HG and miR-497/195 cluster analyzed by qRT-PCR in 27 paired BCa tissues and adjacent normal tissues. $^{**}P < 0.01$ and $^{***}P < 0.001$ by paired-samples *t* test. **(E–G)** TGCA bladder cancer datasets were analyzed for MIR497HG and miR-497/195 cluster expression. $^{*}P < 0.05$. **(H)** The qRT-PCR analysis of MIR497HG, miR-497, and miR-195 expression levels among a panel of 7 BCa cell lines. GAPDH or U6 snRNA served as the internal control.

Protein concentrations were determined using bicinchoninic acid kit (Sigma–Aldrich) according to the manufacturer's protocol. sodium dodecyl sulfate–polyacrylamide gel electrophoresis was used to resolve cell lysates and transferred onto polyvinylidene fluoride membranes. Membranes were incubated for 1 h with non-fat milk in Tris Buffered Saline Tween (TBST) buffer and incubated overnight at 4°C with primary antibodies and required secondary antibodies conjugated to horseradish peroxidase and developed by chemiluminescent substrates.

Reverse Transcription–Quantitative Polymerase Chain Reaction and Chromatin Immunoprecipitation

TRIzol™ Reagent (Invitrogen) was utilized to extract total RNA, and RNA was purified using RNeasy Mini Columns (Qiagen), according to the manufacturer's protocol. For mRNA and lncRNA MIR497HG detection, cDNA was generated using SureScript™ First-Strand cDNA Synthesis Kit (GeneCopoeia). Quantitative polymerase chain reaction (qPCR) was then performed using the SYBR Green qPCR MasterMix (Takara). To analyze the expression level of miR-195 and miR-497, cDNA was synthesized by a mir-X miRNA First-Strand Synthesis Kit (Takara, Dalian, China). MiRNA expression was used for mir-X miRNA quantitative reverse transcription (qRT)–PCR SYBR kit (Toyobo, Osaka, Japan) according to the manufacturer's instructions, with U6 as the control.

Chromatin Immunoprecipitation

Chromatin immunoprecipitation (ChIP) assays were performed according to manufacturer's instructions using

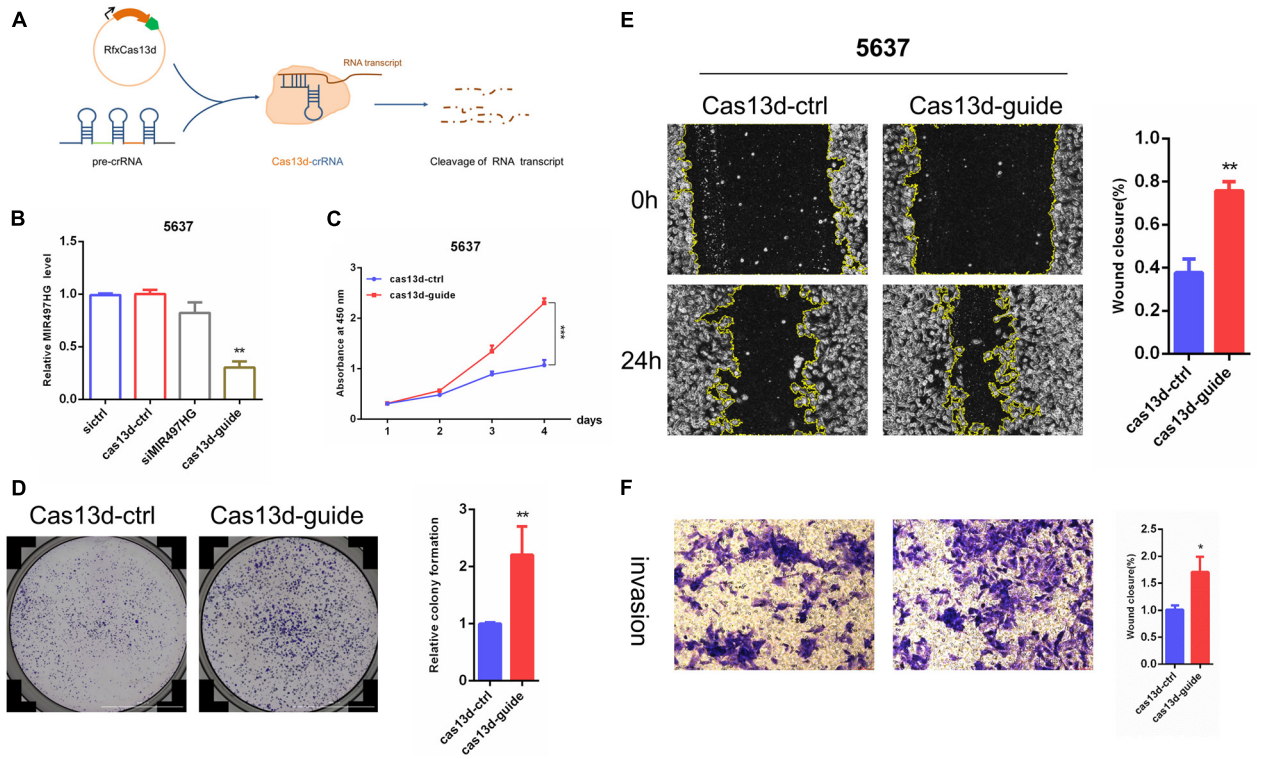

FIGURE 2 | MIR497HG suppresses BCa cell growth, migration, and invasion *in vitro*. **(A)** The schematic of CRISPR/Cas13d system. **(B)** Knockdown of MIR497HG with Cas13d compared with corresponding RNAi. **(C)** The CCK-8 assays showed that silencing of MIR497HG promotes BCa cell proliferation in 5637 cell line. **(D)** Clonogenic assay was performed to measure the capacity of foci formation in 5637 cells stably expressing indicated plasmids. **(E)** Wound healing assay of 5637 cells stably expressing indicated plasmids. **(F)** Representative images of Transwell invasion assay for MIR497HG-silencing 5637 cells. Cell number was counted in six randomly captured pictures. Invasive ability was normalized to control. Data are shown as mean ± SD. $n = 3$ for technical replicates. $^{*}P < 0.05$, $^{**}P < 0.01$, and $^{***}P < 0.001$. P values are calculated by Student t test.

Cell Signaling Immunoprecipitation Kit (#9002). Briefly, 5637 cells were fixed with paraformaldehyde and lysed in buffer A supplemented with DTT. Protease inhibitor cocktail (PIC) and PMSF were maintained on ice for 10 min. Nuclei were pelleted and resuspended in buffer B + DTT. DNA was digested with 0.5 μL micrococcal nuclease. Nuclei were again pelleted, resuspended in ChIP buffer with PIC and PMSF, and incubated at 4°C. The lysates were clarified by centrifugation, and ChIP was carried out by incubating the sample with rabbit immunoglobulin G or E2F4 antibody (Abcam), followed by immobilization on protein A/G-agarose beads (Life Technologies). The chromatin was eluted from antibody/protein G agarose beads, cross-links were reversed, and DNA was purified using spin columns. The qPCR was performed using MIR497HG promoter or GAPDH primers. Ct values were normalized to input DNA. The detailed primer sequences for RT-qPCR and ChIP assays are listed in **Supplementary Table 1**.

Cell Counting Kit-8 (CCK-8) Assay

Cells were cultured in 96-well plates at a concentration of 3×10^3 cells per well. After treatment, 10 μL CCK-8 reagent (Dojindo, Kumamoto, Kyushu, Japan) was added to each well to react for 0.5 h. The absorbance was measured at 450 nm using a microplate reader.

Colony Formation Assay

One thousand cells cells/well were plated onto six-well plates, which were incubated at 37°C and 5% CO_2 until colonies were formed. After 10 to 15 days, colonies were fixed using 0.05% crystal violet in 4% paraformaldehyde and counted using ImageJ program.

Cell Migration Assay

Cells were seeded in six-well plate (5×10^5/per well) and incubated at 37°C in a humidified incubator containing 5% CO_2 to get 100% confluence before transfection. A clear line was produced with scratching using a sterile 200-μL pipette tip. Images were taken from each well quickly. After 24 h, pictures were taken again with the help of a digital camera system. The time of 0 and 24 h of migration distance was calculated, and assays were performed at least three times.

Cell Invasion Assay

Cells were transfected with siRNAs/plasmids for 48 h and then trypsinized and resuspended in serum-free medium. Cells

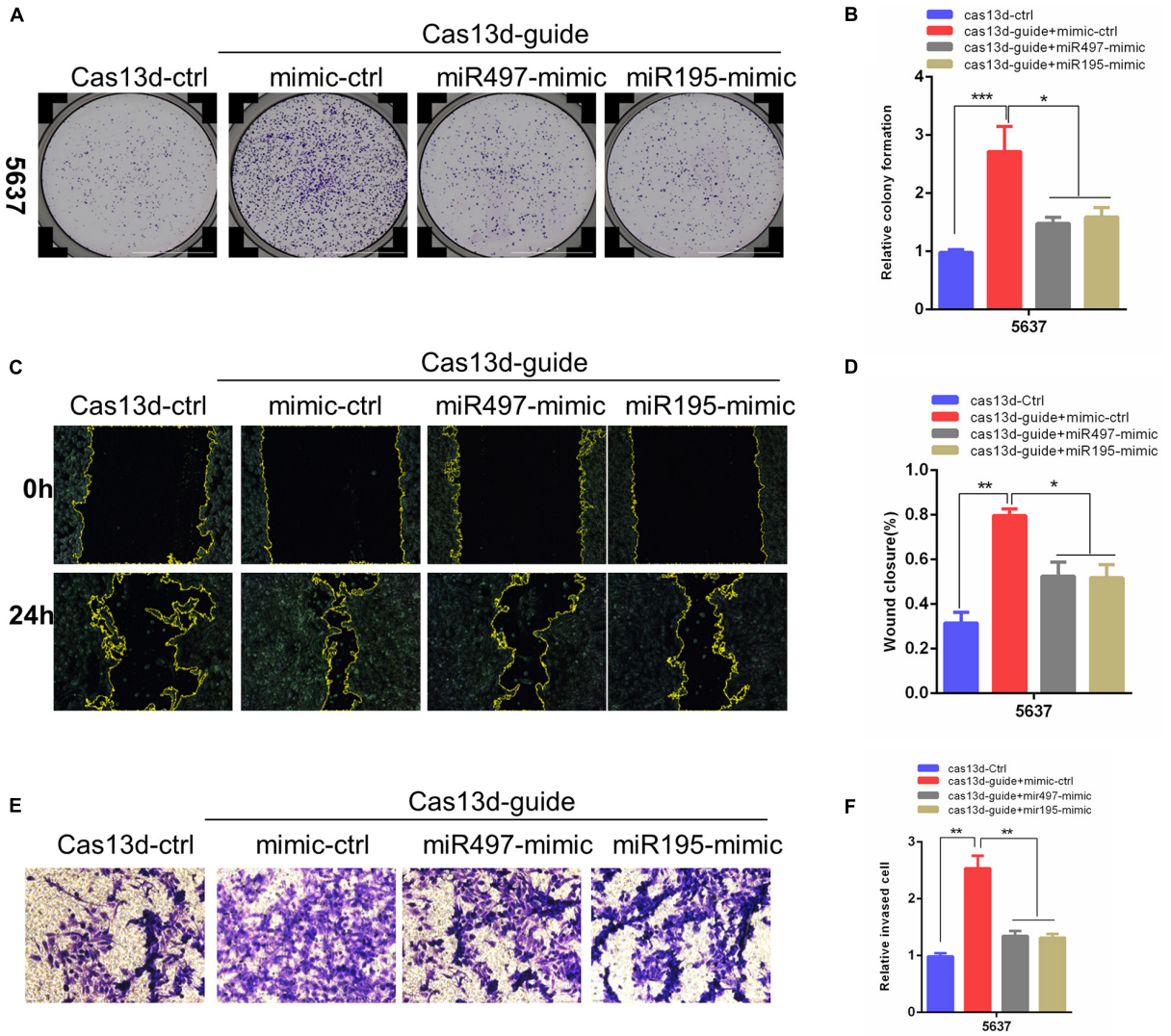

FIGURE 3 | MiR-497 and miR-195 rescued the enhancing effects of MIR497HG inhibition via CRISPR/Cas13d on BCa progression. **(A, B)** Clonogenic assay showed that miR-497 or miR-195 mimics reversed partial Cas13d-mediated silenced MIR497HG enhancing growth of BCa cell. Wound healing assays **(C, D)** and Transwell assays **(E, F)** indicated that miR-497 or miR-195 mimics rescued the enhancing function of Cas13d-mediated MIR497HG knockdown on migratory and invasive activity of 5637 cells. Data are shown as mean ± SD. $n = 3$ for technical replicates. $^{*}P < 0.05$, $^{**}P < 0.01$, and $^{***}P < 0.001$. P values are calculated by Student t test.

(1×10^5) were then added to the upper chambers of the Transwell inserts (Millicell; Merck KGaA) and allowed to migrate toward the bottom of the chambers. After 24 h, the remaining cells in the upper chamber were removed, and at room temperature, cells on the underside were fixed in 4% paraformaldehyde for 30 min and stained with 0.1% crystal violet for 30 min and captured using an Olympus-type light microscope sz30. Quantification of the migrated cells was performed by counting cell numbers.

Plasmids, Lentiviral Production, and Transfection

Yes-associated protein1 and SMAD3 coding sequence was cloned into pCMV-HA-N expression vector (*Sal*I/*Bgl*II and *Kpn*I/*Not*I). Cas13d vector was obtained from Addgene 109049, and crRNA was designed according to the previous study (Abudayyeh et al., 2017). The crRNA sequence was designed according to the website, https://cas13design.nygenome.org/, and the top three crRNA sequences were chosen for this study (AAGAGCAAAATTTAGGGTGCA TC, GA GCAAAATTTAGGGTGCATCCC, and AGAGCAAAATT TAGGGTGCAT CC). The primer sequences are presented in **Supplementary Table 1**. pLemiR control, pLemiR-195, or pLemiR-497 plasmid was packaged with pMDL, VSVG, and pRSV-Rev into HEK-293T cells. To establish stable cell lines, the concentrated lentivirus was directly added into cancer cells and incubated at 37°C for 48 h before they were washed out with phosphate-buffered saline. Finally, cells were selected with

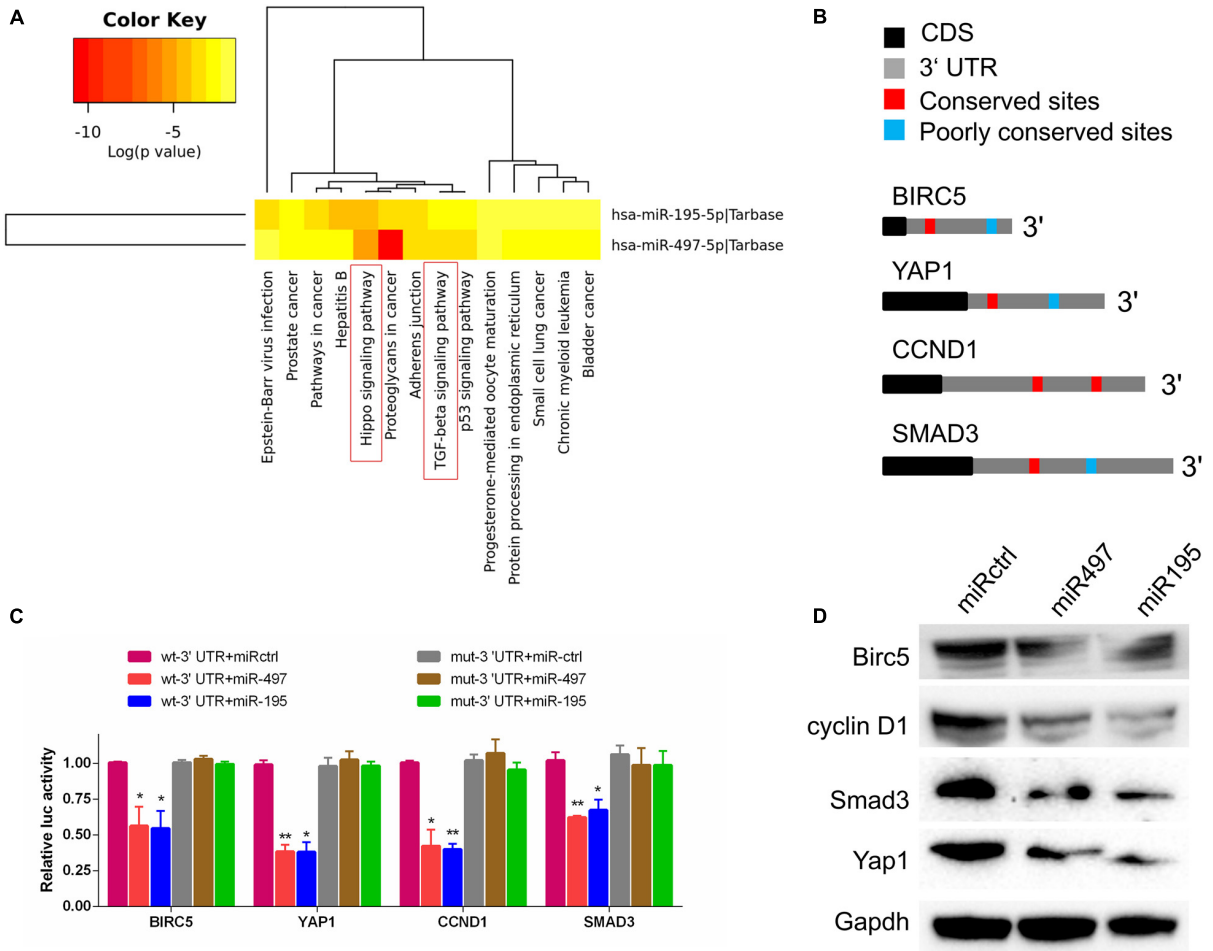

FIGURE 4 | MiR-497 and miR-195 directly suppressed multiple key components in Hippo/Yap and TGF-β signaling. **(A)** The Kyoto Encyclopedia of Genes and Genomes analysis of miR-497 and miR-195 target genes. **(B)** Predicted miR-497 and miR-195 binding conversed (red) and poorly conversed (blue) sites in 3′ UTRs of Birc5, Yap1, CCND1, and Smad3. CDS, coding sequence. **(C)** Luciferase reporter assay of candidates predicted to be regulated by miR-497 or miR-195. Renilla luciferase activity was normalized to firefly activity. $n = 3$ independent experiments. $^{*}P < 0.01$ and $^{**}P < 0.01$ by Student t test. **(D)** Western blot analysis of Birc5, cyclin D1, Smad3, and Yap1 in the indicated cells. Gapdh served as the loading control. Representative of three independent experiments.

2.5 mg/mL puromycin for 4 days. The 3′ UTR fragments of Yap1, SMAD3, CCND1, and BIRC5 containing the wild-type or mutant miR-497∼195 cluster putative target sites were directly synthesized from GeneCreate (Wuhan, China) and cloned downstream of the Renilla luciferase cassette in psiCHECK-2 (Promega). The connective tissue growth factor (CTGF)–luc plasmids were generated as described previously (Zhao et al., 2008). The promoter fragments of human MIR497HG were directly synthesized from GeneCreate (Wuhan, China) and cloned into pGL3-Basic vector (Promega). A site-directed mutagenesis kit (Thermo Fisher Scientific) was used to mutate the miR-497∼195 cluster or E2F4-binding sites of these vectors. The primer sequences used for the site-directed mutagenesis are provided in **Supplementary Table 1**. All sequences were confirmed by sequencing.

The miRNA inhibitors and mimics of miR-ctrl, miR-195, and miR-497 were obtained from Ribobio (Guangzhou, China). Lipofectamine 3000 (Invitrogen, Carlsbad, CA, United States) was used to transfect 50 nM of mimic or inhibitor of miR-ctrl, miR-195, and miR-497 into indicated cancer cells according to the manufacturer's protocol. The expression levels of miR-195 and miR-497 were quantified after 48-h transfection.

Luciferase Reporter Assay

miR-497 or miR-195 mimic or control mimic (Ambion) and indicated psiCHECK-2-3′ UTR wild-type or mutant plasmids were co-transfected into 5637 cells cultured in 24-well plates using Lipofectamine 3000 (Thermo Fisher Scientific). Renilla and firefly luciferase activities were tested with the dual-luciferase reporter assay system (Promega, Madison, WI, United States) according to the manufacturer's manual.

In order to measure promoter activities, the MIR497HG promoter fragment sequence was inserted into pGL3-basic plasmid, named pGL3-MIR497HG. Then pcDNA3.1-E2F4 expression plasmid or empty vector control and pGL3-MIR497HG or pGL3-MIR497HG-mut were co-transfected into

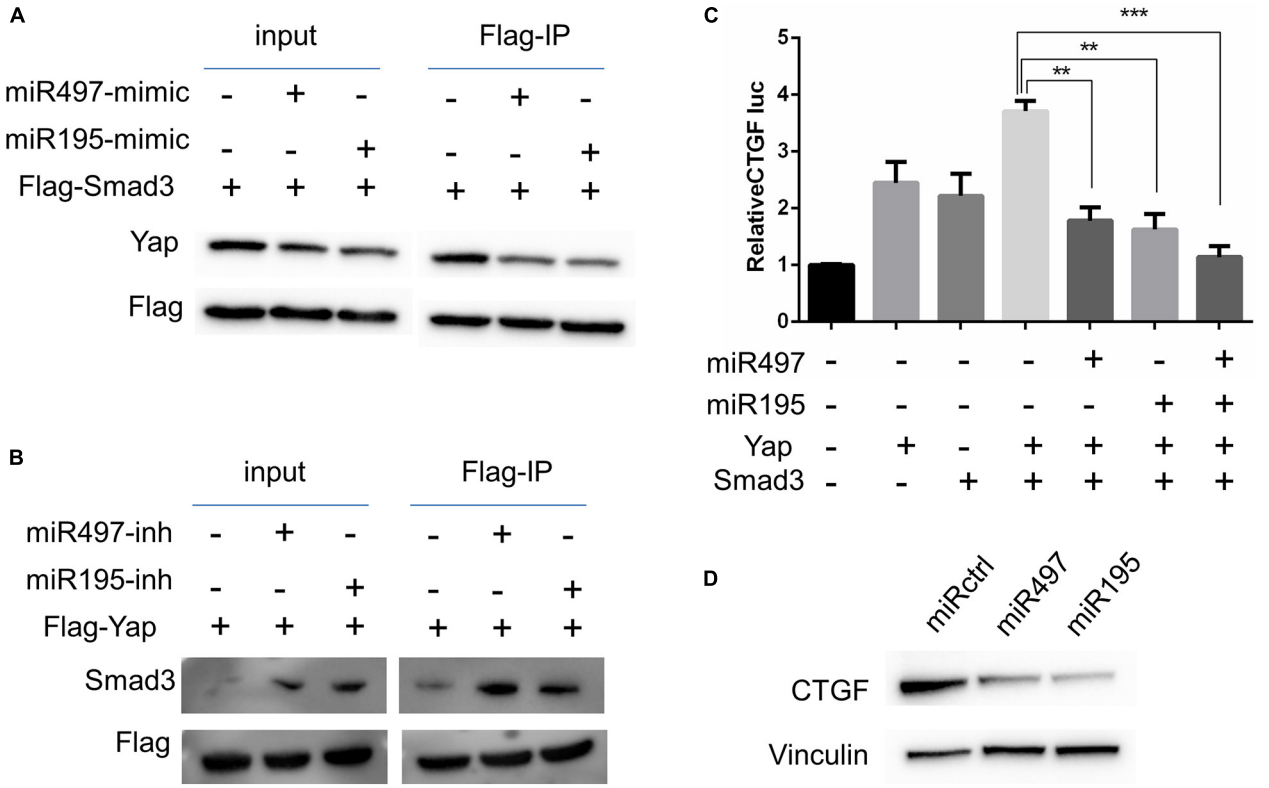

FIGURE 5 | MiR-497 and miR-195 co-ordinately attenuated Yap and Smad3 dependent transcriptional activity. **(A, B)** 5637 cells were transfected with expression vectors as indicated. Cell lysates were subjected to immunoprecipitation (IP) with an anti-Flag antibody and subsequent WB with indicated antibodies. **(C)** CTGF-luciferase reporter was co-transfected with other plasmids into 5637 cells as indicated for luciferase assay. Results are expressed as mean ± SD. $^{**}P < 0.01$ and $^{***}P < 0.001$. **(D)** Western blot analysis of CTGF in the cells transfected with miR-497 and miR-195 mimics.

5637 cells cultured in 24-well plates using Lipofectamine 3000 (Thermo Fisher Scientific). The firefly and Renilla luciferase activity was measured after 48 h with the dual-luciferase reporter assay system (Promega). Firefly luciferase activity was normalized to Renilla activity.

Statistical Analysis

Statistical analysis was performed by the SPSS 21 (SPSS Inc., Chicago, IL, United States). Two-tailed unpaired or paired Student *t* test, analysis of variance (ANOVA; Dunnett or least significant difference *post hoc* test), and Pearson correlation coefficients were used according to the type of experiment. The statistical significance between data sets was expressed as *P* values, and $P < 0.05$ was considered significant, $^{*}P < 0.05$, $^{**}P < 0.01$, and $^{***}P < 0.001$.

RESULTS

MIR497HG and MIR497HG-Derived miR-497 and miR-195 Were Downregulated in BCa

MIR497HG is the host gene of the miR-497∼195 cluster on chromosome 17 (**Figure 1A**). We first examined the expression of MIR497HG, miR-497, and miR-195. The RT-qPCR analysis confirmed the downregulation of endogenous MIR497HG, miR-497, and miR-195 expression in BCa tissues compared with normal adjacent tissues (**Figures 1B–D**). Furthermore, we analyzed The Cancer Genome Atlas (TCGA) bladder urothelial carcinoma RNA sequencing data and revealed that the expression levels of miR-497 and miR-195 were inhibited in various stage of BCa (**Figures 1E,F**), and these data also showed that MIR497HG was downregulated in BCa (**Figure 1G**). Similarly, the expression levels of MIR497HG, miR-195, and miR-497 were repressed in different BCa cell lines including 5637, T24, UMUC-3, SW780, RT4, and TCCSUP. Thus, MIR497HG, miR-497, and miR-195 were downregulated in both human BCa tissues and cell lines (**Figure 1H**). These data suggest that MIR497HG, miR-497, and miR-195 may be involved in the progression of BCa.

MIR497HG Suppressed BCa Cell Growth, Migration, and Invasion *in vitro*

Forward and reverse validation of the function of MIR497HG was verified in BCa cells. The expression level of MIR497HG was not changed after transfection of three different siRNAs targeting MIR497HG (**Supplementary Figure 1**). Thus, CRISPR/Cas13d system (crRNA and Cas13d) was used in this study, and the schematic of this system is shown in **Figure 2A**. Although

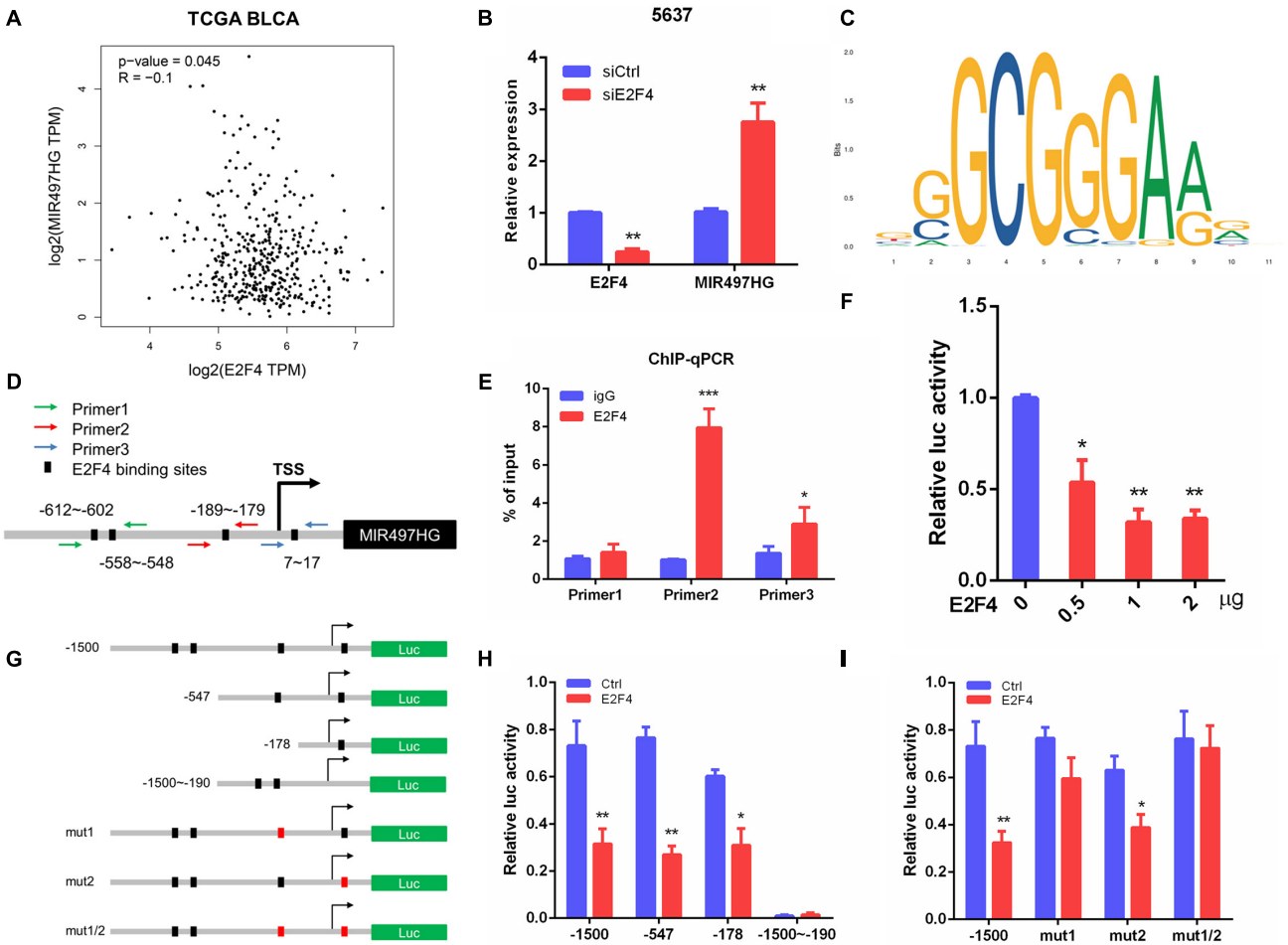

FIGURE 6 | E2F4 transcriptionally repressed MIR497HG expression in BCa cells. **(A)** The correlation between E2F4 gene expression and MIR497HG level in TCGA datasets. **(B)** 5637 cells expressing either E2F4 or non-silencing control siRNA were analyzed for E2F4 (left) or MIR497HG (right) mRNA expression using qRT-PCR. **(C)** E2F4-binding motif. **(D)** E2F4 binding in the MIR497HG promoter and primer designation. **(E)** Chromatin immunoprecipitation was performed in 5637 cells with either IgG or E2F4 and subsequently subjected to qPCR analysis with the indicated primers. Student *t* test, $^{*}P < 0.05$ and $^{***}P < 0.001$. **(F)** HIF-1a promoter activity was determined in 5637 with E2F4 overexpression. One-way ANOVA with Dunnett posttest, $^{*}P < 0.05$ and $^{**}P < 0.01$. **(G)** A schematic representation of deletion or mutation constructs spanning the −1,500 to + 200 region of the MIR497HG promoter. **(H, I)** The luciferase vector pGL3 driven by either wild-type, deletion, or mutant MIR497 promoter was transfected in 5637 cells, and luciferase activity was measured. $n = 3$ independent experiments. $^{*}P < 0.05$ and $^{**}P < 0.01$ by Student *t* test.

the expression level of MIR497HG was decreased significantly in both 5637 and T24 cells, it was higher in 5637 than that in T24. Thus, the expression of MIR497HG was inhibited significantly using CRISPR/Cas13d targeting MIR497HG in BCa 5637 cells (**Figure 2B**). CCK-8 assays and colony formation assays showed that inhibition of MIR497HG via CRISPR/Cas13d significantly promoted cell proliferation, migration, and invasion in 5637 (**Figures 2C–F**). Conversely, overexpression of MIR497HG in BCa T24 cells restrained significantly cell growth (**Supplementary Figures 2A–C**), scratch wound healing (**Supplementary Figures 2D,E**), and invasion abilities (**Supplementary Figures 2F,G**) compared with vector control. However, MIR497HG has no effects on cell apoptosis in BCa cells (data was not shown). Thus, MIR497HG was regarded as a tumor suppressor gene in BCa.

MiR-497 and miR-195 Rescued the Enhancing Effects of MIR497HG Inhibition via CRISPR/Cas13d on BCa Progression

Considering that a major role of miRNA-host gene lncRNAs (lncmiRHGs) depends on their derived miRNAs (Augoff et al., 2012; Keniry et al., 2012; Lu et al., 2017; Wu et al., 2017), we test whether the phenotypes associated with MIR497HG are mediated by miR-497 and miR-195 in BCa cell lines. miR-497 and miR-195 mimics were transiently transfected into 5637 cells after MIR497HG inhibition through CRISPR/Cas13d tool. The most significant suppressive effect was detected using crRNA sequence 1, and we picked these sequences for further study (data was not presented). As shown in **Figure 3**, miR-497 or miR-195 mimics partially

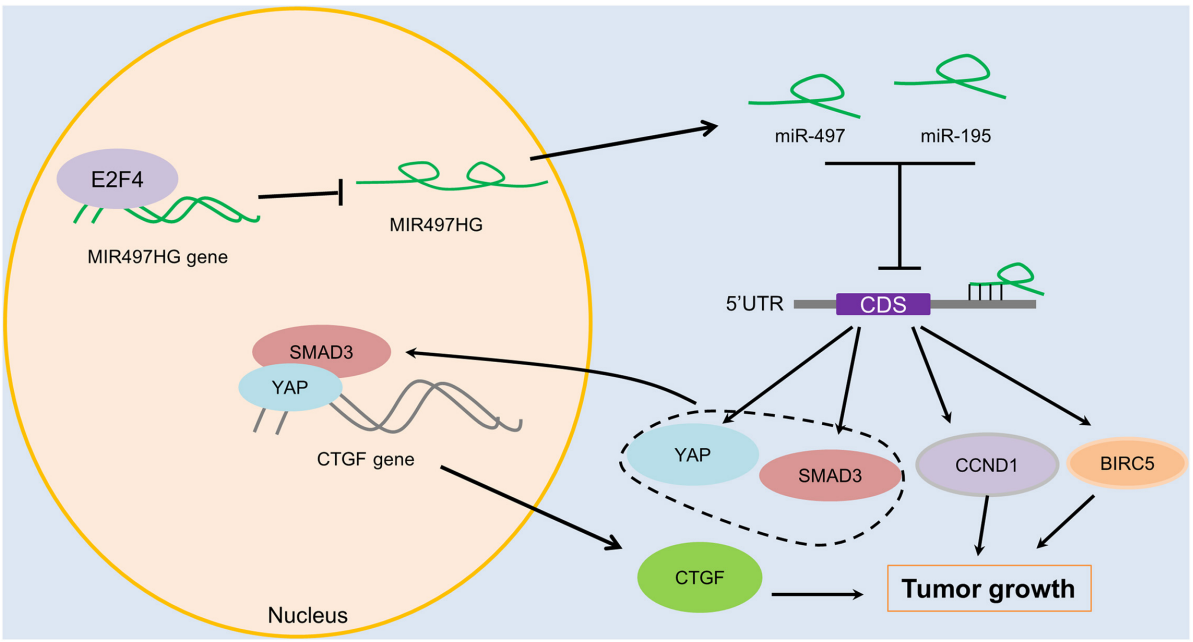

FIGURE 7 | The schematic diagram of mechanism of lncRNA MIR497HG in BCa. E2F4 bound to the promoter of MIR497HG to act as inhibitory transcription factors to suppress the expression of MIR497HG. miR-497 and miR-195 were derived from MIR497HG, and they suppressed the crosstalk of Yap and SMAD3, which were key components in Hippo/Yap and TGF-β/Smad signaling. Then, the downstream of Yap/SMAD3 complex, oncogenic CTGF, was restrained to curb cell progression of BCa.

reversed the promotion of cell proliferation (**Figures 3A,B**), migration (**Figures 3C,D**), and invasion (**Figures 3E,F**) induced by MIR497HG suppression. Collectively, these data suggested that miR-497 and miR-195 are indispensable in the biological function of MIR497HG in BCa.

MiR-497 and miR-195 Directly Suppressed Multiple Key Components in Hippo/Yap and TGF-β Signaling

To explore the molecular pathways of miR-195 and miR-497 in BCa cells, we performed *in silico* analyses using mirPath v.3 and TargetScan. Based on the Kyoto Encyclopedia of Genes and Genomes pathway enrichment analysis, 14 pathways were enriched in miR-195/497 cluster putative targets (**Figure 4A** and **Supplementary Table 2**). Then, we focused on genes predicted as miR-195/497 cluster targets and involved in Hippo signaling and TGF-β pathway. Analyses of TargetScan database and previous studies (Li et al., 2011; Itesako et al., 2014; Jafarzadeh et al., 2016; Zhang L. et al., 2016) revealed that 3′ UTRs of Yap, SMAD3, CCND1, and BIRC5 contained at least one conserved binding site for miR-497∼195 cluster (**Figure 4B**). These genes are the key components in the Hippo signaling and TGF-β pathway. Next, luciferase reporter assays confirmed that miR-497 and miR-195 directly target the 3′ UTR of these candidates (**Figure 4C**). The RT-qPCR and Western blot analysis showed that miR-497 or miR-195 mimics dramatically inhibited Yap, Smad3, Ccnd1, and Birc5 expression in BCa 5637 cells (**Figure 4D** and **Supplementary Figure 3**).

MiR-497 and miR-195 Co-ordinately Attenuated Yap- and Smad3-Dependent Transcriptional Activity

Previous studies suggest that Yap–Smad3 interaction is essential for the crosstalk between Hippo signaling and TGF-β pathway (Varelas et al., 2008; Fujii et al., 2012; Luo, 2017). To examine whether miR-497∼195 clusters affect the formation of Yap–Smad complex, we performed immunoprecipitations to detect Yap–Smad3 interaction in 5637 cell lines. Our results showed that the interaction between Yap and Smad3 was inhibited/enhanced via miR-497 or miR-195 mimic/inhibitor treatment, respectively, (**Figures 5A,B**). Interaction between Yap and Smad3 is required to positively regulate transcriptional activity of their common downstream genes including CTGF, a critically oncogenic target (Fujii et al., 2012). Next, CTGF luciferase assays showed that miR-497∼195 clusters blocked CTGF promoter transcriptional activity mediated by Yap and Smad3 (**Figure 5C**). CTGF protein expression was decreased with miR-497 or miR-195 overexpression (**Figure 5D**). These data suggest that miR-497 and miR-195 synergistically repress Yap- and Smad3-mediated transcriptional activity of CTGF.

E2F4 Transcriptionally Repressed MIR497HG Expression in BCa Cells

To determine the mechanism of downregulation of miR-497∼195 clusters in BCa, we analyzed the host gene MIR497HG promoter sequence using MethPrimer and JASPAR. First, no CpG island exists in the promoter region of MIR497HG predicted

by MethPrimer. It suggested that MIR497HG expression might not be repressed by promoter methylation. Then we identified conserved DNA-binding sites for fork head/winged helix transcription factors. Among these transcription factors, we focused on E2F transcription factor 4 (E2F4), which was negatively correlated with MIR497HG expression (**Figure 6A**) and had relatively high scores (**Supplementary Table 3**). Therefore, we individually knocked down E2F4 or E2F6 (another high score transcription factor) in 5637 cell line using siRNA and analyzed the effect of these knockdowns on MIR497HG expression. Silencing of E2F4 significantly promoted MIR497HG expression (**Figure 6B**), except knockdown of E2F6 (**Supplementary Figure 4**). It inspired us to determine whether the transcription factor E2F4 directly targets MIR497HG. Thus, we first utilized the Ensembl and JASPAR to identify forkhead/winged helix motif (GGCGGGAA) in the MIR497HG 1.5-kb promoter region and found four potential binding sites (**Figures 6C,D**). Next, real-time PCR after ChIP confirmed that E2F4 was significantly enriched at the MIR497HG promoter (**Figure 6E**). We further confirmed that E2F4 directly regulates MIR497HG expression using luciferase reporter assays. E2F4 overexpression significantly decreased the activity of the MIR497HG promoter (**Figure 6F**). Sequential mutations and deletions of four binding sites revealed that forkhead/winged helix-binding site "−189∼−179" was the major site for E2F4 repressing MIR497HG transcriptional activity (**Figures 6G–I**). Altogether, these data clearly demonstrate that E2F4 inhibited MIR497HG transcription by directly binding to its promoter in BCa cells. The schematic diagram of mechanism of lncRNA MIR497HG is shown in **Figure 7**. E2F4 bound to the promoter of MIR497HG to inhibit the expression of MIR497HG. miR-497 and miR-195 were derived from MIR497HG and suppressed the crosstalk of Yap and SMAD3, which were key components in Hippo/Yap and TGF-β/Smad signaling. Then, the downstream of Yap/SMAD3 complex, oncogenic CTGF, was restrained to curb cell proliferation of BCa.

DISCUSSION

MIR497HG is a host gene of the miR-497 and miR-195 embedded in its first intron. MIR497HG was significantly downregulated and might serve as a potential diagnostic marker in BCa (Eissa et al., 2019). MiR-495 and miR-195 were also reduced in BCa and inhibited cancer cell progression (Han et al., 2011; Itesako et al., 2014; Zhang Y. et al., 2016). Consistent with these findings, we confirmed that concomitant low expression of MIR497HG, miR-497, and miR-195 occurred in BCa and that miR-497 and miR-195 co-ordinately play critical antioncogenic roles in BCa cells. *In vitro*, we found that inhibition/overexpression of MIR497HG significantly promotes/inhibits the viability and proliferation of BCa cells. No properly designed siRNAs may be the possible reason for the ineffectiveness of the siRNAs targeting MIR497HG. CRISPR/Cas13d was used to knock down the expression of MIR497HG. Compared with other type VI effectors, the size of Cas13d is smaller and has been verified as effective tools for RNA targeting and editing (Yan et al., 2018). However, more work about the construction of synthetic CRISPR/Cas13d sensing RNA will be performed in the future. Besides, mechanistically, integrated *in silico* analyses and luciferase reporter assays revealed that miR-195/497 cluster directly targeted Yap, SMAD3, BIRC5, and CCND1, the key components in the Hippo and TGF-β pathway. Moreover, we found that miR-195/497 cluster decreased the formation of regulatory transcription complex containing Yap and Smad3, while decreasing their common target genes, such as the gene-encoding CTGF (Luo, 2017). Various studies have revealed that CTGF is critical in cancer progression and initiation (Chen et al., 2019; Pu et al., 2019; Zhou et al., 2020).

Although we focused on the target genes in the Hippo and TGF-β pathway, it is likely that other genes or pathways are changed in BCa cells as a result of miR-195/497 cluster–mediated posttranscriptional gene silencing. For example, miR-195/497 cluster maintained Notch activity and HIF-1α protein expression by targeting FBXW7 in endothelial cells (Yang et al., 2017). However, we observed no similar changes of HIF-1α and FBXW7 expression after miR-195/497 mimic treatment in BCa cells (data was not shown). The reasons for the disparities remain unclear. One possibility is that miRNA performs distinct genetic programs in the different cells and microenvironments in which the cells reside.

Numerous studies points toward an important role for E2F4 with reports of transcriptional stimulatory or repressive effects of E2F4 in different cell type or tissue context (López-Díaz et al., 2013; Cuitiño et al., 2019; Hsu et al., 2019; Kanakkanthara et al., 2019). It is possible that E2F4 serves as a transcriptional activator or repressor upon binding distinct transcriptional cofactors. E2F4 drives genes transcription by interacting with acetyltransferase GCN5 and the essential cofactors TRRAP (Lang et al., 2001). Conversely, E2F4 silence target genes rely on its interaction with the "pocket protein," such as retinoblastoma (Rb), p107, and p130 that recruit DNA methyltransferases (DNMTs) (Iaquinta and Lees, 2007; López-Díaz et al., 2013). Our data showed that E2F4 represses MIR497HG transcriptional activity, while inhibiting its embedded miR-497 and miR-195 expression. Further studies are needed to investigate whether a novel co-repressor that interacts with E2F4 exists.

In conclusion, E2F4 suppressed the expression of MIR497HG, and MIR497HG suppresses BCa progression through disrupting the crosstalk between Hippo/Yap and TGF-β/Smad signaling by reducing expression of four key genes involved in these two pathways and Yap–Smad3 interaction. Our findings may open up avenues for developing effective therapeutic strategies to treat BCa.

DATA AVAILABILITY STATEMENT

The original contributions presented in the study are included in the article/**Supplementary Materials**, further inquiries can be directed to the corresponding author/s.

ETHICS STATEMENT

The studies involving human participants were reviewed and approved by The experimental protocol was established,

according to the ethical guidelines of the Helsinki Declaration and was approved by the Human Ethics Committee of the Ethics Committee of Shenzhen University Nanshan Hospital. Written informed consent was obtained from individual or guardian participants. The patients/participants provided their written informed consent to participate in this study.

AUTHOR CONTRIBUTIONS

CEZ, CAZ, and YL conceived the project, designed, and performed the research. CAZ, SF, and WY analyzed the data. YL and SF wrote the manuscript. CY, WY, XH, and JL provided assistance in some experiments and reviewing of the manuscript. CEZ and WX provided financial support. All authors contributed to the article and approved the submitted version.

FUNDING

This research was supported by the "San-ming" Project of Medicine in Shenzhen (SZSM201612066).

ACKNOWLEDGMENTS

We thank Dr. Xinbo Huang for discussions and suggestions. We also thank Dr. Ming Ma at The First Affiliated Hospital of Nanchang University for providing the cas13d expression vector.

SUPPLEMENTARY MATERIAL

The Supplementary Material for this article can be found online at: https://www.frontiersin.org/articles/10.3389/fmolb.2020.616768/full#supplementary-material

Supplementary Figure 1 | Knockdown efficiency of MIR497HG with three diferent siRNA. RT-qPCR assays showed no significant change of MIR497HG in 3 siRNAs transfected cells.

Supplementary Figure 2 | MIR497HG suppressed T24 cell growth, migration and invasion *in vitro*. The CCK-8 assay **(A)** and colony formation assays **(B, C)** showed that MIR497HG overexpression repressed T24 cell proliferation. Wound healing assays **(D, E)** and transwell assays **(F, G)** suggested that overexpression of MIR497HG significantly inhibited migratory and invasive activity of T24 cells. Data are shown as mean ± SD. $n = 3$ for technical replicates. $^{**}P < 0.01$ and $^{***}P < 0.001$.

Supplementary Figure 3 | Expression analysis of selected genes after miR-497 or miR-195 overexpression. Birc5 **(A)**, CCND1 **(B)**, Smad3 **(C),** and Yap **(D)** mRNA levels were detected by RT-qPCR in miR-497 mimic, miR-195 mimic, and mimic-ctrl transfected cells. Data are shown as mean ± SD. $n = 3$ for technical replicates. $^{**}P < 0.01$ and $^{***}P < 0.001$.

Supplementary Figure 4 | RT-qPCR suggested that the expression of MIR497HG was no changed after knock down of E2F6. $^{***}p < 0.001$.

Supplementary Table 1 | Sequences for cloning, site directed mutagenesis, ChIP-qPCR and RT-qPCR in this work.

Supplementary Table 2 | KEGG pathway enrichment analysis showed that miR-195/497 cluster putative targets involve in different biological pathways.

Supplementary Table 3 | The binding of transcription factor and promoter of MIR497HG was predicted by JASPAR database.

REFERENCES

Abbosh, P. H., McConkey, D. J., and Plimack, E. R. (2015). Targeting signaling transduction pathways in bladder cancer. *Curr. Oncol. Rep.* 17:58.

Abudayyeh, O. O., Gootenberg, J. S., Essletzbichler, P., Han, S., Joung, J., Belanto, J. J., et al. (2017). RNA targeting with CRISPR-Cas13. *Nature* 550, 280–284.

Ameres, S. L., and Zamore, P. D. (2013). Diversifying microRNA sequence and function. *Nat. Rev. Mol. Cell Biol.* 14, 475–488. doi: 10.1038/nrm3611

Augoff, K., McCue, B., Plow, E. F., and Sossey-Alaoui, K. (2012). miR-31 and its host gene lncRNA LOC554202 are regulated by promoter hypermethylation in triple-negative breast cancer. *Mol. Cancer* 11:5. doi: 10.1186/1476-4598-11-5

Burger, M., Catto, J. W., Dalbagni, G., Grossman, H. B., Herr, H., Karakiewicz, P., et al. (2013). Epidemiology and risk factors of urothelial bladder cancer. *Eur. Urol.* 63, 234–241.

Cai, X., and Cullen, B. R. (2007). The imprinted H19 noncoding RNA is a primary microRNA precursor. *RNA* 13, 313–316. doi: 10.1261/rna.351707

Chae, D. K., Park, J., Cho, M., Ban, E., Jang, M., Yoo, Y. S., et al. (2019). MiR-195 and miR-497 suppress tumorigenesis in lung cancer by inhibiting SMURF2-induced TGF-β receptor I ubiquitination. *Mol. Oncol.* 13, 2663–2678. doi: 10.1002/1878-0261.12581

Chen, J. Q., Ou, Y. L., Huang, Z. P., Hong, Y. G., Tao, Y. P., Wang, Z. G., et al. (2019). MicroRNA-212-3p inhibits the proliferation and invasion of human hepatocellular carcinoma cells by suppressing CTGF expression. *Sci. Rep.* 9:9820.

Ciamporcero, E., Shen, H., Ramakrishnan, S., Yu Ku, S., Chintala, S., Shen, L., et al. (2016). Yap activation protects urothelial cell carcinoma from treatment-induced DNA damage. *Oncogene* 35, 1541–1553. doi: 10.1038/onc.2015.219

Cuitiño, M. C., Pécot, T., Sun, D., Kladney, R., Okano-Uchida, T., Shinde, N., et al. (2019). Two distinct E2F transcriptional modules drive cell cycles and differentiation. *Cell Rep.* 27, 3547.e5–3560.e5.

Dhir, A., Dhir, S., Proudfoot, N. J., and Jopling, C. L. (2015). Microprocessor mediates transcriptional termination of long noncoding RNA transcripts hosting microRNAs. *Nat. Struct. Mol. Biol.* 22, 319–327. doi: 10.1038/nsmb.2982

Dong, H., Diao, H., Zhao, Y., Xu, H., Pei, S., Gao, J., et al. (2019). Overexpression of matrix metalloproteinase-9 in breast cancer cell lines remarkably increases the cell malignancy largely via activation of transforming growth factor beta/SMAD signalling. *Cell Prolif.* 52:e12633.

Eissa, S., Safwat, M., Matboli, M., Zaghloul, A., El-Sawalhi, M., and Shaheen, A. (2019). Measurement of urinary level of a specific competing endogenous RNA network (FOS and RCAN mRNA/ miR-324-5p, miR-4738-3p, /lncRNA miR-497-HG) enables diagnosis of bladder cancer. *Urol. Oncol.* 37, 292.e19–292.e27.

Felsenstein, K. M., and Theodorescu, D. (2018). Precision medicine for urothelial bladder cancer: update on tumour genomics and immunotherapy. *Nat. Rev. Urol.* 15, 92–111. doi: 10.1038/nrurol.2017.179

Fujii, M., Toyoda, T., Nakanishi, H., Yatabe, Y., Sato, A., Matsudaira, Y., et al. (2012). TGF-β synergizes with defects in the Hippo pathway to stimulate human malignant mesothelioma growth. *J. Exp. Med.* 209, 479–494. doi: 10.1084/jem.20111653

Furuta, M., Kozaki, K., Tanimoto, K., Tanaka, S., Arii, S., Shimamura, T., et al. (2013). The tumor-suppressive miR-497-195 cluster targets multiple cell-cycle regulators in hepatocellular carcinoma. *PLoS One* 8:e60155. doi: 10.1371/journal.pone.0060155

Granados-Riveron, J. T., and Aquino-Jarquin, G. (2018). CRISPR-Cas13 precision transcriptome engineering in cancer. *Cancer Res.* 78, 4107–4113. doi: 10.1158/0008-5472.can-18-0785

Guo, G., Sun, X., Chen, C., Wu, S., Huang, P., Li, Z., et al. (2013). Whole-genome and whole-exome sequencing of bladder cancer identifies frequent alterations in genes involved in sister chromatid cohesion and segregation. *Nat. Genet.* 45, 1459–1463. doi: 10.1038/ng.2798

Guo, S. T., Jiang, C. C., Wang, G. P., Li, Y. P., Wang, C. Y., Guo, X. Y., et al. (2013). MicroRNA-497 targets insulin-like growth factor 1 receptor and has a tumour suppressive role in human colorectal cancer. *Oncogene* 32, 1910–1920. doi: 10.1038/onc.2012.214

Han, Y., Chen, J., Zhao, X., Liang, C., Wang, Y., Sun, L., et al. (2011). MicroRNA expression signatures of bladder cancer revealed by deep sequencing. *PLoS One* 6:e18286. doi: 10.1371/journal.pone.0018286

Hsu, J., Arand, J., Chaikovsky, A., Mooney, N. A., Demeter, J., Brison, C. M., et al. (2019). E2F4 regulates transcriptional activation in mouse embryonic stem cells independently of the RB family. *Nat. Commun.* 10:2939.

Iaquinta, P. J., and Lees, J. A. (2007). Life and death decisions by the E2F transcription factors. *Curr. Opin. Cell Biol.* 19, 649–657. doi: 10.1016/j.ceb.2007.10.006

Itesako, T., Seki, N., Yoshino, H., Chiyomaru, T., Yamasaki, T., Hidaka, H., et al. (2014). The microRNA expression signature of bladder cancer by deep sequencing: the functional significance of the miR-195/497 cluster. *PLoS One* 9:e84311. doi: 10.1371/journal.pone.0084311

Jafarzadeh, M., Soltani, B. M., Dokanehiifard, S., Kay, M., Aghdami, N., and Hosseinkhani, S. (2016). Experimental evidences for hsa-miR-497-5p as a negative regulator of SMAD3 gene expression. *Gene* 586, 216–221. doi: 10.1016/j.gene.2016.04.003

Kamoun, A., de Reynies, A., Allory, Y., Sjodahl, G., Robertson, A. G., Seiler, R., et al. (2020). A consensus molecular classification of muscle-invasive bladder cancer. *Eur. Urol.* 77, 420–433.

Kanakkanthara, A., Huntoon, C. J., Hou, X., Zhang, M., Heinzen, E. P., O'Brien, D. R., et al. (2019). ZC3H18 specifically binds and activates the BRCA1 promoter to facilitate homologous recombination in ovarian cancer. *Nat. Commun.* 10:4632.

Keniry, A., Oxley, D., Monnier, P., Kyba, M., Dandolo, L., Smits, G., et al. (2012). The H19 lincRNA is a developmental reservoir of miR-675 that suppresses growth and Igf1r. *Nat. Cell Biol.* 14, 659–665. doi: 10.1038/ncb2521

Lang, S. E., McMahon, S. B., Cole, M. D., and Hearing, P. (2001). E2F transcriptional activation requires TRRAP and GCN5 cofactors. *J. Biol. Chem.* 276, 32627–32634. doi: 10.1074/jbc.m102067200

Li, D., Zhao, Y., Liu, C., Chen, X., Qi, Y., Jiang, Y., et al. (2011). Analysis of MiR-195 and MiR-497 expression, regulation and role in breast cancer. *Clin. Cancer Res.* 17, 1722–1730. doi: 10.1158/1078-0432.ccr-10-1800

Liu, J. Y., Li, Y. H., Lin, H. X., Liao, Y. J., Mai, S. J., Liu, Z. W., et al. (2013). Overexpression of Yap 1 contributes to progressive features and poor prognosis of human urothelial carcinoma of the bladder. *BMC Cancer* 13:349. doi: 10.1186/1471-2407-13-349

López-Díaz, F. J., Gascard, P., Balakrishnan, S. K., Zhao, J., Del Rincon, S. V., Spruck, C., et al. (2013). Coordinate transcriptional and translational repression of p53 by TGF-β1 impairs the stress response. *Mol. Cell* 50, 552–564. doi: 10.1016/j.molcel.2013.04.029

Lu, Y., Zhao, X., Liu, Q., Li, C., Graves-Deal, R., Cao, Z., et al. (2017). lncRNA MIR100HG-derived miR-100 and miR-125b mediate cetuximab resistance via Wnt/beta-catenin signaling. *Nat. Med.* 23, 1331–1341. doi: 10.1038/nm.4424

Luo, K. (2017). Signaling cross talk between TGF-beta/smad and other signaling pathways. *Cold Spring Harb. Perspect. Biol.* 9:a022137. doi: 10.1101/cshperspect.a022137

Massagué, J. (2012). TGFβ signalling in context. *Nat. Rev. Mol. Cell Biol.* 13, 616–630.

Mirzamohammadi, F., Kozlova, A., Papaioannou, G., Paltrinieri, E., Ayturk, U. M., and Kobayashi, T. (2018). Distinct molecular pathways mediate Mycn and Myc-regulated miR-17-92 microRNA action in Feingold syndrome mouse models. *Nat. Commun.* 9:1352.

Mo, J. S., Park, H. W., and Guan, K. L. (2014). The Hippo signaling pathway in stem cell biology and cancer. *EMBO Rep.* 15, 642–656. doi: 10.15252/embr.201438638

Pu, N., Gao, S., Yin, H., Li, J. A., Wu, W., Fang, Y., et al. (2019). Cell-intrinsic PD-1 promotes proliferation in pancreatic cancer by targeting CYR61/CTGF via the hippo pathway. *Cancer Lett.* 460, 42–53. doi: 10.1016/j.canlet.2019.06.013

Robertson, A. G., Kim, J., Al-Ahmadie, H., Bellmunt, J., Guo, G., Cherniack, A. D., et al. (2018). Comprehensive molecular characterization of muscle-invasive bladder cancer. *Cell* 174:1033.

Rodriguez, A., Griffiths-Jones, S., Ashurst, J. L., and Bradley, A. (2004). Identification of mammalian microRNA host genes and transcription units. *Genome Res.* 14, 1902–1910. doi: 10.1101/gr.2722704

Sanli, O., Dobruch, J., Knowles, M. A., Burger, M., Alemozaffar, M., Nielsen, M. E., et al. (2017). Bladder cancer. *Nat. Rev. Dis. Prim.* 3:17022.

Smargon, A. A., Cox, D. B. T., Pyzocha, N. K., Zheng, K., Slaymaker, I. M., Gootenberg, J. S., et al. (2017). Cas13b is a type VI-B CRISPR-associated RNA-guided RNase differentially regulated by accessory proteins Csx27 and Csx28. *Mol. Cell* 65, 618.e7–630.e7.

Spitale, R. C., Tsai, M. C., and Chang, H. Y. (2011). RNA templating the epigenome: long noncoding RNAs as molecular scaffolds. *Epigenetics* 6, 539–543. doi: 10.4161/epi.6.5.15221

Varelas, X., Sakuma, R., Samavarchi-Tehrani, P., Peerani, R., Rao, B. M., Dembowy, J., et al. (2008). TAZ controls Smad nucleocytoplasmic shuttling and regulates human embryonic stem-cell self-renewal. *Nat. Cell Biol.* 10, 837–848. doi: 10.1038/ncb1748

Wang, F., Wang, L., Zou, X., Duan, S., Li, Z., Deng, Z., et al. (2019). Advances in CRISPR-Cas systems for RNA targeting, tracking and editing. *Biotechnol. Adv.* 37, 708–729. doi: 10.1016/j.biotechadv.2019.03.016

Wu, X., Wang, Y., Yu, T., Nie, E., Hu, Q., Wu, W., et al. (2017). Blocking MIR155HG/miR-155 axis inhibits mesenchymal transition in glioma. *Neuro Oncol.* 19, 1195–1205. doi: 10.1093/neuonc/nox017

Xia, J., Zeng, M., Zhu, H., Chen, X., Weng, Z., and Li, S. (2018). Emerging role of Hippo signalling pathway in bladder cancer. *J. Cell. Mol. Med.* 22, 4–15. doi: 10.1111/jcmm.13293

Yan, W. X., Chong, S., Zhang, H., Makarova, K. S., Koonin, E. V., Cheng, D. R., et al. (2018). Cas13d is a compact RNA-targeting type VI CRISPR effector positively modulated by a WYL-domain-containing accessory protein. *Mol. Cell* 70, 327.e5–339.e5.

Yang, M., Li, C. J., Sun, X., Guo, Q., Xiao, Y., Su, T., et al. (2017). MiR-497∼195 cluster regulates angiogenesis during coupling with osteogenesis by maintaining endothelial Notch and HIF-1α activity. *Nat. Commun.* 8:16003.

Zhang, L., Yu, Z., Xian, Y., and Lin, X. (2016). microRNA-497 inhibits cell proliferation and induces apoptosis by targeting Yap1 in human hepatocellular carcinoma. *FEBS Open Biol.* 6, 155–164.

Zhang, Y., Zhang, Z., Li, Z., Gong, D., Zhan, B., Man, X., et al. (2016). MicroRNA-497 inhibits the proliferation, migration and invasion of human bladder transitional cell carcinoma cells by targeting E2F3. *Oncol. Rep.* 36, 1293–1300. doi: 10.3892/or.2016.4923

Zhao, B., Ye, X., Yu, J., Li, L., Li, W., Li, S., et al. (2008). TEAD mediates Yap-dependent gene induction and growth control. *Genes Dev.* 22, 1962–1971. doi: 10.1101/gad.1664408

Zhou, Y., Zhang, J., Li, H., Huang, T., Wong, C. C., Wu, F., et al. (2020). AMOTL1 enhances Yap1 stability and promotes Yap1-driven gastric oncogenesis. *Oncogene* 39, 4375–4389. doi: 10.1038/s41388-020-1293-5

Conflict of Interest: The authors declare that the research was conducted in the absence of any commercial or financial relationships that could be construed as a potential conflict of interest.

frontiers in Molecular Biosciences

CORRECTION
published: 23 September 2021
doi: 10.3389/fmolb.2021.664616

Corrigendum: Silencing of lncRNA MIR497HG via CRISPR/Cas13d Induces Bladder Cancer Progression Through Promoting the Crosstalk Between Hippo/Yap and TGF-β/Smad Signaling

Changshui Zhuang[1†], Ying Liu[2†], Shengqiang Fu[3†], Chaobo Yuan[4], Jingwen Luo[5], Xueting Huang[6], Weifeng Yang[1], Wuwei Xie[7] and Chengle Zhuang[7]**

[1]Department of Urology, Union Shenzhen Hospital, Huazhong University of Science and Technology, Shenzhen, China, [2]Shenzhen People's Hospital, The First Affiliated Hospital of Southern University of Science and Technology, The Second Clinical Medical College of Jinan University, Shenzhen, China, [3]Department of Urology, The First Affiliated Hospital of Nanchang University, Nanchang, China, [4]Emergency Department, Union Shenzhen Hospital, Huazhong University of Science and Technology, Shenzhen, China, [5]Shenzhen Yantian District People's Hospital, Shenzhen, China, [6]Department of Thoracic Surgery, Union Shenzhen Hospital, Huazhong University of Science and Technology, Shenzhen, China, [7]Department of Urology, Peking University Shenzhen Hospital, Shenzhen, China

Keywords: bladder cancer, MIR497HG, CRISPR/Cas13days, YAP, TGF-b

OPEN ACCESS

Edited and Reviewd by:
Yuchen Liu,
Shenzhen University, China

***Correspondence:**
Chengle Zhuang
clzhuang@pku.edu.cn
Wuwei Xie
253663153@qq.com

[†]These authors have contributed equally to this work.

Specialty section:
This article was submitted to Molecular Diagnostics and Therapeutics, a section of the journal Frontiers in Molecular Biosciences

Received: 05 February 2021
Accepted: 16 February 2021
Published: 23 September 2021

Citation:
Zhuang C, Liu Y, Fu S, Yuan C, Luo J, Huang X, Yang W, Xie W and Zhuang C (2021) Corrigendum: Silencing of lncRNA MIR497HG via CRISPR/Cas13d Induces Bladder Cancer Progression Through Promoting the Crosstalk Between Hippo/Yap and TGF-β/Smad Signaling. Front. Mol. Biosci. 8:664616. doi: 10.3389/fmolb.2021.664616

A Corrigendum on

Silencing of lncRNA MIR497HG via CRISPR/Cas13d Induces Bladder Cancer Progression Through Promoting the Crosstalk Between Hippo/Yap and TGF-β/Smad Signaling
by Zhuang, C., Liu, Y., Fu, S., Yuan, C., Luo, J., Huang, X., Yang, W., Xie, W., Zhuang, C. (2020), Front Mol Biosci. 7:616768. doi: 10.3389/fmolb.2020.616768

In the original article (Zhuang et al., 2020), there were two errors in Supplementary Figure 2. The "T24 Wound Healing" images of 24 h of "ctrl" in Supplementary Figure 2D and the Supplementary Figure 2F (right) mistakenly used the 5,637 cells data. We then proceed to re-check all original data, found that the inadvertent errors happened during figure processing. All the original pictures of Wound Healing and migration assays of 5,637 and T24 cells were put in a same folder for faster processing and mistakes were happened in the process of image processing using Adobe Illustrator CS6. The authors truly apologize for the oversight on this matter to the editors, reviewers and readers for any confusion that has been caused by these unintentional errors.

The authors apologize for this error and state that this does not change the scientific conclusions of the article in any way. The original article has been updated.

REFERENCE

Zhuang, C., Liu, Y., Fu, S., Yuan, C., Luo, J., Huang, X., et al. (2020). Silencing of lncRNA MIR497HG via CRISPR/Cas13d Induces bladder cancer progression through promoting the Crosstalk between hippo/yap and TGF-β/smad signaling. *Front. Mol. Biosci.* 7, 616768. doi:10.3389/fmolb.2020.616768.eCollection2020

frontiers in Molecular Biosciences

ORIGINAL RESEARCH
published: 05 January 2021
doi: 10.3389/fmolb.2020.627848

A Light-Inducible Split-dCas9 System for Inhibiting the Progression of Bladder Cancer Cells by Activating p53 and E-cadherin

Xinbo Huang[1], Qun Zhou[2], Mingxia Wang[1], Congcong Cao[1], Qian Ma[1], Jing Ye[1] and Yaoting Gui[1]**

[1] *Guangdong and Shenzhen Key Laboratory of Male Reproductive Medicine and Genetics, Institute of Urology, Peking University Shenzhen Hospital, Shenzhen-Peking University-The Hong Kong University of Science and Technology Medical Center, Shenzhen, China,* [2] *Department of Urology, The Affiliated Nanhua Hospital of University of South China, Hengyang, China*

OPEN ACCESS

Edited by:
Yonghao Zhan, Zhengzhou University, China

Reviewed by:
Hongzhou Cui, First Hospital of Shanxi Medical University, China
Shuai Shao, The Ohio State University, United States

***Correspondence:**
Jing Ye
ye2013j@163.com
Yaoting Gui
guiyaoting2007@aliyun.com

Specialty section:
This article was submitted to Molecular Diagnostics and Therapeutics, a section of the journal Frontiers in Molecular Biosciences

Received: *10 November 2020*
Accepted: *02 December 2020*
Published: *05 January 2021*

Citation:
Huang X, Zhou Q, Wang M, Cao C, Ma Q, Ye J and Gui Y (2021) A Light-Inducible Split-dCas9 System for Inhibiting the Progression of Bladder Cancer Cells by Activating p53 and E-cadherin. Front. Mol. Biosci. 7:627848. doi: 10.3389/fmolb.2020.627848

Optogenetic systems have been increasingly investigated in the field of biomedicine. Previous studies had found the inhibitory effect of the light-inducible genetic circuits on cancer cell growth. In our study, we applied an AND logic gates to the light-inducible genetic circuits to inhibit the cancer cells more specifically. The circuit would only be activated in the presence of both the human telomerase reverse transcriptase (hTERT) and the human uroplakin II (hUPII) promoter. The activated logic gate led to the expression of the p53 or E-cadherin protein, which could inhibit the biological function of tumor cells. In addition, we split the dCas9 protein to reduce the size of the synthetic circuit compared to the full-length dCas9. This light-inducible system provides a potential therapeutic strategy for future bladder cancer.

Keywords: CRISPR, split-dCas9, light-inducible, bladder cancer, logic gate

INTRODUCTION

Bladder cancer ranks as the tenth highest incidence with ∼550 thousand people diagnosed worldwide in 2018. The incidence in males is significantly higher than in females, and the highest incidence is observed in men from Europe and North America (https://gco.iarc.fr/today/data/factsheets/cancers/30-Bladder-fact-sheet.pdf). Bladder cancer is often associated with a poor prognosis since the surgery naturally involves the urogenital tract, which leads to a profound psychological impact as well as the physical impact (2017). In addition to the surgery, chemotherapy is often considered as a part of the combination therapy (Leow et al., 2014). However, poor patient compliance due to the side effects and the lack of durable response evokes an urgent need for more targeted and personalized approaches (Vasekar et al., 2016).

Synthetic biology and gene therapy have enormous potential in satisfying these requirements (Rivière and Sadelain, 2017; Sedlmayer et al., 2018). After several decades of development, we now acquire various genetic editing methods, like TALEN(transcription activator-like effector nucleases) (Beerli et al., 2000), ZFNs(zinc-finger nucleases) (Zhang et al., 2011) and CRISPR (clustered regularly interspaced short palindromic repeats) technology. (Jinek et al., 2012; Qi et al., 2013). The high efficiency, ease of use and low cost soon make the CRISPR a preferable tool in the field of gene editing (Zhan et al., 2019).

Small molecules have long been the preferential choice for regulating gene expression (Gossen et al., 1995; Schenone et al., 2013). They present great regulatory performance *in vitro* and *in vivo*, however, they often trigger side effects for therapeutic use (Muller and Milton, 2012). Thus, scientists proposed that the future transcription-control systems will be a molecule-free or traceless remote control (Folcher et al., 2014; Ye and Fussenegger, 2019). Following this, increasing investigation upon light-inducible gene-regulating devices was conducted during the recent decade. Other than molecule-free, light control systems allow precise spatial and temporal regulation of cell behavior, which makes it ideal for gene regulation (Polstein and Gersbach, 2015).

Previous studies found that under blue light illumination, the cryptochrome 2 (CRY2) photoreceptor could form a heterodimer with its specific binding CIB1 protein (cryptochrome-interacting basic-helix-loop-helix 1) (Yamada et al., 2020; Zhao et al., 2020). Incorporated this light-responsive module to the dCas9 protein and the transcriptional activation domain could flexibly tune the transcriptional regulatory function of dCas9 protein. However, applying the CRISPR-dCas9 circuits to clinical use is hindered by the cargo size of current viral delivery vehicles (Truong et al., 2015; Li et al., 2018). To solve this problem, researchers proposed that dCas9 protein can be split into different domains and integrated inside the cells (Nihongaki et al., 2015; Zetsche et al., 2015; Ma et al., 2016).

In this study, we established a light-induced gene expression device based on the dCas9 protein and the CRY2-CIB1 photosensitive module. Then, we incorporated a modular AND logic gate with a CRISPR-dCas9 system for improved specificity. The system would only activate the output gene in the presence of both inputs and the blue light (Liu et al., 2014). In addition, for better practicality, we reduced the size of the dCas9 protein by splitting it in half. Our results demonstrated that by activating the exogenous p53 or endogenous E-cadherin via this system, the cancer cell proliferation and invasion could be effectively inhibited *in vitro*, while apoptosis was promoted. This device not only presented a more advanced specificity and modularity, but also easier to transport, which had the potential of being a promising cancer therapeutic strategy.

RESULTS

Construction of the Split CRISPR-dCas9-Based Light-Inducible System

We constructed a light-inducible genetic circuit that only activates the target gene expression in the presence of blue light illumination. The circuit composed of a dCas9-CIB1 fusion protein which anchored to the target gene, and a CRY2-AD (activator domain) fusion protein which acted as the transcriptional activator (**Figure 1**). Under the blue light condition, the CRY2 and CIBI domains were heterodimerized. Then the AD domain could activate the target gene transcription (**Figure 1B**). Whereas, without the blue light, the CRY2-AD component freely diffuses within the nucleus (**Figure 1A**).

In addition, we combined the logical AND gate with split dCas9 protein which allows the reconstitution of dCas9 only when both input promoters worked. The dCas9 protein was divided into C-terminal (IntC) and N-terminal (IntN) split inteins. The input promoter A drives the transcription of dCas9 IntN and a light-sensitive CIBN domain. The input promoter B drives the transcription of dCas9 IntC and a light-sensitive CIBN domain (**Figure 1C**).

Dose-Dependent Reporter Gene Expression Induced by Blue Light Illumination

A light-inducible CMV promoted dCas9 expression circuit was constructed to assess the efficiency of this light-inducible device. The results showed that the relative activity of hRluc luciferase production in the light group was significantly higher than that in the dark group in 293T and 5,637 cell lines (**Figures 2A,C**). The performance of the full-length dCas9 was better than the split dCas9. In addition, with a higher illumination dose, the relative luciferase activity increased (**Figures 2B,D**). Then, the time-course analysis of the expression of the fluorescence reporter gene in 5,637 cells showed that the expression level of the fluorescence gene increased with the prolongation of light (**Figures 2E,F**).

Construction of the Two-Input Logic and Gate

Next, we modified this system to increase its specificity toward bladder cancer cells by changing the input CMV promoter to hTERT and hUPII promoters, which are specific cancer cell and bladder cell markers (**Figure 3A**). The CMV circuit acted as a positive control and had higher effector expression compared to the hTERT/hUPII circuit when activated. In both 5,637 and T24 cells, both circuits were activated under light condition. Whereas, in 293T cells, only the CMV circuit was activated under light condition, no significant change was observed using the hTERT/hUPII circuit between the dark and light condition (**Figure 3B**).

Construction and Optimisation of the Two-Input and Logic Circuit

To investigate the potential therapeutic use of this system in bladder cancer, we altered the effector to exogenous p53 and endogenous E-cadherin protein. Both of them are well-known tumor suppressors (**Figure 4A**). When both hTERT/hUPII promoters were activated, the dCas9-CIB1 fusion protein would be reconstituted. Under the light condition, the heterodimerized CRY2-AD and dCas9-CIBI would activate the target gene transcription under gRNA guidance. We designed gRNAs specifically targeting CHD1 gene (**Figure 4C**) and exogenous TRE promoter which regulate the activation of p53 expression (**Figure 4B**).

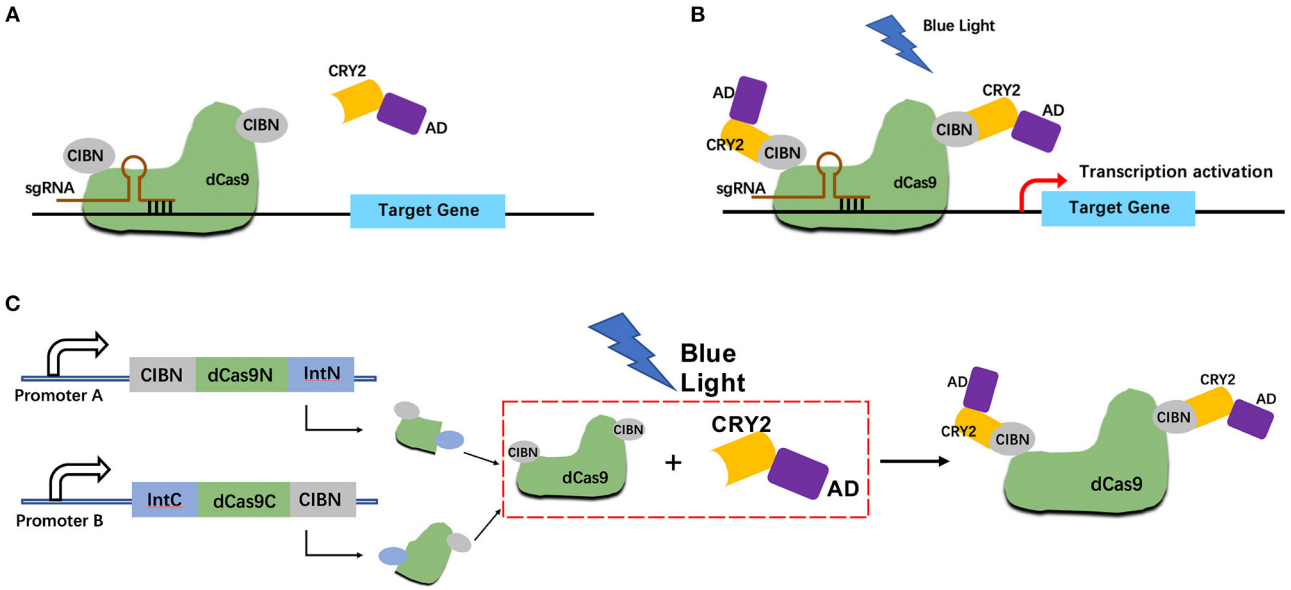

FIGURE 1 | Design strategy for light-inducible split CRISPR-dCas9 gene expression system. **(A,B)** Schematic of the light-inducible CRISPR-dCas9 gene expression system without blue light illumination **(A)** and with blue light illumination **(B)**; **(C)** Schematic of the light-inducible split CRISPR-dCas9 gene expression system with blue light illumination.

The Inhibitory Effect of Dcas9-Based Light-Induced p53 Expression in Bladder Cancer Cells

Furthermore, we detected the expression of p53 mRNA induced by light (**Supplementary Figure 1b**), and examined the effect of the synthetic circuit and elevated exogenous p53 expression on the bladder cancer cells via a set of functional assays. The cell proliferation assay, CCK8 and the cell colonization assay indicated that the light-induced p53 expression significantly reduced both 5,637 and T24 cell growth in light condition (**Figures 5A,C**). The light-dark group significantly decreased the cell colonization in T24 cells compared to the dark control, yet in 5,637 cells, no obvious difference was observed (**Figure 5A**).

Then the cell invasion assay was performed. According to **Figure 5B**, relative cell invasion was significantly reduced in both cell lines under light condition and light-dark condition compared to the dark condition (**Figure 5B**). Finally, the cell apoptosis was examined using caspase-3/ELISA (enzyme-linked immunosorbent assay). The light-induced p53 expression significantly increased the cell apoptosis in both cell lines in the light group and light-dark group compared to the dark control (**Figure 5D**).

The Inhibitory Effect of Dcas9-Based Light-Induced E-cadherin Circuit in Bladder Cancer Cells

The effect of the activated E-cadherin expression was assessed on the bladder cancer cells. In addition, to optimize the efficiency of CRISPR-dCas9 system, we selected three sgRNAs for verification. The efficiency of the sgRNAs was assessed by comparing the relative CHD1 mRNA level between the experimental and control groups, and only sgRNA3 was proved to have high efficiency (**Supplementary Figure 1a**). The cell proliferation and colonization assay showed that the light-induced E-cadherin expression reduced both 5,637 and T24 cell growth in light condition significantly (**Figures 6A,C**). The light-dark group showed a decrease in cell growth, yet not as significant as the light group.

According to **Figure 6B**, cell invasion was also significantly affected by the expression of light-induced E-cadherin. Even under light-dark condition, the cells exhibited a large decrease in their invasion ability (**Figure 6B**). Finally, caspase-3/ELISA (enzyme-linked immunosorbent assay) performed to assess the bladder cancer cell apoptosis. The light-induced E-cadherin expression significantly promoted the cell apoptosis in both cell lines. In T24 the cell apoptosis was higher in the light-dark group compared to the dark control, yet no significant difference was observed in the 5,637 cells (**Figure 6D**).

DISCUSSION

In this study, we demonstrated that in the presence of input signals, the split dCas9 can be reconstituted and carry out its transcriptional regulatory function *in vitro*. In addition, the dose-dependent reporter gene expression induced by blue light illumination suggested a successful integration of the CRY2-CIB1 light-sensitive module with the dCas9 protein. Upon optimizing the light-induced dCas9 system, we performed functional assays to examined the effect of our system on bladder cancer cell lines and profound effects were observed.

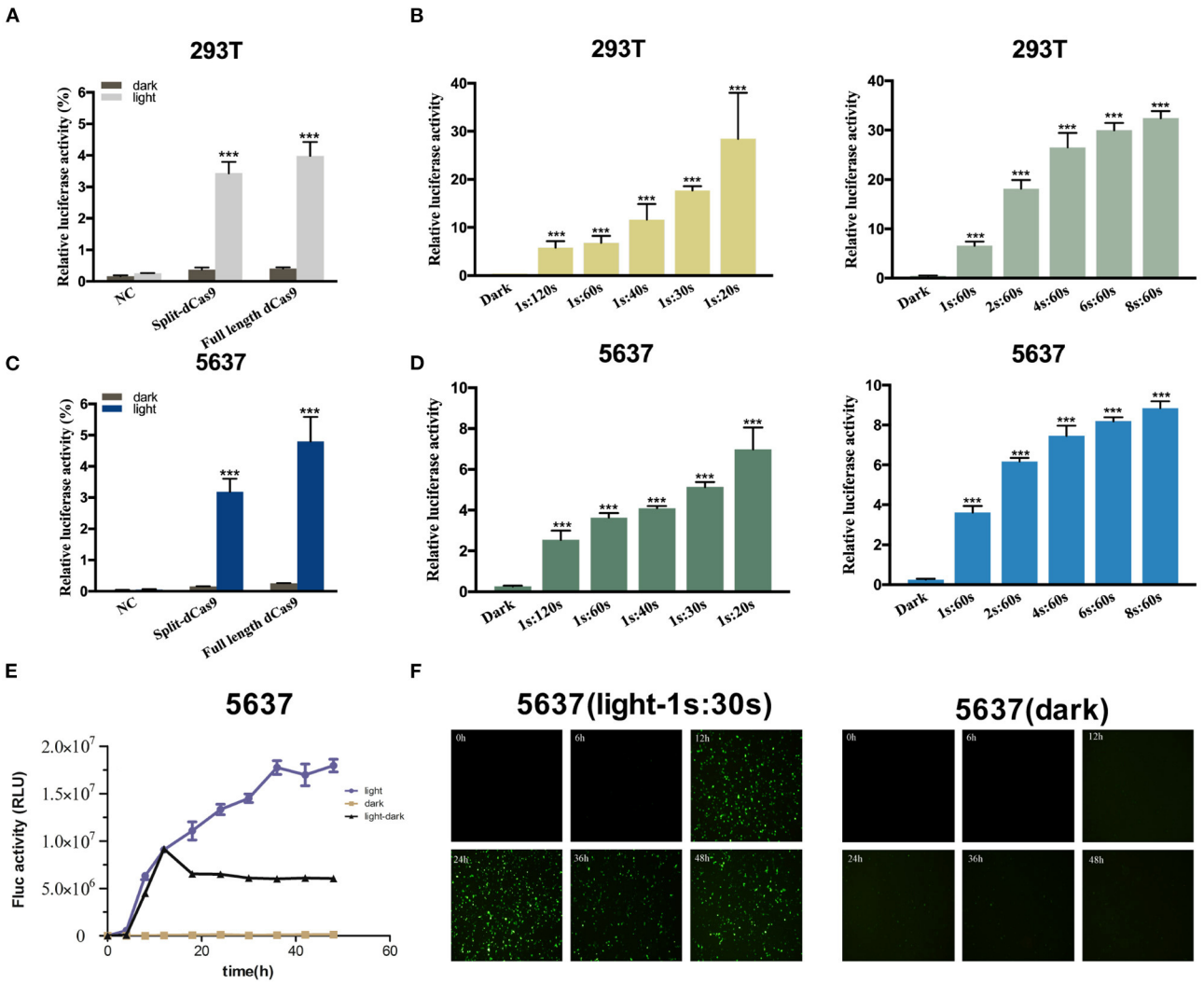

FIGURE 2 | Dose-dependent luciferase activity induced by light in the cancer cell. **(A,C)** Relative luciferase activity examined of full-length dCas9 group, split dCas9 group and the negative control under dark and light condition in 293T **(A)** and 5637 **(C)** cells. **(B,D)** The relative luciferase activity increases with increasing light dose in 293T **(B)** and 5637 **(D)** [1s:20s-1s:120s represents 1 s illumination (0.84 W/m^2) every 20–120 s]. **(E)** The EYFP reporter assay was used to detect changes in the expression of EYFP over time in 5,637 cells under light, dark, and light-dark conditions. **(F)** Time course of EYFP gene expression under light, dark, and light-dark conditions in 5,637 cell using fluorescence microscope. Data are means ± SD. ($n = 3$, $^*p < 0.05$, $^{**}p < 0.01$, $^{***}p < 0.001$).

Utilization of light-inducible gene-regulating devices in synthetic biology caught researchers' attention these years due to its precise spatial and temporal control (Polstein and Gersbach, 2015; Yamada et al., 2020; Zhao et al., 2020). The previous studies showed that a CRISPR-dCas9 based light-sensitive gene expression system could regulate an exogenous p53 expression in a dose-dependent manner (Lin et al., 2016). Via controlling the p53 expression, the bladder cancer cell proliferation was successfully inhibited. Here we adopted the idea of a light-sensitive gene-regulating device, and improved it by integrating AND logic gate with split dCas9 protein. The AND logic gate was composed of two inputs: hTERT and hUPII, which are the cancer-specific promoter and bladder specific promoter, respectively (Zhu et al., 2004; Jusiak et al., 2016). The CMV promoter, a strong promoter in eukaryotes was used as a control logic gate (**Figure 3**) (Zarrin et al., 1999). Through the AND logic gate, we aimed to selectively identify the bladder cancer cells and trigger the following output gene expression.

Besides the AND logic gate, we used split dCas9 protein to restrict the cargo size. This is particularly appealing to future *in vivo* applications, where the adeno-associated viral vectors (AAV) are commonly used (Santiago-Ortiz and Schaffer, 2016; George et al., 2017). They are well-known for the low immunogenicity and having various serotypes suitable for a tissue-specific infection (Verdera et al., 2020). However, the packaging of Streptococcus pyogenes (SpCas9) and gRNA is challenging due to the payload capacity of AAV is limited to ∼4.7 kb (Wu et al., 2010; Senís et al., 2014). In order to solve

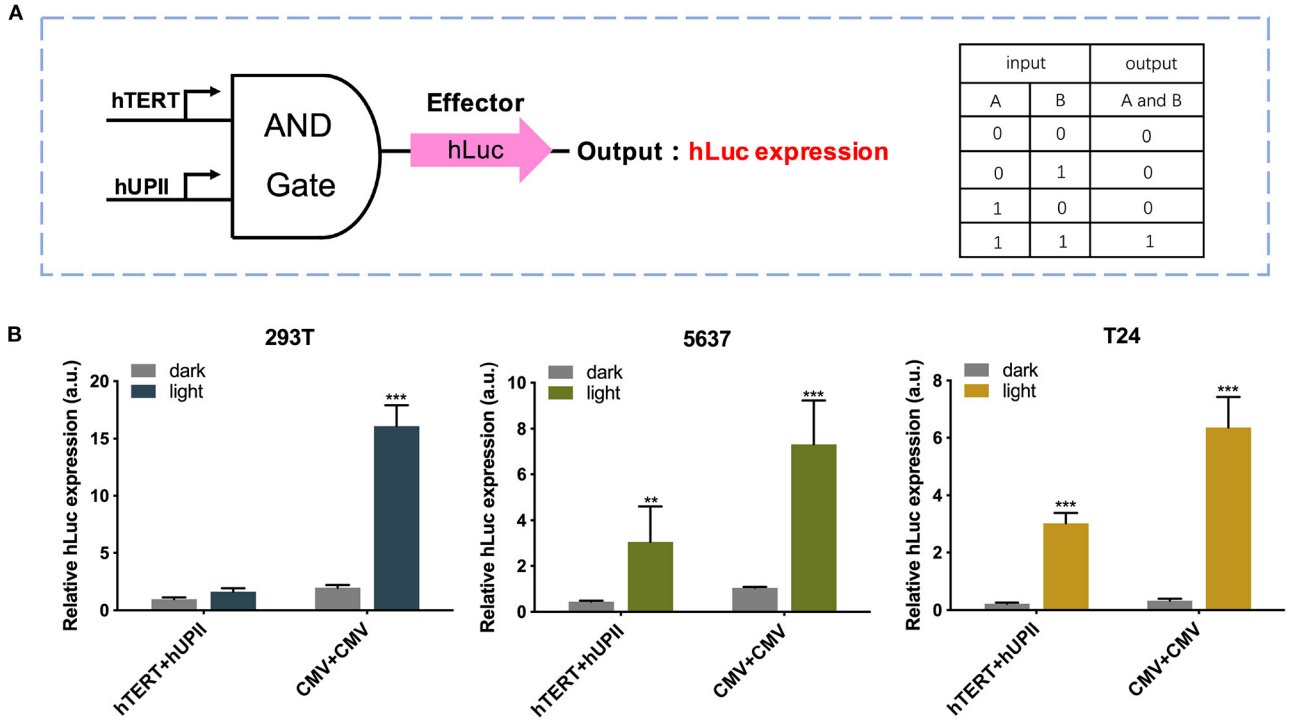

FIGURE 3 | Design and validation of the AND gate genetic circuits. **(A)** The logic AND gate has the hUP II and hTERT promoters as the inputs. In the presence of both inputs, the effector hLuc expression will be activated. **(B)** Luciferase expression levels of 293T, 5,637, and T24 cell lines transfected with the hTERT/hUPII circuit under dark or blue light condition, compared to the CMV control circuit. Data are means ± SD. ($n = 3$, $^{*}p < 0.05$, $^{**}p < 0.01$, $^{***}p < 0.001$).

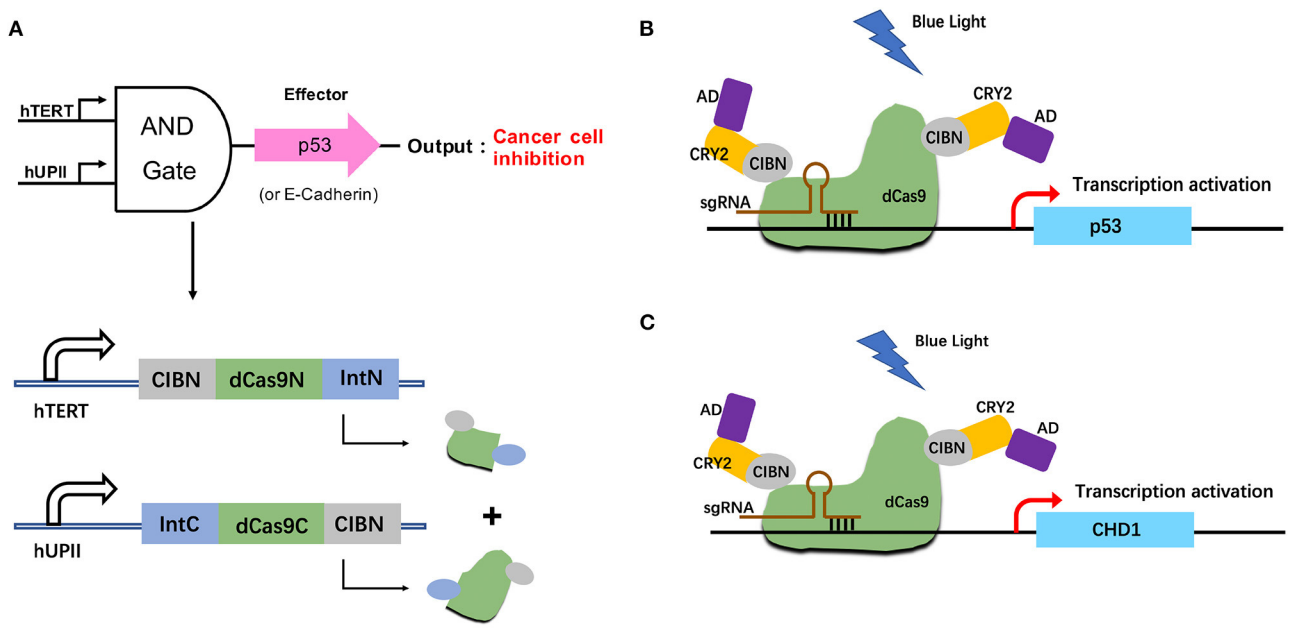

FIGURE 4 | Construction of the p53/E-cadherin circuit. **(A)** The hUP II and hTERT promoters are designed to be the AND logic gate inputs, and the outputs are exogenous p53 or endogenous E-cadhenrin. **(B,C)** In the presence of both inputs and light condition, the effector p53 **(B)** or E-cadherin **(C)** gene expression will be activated.

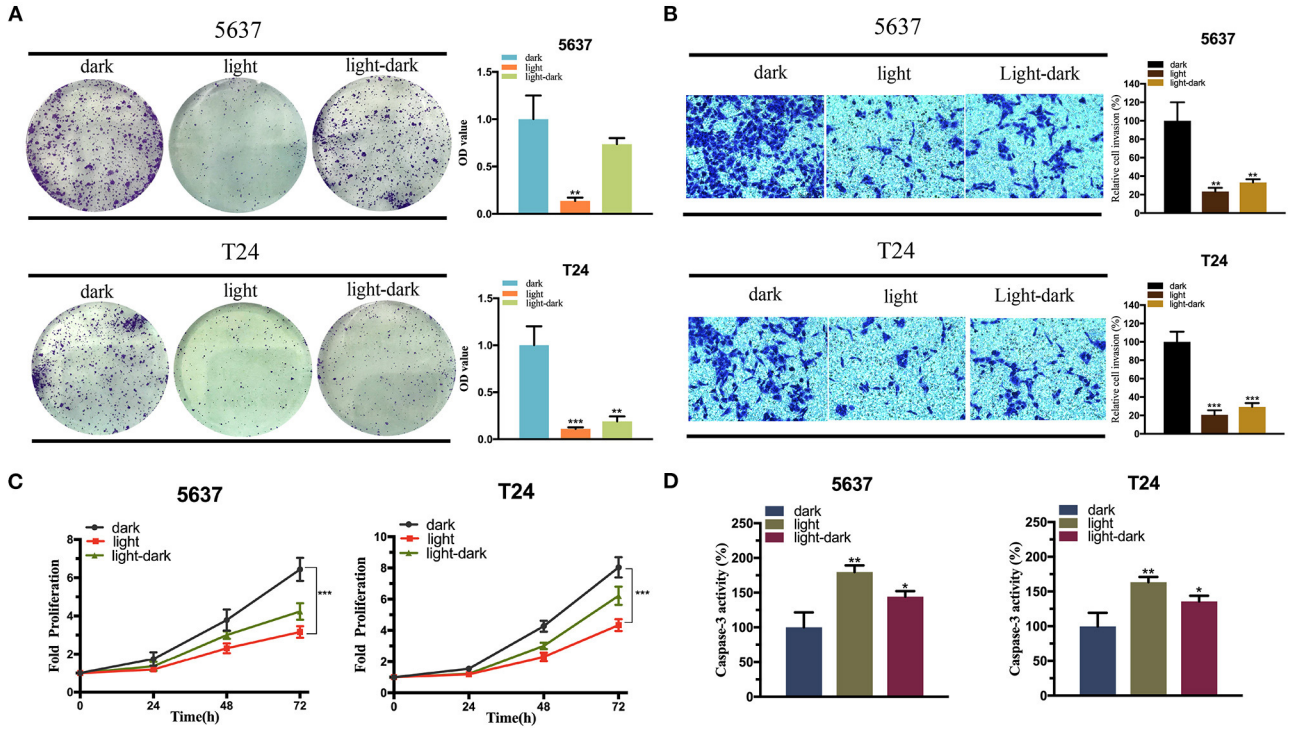

FIGURE 5 | The expression of exogenous p53 inhibits the bladder cancer cell function. **(A,C)** Colony-formation assay **(A)** and CCK-8 assay **(C)** indicating the effect of light-induced exogenous p53 expression under blue-light, dark, or light-dark condition on 5,637 and T24 cell proliferation. **(B)** Transwell assay diaplaying the effect of light-induced exogenous p53 expression under blue-light, dark, or light-dark condition on 5,637 and T24 cell invasion. **(D)** Caspase-3/ELISA suggesting the effect of light-inducible exogenous p53 expression under blue-light, dark, or light-dark condition on 5,637 and T24 cell apoptosis. Data are means ± SD. ($n = 3$, $^{*}p < 0.05$, $^{**}p < 0.01$, $^{***}p < 0.001$).

this problem, scientists proposed various ways including finding shorter and equally efficient Cas9 analogs (Ran et al., 2015). Some researchers have applied full-length Cas9 and split Cas9 to disease treatment and compared them (Hoffmann et al., 2019).Others worked on splitting the Cas9 protein and packaged each section into an individual AAV (Moreno et al., 2018). After transfecting the cell with both AAVs, the whole protein can be reconstituted (Chew et al., 2016; Ma et al., 2016). In addition, there was also a study to expand split-Cas9 into a platform for genome-engineering applications (Wright et al., 2015). In general, the AND logic circuit and split dCas9 protein system we generated could increase the specificity and reduce the size of the device, which could potentially benefit the future therapeutic use.

The output targets of the AND logic gate was exogenous p53 or endogenous E-cadherin, whose inactivation were well-known factors that contributed to cancer development (van Roy and Berx, 2008; Valente et al., 2018; Manshouri et al., 2019; Miller et al., 2020). p53 is the most frequently mutated tumor suppressor gene in cancer. Its mutation has direct association with tumor development and functions as an oncogene (Mircetic et al., 2017; Zhan et al., 2018). E-cadherin was found to be partially or even completely lost in the malignant progression of epithelial tumors (Strumane et al., 2004; Onder et al., 2008). Others also showed that E-cadherin had strong anti-invasion and anti-metastasis effects (Mendonsa et al., 2018; Wong et al., 2018). Our results were in line with previous findings, the activation of p53 and E-cadherin had a profound effect on bladder cancer cell proliferation, invasion and apoptosis.

In conclusion, our results validated the inhibitory effect of our light-induced split dCas9 system on the bladder cancer cells. In addition, based on the previous studies, we improved the specificity and practicality of this transcriptional regulatory tool by combining the light-inducible CRISPR system with the split CRISPR-dCas9 system. This work provides a potential strategy for precise and quantitative inhibition of bladder cancer cells.

MATERIALS AND METHODS

Plasmids Construction

The anchor domain [CMV-CIBN-dCas9(1-1153)-IntN, CMV-IntN-dCas9(1154-1368)-CIBN, hTERT-CIBN-dCas9(1-1153)-IntN, hUPII-IntN-dCas9(1154-1368)-CIBN], activator domain (CRY2PHR-VPR), EYFP reporting vector driven by Tet promoter (Tet-EYFP), dual-luciferase reporter vector driven by Tet promoter (TRE-hluc-SV40-hRluc) were purchased from Syngentech Co., Ltd. (Beijing, China). The sequence of sgRNA targeting Tet promoter of TRE-p53 vector and luciferase reporter vector: TACGTTCTCTATCACTGATA. The above

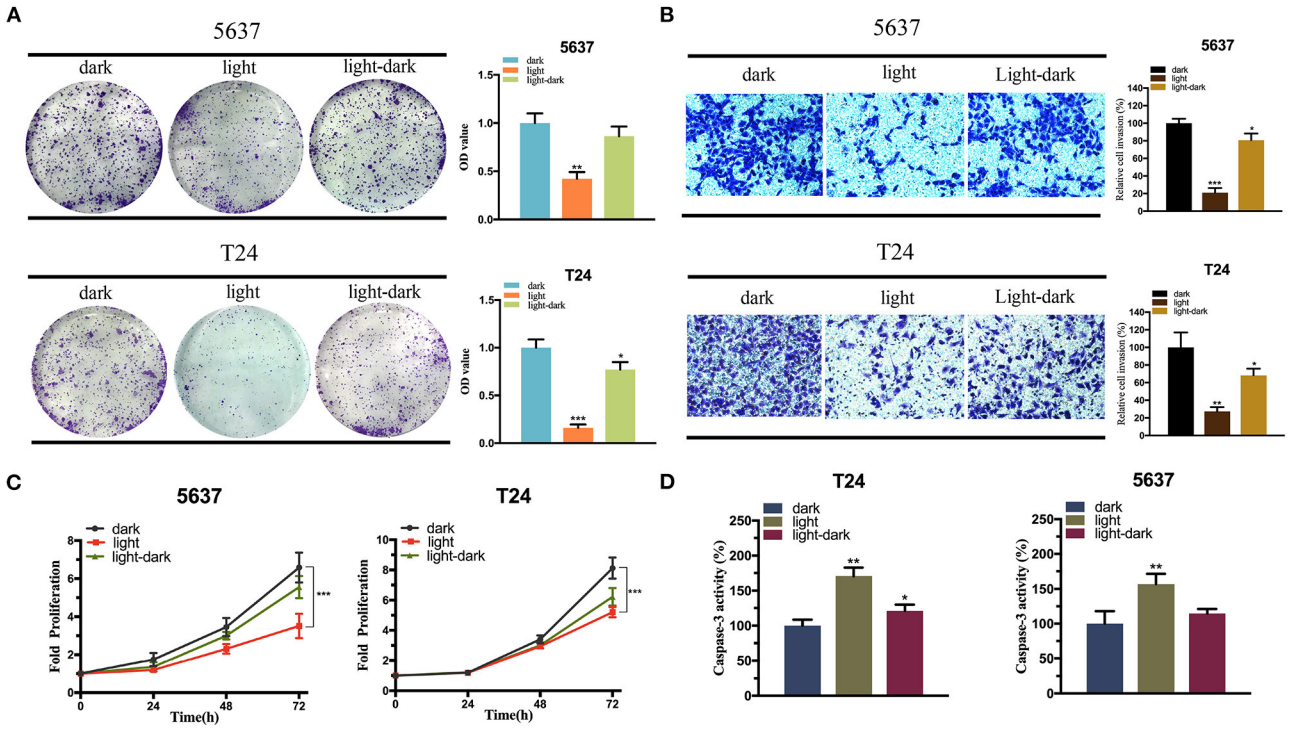

FIGURE 6 | The expression of E-cadherin inhibits the bladder cancer cell function. **(A,C)** The effect of light-induced E-cadherin expression on cell proliferation examined by colony-formation assay **(A)** and CCK-8 assay **(C)** under blue-light, dark, or light-dark condition in 5,637 and T24 cells. **(B)** The effect of light-induced E-cadherin expression on cell invasion examined by Transwell assay under blue-light, dark, or light-dark condition in 5,637 and T24 cells. **(D)** The effect of light-induced E-cadherin expression on cell apoptosis examined by Caspase-3/ELISA under blue-light, dark, or light-dark condition in 5,637 and T24 cells. Data are means ± SD. ($n = 3$, $^{*}p < 0.05$, $^{**}p < 0.01$, $^{***}p < 0.001$).

plasmid abbreviations were listed in **Supplementary Table 1**. The relative sequences were listed in **Supplementary Table 2**.

Cell Lines and Cell Culture

HEK 2923T (Human embryonic kidney cell line) was purchased from the Institute of Cell Research, Chinese Academy of Sciences (Shanghai, China). 5,637 and T24 (human bladder cancer cell lines) were purchased from American Type Culture Collection (ATCC). 293T and T24 were cultured in DMEM media (Invitrogen), 5,637 was maintained in RPMI-1640 media (Invitrogen). All cells were maintained by adding 10% fetal bovine serum, 1% penicillin/streptomycin (100 U/ml penicillin and 100 μg/ml streptomycin), and cultured in an atmosphere of 37°C and 5% CO_2.

Cell Transfection and Illumination

The plasmids were extracted by E.Z.N.A Fastfiler Endo-free Plasmid Maxiprep kits (Omega, Norcross, USA) from *E.coli* bacteria. Cells were transfected with a mixture of plasmids with lipofectamine 3000 (Invitrogen) according to the manufacturer's protocols. Anchor domain vector [CIBN-dCas9(1-1153)-IntN, IntN-dCas9(1154-1368)-CIBN], sgRNA-activator vector and effector vector were mixed in an amount of 0.8 μg per component in a 6-well and transfected at a ratio of 1:1:1:1. After 12 h of transfection, kept the cells in dark or under an LED lamp (460 nm, average irradiance of 0.84 W/m^2) for culture. The illumination dose depended on the frequency and intensity of light and was controlled by a timer.

Quantitative Real-Time PCR

According to the manufacturer's protocol, RNAeasy™ RNA Isolation Kit (Beyotime Biotechnology, China) was used to isolate total RNA from cells under different illumination conditions. cDNA was synthesized using BeyoRT™ II cDNA Synthesis Kit (Beyotime Biotechnology, China). The mRNA expression was performed using SYBR Green qPCR MasterMix (Takara, Dalian, China), with *gapdh* as the control. The relative mRNA (CDH1) level was calculated by ΔΔCt method. The primers for *gapdh* and *chd1* were shown in the following sequences, with directions ranging from 5′to 3′:

gapdh (F): TCCCATCACCATCTTCCA
gapdh (R): CATCACGCCACAGTTTCC
p53 (F): CCTCAGCATCTTATCCGAGTGG
p53 (R): TGGATGGTGGTACAGTCAGAGC
cdh1 (F): ACCAGAATAAAGACCAAGTGACCA
cdh1 (R): AGCAAGAGCAGCAGAATCAGAAT

Cell Proliferation Assay

The effect of blue light illumination on bladder cancer cells was detected by Cell Counting Kit (CCK-8). After dark and

illumination treatment, cells were seeded in 96-well-plates with 2 3 $\times$ 10^3 cells per well and pre-incubated for 12 h. At 0, 24, 48, and 72 h, replace the medium with 100 μl fresh medium containing 10 μl of CCK reagent (Transgen, China). After incubation for 1 h, the microplate reader (Bio-Rad) was used to determine the absorbance at 450 nm of the wells. At the same time, the colony formation assay was performed to detect the clones of 5,637 and T24. The related control and light-inducible vectors were packaged by lentiviruses to infect tumor cells. The infected 5,637 and T24 cells were cultured in 6 cm culture dishes at a density of 3,000 cells per well and incubated about 10 days, during which the cells were cultured in dark, light [1s:30s, 1 second light illumination (0.84 W/m^2) every 30 s] and light-dark (after 12 h of 1s:30s light illumination, cells were cultured in dark) condition. Finally, in order to quantify the number of cells, the cells were stained with 0.1% crystal violet and imaged. Then wash the stained cells with 33% glacial acetic acid, and measure the absorbance of each sample at 550 nm with the microplate reader.

Cell Invasion Assay

The transwell assay was used to detect the effect of dark and light conditions on cell invasion. Digest the transfected cells and inoculate 200 μl into the transwell chamber at a density of 3 $\times$ 10^5/ml, and the chamber was pre-plated with Matrigel (Corning, USA). The chamber was placed in the 24-well-plate, with 10% FBS medium under the cell and serum-free medium in the cell, so that cells could migrate to the medium containing serum in the lower chamber. After incubation for 24 h, the cells passing through the membrane were fixed by paraformaldehyde and stained with 0.1% crystal violet (2 mg/ml). The number of cells migrated through the membrane pores was counted under an optical microscope.

Cell Apoptosis Assay

Cells transfected with negative control vector and light-controlled vectors were inoculated on a 12-well-plate (2 $\times$ 10^5/well) with 70–80% confluency. After 48 h, the cell apoptosis was detected by the caspase-3/ELISA (enzyme-linked immunosorbent assay) assay (Hcusabio, China). The caspase-3 enzyme is a marker for inflammation and apoptosis signaling, since it can regulate the destruction of DNA or cytoskeletal proteins. Each test was performed at least three times.

Statistical Analysis

All statistical data was analyzed by SPSS 21.0 software for Windows (SPSS Inc. Chicago, IL, USA). Statistical analysis was conducted using Student's t-test or ANOVA and $p<0.05$ was considered statistically significant.

DATA AVAILABILITY STATEMENT

The original contributions presented in the study are included in the article/**Supplementary Material**, further inquiries can be directed to the corresponding author/s.

AUTHOR CONTRIBUTIONS

XH, QZ, and MW performed the experiments and data analysis. XH and MW prepared diagrams and wrote the manuscript. XH and QZ designed the project. YG and JY supervised the project and provided financial support. All authors contributed to the article and approved the submitted version.

FUNDING

This work was supported by grants from the National Key R&D Program of China (2019YFA0906003) and National Natural Science Foundation of China (82073364).

SUPPLEMENTARY MATERIAL

The Supplementary Material for this article can be found online at: https://www.frontiersin.org/articles/10.3389/fmolb.2020.627848/full#supplementary-material

REFERENCES

(2017). Bladder cancer: diagnosis and management of bladder cancer: © NICE (2015) Bladder cancer: diagnosis and management of bladder cancer. *BJU Int.* 120, 755–765. doi: 10.1111/bju.14045

Beerli, R. R., Dreier, B., and Barbas, C. F., III. (2000). Positive and negative regulation of endogenous genes by designed transcription factors. *Proc. Natl. Acad. Sci. U.S.A.* 97, 1495–1500. doi: 10.1073/pnas.040552697

Chew, W. L., Tabebordbar, M., Cheng, J. K., Mali, P., Wu, E. Y., Ng, A. H., et al. (2016). A multifunctional AAV-CRISPR-Cas9 and its host response. *Nat. Methods* 13, 868–874. doi: 10.1038/nmeth.3993

Folcher, M., Oesterle, S., Zwicky, K., Thekkottil, T., Heymoz, J., Hohmann, M., et al. (2014). Mind-controlled transgene expression by a wireless-powered optogenetic designer cell implant. *Nat. Commun.* 5:5392. doi: 10.1038/ncomms6392

George, L. A., Sullivan, S. K., Giermasz, A., Rasko, J. E. J., Samelson-Jones, B. J., Ducore, J., et al. (2017). Hemophilia B gene therapy with a high-specific-activity factor IX variant. *N. Engl. J. Med.* 377, 2215–2227. doi: 10.1056/NEJMoa1708538

Gossen, M., Freundlieb, S., Bender, G., Müller, G., Hillen, W., and Bujard, H. (1995). Transcriptional activation by tetracyclines in mammalian cells. *Science* 268, 1766–1769. doi: 10.1126/science.7792603

Hoffmann, M. D., Aschenbrenner, S., Grosse, S., Rapti, K., Domenger, C., Fakhiri, J., et al. (2019). Cell-specific CRISPR-Cas9 activation by microRNA-dependent expression of anti-CRISPR proteins. *Nucleic Acids Res.* 47:e75. doi: 10.1093/nar/gkz271

Jinek, M., Chylinski, K., Fonfara, I., Hauer, M., Doudna, J. A., and Charpentier, E. (2012). A programmable dual-RNA-guided DNA endonuclease in adaptive bacterial immunity. *Science* 337, 816–821. doi: 10.1126/science.1225829

Jusiak, B., Cleto, S., Perez-Piñera, P., and Lu, T. K. (2016). Engineering synthetic gene circuits in living cells with CRISPR technology. *Trends Biotechnol.* 34, 535–547. doi: 10.1016/j.tibtech.2015.12.014

Leow, J. J., Martin-Doyle, W., Rajagopal, P. S., Patel, C. G., Anderson, E. M., Rothman, A. T., et al. (2014). Adjuvant chemotherapy for invasive bladder cancer: a 2013 updated systematic review and meta-analysis of randomized trials. *Eur. Urol.* 66, 42–54. doi: 10.1016/j.eururo.2013.08.033

Li, L., Hu, S., and Chen, X. (2018). Non-viral delivery systems for CRISPR/Cas9-based genome editing: challenges and opportunities. *Biomaterials* 171, 207–218. doi: 10.1016/j.biomaterials.2018.04.031

Lin, F., Dong, L., Wang, W., Liu, Y., Huang, W., and Cai, Z. (2016). An efficient light-inducible P53 expression system for inhibiting proliferation of bladder cancer cell. *Int. J. Biol. Sci*. 12, 1273–1278. doi: 10.7150/ijbs.16162

Liu, Y., Zeng, Y., Liu, L., Zhuang, C., Fu, X., Huang, W., et al. (2014). Synthesizing AND gate genetic circuits based on CRISPR-Cas9 for identification of bladder cancer cells. *Nat. Commun*. 5:5393. doi: 10.1038/ncomms6393

Ma, D., Peng, S., and Xie, Z. (2016). Integration and exchange of split dCas9 domains for transcriptional controls in mammalian cells. *Nat. Commun*. 7:13056. doi: 10.1038/ncomms13056

Manshouri, R., Coyaud, E., Kundu, S. T., Peng, D. H., Stratton, S. A., Alton, K., et al. (2019). ZEB1/NuRD complex suppresses TBC1D2b to stimulate E-cadherin internalization and promote metastasis in lung cancer. *Nat. Commun*. 10:5125. doi: 10.1038/s41467-019-12832-z

Mendonsa, A. M., Na, T. Y., and Gumbiner, B. M. (2018). E-cadherin in contact inhibition and cancer. *Oncogene* 37, 4769–4780. doi: 10.1038/s41388-018-0304-2

Miller, J. J., Gaiddon, C., and Storr, T. (2020). A balancing act: using small molecules for therapeutic intervention of the p53 pathway in cancer. *Chem. Soc. Rev*. 49, 6995–7014. doi: 10.1039/D0CS00163E

Mircetic, J., Dietrich, A., Paszkowski-Rogacz, M., Krause, M., and Buchholz, F. (2017). Development of a genetic sensor that eliminates p53 deficient cells. *Nat. Commun*. 8:1463. doi: 10.1038/s41467-017-01688-w

Moreno, A. M., Fu, X., Zhu, J., Katrekar, D., Shih, Y. V., Marlett, J., et al. (2018). *In situ* gene therapy via AAV-CRISPR-Cas9-mediated targeted gene regulation. *Mol. Ther*. 26, 1818–1827. doi: 10.1016/j.ymthe.2018.04.017

Muller, P. Y., and Milton, M. N. (2012). The determination and interpretation of the therapeutic index in drug development. *Nat. Rev. Drug Discov*. 11, 751–761. doi: 10.1038/nrd3801

Nihongaki, Y., Kawano, F., Nakajima, T., and Sato, M. (2015). Photoactivatable CRISPR-Cas9 for optogenetic genome editing. *Nat. Biotechnol*. 33, 755–760. doi: 10.1038/nbt.3245

Onder, T. T., Gupta, P. B., Mani, S. A., Yang, J., Lander, E. S., and Weinberg, R. A. (2008). Loss of E-cadherin promotes metastasis via multiple downstream transcriptional pathways. *Cancer Res*. 68, 3645–3654. doi: 10.1158/0008-5472.CAN-07-2938

Polstein, L. R., and Gersbach, C. A. (2015). A light-inducible CRISPR-Cas9 system for control of endogenous gene activation. *Nat. Chem. Biol*. 11, 198–200. doi: 10.1038/nchembio.1753

Qi, L. S., Larson, M. H., Gilbert, L. A., Doudna, J. A., Weissman, J. S., Arkin, A. P., et al. (2013). Repurposing CRISPR as an RNA-guided platform for sequence-specific control of gene expression. *Cell* 152, 1173–1183. doi: 10.1016/j.cell.2013.02.022

Ran, F. A., Cong, L., Yan, W. X., Scott, D. A., Gootenberg, J. S., Kriz, A. J., et al. (2015). *In vivo* genome editing using *Staphylococcus aureus* Cas9. *Nature* 520, 186–191. doi: 10.1038/nature14299

Rivière, I., and Sadelain, M. (2017). Chimeric antigen receptors: a cell and gene therapy perspective. *Mol. Ther*. 25, 1117–1124. doi: 10.1016/j.ymthe.2017.03.034

Santiago-Ortiz, J. L., and Schaffer, D. V. (2016). Adeno-associated virus (AAV) vectors in cancer gene therapy. *J. Control. Release* 240, 287–301. doi: 10.1016/j.jconrel.2016.01.001

Schenone, M., Dančík, V., Wagner, B. K., and Clemons, P. A. (2013). Target identification and mechanism of action in chemical biology and drug discovery. *Nat. Chem. Biol*. 9, 232–240. doi: 10.1038/nchembio.1199

Sedlmayer, F., Aubel, D., and Fussenegger, M. (2018). Synthetic gene circuits for the detection, elimination and prevention of disease. *Nat. Biomed. Eng*. 2, 399–415. doi: 10.1038/s41551-018-0215-0

Senís, E., Fatouros, C., Große, S., Wiedtke, E., Niopek, D., Mueller, A. K., et al. (2014). CRISPR/Cas9-mediated genome engineering: an adeno-associated viral (AAV) vector toolbox. *Biotechnol. J*. 9, 1402–1412. doi: 10.1002/biot.201400046

Strumane, K., Berx, G., and Van Roy, F. (2004). Cadherins in cancer. *Handb. Exp. Pharmacol*. 2004, 69–103. doi: 10.1007/978-3-540-68170-0_4

Truong, D. J., Kühner, K., Kühn, R., Werfel, S., Engelhardt, S., Wurst, W., et al. (2015). Development of an intein-mediated split-Cas9 system for gene therapy. *Nucleic Acids Res*. 43, 6450–6458. doi: 10.1093/nar/gkv601

Valente, J. F. A., Queiroz, J. A., and Sousa, F. (2018). p53 as the focus of gene therapy: past, present and future. *Curr. Drug Targets* 19, 1801–1817. doi: 10.2174/1389450119666180115165447

van Roy, F., and Berx, G. (2008). The cell-cell adhesion molecule E-cadherin. *Cell. Mol. Life Sci*. 65, 3756–3788. doi: 10.1007/s00018-008-8281-1

Vasekar, M., Degraff, D., and Joshi, M. (2016). Immunotherapy in bladder cancer. *Curr. Mol. Pharmacol*. 9, 242–251. doi: 10.2174/1874467208666150716120945

Verdera, H. C., Kuranda, K., and Mingozzi, F. (2020). AAV vector immunogenicity in humans: a long journey to successful gene transfer. *Mol. Ther*. 28, 723–746. doi: 10.1016/j.ymthe.2019.12.010

Wong, S. H. M., Fang, C. M., Chuah, L. H., Leong, C. O., and Ngai, S. C. (2018). E-cadherin: its dysregulation in carcinogenesis and clinical implications. *Crit. Rev. Oncol. Hematol*. 121, 11–22. doi: 10.1016/j.critrevonc.2017.11.010

Wright, A. V., Sternberg, S. H., Taylor, D. W., Staahl, B. T., Bardales, J. A., Kornfeld, J. E., et al. (2015). Rational design of a split-Cas9 enzyme complex. *Proc. Natl. Acad. Sci. U.S.A*. 112, 2984–2989. doi: 10.1073/pnas.1501698112

Wu, Z., Yang, H., and Colosi, P. (2010). Effect of genome size on AAV vector packaging. *Mol. Ther*. 18, 80–86. doi: 10.1038/mt.2009.255

Yamada, M., Nagasaki, S. C., Suzuki, Y., Hirano, Y., and Imayoshi, I. (2020). Optimization of light-inducible Gal4/UAS gene expression system in mammalian cells. *iScience* 23:101506. doi: 10.1016/j.isci.2020.101506

Ye, H., and Fussenegger, M. (2019). Optogenetic medicine: synthetic therapeutic solutions precision-guided by light. *Cold Spring Harb. Perspect. Med*. 9:a034371. doi: 10.1101/cshperspect.a034371

Zarrin, A. A., Malkin, L., Fong, I., Luk, K. D., Ghose, A., and Berinstein, N. L. (1999). Comparison of CMV, RSV, SV40 viral and Vlambda1 cellular promoters in B and T lymphoid and non-lymphoid cell lines. *Biochim. Biophys. Acta* 1446, 135–139. doi: 10.1016/S0167-4781(99)00067-6

Zetsche, B., Volz, S. E., and Zhang, F. (2015). A split-Cas9 architecture for inducible genome editing and transcription modulation. *Nat. Biotechnol*. 33, 139–142. doi: 10.1038/nbt.3149

Zhan, H., Xie, H., Zhou, Q., Liu, Y., and Huang, W. (2018). Synthesizing a genetic sensor based on CRISPR-Cas9 for specifically killing p53-deficient cancer cells. *ACS Synth. Biol*. 7, 1798–1807. doi: 10.1021/acssynbio.8b00202

Zhan, T., Rindtorff, N., Betge, J., Ebert, M. P., and Boutros, M. (2019). CRISPR/Cas9 for cancer research and therapy. *Semin. Cancer Biol*. 55, 106–119. doi: 10.1016/j.semcancer.2018.04.001

Zhang, F., Cong, L., Lodato, S., Kosuri, S., Church, G. M., and Arlotta, P. (2011). Efficient construction of sequence-specific TAL effectors for modulating mammalian transcription. *Nat. Biotechnol*. 29, 149–153. doi: 10.1038/nbt.1775

Zhao, W., Wang, Y., and Liang, F. S. (2020). Chemical and light inducible epigenome editing. *Int. J. Mol. Sci*. 21:998. doi: 10.3390/ijms21030998

Zhu, H. J., Zhang, Z. Q., Zeng, X. F., Wei, S. S., Zhang, Z. W., and Guo, Y. L. (2004). Cloning and analysis of human UroplakinII promoter and its application for gene therapy in bladder cancer. *Cancer Gene Ther*. 11, 263–272. doi: 10.1038/sj.cgt.7700672

Conflict of Interest: The authors declare that the research was conducted in the absence of any commercial or financial relationships that could be construed as a potential conflict of interest.

frontiers in Molecular Biosciences

ORIGINAL RESEARCH
published: 18 January 2021
doi: 10.3389/fmolb.2020.627774

CRISPR-Cas13-Mediated Knockdown of lncRNA-GACAT3 Inhibited Cell Proliferation and Motility, and Induced Apoptosis by Increasing p21, Bax, and E-Cadherin Expression in Bladder Cancer

Zhongfu Zhang[1,2,3,4], *Jieqing Chen*[3,4], *Zhongshuang Zhu*[5], *Zhongqing Zhu*[6], *Xinhui Liao*[3,4], *Jianting Wu*[3,4], *Jianli Cheng*[3,4], *Xintao Zhang*[3,4], *Hongbing Mei*[3,4] *and Guosheng Yang*[1,2,7]*

[1] The Second School of Clinical Medicine, Southern Medical University Affiliated Guangdong Second Provincial General Hospital, Southern Medical University, Guangzhou, China, [2] Department of Urology, Guangdong Second Provincial General Hospital, Guangzhou, China, [3] Guangdong Key Laboratory of Systems Biology and Synthetic Biology for Urogenital Tumors, Shenzhen Second People's Hospital, First Affiliated Hospital of Shenzhen University, Shenzhen, China, [4] Shenzhen Key Laboratory of Genitourinary Tumor, Shenzhen Second People's Hospital, First Affiliated Hospital of Shenzhen University, Shenzhen, China, [5] Peking University Shenzhen Hospital, Shenzhen, China, [6] Hong Kong University Shenzhen Hospital, Shenzhen, China, [7] Shanghai East Hospital, Tongji University School of Medicine, Shanghai, China

The current study is to investigate the expression pattern and biological function of long non-coding RNA Focally gastric cancer-associated transcript3 (GACAT3) in bladder cancer. Real-time quantitative qPCR was used to detect the expression level of GACAT-3 in tumor tissues and paired normal tissues. Human bladder cancer T24 and 5637 cell lines were transiently transfected with specific CRISPR-Cas13 or negative control CRISPR-Cas13. Cell migration, proliferation, and apoptosis were measured by using wound healing assay CCK-8 assay and Caspase-3 ELISA assay, respectively. The expression changes of p21, Bax, and E-cadherin after knockdown of GACAT3 were detected by using Western blot. The results demonstrated that GACAT3 was up-regulated in bladder cancer tissues than that in the paired normal tissues. Inhibition of cell proliferation, increased apoptosis, and decreased motility were observed in T24 and 5637 cell lines transfected by CRISPR-Cas13 targeting GACAT3. Downregulation of GACAT3 increased p21, Bax, and E-cadherin expression and silencing these genes could eliminate the phenotypic changes induced by knockdown of GACAT3. A ceRNA mechanism for GACAT3 was also revealed. By using CRISPR-Cas13 biotechnology, we suggested that GACAT3 may be a novel target for diagnosis and treatment of bladder cancer.

Keywords: long non-coding RNA, GACAT3, bladder cancer, CRISPR-Cas13, cancer development

OPEN ACCESS

Edited by:
Yonghao Zhan,
Zhengzhou University, China

Reviewed by:
Kai Yang,
Zhejiang University, China
Yingying Zhang,
Northwest A and F University, China

***Correspondence:**
Guosheng Yang
2008yangguosheng@sina.com

Specialty section:
This article was submitted to Molecular Diagnostics and Therapeutics, a section of the journal Frontiers in Molecular Biosciences

Received: *10 November 2020*
Accepted: *27 November 2020*
Published: *18 January 2021*

Citation:
Zhang Z, Chen J, Zhu Z, Zhu Z, Liao X, Wu J, Cheng J, Zhang X, Mei H and Yang G (2021) CRISPR-Cas13-Mediated Knockdown of lncRNA-GACAT3 Inhibited Cell Proliferation and Motility, and Induced Apoptosis by Increasing p21, Bax, and E-Cadherin Expression in Bladder Cancer. Front. Mol. Biosci. 7:627774. doi: 10.3389/fmolb.2020.627774

INTRODUCTION

Bladder cancer (BC) is the most common type in malignancy tumors of the urinary system all over the world. The cause of bladder cancer is complex, which include both genetic factors and external environmental factors (Czerniak et al., 2016). Under the action of internal and external factors, the signal networks changed in the bladder epithelial cells lead to the occurrence of bladder cancer. Therefore, the development of bladder cancer is the result of a sophisticated multi-molecule effect (Sathe and Nawroth, 2018). These disrupted molecular networks are the root of the appearance of the malignant phenotypes of bladder cancer. For a long time, we have been trying to find the signal molecules which are located in the center of the signal network and attempt to achieve the goal of interfering with the progression of bladder cancer by acting on these molecules. Although traditional treatment such as surgery, chemotherapy and radiation can treat with bladder cancer to a certain extent, they usually cause severe side effect (Amit and Hochberg, 2010). Thus, it is necessary to develop a new method to deal with bladder cancer specifically.

A growing number body of evidences demonstrated that long non-coding RNAs (lncRNAs) play an important role in the pathological and physiological processes of cells, including the formation of cancers (Huarte, 2015). Compared with other types of RNA such as siRNA, piRNA, or miRNA, the mechanisms of lncRNAs are more sophisticated. Through interaction with RNAs, DNA, or other protein molecules, lncRNAs regulate the expression of many proteins (Jariwala and Sarkar, 2016). LncRNA-DILC inhibits the expression of IL-6 by binding to the IL-6 promoter DNA in hepatocellular carcinoma, thereby inhibiting the growth of cancer stem cells (Wang et al., 2016). In breast cancer, lncRNA-LINP1 was found to serve as an important regulator which enhances DNA-repair activity by interacting with DNA-PKcs and Ku80 proteins (Zhang et al., 2016). Moreover, the dysregulation of hundreds of lncRNAs are closely related to the clinical pathologies of gastric cancer in one previous research (Zhao et al., 2015).

LncRNA-GACAT3 is located on human Chr 2p24.3 and it was reported to be upregulated in some types of cancer tissues, such as gastric cancer (Feng et al., 2018), colorectal cancer (Zhou et al., 2018) and non-small cell lung cancer (Yang et al., 2018). The potential of lncRNA-GACAT3 as an important regulatory point in cancer is gradually developed. Although the role of lncRNA-GACAT3 in regulating cell function has been reported in previous studies, its biological function and molecular mechanism in BC is not clear yet (Shen et al., 2016; Feng et al., 2018; Zhou et al., 2018).

In this study, we found that lncRNA-GACAT3 was upregulated in bladder cancer and can promote malignant phenotypes for the first time. Moreover, we also found that GACAT3 can inhibit cell apoptosis, and promote cell proliferation and migration by downregulating the expression of P21, Bax, and E-cadherin proteins in bladder cancer. These results might provide a novel potential methods for targeted therapy or diagnosis of bladder cancer.

METHODS

Cell Culture

We purchased the bladder cancer cell lines T24 and 5637 from the Institute of Cell Research, Chinese Academy of Sciences, Shanghai, China. These cells were cultured in DMEM medium which had added 10% fetal bovine serum. We grew the cells in the 37°C atmosphere which contains 5% CO_2.

qRT-PCR Assay

The TRIzol reagent (Invitrogen, Carlsbad, CA, USA) was used to extract the total RNAs from the cancer simple tissues and bladder cancer cell lines. The cDNAs all were synthesized from the total extracted RNAs and put into effect with the RevertAid™ First Strand cDNA Synthesis Kit (Fermentas, Hanover, MD, USA). We used the All-in-One™ qPCR Mix (GeneCopoiea Inc, Rockville, MD, USA) to carry out the qRT-PCR assay in our study.

Western Blot Assay

The antibodies of P21 protein, Bax protein and E-cadherin protein were got from Cell Signaling Technology (Boston, MA, USA). The process of the western blot assay in our study is carried out according to the traditional western blot assay method.

Cell Counting Kit-8 Assay

We evaluated the level of cell proliferation by using Cell Counting Kit-8 (CCK-8) assay (Beyotime Institute of Biotechnology, shanghai, China). The CCK-8 assay was put into effect according to the instructions of the manufacturer.

Caspase-3 ELISA Assay

The Caspase-3 ELISA assay kit (R&D, Minneapolis, MN, USA) was used to evaluate the level of cell apoptosis in our study. The operation step of this experiment was performed according to the instructions of manufacturer.

Wound Healing Assay

The migration level of bladder cancer cells in our study was evaluated by using wound healing assay. We carried out this experiment according to the traditional method.

Nuclear/Cytoplasmic Fractionation

Nuclear/cytoplasmic fractionation was performed with PARIS Kit (Life Technologies, MA) based on the manufacturer's instructions. After the cell nuclear and cytoplasmic fractionating, the expression level of GACAT3 were determined by RT-qPCR with GAPDH as internal controls, respectively.

Dual-Luciferase Reporter Assay

The vectors of lncRNA GACAT3 Wild Type or Mutant were constructed and co-transfected with miR-497 mimics or corresponding negative control (miR-NC) into bladder cancer cells. Forty-eight hours after transfection, luciferase activity was measured by using the Dual-Luciferase Reporter Assay System (Promega).

Statistical Analysis

The different expression level of GACAT3 RNA between bladder cancer tissues and the paired normal tissues were analyzed by using paired samples *t*-test. The GACAT3 RNA expression differences between cancer subgroups were analyzed using independent samples *t*-test. The diversities between different groups in the CCK-8 assay were analyzed by utilizing ANOVA. Cell apoptosis assays and wound healing assays were analyzed using independent samples *t*-test. Pearson's coefficient correlation was used for expression correlation assay. All these statistical analyses were carried out in SPSS (Version 19.0 SPSS Inc.). A *P*-value of <0.05 was thought to be statistically significant.

RESULTS

lncRNA-GACAT3 Was Upregulated in Bladder Cancer Tissues

In our work, a total of 32 sets of urothelial malignant tumor specimens were collected. All these specimens were collected from the patients who diagnosed with bladder cancer and treated with surgical treatment in the Shenzhen second people's

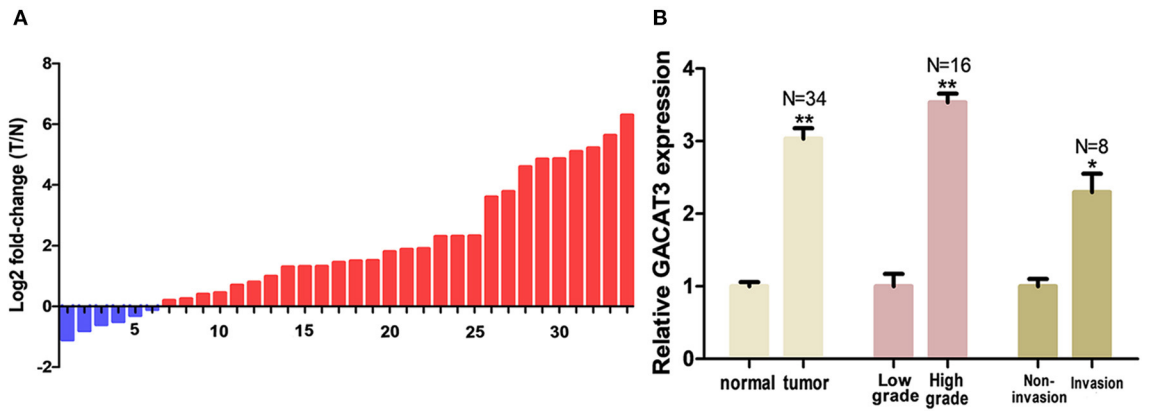

FIGURE 1 | GACAT3 was overexpressed in bladder cancer. Relative GACAT3 expression was detected using Real-Time qPCR. The relative GACAT3 expression value was set as the base value of 1 in each control group. N, number of study population in each group. **(A)** T represents tumor, N represents normal. The heights of the columns in the chart represent the log2-transformed fold changes (tumor/normal) in GACAT3 expression in 36 patients. **(B)** GACAT3 expression levels were higher in tumors than those in normal tissues (**$p < 0.01$). GACAT3 expression levels were higher in high grade cancers than those in low grade cancers (**$p < 0.01$). GACAT3 expression levels were higher in invasive cancers than those in non-invasive cancers (*$p < 0.05$).

TABLE 1 | Clinical features of patients with bladder cancer.

No.	Sex	Age	Grade	Stage	Surgery	No.	Sex	Age	Grade	Stage	Surgery
1	M	57	Low	T2N0M0	Partial	18	M	61	Low	T1N0M0	Partial
2	M	64	Low	T1N0M0	Partial	19	M	64	High	T2N0M0	Radical
3	M	51	Low	T2N0M0	Partial	20	M	61	Low	T1N0M0	Partial
4	M	64	High	T3N0M0	Radical	21	M	54	High	T2N0M0	Radical
5	M	65	Low	T2N0M0	Partial	22	M	58	High	T2N0M0	Radical
6	M	58	Low	T1N0M0	Partial	23	M	50	High	T3N0M0	Radical
7	M	53	High	T2N0M0	Radical	24	M	42	High	T2N0M0	Radical
8	M	61	Low	T2N0M0	Partial	25	M	58	High	T2N0M0	Radical
9	M	41	Low	T1N0M0	Partial	26	M	57	High	T3N0M0	Radical
10	M	54	High	T2N0M0	Radical	27	F	58	High	T3N0M0	Radical
11	M	51	High	T2N0M0	Radical	28	F	56	High	T3N0M0	Partial
12	M	55	Low	T2N0M0	Partial	29	F	51	Low	T1N0M0	Partial
13	M	55	Low	T2N0M0	Partial	30	F	52	Low	T1N0M0	Partial
14	M	73	High	T2N0M0	Radical	31	F	51	High	T3N0M0	Partial
15	M	55	Low	T1N0M0	Partial	32	F	52	High	T3N0M0	Radical
16	M	50	Low	T1N0M0	Partial	33	F	43	High	T3N0M0	Radical
17	M	57	High	T2N0M0	Radical	34	F	69	High	T3N0M0	Radical

No., patient number; M, male; F, female; Age, years old; Grade, the 2004 WHO classification; Stage, AJCC TNM classification; Radical, radical cystectomy; Partial, partial cystectomy.

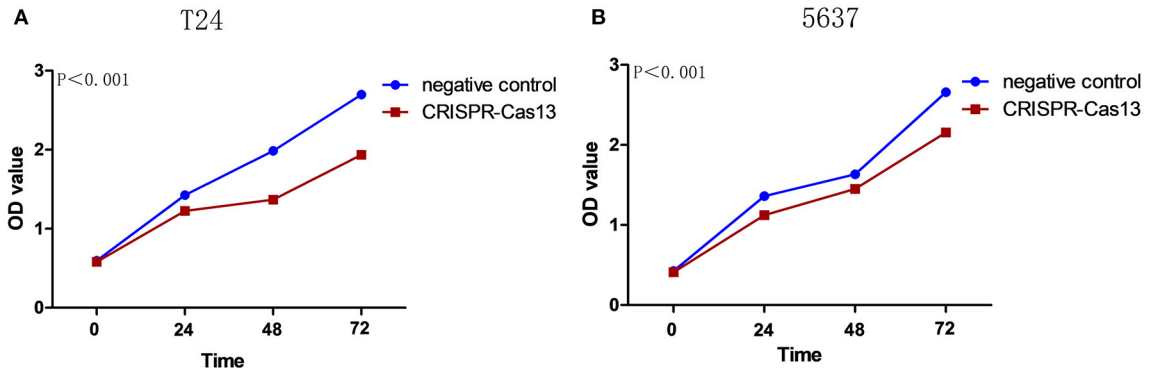

FIGURE 2 | Knockdown of GACAT3 inhibited cell proliferation. Cell proliferation was measured by CCK-8 assay. After transfection of CACAT3 CRISPR-Cas13 or negative control CRISPR-Cas13, OD values were measured and converted to cell numbers. ANOVA was used for the comparison of curves of cell proliferation. **(A)** Inhibition of cell proliferation was observed in bladder cancer 5637 cells (**$p < 0.01$). **(B)** Inhibition of cell proliferation was observed in bladder cancer T24 cells (**$p < 0.01$). Data are shown as mean ± SD. Each experiment in both cell lines was performed in double for three independent times.

Hospital. We conserved the tumor specimens and the normal paired cancer tissues in the liquid nitrogen environment. A written informed consent form is gained from each patient. The study was approved by the first affiliated Hospital of Shenzhen University (Shenzhen, China).

The relative expression level of GACAT3 was detected by utilizing the Real-Time qPCR in a total of 32 patients with bladder cancer. The expression fold change of GACAT3 (bladder cancer tissue/matched histologically normal tissue) in each patient is indicated in **Figure 1A**. The clinical features of this set of patients are displayed in **Table 1**. GACAT3 was upregulation in bladder cancer compared to the paired normal tissues (**Figure 1B**). We analyzed expression differences according to grading and staging. The column diagram indicates the relative expression of GACAT3 in each group. GACAT3 expression levels were higher in high grade tumors than in low grade tumors (**Figure 1B**). GACAT3 expression levels were higher in invasive tumors than in non-invasive tumors (**Figure 1B**).

Specific CRISPR-Cas13 Down-Regulated the Expression of lncRNA-GACAT3

Bladder cancer cell lines T24 and 5637 were grown and transfected with CRISPR-Cas13 or negative control CRISPR-Cas13. Forty-eight hours after transfection, the GACAT3 RNA expression levels were analyzed by Real-Time qPCR. The inhibitory rate (GACAT3 CRISPR-Cas13/negative control CRISPR-Cas13) was 80.23 ± 2.19% in T24 cells and 79.31 ± 4.81% in 5637 cells, respectively. Data are shown as mean ± SD. Each experiment in both cell lines was performed in triplicate for three independent times.

Knockdown of lncRNA-GACAT3 Inhibited Cell Proliferation

Bladder cancer T24 and 5637 cells were transfected with GACAT3 related CRISPR-Cas13 or negative control CRISPR-Cas13 and the cell proliferation rates of bladder cancer cells were determined by CCK-8 assay. Cell proliferation was inhibited in both T24 cells (**Figure 2A**) and 5637 cells after knockdown of GACAT3 (**Figure 2B**).

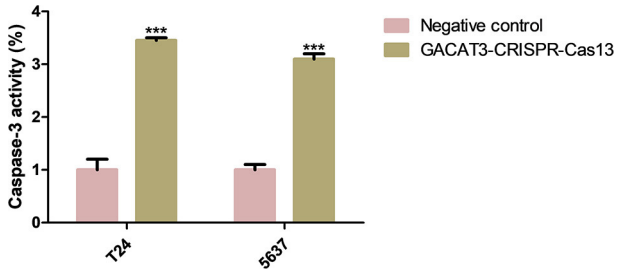

FIGURE 3 | Knockdown of GACAT3 induced apoptosis. Forty-eight hours after transfection of GACAT3 CRISPR-Cas13 or negative control CRISPR-Cas13, the cell apoptosis changes were determined by ELISA. Cell apoptosis induction was observed in GACAT3 CRISPR-Cas13-transfected bladder cancer 5637 (***$p < 0.01$) and T24 (***$p < 0.01$) cells using ELISA. Data are shown as mean ± SD. Each experiment in both cell lines was performed in triplicate for three independent times.

Knockdown of lncRNA-GACAT3 Induced Apoptosis and Inhibited Cell Migration

Bladder cancer T24 and 5637 cell lines were transfected with GACAT3 related CRISPR-Cas13 or negative control CRISPR-Cas13. Forty-eight hours after transfection, the cell apoptosis and migration of bladder cancer T24 and 5637 cells were determined using ELISA (**Figure 3**) and wound healing analysis (**Figures 4A,B**). Induced cell apoptosis and suppressed cell migration were observed in both bladder cancer cell lines after knockdown of GACAT3.

Knockdown of GACAT3 Increased p21, Bax, and E-Cadherin Protein Expression

To investigate the potential bio-markers that induce the above phenotypic changes after knockdown of GACAT3, we used

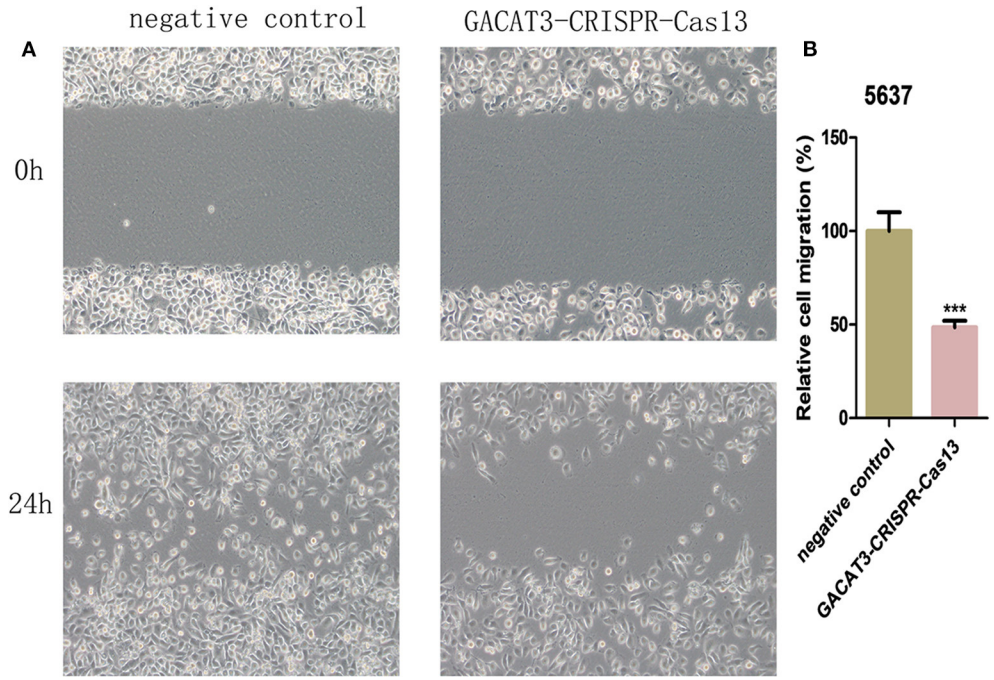

FIGURE 4 | Knockdown of GACAT3 decreased cell motility. After transfection of GACAT3 CRISPR-Cas13 or negative control CRISPR-Cas13, wound healing assay was used to detect cell motility changes in bladder cancer cells. **(A)** Representative images of wound healing assay in 5637 and T24 cells. **(B)** Decreased cell motility was observed in 5637 and T24 cells. Data are indicated as mean ± SD. Each experiment in both cell lines was performed in triplicate for three independent times.

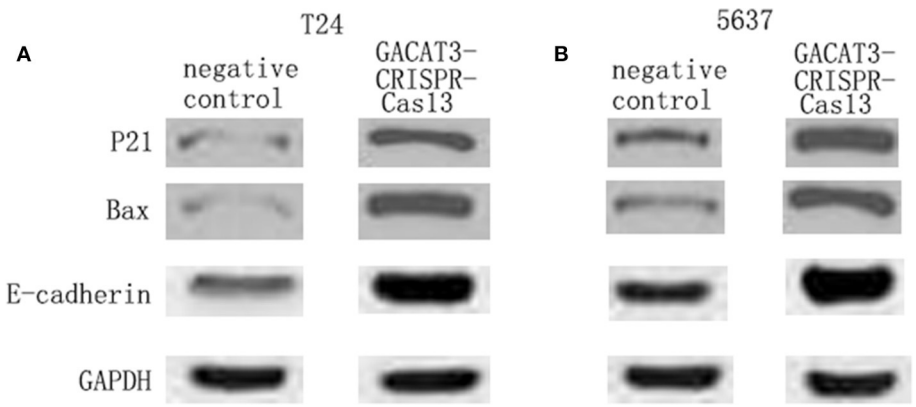

FIGURE 5 | Knockdown of GACAT3 increased p21, Bax, and E-cadherin protein expression. After transfection of GACAT3 CRISPR-Cas13 or negative control CRISPR-Cas13, western blot assay was used to detect expression changes of p21, Bax, and E-cadherin in bladder cancer cells. **(A)** Representative images of western blot assay in 5637 cells. **(B)** Representative images of western blot assay in T24 cells.

western blot assay to determine the protein levels of p21, Bax, and E-cadherin that are well-known for bladder cancer development. GACAT3 CRISPR-Cas13 significantly up-regulated the expression of p21, Bax, and E-cadherin at protein levels in T24 (**Figure 5A**) and 5637 cells (**Figure 5B**). To further verify the functional roles of these markers in GACAT3 knockdown experiments, we also performed double knockdown using two CRISPR-Cas13. p21 CRISPR-Cas13 eliminated the proliferation inhibition effects induced by GACT3 CRISPR-Cas13 in T24 and 5637 (**Figure 6A**). E-cadherin CRISPR-Cas13 eliminated the migration inhibition effects induced by GACAT3 CRISPR-Cas13 in T24 and 5637 (**Figure 6B**). Bax CRISPR-Cas13 eliminated the apoptosis-promoting effects induced by GACAT3 CRISPR-Cas13 in T24 and 5637 (**Figure 6C**). p21 CRISPR-Cas13 did not reverse the migration inhibition effects (**Figure 6B**) and apoptosis-promoting effects (**Figure 6C**) induced by

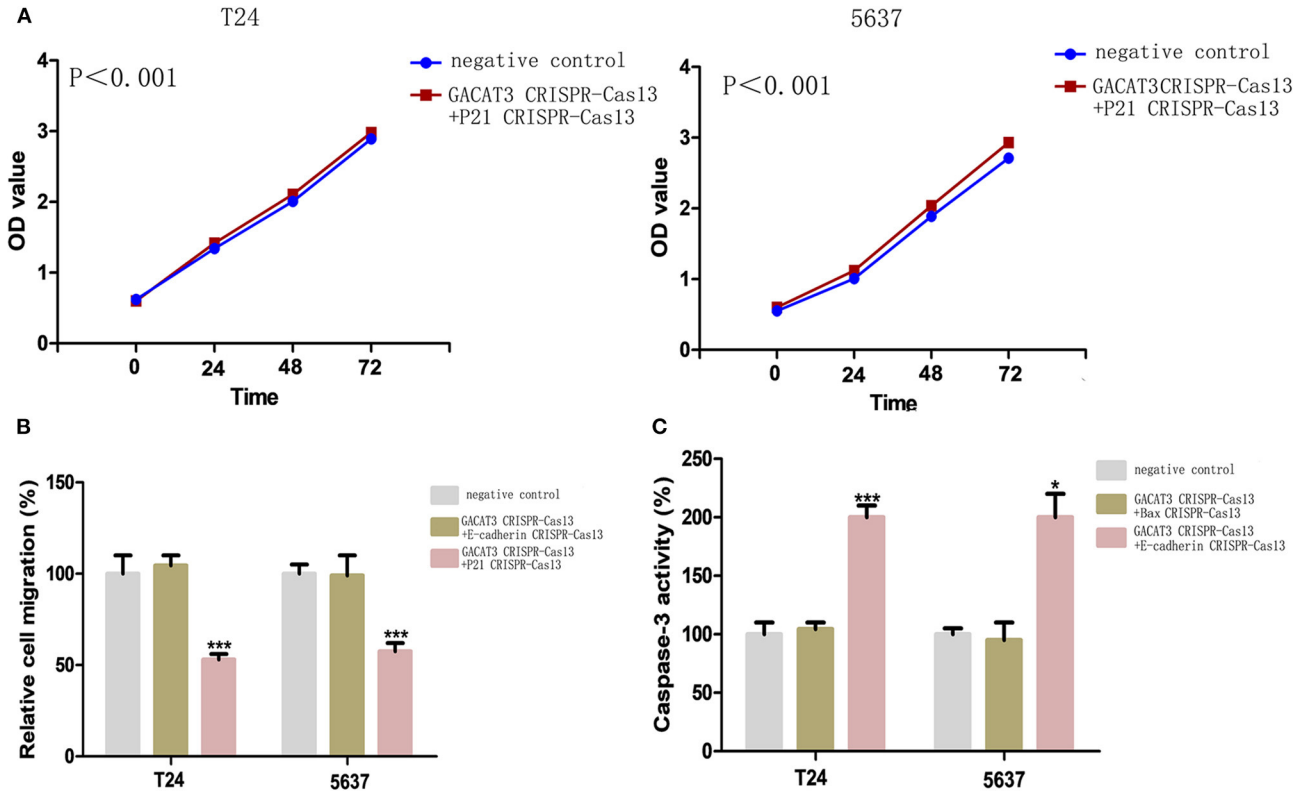

FIGURE 6 | Knockdown of GACAT3 induced cellular phenotypic changes *via* p21, Bax, and E-cadherin regulation. After transfection of CRISPR-Cas13, CCK-8 assay, wound healing assay, and ELISA assay were used to detect cell proliferation, migration and apoptosis, respectively. **(A)** p21 CRISPR-Cas13 eliminated the proliferation inhibition effects induced by GACAT3 CRISPR-Cas13 in T24 and 5637 ($p < 0.05$). **(B)** E-cadherin CRISPR-Cas13 eliminated the migration inhibition effects induced by GACAT3 CRISPR-Cas13 in T24 and 5637, whereas p21 CRISPR-Cas13 has no such function (***$p < 0.001$). **(C)** Bax CRISPR-Cas13 eliminated the apoptosis-promoting effects induced by GACAT3 CRISPR-Cas13 in T24 and 5637, whereas E-cadherin CRISPR-Cas13 has no such function (*$p < 0.05$).

GACAT3 CRISPR-Cas13 in these cells, possibly because p21 could not induce cell death or inhibit cell migration on its own.

lncRNA GACAT3 Was Predominantly Distributed in Cytoplasm and Acted as a Sponge for miR-497

To further explore the mechanism how lncRNA GACAT3 modulates tumorigenesis, we used nuclear/cytoplasmic fractionation assay. The experimental results showed that lncRNA GACAT3 was primarily distributed in cytoplasm of Bca cells (**Figure 7A**). miRDB database (http://mirdb.org/miRDB/) predicted that miR-497 has a sequence complementary to that of GACAT3 (**Figure 7B**). The potential sequence of lncRNA GACAT3 which was predicted complementary to the seed sequence of miR-497 were mutated and used to construct dual-luciferase reporter vector. Dual-luciferase reporter assay showed that co-transfection of lncRNA GACAT3-WT and miR-515-5p significantly inhibited luciferase activity than that of control group (**Figures 7C,D**). It demonstrated the ceRNA mechanism for GACAT3.

DISCUSSION

Recent research indicated that human cancers are caused by dysregulation of a large number of lncRNAs. It has been believed that lncRNAs have great clinical potential as a group of cancer biomarkers and therapeutic targets (Sahu et al., 2015; Sun and Kraus, 2015). For example, lncRNAs MALAT1 (Tian and Xu, 2015), SUMO1P3 (Zhan et al., 2016), and CCAT2 (Li et al., 2016) have been reported to promote cell proliferation and suppress cell apoptosis in bladder cancer. As a recently discovered lncRNA, several previous works were conducted to characterize the oncogenic properties of GACAT3. It may represent a therapeutic target in cancers and increases the transcription of genes including p21 *via* stabilization of BMI1 (Hu et al., 2014; Jeong et al., 2016). It has been reported that p21 is a gene that involved in several processes, such as cell proliferation and apoptosis. Knockdown of GACAT3 stimulated cell-cycle arrest and senescence. GACAT3 plays an important role in cell-cycle progression and was associated with aggressive tumor behavior. These data demonstrated that GACAT3 may be a cancer driver during tumor development.

Since GACAT3 displayed striking oncogenic activity in previous studies (Feng et al., 2018), it is intriguing to explore

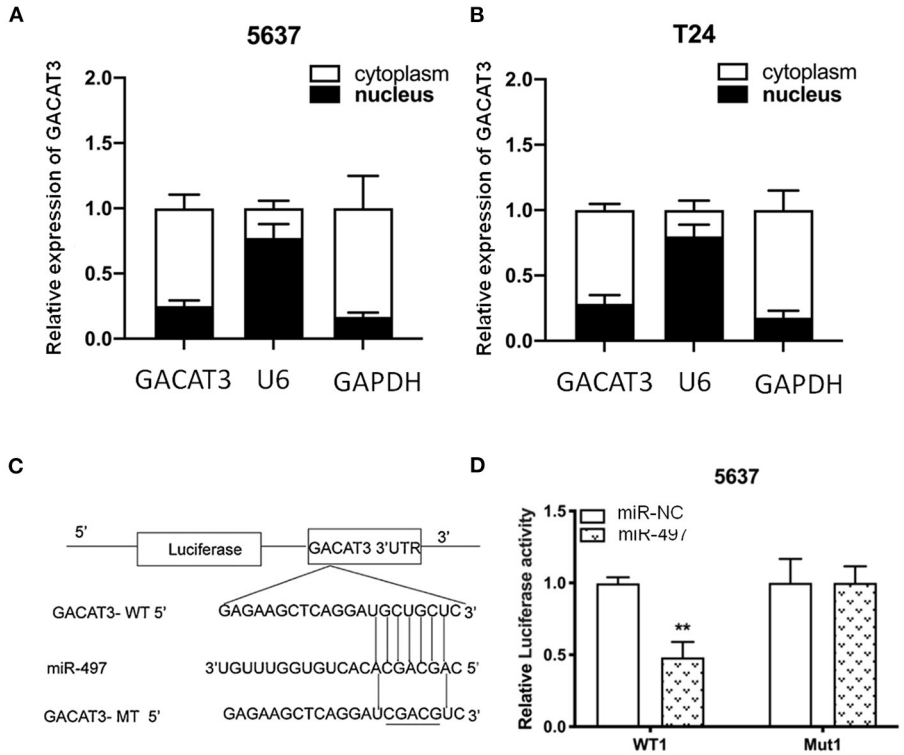

FIGURE 7 | lncRNA GACAT3 directly interacted with miRNA-497. **(A)** Nuclear/cytoplasmic fractionation assay revealed that lncRNA GACAT3 primarily distributed in cytoplasm of Bca 5637 cells. **(B)** Nuclear/cytoplasmic fractionation assay revealed that lncRNA GACAT3 primarily distributed in cytoplasm of Bca T24 cells. **(C)** Bioinformatics analysis predicted the probable sequences of lncRNA GACAT3 that are complementary to the seed sequence of miR-497. **(D)** Dual-luciferase assay showed that co-transfection of lncRNA GACAT3 and miR-497 significantly inhibited luciferase activity (**$p < 0.01$).

its biological function in bladder cancer. With this aim, in this study, we found that GACAT3 was overexpressed in bladder cancer compared to matched normal tissue. High level expression of GACAT3 was associated with high grade and stage bladder cancer. The differential expression patterns of GACAT3 between bladder cancer and control and the association of GACAT3 with clinicopathological features suggest that long non-coding RNA GACAT3 emerges as a novel player in the development and progression of the bladder cancer.

To understand the possible impacts of GACAT3 on bladder cancer, we determined the changes in cell proliferation, apoptosis and motility induced by knockdown of GACAT3 in bladder cancer by using CRISPR-Cas13 biotechnology, which has a better targeting performance than that of siRNA/shRNA. Inhibition of cell proliferation, increased apoptosis, and decreased motility were observed in GACAT3 CRISPR-Cas13-transfected bladder cancer T24 and 5637 cell lines.

To investigate the potential pathways that induce the above phenotypes, we also performed western blot assay and found that knockdown of GACAT3 increased p21, Bax, and E-cadherin protein expression. This result was consistent with the previous studies which indicated that p21 is one GACAT3 downstream target. In other studies on bladder cancer, inactivation of p21 was also shown to promote tumorigenesis and cell proliferation (Tang et al., 2015). Bax, an important homolog of Bcl-2, is a promoter of cell apoptosis and serves as an independent parameter to envisage clinical outcome for patients with bladder cancer (Golestani Eimani et al., 2014; Liu et al., 2016). E-cadherin is a cell-cell junction protein that is frequently absent during the migration of bladder cancer cells (Liu et al., 2014; Zhao et al., 2014). Using double knockdown experiments, we further showed that the expression changes of these bio-markers can at least partly explain the phenotypic changes after knockdown of GACAT3. GACAT3 may associate with the epigenetic repressors, thus regulating the transcription of Bax or E-cadherin. Further studies demonstrated that miR-497 is a direct target of GACAT3, which indicated a ceRNA mechanism.

These findings suggest that GACAT3 functions as an oncogene in carcinogenesis of bladder cancer. Targeting GACAT3 may be a promising approach to the treatment of bladder cancer. More works will be needed to determine the potential molecular mechanism of GACAT3 in the regulation of Bax and E-cadherin in bladder cancer. CRISPR-Cas13-based therapies (Gao et al., 2020; Li et al., 2020) that target GACAT3 are also should under intensive investigation.

DATA AVAILABILITY STATEMENT

The original contributions presented in the study are included in the article/Supplementary Materials, further inquiries can be directed to the corresponding author.

AUTHOR CONTRIBUTIONS

ZhongfZ, JC, ZhongsZ, ZhongqZ, XL, JW, JC, XZ, and HM performed experiments and conducted data analysis. GY supervised the project. All authors contributed to the article and approved the submitted version.

FUNDING

This work was supported by Natural Science Foundation of Shenzhen Science and Technology Innovation Committee (JCYJ20190806164616292), Shenzhen Key Medical Discipline Construction Fund-No.SZXK020) and Science and Technology Plan of Guangzhou (201804010087).

REFERENCES

Amit, D., and Hochberg, A. (2010). Development of targeted therapy for bladder cancer mediated by a double promoter plasmid expressing diphtheria toxin under the control of H19 and IGF2-P4 regulatory sequences. *J. Transl. Med.* 8:134. doi: 10.1186/1479-5876-8-134

Czerniak, B., Dinney, C., and McConkey, D. (2016). Origins of bladder cancer. *Annu. Rev. Pathol.* 11, 149–174. doi: 10.1146/annurev-pathol-012513-104703

Feng, L., Zhu, Y., Zhang, Y., and Rao, M. (2018). LncRNA GACAT3 promotes gastric cancer progression by negatively regulating miR-497 expression. *Biomed. Pharmacother.* 97, 136–142. doi: 10.1016/j.biopha.2017.10.074

Gao, J., Luo, T., Lin, N., Zhang, S., and Wang, J. (2020). A new tool for CRISPR-Cas13a-based cancer gene therapy. *Mol. Ther. Oncolytics* 19, 79–92. doi: 10.1016/j.omto.2020.09.004

Golestani Eimani, B., Sanati, M. H., Houshmand, M., Ataei, M., Akbarian, F., and Shakhssalim, N. (2014). Expression and prognostic significance of bcl-2 and bax in the progression and clinical outcome of transitional bladder cell carcinoma. *Cell. J.* 15, 356–363. doi: 10.1002/jcp.24679

Hu, X., Feng, Y., Zhang, D., Zhao, S. D., Hu, Z., Greshock, J., et al. (2014). A functional genomic approach identifies FAL1 as an oncogenic long noncoding RNA that associates with BMI1 and represses p21 expression in cancer. *Cancer Cell* 26, 344–357. doi: 10.1016/j.ccr.2014.07.009

Huarte, M. (2015). The emerging role of lncRNAs in cancer. *Nat. Med.* 21, 1253–1261. doi: 10.1038/nm.3981

Jariwala, N., and Sarkar, D. (2016). Emerging role of lncRNA in cancer: a potential avenue in molecular medicine. *Ann. Transl. Med.* 4:286. doi: 10.21037/atm.2016.06.27

Jeong, S., Lee, J., Kim, D., Seol, M. Y., Lee, W. K., Jeong, J. J., et al. (2016). Relationship of focally amplified long noncoding on chromosome 1 (FAL1) lncRNA with E2F transcription factors in thyroid cancer. *Medicine* 95:e2592. doi: 10.1097/MD.0000000000002592

Li, C., Guo, L., Liu, G., Guo, M., Wei, H., Yang, Q., et al. (2020). Reprogrammed CRISPR-Cas13a targeting the HPV16/18 E6 gene inhibits proliferation and induces apoptosis in E6-transformed keratinocytes. *Exp. Ther. Med.* 19, 3856–3860. doi: 10.3892/etm.2020.8631

Li, J., Zhuang, C., Liu, Y., Chen, M., Zhou, Q., Chen, Z., et al. (2016). shRNA targeting long non-coding RNA CCAT2 controlled by tetracycline-inducible system inhibits progression of bladder cancer cells. *Oncotarget* 7, 28989–28997. doi: 10.18632/oncotarget.8259

Liu, Y., Zeng, Y., Liu, L., Zhuang, C., Fu, X., Huang, W., et al. (2014). Synthesizing AND gate genetic circuits based on CRISPR-Cas9 for identification of bladder cancer cells. *Nat. Commun.* 5:5393. doi: 10.1038/ncomms6393

Liu, Y., Zhan, Y., Chen, Z., He, A., Li, J., Wu, H., et al. (2016). Directing cellular information flow via CRISPR signal conductors. *Nat. Methods* 13, 938–944. doi: 10.1038/nmeth.3994

Sahu, A., Singhal, U., and Chinnaiyan, A. M. (2015). Long noncoding RNAs in cancer: from function to translation. *Trends Cancer* 1, 93–109. doi: 10.1016/j.trecan.2015.08.010

Sathe, A., and Nawroth, R. (2018). Targeting the PI3K/AKT/mTOR pathway in bladder cancer. *Methods Mol. Biol.* 1655, 335–350. doi: 10.1007/978-1-4939-7234-0_23

Shen, W., Yuan, Y., Zhao, M., Li, J., Xu, J., Lou, G., et al. (2016). Novel long non-coding RNA GACAT3 promotes gastric cancer cell proliferation through the IL-6/STAT3 signaling pathway. *Tumour Biol.* 37, 14895–14902. doi: 10.1007/s13277-016-5372-8

Sun, M., and Kraus, W. L. (2015). From discovery to function: the expanding roles of long noncoding RNAs in physiology and disease. *Endocr. Rev.* 36, 25–64. doi: 10.1210/er.2014-1034

Tang, K., Wang, C., Chen, Z., Xu, H., and Ye, Z. (2015). Clinicopathologic and prognostic significance of p21 (Cip1/Waf1) expression in bladder cancer. *Int. J. Clin. Exp. Pathol.* 8, 4999–5007. doi: 10.1155/2020/6520259

Tian, X., and Xu, G. (2015). Clinical value of lncRNA MALAT1 as a prognostic marker in human cancer: systematic review and meta-analysis. *BMJ Open* 5:e008653. doi: 10.1136/bmjopen-2015-008653

Wang, X., Sun, W., Shen, W., Xia, M., Chen, C., Xiang, D., et al. (2016). Long non-coding RNA DILC regulates liver cancer stem cells via IL-6/STAT3 axis. *J. Hepatol.* 64, 1283–1294. doi: 10.1016/j.jhep.2016.01.019

Yang, X., Zhang, W., Cheng, S. Q., and Yang, R. L. (2018). High expression of lncRNA GACAT3 inhibits invasion and metastasis of non-small cell lung cancer to enhance the effect of radiotherapy. *Eur. Rev. Med. Pharmacol. Sci.* 22, 1315–1322. doi: 10.26355/eurrev_201803_14473

Zhan, Y., Liu, Y., Wang, C., Lin, J., Chen, M., Chen, X., et al. (2016). Increased expression of SUMO1P3 predicts poor prognosis and promotes tumor growth and metastasis in bladder cancer. *Oncotarget* 7, 16038–16048. doi: 10.18632/oncotarget.6946

Zhang, Y., He, Q., Hu, Z., Feng, Y., Fan, L., Tang, Z., et al. (2016). Long noncoding RNA LINP1 regulates repair of DNA double-strand breaks in triple-negative breast cancer. *Nat. Struct. Mol. Biol.* 23, 522–530. doi: 10.1038/nsmb.3211

Zhao, J., Dong, D., Sun, L., Zhang, G., and Sun, L. (2014). Prognostic significance of the epithelial-to-mesenchymal transition markers e-cadherin, vimentin and twist in bladder cancer. *Int. Braz. J. Urol.* 40, 179–189. doi: 10.1590/S1677-5538.IBJU.2014.02.07

Zhao, J., Liu, Y., Zhang, W., Zhou, Z., Wu, J., Cui, P., et al. (2015). Long non-coding RNA Linc00152 is involved in cell cycle arrest, apoptosis, epithelial to mesenchymal transition, cell migration and invasion in gastric cancer. *Cell. Cycle* 14, 3112–3123. doi: 10.1080/15384101.2015.1078034

Zhou, W., Wang, L., Miao, Y., and Xing, R. (2018). Novel long noncoding RNA GACAT3 promotes colorectal cancer cell proliferation, invasion, and migration through miR-149. *OncoTargets Ther.* 11, 1543–1552. doi: 10.2147/OTT.S144103

Conflict of Interest: The authors declare that the research was conducted in the absence of any commercial or financial relationships that could be construed as a potential conflict of interest.

frontiers in Molecular Biosciences

ORIGINAL RESEARCH
published: 09 March 2021
doi: 10.3389/fmolb.2021.638995

CRISPR-CasRx Targeting LncRNA LINC00341 Inhibits Tumor Cell Growth *in vitro* and *in vivo*

Chunjing Li[1,2†], Yu Cao[3†], Li Zhang[1,4†], Jierong Li[1,4†], Jianfeng Wang[1,4], Yanfen Zhou[1], Huiling Wei[1], Mingjuan Guo[1], Liang Liu[4], Chunxiao Liu[2], Shilin Zhang[1,4] and Guoqing Liu[1,4]*

[1]Affiliated Foshan Maternal and Child Healthcare Hospital, Southern Medical University, Foshan, China, [2]Department of Urology, Zhujiang Hospital of Southern Medical University, Guangzhou, China, [3]Ningxiang Hospital, Hunan University of Traditional Chinese Medicine, NingXiang, China, [4]The Second School of Clinical Medicine, Southern Medical University, Guangzhou, China

OPEN ACCESS

Edited by:
Yonghao Zhan, Zhengzhou University, China

Reviewed by:
Hongzhou Cui, First Hospital of Shanxi Medical University, China
Xiaoli Zhang, Wuhan University, China

***Correspondence:**
Liang Liu
40881892@qq.com
Chunxiao Liu
liuchx888@163.com
Shilin Zhang
zhang_40_1@163.com
Guoqing Liu
13929974636@163.com

[†]*These authors have contributed equally to this work*

Specialty section:
This article was submitted to Molecular Diagnostics and Therapeutics, a section of the journal Frontiers in Molecular Biosciences

Received: *08 December 2020*
Accepted: *19 January 2021*
Published: *09 March 2021*

Citation:
Li C, Cao Y, Zhang L, Li J, Wang J, Zhou Y, Wei H, Guo M, Liu L, Liu C, Zhang S and Liu G (2021) CRISPR-CasRx Targeting LncRNA LINC00341 Inhibits Tumor Cell Growth in vitro *and* in vivo. *Front. Mol. Biosci. 8:638995. doi: 10.3389/fmolb.2021.638995*

CRISPR-CasRx technology provides a new and powerful method for studying cellular RNA in human cancer. Herein, the pattern of expression of long noncoding RNA 00341 (LINC00341) as well as its biological function in bladder cancer were studied using CRISPR-CasRx. qRT-PCR was employed to quantify the levels of expression of LINC00341 in tumor tissues along with the matched non-tumor tissues. sgRNA targeting LINC00341 or the sgRNA negative control were transiently transfected into the T24 as well as 5,637 human bladder cancer cell lines. CCK-8, ELISA as well as wound healing methods were employed to explore cell proliferation, apoptosis and migration, respectively. The tumorigenicity experiment in nude mice also performed to detect cell proliferation. The expression of p21, Bax as well as E-cadherin were assayed using western blot. The results demonstrated that LINC00341 was overexpressed in bladder cancer in contrast with the healthy tissues. The LINC00341 expression level in high-grade tumors was higher in contrast with that in low-grade tumors. The expression of linc00341 was higher relative to that of non-invasive tumors. In T24 as well as 5637-cell lines harboring LINC00341-sgRNA, inhibition of cell proliferation (*in vitro* and *in vivo*), elevated apoptosis rate and diminished migration ability. Moreover, silencing LINC00341 upregulated the expressions of p21, Bax as well as E-cadherin. Knockout of these genes could eliminate the phenotypic changes caused by sgRNA targeting LINC00341. Our data demonstrate that LINC00341 has a carcinogenic role in human bladder cancer.

Keywords: long noncoding RNA, LINC00341, cancer, CRISPR-CasRx 3, CRISPR

INTRODUCTION

Bladder cancer constitutes one of the most frequent malignancies in male urinary system worldwide and the ninth most frequent malignancy worldwide. Its most common histopathologic type is urothelial carcinoma. The genetic modulation is found to be responsible for the pathogenesis of bladder cancer, and the genetic mutations and epigenetic modifications that account to the development as well as progression of bladder cancer are to be identified (Chen et al., 2014; Wang et al., 2015).

Long non-coding RNAs (lncRNAs) comprise non-protein coding RNA transcripts that are larger than 200 nt in length (Gloss and Dinger, 2016). The investigations on lncRNAs have revealed that they can function as scaffolds or intermediators to form gene-gene networks and thus serve pivotal

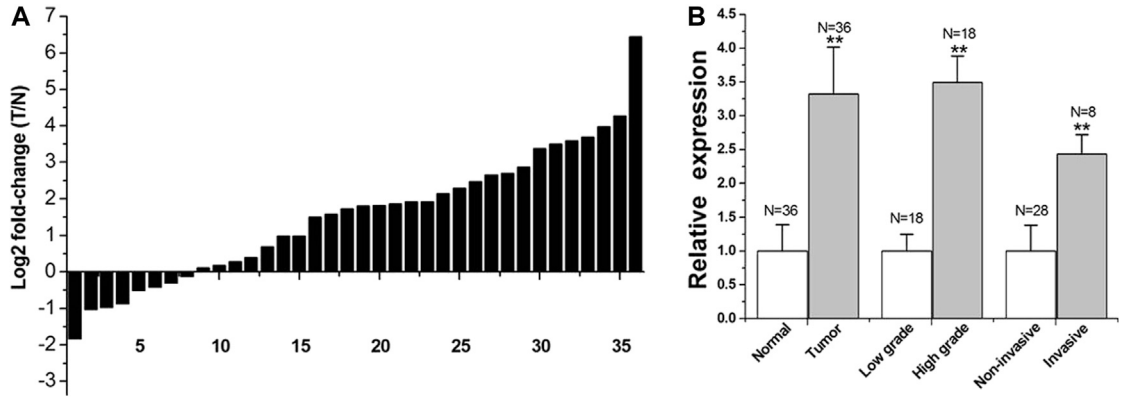

FIGURE 1 | LINC00341 was overexpressed in bladder cancer.qRT-PCR was employed to explore LINC00341 relative expression. In each control group, the relative expression value of LINC00341 was set to a basic value of 1. N, the number of samples in each group. **(A)**. T stands for tumor and N stands for normal. The height of each column in the chart indicates the fold change (tumor/non-tumor) expressed by LINC00341 in 36 patients after log 2 conversion. **(B)**. Comparing the expression level of LINC00341 between tumor and healthy tissues (**$p < 0.01$). Differences in the expression of LINC00341 between high-grade cancer and low-grade cancer was compared (**$p < 0.01$). The expression level of LINC00341 in invasive cancer and non-invasive cancer was compared (**$p < 0.01$).

TABLE 1 | Clinical characteristics of patients with bladder cancer.

No.	Sex	Age	Grade	Stage	Surgery	No.	Sex	Age	Grade	Stage	Surgery
1	M	56	Low	T2N0M0	Partial	19	M	60	Low	T1N0M0	Partial
2	M	68	Low	T1N0M0	Partial	20	M	63	High	T2N0M0	Radical
3	M	52	Low	T2N0M0	Partial	21	M	62	Low	T1N0M0	Partial
4	M	62	High	T3N0M0	Radical	22	M	53	High	T2N0M0	Radical
5	M	67	Low	T2N0M0	Partial	23	M	59	High	T2N0M0	Radical
6	M	56	Low	T1N0M0	Partial	24	M	49	High	T3N0M0	Radical
7	M	53	High	T2N0M0	Radical	25	M	41	High	T2N0M0	Radical
8	M	62	Low	T2N0M0	Partial	26	M	59	High	T2N0M0	Radical
9	M	42	Low	T1N0M0	Partial	27	M	57	High	T3N0M0	Radical
10	M	76	Low	T2N0M0	Partial	28	M	54	High	T3N0M0	Radical
11	M	55	High	T2N0M0	Radical	29	M	57	High	T3N0M0	Radical
12	M	55	High	T2N0M0	Radical	30	M	55	Low	T1N0M0	Partial
13	M	51	Low	T2N0M0	Partial	31	F	50	Low	T1N0M0	Partial
14	M	52	Low	T2N0M0	Partial	32	F	53	Low	T1N0M0	Partial
15	M	70	High	T2N0M0	Radical	33	F	50	Low	T1N0M0	Partial
16	M	54	Low	T1N0M0	Partial	34	F	51	High	T3N0M0	Radical
17	M	52	Low	T1N0M0	Partial	35	F	43	High	T3N0M0	Radical
18	M	58	High	T2N0M0	Radical	36	F	68	High	T3N0M0	Radical

No., patient number; M, Male; F, Female. Age, years old, Grade, the 2004 WHO classification. Stage, AJCC TNM classification. Radical, radical cystectomy. Partial, partial cystectomy.

roles in the mediation of gene expression as well as disease progressions (Zhou et al., 2015). The dysregulation of lncRNAs is associated with the process of tumorigenesis, invasion, and metastasis, which makes them potential diagnostic and therapeutic biomarkers of human cancers (Hu et al., 2014; Jeong et al., 2016). LINC00341, a new long intergenic non-protein-coding RNA , whose role is unclear and no literatures have studied the biological role of this lncRNA in any diseases including cancers.

Herein, we established that LINC00341 is overexpressed in bladder cancer in contrast with the corresponding non-tumor bladder tissue. Moreover, the LINC00341 expression in high-grade tumors is elevated in contrast with low-grade tumors. LINC00341 RNA is more enriched in invasive tumors in contrast with non-invasive tumors. The knockdown of LINC00341 with CRISPR--CasRx technology can repress bladder cancer cell proliferation, trigger cell apoptosis, as well as reduce cell motility.

MATERIALS AND METHODS

Patient Samples

To determine the expression of LINC00341 in tissue samples, we enrolled 36 patients diagnosed with urothelial carcinoma of the bladder who underwent partial or radical cystectomy into the study. Tumor histology was reviewed by two urological pathologists. The bladder cancer tissues along with the matched histologically non-tumor tissues acquired from the subjects were immediately snap-frozen in liquid nitrogen after

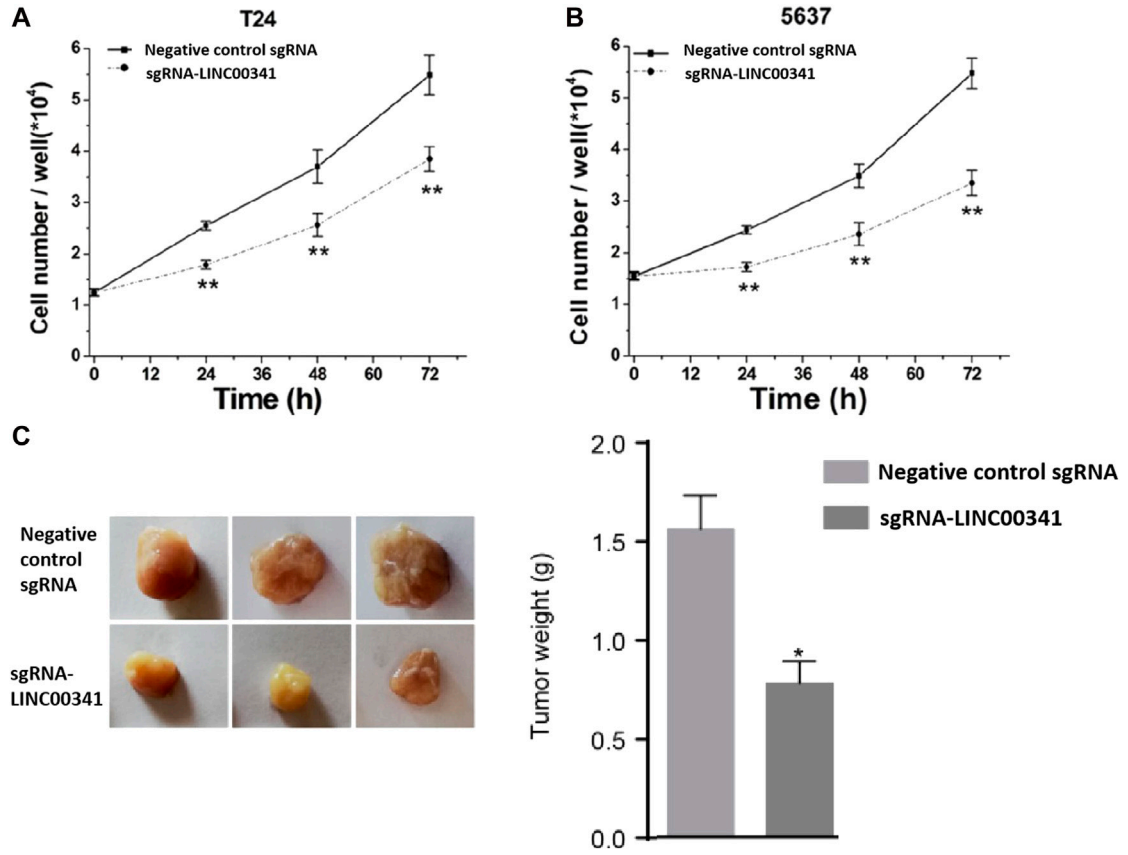

FIGURE 2 | Knockdown of LINC00341 by CRISPR-CasRx suppressed cell proliferation. CCK-8 assay was employed to explore cell proliferation. After transfection with LINC00341 sgRNA or negative control sgRNA, the OD value was determined and converted into cell number. Analysis of variance is used to compare cell proliferation curves. **(A)**. There was suppression of cell proliferation in T24 bladder cancer cells (** $p < 0.01$). **(B)**. There was suppression of cell growth in 5,637 cells (**$p < 0.01$). The data is shown as the average ± SD. The experiments were conducted in triplicates. **(C)**. There was inhibition of tumor growth *in vivo* in 5,637 bladder cancer cells (**$p < 0.01$). The data is indicated as the average ± SD.

surgical operation. All the subjects provided a written informed consent. Moreover, the Institutional Review Board of the Foshan Women and Children's Hospital (Foshan, China) approved the study as per the declaration of Helsinki. subjects signed informed consents prior to sample collection.

Cell Culture

To study the biological function of LINC00341 in cells, the T24 as well as 5,637 human bladder cancer cell lines were acquired from the Cell Bank of the Chinese Academy of Sciences (Shanghai, China). These cells were inoculated in minimal essential medium (DMEM) (Invitrogen, Carlsbad, CA, United States) enriched with 10% fetal bovine serum (Invitrogen, Carlsbad, CA, Unitd States) and allowed to grow. All media contained 1% penicillin/streptomycin. The culture environment was humidified air enriched with 5% CO_2 at 37°C.

Real-Time Quantitative PCR

To investigate the RNA expression of LINC00341, Trizol (Ambion, Austin, TX, United States) was employed to isolate total RNA as described by the manufacturer. RNA was reverted into complementary DNA (cDNA) using the Promega M-MLV kit. The sequences of the primers were: LINC00341 primers (Hu et al., 2014) forward: 5'- GCAGGACTCAGCATCTCCCA -3', reverse: 5'-CTCGGCTGGACAAGGTGGTT -3'; p21 primers forward: 5'-GGGATGAGTTGGGAGGAGG -3', reverse: 5'-CGGCGTTTG GAGTGGTAG -3'; Bax primers forward: 5'- TGGCAGCTG ACATGTTTTCTGAC-3', reverse: 5'- TCACCCAACCACCCT GGTCTT-3'; E-cadherin primers forward: 5'- CGCATTGCC ACATACACTCT -3', reverse: 5'- TTGGCTGAGGATGGTGTA AG -3'; GAPDH primers forward: 5'-CGCTCTCTGCTCCTCCTG TTC-3', reverse: 5'-ATCCGTTGACTCCGACCTTCAC-3'. The PCR reaction volume of 20 µl consisted of 10 µl of 2 × All-in-OneTM qPCR Mix (GeneCopoiea Inc., Rockville, MD, United States), 0.4 µl ROX Reference Dye, 0.4 µl forward primer, 0.4 µl reverse primer, 1 µl First-Strand cDNA, as well as 7.8 µl DEPC treated water. The PCR was run and analyzed on an ABI PRISM 7000 Fluorescent Quantitative PCR System (Applied Biosystems, Foster City, CA, United States). Each PCR reaction was replicated thrice. GAPDH served as the internal standard. The PCR cycling conditions were: 10 min initial denaturation step at 95°C, 40 cycles constituting of 15 s denaturation at 95°C, 20 s annealing at 55°C, and 30 s extension at 70°C. In each triplicate, the median was employed to compute the relative LINC00341 level via the

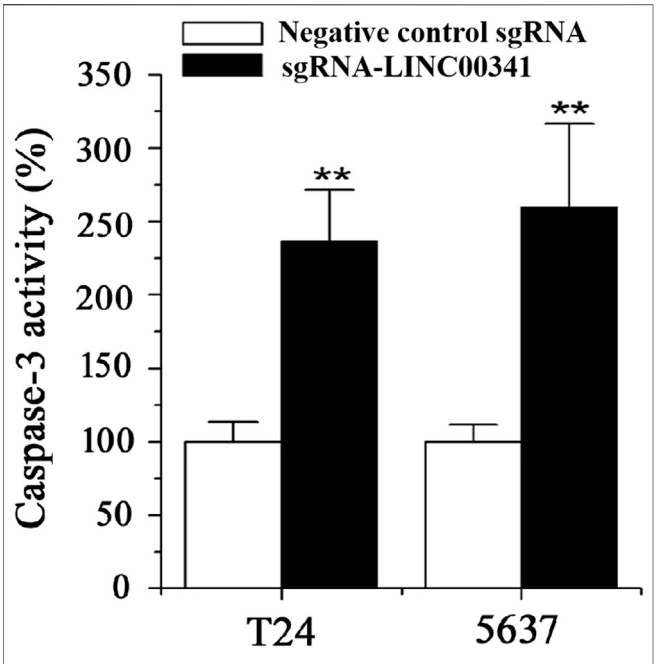

FIGURE 3 | Knockdown of LINC00341 by CRISPR-CasRx triggered apoptosis. 48 h post transfection with LINC00341 sgRNA or the negative control sgRNA, the changes of apoptosis were measured by ELISA. Apoptosis induction was observed in T24 cells (**$p < 0.01$) and 5,637 cells (**$p < 0.01$) transfected with LINC00341 sgRNA via ELISA. The data is indicated as the average ± SD. The experiments were conducted in triplicates for three independent times for both cell lines.

comparative ΔCt approach (value of 2-ΔCt (LINC00341-GAPDH)). After normalization with reference to GAPDH expression, expression fold changes were computed through the 2-ΔΔCt approach (VanGuilder et al., 2008).

CRISPR-CasRx Plasmid Construction and sgRNA/siRNA Transfection

The sgRNA targeting LINC00341 has been designed, synthesized and inserted into the downstream of the U6 promoter, while the -CasRx gene was driven by the CMV promoter.

Genepharma Co., Ltd. (Suzhou, China) synthesized the p21 siRNA for the knockdown of gene expression. The p21 siRNA sequence (Sense) 5'- GAUGGAACUUCGACUUUGUUU-3'; (Antisense) 5'- ACAAAGUCGAAGUUCCAUCUU-3'. siRNAs targeting Bax along with E-cadherin were supplied by Genepharma (Suzhou, China). The negative control siRNA was also purchased from Genepharma Co., Ltd., Suzhou, China. Transfection of either the specific siRNAs or the siRNA negative control into the cell lines was done using the Lipofectamine 2000 Transfection system (Invitrogen, Carlsbad, CA, United States) as described by the manufacturer.

Cell Counting Kit-8 (CCK-8) Assay

To explore the impact of LINC00341 on cell growth, the Cell Counting Kit-8, CCK-8 (Beyotime Institute of Biotechnology, shanghai, China) was employed to explore cell growth as per the protocol provided by the manufacturer. Cells were planted into 96-well plates and maintained overnight at 37°C. Afterwards, transfection of these cells with LINC00341 sgRNA/-CasRx or the negative control sgRNA/CasRx was conducted. At 0, 24, 48 as well as 72 h post-transfection, we introduced 10 μl of CCK-8 (5 mg/ml) into each well, allowed the cells to grow for an additional 1 h. After that, a microplate reader (Bio-Rad, Hercules, CA, Unites States) was employed to read the OD values of the samples at a wavelength of 450 nm. Finally, we converted the OD values into cell numbers via standard curves.

Cell Apoptosis Assessment

To study the impact of LINC00341 on cell apoptosis, the caspase three ELISA assay kit (R&D, Minneapolis, MN, Unites States) was utilized to explore cell apoptosis as described by the manufacturer. The bladder cancer cells were grown and then transfection of either the LINC00341 sgRNA/-CasRx or the sgRNA/-CasRx negative control into cells was performed with the lipofectamine 2000 transfection system as per the manufacturer provided protocol. Thereafter, the cells were allowed to grow for 48 h, and then apoptosis triggered by LINC00341 knockdown was explored through exploring the caspase three activity as described by the manufacturer. Afterwards, the OD values were mesured with the microplate reader (Bio-Rad, Hercules, CA, Unites States). Data are indicated as the ratios of the OD values of LINC00341 sgRNA-transfected cells to the sgRNA negative control -transfected cells.

Wound Healing Assessment

To study the impact of LINC00341 on cell migration, we cultured the bladder cancer cell lines and transfected them with either LINC00341 sgRNA or negative control sgRNA. Thereafter, a monolayer of the cells was scratched and then grown under normal parameters. The migration distances were finally determined at 0, 24 h after scratching for T24 and 5,637 cells, respectively.

Tumorigenicity Assay in Nude Mice

Cells suspensions (5 × 10 7 cells/ml) were prepared using normal saline. We enrolled six 4-6-week-old male nude mice of specific-pathogen free (SPF) (weight: 18–20 g, an average of 18.81 ± 0.78 g) supplied by Shanghai SLAC Laboratory Animal Co., Ltd. (Shanghai, China). Following anesthesia with pentobarbital sodium, we routinely disinfected the nude mice followed by subcutaneous administration of 200 μl of tumor cell suspension. Afterwards, the mice underwent culture under SPF conditions.

Western Blot Assay

To study the influence of LINC00341 on target gene expression, PBS was employed to rinse the T24 as well as 5,637 cells, followed by lysing with the RIPA buffer. Thereafter, quantitation of the proteins was performed via the BCA protein assay. An equivalent amount of the whole protein isolates were fractionated on an SDS-PAGE , and then blotting onto the PVDF membrane (Millipore, Billerica, MA, United States) performed. Subsequently, blocking of the samples was conducted using 5% dry milk. Thereafter, the samples were inoculated with the

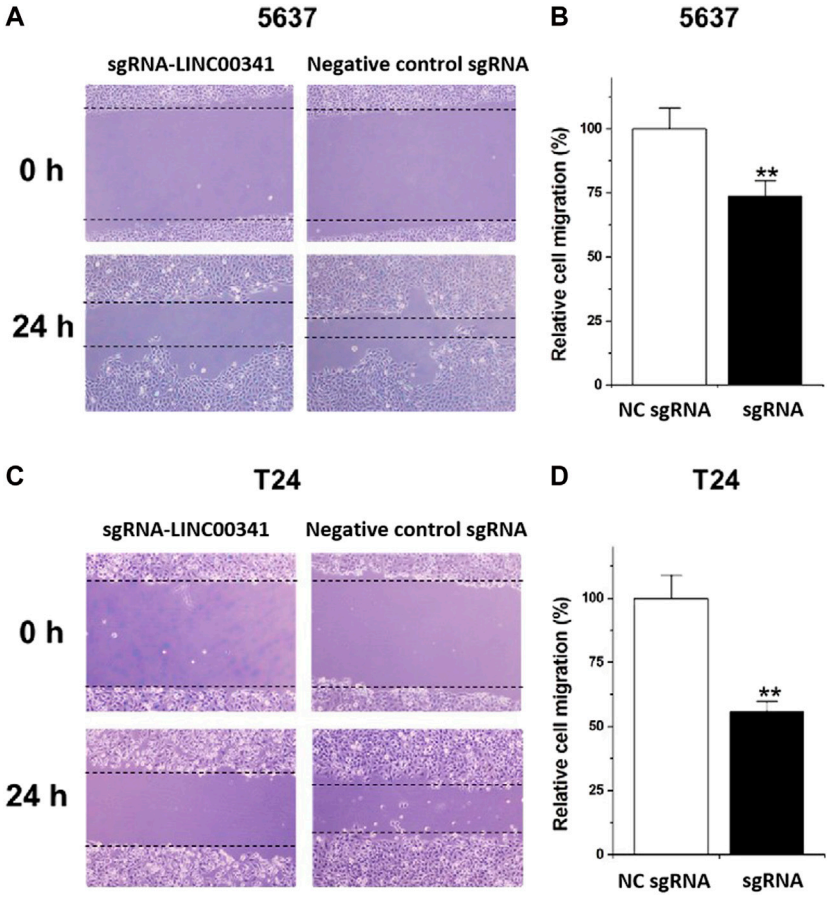

FIGURE 4 | Knockdown of LINC00341 by CRISPR-CasRx decreased cell motility. Following the transfection with LINC00341 sgRNA or the negative control sgRNA, we performed the wound healing analysis to explore the cell motility alterations in T24 as well as 5,637 cells. **(A)**. Wound healing assay illustrative images in 5,637 cells. **(B)**. Diminished cell motility was seen in 5,637 cells (**$p < 0.01$). **(C)**. Wound healing assay illustrative images of T24 cells. **(D)**. Diminished cell motility occurred in T24 cells (**$p < 0.01$). Data are indicated as mean ± SD. The experiments were conducted in triplicates for three independent times for both cell lines.

primary antibody against E-cadherin (1: 200; Santa Cruz Biotechnology, Santa Cruz, CA, United States), hBAX (1:1,000; Santa Cruz Biotechnology, Santa Cruz, CA, United states), as well as p21 (1:200; Santa Cruz Biotechnology, Santa Cruz, CA, United States), and GAPDH (1:10,000; Sigma-Aldrich) and incubated overnight. Afterwards, inoculation of the samples with HRP-labelled secondary antibodies (Amersham, Piscataway, NJ, United States) was performed, and Western blots were performed with the SuperSignal chemiluminescence reagents (Pierce Chemical Co.).

Statistical Analysis

A paired sample t-test was employed to analyze the difference in LINC00341 RNA expression between bladder cancer tissue and matched non-tumor tissue. The independent samples t-test was employed to explore the differences in LINC00341 RNA expression between cancer subgroups. ANOVA was applied to examine the differences between the different groups in the CCK-8 analysis. Moreover, an independent sample t-test was utilized to analyze the apoptosis assay and wound healing assay. Pearson's coefficient correlation is applied to measure the expression correlation. The SPSS (version 19.0 SPSS Inc.) as well as GraphPad Prism 8.0 (GraphPad Software, San Diego, CA, Unites States) softwares were employed to perform all the statistical analyses. p <0.05 signified statistical significance. All data are indicated as the mean ± SD.

RESULTS

LINC00341 was Overexpressed in Bladder Cancer

The relative LINC00341 expression in 36 bladder cancer patients was explored via qRT-PCR. **Figure 1A** shows the fold change in the expression of LINC00341 (bladder cancer tissue/ corresponding histological non-tumor tissue) in every patient. **Table 1** indicates the clinical features of this group of patients. In contrast with the matched non-tumor tissues, LINC00341 was overexpressed in bladder cancer (**Figure 1B**).

We examined differences in expression based on grade and stage. The bar graph indicates the lncRNA-LINC00341 relative expression in all the groups. The LINC00341 expression level in

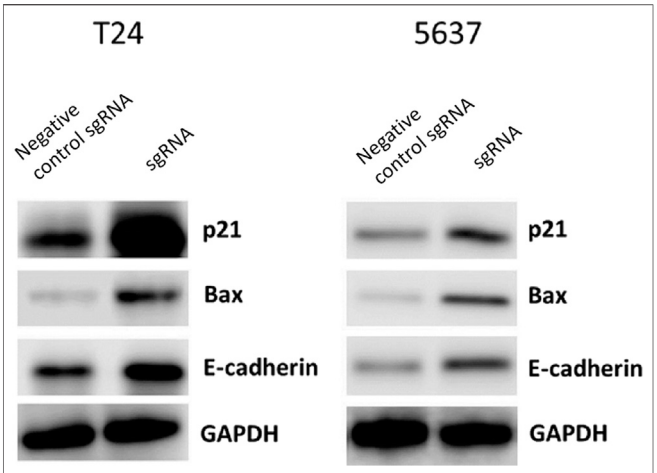

FIGURE 5 | Knockdown of LINC00341 by CRISPR-CasRx increased p21, Bax and E-cadherin protein expression. LINC00341 sgRNA or negative control sgRNA transfected cells were subjected to western blot assay to examine expression changes of p21, E-cadherin, as well as Bax in bladder cancer cells. **(A)**. Western blot results showing protein expression T24 cells. **(B)**. Western blot assay images showing protein expression in 5,637 cells.

high-grade tumors is higher in contrast with that in low-grade tumors (**Figure 1B**). The LINC00341 expression level in infiltrating tumors was higher relative to that in non-infiltrating tumors (**Figure 1B**).

Specific sgRNA/-CasRx Down-Regulated LINC0034l Expression

The T24 as well as 5,637 bladder cancer cells were grown and inserted with LINC00341 sgRNA/-CasRx or negative control sgRNA/-CasRx. The RNA expression of LINC00341 was assayed 48 h after transfection via qRT-PCR. Consequently, the inhibition rate (LINC00341 sgRNA/negative control sgRNA) was 82.14 ± 2.67% and 78.31 ± 3.82% in T24 cells and 5,637 cells, respectively. The data are expressed as mean ± SD. Each sample was assayed in triplicates.

Knockdown of LINC00341 by CRISPR-CasRx Repressed Cell Proliferation

We transfected the T24 as well as 5,637 bladder cancer cells with LINC00341 sgRNA or negative control sgRNA, and then determined the rate of growth of bladder cancer cells proliferation via the CCK-8 assay. After knocking down LINC00341 (**Figure 2B**), the cell proliferation of T24 cells (**Figure 2A**) as well as 5,637 cells were inhibited. The inhibitory effect of LINC00341on the growth of tumors *in vivo* was also confirmed (**Figure 2C**), which indicated that LINC00341 repressed bladder cancer cell proliferation.

Knockdown of LINC00341 by CRISPR-CasRx Induced Apoptosis

Transfection of T24 as well as 5,637 bladder cancer cell lines with LINC00341 sgRNA or negative control sgRNA was performed. 48 h post transfection, we utilized ELISA to assay for the apoptosis of T24 as well as 5,637 bladder cancer cells (**Figure 3**). After knocking down LINC00341, induced apoptosis occurred in T24 as well as 5,637 bladder cancer cell lines.

Motility Changes Triggered by Knockdown of LINC00341 Using CRISPR-CasRx

We employed the wound healing to explore the changes in motility of the cells triggered by LINC00341 knockdown in bladder cancer cells. Diminished motility of the cells was reported in 5,637 cells as indicated in **Figures 4A,B**, as well as T24 cells as indicated in **Figures 4C,D**.

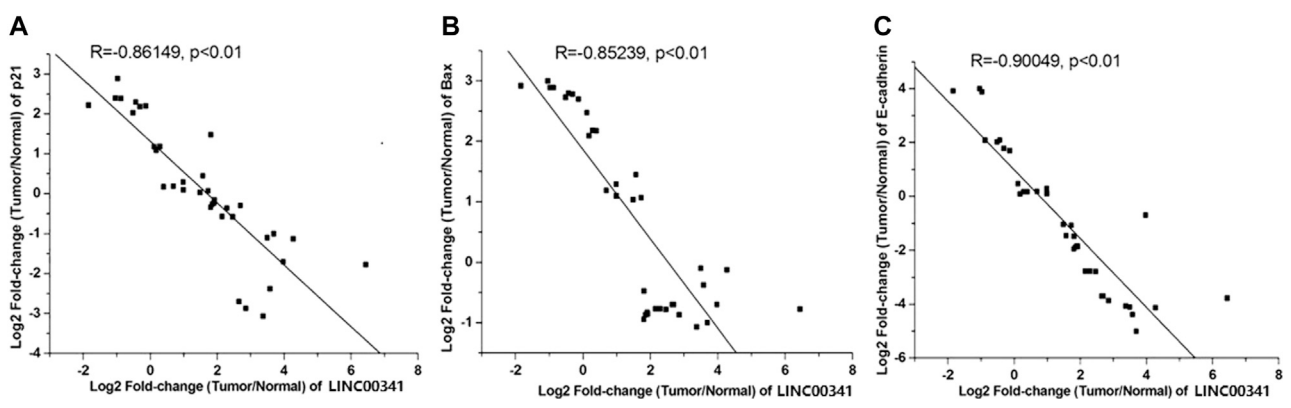

FIGURE 6 | Negative correlation of LINC00341 with p21, Bax and E-cadherin expression. qPCR was employed to assay the expression changes of p21, E-cadherin, as well as Bax in bladder cancers compared to non-tumor tissues (N = 36). **(A)**. Inversely expressed LINC00341 and p21 in bladder cancer. **(B)**. Inversely expressed LINC00341 and Bax in bladder cancer. **(C)**. Inversely expressed LINC00341 and E-cadherin in bladder cancer.

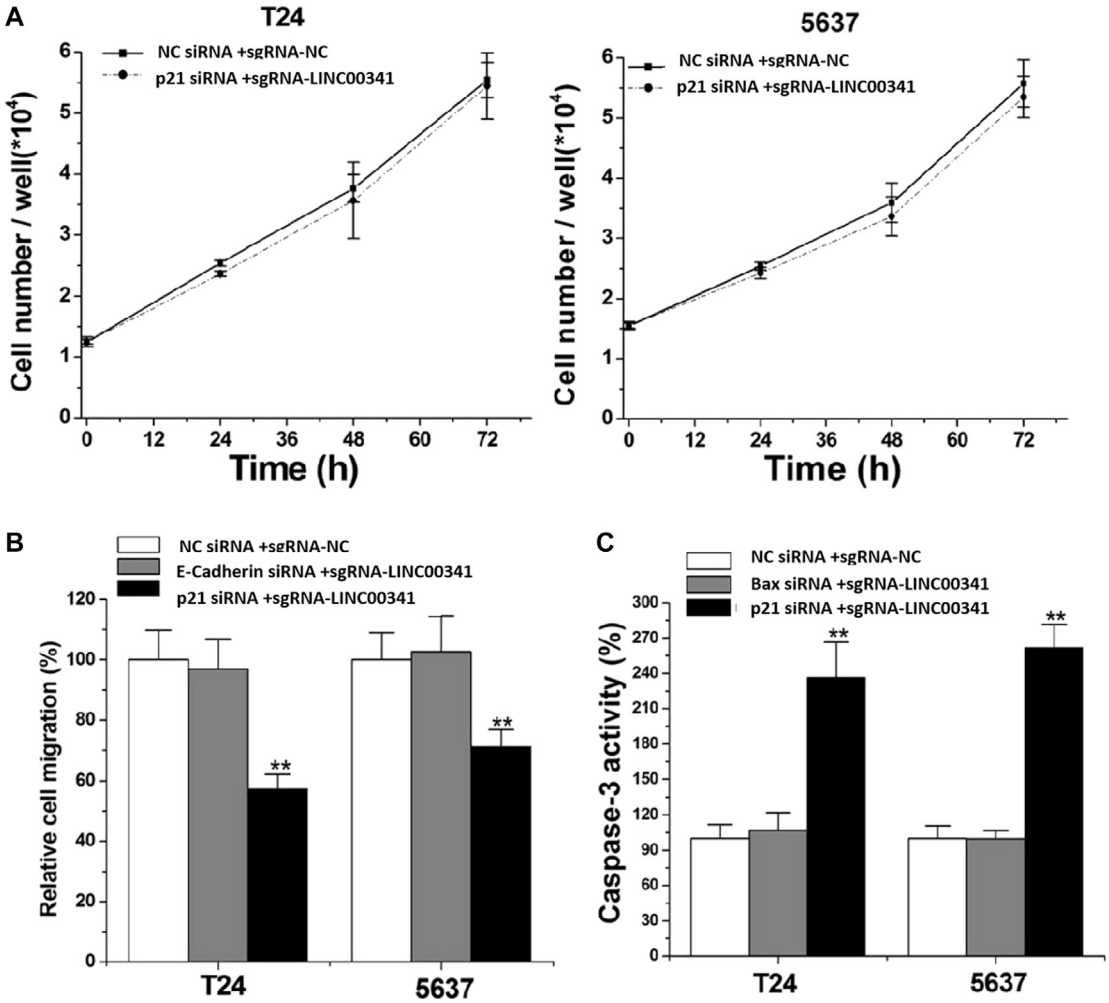

FIGURE 7 | Knockdown of LINC00341 by CRISPR-CasRx induced cellular phenotypic changes via p21, Bax as well as E-cadherin regulation. After siRNA transfection, CCK-8, wound healing as well as ELISA analyses were respectively employed to detect cell proliferation, migration as well as apoptosis. **(A)**. p21 siRNA eliminated the proliferation inhibitory effect induced by LINC00341 sgRNA in T24 as well as 5,637 ($p > .05$). **(B)**. E-cadherin siRNA eliminates the migration inhibitory effect induced by LINC00341 sgRNA in T24 and 5,637, while p21 siRNA does not have this function. $^{**}p < 0.01$. **(C)**. Bax siRNA eliminates the apoptosis-promoting effect induced by LINC00341 sgRNA in T24 and 5,637, while p21 siRNA does not have this function. $^{**}p < 0.01$.

Knockdown of LINC00341 by CRISPR-CasRx Increased p21, Bax as well as E-Cadherin Protein Expression

To assess the prospective biomarkers that trigger the aforementioned phenotypic alterations after knocking down LINC00341, Western blot was conducted to assess the protein contents of p21, Bax, as well as E-cadherin that have vital roles in the bladder cancer development. LINC00341 sgRNA significantly up-regulated the p21, Bax as well as E-cadherin expressions in T24 and 5,637 cells as indicated in **Figures 5A,B** at the protein level. In addition, clinical samples also showed that LINC00341 was negatively correlated with p21 (**Figure 6A**), Bax (**Figure 6B**) and E-cadherin expression (**Figure 6C**). To further verify the functional role of these markers in the LINC00341 knockdown experiment, we also used two siRNAs for double knockdown. p21 siRNA abolished the proliferation inhibitory effect induced by LINC00341 sgRNA in T24 and 5,637 (**Figure 7A**). E-cadherin siRNA abolished the migration inhibitory effects induced by LINC00341 sgRNA in T24 and 5,637 (**Figure 7B**). Bax siRNA eliminated the apoptosis-promoting effect induced by LINC00341 sgRNA in T24 and 5,637 (**Figure 7C**). p21 siRNA could not reverse the migration inhibitory effect (**Figure 7B**) and apoptosis promotion effect (**Figure 7C**) induced by LINC00341 sgRNA in these cells, possibly because p21 alone could not induce cell death or inhibit cell migration.

DISCUSSION

Recent studies have shown that human cancer is caused by a large number of lncRNA disorders. It is thought that lncRNA has great clinical significance as a set of cancer molecular markers as well as treatment targets(Sahu et al., 2015; Sun and Kraus, 2015). For

example, it is reported that lncRNA PVT1 (Zhuang et al., 2015), SUMO1P3 (Zhan et al., 2016) and CCAT2 (Li et al., 2016) can facilitate cell proliferation as well as repress cell apoptosis in bladder cancer. As a recently discovered lncRNA, no work has been done to characterize the carcinogenic properties of LINC00341. It may provide the potential target of cancer treatment (Zhong et al., 2015).

LINC00341 may be a cancer driving factor in tumor development. Therefore, it is very interesting to explore its biological role in bladder cancer. For this purpose, herein, we established that LINC00341 is overexpressed in bladder cancer in contrast with the corresponding non-tumor tissues. The high expression of LINC00341 is related to high-grade as well as staged bladder cancer. The differential expression pattern of LINC00341 between bladder cancer and control along with the association of LINC00341 with clinicopathological characteristics indicate that the lnRNA LINC00341 has a new role in the occurrence and development of bladder cancer. To elucidate the possible influences of LINC00341 on bladder cancer, we assessed the changes in cell proliferation, apoptosis, as well as motility induced by LINC00341 silencing by CRISPR-CasRx in bladder cancer. Although traditional methods including siRNA/shRNA also offers a possibility for inhibiting LINC00341, the unexpected off-target effects significantly limit their applications. As a newly identified Cas system from RNA-targeting CRISPR enzymes, CRISPR-CasRx exhibits high efficiency and specificity for RNA cleavage (Jiang et al., 2020; Zhou et al., 2020). Inhibition of cell proliferation, escalated the rate of apoptosis, and reduced the motility rate in LINC00341 sgRNA-transfected T24 as well as 5,637 bladder cancer cell lines.

In order to study the potential ways to induce the above phenotype, we also performed a Western blot experiment and found that knocking down LINC00341 by CRISPR-CasRx can increase the expression of p21, Bax and E-cadherin. This finding is congruent with previous studies, which indicated that p21 is a downstream target of LINC00341. In other studies on bladder cancer, inactivation of p21 has also been shown to promote tumorigenesis and cell proliferation (Tang et al., 2015). Bax is a vital homologue of Bcl-2, an enhancer of apoptosis, and can be used as an independent parameter for predicting the clinical prognosis of individuals with bladder cancer (Golestani Eimani et al., 2014; Liu et al., 2016). E-cadherin is a cell-cell junction protein that is often absent during the migration of bladder cancer cells (Liu et al., 2014; Zhao et al., 2014). Using double knockdown experiments, we further show that the expression changes of these biomarkers can at least partially explain the phenotypic changes after LINC00341 knockdown. LINC00341 may be associated with an epigenetic repressor, thereby regulating the transcription of Bax or E-cadherin.

In summary, the above data indicate that LINC00341 serves as an oncogene in the carcinogenesis of bladder cancer. Targeting LINC00341 may be a promising method for human cancer gene therapy. More work is required to establish the prospective molecular mechanism of LINC00341 in the regulation of Bax as well as E-cadherin in bladder cancer. The treatment of LINC00341 should also be studied in depth.

DATA AVAILABILITY STATEMENT

The original contributions presented in the study are included in the article/Supplementary material, further inquiries can be directed to the corresponding author.

ETHICS STATEMENT

The studies involving human participants were reviewed and approved by the Institutional Review Board of Foshan Women and Children's Hospital. The patients/participants provided their written informed consent to participate in this study. The animal study was reviewed and approved by the Institutional Review Board of Foshan Women and Children's Hospital.

AUTHOR CONTRIBUTIONS

CL, YC, LZ, and JW performed most experiments and data analyses. LL, CL, SZ, and GL supervised the whole project and wrote the manuscript. HL, YZ, HW, MG, and JL also performed some experiments and provided some data.

FUNDING

This work was supported by Foshan medical science and technology research project (No. 1920001000300), Medical Research Fund Project of Guangdong Province (B2020059), Science and Technology Plan Project of Changsha (kq1907033), Project of Hunan Provincial Health Commission (20201100), and Project of Hunan Provincial Department of Education (19C1408).

REFERENCES

Chen, L. M., Chang, M., Dai, Y., Chai, K. X., Dyrskjøt, L., Sanchez-Carbayo, M., et al. (2014). External validation of a multiplex urinary protein panel for the detection of bladder cancer in a multicenter cohort. *Cancer Epidemiol. Biomarkers Prev.* 23 (9), 1804–1812. doi:10.1158/1055-9965.EPI-14-0029

Gloss, B. S., and Dinger, M. E. (2016). The specificity of long noncoding RNA expression. *Biochim. Biophys. Acta* 1859 (1) 16–22. doi:10.1016/j.bbagrm.2015.08.005

Golestani Eimani, B., Sanati, M. H., Houshmand, M., Ataei, M., Akbarian, F., and Shakhssalim, N. (2014). Expression and prognostic significance of bcl-2 and bax in the progression and clinical outcome of transitional bladder cell carcinoma. *Cell J.* 15 (4), 356–363. doi:10.1002/jcp.24679

Hu, X., Feng, Y., Zhang, D., Zhao, S. D., Hu, Z., Greshock, J., et al. (2014). A functional genomic approach identifies FAL1 as an oncogenic long noncoding RNA that associates with BMI1 and represses p21 expression in cancer. *Cancer Cell* 26 (3) 344–357. doi:10.1016/j.ccr.2014.07.009

Jeong, S., Lee, J., Kim, D., Seol, M. Y., Lee, W. K., Jeong, J. J., et al. (2016). Relationship of focally amplified long noncoding on chromosome 1 (FAL1)

lncRNA with E2F transcription factors in thyroid cancer. *Medicine (Baltimore)* 95 (4) e2592. doi:10.1097/MD.0000000000002592

Jiang, W., Li, H., Liu, X., Zhang, J., Zhang, W., Li, T., et al. (2020). Precise and efficient silencing of mutant $Kras^{G12D}$ by CRISPR-CasRx controls pancreatic cancer progression. *Theranostics* 10 (25), 11507–11519. doi:10.7150/thno.46642

Li, J., Zhuang, C., Liu, Y., Chen, M., Zhou, Q., Chen, Z., et al. (2016). shRNA targeting long non-coding RNA CCAT2 controlled by tetracycline-inducible system inhibits progression of bladder cancer cells. *Oncotarget* 7 (20), 28989–28997. doi:10.18632/oncotarget.8259

Liu, Y., Zeng, Y., Liu, L., Zhuang, C., Fu, X., Huang, W., et al. (2014). Synthesizing AND gate genetic circuits based on CRISPR-Cas9 for identification of bladder cancer cells. *Nat. Commun.* 5, 5393. doi:10.1038/ncomms6393

Liu, Y., Zhan, Y., Chen, Z., He, A., Li, J., Wu, H., et al. (2016). Directing cellular information flow via CRISPR signal conductors. *Nat. Methods* 13 (11), 938–944. doi:10.1038/nmeth.3994

Sahu, A., Singhal, U., and Chinnaiyan, A. M. (2015). Long noncoding RNAs in cancer: from function to translation. *Trends Cancer* 1 (2) 93–109. doi:10.1016/j.trecan.2015.08.010

Sun, M., and Kraus, W. L. (2015). From discovery to function: the expanding roles of long noncoding RNAs in physiology and disease. *Endocr. Rev.* 36 (1), 25–64. doi:10.1210/er.2014-1034

Tang, K., Wang, C., Chen, Z., Xu, H., and Ye, Z. (2015). Clinicopathologic and prognostic significance of p21 (Cip1/Waf1) expression in bladder cancer. *Int. J. Clin. Exp. Pathol.* 8 (5), 4999–5007. doi:10.1016/j.trecan.2015.08.010

VanGuilder, H. D., Vrana, K. E., and Freeman, W. M. (2008). Twenty-five years of quantitative PCR for gene expression analysis. *Biotechniques* 44 (5) 619–626. doi:10.2144/000112776

Wang, J., Zhang, X., Wang, L., Dong, Z., Du, L., Yang, Y., et al. (2015). Downregulation of urinary cell-free microRNA-214 as a diagnostic and prognostic biomarker in bladder cancer. *J. Surg. Oncol.* 111 (8), 992–999. doi:10.1002/jso.23937

Zhan, Y., Liu, Y., Wang, C., Lin, J., Chen, M., Chen, X., et al. (2016). Increased expression of SUMO1P3 predicts poor prognosis and promotes tumor growth and metastasis in bladder cancer. *Oncotarget* 7 (13), 16038–16048. doi:10.18632/oncotarget.6946

Zhao, J., Dong, D., Sun, L., Zhang, G., and Sun, L. (2014). Prognostic significance of the epithelial-to-mesenchymal transition markers e-cadherin, vimentin and twist in bladder cancer. *Int. Braz. J. Urol.* 40 (2), 179–189. doi:10.1590/S1677-5538.IBJU.2014.02.07

Zhong, X., Hu, X., and Zhang, L. (2015). Oncogenic long noncoding RNA FAL1 in human cancer. *Mol. Cell. Oncol.* 2 (2), e977154. doi:10.4161/23723556.2014.977154

Zhou, C., Ye, L., Jiang, C., Bai, J., Chi, Y., and Zhang, H. (2015). Long noncoding RNA HOTAIR, a hypoxia-inducible factor-1α activated driver of malignancy, enhances hypoxic cancer cell proliferation, migration, and invasion in non-small cell lung cancer. *Tumour Biol.* 36 (12), 9179–9188. doi:10.1007/s13277-015-3453-8

Zhou, H., Su, J., Hu, X., Zhou, C., Li, H., Chen, Z., et al. (2020). Glia-to-neuron conversion by CRISPR-CasRx alleviates symptoms of neurological disease in mice. *Cell* 181 (3), 590–603. doi:10.1016/j.cell.2020.03.024

Zhuang, C., Li, J., Liu, Y., Chen, M., Yuan, J., Fu, X., et al. (2015). Tetracycline-inducible shRNA targeting long non-coding RNA PVT1 inhibits cell growth and induces apoptosis in bladder cancer cells. *Oncotarget* 6 (38), 41194–41203. doi:10.18632/oncotarget.5880

Conflict of Interest: The authors declare that the research was conducted in the absence of any commercial or financial relationships that could be construed as a potential conflict of interest.

frontiers in Molecular Biosciences

ORIGINAL RESEARCH
published: 11 March 2021
doi: 10.3389/fmolb.2021.652392

Transcriptional Inhibition of lncRNA gadd7 by CRISPR/dCas9-KRAB Protects Spermatocyte Viability

*Jun Zhao†, Wenmin Ma†, Yucheng Zhong†, Hao Deng†, Bingyu Zhou, Yaqin Wu, Meiqiong Yang and Huan Li**

Assisted Reproductive Technology Center, Foshan Maternal and Child Health Care Hospital, Foshan, China

Our previous study found that lncRNA gadd7 was up-regulated in the semen of varicocele patients, and could promote the apoptosis of mouse spermatocytes and inhibit their proliferation. Therefore, we further explored whether down-regulation of Gadd seven expression could protect the viability of spermatocytes. Here we designed specific sgRNAs targeting the ORF region of gadd7, and constructed a CRISPR-dCas9-KRAB system that effectively inhibits gadd7 at the transcriptional level. The CRISPRi system can effectively prevent the apoptosis of spermatocytes and enhance their proliferation, which is expected to provide a potentially effective molecular intervention method for the treatment of male infertility caused by varicocele.

Keywords: lncRNA gadd7, CRISPR, varicocele, infertility, male

OPEN ACCESS

Edited by:
Yonghao Zhan,
Zhengzhou University, China

Reviewed by:
Kai Yang,
Zhejiang University, China
Xiaoli Zhang,
Wuhan University, China

****Correspondence:***
Huan Li
421991218@qq.com

†These authors have contributed equally to this work.

Specialty section:
This article was submitted to Molecular Diagnostics and Therapeutics, a section of the journal Frontiers in Molecular Biosciences

Received: *12 January 2021*
Accepted: *29 January 2021*
Published: *11 March 2021*

Citation:
Zhao J, Ma W, Zhong Y, Deng H, Zhou B, Wu Y, Yang M and Li H (2021) Transcriptional Inhibition of lncRNA gadd7 by CRISPR/dCas9-KRAB Protects Spermatocyte Viability. Front. Mol. Biosci. 8:652392. doi: 10.3389/fmolb.2021.652392

INTRODUCTION

Varicocele is a common disease of the male reproductive system (Hyun, 2020). The incidence rate in the general male population is 15%, and the incidence rate in the infertile population is as high as 39% (Alsaikhan et al., 2016; Barratt et al., 2017). It is considered by the World Health Organization to be one of the most common causes of male infertility. It affects the spermatogenic function of the testis through a variety of pathophysiological changes. The theory of renal venous reflux is considered to be a possible cause of damage to spermatogenesis (Sayfan and Adam, 1978; Graif et al., 2000). Toxic metabolites from the reflux of kidneys/adrenal glands cause local microenvironmental changes in spermatogenesis of testis. Clinically, semen quality testing is often used to determine the effect of varicocele on men. For patients with moderate to severe varicocele, surgical treatment is the most effective treatment method, and microscopy is the current gold standard for surgical treatment (Johnson and Sandlow, 2017).

Long noncoding RNAs (LncRNAs) are a type of RNA molecules with a transcript length of more than 200 nt (Kopp and Mendell, 2018). They are widely present in mammals and participate in various normal activities of cells, such as genome imprinting, transcription regulation, X Chromosome silencing and nuclear transport (Chen, 2016). They also participate in the pathological process of tumors and other diseases. LncRNAs do not encode proteins, but they regulate gene expression at multiple levels in the form of RNA, and are related to a series of major human diseases, especially neurological diseases and cancers (Renganathan and Felley-Bosco, 2017; Choudhari et al., 2020).

In recent years, the research on LncRNAs has progressed rapidly, but the function and mechanism of most LncRNAs are still unclear. The gene expressing gadd7 was cloned from Chinese hamster ovary cells exposed to ultraviolet light in 1988 (Hollander et al., 1996). It is a LncRNA specifically expressed in hamster cells. Basically all factors such as growth arrest, DNA

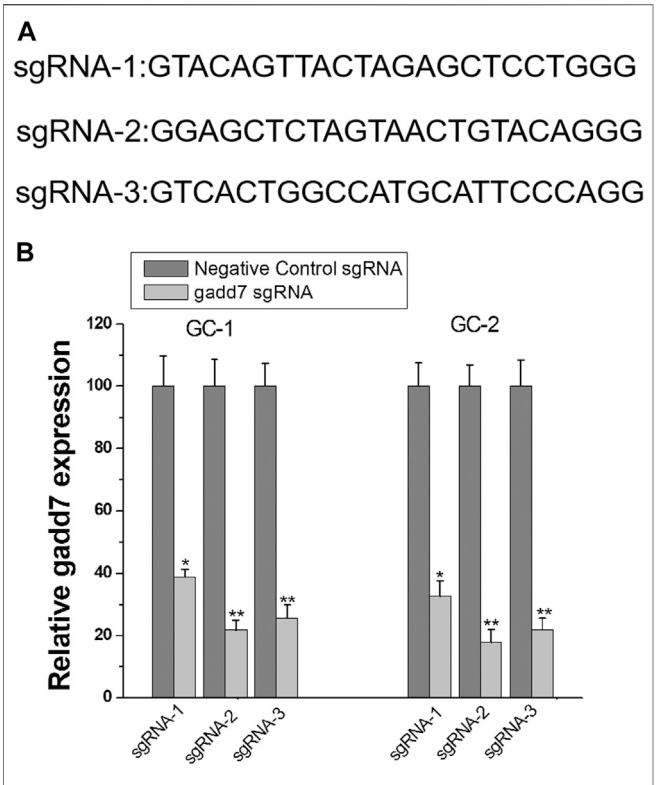

FIGURE 1 | CRISPR-dCas9-KRAB inhibits lncRNA gadd7 expression. **(A)** cDNA sequences of the first 20 nt of the sgRNAs targeting the ORF region of gadd7. **(B)** Inhibition of gadd7 expression using the designed sgRNAs in GC-1 and GC-2 cells. The relative expression level of gadd7 wad determined by qRT-PCR. *$p < 0.05$, relative to the negative control by paired, one-sided *t*-test. **$p < 0.01$, relative to the negative control by paired, one-sided *t*-test.

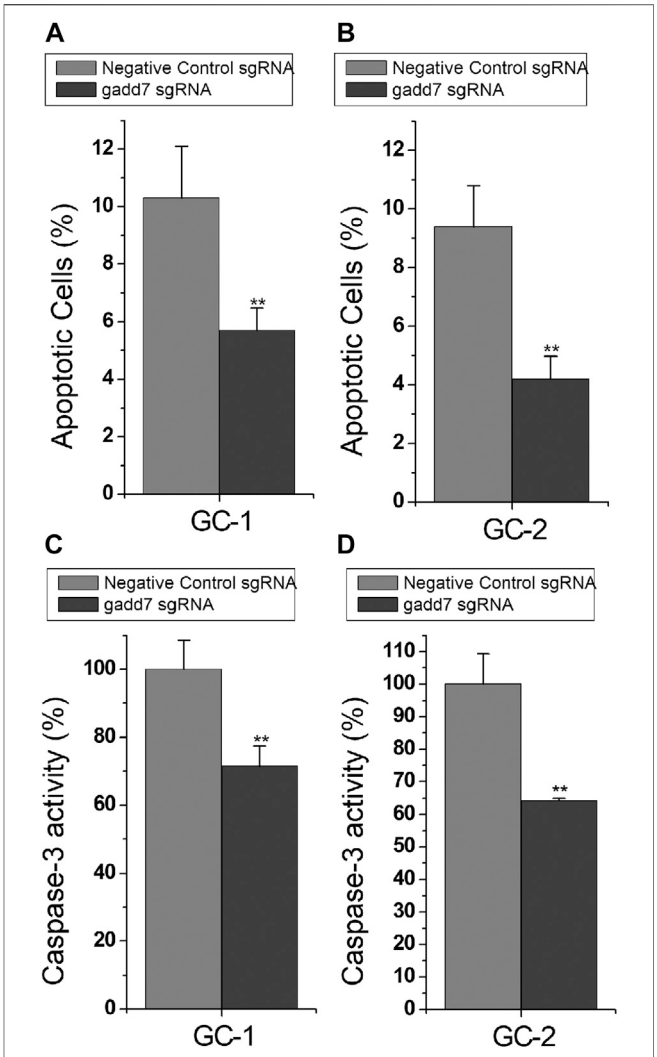

FIGURE 2 | Inactivation of gadd7 by CRISPR-dCas9-KRAB prevents cell apoptosis. **(A)** Cell apoptosis changes were determined using flow cytometry analysis in GC-1 cells. **(B)** Cell apoptosis changes in GC-2 cells. **(C)** Caspase-3 activity was determined using ELISA in GC-1 cells. **(D)** Caspase-3 activity was determined using ELISA in GC-2 cells. The error bars indicate the S.D. from three different experiments. NC, negative control. **$p < 0.01$, relative to the negative control group by paired, one-sided *t*-test.

damage, and excessive oxidative stress can induce its expression (Mizenina et al., 1998). Currently, there still lacks much research on the function and mechanism of its action. Studies have found that, in addition to inhibiting cell clone formation, the lncRNA gadd7 also plays an important regulatory role in lipotoxicity-induced cell death. Our previous studies have found that gadd7 is elevated in the sperm of patients with varicocele, and can promote the apoptosis of mouse spermatocytes and inhibit their proliferation (Zhao et al., 2018).

A more interesting idea is whether down-regulation of lncRNA gadd7 can protect spermatocytes. However, traditional RNAi technology is difficult to achieve effective knockdown of lncRNA, which limits the implementation of this idea. The CRISPRi transcription suppression technology developed in recent years is expected to inhibit the expression of lncRNA (Liu et al., 2017; Stojic et al., 2018; Liu et al., 2020). The dCas9 protein targeted to the ORF region of the gene can silence the expression of specific lncRNA by fusing the KRAB transcription repressor. In this study, we designed a specific sgRNA for the ORF region of gadd7, and screened and obtained a CRISPRi system that effectively inhibits gadd7. This system can effectively slow down the apoptosis of spermatocytes and promote their proliferation, which is expected to provide a potentially effective molecular intervention method for the treatment of male infertility caused by varicocele.

MATERIALS AND METHODS

Cell Lines and Cell Culture

The two mouse germ cell lines, GC-1 and GC-2, had been purchased from the Institute of Cell Research, Chinese Academy of Sciences (Shanghai, China). Cells were grown in RPMI 1640 medium supplemented with 10% fetal bovine serum (Invitrogen) at 37°C in a 5% CO_2 atmosphere.

Construction of CRISPR-dCas9-KRAB and Transfection

The plasmid vectors pcDNA-dCas9-KRAB (#110820, Addgene) was used to transiently express dCas9-KRAB fusion protein (for CRISPR-based interference) in mouse germ cells. The designed cDNA sequence for each sgRNA was designed using the online software tool (http://crispr-era.stanford.edu/), and synthesized and inserted into pGPU6/GFP/Neo vector which was digested with Bam HI/Bbs I. The leader sequence of sgRNA negative control was 5′-GTACGTTCTCTATCACTGATA-3′.

The above plasmids were transfected into GC-1 and GC-2 cells using Nanofectin™ Transfection reagent (Excell Bio, Shanghai, China) according to the supplier's protocol. The final concentration of plasmid was 1 μg/ml.

Quantitative Real-Time PCR (qRT-PCR)

Total RNA was extracted from indicated cells or frozen specimens using Trizol reagents (Invitrogen). Reverse transcription was performed using M-MLV Reverse transcriptase (Invitrogen) and the extracted RNA. qRT-PCR was conducted on the Applied Biosystems 7,300 Fast Real-Time PCR System (Applied Biosystems, Foster City, CA, United States) using SYBR® Green Realtime PCR Master Mix (Toyobo, Osaka, Japan) and the primers 5′-ACAATGACGCCA TCGTTTTCT-3' (forward) and 5′- TGTCCTCCATCTGGG CATTT-3-3' (reverse) for gadd7. The expression levels were calculated using the comparative CT method for relative quantification against GAPDH. The primers for GAPDH were forward 5′-CGCTCTCTGCTCCTCCTGTTC-3′, and reverse 5′-ATCCGTTGACTCCGACCTTCAC-3′.

Cell Proliferation Assay

Cell proliferation abilities were evaluated using Cell counting kit-8 (CCK-8).Briefly, 3,000 indicated GC-1/GC-2 cells were plated into 96-well plates per well. After incubation for 24 h, 48 h, or 72 h, 10 μL CCK-8 solution (Biyuntian Biological Engineering Co. Ltd., Shanghai, China) was added to per well. After incubation for 2 h, the absorbance at 450 nm was measured at 490 nm by a microplate reader (Bio-Rad, Hercules, CA). Each experiment was done at least three times.

Cell Apoptosis Assays

GC-1 and GC-2 cells were transiently transfected with plasmid vectors, and then cells were harvested and resuspended in fixation fluid 48 h after transfection. 5 μl of Annexin V—FIFC and 2 μl of propidium iodide were added to 500 μl of cell suspension. Cell apoptosis was then determined using flow cytometry (EPICS, XL-4, Beckman, CA, United States). Each experiment was done at least three times.

The caspase-3 activity in GC-1 and GC-2 cells was determined by ELISA using a Caspase-3 Activity Assay kit (Fluorometric). At 48 h after transfection, cells were reaped and cultured in lysis buffer for 15 min at 4°C, followed by centrifugation and supernatant collection. The final absorbance (at 405 nm) was determined using a microplate reader.

Statistical Methods

The *t* test (homogeneity of variance) or t 'test (heterogeneity of variance) of two or more independent samples was used for the normal distribution data. SPSS 17.0 software was used for analysis, and $p < 0.05$ was considered statistically significant.

RESULTS

Design and Construction of CRISPR-dCas9-KRAB Targeting gadd7

To determine whether the CRISPRi technology can be used to inhibit the expression of lncRNA gadd7, we targeted the dCas9-KRAB protein to the ORF regions of gadd7 using designed sgRNAs (sgRNA1~3) (**Figure 1A**). Then, we introduced dCas9-KRAB and sgRNA combination into GC-1 and GC-2 cells. The expression of these sgRNAs induced various

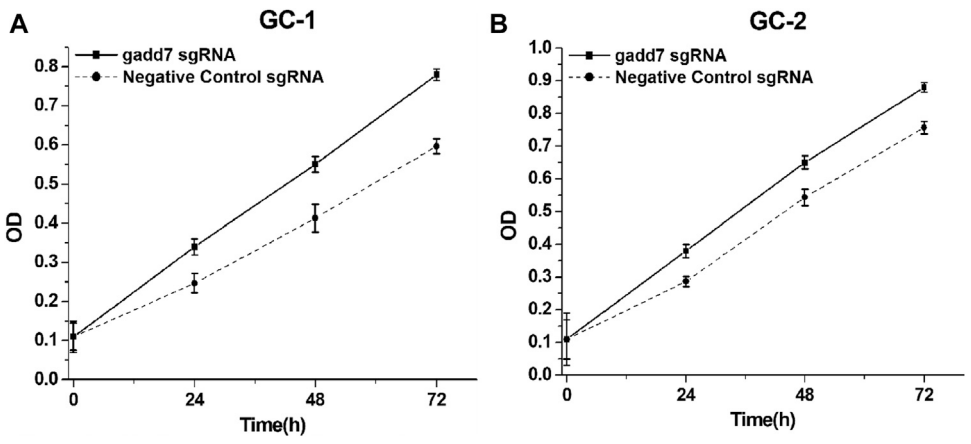

FIGURE 3 | Inactivation of gadd7 by CRISPR-dCas9-KRAB enhances cell proliferation. Cell proliferation was detected by CCK-8 assay. **(A)** Compared to the negative control group, the proliferative ability of GC-1 cells transfected with gadd7 sgRNA was significantly increased ($p < 0.01$). **(B)** Compared to the negative control group, the proliferative ability of GC-2 cells transfected with gadd7 sgRNA was significantly increased ($p < 0.01$).

significant decreases in gadd7 expression, and the strongest inhibition was achieved with sgRNA-2 (**Figure 1B**). Therefore, we chose sgRNA-2 to do the following experiments.

Downregulation of gadd7 by CRISPR-dCas9-KRAB Reduced Cell Apoptosis

To investigate the downstream effect of downregulation of gadd7 on the apoptosis of GC-1 and GC-2 cells, the cell apoptotic rates of these cells were determined using the Flow cytometry assay. The results shown in **Figure 2** demonstrated that the apoptotic cells (%) of GC-1 (**Figure 2A**) and GC-2 (**Figure 2B**) cell lines transfected with the CRISPR-dCas9-KRAB system were much lower than those transfected with the negative control plasmid. These results suggested that downregulation of gadd7 by CRISPR-dCas9-KRAB could prevent the apoptosis of germ cells.

Downregulation of gadd7 by CRISPR-dCas9-KRAB Enhanced Cell Proliferation

To investigate the downstream effect of downregulation of gadd7 on the proliferation of GC-1 and GC-2 cells, the cell proliferation rates of these cells were determined using the CCK-8 assay. The results shown in **Figure 2** demonstrated that the proliferation rate of GC-1 (**Figure 3A**) and GC-2 (**Figure 3B**) cell lines transfected with the CRISPR-dCas9-KRAB system were much higher than those transfected with the negative control plasmid. These results suggested that downregulation of gadd7 by CRISPR-dCas9-KRAB could enhance the proliferation of germ cells.

DISCUSSION

It has always been the dream of many biologists to have a technology that can control gene expression at will. The emergence of CRISPR/Cas9 system meets this need. Cas9 is like a DNA scissors. Under the guidance of sgRNA, it specifically cuts the target sequence and forms DNA double strand breaks (Jiang and Doudna, 2017; Kosicki et al., 2018). Later studies obtained dead Cas9 (dCas9) by inactivating the endonuclease activity of Cas9. dCas9 only binds to the target site under the guidance of sgRNA, but does not cleave DNA. The coupling of dCas9 with epigenetic modifiers can efficiently regulate the transcription of specific genes (Komor et al., 2016; Savić and Schwank, 2016). When the kox1 domain of KRAB is fused with dCas9, the CRISPR system can be used to induce transcriptional suppression. In addition to the regulation of protein coding region, CRISPR-dCas9 system can also act on non coding RNAs including lncRNAs.

In this study, we designed a CRISPR-dCas9-KRAB transcriptional regulation system which inhibits mouse lncRNA gadd7. To the best of our knowledge, this is the first report which used CRISPR-dCas9 to regulate gene expression in spermatocytes. By inhibiting the expression of gadd7, this system can protect the viability of spermatocytes, which is manifested in the reduction of apoptosis and enhancement of proliferation. These results suggest that CRISPRi technique may be used in male oligoasthenospermia caused by varicocele. There may be other lncRNAs with functions similar to gadd7 that can affect spermatocytes, which need to be further explored.

In the future, further animal experiments are needed to verify the biological protection effect of the system *in vivo*.

DATA AVAILABILITY STATEMENT

The original contributions presented in the study are included in the article/Supplementary Material, further inquiries can be directed to the corresponding authors.

AUTHOR CONTRIBUTIONS

JZ, WM, YZ, HD, BZ, YW, and MY performed experiments and conducted data analyses. HL supervised the whole project.

REFERENCES

Alsaikhan, B., Alrabeeah, K., Delouya, G., and Zini, A. (2016). Epidemiology of varicocele. *Asian J. Androl.* 18 (2), 179–181. doi:10.4103/1008-682X.172640

Barratt, C. L. R., Björndahl, L., De Jonge, C. J., Lamb, D. J., Osorio Martini, F., McLachlan, R., et al. (2017). The diagnosis of male infertility: an analysis of the evidence to support the development of global WHO guidance-challenges and future research opportunities. *Hum. Reprod. Update* 23 (6), 660–680. doi:10.1093/humupd/dmx021

Chen, L. L. (2016). Linking long noncoding RNA localization and function. *Trends Biochem. Sci.* 41 (9), 761–772. doi:10.1016/j.tibs.2016.07.003

Choudhari, R., Sedano, M. J., Harrison, A. L., Subramani, R., Lin, K. Y., Ramos, E. I., et al. (2020). Long noncoding RNAs in cancer: from discovery to therapeutic targets. *Adv. Clin. Chem.* 95, 105–147. doi:10.1016/bs.acc.2019.08.003

Graif, M., Hauser, R., Hirshebein, A., Botchan, A., Kessler, A., and Yabetz, H. (2000). Varicocele and the testicular-renal venous route: hemodynamic doppler sonographic investigation. *J. Ultrasound Med.* 19 (9), 627–631. doi:10.7863/jum.2000.19.9.627

Hollander, M. C., Alamo, I., and Fornace, A. J., Jr (1996). A novel DNA damage-inducible transcript, gadd7, inhibits cell growth, but lacks a protein product. *Nucleic Acids Res.* 24 (9), 1589–1593. doi:10.1093/nar/24.9.1589

Hyun, G. (2020). Adolescent varicocele: NYU case of the month, may 2020. *Rev. Urol.* 22 (2), 77–79.

Jiang, F., and Doudna, J. A. (2017). CRISPR-Cas9 structures and mechanisms. *Annu. Rev. Biophys.* 46, 505–529. doi:10.1146/annurev-biophys-062215-010822

Johnson, D., and Sandlow, J. (2017). Treatment of varicoceles: techniques and outcomes. *Fertil. Steril.* 108 (3), 378–384. doi:10.1016/j.fertnstert.2017.07.020

Komor, A. C., Kim, Y. B., Packer, M. S., Zuris, J. A., and Liu, D. R. (2016). Programmable editing of a target base in genomic DNA without double-stranded DNA cleavage. *Nature* 533 (7603), 420–424. doi:10.1038/nature17946

Kopp, F., and Mendell, J. T. (2018). Functional classification and experimental dissection of long noncoding RNAs. *Cell* 172 (3), 393–407. doi:10.1016/j.cell.2018.01.011

Kosicki, M., Tomberg, K., and Bradley, A. (2018). Repair of double-strand breaks induced by CRISPR-Cas9 leads to large deletions and complex rearrangements. *Nat. Biotechnol.* 36 (8), 765–771. doi:10.1038/nbt.4192

Liu, S. J., Horlbeck, M. A., Cho, S. W., Birk, H. S., Malatesta, M., He, D., et al. (2017). CRISPRi-based genome-scale identification of functional long noncoding RNA loci in human cells. *Science* 355 (6320), aah7111. doi:10.1126/science.aah7111

Liu, S. J., Malatesta, M., Lien, B. V., Saha, P., Thombare, S. S., Hong, S. J., et al. (2020). CRISPRi-based radiation modifier screen identifies long non-coding RNA therapeutic targets in glioma. *Genome Biol.* 21 (1), 83. doi:10.1186/s13059-020-01995-4

Mizenina, O., Yanushevich, Y., Musatkina, E., Rodina, A., Camonis, J., Tavitian, A., et al. (1998). C-terminal end of v-src protein interacts with peptide coded by gadd7/adapt15-like RNA in two-hybrid system. *FEBS Lett.* 422 (1), 79–84. doi:10.1016/s0014-5793(97)01568-8

Renganathan, A., and Felley-Bosco, E. (2017). Long noncoding RNAs in cancer and therapeutic potential. *Adv. Exp. Med. Biol.* 1008, 199–222. doi:10.1007/978-981-10-5203-3_7

Savić, N., and Schwank, G. (2016). Advances in therapeutic CRISPR/Cas9 genome editing. *Transl Res.* 168, 15–21. doi:10.1016/j.trsl.2015.09.008

Sayfan, J., and Adam, Y. G. (1978). Intraoperative internal spermatic vein phlebography in the subfertile male with varicocele. *Fertil. Steril.* 29 (6), 669–675. doi:10.1016/s0015-0282(16)43343-1

Stojic, L., Lun, A. T. L., Mangei, J., Mascalchi, P., Quarantotti, V., Barr, A. R., et al. (2018). Specificity of RNAi, LNA and CRISPRi as loss-of-function methods in transcriptional analysis. *Nucleic Acids Res.* 46 (12), 5950–5966. doi:10.1093/nar/gky437

Zhao, J., Li, H., Deng, H., Zhu, L., Zhou, B., Yang, M., et al. (2018). LncRNA gadd7, increased in varicocele patients, suppresses cell proliferation and promotes cell apoptosis. *Oncotarget* 9 (4), 5105–5110. doi:10.18632/oncotarget.23696

Conflict of Interest: The authors declare that the research was conducted in the absence of any commercial or financial relationships that could be construed as a potential conflict of interest.

frontiers in Molecular Biosciences

ORIGINAL RESEARCH
published: 16 March 2021
doi: 10.3389/fmolb.2021.655126

Silencing of the *TRIM58* Gene by Aberrant Promoter Methylation is Associated with a Poor Patient Outcome and Promotes Cell Proliferation and Migration in Clear Cell Renal Cell Carcinoma

Ying Gan[1,2,3†], *Congcong Cao*[4†], *Aolin Li*[1,2,3†], *Haifeng Song*[1,2,3], *Guanyu Kuang*[1,2,3], *Binglei Ma*[1,2,3], *Quan Zhang*[1,2,3] *and Qian Zhang*[1,2,3*]

[1]*Department of Urology, Peking University First Hospital and Institute of Urology, Peking University, Beijing, China,* [2]*National Urological Cancer Center, Beijing, China,* [3]*Beijing Key Laboratory of Urogenital Diseases (male) Molecular Diagnosis and Treatment Center, Beijing, China,* [4]*The Guangdong and Shenzhen Key Laboratory of Male Reproductive Medicine and Genetics, Peking University Shenzhen Hospital, Institute of Urology of Shenzhen PKU-HKUST Medical Center, Shenzhen, China*

OPEN ACCESS

Edited by:
Yuchen Liu,
Shenzhen University, China

Reviewed by:
Wanru Ma,
Beijing Hospital, China
Xiaojing Wang,
Tsinghua University, China

***Correspondence:**
Qian Zhang
zhangqianbjmu@126.com

[†]These authors have contributed equally to this work.

Specialty section:
This article was submitted to Molecular Diagnostics and Therapeutics, a section of the journal Frontiers in Molecular Biosciences

Received: *18 January 2021*
Accepted: *27 January 2021*
Published: *16 March 2021*

Citation:
Gan Y, Cao C, Li A, Song H, Kuang G, Ma B, Zhang Q and Zhang Q (2021) Silencing of the TRIM58 *Gene by Aberrant Promoter Methylation is Associated with a Poor Patient Outcome and Promotes Cell Proliferation and Migration in Clear Cell Renal Cell Carcinoma. Front. Mol. Biosci. 8:655126. doi: 10.3389/fmolb.2021.655126*

To investigate the underlying molecular mechanism of tripartite motif-containing 58 (TRIM58) in the development of clear cell renal cell carcinoma (ccRCC), we explored TRIM58 expression and methylation in tumor tissues and the association with clinicopathological features and prognosis of tissue samples; Moreover, we examined the direct gene transcription of TRIM58-specific DNA demethyltransferase (TRIM58-TET1) by the CRISPR-dCas9 fused with the catalytic domain of TET1 and the biological functions in RCC cells. In this study, we demonstrate that TRIM58 is frequently downregulated by promoter methylation in ccRCC tissues, associated significantly with tumor nuclear grade and poor patient survival. TRIM58-TET1 directly induces demethylation of TRIM58 CpG islands, and activates TRIM58 transcription in RCC cell lines. Besides, DNA demethylation of TRIM58 by TRIM58-TET1 significantly inhibits cell proliferation and migration Overall, our results demonstrate that TRIM58 is inactivated by promoter methylation, associates with tumor nuclear grade and poor survival, and TRIM58 DNA demethylation could directly activate TRIM58 transcription and inhibit cell proliferation and migration in RCC cell lines.

Keywords: clear cell renal cell carcinoma, TRIM58, DNA methylation, engineered demethyltransferase, CRISPR-dCas9

INTRODUCTION

Renal cell carcinoma (RCC) is one of the most common malignancies of the urinary system and accounts for approximately 2–3% of adult malignant solid tumors. The incidence of this disease has been steadily increasing in recent decades, partially because of increase in life expectancy and advance in medical imaging techniques (Ferlay et al., 2015; Bray et al., 2018). RCC lacks specific clinical manifestations, and approximately 20–30% of patients were reported to be initially diagnosed with distant metastasis (Alt et al., 2011). The response rate to targeted therapy and immunotherapy for metastatic patients is only approximately 30%. With the emergence of drug resistance, the vast

majority of patients will eventually die from tumor progression (Linehan and Ricketts, 2014). Clear cell renal cell carcinoma (ccRCC) is the most common pathological subtype of RCC (accounting for 75–80%) (Moch, 2013). Therefore, it is of great significance to further investigate the molecular mechanism underlying ccRCC occurrence and development, which will benefit future research in discovering effective biomarkers and therapeutic targets.

Genome-wide epigenetic alterations are associated with human tumorigenesis. The silence of tumor suppressor genes (TSGs) by aberrant promoter methylation happens frequently and is recognized as a hallmark of the occurrence and development of cancers, including RCC (Sharma et al., 2010; Klutstein et al., 2016). Many critical TSGs have been reported to be inactivated by promoter methylation in RCC, such as APAF-1, RASSF1A, SFRP, CADM2, CDKN2A, DKK1, IRF8, and SOX7 (Morrissey et al., 2001; Christoph et al., 2006; Hirata et al., 2011; He et al., 2013; Ricketts et al., 2014; Zhang et al., 2014; Ricketts et al., 2018; Wang et al., 2019), among others. TRIM58 (tripartite motif-containing 58), a member of the TRIM family, which is located at 1q44, encodes a protein that exhibits E3 ubiquitin ligase activity. It was found to participate in a wide range of physiological processes, such as innate immunity, cell proliferation, and DNA damage repair, as well as many genetic diseases and cancers (Hatakeyama, 2011). Studies have revealed that the TRIM58 gene is hypermethylated and downregulated in a variety of malignancies including lung cancer, liver cancer, and pancreatic ductal adenocarcinoma (Tao et al., 2011; Kajiura et al., 2017; Xu et al., 2019). Moreover, TRIM58 protein can inhibit proliferation and invasion in gastrointestinal cancer cells, indicating the tumor-suppressive role in such cancers (Liu M. et al., 2018; Liu et al., 2020). However, the direct methylation–expression pattern and biological function of TRIM58 in ccRCC remains unclear.

To dissect the functional significance of DNA methylation events in human cancer, CRISPR–dCas9 has been used for targeted epigenome editing by fusion with epigenome modifying enzymes such as Dnmt3a (a DNA methyltransferase enzyme) and TET (catalyze active DNA demethylation) (Sasaki and Matsui, 2008; Morita et al., 2016; Vojta et al., 2016; Xu et al., 2016). A catalytically inactive dead Cas9 (dCas9)-based system fused to the catalytic domain of TET1 (TET1CD) that hydroxylates specific loci. This system has been designed to activate site-specific demethylation in the genome DNA (Yin and Xu, 2016; Gallego-Bartolome et al., 2018; Liu X. S. et al., 2018). Here, a TRIM58-specific DNA demethyltransferase (TRIM58-TET1) was used to directly activate TRIM58 transcription and the subsequent functional effects.

In this study, we investigated whether TRIM58 was a newly identified tumor suppressor gene with aberrant promoter methylation for ccRCC. To get this conclusion, we explored TRIM58 expression and methylation status in primary tumors, as well as its relationship with clinicopathological characteristics and survival. We also examined its tumor-suppressive functions by TRIM58-TET1 in RCC cells.

RESULTS

TRIM58 was Frequently Silenced and Promoter Methylated in ccRCC Samples

To evaluate TRIM58 expression in ccRCC tissues, the mRNA transcription level of TRIM58 was examined by qRT-PCR in ccRCC samples compared to that in adjacent non-malignant renal tissues from our center. Compared with the adjacent non-malignant renal tissues, TRIM58 was significantly decreased in 15 paired renal tumor tissues ($p < 0.001$, **Figure 1A**). TRIM58 protein expression levels were also decreased in ccRCC samples according to IHC, as compared to those in adjacent non-malignant renal tissue (**Figure 1B**). We next validated the expression pattern of TRIM58 in KIRC using the TCGA database. According to RNA-sequence data from 530 KIRC patients, KIRC exhibited significantly decreased expression of *TRIM58* mRNA compared to that in normal renal tissues ($p < 0.001$, **Figure 1C**).

It is generally known that DNA methylation in the promoter region may directly in-activate gene transcription. By exploring the UCSC Genome Browser, we found there is a CpG island near the TRIM58 promoter region. It is attractive that if there are any change of DNA methylation status of TRIM58 promoter region in ccRCC. TRIM58 methylation status was analyzed in 92 ccRCC samples and 22 adjacent non-malignant renal tissues from our center. Primers targeting this region were designed for MSP and BGS (**Figure 1D**). MSP analysis showed that methylation of the TRIM58 promoter could be detected in 80.4% (74/92) of ccRCC samples but in only 18.2% (4/22) of adjacent non-malignant renal tissues ($p < 0.001$, **Figure 1E**). As expected, BGS analysis of five ccRCC samples with paired adjacent non-malignant tissues demonstrated that TRIM58 methylation levels were greater in ccRCC tissues based on 32 CpG sites (**Figure 1F**). Meanwhile, we analyzed the methylation data of 317 KIRC patients from UALCAN and found TRIM58 promoter methylation level in KIRC was significantly higher than that in normal renal tissue ($p < 0.001$, **Figure 1G**). To investigate the relationship between the expression and promoter methylation of TRIM58, we performed correlation analysis. The results showed a significant negative correlation between mRNA expression and promoter methylation levels for this gene ($R = -0.21$, $p < 0.001$, **Figure 1H**).

TRIM58 Hypermethylation and Low Expression was Associated With Clinicopathological Features and Poor Prognosis in ccRCC Samples

We evaluated the relationship between TRIM58 methylation and clinicopathological features of RCC patients from our center. According to their TRIM58 methylation status of tumor tissue samples, 92 KIRC patients were allocated into a methylated group and a non-methylated group, with their corresponding clinicopathological characteristics analyzed. Among the 92 patients, 63 were males and 29 were females, with an average age of 57.28 ± 12.42 years. We found that the TRIM58 promoter methylation was significantly associated with nuclear grade. Nuclear grade was higher in the methylated group compared

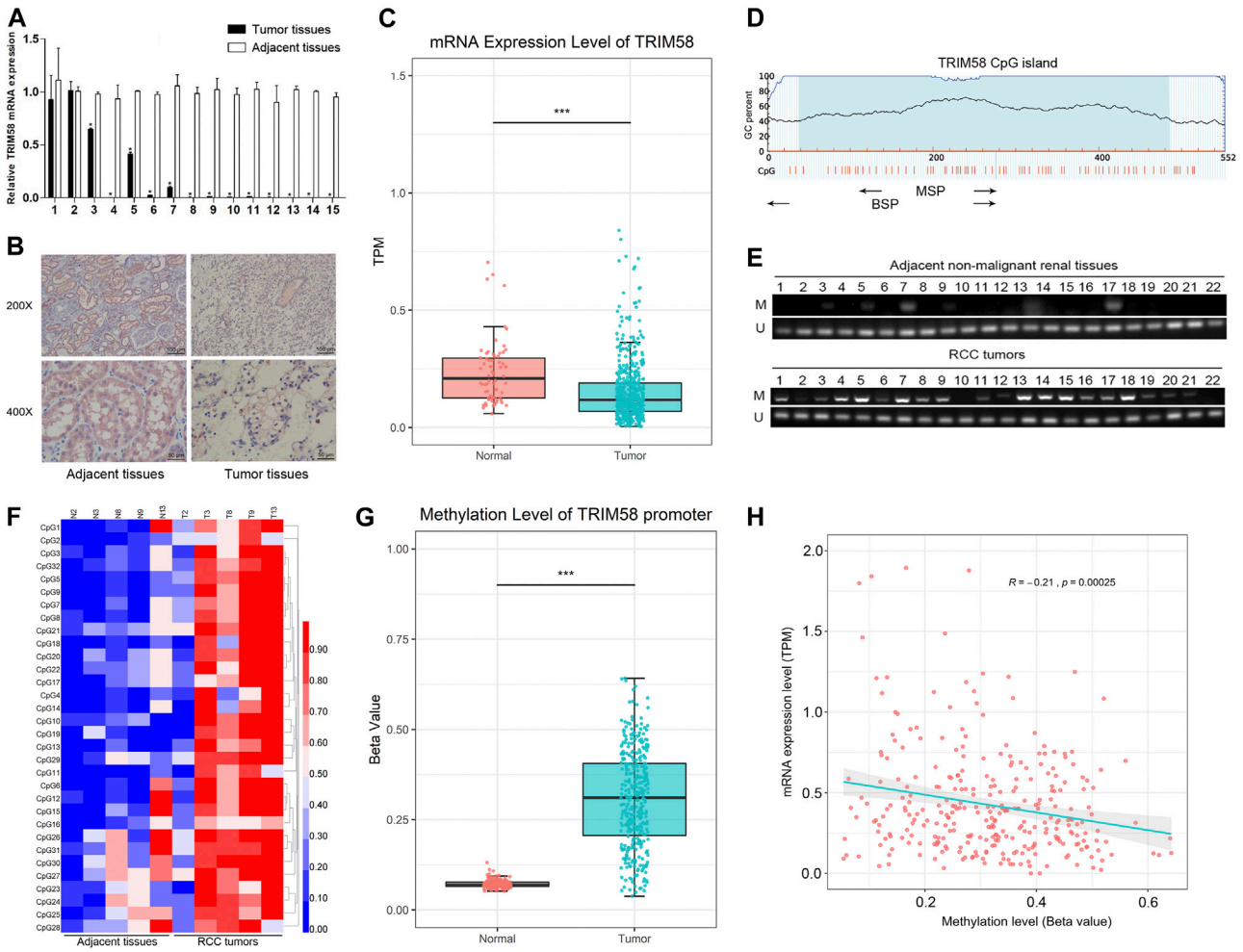

FIGURE 1 | TRIM58 is frequently silenced and hypermethylated in ccRCC samples. **(A)** The relative mRNA transcription level of TRIM58 in 15 paired renal tumor tissues and the adjacent non-malignant renal tissues; **(B)** Representative IHC staining for TRIM58 in human ccRCC cancer **(right panels)** and adjacent normal renal tissues **(left panels)**; **(C)** mRNA transcription level of TRIM58 in KIRC from TCGA database; **(D)** Primers targeting TRIM58 promoter region designed for MSP and BGS; **(E)** MSP analysis in 92 ccRCC samples and 22 adjacent non-malignant renal tissues from our center; **(F)** BGS analysis on TRIM58 promoter 32 CpG sites of five ccRCC samples with paired adjacent tissues; **(G)** Methylation level of 317 KIRC patients from UALCAN; **(H)** Correlation analysis between the expression and methylation of TRIM58.

to the unmethylated group ($p = 0.02$). Moreover, methylation of the TRIM58 promoter was not significantly associated with patient age, sex, and T stage (**Table 1**). UALCAN patients were then divided into high and low methylation groups according to the median TRIM58 methylation level. Chi-square test showed that the methylation of TRIM58 was significantly associated with T stage and nuclear grade in ccRCC; patients with a high methylation level had higher T stages ($p < 0.001$) and nuclear grades ($p < 0.001$, **Table 1**).

To further explore the correlation between TRIM58 DNA methylation inactivation and the prognosis of KIRC patients, the median mRNA expression level of TRIM58 was separately set as the cut-off value using the TCGA database. Survival analysis indicated significant differences between high and low expression groups in terms of both overall survival (OS) and disease-free survival (DFS); patients with high *TRIM58* expression had a longer OS ($p = 0.025$, **Supplementary Figure S1A**) and DFS ($p = 0.02$, **Supplementary Figure S1B**). In addition, patients from UALCAN with a high TRIM58 methylation level had significant worse OS ($p = 0.014$, **Supplementary Figure S1C**) and DFS ($p < 0.001$, **Supplementary Figure S1D**) than patients with low methylation. These results indicate that TRIM58 methylation inactivation is correlated with the poor prognosis of KIRC.

Methylation of TRIM58 Promoter Correlated With Its Downregulation in RCC Cell Lines

To evaluate the expression level of TRIM58 in RCC cell lines, we examined mRNA and protein expression in RCC cell lines (786-O, 769-P, ACHN and OS-RC-2). The TRIM58 expression was significantly reduced and even silenced, when compared to that in HK-2 normal human kidney proximal tubular epithelial cells using qRT-PCR (**Figure 2A**) and Western Blot (**Figure 2B**). We

TABLE 1 | Association of TRIM58 promotor methylation with clinicopathological features in ccRCC.

Features	PKUFH (n = 92)			TCGA (n = 317)		
	Methylated (%)	Unmethylated (%)	p	High (%)	Low (%)	*p*
Age			0.056			0.154
<65	145 (54.9%)	119 (45.1%)		67 (44.7%)	83 (55.3%)	
≥65	124 (46.6%)	142 (53.4)		88 (52.7%)	79 (47.3%)	
Gender			0.637			0.055
Male	172 (50%)	172 (50%)		107 (53.0%)	95 (47.0%)	
Female	97 (52.2)	89 (47.8%)		48 (41.7%)	67 (58.3%)	
T stage			0.142			**<0.001**
T1-T2	59 (77.6%)	17 (22.4%)		73 (36.5%)	127 (63.5%)	
T3-T4	15 (93.7%)	1 (6.2%)		82 (70.1%)	35 (29.9%)	
Nuclear grade			**0.020**			**<0.001**
G1-G2	56 (75.7%)	18 (24.3%)		52 (35.6%)	94 (64.4%)	
G3-G4	18 (100%)	0 (0%)		103 (60.2%)	68 (39.8%)	

Bold values indicate statistical significance.
PKUFH, Peking University First Hospital; TCGA, The Cancer Genome Atlas.

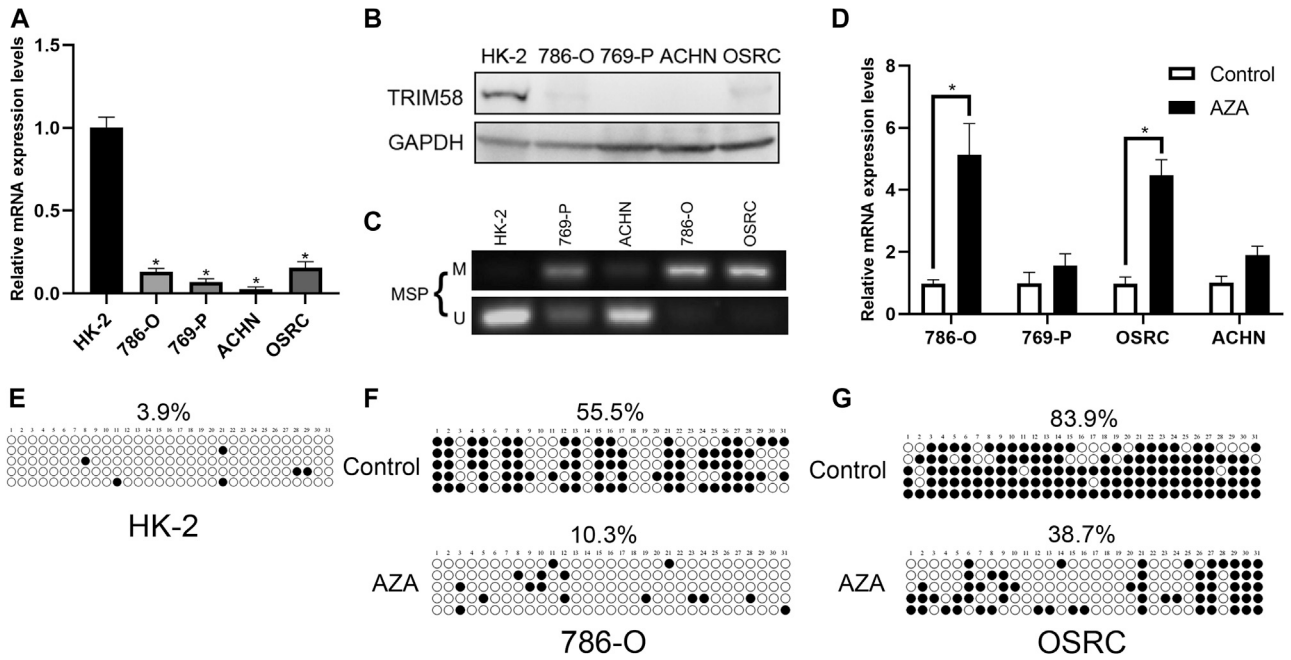

FIGURE 2 | TRIM58 methylation correlates with its downregulation in RCC cell lines. **(A**, **B)** TRIM58 expression in RCC cell lines (786-O, 769-P, ACHN and OSRC) and HK-2 normal cells using qRT-PCR **(A)** and Western Blot **(B)**; **(C)** MSP for methylation status of the TRIM58 promoter; **(D)** TRIM58 mRNA expression level after treating with the demethylation drug 5-AZA; **(E)** Methylation pattern of TRIM58 in HK-2 cells; **(F**, **G)** TRIM58 promoter CpG site methylation after treating with 5-AZA in 786-O and OS-RC-2 cells.

then examined the methylation status of the TRIM58 promoter in those cells. MSP results showed that the RCC cell lines, especially 786-O and OS-RC-2, exhibited DNA hypermethylation in the promoter region of TRIM58 compared to HK-2 cells (**Figure 2C**).

To determine whether TRIM58 expression was directly repressed by DNA methylation, we examined the TRIM58 mRNA expression level and DNA methylation status in RCC cell lines after treating them with the demethylation drug 5-AZA. The TRIM58 mRNA levels were restored after the treatments (**Figure 2D**), accompanied with a decrease of TRIM58 promoter CpG site methylation from ~55.5% to ~10.3% in 786-O, and from ~83.9% to ~38.7% in OS-RC-2, respectively (**Figures 2E–G**). These results suggested that TRIM58 promoter methylation mediates its decreased expression in RCC cells.

TRIM58 DNA Demethylation Directly Activated Gene Transcription

To explore whether DNA demethylation is essential for re-activation of TRIM58, TRIM58 promoter-specific DNA

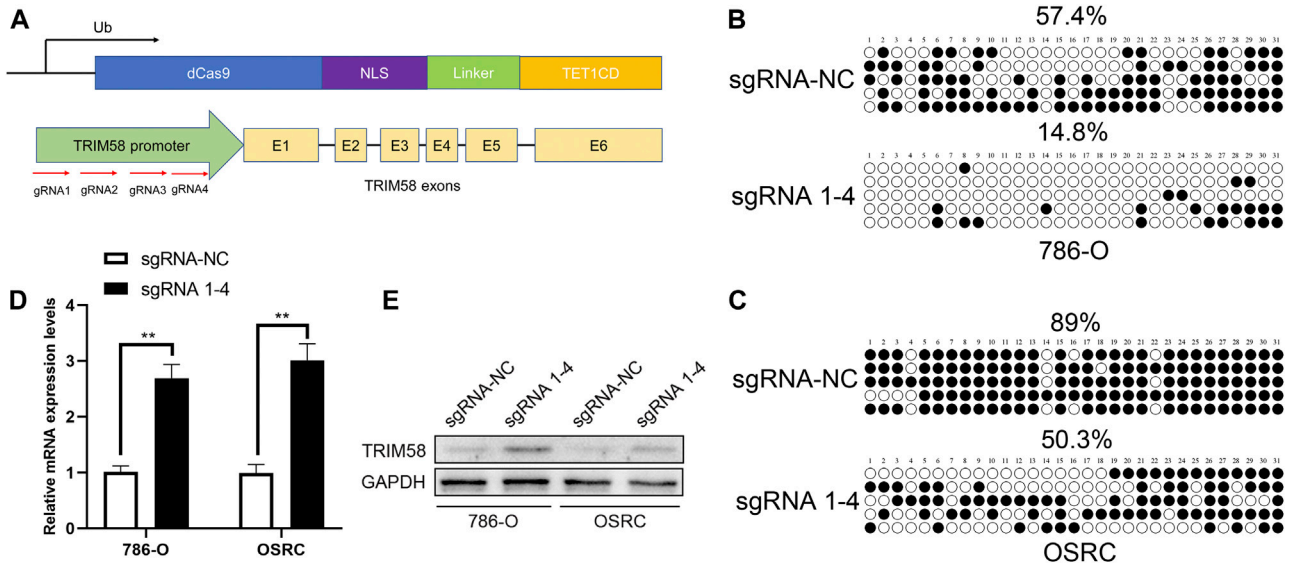

FIGURE 3 | TRIM58 targeted demethylation directly activates gene transcription. **(A)** Contruction of TRIM58-TET1 using CRISPR-dCas9 systems with 4 gRNAs targeting TRIM58 promoter region and the catalytic domain of DNA hydroxymethylase; **(B, C)** Bisulfite clone-sequencing results from 786-O and OS-RC-2 cells transiently transfected with TRIM58-TET1; **(D, E)** TRIM58 gene transcription **(D)** and protein expression **(E)** following TRIM58-TET1 transfection.

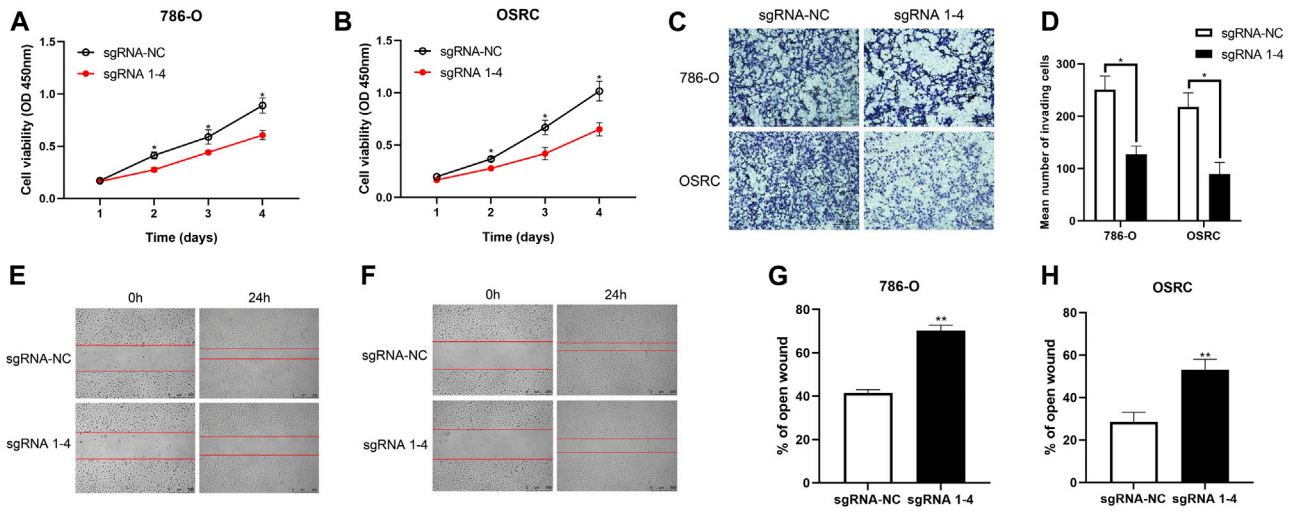

FIGURE 4 | Proliferation and migration assays carried out with RCC cells transient transfected with TRIM58-TET1 vector. **(A, B)** CCK-8 assay for cell proliferation of TRIM58-TET1 transient transfected 786-O and OS-RC-2 cells; **(C, D)** Transwell assays for the migration ability of 786-O and OS-RC-2 cells; **(E–H)** The wound-healing assays for TRIM58 demethylation in both RCC cells.

demethyltransferase (TRIM58-TET1) leading by four guide RNAs (sgRNA1-4) using CRISPR-dCas9 systems (**Figure 3A**) was transfected transiently into 786-O and OS-RC-2 RCC cell lines. Then, methylation of CpG islands within the TRIM58 promoter region was detected using bisulfite-sequencing. As expected, TRIM58-TET1 induced TRIM58 DNA demethylation in both 786-O and OS-RC-2 cells (**Figures 3B,C**) and significantly activated TRIM58 gene transcription and protein expression (**Figures 3D,E**). Taken together, these results indicated that TRIM58 promoter region demethylation could directly activate gene transcription and expression.

TRIM58 DNA Demethylation Suppressed Cell Proliferation and Migration in RCC Cells

To characterize the biological behaviors of cancer cells following TRIM58-specific activation by DNA demethylation, we determined whether TRIM58 demethylation inhibited RCC

cell proliferation. As shown in **Figures 4A,B**, we found that TRIM58 demethylation in 786-O and OS-RC-2 cells significantly inhibited cell proliferation by CCK-8 assay. Next, we evaluated the migration ability of TRIM58 demethylation in RCC cell lines by transwell migration assays and wound healing. The migration ability of 786-O and OS-RC-2 cells was significantly decreased following TRIM58 demethylation (**Figures 4C,D**). The wound-healing assays showed that TRIM58 demethylation in both RCC cells closed the wound much slower than controls (**Figures 4E–H**). Taken together, these results implied that TRIM58 DNA demethylation reduced the proliferation and migration phenotypes of RCC cells.

DISCUSSION

Methylation-mediated silencing of tumor-suppressor genes is a critical event in the occurrence and development of various malignancies, including ccRCC(Malouf et al., 2016; Morris and Latif, 2017; Joosten et al., 2018). In the previous series of research, we identified some tumor-specifically methylated genes in RCC, such as DLC1, DLEC1, IRF8, ADAMTS18 (Zhang et al., 2007; Zhang et al., 2010; Zhang et al., 2014). TRIM58, a member of the TRIM family, has been reported to play a tumor suppressive role and to be regulated by DNA methylation in lung cancer, colorectal cancer, and gastric cancer (Kajiura et al., 2017; Liu M. et al., 2018; Liu et al., 2020). However, its DNA methylation status and biological function in ccRCC remained unclear. In the present study, we preliminarily verified that TRIM58 is silenced and hypermethylated in ccRCC based on the TCGA database. The methylation level of TRIM58 was strongly associated with nuclear grade in both our samples and database, as well as with tumor stage in database. Although patients with higher T stages had higher methylation rates of TRIM58 than patients with lower T stages in our center, no statistical difference was found between them. We speculated that this was because of the small sample size of high T stage patients. In addition, ccRCC patients with high TRIM58 expression and hypomethylation levels of TRIM58 have better OS and DFS.

In vitro, we confirmed the methylation of TRIM58 in several RCC cell lines. RCC cells with low TRIM58 expression were found to be hypermethylated and the demethylation drug 5-AZA upregulated the expression of TRIM58, suggesting that the low expression of TRIM58 in ccRCC was probably induced by promoter methylation. We found TRIM58 was frequently inactivated and methylated in RCC cell lines and in primary RCC tissues. Thus, we investigated whether TRIM58 demethylation is capable of activating transcription. To target specific epigenetic alterations in cancer cells, we selected the CRISPR-dCas9 system. CRISPR-dCas9 was derived from the CRISPR-Cas9 system, and has been used in many fields such as gene regulation, epigenetic regulation and high throughput screening. dCas9 lacks nuclease activity but maintains its ability to bind both the sgRNA and targeted DNA. Several groups have developed modified versions of Cas9 for applications that go beyond genome editing (Bikard et al., 2013; Chavez et al., 2015; Kardooni et al., 2018). Here, we used dCas9-TET1 and gRNAs targeting the TRIM58 gene promoter to induce DNA demethylaton and activate transcription.

In lung squamous cell carcinoma, TRIM58 methylation is associated with eight prognostic genes, and may be used as a potential prognostic biomarker (Zhang et al., 2018). In gastric cancer, TRIM58 may function as a tumor suppressor and potentially suppress the tumor growth (Liu et al., 2020). In early-stage lung adenocarcinoma, TRIM58 was robustly silenced by hypermethylation and the restoration of TRIM58 expression in cell lines inhibited cell growth *in vitro* and *in vivo* (Kajiura et al., 2017). In the present study, we have provided evidence to demonstrate that TRIM58-TET1 induced demethylation could directly inhibit proliferation and migration of cancer cells *in vitro*. These facts strongly implicate the inactivation of TRIM58 by DNA methylation as a possible promoter of proliferation and migration in RCC.

MATERIALS AND METHODS

Patients and Tissue Specimen Collection

92 primary clear cell renal cell carcinoma (ccRCC) samples and 22 adjacent non-malignant renal tissues with patients' informed consent were obtained from the Urology Department of Peking University First Hospital (PKUFH), Beijing, China. This study followed the Helsinki declaration and was approved by the Institutional Ethical Review Board of PKUFH. Samples were collected immediately in the operating room after surgical removal and were stored in liquid nitrogen after rapid freezing in liquid nitrogen. The pathological diagnosis was made by professional urological pathologists.

Further, mRNA expression and clinical information for 530 kidney renal clear cell carcinoma (KIRC) patients with available RNA-sequence data were downloaded from The Cancer Genome Atlas (TCGA). Methylation data (Illumina Human Methylation 450K BeadChip) of 317 KIRC patients were downloaded from UALCAN (http://ualcan.path.uab.edu/).

Cell Lines Culture and Demethylation Treatment

RCC cell lines (786-O, 769-P, ACHN and OS-RC-2) were used in this study. HK-2 human kidney proximal tubular epithelial cells were used as normal controls. These cell lines were purchased from the American Type Culture Collection (ATCC, Manassas, VA, United States) and National Infrastructure of Cell Line Resource, China. Cell lines were routinely cultured in RPMI 1640 or DMEM, which was supplemented with 10% fetal bovine serum (Invitrogen, Carlsbad, CA, United States) and incubated in a 5% CO_2 environment at 37°C. These cells were split to a low density (30% confluence) for 12 h before drug treatment, then incubated with 5-aza-2′-deoxycytidine (5-Aza; Sigma, St. Louis, MO, United States) at a concentration of 10 μM in the optional medium, which was exchanged every 24 h. After 5-Aza treatment for 72 h, the cells were harvested for further analysis.

Construction of Vectors and Transfection

The sequences of the TRIM58 gene promoter region containing the CpG islands were extracted using the UCSC genome browser.

TABLE 2 | Primers for RT-qPCR, MSP, BGS and sequence of gRNAs.

Target	Sequence (5′-3′)	Application
TRIM58	F: GGTGTGTTTGGATTTTTTGTAGGAG R: CCACAACCAAAACAAAAAAACC	RT-qPCR
GAPDH	F: GGAGCGAGATCCCTCCAAAAT R: GGCTGTTGTCATACTTCTCATGG	RT-qPCR
TRIM58	M-F: CGTTTACGTTTGTTCGTAGTGTC M-U: CAAAAACGACTCAAATCCTCG	MSP
TRIM58	U-F: TGTTTATGTTTGTTTGTAGTGTTG U-R: CAAAAACAACTCAAATCCTCACC	MSP
TRIM58	F: GAGGAGGGATTTTAGTTAGAAATGTTT R: ACTCCTACAAAAAATCCAAACACAC	BGS
TRIM58-sgRNA-1	F: TTGGGTACGTTTGTTCGTAGTGTCGGGGC R: GAACAACCCATGCAAACAAGCATCACAGC CCCGAGCT	dcas9-TET1CD
TRIM58-sgRNA-2	F: TTGGGAGTCGGTTAGCGTGGATTGGGGC R: GAACAACCCTCAGCCAATCGCACCTAAC CCCGAGCT	dcas9-TET1CD
TRIM58-sgRNA-3	F: TTGGGCCTCGGGCTTTCGCCCCAACGGGC R: GAACAACCCCGGTTGGGGCGAAAGCCCGA CCCGAGCT	dcas9-TET1CD
TRIM58-sgRNA-4	F: TTGGGCGGGCCTGGTGGAGAGCGTGGGGC R: GAACAACCCCACGCTCTCCACCAGGCCCG CCCGAGCT	dcas9-TET1CD
TRIM58-sgRNA-NC	F:TTGGGGTAATGCCTGGCTTGTCGACGCATAGTCTGGGGC R:GAACAACCCCAGACTATGCGTCGACAAGCCAGGCATTACCCCGAGCT	dcas9-TET1CD

The CRISPR dCas9 plasmid dCas9-Tet1CD (#84475) and pgRNA-humanized (#44248) were purchased from Addgene. Four gRNAs that target the TRIM58 promoter were cloned into pgRNA-humanized and listed in **Table 2**. All designed gRNAs were subjected to MEGABLAST (https://blast.ncbi.nlm.nih.gov/Blast.cgi) to avoid mismatch to unexpected genes in the human genome.

DNA and RNA Extraction

Total RNA and genomic DNA of primary RCC tissues and cell lines were extracted using an RNA-easy Isolation Reagent (Vazyme Biotech, Nanjing, China) and TIANamp Genomic DNA Kits (TIANGEN, Shanghai, China) according to their instructions, respectively, as previously described (Zhang et al., 2014; Wang et al., 2019).

Bisulfite Treatment and Promoter Methylation Analysis

The bisulfite modification of genomic DNA was performed using the EZ DNA Methylation-Gold™ Kit (Zymo Research, Menlo Park, CA, United States). Methylation specific PCR (MSP) and bisulfite genomic sequencing (BGS) were used to analyze methylation status of TRIM58 promoter region. The primers for TRIM58 used for MSP and BGS were listed in **Table 2**. For BGS, PCR products were subcloned into the fast-T1 clone vector (Vazyme Biotech, Nanjing, China) and 8–10 colonies were randomly selected and sequenced.

Quantitative RT-PCR, Western Blot and Immunohistochemistry Staining of TRIM58 Expression

cDNA was synthesized using HiScript III RT SuperMix for qPCR (Vazyme Biotech, Nanjing, China). qRT-PCR was performed using spectrophotometry (ABI Prism 7500TM instrument, Applied Biosystems) with Universal SYBR Green qPCR Master Mix (Vazyme Biotech, Nanjing, China). Glyceraldehyde 3-phosphate dehydrogenase (GAPDH) was used as reference gene. Primers used for TRIM58 and GAPDH qRT-PCR were listed in **Table 2**.

Total protein was extracted by KeyGEN Bio TECH protein extraction kit (KGP1100) and separated on 10% SDS-PAGE and transferred onto nitrocellulose membrane. After blocking, blots were immunostained with primary antibodies and secondary antibodies respectively as previously described (Wang et al., 2017). The antibodies were as follows: TRIM58 (ab254786, Abcam, 1:500); GAPDH (0494-1-AP, proteinteach, 1:10000).

Immunohistochemistry staining was performed using a primary antibody of TRIM58 (ab254786, Abcam) at a 1:300 dilution following a protocol described previously (Liu et al., 2015). All photographs were taken randomly and measured using Image Pro Plus (Media Cybernetics, Rockville, MD, United States).

Wound-Healing Assay

The cell motility was assessed by scratch wound healing assay. 786-O and OS-RC-2 cells ($2–3\times10^6$ per well) were plated in a 6-well plate for 1 day and then transfected with vectors for 24 h. The cell layers were washed with PBS after carefully scratching by sterile tips. After incubation for 0 and 24 h, photos were taken. The assays were performed in triplicate.

Transwell Migration Assay

The 786-O and OS-RC-2 cells suspended in 150 uL serum-free medium (2×10^5 cells/mL) were placed on the upper layer of a cell permeable membrane. Following another 24–48 h incubation, the cells migrated through the membrane were stained with 1% Crystal Violet and counted.

Statistical Analysis

When comparing two groups of measurement data, *t* test was used for data conforming to normal distribution, whereas a Wilcoxon test was used for data not conforming to normal distribution, and the measurement data were expressed as the mean ± standard deviation (SD). A Chi-square test was used to analyze comparisons between groups for enumeration data. Pearson correlation analysis was used to investigate the relationship between mRNA expression levels and methylation levels of TRIM58. The Kaplan–Meier method was used for survival analysis, and a log-rank test was applied for comparations between groups. R packages used in this study included "GDCRNATools," "clusterProfiler," "org.Hs.eg.db," "tidyr," "dplyr," "ggplot2," "ggsignif," "survival," and "survimier." Annotation gene sets used in GSEA were hallmark gene sets from the Molecular Signatures Database (MSigDB). All statistical analyses were performed and visualized using RStudio (Version1.2.1335, Boston, MA, United States), GSEA (Version4.0, UC San Diego and Broad Institute, United States) 23, Medcalc (Version16.8, Ostend, Belgium), and GraphPad Prism (Version 8.0, GraphPad, Inc., La Jolla, CA, United States). A two-tailed $p < 0.05$ was considered statistically significant.

DATA AVAILABILITY STATEMENT

The original contributions presented in the study are included in the article/**Supplementary Material**, further inquiries can be directed to the corresponding author.

ETHICS STATEMENT

The studies involving human participants were reviewed and approved by the Ethics Committee of Peking University First Hospital. The patients/participants provided their written informed consent to participate in this study.

AUTHOR CONTRIBUTIONS

YG, CC, and AL designed the project and wrote the manuscript. YG, CC, AL, HS, GK, BM and QuZ performed experiments and data analysis. QiZ and YG supervised the project and provided financial support for the project. All authors contributed to the article and approved the submitted version.

FUNDING

This work was supported by grants from the National Natural Science Foundation of China to Qi.Z. (No. 82072826 and 81872088).

SUPPLEMENTARY MATERIAL

The Supplementary Material for this article can be found online at: https://www.frontiersin.org/articles/10.3389/fmolb.2021.655126/full#supplementary-material.

REFERENCES

Alt, A. L., Boorjian, S. A., Lohse, C. M., Costello, B. A., Leibovich, B. C., and Blute, M. L. (2011). Survival after complete surgical resection of multiple metastases from renal cell carcinoma. *Cancer* 117, 2873–2882. doi:10.1002/cncr.25836

Bikard, D., Jiang, W., Samai, P., Hochschild, A., Zhang, F., and Marraffini, L. A. (2013). Programmable repression and activation of bacterial gene expression using an engineered CRISPR-Cas system. *Nucleic Acids Res.* 41, 7429–7437. doi:10.1093/nar/gkt520

Bray, F., Ferlay, J., Soerjomataram, I., Siegel, R. L., Torre, L. A., and Jemal, A. (2018). Global cancer statistics 2018: GLOBOCAN estimates of incidence and mortality worldwide for 36 cancers in 185 countries. *CA Cancer J. Clin.* 68, 394–424. doi:10.3322/caac.21492

Chavez, A., Scheiman, J., Vora, S., Pruitt, B. W., Tuttle, M., RIE, P., et al. (2015). Highly efficient Cas9-mediated transcriptional programming. *Nat. Methods* 12, 326–328. doi:10.1038/nmeth.3312

Christoph, F., Weikert, S., Kempkensteffen, C., Krause, H., Schostak, M., Köllermann, J., et al. (2006). Promoter hypermethylation profile of kidney cancer with new proapoptotic p53 target genes and clinical implications. *Clin. Cancer Res.* 12, 5040–5046. doi:10.1158/1078-0432.CCR-06-0144

Ferlay, J., Soerjomataram, I., Dikshit, R., Eser, S., Mathers, C., Rebelo, M., et al. (2015). Cancer incidence and mortality worldwide: sources, methods and major patterns in GLOBOCAN 2012. *Int. J. Cancer* 136, E359–E386. doi:10.1002/ijc.29210

Gallego-Bartolome, J., Gardiner, J., Liu, W., Papikian, A., Ghoshal, B., Kuo, H. Y., et al. (2018). Targeted DNA demethylation of the arabidopsis genome using the human TET1 catalytic domain. *Proc. Natl. Acad. Sci. U.S.A.* 115, E2125–E2134. doi:10.1073/pnas.1716945115

Hatakeyama, S. (2011). TRIM proteins and cancer. *Nat. Rev. Cancer* 11, 792–804. doi:10.1038/nrc3139

He, W., Li, X., Xu, S., Ai, J., Gong, Y., Gregg, J. L., et al. (2013). Aberrant methylation and loss of CADM2 tumor suppressor expression is associated with human renal cell carcinoma tumor progression. *Biochem. Biophys. Res. Commun.* 435, 526–532. doi:10.1016/j.bbrc.2013.04.074

Hirata, H., Hinoda, Y., Nakajima, K., Kawamoto, K., Kikuno, N., Ueno, K., et al. (2011). Wnt antagonist DKK1 acts as a tumor suppressor gene that induces apoptosis and inhibits proliferation in human renal cell carcinoma. *Int. J. Cancer* 128, 1793–1803. doi:10.1002/ijc.25507

Joosten, S. C., Smits, K. M., Aarts, M. J., Melotte, V., Koch, A., Tjan-Heijnen, V. C., et al. (2018). Epigenetics in renal cell cancer: mechanisms and clinical applications. *Nat. Rev. Urol.* 15, 430–451. doi:10.1038/s41585-018-0023-z

Kajiura, K., Masuda, K., Naruto, T., Kohmoto, T., Watabnabe, M., Tsuboi, M., et al. (2017). Frequent silencing of the candidate tumor suppressor TRIM58 by promoter methylation in early-stage lung adenocarcinoma. *Oncotarget* 8, 2890–2905. doi:10.18632/oncotarget.13761

Kardooni, H., Gonzalez-Gualda, E., Stylianakis, E., Saffaran, S., Waxman, J., and Kypta, R. M. (2018). CRISPR-mediated reactivation of DKK3 expression attenuates TGF-β signaling in prostate cancer. *Cancers* 10 (6), 165. doi:10.3390/cancers10060165

Klutstein, M., Nejman, D., Greenfield, R., and Cedar, H. (2016). DNA methylation in cancer and aging. *Cancer Res.* 76, 3446–3450. doi:10.1158/0008-5472.CAN-15-3278

Linehan, W. M., and Ricketts, C. J. (2014). Decade in review-kidney cancer: discoveries, therapies and opportunities. *Nat. Rev. Urol.* 11, 614–616. doi:10.1038/nrurol.2014.262

Liu, M., Zhang, X., Cai, J., Li, Y., Luo, Q., Wu, H., et al. (2018). Downregulation of TRIM58 expression is associated with a poor patient outcome and enhances colorectal cancer cell invasion. *Oncol. Rep.* 40, 1251–1260. doi:10.3892/or.2018.6525

Liu, Q., Jin, J., Ying, J., Sun, M., Cui, Y., Zhang, L., et al. (2015). Frequent epigenetic suppression of tumor suppressor gene glutathione peroxidase 3 by promoter

hypermethylation and its clinical implication in clear cell renal cell carcinoma. *Int. J. Mol. Sci.* 16, 10636–10649. doi:10.3390/ijms160510636

Liu, X., Long, Z., Cai, H., Yu, S., and Wu, J. (2020). TRIM58 suppresses the tumor growth in gastric cancer by inactivation of β-catenin signaling via ubiquitination. *Cancer Biol. Ther.* 21, 203–212. doi:10.1080/15384047.2019.1679554

Liu, X. S., Wu, H., Krzisch, M., Wu, X., Graef, J., Muffat, J., et al. (2018). Rescue of fragile x syndrome neurons by DNA methylation editing of the FMR1 gene. *Cell* 172, 979–992. doi:10.1016/j.cell.2018.01.012

Malouf, G. G., Su, X., Zhang, J., Creighton, C. J., Ho, T. H., Lu, Y., et al. (2016). DNA methylation signature reveals cell ontogeny of renal cell carcinomas. *Clin. Cancer Res.* 22, 6236–6246. doi:10.1158/1078-0432.CCR-15-1217

Moch, H. (2013). An overview of renal cell cancer: pathology and genetics. *Semin. Cancer Biol.* 23, 3–9. doi:10.1016/j.semcancer.2012.06.006

Morita, S., Noguchi, H., Horii, T., Nakabayashi, K., Kimura, M., Okamura, K., et al. (2016). Targeted DNA demethylation *in vivo* using dCas9-peptide repeat and scFv-TET1 catalytic domain fusions. *Nat. Biotechnol.* 34, 1060–1065. doi:10.1038/nbt.3658

Morris, M. R., and Latif, F. (2017). The epigenetic landscape of renal cancer. *Nat. Rev. Nephrol.* 13, 47–60. doi:10.1038/nrneph.2016.168

Morrissey, C., Martinez, A., Zatyka, M., Agathanggelou, A., Honorio, S., Astuti, D., et al. (2001). Epigenetic inactivation of the RASSF1A 3p21.3 tumor suppressor gene in both clear cell and papillary renal cell carcinoma. *Cancer Res.* 61, 7277–7281.

Ricketts, C. J., De Cubas, A. A., Fan, H., Smith, C. C., Lang, M., Reznik, E., et al. (2018). The cancer genome atlas comprehensive molecular characterization of renal cell carcinoma. *Cell Rep.* 23, 313–326. doi:10.1016/j.celrep.2018.03.075

Ricketts, C. J., Hill, V. K., and Linehan, W. M. (2014). Tumor-specific hypermethylation of epigenetic biomarkers, including SFRP1, predicts for poorer survival in patients from the TCGA kidney renal clear cell carcinoma (KIRC) project. *PLoS One* 9, e85621. doi:10.1371/journal.pone.0085621

Sasaki, H., and Matsui, Y. (2008). Epigenetic events in mammalian germ-cell development: reprogramming and beyond. *Nat. Rev. Genet.* 9, 129–140. doi:10.1038/nrg2295

Sharma, S., Kelly, T. K., and Jones, P. A. (2010). Epigenetics in cancer. *Carcinogenesis* 31, 27–36. doi:10.1093/carcin/bgp220

Tao, R., Li, J., Xin, J., Wu, J., Guo, J., Zhang, L., et al. (2011). Methylation profile of single hepatocytes derived from hepatitis B virus-related hepatocellular carcinoma. *PLoS One* 6, e19862. doi:10.1371/journal.pone.0019862

Vojta, A., Dobrinić, P., Tadić, V., Bočkor, L., Korać, P., Julg, B., et al. (2016). Repurposing the CRISPR-Cas9 system for targeted DNA methylation. *Nucleic Acids Res.* 44, 5615–5628. doi:10.1093/nar/gkw159

Wang, L., Cui, Y., Sheng, J., Yang, Y., Kuang, G., Fan, Y., et al. (2017). Epigenetic inactivation of HOXA11, a novel functional tumor suppressor for renal cell carcinoma, is associated with RCC TNM classification. *Oncotarget* 8, 21861–21870. doi:10.18632/oncotarget.15668

Wang, L., Fan, Y., Zhang, L., Li, L., Kuang, G., Luo, C., et al. (2019). Classic SRY-box protein SOX7 functions as a tumor suppressor regulating WNT signaling and is methylated in renal cell carcinoma. *Faseb J.* 33, 254–263. doi:10.1096/fj.201701453RR

Xu, R., Xu, Q., Huang, G., Yin, X., Zhu, J., Peng, Y., et al. (2019). Combined analysis of the aberrant epigenetic alteration of pancreatic ductal adenocarcinoma. *Biomed. Res. Int.* 2019, 9379864. doi:10.1155/2019/9379864

Xu, X., Tao, Y., Gao, X., Zhang, L., Li, X., Zou, W., et al. (2016). A CRISPR-based approach for targeted DNA demethylation. *Cell Discov.* 2, 16009. doi:10.1038/celldisc.2016.9

Yin, X., and Xu, Y. (2016). Structure and function of TET enzymes. *Adv. Exp. Med. Biol.* 945, 275–302. doi:10.1007/978-3-319-43624-1_12

Zhang, Q., Ying, J., Li, J., Fan, Y., Poon, F. F., Ng, K. M., et al. (2010). Aberrant promoter methylation of DLEC1, a critical 3p22 tumor suppressor for renal cell carcinoma, is associated with more advanced tumor stage. *J. Urol.* 184, 731–737. doi:10.1016/j.juro.2010.03.108

Zhang, Q., Ying, J., Zhang, K., Li, H., Ng, K. M., Zhao, Y., et al. (2007). Aberrant methylation of the 8p22 tumor suppressor gene DLC1 in renal cell carcinoma. *Cancer Lett.* 249, 220–226. doi:10.1016/j.canlet.2006.08.019

Zhang, Q., Zhang, L., Li, L., Wang, Z., Ying, J., Fan, Y., et al. (2014). Interferon regulatory factor 8 functions as a tumor suppressor in renal cell carcinoma and its promoter methylation is associated with patient poor prognosis. *Cancer Lett.* 354, 227–234. doi:10.1016/j.canlet.2014.07.040

Zhang, W., Cui, Q., Qu, W., Ding, X., Jiang, D., and Liu, H. (2018). TRIM58/cg26157385 methylation is associated with eight prognostic genes in lung squamous cell carcinoma. *Oncol. Rep.* 40, 206–216. doi:10.3892/or.2018.6426

Conflict of Interest: The authors declare that the research was conducted in the absence of any commercial or financial relationships that could be construed as a potential conflict of interest.

frontiers in Molecular Biosciences

ORIGINAL RESEARCH
published: 19 March 2021
doi: 10.3389/fmolb.2021.646412

Engineered CRISPR/Cas13d Sensing hTERT Selectively Inhibits the Progression of Bladder Cancer *In Vitro*

Chengle Zhuang[1†], Changshui Zhuang[2†], Qun Zhou[3†], Xueting Huang[4], Yaoting Gui[1], Yongqing Lai[1] and Shangqi Yang[1]**

[1]Department of Urology, Peking University Shenzhen Hospital, Shenzhen, China, [2]Department of Urology, Union Shenzhen Hospital, Huazhong University of Science and Technology, Shenzhen, China, [3]Department of Urology, the Affiliated Nanhua Hospital of University of South China, Hengyang, China, [4]Department of Nephrorheumatology, Shenzhen Yantian District People's Hospital, Shenzhen, China

Aptazyme and CRISPR/Cas gene editing system were widely used for regulating gene expression in various diseases, including cancer. This work aimed to reconstruct CRISPR/Cas13d tool for sensing hTERT exclusively based on the new device OFF-switch hTERT aptazyme that was inserted into the 3' UTR of the Cas13d. In bladder cancer cells, hTERT ligand bound to aptamer in OFF-switch hTERT aptazyme to inhibit the degradation of Cas13d. Results showed that engineered CRISPR/Cas13d sensing hTERT suppressed cell proliferation, migration, invasion and induced cell apoptosis in bladder cancer 5637 and T24 cells without affecting normal HFF cells. In short, we constructed engineered CRISPR/Cas13d sensing hTERT selectively inhibited the progression of bladder cancer cells significantly. It may serve as a promising specifically effective therapy for bladder cancer cells.

Keywords: CRISPR/Cas13d, hTERT, bladder cancer, aptazyme, degradation

OPEN ACCESS

Edited by:
Tao Xu,
Anhui Medical University, China

Reviewed by:
Yuhan Chen,
Southern Medical University, China
Qing Zhou,
Chinese Academy of Sciences (CAS), China

****Correspondence:***
Yongqing Lai
yqlord@163.com
Shangqi Yang
yangshangqi88@aliyun.com

†Those authors contributed equally to this work

Specialty section:
This article was submitted to Molecular Diagnostics and Therapeutics, a section of the journal Frontiers in Molecular Biosciences

Received: *26 December 2020*
Accepted: *01 February 2021*
Published: *19 March 2021*

Citation:
Zhuang C, Zhuang C, Zhou Q, Huang X, Gui Y, Lai Y and Yang S (2021) Engineered CRISPR/Cas13d Sensing hTERT Selectively Inhibits the Progression of Bladder Cancer In Vitro. *Front. Mol. Biosci. 8:646412. doi: 10.3389/fmolb.2021.646412*

INTRODUCTION

Bladder cancer is one of the most common urologic neoplasms all over the world (Siegel et al., 2020). About 50% of bladder cancer patients will develop metastases within two years after diagnosis of bladder cancer (Sternberg et al., 2013). For bladder cancer patients with advanced metastasis, chemotherapy is the main treatment (Lenis et al., 2020). However, severe adverse reactions are caused due to poor specificity of chemotherapy drugs (Lenis et al., 2020). Thus, finding a highly specific targeted therapy for bladder cancer is of great value for bladder cancer patients.

Gene expression can be controlled by various tools including ligand-dependent small self-cleaving ribozymes (Lee et al., 2016). These ribozymes are named as aptazymes with properties of small, modular and no need of regulatory protein factors and have promising use in clinical applications (Felletti et al., 2016). Ribozyme platform, a communication module and aptamer are three main parts of the aptazymes (Nomura et al., 2012). The hammerhead ribozyme (HHR) is the common ribozyme platform (Zhong et al., 2016). When aptamer combines with ligand, the induced conformational change will be transferred to HHR via the communication module, generating cleavage activity (Spöring et al., 2020). OFF-switch and ON-switch are two types of aptazymes (Nomura et al., 2013; Beilstein et al., 2015; Yokobayashi, 2019). OFF-switch represents that gene expression is suppressed without corresponding ligand (Yokobayashi, 2019).

CRISPR/Cas13 is the class II type VI CRISPR (clustered regularly interspaced short palindromic repeats) gene editing tool (Huynh et al., 2020). A guide RNA (CRISPR-RNA, crRNA) and Cas13 are

two components in this system (Huynh et al., 2020). It can target RNA substrate instead of DNA (Makarova et al., 2020). There are four subtypes of Cas13, including Cas13a, Cas13b, Cas13c and Cas13d and Cas13d is the smallest protein (Makarova et al., 2020). Compared with RNA interference (RNAi), CRISPR/Cas13 shows high efficiencies and on-target effects (O'Connell, 2019). CRISPR/Cas13 has been used in various fields. For example, Gootenberg et al. (2017) . had created a CRISPR/Cas13a-based molecular detection platform to distinguish genotype human DNA, pathogenic bacteria and identify mutations in cell-free tumor DNA (Gootenberg et al., 2017). Wang et al. (2019). reported that the formation of glioma intracranial tumors in mice was inhibited significantly using the collateral effect of CRISPR/Cas13a (Wang et al., 2019). A recent study showed that lung cancer cell viability was decreased significantly via CRISPR/Cas13a targeting EML4-ALK (Saifullah et al., 2020).

In our previous studies, we have shown that compared with normal cells, hTERT only existed in bladder cancer cells and it may be regarded as a specific ligand in bladder cancer (Liu et al., 2014; Huang et al., 2017). In this study, engineered CRISPR/Cas13d was constructed to selectively suppress the progression of bladder cancer via sensing hTERT ligand. The hTERT OFF-switch aptazyme was synthesized and inserted into the 3'UTR of Cas13d. MYC is an oncogene in bladder cancer and crRNA was designed to target MYC. As we expected, engineered CRISPR/Cas13d inhibited the mRNA and protein levels of MYC, and thus suppressed cell proliferation, migration, invasion and induced apoptosis of bladder cancer cells *in vitro*. However, there was no effects in normal human foreskin fibroblast (HFF) cells. In short, engineered CRISPR/Cas13d sensing hTERT may be another highly effective approach for kill bladder cancer cells specifically.

MATERIALS AND METHODS

Cell Culture

Human foreskin fibroblast (HFF) was purchased from the Type Culture Collection of the Chinese Academy of Sciences, Shanghai, China. Human bladder cancer cell lines T24 and 5637 were purchased from the American Type Culture Collection (ATCC, Manassas, VA). T24 and 5637 were cultured from bladder cancer tissues with the histological grade of G3 and G2, respectively. These cells were cultured according to the manufacturer's protocol.

Cell Transfection

HFF or bladder cancer cells were seeded in plates. The corresponding plasmids were transfected into cells with Lipofectamine 3000 (Invitrogen, Carlsbad, CA, United States) according to the manufacturer's instructions.

RT-qPCR

TRIzol reagent was used to isolate total RNA from cells. A PrimeScript RT Reagent Kit with gDNA Eraser (Takara, Dalian, China) was utilized to synthesize the first strand of cDNA for detection of MYC and GAPDH. Quantitative PCR was then performed using the SYBR Premix Ex TaqTM kit (Takara, Dalian, China) on the Roche lightcycler 480 Real-Time PCR System. The comparative $2^{-\Delta\Delta CT}$ method was used to analyze the expression levels.

Vector Construction

Inactivated aptazyme sensing hTERT included hTERT aptamer and hammerhead ribozyme. The sequence of hTERT aptamer or hammerhead ribozyme was shown in the previous studies (Chen et al., 2010; Varshney et al., 2017). The sequence of hTERT aptamer is 5'-AGACAAGAAUAAAACGCUCAAUAUUGG GCUUUUAGCUUCUUGGUUGGAUAAUAGAUACACAUU CGACAGGAGGCUCACAACAGGC-3'. The inactivated aptazyme sensing hTERT was inserted into 3' UTR of the Cas13d (Addgene 109049) or downstream of the Renilla luciferase cassette in psiCHECK-2 (Promega). The crRNA targeting MYC mRNA was designed according to a previous study (Zhu et al., 2018). The sequence of crRNA used in this study was 5'-ACUCGCUGUAGUAAUUCCAGCGAGAGGCA-3'.

Luciferase Reporter Assay

The psiCHECK-2 vectors with inactivated aptazyme sensing hTERT were transfected into HFF or bladder cancer cells. Renilla and firefly luciferase activities were tested with the dual-luciferase reporter assay system (Promega, Madison, WI, United States) according to the user manuals.

Cell Proliferation Assays

Cell Counting Kit-8 (CCK-8) assay and colony formation assay were used to detect engineered CRISPR/Cas13d on cell proliferation. For CCK-8 assay, 2,000 cells/well were cultured in 96-well plates. 10 μl CCK-8 reagent was added to each well for 0.5 h. The absorbance was measured at 450 nm using a microplate reader. For colony formation assay, 1,000 cells/well were plated onto six-well plates, and were incubated at 37°C and 5% CO_2. After about 2°weeks, colonies were fixed using 0.05% crystal violet in 4% paraformaldehyde and counted using Image J program.

Cell Apoptosis Assay

The FITC Annexin V Apoptosis Detection Kit (TransGen, Peking, China) was utilized to double stain cells with FITC-Annexin V and PI according to the manufacturer's instructions. Right lower quadrant represents the percentage of early apoptosis cells.

Cell Migration and Invasion Assays

100% confluence of bladder cancer/normal cells were scratched via a sterile 200 μl pipette tip. Images were taken from per well at 0 and 24 h. The migration distance between 0 and 24 h in each group was calculated. For cell invasion assay, cells were seeded to the upper chambers of the Transwell (Millicell, Merk KGaA). After 24 h, cells on the underside chambers were fixed in 4% paraformaldehyde for 30 min and stained with 0.1% crystal violet for 30 min and captured using a microscope. Quantification of the migrated cells was performed by counting cell numbers.

Western Blot

RIPA Lysis Buffer (#P0013B; Beyotime) was used to extract protein. Protein concentrations were measured using

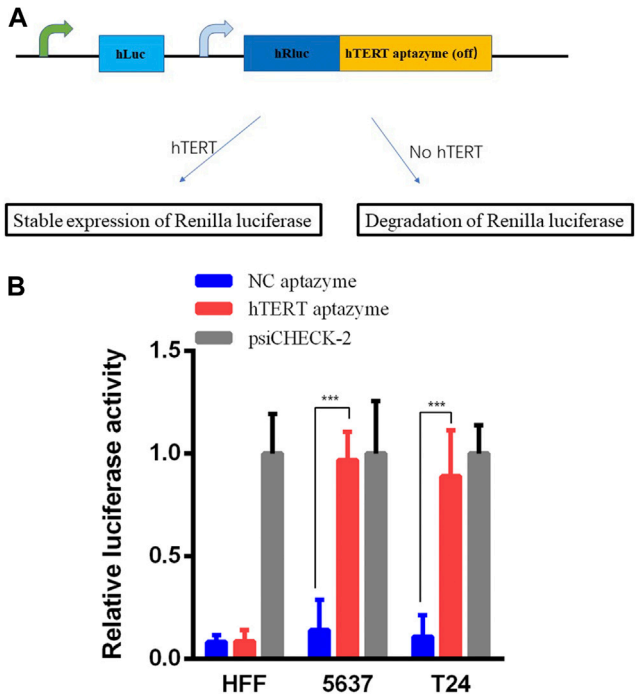

FIGURE 1 | Relative luciferase activities were stable expressed in hTERT aptazyme group compared with NC aptazyme **(A)** The hTERT aptazyme was inserted into the 3' UTR of Renilla luciferase gene and the schematic diagram of the hTERT aptazyme mode **(B)** Relative luciferase activities were stable expressed in hTERT aptazyme group in bladder cancer 5637 and T24 cells. However, Renilla luciferase was degraded significantly in normal cell HFF. *** represents $p < 0.001$.

Bicinchoninic Acid Kit (Sigma-Aldrich) according to the manufacturer's protocol. Cell lysates were resolved by SDS-PAGE and transferred onto PVDF membranes. Membranes were blocked for 1 h with 5% non-fat milk in TBST and incubated overnight at 4°C with primary antibodies and required secondary antibodies conjugated to horseradish peroxidase and developed by chemiluminescent substrates.

Statistical Analysis

All the above experiments were performed at least three times in this study. SPSS software version 22.0 (SPSS Inc., Chicago, IL, United States) was used to analyze all statistical analysis. All data are presented as the mean ± standard error (SD). Student's *t*-test, was used to analyze the group difference. A p-value < 0.05 (two-sided) was regarded as statistical significance.

RESULTS

The Expression of Renilla Luciferase Was Stable in Bladder Cancer Cells

The hTERT OFF-switch aptazyme was constructed as described in the Materials and Methods section. The hTERT aptazyme was synthesized and inserted into the 3'UTR of Renilla luciferase gene in psiCHECK-2 vector (**Figure 1A**). As shown in **Figure 1B**, compared with the NC aptazyme group, the relative luciferase activities of hTERT aptazyme group were no difference in HFF. However, the relative luciferase activities of hTERT aptazyme group was increased significantly in bladder cancer 5637 and T24 cells. It represents that hTERT ligand bound to OFF-switch aptazyme and restrained the degradation of Renilla luciferase.

Engineered CRISPR/Cas13d Sensing hTERT Selectively Suppressed the mRNA and Protein Levels of MYC

As shown in schematic diagram in **Figure 2A**, the sequence of hTERT OFF-switch aptazyme was inserted into the 3'UTR of Cas13d. The crRNA targeting oncogene MYC mRNA was designed. In HFF, the expression of hTERT ligand was very low or loss, and induces the degradation of Cas13d. However, Cas13d is highly expressed in cancer cells and with the guidance of crRNA targeting MYC mRNA, Cas13d binds to MYC mRNA results in degradation of MYC expression at mRNA and protein levels. Finally, the progression of bladder cancer is suppressed. In order to validate this mechanism of engineered CRISPR/Cas13d sensing hTERT, we detected the mRNA and protein expression levels of MYC. The MYC mRNA expression levels were decreased significantly between NC aptazyme and hTERT aptazyme group in bladder cancer 5637 and T24 cells. However, it was no difference in HFF (**Figure 2B**). Similarly, the MYC protein levels were selectively inhibited markedly in bladder cancer 5637 and T24 cells except HFF. In short, the mRNA and protein levels of MYC were restrained selectively in bladder cancer without affecting normal cells via engineered CRISPR/Cas13d sensing hTERT.

Bladder Cancer Cell Proliferation Was Selectively Inhibited by Engineered CRISPR/Cas13d Sensing hTERT

Next, the effects of engineered CRISPR/Cas13d sensing hTERT were detected in bladder cancer cells using CCK-8 and colony formation assay. Cell growth was not changed in HFF between NC aptazyme and hTERT aptazyme group (**Figure 3A**). However, compared with NC aptazyme set, cell proliferation of bladder cancer 5637 and T24 cells was suppressed significantly (**Figures 3B,C**). Analogously, colony formation was no difference between these two objects. Nonetheless, bladder cancer 5637 and T24 cell colony was inhibited dramatically between NC aptazyme and hTERT aptazyme group (**Figure 3D**). All in all, these results demonstrated that engineered CRISPR/Cas13d sensing hTERT selectively restrained bladder cancer cell proliferation.

Bladder Cancer Cell Apoptosis Was Selectively Promoted by Engineered CRISPR/Cas13d Sensing hTERT

The FITC Annexin V Apoptosis Detection Kit was used to measure the effects of engineered CRISPR/Cas13d on cell apoptosis in bladder cancer cells. As shown in **Figure 4A**, cell apoptosis was not changed between NC aptazyme and hTERT

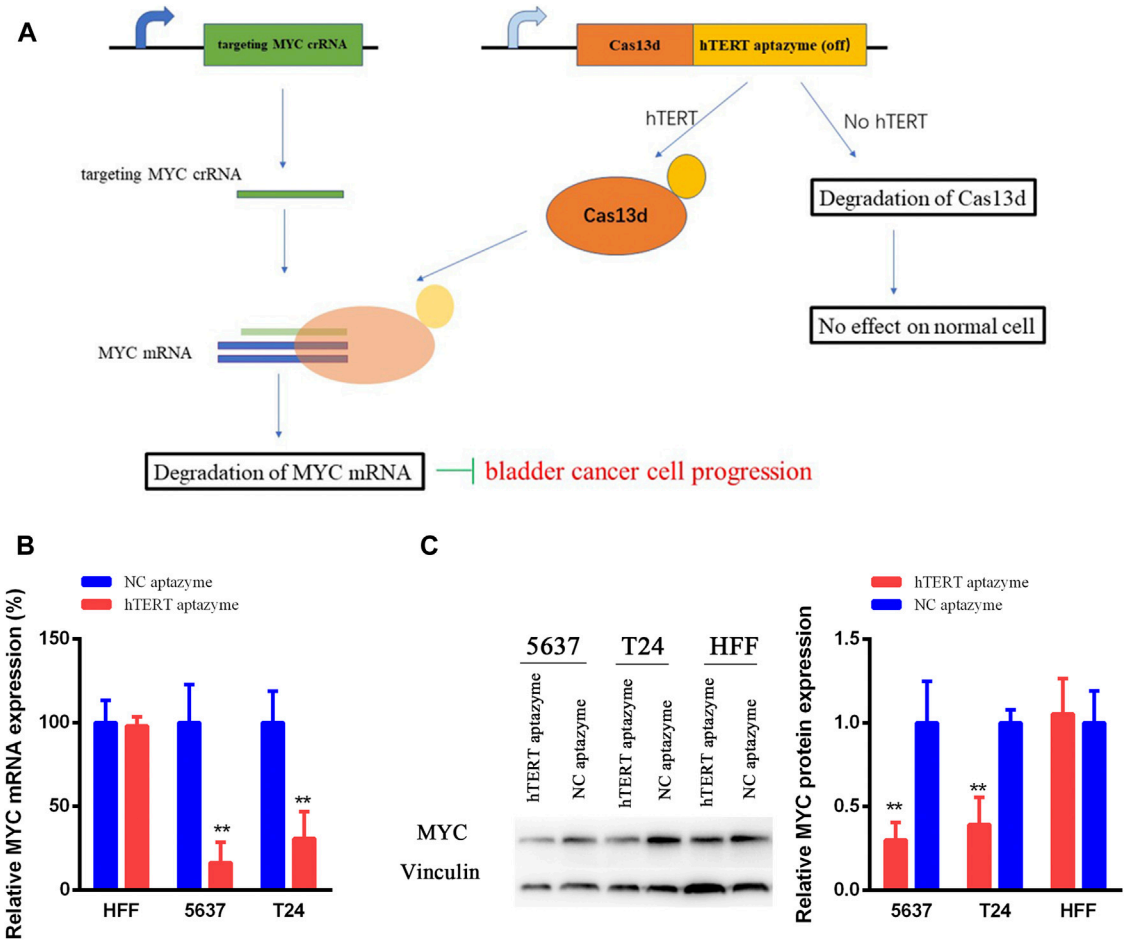

FIGURE 2 | Schematic diagram of engineered CRISPR/Cas13d sensing hTERT in bladder cancer **(A)** The working mechanism of engineered CRISPR/Cas13d sensing hTERT in bladder cancer cells **(B and C)** Engineered CRISPR/Cas13d sensing hTERT selectively suppressed the MYC mRNA and protein expression levels without affecting HFF. *represents $p < 0.05$, ** means $p < 0.01$.

aptazyme group. However, the cell apoptosis of hTERT aptazyme group was increased significantly compared with NC aptazyme object in bladder cancer 5637 cells (**Figure 4B**). Homoplastically, engineered CRISPR/Cas13d sensing hTERT promoted apoptosis obviously in bladder cancer T24 cells compared with the negative control (**Figure 4C**). In short, the above results illustrated that engineered CRISPR/Cas13d sensing hTERT selectively promoted bladder cancer cell apoptosis.

Bladder Cancer Cell Migration and Invasion Were Selectively Suppressed by Engineered CRISPR/Cas13d Sensing hTERT

Engineered CRISPR/Cas13d sensing hTERT had no effects on cell migration and invasion in HFF and bladder cancer cells (**Figures 5A,D–F**). However, cell migration and invasion were inhibited significantly via engineered CRISPR/Cas13d in bladder cancer 5637 and T24 cells (**Figures 5B–F**). These results demonstrated that engineered CRISPR/Cas13d sensing hTERT could selectively inhibit bladder cancer cell migration and invasion.

DISCUSSION

The role of hTERT was in-depth study in recent years and hTERT involves in the development of diseases including cancer. The hTERT is highly expressed in all human cancers except normal human cells (not include embryonic stem cells and germ cells) (Chen et al., 2020). Studies have demonstrated that hTERT maintains cancer cell immortalization and involves closely in cancer growth, metastasis and transformation (Liu et al., 2017; Chen et al., 2018b). Lots of studies have reported that hTERT is a promising cancer biomarker in various kinds of cancer (Shi et al., 2014; Chen et al., 2017). In our previous studies (Huang et al., 2017; Zhuang et al., 2017), we have validated that hTERT was only expressed in bladder cancer cells except normal cells HFF. The strategy of utilization of hTERT will be a valuable method to distinguish bladder cancer cells and normal cells.

Artificial riboswitch (aptazyme) has been used to regulate gene expression precisely via binding between RNA and

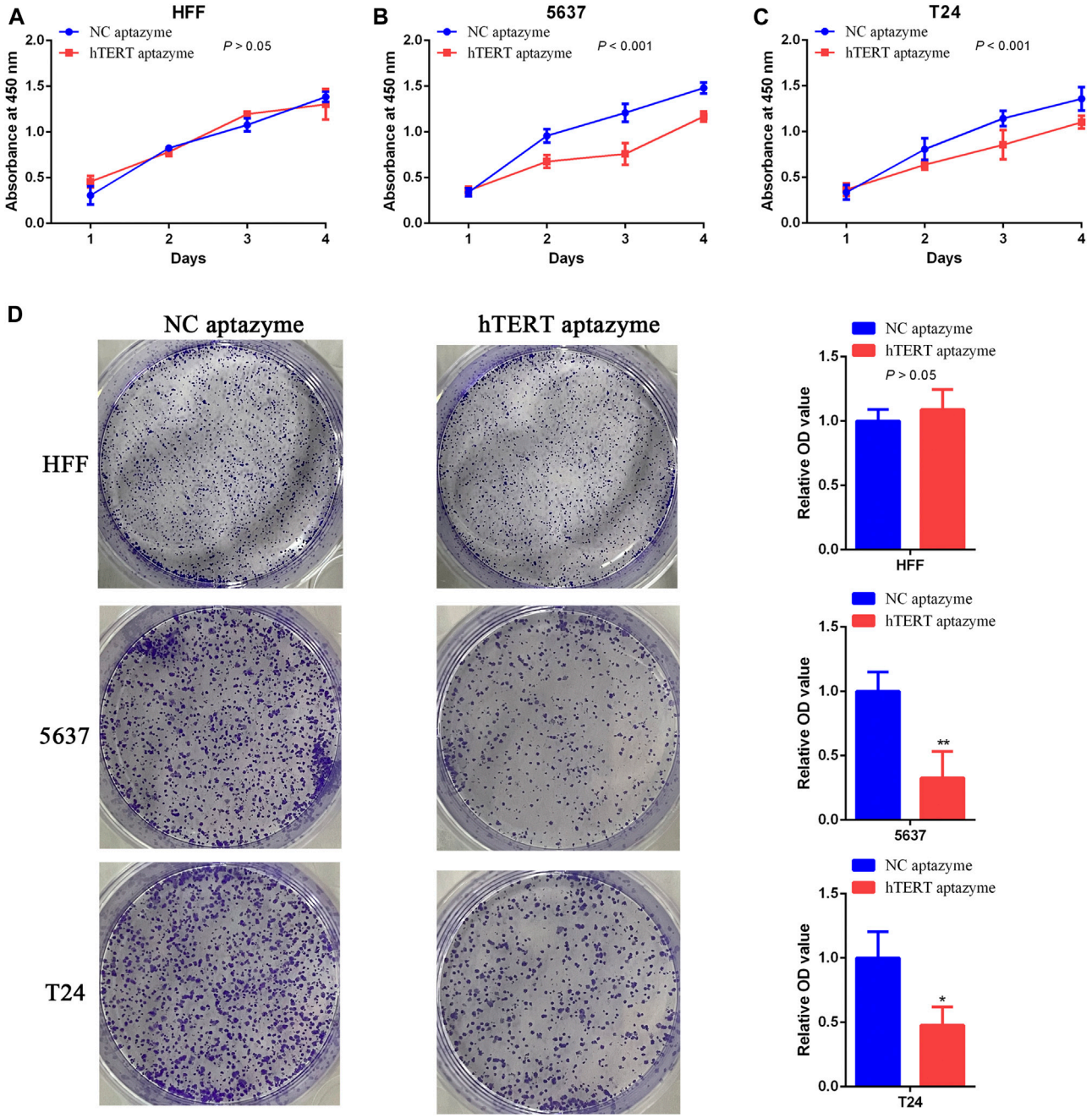

FIGURE 3 | Engineered CRISPR/Cas13d sensing hTERT selectively inhibited bladder cancer cell proliferation **(A–C)** Cell growth was suppressed by engineered CRISPR/Cas13d sensing hTERT without affecting HFF through CCK-8 assay **(D)** Results of colony formation assay illustrated that bladder cancer cell proliferation was selectively inhibited via engineered CRISPR/Cas13d sensing hTERT.

ligand (Pu et al., 2020). Aptazyme was utilized to control mRNA cleavage through self-cleavage within the mRNA (Takahashi and Yokobayashi, 2019; Spöring et al., 2020). Aptazyme can be inserted into 5' or 3' UTR of gene mRNA for controlling gene expression (Chen et al., 2018a). A previous study has reported that an optimal hTERT aptamer was synthesized, screened and can exclusively bind to hTERT *in vitro* and *in vivo* (Varshney et al., 2017).

Various studies demonstrated that CRISPR/Cas gene editing tools have been used for gene expression in cancer (Sharma et al., 2020). Targeting DNA of CRISPR/Cas9 system was widely reconstructed to create new gene circuits for cancer treatment (Liu et al., 2020). However,

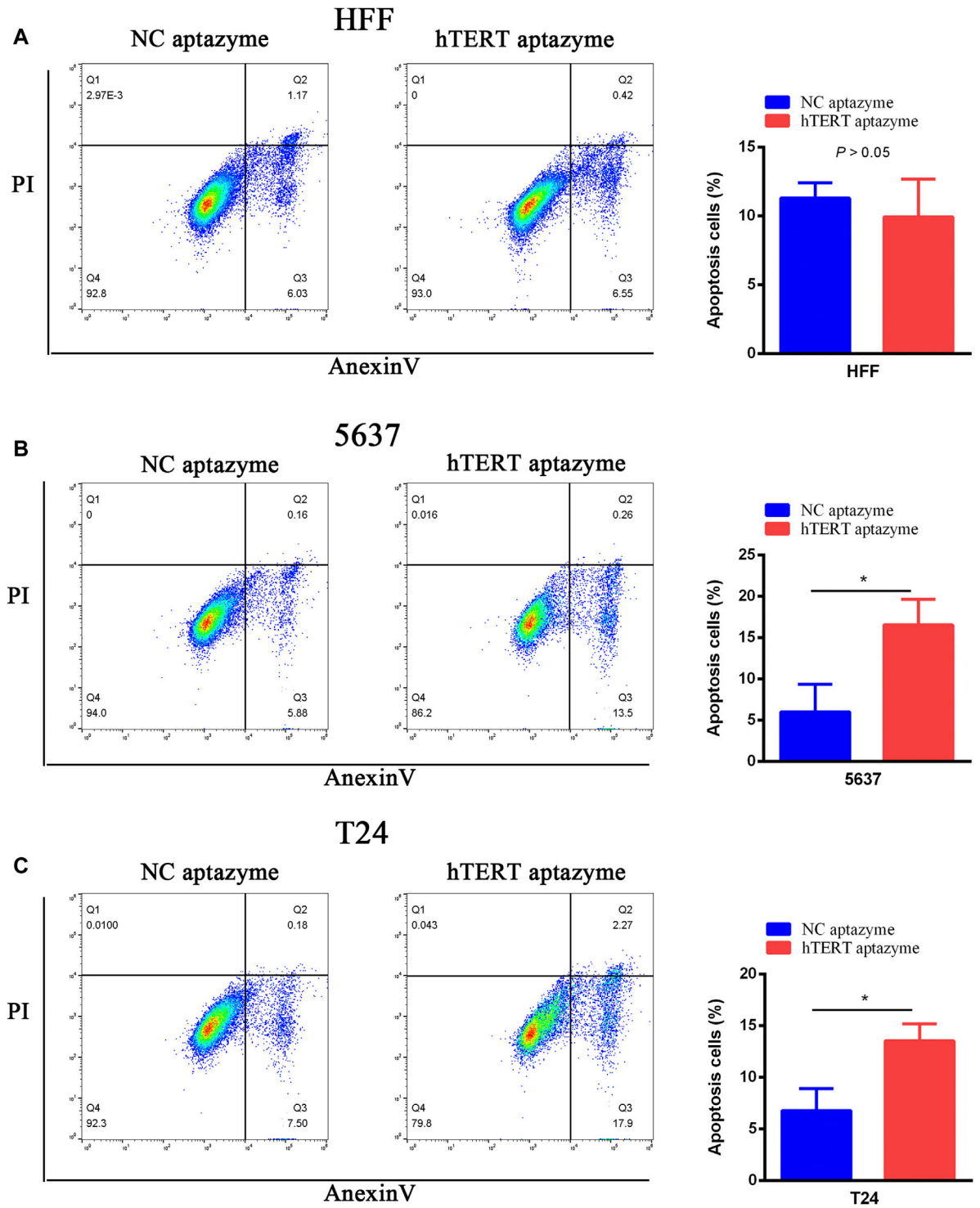

FIGURE 4 | Engineered CRISPR/Cas13d sensing hTERT selectively induced bladder cancer cell apoptosis. Engineered CRISPR/Cas13d sensing hTERT have no effects on apoptosis in HFF **(A)**. However, cell apoptosis was significantly increased by engineered CRISPR/Cas13d sensing hTERT in bladder cancer 5637 **(B)** and T24 **(C)** cells.

high off-target effect is inevitable for CRISPR/Cas9 (Pruett-Miller, 2020). CRISPR/Cas13d was another gene editing method to targeting RNA molecules (Lin et al., 2020). It showed higher efficiencies and on-target effects in cells (Lin et al., 2020). In this study, we synthesized the OFF-switch hTERT aptazyme and inserted into 3'UTR of the Cas13d

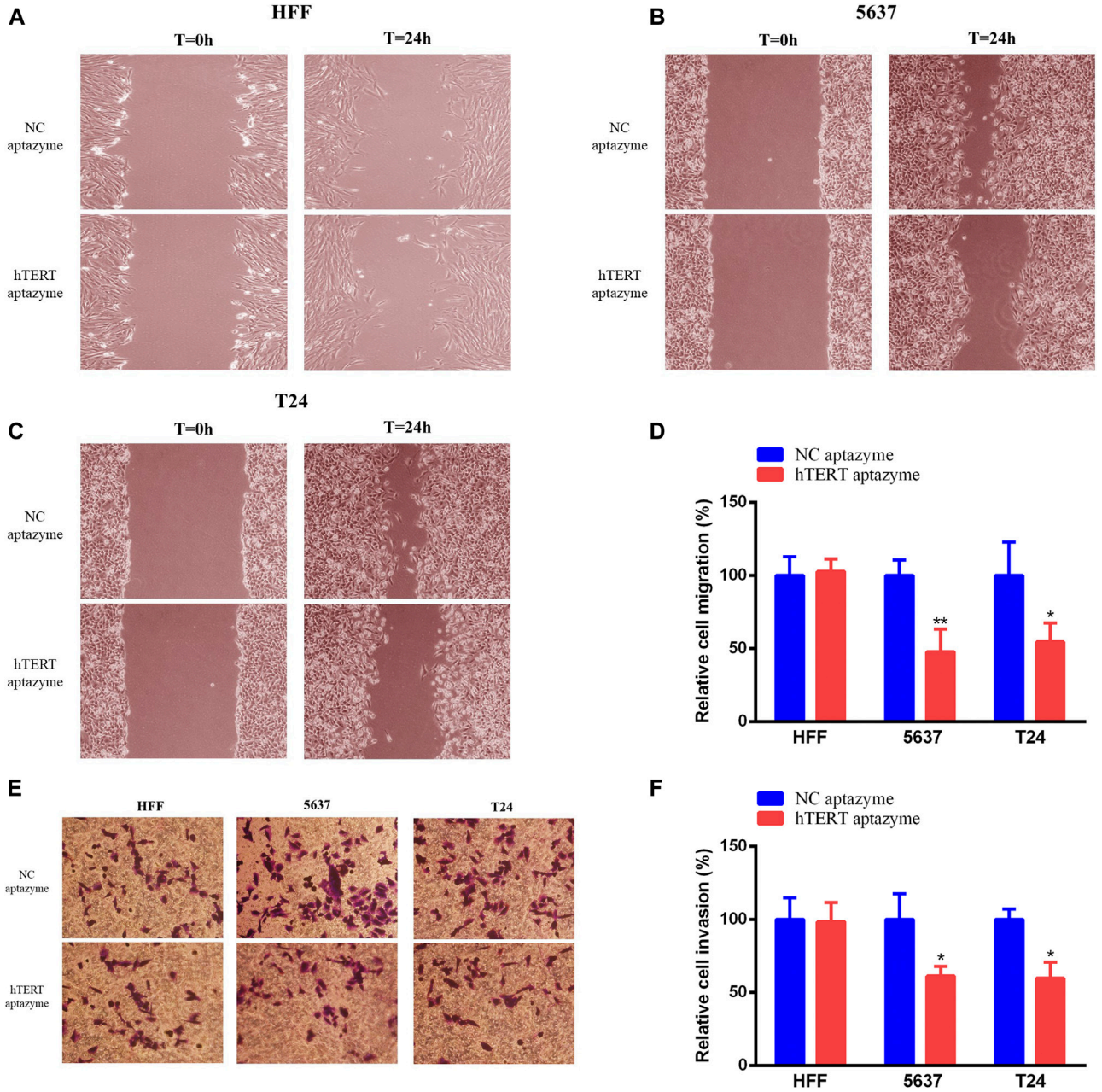

FIGURE 5 | Engineered CRISPR/Cas13d sensing hTERT selectively suppressed bladder cancer cell migration and invasion. Engineered CRISPR/Cas13d sensing hTERT have no effects on cell migration and invasion in HFF **(A,E,F)**. However, cell migration and invasion were significantly suppressed by engineered CRISPR/Cas13d sensing hTERT in bladder cancer 5637 and T24 cells **(B–F)**.

according to previous studies. When hTERT existed in cells, hTERT bound to OFF-switch hTERT aptazyme and restrained the degradation of Cas13d. On the contrary, Cas13d was degraded without hTERT in normal cells. This engineered CRISPR/Cas13d sensing hTERT was tested in bladder cancer 5637 and T24 cells in this subject. Results showed that engineered CRISPR/Cas13d sensing hTERT selectively suppressed the progression of bladder cancer cells except normal cell HFF. However, deficiencies of this study still existed. The protein expression levels of Cas13d were not shown in this study owing to lack of Cas13d antibody at present. The role of engineered CRISPR/Cas13d sensing hTERT *in vivo* is lack. We will further confirm this *in vivo* effect in the near future.

In short, engineered CRISPR/Cas13d sensing hTERT was constructed and selectively suppressed the progression of bladder cancer cells. It may provide a promising precise exclusively method for bladder cancer.

Data Availability Statement

The original contributions presented in the study are included in the article/Supplementary Material, further inquiries can be directed to the corresponding authors.

AUTHOR CONTRIBUTIONS

CLZ, CSZ, and QZ conceived the project, designed and performed the research; XH provided assistance in some experiments and reviewing of the manuscript; YG, YL, and SY provided financial support.

FUNDING

This research was supported by the "San-ming" Project of Medicine in Shenzhen (SZSM201612066) and Research Foundation of Peking University Shenzhen Hospital (JCYJ2020005).

ACKNOWLEDGMENTS

The authors thank all the donors whose names were not included in the author list, but who participated in this program.

REFERENCES

Beilstein, K., Wittmann, A., Grez, M., and Suess, B. (2015). Conditional control of mammalian gene expression by tetracycline-dependent hammerhead ribozymes. *ACS Synth. Biol.* 4, 526–534. doi:10.1021/sb500270h

Chen, Y. Y., Jensen, M. C., and Smolke, C. D. (2010). Genetic control of mammalian T-cell proliferation with synthetic RNA regulatory systems. *Proc. Natl. Acad. Sci. USA* 107, 8531–8536. doi:10.1073/pnas.1001721107

Chen, P., Gu, W.-L., Gong, M.-Z., Wang, J., and Li, D.-Q. (2017). shRNA-mediated silencing of hTERT suppresses proliferation and promotes apoptosis in osteosarcoma cells. *Cancer Gene Ther.* 24, 325–332. doi:10.1038/cgt.2017.22

Chen, H., Li, Y., Du, C., Li, Y., Zhao, J., Zheng, X., et al. (2018a). Aptazyme-mediated direct modulation of post-transcriptional sgRNA level for conditional genome editing and gene expression. *J. Biotechnol.* 288, 23–29. doi:10.1016/j.jbiotec.2018.10.011

Chen, L., Chen, C., Chen, W., Li, K., Chen, X., Tang, X., et al. (2018b). Biodegradable black phosphorus nanosheets mediate specific delivery of hTERT siRNA for synergistic cancer therapy. *ACS Appl. Mater. Inter.* 10, 21137–21148. doi:10.1021/acsami.8b04807

Chen, K., Li, L., Qu, S., Pan, X., Sun, Y., Wan, F., et al. (2020). Silencing hTERT attenuates cancer stem cell-like characteristics and radioresistance in the radioresistant nasopharyngeal carcinoma cell line CNE-2R. *Aging* 12, 25599–25613. doi:10.18632/aging.104167

Felletti, M., Stifel, J., Wurmthaler, L. A., Geiger, S., and Hartig, J. S. (2016). Twister ribozymes as highly versatile expression platforms for artificial riboswitches. *Nat. Commun.* 7, 12834. doi:10.1038/ncomms12834

Gootenberg, J. S., Abudayyeh, O. O., Lee, J. W., Essletzbichler, P., Dy, A. J., Joung, J., et al. (2017). Nucleic acid detection with CRISPR-Cas13a/C2c2. *Science* 356, 438–442. doi:10.1126/science.aam9321

Huang, X., Zhuang, C., Zhuang, C., Xiong, T., Li, Y., and Gui, Y. (2017). An enhanced hTERT promoter-driven CRISPR/Cas9 system selectively inhibits the progression of bladder cancer cells. *Mol. Biosyst.* 13, 1713–1721. doi:10.1039/c7mb00354d

Huynh, N., Depner, N., Larson, R., and King-Jones, K. (2020). A versatile toolkit for CRISPR-Cas13-based RNA manipulation in drosophila. *Genome Biol.* 21, 279. doi:10.1186/s13059-020-02193-y

Lee, C. H., Han, S. R., and Lee, S.-W. (2016). Therapeutic applications of aptamer-based riboswitches. *Nucleic acid Ther.* 26, 44–51. doi:10.1089/nat.2015.0570

Lenis, A. T., Lec, P. M., Chamie, K., and Mshs, M. D. (2020). Bladder cancer: a review. *Jama* 324, 1980–1991. doi:10.1001/jama.2020.17598

Lin, P., Qin, S., Pu, Q., Wang, Z., Wu, Q., Gao, P., et al. (2020). CRISPR-Cas13 inhibitors block RNA editing in bacteria and mammalian cells. *Mol. Cel.* 78, 850–861. doi:10.1016/j.molcel.2020.03.033

Liu, Y., Zeng, Y., Liu, L., Zhuang, C., Fu, X., Huang, W., et al. (2014). Synthesizing AND gate genetic circuits based on CRISPR-Cas9 for identification of bladder cancer cells. *Nat. Commun.* 5, 5393. doi:10.1038/ncomms6393

Liu, T., Li, W., Lu, W., Chen, M., Luo, M., Zhang, C., et al. (2017). RBFOX3 promotes tumor growth and progression via hTERT signaling and predicts a poor prognosis in hepatocellular carcinoma. *Theranostics* 7, 3138–3154. doi:10.7150/thno.19506

Liu, Y., Huang, W., and Cai, Z. (2020). Synthesizing AND gate minigene circuits based on CRISPReader for identification of bladder cancer cells. *Nat. Commun.* 11, 5486. doi:10.1038/s41467-020-19314-7

Makarova, K. S., Wolf, Y. I., Iranzo, J., Shmakov, S. A., Alkhnbashi, O. S., Brouns, S. J. J., et al. (2020). Evolutionary classification of CRISPR-Cas systems: a burst of class 2 and derived variants. *Nat. Rev. Microbiol.* 18, 67–83. doi:10.1038/s41579-019-0299-x

Nomura, Y., Kumar, D., and Yokobayashi, Y. (2012). Synthetic mammalian riboswitches based on guanine aptazyme. *Chem. Commun. (camb).* 48, 7215–7217. doi:10.1039/c2cc33140c

Nomura, Y., Zhou, L., Miu, A., and Yokobayashi, Y. (2013). Controlling mammalian gene expression by allosteric hepatitis delta virus ribozymes. *ACS Synth. Biol.* 2, 684–689. doi:10.1021/sb400037a

O'Connell, M. R. (2019). Molecular mechanisms of RNA targeting by cas13-containing type VI CRISPR-cas systems. *J. Mol. Biol.* 431, 66–87. doi:10.1016/j.jmb.2018.06.029

Pruett-Miller, S. M. (2020). Assessing off-target editing of CRISPR-cas9 systems. *CRISPR J.* 3, 430–432. doi:10.1089/crispr.2020.29116.smi

Pu, Q., Zhou, S., Huang, X., Yuan, Y., Du, F., Dong, J., et al. (2020). Intracellular selection of theophylline-sensitive hammerhead aptazyme. *Mol. Ther. Nucleic Acids* 20, 400–408. doi:10.1016/j.omtn.2020.03.001

SaifullahSakari, . M., Suzuki, T., Yano, S., and Tsukahara, T. (2020). Effective RNA knockdown using CRISPR-cas13a and molecular targeting of the EML4-ALK transcript in H3122 lung cancer cells. *Int. J. Mol. Sci.* 21, 8904. doi:10.3390/ijms21238904

Sharma, G., Sharma, A. R., Bhattacharya, M., Lee, S. S., and Chakraborty, C. (2020). CRISPR-Cas9: a preclinical and clinical perspective for the treatment of human diseases. *Mol. Ther.* 29, 571–586. doi:10.1016/j.ymthe.2020.09.028

Shi, Y.-A., Zhao, Q., Zhang, L.-H., Du, W., Wang, X.-Y., He, X., et al. (2014). Knockdown of hTERT by siRNA inhibits cervical cancer cell growth *in vitro* and *in vivo*. *Int. J. Oncol.* 45, 1216–1224. doi:10.3892/ijo.2014.2493

Siegel, R. L., Miller, K. D., and Jemal, A. (2020). Cancer statistics, 2020. *CA: Cancer J. Clin.* 70, 7–30. doi:10.3322/caac.21590

Spöring, M., Boneberg, R., and Hartig, J. S. (2020). Aptamer-Mediated control of polyadenylation for gene expression regulation in mammalian cells. *ACS Synth. Biol.* 9, 3008–3018. doi:10.1021/acssynbio.0c00222

Sternberg, C. N., Bellmunt, J., Sonpavde, G., Siefker-Radtke, A. O., Stadler, W. M., Bajorin, D. F., et al. (2013). ICUD-EAU international consultation on bladder cancer 2012: chemotherapy for urothelial carcinoma-neoadjuvant and adjuvant settings. *Eur. Urol.* 63, 58–66. doi:10.1016/j.eururo.2012.08.010

Takahashi, K., and Yokobayashi, Y. (2019). Reversible gene regulation in mammalian cells using riboswitch-engineered vesicular stomatitis virus vector. *ACS Synth. Biol.* 8, 1976–1982. doi:10.1021/acssynbio.9b00177

Varshney, A., Bala, J., Santosh, B., Bhaskar, A., Kumar, S., and Yadava, P. K. (2017). Identification of an RNA aptamer binding hTERT-derived peptide and inhibiting telomerase activity in MCF7 cells. *Mol. Cel Biochem* 427, 157–167. doi:10.1007/s11010-016-2907-7

Wang, Q., Liu, X., Zhou, J., Yang, C., Wang, G., Tan, Y., et al. (2019). The CRISPR-cas13a gene-editing system induces collateral cleavage of RNA in glioma cells. *Adv. Sci. (Weinh)* 6, 1901299. doi:10.1002/advs.201901299

Yokobayashi, Y. (2019). Aptamer-based and aptazyme-based riboswitches in mammalian cells. *Curr. Opin. Chem. Biol.* 52, 72–78. doi:10.1016/j.cbpa.2019.05.018

Zhong, G., Wang, H., Bailey, C. C., Gao, G., and Farzan, M. (2016). Rational design of aptazyme riboswitches for efficient control of gene expression in mammalian cells. *eLife* 5, 18858. doi:10.7554/elife.18858

Zhuang, C., Huang, X., Zhuang, C., Luo, X., Zhang, X., Cai, Z., et al. (2017). Synthetic regulatory RNAs selectively suppress the progression of bladder cancer. *J. Exp. Clin. Cancer Res. CR* 36, 151. doi:10.1186/s13046-017-0626-x

Zhu, H., Richmond, E., and Liang, C. (2018). CRISPR-RT: a web application for designing CRISPR-C2c2 crRNA with improved target specificity. *Bioinformatics* 34, 117–119. doi:10.1093/bioinformatics/btx580

Conflict of Interest: The authors declare that the research was conducted in the absence of any commercial or financial relationships that could be construed as a potential conflict of interest.

frontiers in Molecular Biosciences

ORIGINAL RESEARCH
published: 26 March 2021
doi: 10.3389/fmolb.2021.653787

Knockdown of LncRNA PANDAR by CRISPR-dCas9 Decreases Proliferation and Increases Apoptosis in Oral Squamous Cell Carcinoma

Tingting Jia[1], Fengze Wang[2], Bo Qiao[1], Yipeng Ren[1], Lejun Xing[1], Haizhong Zhang[1] and Hongbo Li[1]**

[1]Department of Stomatology, The First Medical Center of Chinese PLA General Hospital, Beijing, China, [2]Clinic of Oral and Cranio-Maxillofacial Surgery, University Hospital Basel, Basel, Switzerland

Oral squamous cell carcinoma (OSCC) is the most common malignant epithelial tumor in the oral cavity. Emerging evidence has demonstrated the important function roles of long noncoding RNAs (lncRNAs) in human cancers. LncRNA promoter of CDKN1A antisense DNA damage activated RNA (PANDAR) functions as an oncogene in multiple carcinomas, whereas its function in OSCC has not been investigated yet. The aim of our study is to investigate the possible regulatory mechanism of PANDAR in OSCC. First of all, PANDAR was highly expressed in OSCC cells and loss-of-function assays mediated by CRISPR-dCas9 observed that PANDAR silencing restrained cell proliferation and promoted cell apoptosis. Then we found and confirmed the interaction between PANDAR and serine and arginine rich splicing factor 7 (SRSF7). Subsequently, serine/threonine-protein kinase pim-1 (PIM1) was proved to be regulated by PANDAR in SRSF7-dependant way. Rescue experiments validated that PANDAR modulated the proliferation and apoptosis in OSCC through PIM1. In conclusion, PANDAR bound with SRSF7 to increase PIM1 expression, hence promoting the development of OSCC. These data shed new lights into the seeking for effective diagnostic biomarkers and therapeutic targets for OSCC patients.

Keywords: CRISPR-dCas9, oral squamous cell carcinoma, PANDAR, SRFS7, PIM1

OPEN ACCESS

Edited by:
Yuchen Liu,
Shenzhen University, China

Reviewed by:
Aolin Li,
Peking University First Hospital, China
Xiaoli Zhang,
Wuhan University, China

****Correspondence:***
Haizhong Zhang
zhang126301@126.com
Hongbo Li
hongbolii@sina.com

Specialty section:
This article was submitted to Molecular Diagnostics and Therapeutics, a section of the journal Frontiers in Molecular Biosciences

Received: *15 January 2021*
Accepted: *27 January 2021*
Published: *26 March 2021*

Citation:
Jia T, Wang F, Qiao B, Ren Y, Xing L, Zhang H and Li H (2021) Knockdown of LncRNA PANDAR by CRISPR-dCas9 Decreases Proliferation and Increases Apoptosis in Oral Squamous Cell Carcinoma. Front. Mol. Biosci. 8:653787. doi: 10.3389/fmolb.2021.653787

INTRODUCTION

Oral squamous cell carcinoma (OSCC) is a well-known cancer that accounts for more than 90% of all types of oral cancers (Bagan et al., 2010). Due to efforts made on cancer therapy, such as radiotherapy, chemotherapy, and molecular target therapy, the 5-year relative survival more than doubled in the last 26 years for OSCC (Sutton et al., 2003; Jerjes et al., 2010; van Putten et al., 2018). Nevertheless, the pathogenesis and molecular mechanism of OSCC have not been clear, and further research is needed.

Long noncoding RNAs (lncRNAs) are noted as nonprotein coding transcripts which are longer than 200 nucleotides (nt) in length (Xing et al., 2016). Over the past years, researchers have identified thousands of lncRNAs and also demonstrated their roles in physiological and pathological processes of diseases (Du et al., 2018; Ye et al., 2018). For example, SP1-induced lncRNA CASC11 promotes the tumorigenesis of glioma by targeting FOXK1 through sponging miR-498 (Jin et al., 2019). APF lncRNA affects autophagy and myocardial infarction by sponging miR-188-3p (Wang et al., 2015). DLX6-AS1 promotes pancreatic cancer development by regulating miR-497-5p/FZD4/FZD6/

Wntβ-catenin pathway (Yang et al., 2019). Although lncRNAs have been widely studied in many diseases, more investigations about the aberrant lncRNAs in OSCC are urgently needed.

LncRNA promoter of CDKN1A antisense DNA damage activated RNA (PANDAR), which is located in chromosome 6p21.2, functions an oncogene in many kinds of tumors, such as pancreatic ductal adenocarcinoma (Jiang et al., 2017), breast cancer (Li et al., 2019), gastric cancer (Liu et al., 2018), acute myeloid leukemia (Yang et al., 2018), retinoblastoma (Sheng et al., 2018), ovarian cancer (Wang et al., 2018), and colorectal and cervical cancer (Huang et al., 2017; Rivandi et al., 2019). However, the regulation mechanism of PANDAR in OSCC is to be investigated.

Besides for lncRNAs, the functions of serine/threonine-protein kinase pim-1 (PIM1) in multiple cancers have already been reported by researches. Alpinumisoflavone promotes apoptosis in esophageal squamous cell carcinoma via modulation of miR-370/PIM1 signaling (Han et al., 2016). MicroRNA-33a silencing increases cyclin-dependent kinase 6, cyclin D1, and PIM1 expression and promotes cell proliferation in gastric cancer (Wang et al., 2015). Epstein-Barr virus-encoded LMP1 regulates Pim1 kinase expression to promote proliferation of cancer cells (Ding et al., 2019). Physcion 8-O-β-glucopyranoside represses tumor growth of hepatocellular carcinoma via downregulation of PIM1 (Wang et al., 2017). The investigation for the relationship between lncRNAs and PIM1 in OSCC is vitally imperative.

In this study, we aim to reveal novel regulatory mechanisms of PANDAR in OSCC. First of all, we found that PANDAR was highly expressed in OSCC cells. It was observed from CRISPR-mediated functional assays that PANDAR silencing restrained cell proliferation and promoted cell apoptosis in OSCC. Then we found and confirmed the binding between PANDAR and SRSF7. Next, PIM1 was revealed to be regulated by PANDAR through SRSF7 inhibition. Rescue experiments validated that PANDAR modulated the proliferation and apoptosis in OSCC through PIM1.

MATERIALS AND METHODS

Cell Culture

A human immortalized oral keratinocytes (NOKs) and the five most commonly used OSCC cell lines (SAS, Cal27, SCC9, SCC15, and SCC4) from the Institute of Biochemistry and Cell Biology at the Chinese Academy of Sciences (Shanghai, China) were used in this study. All cell lines were cultured in RPMI 1640 (Gibco, Darmstadt, Germany) supplemented with 10% fetal bovine serum (FBS; Gibco), 100 U/ml penicillin, and 100 mg/ml streptomycin (Invitrogen, Carlsbad, CA) at 37°C in 5% CO_2.

Cell Transfection

At 24 h prior to transfection, cells were cultured in 6-well plates. Then, the cells were transfected using Lipofectamine 2000 (Thermo Fisher Scientific, Inc., Waltham, MA, United States). All cells were harvested after 48 h. Single guide RNAs (sgRNAs) targeting PANDAR and SRSF7 (sgRNA-PANDAR#1/2/3 and sgRNA-SRSF7) and the negative control sgRNA (sgRNA-NC) were constructed by RiboBio (Guangzhou, China). The sequences of sgRNAs targeting PANDAR are as follows: sgRNA-PANDAR#1GGCCAGACCTATAATATTAA; sgRNA-PANDAR#2GCCAGACCTATAATATTAAT; sgRNA-PANDAR#3GGAGATACCACCACTGTCAA. The overexpression of PIM1 was achieved by treating cells with pcDNA3.1/PIM1 and empty control (RiboBio).

RNA Extraction and Quantitative Real-Time PCR Assays

According to the recommendations provided by manufacturer, total RNA was extracted from cells using TRIzol reagent (Invitrogen). Then the PrimeScript reverse transcriptase reagent kit (Takara Bio Inc., Kusatsu, Shiga, Japan) was used to synthesize complementary DNA (cDNA). Real-time PCR amplification was then performed using an SYBR Green Real-Time PCR Kit on the Bio-Rad CFX96 System (Applied Biosystems, Foster City, CA). Furthermore, GADPH was used as the endogenous control. The $2^{-\Delta\Delta CT}$ method was used for transcript quantification. The primers for genes are as follows: PANDAR forward 5′-CTCCATCATGCCAAG TTCTGC-3′ and reverse 5′-GAAGGCAGGCAAGACTCGAA-3′; SRSF7 forward 3′-GCGGTACGGAGGAGAAAC-5′ and reverse 3′-TCGGGAGCCACAAATCAC-5′; Pim1 forward 5′-CTTCGG CTCGGTCTACTCAG-3′, reverse 5′-AGTGCCATTAGGCAG CTCTC-3′; GAPDH forward 5′- TGCACCACCAACTGCTTA GC -3′, and reverse 5′- GGCATGGACTGTGGTCATGAG -3′.

CCK-8 Assays

The proliferation rate of cells was determined via Cell Counting Kit-8 (CCK-8) assay kit. The cells were seeded in 96-well plates (3×10^3 cells/well) and cultured for five periods (0, 24, 48, 72, and 96 h) at 37°C with 5% CO_2. At the same time, each well was added with 10 μL of CCK-8 solution and incubated for 4 h continuously. Finally, the OD value (450 nm) was assessed with a Bio-Rad iMark microplate absorbance reader (Bio-Rad Laboratories Inc., Hercules, CA, United States).

RNA Immunoprecipitation Assay

The EZ-Magna RIP RNA-Binding Protein Immunoprecipitation kit (Millipore, Bedford, Massachusetts, United States) was applied to perform RIP assay. A total of 2×10^7 cells were harvested and lysed in 100 μl lysis buffer (Millipore) for RIP reaction. Anti-IgG or anti-SRSF7 was added into cell lysates, and then the whole-cell extract was incubated with rotation overnight at 4°C. Finally, the immunoprecipitated RNA was purified using TRIzol regent, and binding targets were analyzed with qRT-PCR.

EdU Assays

To examine cellular proliferation, 5′-Ethynyl-2′-deoxyuridine (EdU; RiboBio, Guangzhou, China) incorporation experiment was performed in light of the operational manual. When cell confluence is up to 80%–90%, all cells were incubated by EdU diluent for 2 h at 37°C. Subsequently, cells were fixed and then stained with Apollo 567 working solution for 30 min away from light. After staining, the cells were washed by penetrant. Images were captured and photographed under a fluorescence microscope (Leica, Wetzlar, Germany).

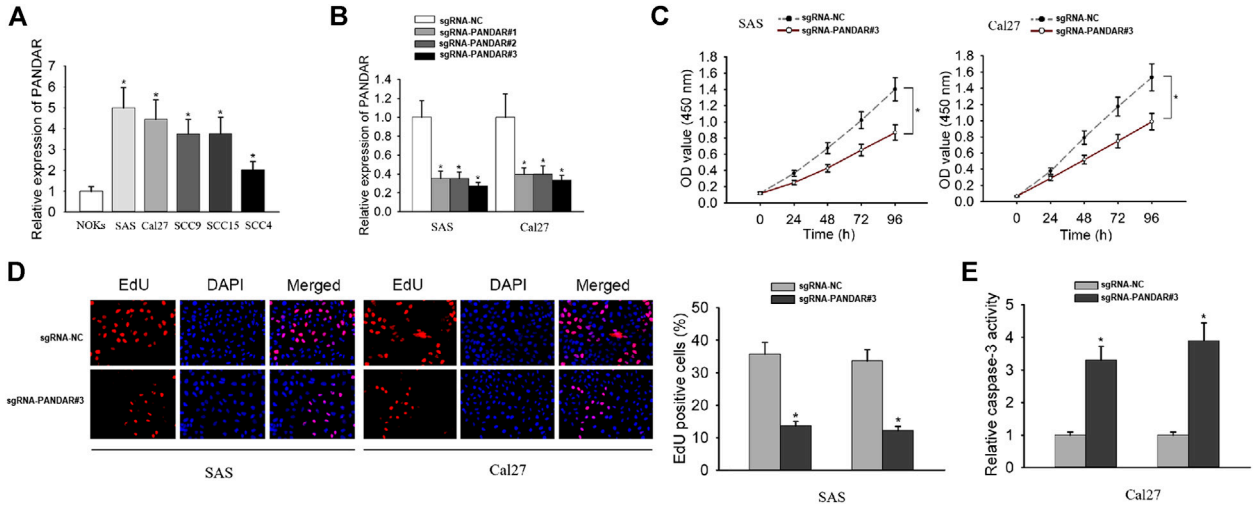

FIGURE 1 | The impact of PANDAR knockdown on proliferation and apoptosis of OSCC cells. **(A)** The relative expression level of PANDAR in cancerous cell lines and normal cell line. **(B)** The knockdown efficiency of specific sgRNAs targeting PANDAR was detected in OSCC cells by qRT-PCR. **(C–E)** Cell proliferation assays (CCK-8 and EdU) and cell apoptosis assay (caspase-3 activity assay) were carried out to assess the functional role of PANDAR knockdown in OSCC. Data were represented as the mean values (±SD) of three independent experiments. *$p < 0.05$, significantly different from the control.

Biotinylated RNA Pull-Down Assays

Chemically synthesized probes for PANDAR-WT, PANDAR-MUT, PIM1-WT, PIM1-MUT, and their relative negative control (NC) were biotin-labeled (they were named as Bio-PANDAR-WT, Bio-PANDAR-MUT, Bio-PIM1-WT, Bio-PIM1-MUT, and Bio-NC) using the Biotin RNA Labeling Mix (Roche Diagnostics, Indianapolis, IN). The biotinylated RNA was incubated overnight with lysates from cells and then treated with magnetic beads with *Streptomyces* for 48 h. Finally, the RNA present in the pull-down material was assessed using qRT-PCR.

Western Blotting Assay

By using RIPA reagent (Beyotime, Beijing, China) and protease inhibitor cocktail, proteins were separated by 10% SDS-PAGE and transferred to PVDF membranes. The membranes were blocked with 5% nonfat milk for 60 min and incubated with primary antibodies at 4°C for 12–16 h. Autoradiograms were monitored by densitometry through Quantity One software (Bio-Rad). Antibodies for PIM1 and GAPDH were obtained from Cell Signaling Technology (Danvers, MA, United States).

Caspase-3 Activity Assays

The activity of Caspase-3 was determined at 48 h after transfection by Caspase-3 activity kit (Beyotime Institute of Biotechnology, Guangzhou, Guangdong, China). Protein samples were obtained through lysis buffer and then diluted to 50 μl of final volume. The diluted protein was subjected to 75 μl of caspase-3 substrate for 3 h, and the hydrolysis of Ac-DEVD-pNA was detected at 405 nm by caspase-3 released free pNA (yellow formazan product).

Statistical Analysis

All the numerical data are presented as the means ± SD. Each experimental procedure was repeated for more than two times. Student's *t*-test and one-way ANOVA were used to analyze significant difference of groups, and $p < 0.05$ was taken as the significance threshold. Statistical analyses were performed with SPSS 13.0 Software (GraphPad Software, San Diego, CA, United States).

RESULTS

PANDAR Was Highly Expressed in OSCC and PANDAR Inhibition Restrained Cell Proliferation and Promoted Cell Apoptosis

To explore whether lncRNA PANDAR affects the biological activities of OSCC cells, we initially examined the expression level of PANDAR in OSCC cells (SAS, Cal27, SCC9, SCC15, and SCC4) and normal oral keratinocytes (NOKs). The high levels of PANDAR in OSCC cells were shown in **Figure 1A**. PANDAR was accordingly silenced by transfecting with sgRNA-PANDAR#1/2/3 in SAS and Cal27 cells and sgRNA#3 achieved the best performance (**Figure 1B**). Therefore, this sgRNA was chosen for the following functional studies. The analysis from CCK-8 assay found that cell proliferation was inhibited after PANDAR silencing (**Figure 1C**). Also, the repression on cell proliferation was observed when PANDAR was knocked down, as tested by EdU assay (**Figure 1D**). Caspase-3 activity assay revealed that PANDAR downregulation had a stimulative effect on cell apoptosis (**Figure 1E**). In order to further prevent the false positive problem caused by potential off-targeting effects of sgRNA, we also used sgRNA # 1 and 2 to repeat the above functional experiments and obtained similar results (**Supplementary Figure S1**). These findings illustrated that silencing of PANDAR inhibited cell proliferation and induced cell apoptosis.

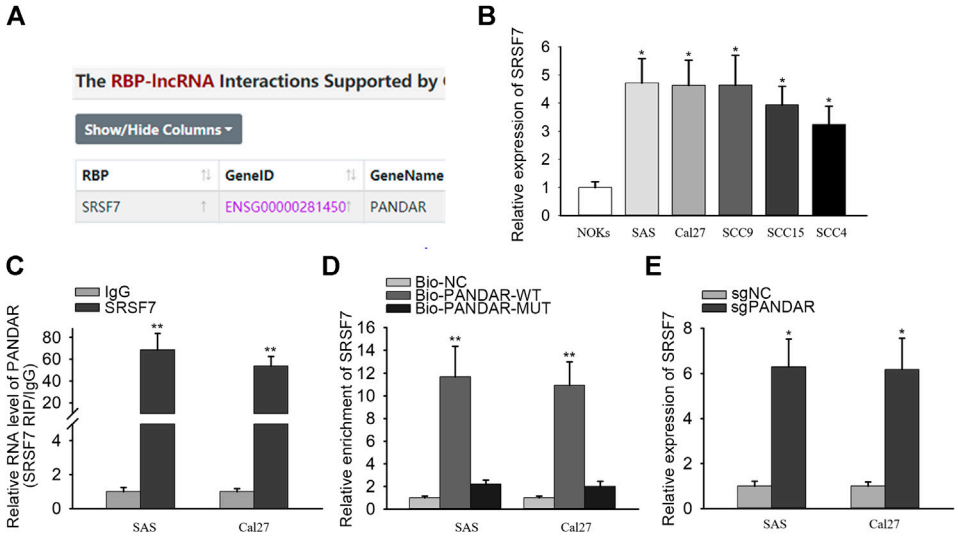

FIGURE 2 | SRSF7 acted as a RBP of PANDAR in OSCC. **(A)** In line with the prediction of starBase, SRSF7 was found to be a RBP of PANDAR. **(B)** The expression level of SRSF7 in cancerous cells and normal cells. **(C,D)** RIP and RNA pull-down assays were conducted for validating the interaction between SRSF7 and PANDAR in OSCC cells. **(E)** PANDAR knockdown increased SRSF7 expression in OSCC cells. Data were represented as the mean values (±SD) of three independent experiments. $^{*}p < 0.05$ and $^{**}p < 0.01$, significantly different from the control.

PANDAR Bound With SRSF7

LncRNAs have been reported to bind with RNA-binding proteins (RBPs) so as to influence cellular processes (Nguyen et al., 2018; Zhang et al., 2018). From starBase v3.0, the binding between PANDAR and SRSF7 was uncovered (**Figure 2A**). SRSF7 expression was upregulated in OSCC cells compared to NOKs cells (**Figure 2B**). Then RIP and RNA pull-down assays were performed and the results demonstrated that PANDAR was only enriched in anti-SRSF7 group and merely bio-PANDAR-WT pulled down SRSF7 protein, suggesting the direct interaction between PANDAR and SRSF7 (**Figures 2C,D**). Moreover, after knocking down of PANDAR, the SRSF7 expression was increased. These results indicated that PANDAR bound with SRSF7 and downregulated SRSF7.

PANDAR Regulated PIM1 Expression Through Binding With SRSF7

RBP interactions with mRNAs are identified in numerous cancers (Chand et al., 2017; Zhong et al., 2019). PIM1 is an oncogene in OSCC and has been known to regulate the proliferation ability of OSCC cells. Strikingly, we found out the interaction between SRSF7 and PIM1 from starBase v3.0 (**Figure 3A**). qRT-PCR analysis detected that PIM1 was highly expressed in OSCC cells (**Figure 3B**). The binding between SRSF7 and PIM1 was also confirmed through RIP and RNA pull-down experiments. In RIP assay, the enrichment of PIM1 was observed in SRSF7 group (**Figure 3C**). In RNA pull-down assay, SRSF7 was simply pulled down by bio-PIM1-WT probe (**Figure 3D**). In addition, PIM1 expression was augmented after SRSF7 was downregulated or PANDAR was knocked down (**Figures 3E–G**). The coinfluences of PANDAR and SRSF7 on PIM1 were measured through qRT-PCR. PIM1 expression was silenced by PANDAR inhibition but recovered partly by SRSF7 downregulation (**Figure 3H**). Taken together, PANDAR modulated PIM1 through binding to SRSF7.

PANDAR Affected the Proliferation and Apoptosis in OSCC Through PIM1

Finally, we performed rescue experiments to validate the whole mechanism in OSCC. SAS cells were transfected with sgRNA-NC, sgRNA#3 + pcDNA3.1, and sgRNA#3 + PIM1, respectively (**Figure 4A**). Through EdU and CCK-8 assays, we observed that the proliferation ability repressed by PANDAR knockdown was rescued by PIM1 overexpression (**Figures 4B,C**). In caspase-3 activity assay, PANDAR repression activated cell apoptosis, and this phenomenon was counteracted when PIM1 was upregulated (**Figure 4D**). All in all, overexpression of PIM1 reversed the corresponding effects of PANDAR inhibition on cell proliferation and apoptosis.

DISCUSSION

Numerous researches have demonstrated the crucial roles of long noncoding RNAs (lncRNAs) in human tumors, including OSCC. However, further explorations are needed.

In this study, we investigated the lncRNA PANDAR in OSCC. We showed that PANDAR expression is upregulated in OSCC cells in comparison with normal oral keratinocytes, and knockdown of PANDAR by CRISPR-dCas9 reduces proliferation and increases apoptosis of OSCC cells. We also demonstrated that those phenotypes are dependent of PIM1 regulation, via binding to SRSF7.

First of all, we investigated the expression pattern and biological function of PANDAR in OSCC. Mounting evidence has illustrated the oncogenic function of PANDAR in other

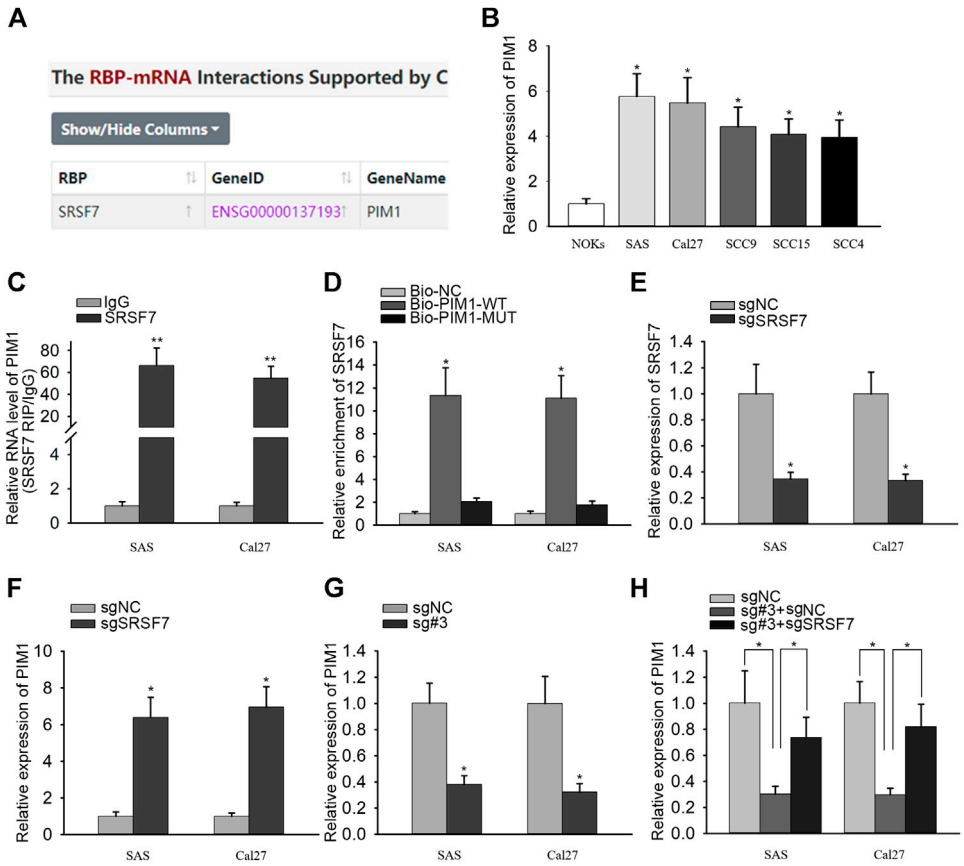

FIGURE 3 | PANDAR affected PIM1 expression by regulating SRSF7 in OSCC. **(A)** According to starBase, SRSF7 was identified as a RBP of PIM1. **(B)**. The high expression level of PIM1 in OSCC cells. **(C,D)** The interaction between SRSF7 and PIM1 was confirmed by RIP and RNA pull-down assays. **(E,F)** The sgRNA targeting SRSF7 decreased SRSF7 and increased PIM1 expression. **(G,H)** PIM1 expression level was reduced by sgRNA PANDAR#3, and this effect was reversed partially by sgRNA SRSF7 in OSCC cells. Data were represented as the mean values (±SD) of three independent experiments. $^{*}p < 0.05$ and $^{**}p < 0.01$, significantly different from the control.

carcinomas except for OSCC. For instances, PANDAR promotes cell proliferation and suppresses cell apoptosis in pancreatic ductal adenocarcinoma (Jiang et al., 2017); inhibition of PANDAR reduces cell proliferation and cell invasion and suppresses EMT process in breast cancer (Li et al., 2019); PANDAR blocks CDKN1A gene transcription via competitive interaction with p53 protein in gastric cancer (Liu et al., 2018); SP1-induced PANDAR regulates cell growth and apoptosis of retinoblastoma cells (Sheng et al., 2018). Our research firstly gives the evidence for the high expression of PANDAR in OSCC cells. Loss-of-function experiments suggest that inhibition of PANDAR restrained the proliferation capacity of OSCC cells.

RNA-binding proteins (RBPs) provide one connector through which lncRNAs regulate mRNAs expression specifically (Glisovic et al., 2008; Barbagallo et al., 2018). According to the data from starBase v3.0, PANDAR was merely predicted to interact with SRSF7. In the past studies, SRSF7 has been revealed to be heightened in carcinomas and promotes cancer progression in various tumors. For example, inhibition of SRSF7 promotes apoptosis in colon and lung cancers (Boguslawska et al., 2016). MicroRNAs modulate the expression of osteopontin splice variants in renal cancer cells by targeting SRSF7 splicing factor (Boguslawska et al., 2016). The comparative expression patterns and diagnostic efficiencies of HNRNPA1 and SR splicing factors were discovered in gastric and colorectal cancers (Park et al., 2016). The present research discovered the interaction between PANDAR and SRSF7. Additionally, increasing reports have indicated that PIM1 is a tumor growth promoter via influencing cell proliferation and apoptosis (Wang et al., 2015; Wang et al., 2017; Ding et al., 2019), which forced us to study the potent relationship among the three genes. Interestingly, the binding between SRSF7 and PIM1 was unveiled though the assistance of starBase v3.0 website. Further investigations validated the regulatory role of PANDAR/SRSF7/PIM1 axis in OSCC, where PANDAR modulated the proliferation and apoptosis of OSCC through PIM1. Therefore, PANDAR/SRSF7/PIM1 axis may be a potential therapeutic target for the treatment of OSCC.

This study also highlights the important role of CRISPR-dCas9 in lncRNA research. Through the flexible regulation of lncRNA expression level, it would be easy to study the function and molecular regulation mechanism of lncRNAs (Dominguez et al., 2016; Pulecio et al., 2017; Gjaltema and Schulz, 2018). This is an unprecedented convenience.

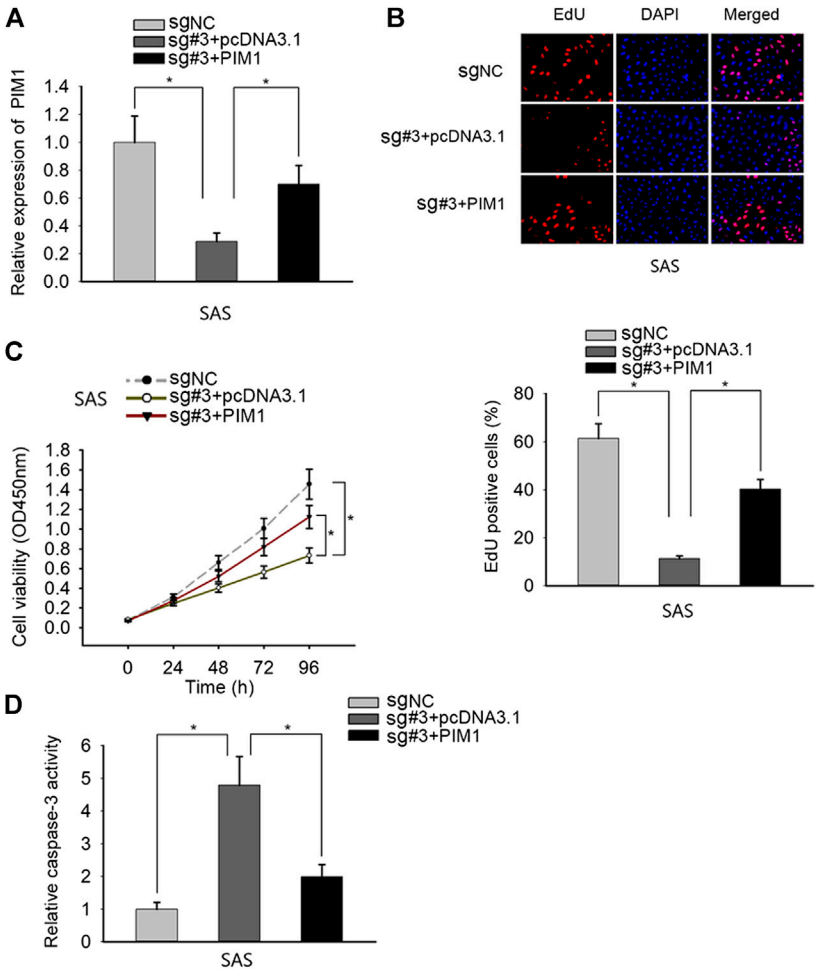

FIGURE 4 | PANDAR modulated OSCC cell proliferation and apoptosis via SRSF7/PIM1 axis. **(A)** The pcDNA3.1/PIM1 reversed the inhibitory effect on PIM1 mediated by knockdown of PANDAR. **(B–D)** The inhibited proliferation and increased apoptosis of OSCC cells caused by PANDAR knockdown were recovered and weakened through overexpressing PIM1. Data were represented as the mean values (±SD) of three independent experiments. *$p < 0.05$, significantly different from the control.

In summary, in OSCC cells, PANDAR interacts with SRSF7 to upregulate PIM1 expression, therefore promoting the proliferation ability of OSCC cells. These data provided novel insights into the seeking for effective biomarkers and therapeutic targets for patients with OSCC.

DATA AVAILABILITY STATEMENT

The original contributions presented in the study are included in the article/**Supplementary Material**; further inquiries can be directed to the corresponding authors.

AUTHOR CONTRIBUTIONS

HL and HZ were involved in conceptualization, project administration, and manuscript review; TJ, FW, BQ, YR, LX, HZ, and HL were involved in experiments, data analysis, and original draft writing. All authors have made substantial contributions to this study.

FUNDING

This study was supported by the National Key R&D Program of China (2017YFB1304300) and the Military Medical Youth Program of the Chinese PLA General Hospital (QNF19054).

SUPPLEMENTARY MATERIAL

The Supplementary Material for this article can be found online at: https://www.frontiersin.org/articles/10.3389/fmolb.2021.653787/full#supplementary-material.

REFERENCES

Bagan, J., Sarrion, G., and Jimenez, Y. (2010). Oral cancer: clinical features. *Oral Oncol.* 46 (6), 414–417. doi:10.1016/j.oraloncology.2010.03.009

Barbagallo, D., Caponnetto, A., Cirnigliaro, M., Brex, D., Barbagallo, C., D'Angeli, F., et al. (2018). CircSMARCA5 inhibits migration of glioblastoma multiforme cells by regulating a molecular axis involving splicing factors SRSF1/SRSF3/PTB. *Int. J. Mol. Sci.* 19, 480. doi:10.3390/ijms19020480

Boguslawska, J., Sokol, E., Rybicka, B., Czubaty, A., Rodzik, K., and Piekielko-Witkowska, A. (2016). microRNAs target SRSF7 splicing factor to modulate the expression of osteopontin splice variants in renal cancer cells. *Gene* 595, 142–149. doi:10.1016/j.gene.2016.09.031

Chand, S. N., Zarei, M., Schiewer, M. J., Kamath, A. R., Romeo, C., Lal, S., et al. (2017). Posttranscriptional regulation of PARG mRNA by HuR facilitates DNA repair and resistance to PARP inhibitors. *Cancer Res.* 77, 5011–5025. doi:10.1158/0008-5472.can-16-2704

Ding, R.-R., Yuan, J.-L., Jia, Y.-N., Liao, X.-M., Wang, S.-S., Shao, Z.-M., et al. (2019). Epstein-Barr virus-encoded LMP1 regulated Pim1 kinase expression promotes nasopharyngeal carcinoma cells proliferation. *Onco. Targets Ther.* 12, 1137–1146. doi:10.2147/ott.s190274

Dominguez, A. A., Lim, W. A., and Qi, L. S. (2016). Beyond editing: repurposing CRISPR-Cas9 for precision genome regulation and interrogation. *Nat. Rev. Mol. Cell Biol.* 17, 5–15. doi:10.1038/nrm.2015.2

Du, M., Huang, T., Wu, J., Gu, J.-J., Zhang, N., Ding, K., et al. (2018). Long non-coding RNA n326322 promotes the proliferation and invasion in nasopharyngeal carcinoma. *Oncotarget* 9, 1843–1851. doi:10.18632/oncotarget.22828

Gjaltema, R. A. F., and Schulz, E. G. (2018). CRISPR/dCas9 switch systems for temporal transcriptional control. *Methods Mol. Biol.* 1767, 167–185. doi:10.1007/978-1-4939-7774-1_8

Glisovic, T., Bachorik, J. L., Yong, J., and Dreyfuss, G. (2008). RNA-binding proteins and post-transcriptional gene regulation. *FEBS Lett.* 582, 1977–1986. doi:10.1016/j.febslet.2008.03.004

Han, Y., Yang, X., Zhao, N., Peng, J., Gao, H., and Qiu, X. (2016). Alpinumisoflavone induces apoptosis in esophageal squamous cell carcinoma by modulating miR-370/PIM1 signaling. *Am. J. Cancer Res.* 6, 2755–2771.

Huang, H. W., Xie, H., Ma, X., Zhao, F., and Gao, Y. (2017). Upregulation of LncRNA PANDAR predicts poor prognosis and promotes cell proliferation in cervical cancer. *Eur. Rev. Med. Pharmacol. Sci.* 21, 4529–4535.

Jerjes, W., Upile, T., Petrie, A., Riskalla, A., Hamdoon, Z., Vourvachis, M., et al. (2010). Clinicopathological parameters, recurrence, locoregional and distant metastasis in 115 T1-T2 oral squamous cell carcinoma patients. *Head neck Oncol.* 2 (1), 9. doi:10.1186/1758-3284-2-9

Jiang, Y., Feng, E., Sun, L., Jin, W., You, Y., Yao, Y., et al. (2017). An increased expression of long non-coding RNA PANDAR promotes cell proliferation and inhibits cell apoptosis in pancreatic ductal adenocarcinoma. *Biomed. Pharmacother.* 95, 685–691. doi:10.1016/j.biopha.2017.08.124

Jin, J., Zhang, S., Hu, Y., Zhang, Y., Guo, C., and Feng, F. (2019). SP1 induced lncRNA CASC11 accelerates the glioma tumorigenesis through targeting FOXK1 via sponging miR-498. *Biomed. Pharmacother.* 116, 108968. doi:10.1016/j.biopha.2019.108968

Li, Y., Su, X., and Pan, H. (2019). Inhibition of lncRNA PANDAR reduces cell proliferation, cell invasion and suppresses EMT pathway in breast cancer. *Cancer Biomark.* 25, 185–192. doi:10.3233/cbm-182251

Liu, J., Ben, Q., Lu, E., He, X., Yang, X., Ma, J., et al. (2018). Long noncoding RNA PANDAR blocks CDKN1A gene transcription by competitive interaction with p53 protein in gastric cancer. *Cell Death Dis.* 9, 168. doi:10.1038/s41419-017-0246-6

Nguyen, E. D., Balas, M. M., Griffin, A. M., Roberts, J. T., and Johnson, A. M. (2018). Global profiling of hnRNP A2/B1-RNA binding on chromatin highlights LncRNA interactions. *RNA Biol.* 15, 901–913. doi:10.1080/15476286.2018.1474072

Park, W. C., Kim, H. R., Kang, D. B., Ryu, J. S., Choi, K. H., Lee, G. O., et al. (2016). Comparative expression patterns and diagnostic efficacies of SR splicing factors and HNRNPA1 in gastric and colorectal cancer. *BMC Cancer* 16, 358. doi:10.1186/s12885-016-2387-x

Pulecio, J., Verma, N., Mejía-Ramírez, E., Huangfu, D., and Raya, A. (2017). CRISPR/Cas9-Based engineering of the epigenome. *Cell Stem Cell* 21, 431–447. doi:10.1016/j.stem.2017.09.006

Rivandi, M., Pasdar, A., Hamzezadeh, L., Tajbakhsh, A., Seifi, S., Moetamani-Ahmadi, M., et al. (2019). The prognostic and therapeutic values of long noncoding RNA PANDAR in colorectal cancer. *J. Cell Physiol.* 234, 1230–1236. doi:10.1002/jcp.27136

Sheng, L., Wu, J., Gong, X., Dong, D., and Sun, X. (2018). SP1-induced upregulation of lncRNA PANDAR predicts adverse phenotypes in retinoblastoma and regulates cell growth and apoptosis *in vitro* and *in vivo*. *Gene* 668, 140–145. doi:10.1016/j.gene.2018.05.065

Sutton, D. N., Brown, J. S., Rogers, S. N., Vaughan, E. D., and Woolgar, J. A. (2003). The prognostic implications of the surgical margin in oral squamous cell carcinoma. *Int. J. Oral Maxill. Surg.* 32 (1), 30–34. doi:10.1054/ijom.2002.0313

van Putten, M., de Vos-Geelen, J., Nieuwenhuijzen, G. A. P., Siersema, P. D., Lemmens, V. E. P. P., Rosman, C., et al. (2018). Long-term survival improvement in oesophageal cancer in The Netherlands. *Eur. J. Cancer* 94, 138–147. doi:10.1016/j.ejca.2018.02.025

Wang, H., Fang, L., Jiang, J., Kuang, Y., Wang, B., Shang, X., et al. (2018). The cisplatin-induced lncRNA PANDAR dictates the chemoresistance of ovarian cancer via regulating SFRS2-mediated p53 phosphorylation. *Cell Death Dis.* 9, 1103. doi:10.1038/s41419-018-1148-y

Wang, K., Liu, C. Y., Zhou, L. Y., Wang, J. X., Wang, M., Zhao, B., et al. (2015). APF lncRNA regulates autophagy and myocardial infarction by targeting miR-188-3p. *Nat. Commun.* 6, 6779. doi:10.1038/ncomms7779

Wang, Q., Jiang, Y., Guo, R., Lv, R., Liu, T., Wei, H., et al. (2017). Physcion 8-O-β-glucopyranoside suppresses tumor growth of Hepatocellular carcinoma by downregulating PIM1. *Biomed. Pharmacother.* 92, 451–458. doi:10.1016/j.biopha.2017.05.110

Wang, Y., Zhou, X., Shan, B., Han, J., Wang, F., Fan, X., et al. (2015). Downregulation of microRNA-33a promotes cyclin-dependent kinase 6, cyclin D1 and PIM1 expression and gastric cancer cell proliferation. *Mol. Med. Rep.* 12, 6491–6500. doi:10.3892/mmr.2015.4296

Xing, Y.-H., Bai, Z., Liu, C.-X., Hu, S.-B., Ruan, M., and Chen, L.-L. (2016). Research progress of long noncoding RNA in China. *IUBMB life* 68, 887–893. doi:10.1002/iub.1564

Yang, J., Ye, Z., Mei, D., Gu, H., and Zhang, J. (2019). Long noncoding RNA DLX6-AS1 promotes tumorigenesis by modulating miR-497-5p/FZD4/FZD6/Wnt/β-catenin pathway in pancreatic cancer. *Cancer Manag. Res.* 11, 4209–4221. doi:10.2147/cmar.s194453

Yang, L., Zhou, J.-D., Zhang, T.-J., Ma, J.-C., Xiao, G.-F., Chen, Q., et al. (2018). Overexpression of lncRNA PANDAR predicts adverse prognosis in acute myeloid leukemia. *Cancer Manag. Res.* 10, 4999–5007. doi:10.2147/cmar.s180150

Ye, B., Liu, B., Yang, L., Zhu, X., Zhang, D., Wu, W., et al. (2018). LncKdm2b controls self-renewal of embryonic stem cells via activating expression of transcription factor Zbtb3. *EMBO J.* 37, e97174. doi:10.15252/embj.201797174

Zhang, S., Leng, T., Zhang, Q., Zhao, Q., Nie, X., and Yang, L. (2018). Sanguinarine inhibits epithelial ovarian cancer development via regulating long non-coding RNA CASC2-EIF4A3 axis and/or inhibiting NF-κB signaling or PI3K/AKT/mTOR pathway. *Biomed. Pharmacother.* 102, 302–308. doi:10.1016/j.biopha.2018.03.071

Zhong, Y., Yang, S., Wang, W., Wei, P., He, S., Ma, H., et al. (2019). The interaction of Lin28A/Rho associated coiled-coil containing protein kinase2 accelerates the malignancy of ovarian cancer. *Oncogene* 38, 1381–1397. doi:10.1038/s41388-018-0512-9

Conflict of Interest: The authors declare that the research was conducted in the absence of any commercial or financial relationships that could be construed as a potential conflict of interest.

frontiers in Molecular Biosciences

ORIGINAL RESEARCH
published: 29 March 2021
doi: 10.3389/fmolb.2021.657145

Knockdown of Long Non-coding RNA SNGH3 by CRISPR-dCas9 Inhibits the Progression of Bladder Cancer

Yu Cao[1†], Qiong Hu[1†], Ruiming Zhang[1†], Ling Li[2†], Mingjuan Guo[3], Huiling Wei[3], Li Zhang[3], Jianfeng Wang[3*] and Chunjing Li[3*]*

[1] Ningxiang Hospital Affiliated to Hunan University of Traditional Chinese Medicine, Ningxiang, China, [2] Medical Basic Teaching Experiment Center, College of traditional Chinese Medicine, Hunan University of Chinese Medicine, Changsha, China, [3] Department of Urology, Affiliated Foshan Maternal and Child Healthcare Hospital, Southern Medical University, Foshan, China

OPEN ACCESS

Edited by:
Yuchen Liu,
Shenzhen University, China

Reviewed by:
Yingying Zhang,
Northwest A&F University, China
Kai Yang,
Zhejiang University, China

****Correspondence:***
Li Zhang
fsfyli@sina.com
Jianfeng Wang
jianfengwang1977@aliyun.com
Chunjing Li
164194249@qq.com

[†] These authors have contributed equally to this work

Specialty section:
This article was submitted to Molecular Diagnostics and Therapeutics, a section of the journal Frontiers in Molecular Biosciences

Received: *22 January 2021*
Accepted: *04 March 2021*
Published: *29 March 2021*

Citation:
Cao Y, Hu Q, Zhang R, Li L, Guo M, Wei H, Zhang L, Wang J and Li C (2021) Knockdown of Long Non-coding RNA SNGH3 by CRISPR-dCas9 Inhibits the Progression of Bladder Cancer. Front. Mol. Biosci. 8:657145. doi: 10.3389/fmolb.2021.657145

Recent research evidence documents that lncRNAs (long non-coding RNAs lncRNAs) play a pivotal role in the tumorigenesis and development of tumors. LncRNA SNGH3 (small nucleolar RNA host gene 3) is highly expressed in numerous forms of cancer, serving as an oncogene in cancer progression. Nonetheless, the clinical relationship, along with the mechanism of SNGH3 in bladder cancer, have not been studied. Herein, the findings exhibited upregulation of SNGH3 in bladder cancer tissues, along with the cell lines. Furthermore, overexpressed SNGH3 was positively linked to the TNM stage, as well as the histological grade of bladder cancer. Moreover, the silencing of SNGH3, using CRISPR-dCas9, suppressed cell growth along with migration, but elevated bladder cancer cell apoptosis. In summary, we established that SNGH3 serves as a bladder cancer oncogene and could be employed as a prospective diagnostic marker for clinical use, and is also a therapeutic target for CRISPR-mediated gene therapy.

Keywords: SNGH3, bladder cancer, CRISPR-dCas9, lncRNA, therapeutic target

INTRODUCTION

Human bladder cancer, which has high incidence and a high mortality, is the most frequent type of the urinary system tumors. According to statistics, there are approximately 549,000 new cases of bladder cancer and 200,000 people died of the disease in 2018 (Bray et al., 2018). Although significant advancements have been made in the treatment of bladder cancer in recent years, the 5 year survival rate and prognosis of patients with advanced bladder cancer remain low (Kamat et al., 2016; Dy et al., 2017; Massari et al., 2018). Early diagnosis and treatment of bladder cancer is strongly linked to the prognosis of patients. Frequent relapse along with distant metastasis of bladder cancer are the primary causes of treatment failure. However, the exact molecular biology of bladder cancer remains unknown. Therefore, it is critical to find new effective biological targets for the diagnosis, as well as the treatment of bladder cancer.

Long non-coding RNA (lncRNA) is a non-coding RNA molecule with a length of more than 200 nt. Because lncRNAs lack (ORFs) open reading frames, they cannot be translated into proteins (Ponting et al., 2009). Recent research findings have documented that lncRNAs have a core role in

cell proliferation, apoptosis, infiltration, and other biological processes, as well as gene regulation, chromatin remodeling, and other molecular levels (Tsai et al., 2010; Quinodoz and Guttman, 2014). In addition, a large number of lncRNAs participate in tumor development along with metastasis (Huarte, 2015). The expression characteristics of lncRNAs have obvious tissue or cell specificity. They can be used as oncogenic factors or tumor repressors (Evans et al., 2016; Chen Y. et al., 2017). In many classical instances, lncRNAs are employed as guides or molecular scaffolds that modulate protein-protein or DNA-protein cross talks, as enhancers that modulate transcription, or as miRNA (microRNA) sponges to adsorb miRNAs (Jandura and Krause, 2017; Marchese et al., 2017). lncRNA can also be used as readouts of active cellular genetic programs or conductors of distinct cellular signaling events, can assess the pathological state of cancers, and offers prognostic ability for cancer patients (Engreitz et al., 2016). For example, lncRNA MALAT-1 has been found to be upregulated in various malignant tumors, and upregulated MALAT-1 is remarkably linked to worse OS (overall survival) or DFS (disease-free survival) in individuals with gastrointestinal carcinomas (Chen D. et al., 2017; Wu et al., 2018). High expression of lncRNA HOTAIR in primary, as well as metastatic breast cancer indicates dismal prognosis. It promotes the infiltration along with the metastasis of breast cancer cells by mediating PRC2 relocation and modulating H3K27 methylation (Milevskiy et al., 2016; Portoso et al., 2017). LncRNA-HOXD-AS1 functions as a sponge of miRNA and competitively bind with miR-130a, thereby upregulating the expression of the EF28 transcription factor, and enhancing the migration and infiltration of glioma cells (Chen et al., 2018). Therefore, it is extremely necessary to conduct a comprehensive genomic and cellular functional study on the changes of lncRNA in tumor development along with metastasis, which will help to uncover new cancer diagnosis and treatment targets.

The dysregulation of lncRNAs is closely linked to multiple cancer types, such as small nucleolar RNA host gene (SNHG) related lncRNA. Recently, accumulating evidence suggests that small nucleolar RNA host genes of lncRNAs participate in the onset of cancer, accelerating the progression of cancer cells. For instance, lncRNA SNHG1 promotes the growth of colon and lung cancer by enhancing the transcriptional level of neighboring gene SLC3A2 and accelerating the phosphorylation of the PI3K/Akt pathway (Sun et al., 2017). The oncogenic lncRNA, SNHG6 enhances genomic hypomethylation by inhibiting the generation of SAMe. Moreover, SNHG6 sponges miR-1297 to increase MAT2A expression, upregulating MAT2A expression in hepatocellular carcinoma (Guo et al., 2018). Shan et al. (2018) documented that lncRNA SNHG7 was highly expressed in colorectal cancer and increased up regulated SNHG7 expression, promoted the cell growth and migration by acting as the miR-216b sponge to affect the expression and GALNT1 and EMT markers.

To the best of our knowledge, there is no study showing the biological function of lncRNA SNHG3 in bladder cancer. Herein, the data revealed lncRNA SNHG3 upregulation in bladder cancer tissues, as well as cell lines in contrast with the matched bladder non-malignant tissues and SV-HUC1 cells, respectively. Elevated SNHG3 expression was positively linked to the TNM stage along with the histological grade of individuals with bladder cancer. In addition, upregulated SNHG3 expression was shown to result in the dismal prognosis of bladder cancer patients, causing lower OS and DFS. Further functional assays illustrated that SNHG3 silencing, by CRISPR-dCas9, repressed the bladder cancer cell growth, as well as migration and enhanced cell apoptosis.

MATERIALS AND METHODS

Patient Samples

Overall, 41 individuals who were diagnosed with bladder cancer and who had undergone partial or radical cystectomy at the Affiliated Foshan Maternal and Child Healthcare Hospital were enrolled in the study. All the bladder cancer tissues along with the matching neighboring non-malignant tissues were stored in RNA later and then immediately snap-frozen in liquid nitrogen.

All subjects who enrolled in the present study approved this research and provided written informed consent. In addition, we performed the study with the approval of the Research Ethics Committee of the Affiliated Foshan Maternal and Child Healthcare Hospital.

Cell Culture

The 5637, SW780, and T24 human bladder cancer cells along with the SV-HUC-1 human non-malignant bladder epithelial cells were all supplied by ATCC. The RPMI-1640 Medium (Gibco) augmented with 10% FBS (Invitrogen, Carlsbad, CA, United States) was utilized to grow all the cells under 37°C and 5% CO_2 growth conditions.

Cell Transfection

SW780 along with the 5637 cells were transiently inserted with specific sgRNA targeting on lncRNA SNHG3 through transfection. The SNHG3 sgRNA sequence was listed as follows: sgRNA-1: 5′-GGACTTCCGGGCACTTCGTA-3′; sg-RNA-2: 5′-GGACTTCCGGGCACTTCGTA-3′; sgRNA-3: 5′-GATGCTTGCCACCGGAGTTG-3′. SNHG3 sgRNA (sg-SNHG3), and the sg-NC (negative control) were synthesized by GenePharma (Suzhou, China). The Lipofectamine 3000 (Invitrogen, Carlsbad, CA) was employed to transfect the bladder cancer cells as described by the manufacturer. Transfection was done after the cultured cells attained 50–70% confluence in six-well plates. We harvested the transfected cells for real-time quantitative PCR after 48 h.

RT-qPCR

The Trizol reagent (Invitrogen, Carlsbad, CA, United States) was utilized to isolate total RNA from the bladder cancer tissues and cells as described in the manual provided by the manufacturer. After that, cDNA was processed from 1 μg total RNA with the PrimeScript RT Reagent Kit with gDNA Eraser (Takara, Dalian, China) *via* reverse transcription. Subsequently, 2 μl of cDNA was employed as the template in qPCR process consisting of 10 μl of SYBR Green PCR kit mix (Takara, Dalian, China), 0.5 μl specific forward primer, 0.5 μl specific reverse primer, and 7 μl

of deionized water. This assay was carried out and analyzed on the ABI7000 system (Applied Biosystems, Foster City, CA, United States). The GAPDH gene served as the internal standard. Each sample was assayed in triplicate.

Cell Proliferation Assessment

The CCK along with the MTT assays were employed to study cell proliferation. At 48 h after transfection with sg-SNHG3 or sg-NC, we harvested the cells and then inoculated them in a 96-well plate for 24 h. Afterward, 10 μl CCK-8 reagent was introduced to every well at intervals of 0, 24, 48, and 72 h post cell attachment. The cells were cultured in darkness for 1 h. Next, a micro-plate reader (Bio-Rad, Hercules, CA, United States) was employed to determine the OD values at 450 nm. The MTT assay was employed to validate the CCK-8 assay data. In brief, we introduced 10 μl of MTT reagent to every well at 0, 24, 48, and 72 h post cell attachment. The cells were cultured in darkness for 1 h and then 100 μl of DMSO was introduced. A micro-plate reader (Bio-Rad, Hercules, CA, United States) was employed to determine the OD values at 450 nm after 10 min of vibration.

Cell Migration Assessment

Cell migration was explored by the scratch assay and transwell assay. The bladder cancer cells were inserted with specified sgRNA oligonucleotides when cells attained 90% confluence. At 24 h after transfection, we used a sterile 200 μl pipette tip to

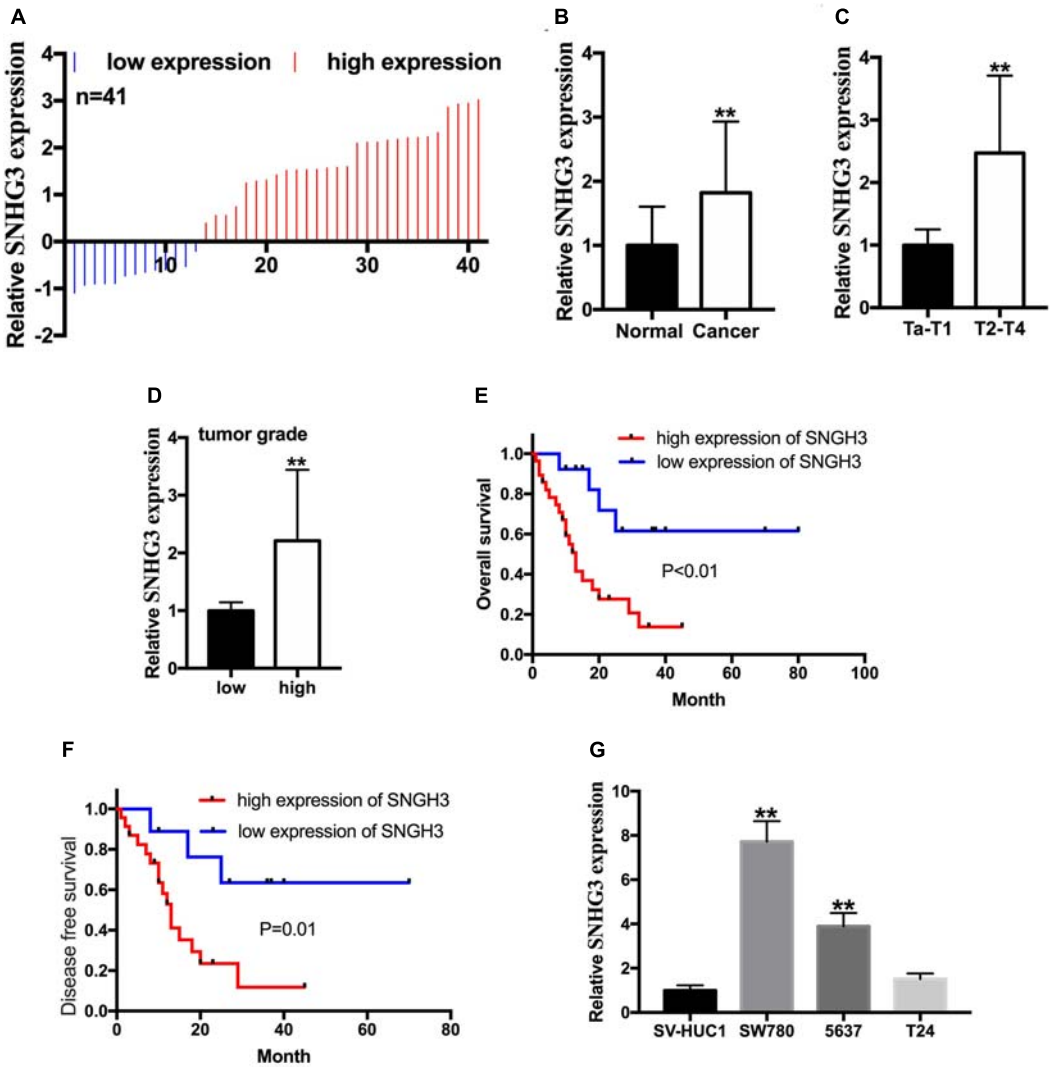

FIGURE 1 | SNGH3 was highly expressed in bladder cancer tissues, and cell lines. **(A)** 41 bladder cancer samples were analyzed herein. SNHG3 was highly expressed in 28 of 41 bladder cancer tissue samples. **(B)** Total SNHG3 expression in bladder cancer tissue was remarkably higher in contrast with that in matched neighboring non-malignant tissues. **(C)** SNGH3 RNA content was higher in T2-T4 stage cancers in contrast with those in Ta-T1 cancers. **(D)** SNGH3 RNA content was higher in high grade cancers in contrast with those in low grade cancers. **(E)** The association of SNGH3 content with OS. **(F)** The association of SNGH3 RNA content with DFS. **(G)** SNGH3 was overexpressed in SW780 and 5637 cells in contrast with that in SV-HUC1. Data were indicated as means ± SD from three independent experiments (**$P < 0.01$).

generate a clear line in the wells. The images of mobilized cells were captured from every well with a digital camera at 0 and 24 h post scratching for bladder cancer cells. Relative migration distance was measured using Photoshop software. To validate the scratch assay data, a transwell assay was also conducted. Approximately 10,000 transfected cells enriched with 100 μl serum-free medium were planted into the upper compartments (24-well plate, pore size 8 μm, Corning). 500 μl of DMEM medium enriched with 10% FBS was introduced into the lower compartments in each well. The cells were grown for 24 h and then the chambers were rinsed with PBS twice. Afterward, 4% paraformaldehyde fixation of the cells under the lower compartment surface was done for 30 min. Subsequently, 0.1% crystal violet staining of the cells was done for 40 min, followed by rinsing twice with PBS. An inverted microscope was employed to observe the migrated cells, which were imaged. Lastly, 600 μl of 33% glacial acetic acid was introduced to each chamber to wash out the crystal violet and was then incubated for 30 min. 100 μl of scrubbing solution was added to 96-well plates and a microplate reader was employed to examine the absorbance at 570 nm.

Caspase 3 ELISA Assay

Caspase 3 ELISA analysis was employed to investigate cell apoptosis. 5637 and SW780 bladder cancer cells were inserted with sg-SNHG3 or sg-NC in 12-well plates through transfection. Forty-eight hours post transfection, the activity of capase-3 was employed to assay the apoptosis caused by decreased SNHG3 expression as described in the manufacturer manual (Cusabio, Wuhan, China). Absorbance was examined by a microplate reader. The ratios between the OD values of the sg-SNHG3 cell transfects and those of the sg-NC cell transfects were employed to present the results. Experiments were replicated at least three times.

Statistical Analyses

All these statistical analyses were executed with SPSS 20.0. The Paired samples *t*-test was employed to explore the SNHG3 RNA expression differences between bladder cancer tissues and matching non-malignant tissues. Moreover, the differences in SNHG3 RNA content between cancer cells and SV-HUC1 were assessed using the independent samples *t*-test. The results of the CCK-8 assay and MTT assay were explored by the independent samples *t*-test at each time point. Cell migration along with an apoptosis assay were assessed by the independent samples *t*-test. $P < 0.05$ designated statistical significance.

RESULTS

LncRNA SNHG3 Is Highly Expressed in Bladder Cancer Tissues and Cell Lines

The relative lncRNA SNHG3 expression was determined by performing a qRT-PCR assay in bladder cancer tissues, as well as the cells. In contrast with the matching non-malignant bladder peritumoral tissues, SNHG3 expression was highly expressed in 68.3% (28 of 41) of bladder cancer tissues (**Figure 1A**). The SNHG3 expression fold change (bladder cancer tissues/corresponding non-malignant tissues) in total bladder cancer patients is shown in **Figure 1B**. Moreover, elevated SNHG3 content was strongly linked to the TNM stage along with histological grade of individuals with bladder cancer, but irrelevant to other clinical features, including gender, lymph node metastasis, age, distant metastasis, as well as tumor size (**Table 1**). The expression differences based on the TNM stage and histological grade were shown as follows. The SNHG3 expression fold change in T2-T4 stage bladder cancer tissues was 2.47 times

TABLE 1 | Relationship of SNGH3 expression with clinicopathological features of bladder cancer patients.

Parameters	Group	Total	Expression		*P*-value
			High	Low	
Gender	Male	26	16	10	0.221
	Female	15	12	3	
Age (years)	<60	10	6	4	0.779
	>>60	31	22	9	
Tumor size	<3	14	10	4	0.756
	>>3	27	18	9	
TNM stage	Ta + Tis + TI	12	5	7	0.009
	T2 or above	29	24	5	
Grade	Low	8	2	6	0.003
	High	33	26	7	
Lymph node metastasis	No	24	15	9	0.344
	N1 or above	17	13	4	
Distant metastasis	No	38	25	13	0.22
	Yes	3	3	0	

$P < 0.05$ signified statistical significance.

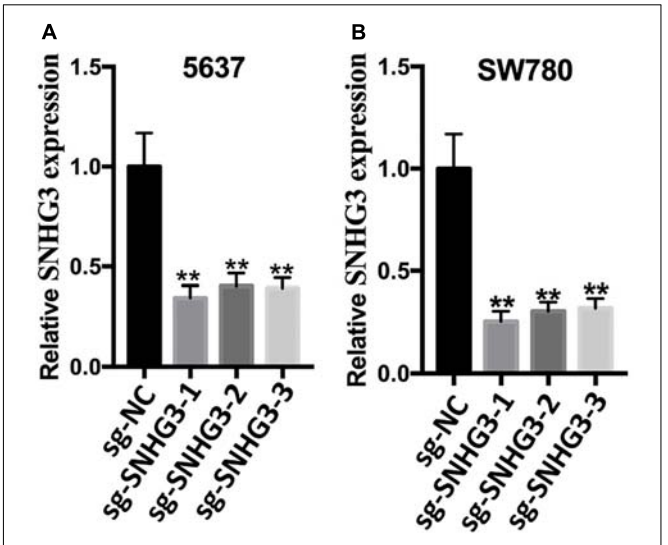

FIGURE 2 | Knockdown of SNGH3 expression. **(A)** Silencing of SNGH3 with sgRNA in 5637 cell. **(B)** Silencing of SNGH3 with sgRNA in SW780 cell. Data were indicated as means ± SD from three independent experiments (** denotes $P < 0.01$). sg: sgRNA.

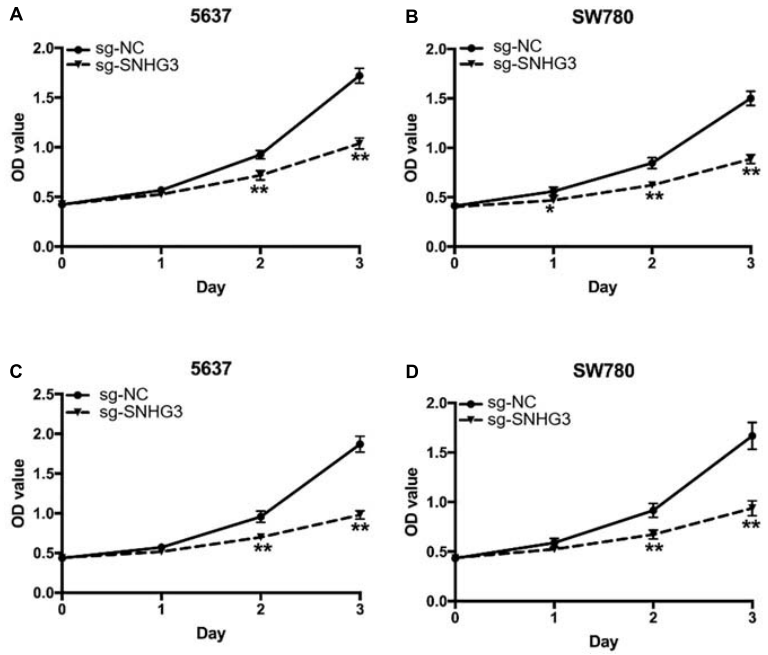

FIGURE 3 | SNGH3 silencing repressed *in vitro* cell proliferation. **(A,B)** CCK-8 assay illustrated that repression of SNGH3 reduced the growth of 5637 and SW780 cells. **(C,D)** MTT assay illustrated that SNGH3 silencing dramatically repressed the growth of 5637 and SW780 cells. Data were indicated as means ± SD from three independent experiments (** denotes $P < 0.01$, * denotes $P < 0.05$). sg: sgRNA.

that in Ta-T1 stage bladder cancer tissues (**Figure 1C**). The SNHG3 expression fold change in high grade bladder cancer tissues was 2.21 times that in low grade bladder cancer tissues (**Figure 1D**). Moreover, the OS (**Figure 1E**) and DFS (**Figure 1F**) in the SNHG3 overexpression group was remarkably lower in contrast to that in the SNHG3 down-regulation group, indicating that SNHG3 could be applied as a prognostic indicator for bladder cancer. Lastly, we established that SNHG3 was highly expressed in the bladder cancer cells (5637 and SW780) in contrast to that in SV-HUC1 (**Figure 1G**), implying that SNHG3 is a bladder cancer oncogene. Hence, 5637 and SW78O cells were selected to perform functional experiments.

Specific sgRNA Inhibited the Expression of SNHG3

According to the promoter sequence of SNHG3, we designed three different sgRNAs (sg-SNHG3-3, sg-SNHG3-2, as well as sg-SNHG3-1) targeting SNHG3 and evaluated their efficiencies in 5637 and SW780 bladder cancer cells inserted with a sg-SNHG3 or sgRNA negative control (sg-NC). At 48 h post transfection, SNHG3 expression was measured. As shown in **Figures 2A,B**, sg-SNHG3-1 induced the maximal knockdown effect of SNHG3 in 5637 and SW780 cells. Therefore, sg-SNHG3-1 was used to perform the functional experiments.

Suppression of SNHG3 Repressed Cell Proliferation

To assess the influence of SNHG3 on cell growth, CCK-8 assay along with MTT assay were carried out. As indicated in

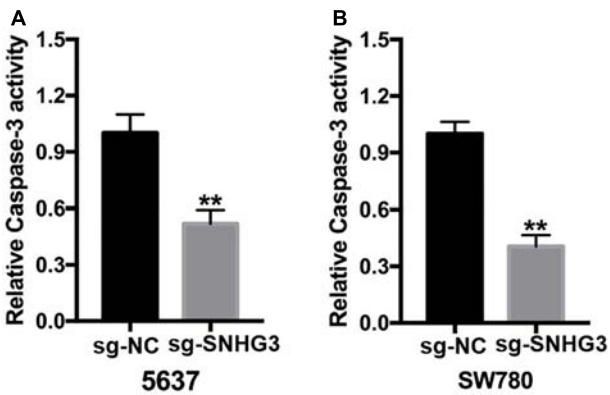

FIGURE 4 | SNGH3 silencing triggered cell apoptosis. **(A)** Relative caspase activity in the 5637 cells transfected with sg-SNGH3 was remarkably increased in contrast with that in the negative control group. **(B)** Relative caspase-3 activity in the sg-SNGH3 transfected SW780 cells was remarkably up-regulated in contrast with that in the negative control group. Data were indicated as means ± SD from three independent experiments (**$P < 0.01$). sg: sgRNA.

Figures 3A,B, the results of CCK-8 demonstrated that sg-SNHG3 repressed cell growth remarkably in both 5637 and SW780 cells. In addition, the results of MTT were congruent with the results of the CCK-8 assay data. As indicated in **Figures 3C,D**, SNHG3 silencing remarkably reduced the growth curve of SW780 and 5637 cells. Collectively, the data confirmed that suppression of SNHG3 inhibited bladder cancer cell growth.

SNHG3 Silencing Promoted Cell Apoptosis

Forty-eight hours post transfection, we harvested the bladder cancer cells and then used them to perform the Capase-3 ELISA assay. As indicated in **Figures 4A,B**, there were remarkably elevated relative Capase-3 activity in sg-SNHG3 bladder cancer cells in contrast with sg-NC cell transfects.

Knockdown of SNHG3 Inhibited Cell Migration and Infiltration

The scratch assay along with the transwell assay were employed to verify the effect of SNHG3 on cell migration, as well as infiltration. The scratch experiment showed that bladder cancer cells transfected with sg-SNHG3 exhibited a slower rate of closing of scratched wounds in contrast with the sg-NC groups (**Figures 5A,B**). Further data analysis indicated that the relative migration distance in the sg-SNHG3 group was decreased by 49% in the 5637 cell (**Figure 5C**) and reduced by 60% in the SW780 cell (**Figure 5D**). The Transwell assay was additionally conducted to explore bladder cancer cell invasion. In contrast with the sg-NC group, cell infiltration potential of the sg-SNHG3 group was extremely inhibited in the 5637 (**Figure 6A**) and SW780 cells (**Figure 6B**). The OD value of washing-up liquid in the sg-SNHG3 transfected 5637 (**Figure 6C**) and SW780 cells (**Figure 6D**) was remarkably lower in contrast with the sg-NC group. Altogether, these data revealed that SNHG3 silencing repressed migration along with the infiltration of bladder cancer cells.

DISCUSSION

LncRNAs are a kind of non-protein coding RNAs with a length of about 200 nucleotides. Mounting research evidence suggest that lncRNAs are involved with gene expression regulation by

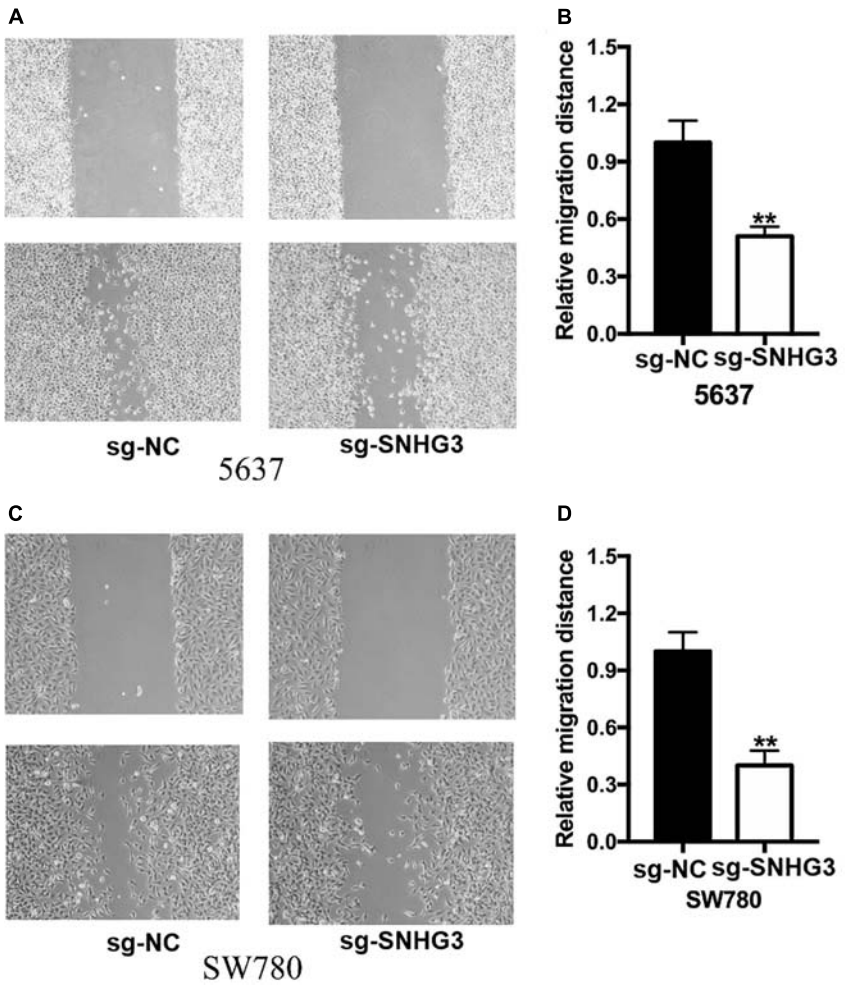

FIGURE 5 | Silencing of SNGH3 repressed migration of cells. The wound healing experiment was applied to examine bladder cancer cell migration. **(A)** Suppression of SNGH3 caused a slower closing of scratch wounds in 5637 cells. **(B)** Reduced cell migration was reported in 5637 cells treated with sg-SNGH3. **(C)** Knockdown of SNGH3 caused a slower closing of scratch wounds in SW780 cells. **(D)** Cell migration inhibition was assayed in SW780 cells treated with sg-SNGH3. Data were indicated as means ± SD from three independent experiments (** denotes $P < 0.01$). sg: sgRNA.

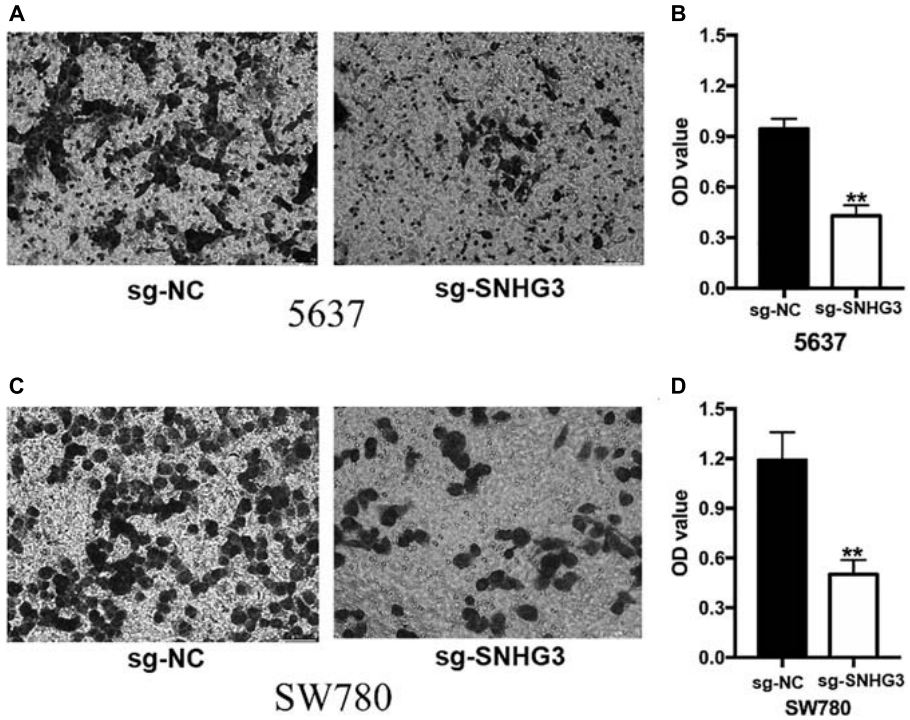

FIGURE 6 | SNGH3silencing inhibited cell infiltration. Transwell assay was employed to explore bladder cancer cell infiltration. **(A)** Images illustrating transwell assay in 5637 cells. **(B)** Inhibition of SNGH3 reduced the invasion of 5637 cells. **(C)** Images illustrating wound healing assay in SW780 cells. **(D)** Inhibition of SNGH3 reduced the invasion of 5637 cells. Data were indicated as means ± SD from three independent experiments (** denotes $P < 0.01$). sg: sgRNA.

affecting the gene transcription, post-transcriptional process, and chromatin modification (Meller et al., 2015; Engreitz et al., 2016). Furthermore, lncRNAs can act as competitive endogenous RNA to capture microRNA which can suppress the transcriptional and translational process by docking to the 3′UTR region of mRNA (Thomson and Dinger, 2016). Hence, lncRNAs participate in modulatory roles in nearly all the biological processes, constituting cell growth, tissue, as well as organ development, cell apoptosis, energy metabolism, and so on (Kopp and Mendell, 2018; Krause, 2018). However, dysregulation of lncRNAs will cause the disorder of the internal environment and multiple types of human diseases, especially cancers. Aberrant expression of lncRNAs can enhance the growth, infiltration, and drug resistance of cancer cells. Moreover, the disorder of lncRNAs can disturb the cell apoptosis process (Parasramka et al., 2016; Schmitt and Chang, 2016). For instance, upregulation of lncRNA HOXD-AS1 has been documented in bladder cancer tissues, as well as cells, and HOXD-AS1 can enhance the cell growth and migration, but can repress cell apoptosis during the progression of bladder cancer (Li et al., 2016). LncRNA SPRY4-IT1 enhances the growth along with the metastasis of bladder cancer cells though sponging miR-101-3p to increase EZH2 expression (Li et al., 2017; Liu et al., 2017). As a recently identified lncRNA, multiple previous studies were summarized to characterize the oncogenic features of lncRNA SNHG3, a 2,238 nt in length lncRNA located on chromosome 1p36.1. SNHG3 is overexpressed in hepatocellular carcinoma (HCC) tissues in contrast with the matched non-malignant tissues. SNHG3 RNA content is positively correlated with portal vein tumor thrombus tumor size and tumor relapse of HCC patients. Increased expression of SNHG3 causes lower OS, poorer recurrence-free survival, as well as lower DFS (Zhang et al., 2016). Zhang et al. (2018) demonstrated that overexpression of SNHG3 facilitates cell infiltration, the epithelial−mesenchymal transition (EMT) progress, along with sorafenib resistance by sponging miR−128 to up-regulate CD151 expression in HCC cells. Huang et al. (2017) extracted the data from the TCGA dataset and documented that SNHG3 was up-regulated in CRC tissues and cells in contrast with neighboring non-malignant tissues and normal cells, respectively. SNHG3 silencing repressed cell growth and tumor growth by capturing miR-182-5p, which can suppress c-Myc expression. Fei et al. (2018) found that SNHG3 could recruit EZH2 to the KLF2 and p21 promoter region to suppress KLF2 and p21 expression in the malignant progression of glioma cells. Li et al. (2018) also extracted the data of ovarian cancer from the TCGA data resource and documented that SNHG3 was closely linked to the OS and energy metabolism. Further analysis suggested that SNHG3 absorbed miRNAs and EIF4AIII to affect the expression of UQCRH, IDH2, PKM, and PDHB and in the energy metabolism related cascades. Moreover, SNGH3 was remarkably overexpressed in lung adenocarcinoma samples in contrast with neighboring samples. Forced SNGH3 expression facilitated A549 cell growth and inhibited A549 cell apoptosis (Liu et al., 2018). In general, SNGH3 is overexpressed in HCC,

CRC, glioma, and lung adenocarcinoma. SNGH3 promotes the malignant phenotype of these cancer cells *via* sponging miRNA or acting as a protein scaffold.

CRISPR-dCas9 is a new gene regulation system which was developed in 2013 (Vigouroux et al., 2018; Lee et al., 2021). It was first used in bacteria and was later widely used in human cells. The mutated dCas9 protein cannot cut DNA but can bind to the promoter region or ORF region of the gene, thus hindering the normal transcription of the gene through steric hindrance. This tool is very suitable for studying the function of lncRNAs.

To the best of our knowledge, this is the first report to explore the role of lncRNA SNGH3 in bladder cancer. Herein, it was discovered that SNGH3 was highly expressed in bladder cancer tissues along with the cell lines, in contrast with the matched non-malignant tissue and cell. Elevated SNGH3 expression was directly linked to the TNM stage, as well as the histological grade of bladder cancer. Moreover, bladder cancer individuals with high SNGH3 expression showed worse OS and DFS. The differential SNGH3 expression trends between bladder cancer tissues and non-malignant tissues and the correlation of SNGH3 with clinic pathological data indicate that SNGH3 emerges as a pivotal player in the onset and progression of bladder cancer. A further functional assay showed that cell proliferation, repression reduced motility, and escalated apoptosis were remarkably detected in the sg-SNGH3 transfected group. These findings demonstrated that SNGH3 played oncogenic roles in the development of bladder cancer. Furthermore, SHGH3 may act as prospective prognostic biomarker and treatment target for bladder cancer. Targeting on SNGH3 using CRISPR technology may be a valuable strategy to fight against bladder cancer.

DATA AVAILABILITY STATEMENT

The original contributions presented in the study are included in the article/supplementary material, further inquiries can be directed to the corresponding author/s.

ETHICS STATEMENT

The studies involving human participants were reviewed and approved by the Research Ethics Committee of the Affiliated Foshan Maternal and Child Healthcare Hospital. The patients/participants provided their written informed consent to participate in this study.

AUTHOR CONTRIBUTIONS

YC, QH, RZ, LL, MG, HW, LZ, and JW performed the biological experiments and data analyses. CL designed and supervised the project. All authors contributed to the article and approved the submitted version.

FUNDING

This work was supported by the Guangdong Provincial Medical Science and Technology Research Funding (No. 20205792148508), the Changsha Science and Technology Bureau project (No. kq1907033), the National Nature Science Foundation of China (No. 81703919), and the Hunan Natural Science Foundation (No. 2020JJ5418).

REFERENCES

Bray, F., Ferlay, J., Soerjomataram, I., Siegel, R. L., Torre, L. A., and Jemal, A. (2018). Global cancer statistics 2018: GLOBOCAN estimates of incidence and mortality worldwide for 36 cancers in 185 countries. *CA Cancer J. Clin.* 68, 394–424. doi: 10.3322/caac.21492

Chen, D., Liu, L., Wang, K., Yu, H., Wang, Y., Liu, J., et al. (2017). The role of MALAT-1 in the invasion and metastasis of gastric cancer. *Scand. J. Gastroenterol.* 52, 790–796. doi: 10.1080/00365521.2017.1280531

Chen, Y., Xie, H., Zou, Y., Lai, X., Ma, L., Liu, Y., et al. (2017). Tetracycline-controllable artificial microRNA-HOTAIR + EZH2 suppressed the progression of bladder cancer cells. *Mol. Biosyst.* 13, 1597–1607. doi: 10.1039/c7mb00202e

Chen, Y., Zhao, F., Cui, D., Jiang, R., Chen, J., Huang, Q., et al. (2018). HOXD-AS1/miR-130a sponge regulates glioma development by targeting E2F8. *Int. J. Cancer* 142, 2313–2322. doi: 10.1002/ijc.31262

Dy, G. W., Gore, J. L., Forouzanfar, M. H., Naghavi, M., and Fitzmaurice, C. (2017). Global Burden of Urologic Cancers, 1990-2013. *Eur. Urol.* 71, 437–446. doi: 10.1016/j.eururo.2016.10.008

Engreitz, J. M., Ollikainen, N., and Guttman, M. (2016). Long non-coding RNAs: spatial amplifiers that control nuclear structure and gene expression. *Nat. Rev. Mol. Cell Biol.* 17, 756–770. doi: 10.1038/nrm.2016.126

Evans, J. R., Feng, F. Y., and Chinnaiyan, A. M. (2016). The bright side of dark matter: lncRNAs in cancer. *J. Clin. Invest.* 126, 2775–2782. doi: 10.1172/jci84421

Fei, F., He, Y., He, S., He, Z., Wang, Y., Wu, G., et al. (2018). LncRNA SNHG3 enhances the malignant progress of glioma through silencing KLF2 and p21. *Biosci. Rep.* 38:BSR20180420.

Guo, T., Wang, H., Liu, P., Xiao, Y., Wu, P., Wang, Y., et al. (2018). SNHG6 Acts as a Genome-Wide Hypomethylation Trigger via Coupling of miR-1297-Mediated S-Adenosylmethionine-Dependent Positive Feedback Loops. *Cancer Res.* 78, 3849–3864. doi: 10.1158/0008-5472.can-17-3833

Huang, W., Tian, Y., Dong, S., Cha, Y., Li, J., Guo, X., et al. (2017). The long non-coding RNA SNHG3 functions as a competing endogenous RNA to promote malignant development of colorectal cancer. *Oncol. Rep.* 38, 1402–1410. doi: 10.3892/or.2017.5837

Huarte, M. (2015). The emerging role of lncRNAs in cancer. *Nat. Med.* 21, 1253–1261. doi: 10.1038/nm.3981

Jandura, A., and Krause, H. M. (2017). The New RNA World: Growing Evidence for Long Noncoding RNA Functionality. *Trends Genet.* 33, 665–676. doi: 10.1016/j.tig.2017.08.002

Kamat, A. M., Hahn, N. M., Efstathiou, J. A., Lerner, S. P., Malmstrom, P. U., Choi, W., et al. (2016). Bladder cancer. *Lancet* 388, 2796–2810.

Kopp, F., and Mendell, J. T. (2018). Functional Classification and Experimental Dissection of Long Noncoding RNAs. *Cell* 172, 393–407. doi: 10.1016/j.cell.2018.01.011

Krause, H. M. (2018). New and Prospective Roles for lncRNAs in Organelle Formation and Function. *Trends Genet.* 34, 736–745. doi: 10.1016/j.tig.2018.06.005

Lee, M. H., Lin, C. C., Thomas, J. L., Li, J. A., and Lin, H. Y. (2021). Cellular reprogramming with multigene activation by the delivery of CRISPR/dCas9 ribonucleoproteins via magnetic peptide-imprinted chitosan nanoparticles. *Mater. Today Bio.* 9:100091. doi: 10.1016/j.mtbio.2020.100091

Li, J., Chen, Y., Chen, Z., He, A., Xie, H., Zhang, Q., et al. (2017). SPRY4-IT1: A novel oncogenic long non-coding RNA in human cancers. *Tumour Biol.* 39:1010428317711406.

Li, J., Zhuang, C., Liu, Y., Chen, M., Chen, Y., Chen, Z., et al. (2016). Synthetic tetracycline-controllable shRNA targeting long non-coding RNA HOXD-AS1 inhibits the progression of bladder cancer. *J. Exp. Clin. Cancer Res.* 35:99.

Li, N., Zhan, X., and Zhan, X. (2018). The lncRNA SNHG3 regulates energy metabolism of ovarian cancer by an analysis of mitochondrial proteomes. *Gynecol. Oncol.* 150, 343–354. doi: 10.1016/j.ygyno.2018.06.013

Liu, D., Li, Y., Luo, G., Xiao, X., Tao, D., Wu, X., et al. (2017). LncRNA SPRY4-IT1 sponges miR-101-3p to promote proliferation and metastasis of bladder cancer cells through up-regulating EZH2. *Cancer Lett.* 388, 281–291. doi: 10.1016/j.canlet.2016.12.005

Liu, L., Ni, J., and He, X. (2018). Upregulation of the Long Noncoding RNA SNHG3 Promotes Lung Adenocarcinoma Proliferation. *Dis. Markers* 2018:5736716.

Marchese, F. P., Raimondi, I., and Huarte, M. (2017). The multidimensional mechanisms of long noncoding RNA function. *Genome Biol.* 18:206.

Massari, F., Santoni, M., di Nunno, V., Cheng, L., Lopez-Beltran, A., Cimadamore, A., et al. (2018). Adjuvant and neoadjuvant approaches for urothelial cancer: Updated indications and controversies. *Cancer Treat. Rev.* 68, 80–85. doi: 10.1016/j.ctrv.2018.06.002

Meller, V. H., Joshi, S. S., and Deshpande, N. (2015). Modulation of Chromatin by Noncoding RNA. *Annu. Rev. Genet.* 49, 673–695. doi: 10.1146/annurev-genet-112414-055205

Milevskiy, M. J., Al-Ejeh, F., Saunus, J. M., Northwood, K. S., Bailey, P. J., Betts, J. A., et al. (2016). Long-range regulators of the lncRNA HOTAIR enhance its prognostic potential in breast cancer. *Hum. Mol. Genet.* 25, 3269–3283.

Parasramka, M. A., Maji, S., Matsuda, A., Yan, I. K., and Patel, T. (2016). Long non-coding RNAs as novel targets for therapy in hepatocellular carcinoma. *Pharmacol. Ther.* 161, 67–78.

Ponting, C. P., Oliver, P. L., and Reik, W. (2009). Evolution and functions of long noncoding RNAs. *Cell* 136, 629–641.

Portoso, M., Ragazzini, R., Brencic, Z., Moiani, A., Michaud, A., Vassilev, I., et al. (2017). PRC2 is dispensable for HOTAIR-mediated transcriptional repression. *EMBO J.* 36, 981–994.

Quinodoz, S., and Guttman, M. (2014). Long noncoding RNAs: an emerging link between gene regulation and nuclear organization. *Trends Cell Biol.* 24, 651–663.

Schmitt, A. M., and Chang, H. Y. (2016). Long Noncoding RNAs in Cancer Pathways. *Cancer Cell* 29, 452–463.

Shan, Y., Ma, J., Pan, Y., Hu, J., Liu, B., and Jia, L. (2018). LncRNA SNHG7 sponges miR-216b to promote proliferation and liver metastasis of colorectal cancer through upregulating GALNT1. *Cell Death Dis.* 9:722.

Sun, Y., Wei, G., Luo, H., Wu, W., Skogerbo, G., Luo, J., et al. (2017). The long noncoding RNA SNHG1 promotes tumor growth through regulating transcription of both local and distal genes. *Oncogene* 36, 6774–6783.

Thomson, D. W., and Dinger, M. E. (2016). Endogenous microRNA sponges: evidence and controversy. *Nat. Rev. Genet.* 17, 272–283.

Tsai, M. C., Manor, O., Wan, Y., Mosammaparast, N., Wang, J. K., Lan, F., et al. (2010). Long noncoding RNA as modular scaffold of histone modification complexes. *Science* 329, 689–693.

Vigouroux, A., Oldewurtel, E., Cui, L., Bikard, D., and van Teeffelen, S. (2018). Tuning dCas9's ability to block transcription enables robust, noiseless knockdown of bacterial genes. *Mol. Syst. Biol.* 14:e7899.

Wu, C., Zhu, X., Tao, K., Liu, W., Ruan, T., Wan, W., et al. (2018). MALAT1 promotes the colorectal cancer malignancy by increasing DCP1A expression and miR203 downregulation. *Mol. Carcinog.* 57, 1421–1431.

Zhang, P. F., Wang, F., Wu, J., Wu, Y., Huang, W., Liu, D., et al. (2018). LncRNA SNHG3 induces EMT and sorafenib resistance by modulating the miR-128/CD151 pathway in hepatocellular carcinoma. *J. Cell Physiol.* 234, 2788–2794.

Zhang, T., Cao, C., Wu, D., and Liu, L. (2016). SNHG3 correlates with malignant status and poor prognosis in hepatocellular carcinoma. *Tumour Biol.* 37, 2379–2385.

Conflict of Interest: The authors declare that the research was conducted in the absence of any commercial or financial relationships that could be construed as a potential conflict of interest.

frontiers in Molecular Biosciences

ORIGINAL RESEARCH
published: 29 March 2021
doi: 10.3389/fmolb.2021.654718

Up-Regulating ERIC by CRISPR-dCas9-VPR Inhibits Cell Proliferation and Invasion and Promotes Apoptosis in Human Bladder Cancer

*Jiangeng Yang, An Xia, Huajie Zhang, Qi Liu, Hongke You, Daoyuan Ding, Yonghua Yin and Bo Wen**

Department of Urology, Shenzhen Hospital of Integrated Traditional Chinese and Western Medicine, Shenzhen, China

LncRNAs are defined as non-coding RNAs that are longer than 200 nucleotides in length. The previous studys has shown that lncRNAs played important roles in the regulation of gene expression and were essential in mammalian development and disease processes. Inspired by the observation that lncRNAs are aberrantly expressed in tumors, we extracted RNA from Bladder urothelial carcinoma and matched histologically normal urothelium from each patient and bladder carcinoma cell lines. Then, we reversed transcribed them into cDNA.Last, we investigated the expression patterns of ERIC by the fluorescence quantitative PCR in bladder cancer tissues and cell lines. CRISPR-dCas9-VPR targeting ERIC plasmid was transfected into T24 and 5637 cells, and cells were classified into two groups: negative control (NC) and ERIC overexpression group. MTT assay, transwell assay, and flow cytometry were performed to examine changes in cell proliferation, invasiveness, and apoptosis. We found that the expression of ERIC was down-regulated in bladder urothelial carcinoma compared to matched histologically normal urotheliam. The differences of the expression of this gene were large in the bladder cancer lines. Compared with the negative control group, the ERIC overexpression group showed significantly decreased cell proliferation rate (t = 7.583, $p = 0.002$; $t = 3.283$, $p = 0.03$) and invasiveness ($t = 11.538$, $p < 0.001$; $t = 8.205$, $p = 0.01$); and increased apoptotic rate (t = –34.083, $p < 0.001$; t = –14.316, $p < 0.001$). Our study lays a foundation for further study of its pathogenic mechanism in bladder cancer.

Keywords: CRISPR-dCas9-VPR, long non coding RNA, ERIC, cancer, bladder

OPEN ACCESS

Edited by:
Yonghao Zhan,
Zhengzhou University, China

Reviewed by:
Congcong CAO,
Peking University Shenzhen Hospital, China
Kai Yang,
Zhejiang University, China

****Correspondence:***
Bo Wen
tjwb001@126.com

Specialty section:
This article was submitted to Molecular Diagnostics and Therapeutics, a section of the journal Frontiers in Molecular Biosciences

Received: *17 January 2021*
Accepted: *08 February 2021*
Published: *29 March 2021*

Citation:
Yang J, Xia A, Zhang H, Liu Q, You H, Ding D, Yin Y and Wen B (2021) Up-Regulating ERIC by CRISPR-dCas9-VPR Inhibits Cell Proliferation and Invasion and Promotes Apoptosis in Human Bladder Cancer. Front. Mol. Biosci. 8:654718. doi: 10.3389/fmolb.2021.654718

INTRODUCTION

Long non-coding RNA (lncRNAs) is an RNA molecule with a length greater than 200bp. It has mrna-like structure and polyA tail and promoter structure after splicing. During differentiation, it has dynamic expression and different splicing modes. LncRNAs are mainly transcribed by RNA polymerase II (RNA PII), polyadenylation and splicing, and most of them are located in the nucleus (Zhang et al., 2013). LncRNAs do not encode proteins, but regulate gene expression in the form of RNA at the epigenetic, transcriptional and post-transcriptional levels (Mattick, 2005).

At first, researchers found that they do not encode proteins, so they were treated as the "noise" of genome transcription, with no biological function (Gershon, 2005). With the deepening of studies on lncRNAs, the regulatory mechanism of lncRNAs in cells has gradually attracted extensive attention. At present, the functions of most of the lncRNAs have not been clearly studied, but most scholars believe that the study of lncRNAs will help to understand the complex gene regulatory network of living organisms, and is expected to provide new molecular basis for the prediction, diagnosis and treatment of complex diseases (Zhang et al., 2013).

Numerous studies have shown that the expression level of certain lncRNAs can be significantly changed in tumor tissues and cells. For example, pcat-1 and PCGEM1 are significantly down-regulated in prostate cancer (Gibb et al., 2011; Prensner et al., 2011). While in breast cancer, GAS5 is overexpressed (Mourtada-Maarabouni et al., 2009). This change may be closely related to many biological processes, so lncRNAs can provide a basis and target for the molecular diagnosis and treatment of malignant tumors. With the rapid development of high-throughput screening sequencing technology and bioinformatics, more lncrnas with important functions in tumors will be discovered, which will also provide new theories and basis for the diagnosis and treatment of these major diseases.

ERIC, e2f1-regulated Inhibitor of Cell Death, is a long non-coding RNA–XLOC 006942. The gene is regulated by E2Fs transcription and inhibits apoptosis induced by E2F1 and DNA damage. On the chromosome diagram, ERIC (also known as TCONS_00014875) is located on chromosome 8 (CHR 8:141646242–141648531), corresponding to a position on band 8q24.3, and transcribed from the positive chain. ERIC is composed of two exons and a transcription sequence with a size of 1745 bp (Feldstein et al., 2013).

Bladder cancer is the most common malignant tumor in the genitourinary system, which is mainly divided into three subtypes: transitional cell carcinoma (TCC), squamous cell carcinoma (SCC) and adenocarcinoma. Its main pathological type is TCC, accounting for more than 90% of cases of bladder cancer (Rahmani et al., 2013). Among them, 70–80% of patients were diagnosed as non-muscular invasive bladder cancer (formerly known as superficial bladder cancer), and the other 20–30% were diagnosed as muscular invasive bladder cancer.

The incidence of bladder cancer ranks 9th among all malignant tumors and 6th among male tumors. Globally, there are 350,000 new cases a year (Griffiths, 2013). In the United States, there are 72,570 new cases of bladder cancer and 15,210 new deaths each year (Siegel et al., 2013). It costs $40 billion a year in the United States alone to treat bladder cancer, which requires repeated examinations and follow-up treatment after surgery. Thus, bladder cancer is the most expensive malignancy in the United States on average per patient. In China, the incidence and mortality of bladder cancer are the highest in urinary system tumors. In the past decade, the incidence of the disease has been increasing year by year and getting younger (Li et al., 2017). The most common treatment for bladder cancer is surgery, chemotherapy, immunotherapy, and radiation (Liu et al., 2012). Many patients were already in the middle and late stage when they went to the doctor. Bladder cancer, like other cancers, has become a major public health problem threatening human health.

Currently, the pathogenesis of bladder cancer is still not clear. However, with the development of molecular biology and genetic technology in recent years, more and more scholars believe that the pathogenesis of bladder cancer is a complex process involving multiple factors, multiple genes and multiple steps. Accumulation of abnormal mutant genotypes and the role of external oncogenic environment eventually led to the emergence of malignant phenotype of bladder cancer. It is an urgent task to explore the pathogenesis of bladder cancer and find specific targets for bladder cancer, so as to achieve early diagnosis, effective treatment and prevent its recurrence.

Currently, some international scholars have proposed the hypothesis of abnormal chromatin remodeling in tumors, including bladder cancer (Michaeleen, 2011). Most studies of long non-coding RNAs have recognized that they regulate the expression of many genes mainly through large region chromatin remodeling (Costa, 2008). So LncRNAs are important regulators of the interaction between gene expression and the important pathways of cell growth, proliferation, differentiation and survival. Changes in the function of lncRNAs promote tumor formation and development, as well as metastasis of prostate cancer, bladder cancer and renal cell carcinoma. LncRNAs can be used as non-invasive tumor markers in malignant tumors of the urinary system. The increasing study on the molecular mechanism of LncRNAs in normal and malignant cells will contribute to a better understanding of tumor biology and may be a new therapeutic target for the treatment of cancer of the urinary system (Chung et al., 2011; Luo et al., 2013; Yang et al., 2013; Martens-Uzunova et al., 2014). Therefore, lncRNAs with significant expression differences in bladder cancer were screened out to further explore their biological functions, which will bring new opportunities for the diagnosis, treatment and postoperative detection of this disease.

METHODS

Sample Collection

A total of 5 bladder cancer samples were obtained. The 4 normal samples were defined as bladder tissues located 2.0 cm outside of visible cancer lesions. All resection samples were confirmed to be bladder cancer by clinical pathology. The collection and use of the patient samples were reviewed and approved by the Institutional Ethics Committee of Shenzhen Shajing Affiliated Hospital of Guangzhou Medical University, and written informed consent from all patients was appropriately obtained.

Cell Culture

The bladder cancer cell lines T24 and 5,637 were purchased from the Institute of Cell Research, Chinese Academy of Sciences, Shanghai, China. These cells were cultured in DMEM medium which had added 10% fetal bovine serum, and were grown in the 37°C atmosphere which contains 5% CO_2.

Total RNA Preparation and Reverse Transcription

Total RNA was extracted from tissue samples, and cell lines using TRIZOL (Invitrogen, United States) according to the manufacture's protocol and evaluated using Agilent 2,100 Bioanalyzer (Agilent Technologies, United States). RT was carried out using Omniscript Reverse Transcriptase kit (Qiagen, Hilden, Germany). The total reaction volume was 20 µl including 1 µg RNA. The reaction mixture was incubated at 42°C for 60 min, heated at 95°C for 10 min and then cooled on ice. The reaction was diluted 1:1 with water and aliquoted for further analysis.

qRT-PCR Assay

The TRIzol reagent (Invitrogen, Carlsbad, CA, United States) was used to extract the total RNAs from the cancer tissues and bladder cancer cell lines. The cDNAs were synthesized from the total extracted RNAs with the RevertAid™ First Strand cDNA Synthesis Kit (Fermentas, Hanover, MD, United States). The All-in-One™ qPCR Mix (GeneCopoiea Inc., Rockville, MD, United States) was used to carry out the qRT-PCR assay in our study. ERIC forward primer:5′- AGCCTGTGGCTACCT CCTTT-3′; reverse primer:5′- CTTGCACCCATATGCAGACA-3′; GAPDH forward primer:5′-CGCTCTCTGCTCCTCCTGTTC-3′; reverse primer:5′-ATCCGTTGACTCCGACCTTCAC-3′.

Plasmid Transfection

The CRISPR-dCas9-VPR targeting ERIC plasmid used in this experiment was purchased from Gima Company. After transforming into competent *Escherichia coli* DH5alpha, the plasmids were extracted by monoclone and sequenced to verify the cloned plasmids. At the logarithmic growth stage, cells were transfected into 24-well plates to adjust the cell density to 4×10^5/well; the fusion degree of cells was 70 –80%. In accordance with the Lipofectamine 2,000 transfection instructions, the plasmids were transfected into T24 and 5,637. The cells were cultured in a constant-temperature incubator with 5% CO_2 at 37°C. After 48 h, the culture plates were taken out and the cells were collected for subsequent experiments.

MTT Assay

Cells in logarithmic growth phase were cultured overnight in an incubator in 5% CO_2 at 37°C for 4 h after adjusting the cell density to 5×10^4 cells/mL. The cells were seeded in a 96-well plate in 100 µL of cell suspension and then cultured in a constant-temperature incubator with 5% CO_2 at 37°C for 4 h. After incubation, 0.15 mL DMSO was added and the suspension was shaken for 10 min. Optical density at 568 nm (OD_{568}) was measured using a microplate reader.

Transwell Assay

After 48 h of successful transfection, the cells of each group were digested, collected with 0.25% trypsin, and centrifuged. The cells were then washed twice with pre-cooled phosphate-buffered saline (PBS). Cells were suspended in a serum-free medium and counted by the plate count method. Next, 0.8 mL medium with 10% FBS was transferred into a 24-well plate, which was then placed in a transwell chamber. Then 1 mg/mL matrigel (100 µL) was added vertically to the bottom of the upper transwell chamber. After the matrigel solidified, 200 mL cell suspension was added to the upper transwell chamber and cultured in 5% CO_2 at 37°C for 24 h. The transwell was then removed; the chamber was washed with PBS; and the cells were fixed in 10% MeOH. After 30 min, the membrane was removed; the cells were subjected to crystal violet (0.5%) staining at room temperature for 20 min and finally washed with PBS. Images were acquired and cell numbers calculated under a microscope.

Flow Cytometry

After 2 days of culture, cells were subjected to trypsin digestion (0.25%) and then collected in a special flow tube. Approximately

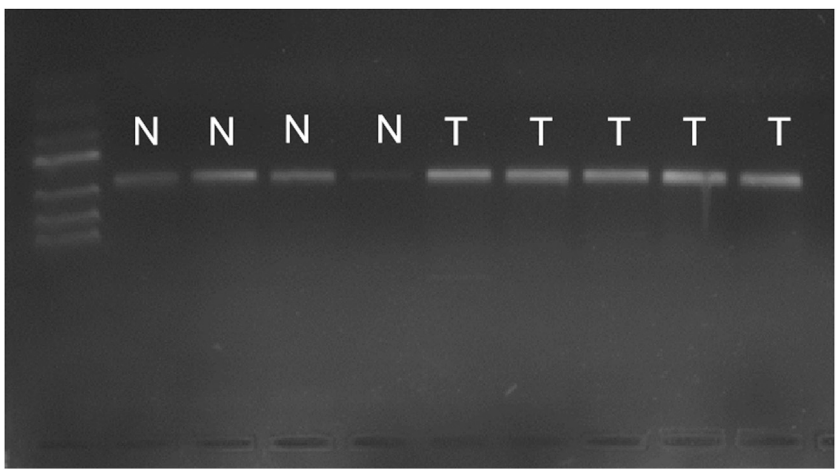

FIGURE 1 | PCR results of cancer tissues and adjacent tissues. Bands of PCR in both the cancerous tissue and the paracancer tissueN, normal bladder tissurs. T, bladder tumor tissues.

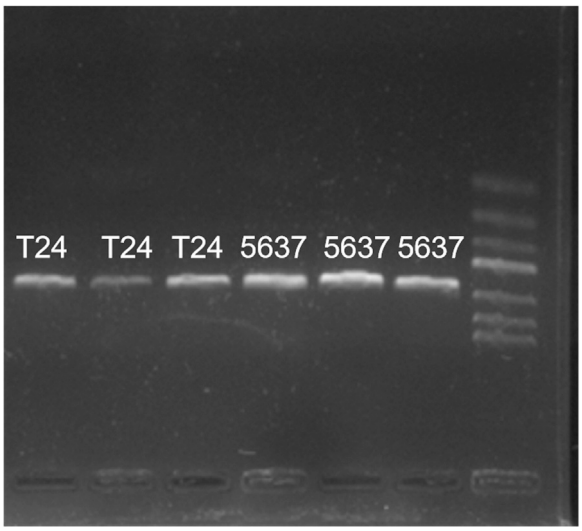

FIGURE 2 | General PCR results of cell lines T24 and 5,637 cDNA. PCR bands were observed in both cell lines T24 and 5,637, while the band brightness of the three groups of 5,637 was lighter than that of T24.

10^5 suspended cells were centrifuged. Detection was conducted following the instructions of the Annexin V-APC/7-AAD detection kit. Binding buffer (0.05 mL, 5×10^5/mL) was added to cells, and cells were resuspended. The 7-AAD solution (5 μL) was added, and cells were incubated for 15 min at room temperature. Finally, 0.45 mL binding buffer and 1 μL Annexin V-APC were added for reaction at room temperature in the dark for 15 min. The samples were investigated through flow cytometry.

Statistical Analysis

Statistical analyses were performed using SPSS (v. 22.0). Data were presented as mean ± SD, and independent t-tests were used to investigate intergroup distinctions. A $p < 0.05$ was considered significant.

RESULTS

PCR Results of Bladder Cancer and Paracancer Tissues

As shown in **Figure 1**, there were bands of PCR in both the cancerous tissue and the paracancer tissue, indicating the success of reverse transcription. However, compared with bands of bladder cancer, the normal bands were lighter in brightness, indicating that the amount of cDNA in reverse transcription was less. Fluorescence quantitative PCR was performed.

General PCR Results of Bladder Cancer Cell Lines T24 and 5,637

Common PCR results of cell lines T24 and 5,637 were shown in **Figure 2**: PCR bands were observed in both cell lines T24 and 5,637, indicating successful reverse transcription. However, the band brightness of the three groups of 5,637 cell lines was lighter than that of T24. Fluorescence quantitative PCR was performed.

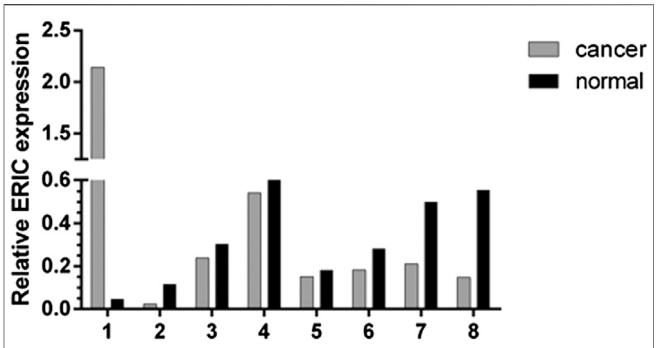

FIGURE 3 | Expression of ERIC gene in bladder cancer tissues and paracancer tissues of 8 patients. The relative expression level of ERIC was determined by qRT-PCR assay. The mean value was shown.

Expression of ERIC Gene in Bladder Cancer

Real-time fluorescence quantitative PCR was used to detect the expression level of ERIC gene in 36 bladder cancer tissues and para-cancer normal tissues. As shown in **Figure 3**, the expression level of ERIC in bladder cancer tissue was higher in seven cases than that in the adjacent group (about 2.48 times on average), and only one case was lower than that in the adjacent group.

Expression of ERIC Gene in Cell Lines T24 and 5,637

The fluorescence quantitative PCR results of cell lines T24 and 5,637 were shown in **Figure 4**: the expression level of T24 was significantly higher than that of 5,637.

Effect of ERIC on T24 and 5,637 Cell Proliferation

Compared with that in the T24 NC group, cell proliferation rate in the T24 ERIC group was significantly decreased ($t = 7.583$, $p <$

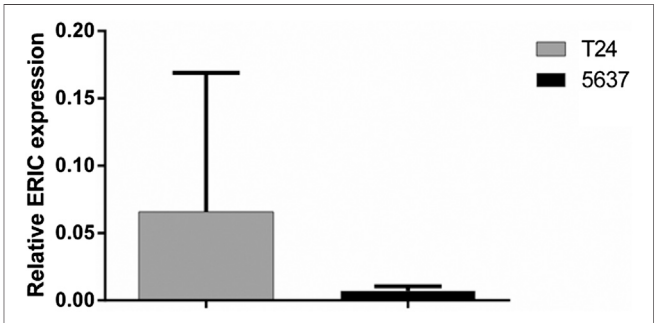

FIGURE 4 | Expression of ERIC gene in bladder cancer cell lines T24 and 5,637. The relative expression level of ERIC was determined by qRT-PCR assay. The mean value ± SD was shown.

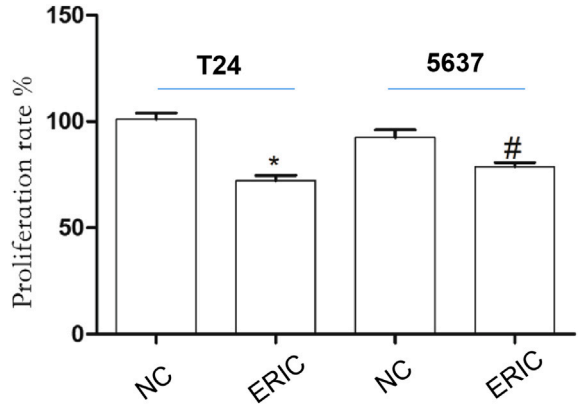

FIGURE 5 | Changes in cell proliferation rate in each group. The proliferation rate was determined by MTT assay. The mean value ± SD was shown. $^{*}p < 0.05$. $^{\#}p < 0.05$.

0.05). Similarly, compared with that in the 5637 NC group, the cell proliferation rate in the 5637 ERIC group was significantly decreased ($t = 3.283$, $p < 0.05$) (**Figure 5**).

Effect of ERIC on T24 and 5,637 Cell Invasion

Compared with that in the ERIC groups (T24 and 5,637 + ERIC), the number of cells in the negative control groups (T24 and 5637 NC) was significantly increased ($t = 11.538$, $p < 0.001$; $t = 8.205$, $p < 0.05$, respectively) (**Figure 6**).

Effects of ERIC Inhibition on T24 and 5,637 Cell Apoptosis

To study the influence of ERIC on BCC apoptosis, flow cytometry was used to detect T24 and 5,637 cell apoptosis. Compared with that in the T24 NC group, the apoptosis rate in the T24 ERIC group was dramatically increased ($t = -34.083$, $p < 0.001$). Compared with that in the 5637 NC group, the apoptosis rate in the 5637 ERIC group was also increased ($t = -14.316$, $p < 0.001$) (**Figure 7**).

DISCUSSION

In China, bladder cancer is the first malignant tumor of the urinary system (Li et al., 2017). Currently, smoking and occupational exposure to aromatic amine are the main risk factors for bladder cancer (Bosetti et al., 2011). The occurrence and development of bladder cancer is a multi-stage and multi-step evolutionary process, and the long-term accumulation of abnormal genotypes leads to the emergence of malignant phenotypes. The purpose of determining the expression status of certain genes in bladder cancer is to determine whether this gene is related to bladder cancer, so as to lay a foundation for the follow-up study on its function and molecular mechanism. Finally, we hope to find specific targets for bladder cancer and provide a new molecular basis for our clinical diagnosis, treatment and prognosis.

Long non-coding RNA (lncRNA) is a class of RNA molecules with a transcript length of more than 200 nt, which does not itself encode proteins or has little function of encoding proteins, and is generally transcribed in mammalian genomes. It was originally thought to be a by-product of the transcription process, with no biological function. With the deepening of research, new lncrnas have been continuously discovered, and more and more evidence shows that lncrnas have complex biological functions and are closely related to human diseases, especially the occurrence of tumors (Gupta et al., 2010).

The long non-coding RNA ERIC transcript is 1745bp in size and is directly regulated by E2F in a p53 independent manner (Feldstein et al., 2013). The expression of ERIC gene is regulated by cell cycle and reaches its peak in G1 phase. Studies have shown that ERIC gene and transcription factor E2F1 constitute a negative feedback pathway, which regulates the activity of E2F1, and ERIC inhibits the cell apoptosis induced by E2F1.

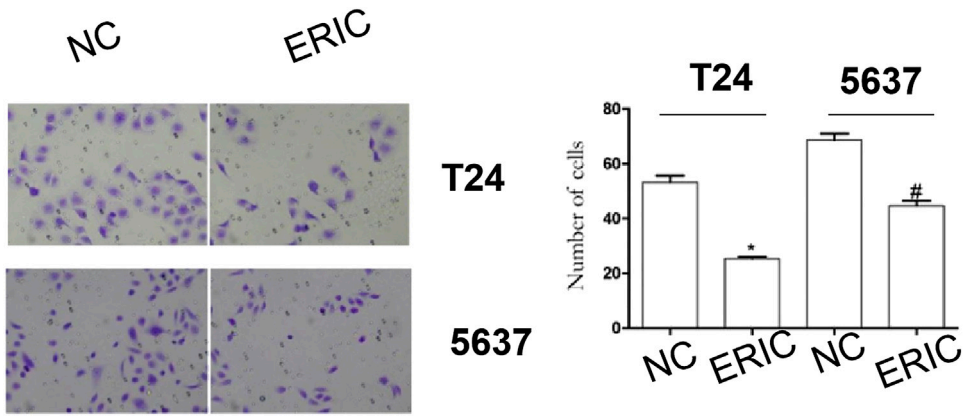

FIGURE 6 | Changes in cell invasion levels in each group (200 times). Cell invasion level was determined by transwell assay. The mean value ± SD was shown. $^{*}p < 0.05$. $^{\#}p < 0.05$.

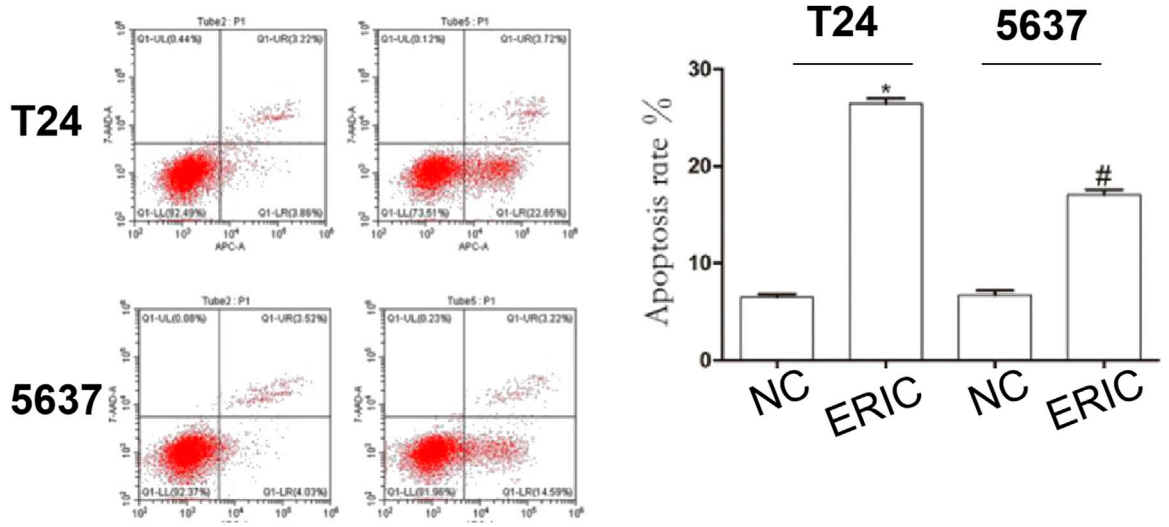

FIGURE 7 | Changes in apoptotic rate in each group. Cell apoptosis level was determined by flow cytometry. The mean value ± SD was shown. $^{*}p < 0.05$. $^{\#}p < 0.05$.

With the increase of E2F1 activity, the expression of ERIC gene also increased.

In this study, this gene was down-regulated in bladder cancer tissues compared with para-cancer tissues, suggesting that this gene may play a role of "tumor suppressor gene". As they are regulated by transcription factors E2F1 and E2F3, these two genes are also down-regulated in bladder cancer. It laid a solid foundation for further research on the function of this gene.

Currently, it has become one of the difficult problems in urology surgery to find specific targets for bladder cancer, explore new treatment methods and overcome the shortcomings of traditional treatment methods such as chemotherapy and surgery. Revealing the expression and function of lncRNAs in bladder cancer is an effective way to find specific targets. Xue M et al. found that the up-regulated expression of lncrna-uca1 can increase the proliferation, migration and invasion ability of cells and inhibit apoptosis under the hypoxia condition (Xue et al., 2014); Fan Y et al. demonstrated a positive correlation between the expression of lncrna-uca1 and Wnt6 *in vivo*, and ultimately demonstrated that UCA1 increased cisplatin resistance in bladder cancer cells by enhancing the expression of Wnt6 (a member of the Wnt6 pterless MMTV integration site family 6), thus identifying potential targets for overcoming chemotherapy resistance (Fan et al., 2014a); Fan Y TGF–such as beta MALAT1 induced bladder cancer cells and epithelial mesenchymal (EMT), MALAT1 excessive expression was significantly associated with bladder cancer patients with low survival rate, the expression of targeted inhibit MALAT1 and suz12 can inhibit the TGF - beta induced cell migration, and invasion characteristics, and think the MALAT1 inhibition may be used to inhibit the development of bladder cancer is a promising treatment (Fan et al., 2014b). These studies will provide theoretical basis for the research and development of new ways and new drugs to treat bladder cancer.

At present, there are few studies on ERIC gene, and its function in tumor has not been reported. Although it was found to be down-regulated in bladder cancer in this study, it was not statistically significant due to the small number of study samples. Thererfore we further study the function of this gene to reveal its role in bladder cancer. CRISPR-dCas9-VPR technology was a new approach for upregulating celluar gene expression without affecting cell viabillity. By binding to the promoter region of targeted gene, it could activate lncRNA transcription (Kardooni et al., 2018; Zhang et al., 2018; Blanas et al., 2019). A CRISPR-dCas9-VPR targeting ERIC plasmid was constructed and transfected into bladder cancer cell lines T24 and 5,637 to detect the effect on proliferation, invasion, apoptosis and other aspects of bladder cancer cell lines and reveal its function. Multi-level research will be helpful to find specific targets for bladder cancer, and provide new scientific basis for clinical targeted treatment of this disease and the research and development of new drugs. In our study, the proliferation and migration of ERIC positive cells were significantly reduced, and cell apoptosis was increased.

In conclusion, downregulated ERIC can inhibit the invasion of human bladder cancer, and promote their apoptosis.

DATA AVAILABILITY STATEMENT

The original contributions presented in the study are included in the article/Supplementary Material, further inquiries can be directed to the corresponding authors.

ETHICS STATEMENT

The collection and use of the patient samples were reviewed and approved by the Institutional Ethics Committee of Shenzhen Shajing Affiliated Hospital of Guangzhou Medical University, and written informed consent from all patients was appropriately obtained.

AUTHOR CONTRIBUTIONS

JY, AX, HZ, QL, HY, DD, and YY have done the experiments and statistical analysis. BW designed the whole project.

FUNDING

We are grateful for the financial support from the the Shenzhen Municipal Government of China (JCYJ20160427190559022).

REFERENCES

Blanas, A., Cornelissen, L. A. M., Kotsias, M., van der Horst, J. C., van de Vrugt, H. J., Kalay, H., et al. (2019). Transcriptional activation of fucosyltransferase (FUT) genes using the CRISPR-dCas9-VPR technology reveals potent N-glycome alterations in colorectal cancer cells. *Glycobiology* 29 (2), 137–150. doi:10.1093/glycob/cwy096

Bosetti, C., Bertuccio, P., Chatenoud, L., Negri, E., La Vecchia, C., and Levi, F. (2011). Trends in mortality from urologic cancers in Europe, 1970–2008. *Eur. Urol.* 60 (1), 1–15. doi:10.1016/j.eururo.2011.03.047

Chung, S., Nakagawa, H., Uemura, M., Piao, L., Ashikawa, K., Hosono, N., et al. (2011). Association of a novel long non-coding RNA in 8q24 with prostate cancer susceptibility. *Cancer Sci.* 102, 245–252. doi:10.1111/j.1349-7006.2010.0173710.1111/j.1349-7006.2010.01737.x

Costa, F. F. (2008). Non-coding RNAs, epigenetics and complexity. *Gene* 410 (1), 9–17. doi:10.1016/j.gene.2007.12.008

Fan, Y., Shen, B., Tan, M., Mu, X., Qin, Y., Zhang, F., et al. (2014a). TGF-β-induced upregulation of malat1 promotes bladder cancer metastasis by associating with suz12. *Clin. Cancer Res.* 20 (6), 1531–1541. doi: doi:10.1158/1078-0432.CCR-13-1455

Fan, Y. Y., ShenB, B. B., Tan, Y. M., Mu, X., Qin, Y., Zhang, F., et al. (2014b). Long non-coding RNA UCA1 increases chemoresistance of bladder cancer cells by regulating Wnt signaling. *FEBS J.* 281 (7), 1750–1758. doi:10.1111/febs.12737

Feldstein, O., Nizri, T., Doniger, T., Jacob, J., Rechavi, G., and Ginsberg, D. (2013). The long non-coding RNA ERIC is regulated by E2F and modulates the cellular response to DNA damage. *Mol. Cancer* 12, 131. doi:10.1186/1476-4598-12-131

Gershon, D. (2005). More than gene expression. *Nature* 437 (7062), 1195–1196. doi:10.1038/4371195a

Gibb, E. A., Brown, C. J., Lam, W. L., and Gibb, E. A. (2011). The functional role of long non-coding RNA in human carcinomas. *Mol. Cancer* 10, 38. doi:10.1186/1476-4598-10-38

Griffiths, T. R. L. (2013). Current perspectives in bladder cancer management. *Int. J. Clin. Pract.* 67, 435–448. doi:10.1111/ijcp.12075

Gupta, R. A., Shah, N., Wang, K. C., Kim, J., Horlings, H. M., Wong, D. J., et al. (2010). Long non-coding RNA HOTAIR reprograms chromatin state to promote cancer metastasis. *Nature* 464, 1071–1076. doi:10.1038/nature08975

Kardooni, H., Gonzalez-Gualda, E., Stylianakis, E., Saffaran, S., Waxman, J., and Kypta, R. (2018). CRISPR-mediated reactivation of DKK3 expression attenuates TGF-β signaling in prostate cancer. *Cancers* 10 (6), 165. doi:10.3390/cancers10060165

Li, Q. Q., Hao, J. J., Zhang, Z., Krane, L. S., Hammerich, K. H., Sanford, T., et al. (2017). Proteomic analysis of proteome and histone post-translational modifications in heat shock protein 90 inhibition-mediated bladder cancer therapeutics. *Sci. Rep.* 7, 201. doi:10.1038/s41598-017-00143-6

Liu, Y., Han, Y., Zhang, H., Nie, L., Jiang, Z., Fa, P., et al. (2012). Synthetic miRNA-mowers targeting miR-183-96-182 cluster or miR-210 inhibit growth and migration and induce apoptosis in bladder cancer cells. *PLoS One* 7, e52280. doi:10.1371/journal.pone.0052280

Luo, M., Li, Z., Wang, W., Zeng, Y., Liu, Z., and Qiu, J. (2013). Long non-coding RNA H19 increases bladder cancer metastasis by associating with EZH2 and inhibiting E-cadherin expression. *Cancer Lett.* 333, 213–221. doi:10.1016/j.canlet.2013.01.033

Martens-Uzunova, E. S., Böttcher, R., Croce, C. M., Jenster, G., Visakorpi, T., and Calin, G. A. (2014). Long noncoding RNA in prostate, bladder, and kidney cancer. *Eur. Urol.* 65 (6), 1140–1151. doi:10.1016/j.eururo.2013.12.003

Mattick, J. S. (2005). The functional genomics of noncoding RNA. *Science* 309 (5740), 1527–1528. doi:10.1126/science.1117806

Michaeleen, D. (2011). Cancer's epigenome. *Adv. Genet.* 147 (1), 5–7. doi:10.1016/j.cell.2011.09.021

Mourtada-Maarabouni, M., Pickard, M. R., Hedge, V. L., Farzaneh, F., and Williams, G. T. (2009). GAS5, a non-protein-coding RNA, controls apoptosis and is downregulated in breast cancer. *Oncogene* 28 (2), 195–208. doi:10.1038/onc.2008.373

Prensner, J. R., Iyer, M. K., Balbin, O. A., Dhanasekaran, S. M., Cao, Q., Brenner, J. C., et al. (2011). Transcriptome sequencing across a prostate cancer cohort identifies PCAT-1, an unannotated lincRNA implicated in disease progression. *Nat. Biotechnol.* 29 (8), 742–749. doi:10.1038/nbt.1914

Rahmani, A. H., Alzohairy, M., Babiker, A. Y., Khan, A. A., Aly, S. M., and Rizvi, M. A. (2013). Implication of androgen receptor in urinary bladder cancer: a critical mini review. *Int. J. Mol. Epidemiol. Genet.* 4, 150–155.

Siegel, R., Naishadham, D., and Jemal, A. (2013). Cancer statistics. *CA Cancer J. Clin.* 63, 11–30. doi:10.1038/nbt.1914

Xue, M., Li, X., Li, Z., and Chen, W. (2014). Urothelial carcinoma associated 1 is a hypoxia-inducible factor-1α-targeted long noncoding RNA that enhances hypoxic bladder cancer cell proliferation, migration, and invasion. *Tumor Biol.* 35 (7), 6901–6912. doi:10.1007/s13277-014-1925-x

Yang, L., Lin, C., Jin ., C., Yang, J. C., Tanasa, B., Li, W., et al. (2013). lncRNA-dependent mechanisms of androgen-receptor-regulated gene activation programs. *Nature* 500, 598–602. doi:10.1038/nature12451

Zhang, H., Chen, Z., Wang, X., Huang, Z., He, Z., and Chen, Y. (2013). Long non-coding RNA: a new player in cancer. *J. Hematol. Oncol.* 6, 37. doi:10.1186/1756-8722-6-37

Zhang, L., Salgado-Somoza, A., Vausort, M., Leszek, P., and Devaux, Y., and Cardiolinc™ network (2018). A heart-enriched antisense long non-coding RNA regulates the balance between cardiac and skeletal muscle triadin. *Biochim. Biophys. Acta Mol. Cell Res.* 1865 (2), 247–258. doi:10.1016/j.bbamcr.2017.11.002

Conflict of Interest: The authors declare that the research was conducted in the absence of any commercial or financial relationships that could be construed as a potential conflict of interest.

frontiers in Molecular Biosciences

ORIGINAL RESEARCH
published: 09 April 2021
doi: 10.3389/fmolb.2021.649976

lncRNA SNHG9 Promotes Cell Proliferation, Migration, and Invasion in Human Hepatocellular Carcinoma Cells by Increasing GSTP1 Methylation, as Revealed by CRISPR-dCas9

Shanting Ye[1,2] *and Yong Ni*[1,2]*

[1] Graduate School of Guangzhou Medical University, Guangzhou, China, [2] Department of Hepatobiliary Surgery, Shenzhen Second People's Hospital, Shenzhen, China

Hepatocellular carcinoma (HCC) is among the major causes of cancer-related mortalities globally. Long non-coding RNAs (LncRNAs), as epigenetic molecules, contribute to malignant tumor incidences and development, including HCC. Although LncRNA SNHG9 is considered an oncogene in many cancers, the biological function and molecular mechanism of SNHG9 in HCC are still unclear. We investigated the effects of lncRNA SNHG9 on the methylation of glutathione S-transferase P1 (GSTP1) and the progression of HCC. Histological data analysis, CRISPR-dCas9, and cytological function experiment were used to study the expression level and biological function of SNHG9 in HCC. There was an upregulated expression of SNHG9 in HCC, which was associated with shorter disease-free survival. Knockdown of SNHG9 can inhibit cell proliferation, block cell cycle progression, and inhibit cell migration and invasion by upregulating GSTP1. LncRNA SNHG9 recruits methylated enzymes (DNMT1, DNMT3A, and DNMT3B) to increase GSTP1 promoter methylation, a common event in the development of HCC. Inhibition of lncRNA SNHG9 demethylates GSTP1, which prevents HCC progression, presents a promising therapeutic approach for HCC patients.

Keywords: SNHG9, hepatocellular carcinoma, CRISPR-dCas9, GSTP1, promoter methylation

OPEN ACCESS

Edited by:
Yonghao Zhan,
Zhengzhou University, China

Reviewed by:
Xiaoli Zhang,
Wuhan University, China
Tingting Jia,
Air Force General Hospital PLA, China

***Correspondence:**
Yong Ni
niyong123456@163.com

Specialty section:
This article was submitted to Molecular Diagnostics and Therapeutics, a section of the journal Frontiers in Molecular Biosciences

Received: *06 January 2021*
Accepted: *10 March 2021*
Published: *09 April 2021*

Citation:
Ye S and Ni Y (2021) lncRNA SNHG9 Promotes Cell Proliferation, Migration, and Invasion in Human Hepatocellular Carcinoma Cells by Increasing GSTP1 Methylation, as Revealed by CRISPR-dCas9. Front. Mol. Biosci. 8:649976. doi: 10.3389/fmolb.2021.649976

INTRODUCTION

Hepatocellular carcinoma (HCC) is a malignant tumor originating from hepatocytes and is the most common primary hepatic malignant tumor. HCC is the sixth most common cancer and the second-leading cause of tumor-related mortalities globally (Zhu et al., 2016; Kim et al., 2017; Zhu and Rhim, 2019). China accounts for approximately 55% of the newly diagnosed HCC cases, attributable to high incidence rates of chronic hepatitis B virus (HBV) infections (Wang et al., 2017). Despite the improvements in clinical therapeutic efficacy, the recovery and long-term survival rate of HCC patients remain low (Shen et al., 2017; Umeda et al., 2019). Recently, the discovery of

targeted therapies has presented novel opportunities for treating liver cancer (Chen et al., 2019; Fu and Wang, 2019); however, the few HCC targeted drugs available are often associated with resistance. Therefore, understanding the pathogenesis of HCC can reveal potential therapeutic targets, which may facilitate the development of novel molecular targeted therapies.

Long non-coding RNAs (lncRNAs) are newly discovered non-protein-coding RNA molecules composed of over 200 nucleotides (Chen et al., 2016; Mathy and Chen, 2017). They are found in the nucleus or cytoplasm and have complex structures that transmit a variety of cellular functions and play an important role in a variety of diseases (Beermann et al., 2016; Chen et al., 2017). There is increasing evidence that lncrNA expression disorders affect gene regulation and promote cancer development (Fang and Fullwood, 2016; Tang et al., 2017; Arun et al., 2018). Small nucleolar RNA host gene 9 (SNHG9) is a membrane-lipid-related LncRNA that has been shown to regulate the proliferation of pancreatic cancer cells (Zhang et al., 2018) and glioblastoma cells (Zhang et al., 2019). However, the role of SNHG9 in HCC remains unclear.

Glutathione s-transferase P1 (GSTP1) catalyzes the Q coupling of electrophilic molecules to glutathione, is involved in detoxification (Crawford and Weerapana, 2016; Gurioli et al., 2018). Research shows that GSTP1 gene polymorphism is associated with HCC among other cancers (Wang et al., 2016; Chatterjee and Gupta, 2018; Ding et al., 2019). Besides, the methylation of the GSTP1 promoter is correlated with gene expression and function (Sophonnithiprasert et al., 2020).

We sought to establish the role of SNHG9 and GSTP1 in HCC pathology. The findings indicated the upregulated expression of SNHG9 in HCC is associated with shorter disease-free survival. Upregulating GSTP-1 expression led to cell proliferation inhibition, cell cycle progression blockage, cell migration, and invasion inhibition. LncRNA SNHG9 recruits methylated enzymes (DNMT1, DNMT3A, and DNMT3B) to promote the GSTP1 promoter's methylation, which is a common event in HCC development. Therefore, we underscore the molecular mechanisms of HCC pathogenesis and potential targets for treatment.

MATERIALS AND METHODS

Clinical Specimens

In this study, HCC specimens and adjacent tissues were obtained from patients from the First Affiliated Hospital of Shenzhen University from 2015 to 2018. All patients received written informed consent. The research was approved by the Ethics and Human Sciences Committee of Shenzhen University and conducted as per the Helsinki Declaration.

Public Data Set Download

Liver cancer genome atlas (TCGA) level 3 RNA sequencing—seq (RNA) data and their medical data were derived from the genomic data sharing (GDC) data portal website[1]. Also, we obtained three datasets (GSE19915 GSE13507 GSE3167) from Gene Expression Omnibus (GEO[2]) based on the microarray data sets (Zhang et al., 2018, 2019).

Real-Time Quantitative Polymerase Chain Reaction

Total RNA was extracted using Trizol reagent (Invitrogen) as per the manufacture's instructions. cDNA was reverse-transcribed to 2–6 g total RNA using M-MLV reverse transcriptase (Promega, Madison, WI, United States). Real-Time Quantitative Polymerase Chain Reaction (Rt-qPCR) was performed by the StepOnePlus real-time PCR system (ABI, United States) using a 20 L reaction mixture consisting of 0.1 M primers, 10 L 2 × FastStart Universal SYBR Green Master (Rox, Switzerland), and 20–100 ng cDNA samples. All the experiments were repeated at least three times. Relative mRNA levels were standardized to -actin mRNA levels, using $2^{-\Delta\Delta CT}$ Methods.

CCK-8 and Clone Formation Tests

About 1×10^4 cells were inoculated into 96-well plates overnight. CCK-8 reagent (Japanese Dojindo) was mixed with 10%FBS + RMI-1640 medium at a ratio of 1:9 and cultured in the dark for 3 h. Absorbance was measured after 0, 24, 48, and 72 h at 450 nm using a multi-tablet reader (Bio-RAD, United States). The ratio of absorbance after 24, 48, and 72 h to absorbance at 0 h was used to investigate the cells' proliferation ability in five independent experiments.

In the clone formation experiment, 200, 400, and 800 cells were cultured in a 6-well plate at 37°C until the clone was visible to the naked eye. The clones were stained in 0.1% crystal violet and 20% methanol, after which they were imaged and counted.

Cell Migration Test

Each group's logarithmically growing cells were seeded into a 6-well plate (1×10^6 cells/well). A line was evenly drawn on the back of the 6-well plate using a marker pen as the subsequent photo position and recorded. When the cells were attached to the plate surface, the old medium was replaced with a fresh culture medium containing 1% fetal bovine serum (FBS), after which the cells were then starved for 12 h. The point of a 200 L spear was scraped out in a straight line using a ruler on the board. Then the cells were washed three times with 2 ml PBS and photographed at 0 h and 24 h. The experiment was replicated thrice. In each image, 15 lines were uniformly distributed, and the distances across the lines were measured and averaged.

Transwell Assay

Matrigel (BD Biosciences, San Jose, CA, United States) was added to a cell medium without serum (1:1 v/v). Matrigel was then polymerized in a Transwell chamber (Corning, NY, United States) at 50 L/well and placed in a 37°C incubator. The cells in the logarithmic growth phase were starved for 24 h in a cell culture medium containing 1% fetal bovine serum. After separation, the cells were resuspended in a 1×10^6

[1]https://portal.gdc.cancer.gov/

[2]http://www.ncbi.nlm.nih.gov/geo/

serum-free medium. 50 L FBS was mixed with a 50 L medium containing 2% FBS and added to the apical chamber of the Transwell. A 600 L cell culture medium containing 10% fetal bovine serum was added to the basal lateral compartment and cultured in an incubator at 37°C and 5% CO_2, saturated humidity and sufficient oxygen for 24 h. The Transwell chamber was then removed, fixed with 4% paraformaldehyde, and stained with crystal violet. Finally, the invasion cells were counted in 5 randomly selected fields under an inverted microscope. Three independent experiments were conducted, and the average value was taken.

Cell Cycle Analysis (Image-Flow Cytometry)

We harvested the transfected cells, washed them twice with cold PBS, and then fixed them with 70% cold ethanol. A cell cycle analysis kit (MultiSciences, China) was used to determine cell cycle distribution. ModFit 5.2 software was used to sequence and calculate cells at different stages of the cell cycle.

Methylation-Specific Polymerase Chain Reaction

The DNA of cells was extracted using a standard procedure. The cells were treated with protease K, after which chloroform was added. The concentration of the extracted DNA was determined using a spectrophotometer. Sodium bisulfite was mixed with the DNA extract to produce vulcanized DNA. The PCR products were then electrophoresed by agarose gel, and the target bands were observed by gel imager.

Double Luciferase Reporter Gene Detection

The GSTP1 promoter and lncRNA SNHG9 full-length sequences were derived from the NCBI database[3]. Four plasmid expression vectors (HA-PCMV5-GSTP1, PCMV5-SNHG9, GSTP1 promoter—LUC, and pCMV5 (control) were constructed from Addgene (Cambridge, MA, United States), including. Then the GSTP1 promoter—LUc and pCMV5 vectors, HA-PCMV5-GSTP1, GSTP1 promoter—Luc, and PCMV5-SNHG9 vectors, were transfected into the cells, respectively. Luciferase activity was then determined using the luciferase reporter assay kit (Promega, Madison, WI, United States). Briefly, 20 L of cell lysate was added to a 1.5 mL centrifuge tube followed by 100 L of LARII solution. After mixing, the absorbance was measured at 460 nm with a luminescence detector (Promega, Madison, WI, United States).

Fluorescence *in situ* Hybridisation

The Fluorescence *in situ* Hybridisation (FISH) technique was performed using the RiboTM lncRNA FISH Probe Mix (Red) to detect the localization of SNHG9 in HCC cells using the procedure described by the manufacturer (Guangzhou RiboBio Co., Ltd., Guangzhou, Guangdong China). Briefly, the cells were inoculated in a six-well culture plate and covered with slides. The cells were 80% confluent after 24 h of culture. The glass was washed with PBS, fixed with 1 mL 4% paraformaldehyde at room temperature, and treated with protease K (2 g/mL), glycine, and acetylation reagent. Subsequently, the additive plate was used with a 250 L prehybridization solution and incubated at 42°C for 1 h. After removing the prehybridization solution, the 250 L hybridization solution consists of an overnight incubation of a detector (300 ng/mL) at 42°C, followed by three and phosphate buffer brine washing Tween-20 (PBST). Then, the nuclei were diluted with PBST for 4′ and stained with 6-diamino-2-pheninindole (DAPI) (1:800). 24-well plates were added for 5 min and washed with PBST for 3 min. Finally, the cells were observed under a fluorescence microscope (Olympus Optical Co., Ltd., Tokyo, Japan).

RNA Binding Protein Immunoprecipitation

The binding analysis of lncRNA SNHG9 with DNMT1, DNMT3A, and DNMT3B was carried out step by step according to the instructions of RNA Binding Protein Immunoprecipitation (RIP) Kit (Millipore, Billerica, MA, United States). Briefly, cells were washed using pre-cooled phosphate-buffered saline (PBS) for 5 min. with 25 eases to L Tris–Hcl (pH 7.5),150 eases to L potassium chloride, and 2 eases to L ediamine tetraacetic acid (EDTA),0.5% NP40 L was more easily associated with sodium fluoride,1 was more easily associated with Deloitte,100 U/ml RNasin ribozyme inhibitor and EDTA-free protease inhibitor, and centrifuged at 14,000 rpm for 10 min at 4°C. A cell extract portion was then taken as an input, and the other part was incubated with an antibody for co-precipitation. To sum up, 50 L magnetic beads were extracted from each co-precipitation reaction system. After washing, they were resuspended in 100 L RIP washing solution, and then 5 g antibody was added in groups for incubation and combination. Subsequently, the magnetic bead—antibody complex was washed and again suspended in 900 L RIP wash solution and incubated at 4°C overnight with 100 L cell extract. The samples were then placed on a magnetic base to collect globin complexes. Samples and inputs were separated by protease K, RNA was extracted, and quantitative polymerase chain reaction (RT-QPCR) was performed. In this study, rabbit anti-human antibodies DNMT1 (1:100, AB13537), DNMT3A (1:100, AB2850), and DNMT3B (1:100, AB2851) were uniformly mixed for 30 min at room temperature. Rabbit anti-human immunoglobulin G (IgG) (1:100, AB109489) was used as the negative control (NC). The antibodies were sourced from Abcam (Cambridge, United Kingdom).

Chromatin Immunoprecipitation

After attaining a 70–80% confluence, cells in each group were harvested and fixed in 1% formaldehyde for 10 min at room temperature to cross-link DNA and proteins. The DNA and proteins were then randomly separated by ultrasound. The cells were centrifuged at 4°C, 13,000 × *g*. The supernatant was mixed with rabbit anti-IgG (AB109489 1:100, Abcam Inc., Cambridge, United Kingdom) CNC antibody and the target protein-specific antibodies (DNMT1 (AB13537 1:100, Abcam

[3]https://www.ncbi.nlm.nih.gov/gene

Inc., Cambridge, United Kingdom), DNMT3A (AB2850 1:100, Abcam Inc., Cambridge, United Kingdom), and DNMT3B (Abcam AB2851, 1:100, Cambridge, United Kingdom), followed by overnight incubation at 4°C. The endogenous DNA-protein complex was then precipitated with protein agarose/agarose. After centrifugation for a while, the supernatant was removed, and the non-specific complex was rinsed. Then, the cross-linking was completed overnight at 65°C, and the DNA fragments were extracted and purified with phenol/chloroform solution. Enrichment of GSTP-1 promoter fragment bound to DNMT1, DNMT3A, and DNMT3B was detected by gSTP-1 promoter fragment specific primer.

Statistical Analysis

Data analysis was performed using SPSS 20.0 software. The quantitative variables were summarized as mean ± standard deviation (SD). The students' *T*-test was used to analyze the differences between the two independent groups. The two-tailed test was considered significant when $P < 0.05$ was calculated.

RESULTS

SNHG9 Expression Was Upregulated in HCC Tissue Samples

To assess the expression of SNHG9 in HCC samples, we downloaded 408 HCC sample and 19 adjacent normal tissue TCGA data. TCGA data showed that SNHG9 was significantly upregulated in HCC ($P = 4.0 \times 10^{-5}$). GEO datasets showed significant increases in SNHG9 in HCC samples ($P = 3.92 \times 10^{-4}$ for GSE3167, $P = 0.003$ for GSE13507, and $P = 0.002$ for GSE19915) (**Figure 1A**). The Receiver Operating Characteristic (ROC) curve was used to analyze the sensitivity and specificity based on TCGA data to evaluate

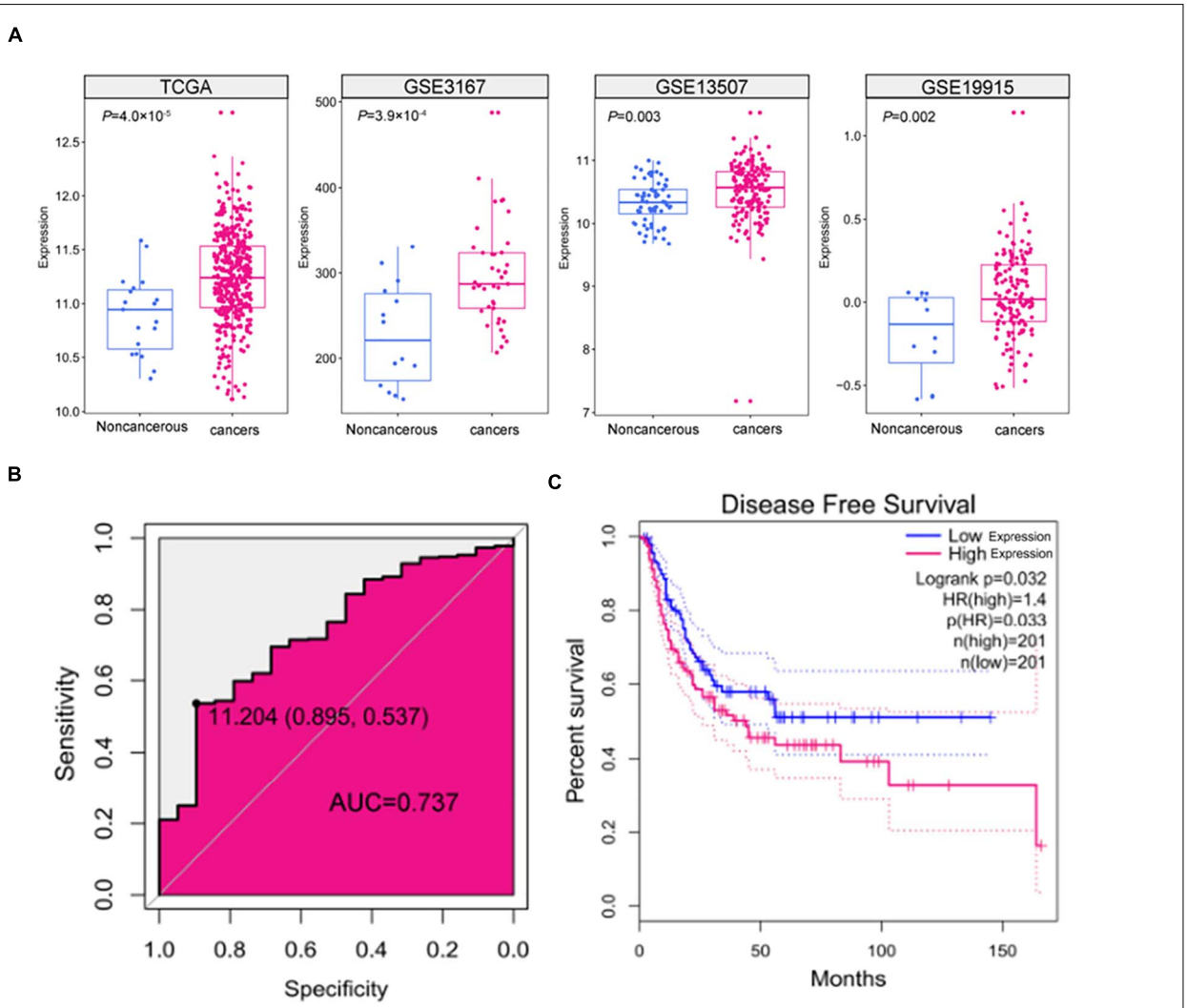

FIGURE 1 | The expression and clinical significance of SNHG9 in HCC. **(A)** SNHG9 expression in non-cancerous liver tissues and HCC samples, based on data from the public dataset. **(B)** ROC curve and AUC of SNHG9. **(C)** Kaplan–Meier survival curves of the two groups of patients based on TCGA data. Red: Patients with high SNHG9 expression. Blue: Patients with low expression of SNHG9.

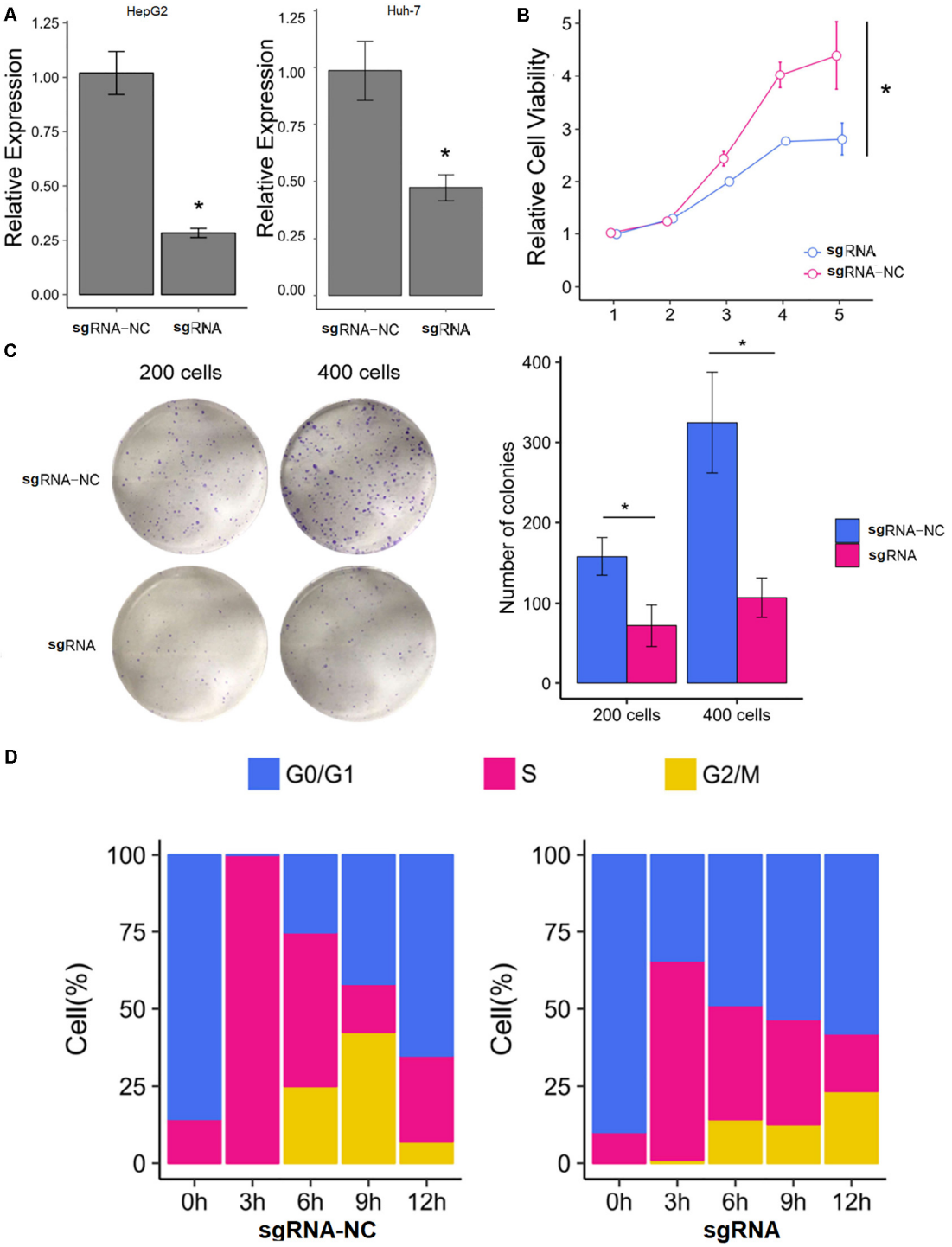

FIGURE 2 | Knockdown of SNHG9 can inhibit the proliferation and cell cycle progression of HCC cells. **(A)** The expression of SNHG9 in sgRNA-NC and sgRNA-SNHG9 transfected cells as detected by RT-qPCR. (n = 3 independent experiments). **(B)** The CCK-8 method was used to evaluate the effect of silencing SNHG9 on cell proliferation. (n = 3 independent preparations) *$P < 0.05$. **(C)** Clones are stained with Giemsa and photographed with a digital camera. The clone number was calculated and statistically analyzed. **(D)** The cell cycle was synchronized with the use of a double thymine block. The stack diagram shows the percentage of cells in each cycle at each time point. Left: Cells transfected with sgRNA-NC. Right: Cells transfected with sgRNA-SNHG9. Blue: Phase G0. Red:S phase. Gold:G2 and M phase.

the diagnostic value of SNHG9 for HCC. The area under the SNHG9 curve (AUC) was 0.737. At the critical value of 11.20, the sensitivity and specificity were 0.54 and 0.90, respectively (**Figure 1B**). Survival analysis showed that high SNHG9 expression was associated with shorter disease-free survival ($P = 0.032$) (**Figure 1C**).

Downregulation of the SNHG9 Gene Inhibited the Proliferation of Hepatocellular Carcinoma Cells and Blocked the Progression of the Cell Cycle

The HepG2 and Huh-7 HCC cell lines were established to effectively express SNHG9 targeting sgRNA (sgRNA-SNHG9) and negative control sgRNA (sgRNA-NC), respectively. Rt-qPCR and Western blot were used to verify the effect of knockout. After transfection of sgRNA-SNHG9, the expression of SNHG9 was significantly decreased (HEPG2: $P = 0.009$; Huh-7: $P = 0.003$; **Figure 2A**). Compared with the control group, the relative expression of lncRNA in HepG2 and Huh-7 cells was reduced by 72.2 and 50.3%, respectively. These results indicated that SNHG9 was effectively knocked out. We compared the proliferation of sgRNA-SNHG9 and sgRNA-NC groups in HEPG2 cells using the CCK-8 method to determine the role of SNHG9 in HCC cells. SNHG9 knockdown significantly reduced cell proliferation ($P = 0.018$) (**Figure 2B**). On day 5, the proliferation of the sgRNA-SNHG9 group decreased by 1.57 ± 0.95. In the clone formation experiment, we found that the clonal formation capacity of Huh-7 cells was significantly inhibited than the negative control cells (**Figure 2C**).

We dynamically compared the cell cycle progression of the sgRNA-SNHG9 group and sgRNA-NC group in HEPG2 cells to establish the function of SNHG9 in the cell cycle. Cell cycle synchronization was first blocked by double thymine at the G1/S boundary and then released simultaneously. We found that most cells in the sgRNA-NC group were in the G0/G1 phase and entered the G2/M phase through the S phase within 6–12 h. In the sgRNA-SNHG9 group, the G0/G1 phase cells slowly entered the S phase from 0 to 12 h, suggesting that SNHG9 knockdown led to cell cycle arrest at the G0/S phase (**Figure 2D**). These results indicated that silencing lncRNA SNHG9 could impede HCC cell growth.

Downregulation of SNHG9 Inhibited the Migration and Invasion of Hepatocellular Carcinoma Cells

The scratch test showed that cell mobility was significantly reduced after sgRNA-SNHG9 treatment ($P < 0.05$; **Figures 3A,B**). The results suggest that silencing lncRNA SNHG9 can inhibit cell migration. Subsequently, Transwell's results showed that sgRNA-SNHG9 significantly reduced cell invasion

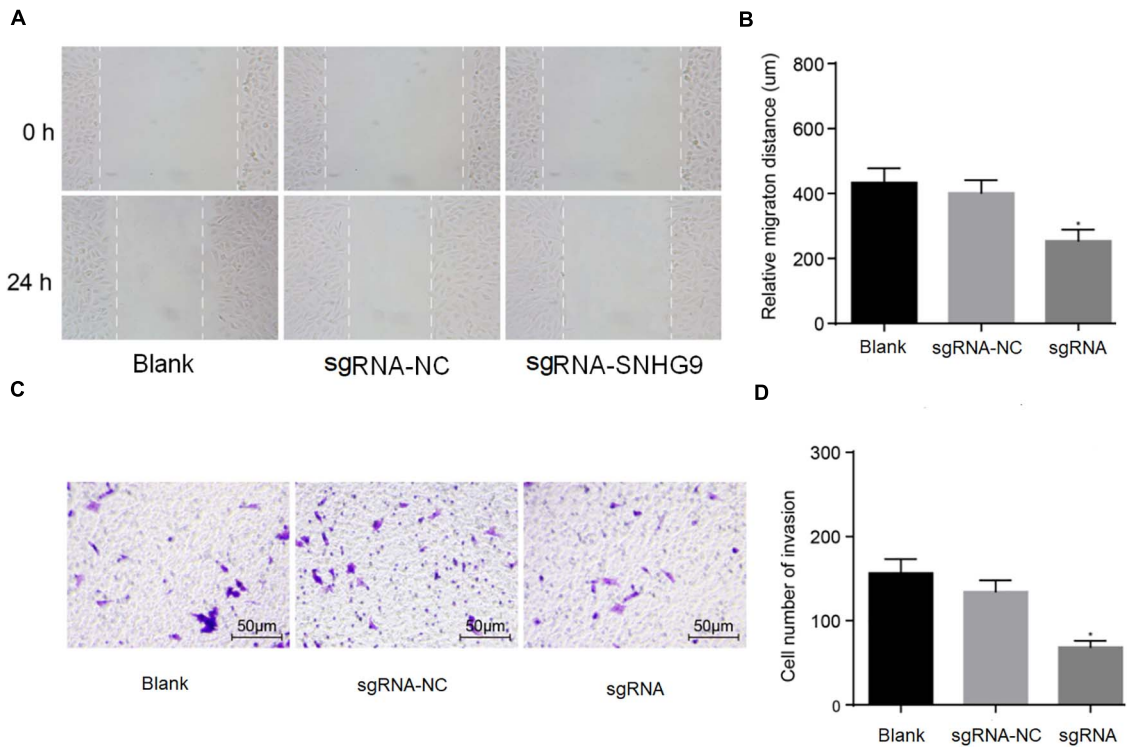

FIGURE 3 | The downregulation of SNHG9 inhibited the migration and invasion of HCC cells. Panles **(A,B)** were used to detect the cell migration after SNHG9 knockdown by scratch test. **(C,D)** Cell invasion after SNHG9 gene knockout was detected by Transwell method. Statistical data were presented as mean ± standard deviation, and One-Way ANOVA was used. The experiment was repeated three times; *$P < 0.05$.

($P < 0.05$; **Figures 3C,D**), indicating that the cell invasion rate could be inhibited after lncRNA SNHG9 was inhibited.

LncRNA SNHG9 Promotes DNA Methylation of the GSTP1

Bioinformatics analysis showed that lncRNA SNHG9 was located in the nucleus, and online CpG prediction software was used to predict the presence of methylated CpG islands in the GSTP1 promoter (**Figure 4A**). The Methylation-Specific Polymerase Chain Reaction (mS-PCR) results showed that after treatment with sgRNA-SNHG9 and SGI-1027, methylation inhibitors of GSTP1, the GSTP1 promoter's methylation degree was significantly reduced (**Figure 4B**). The results of double luciferase reporter gene detection (**Figure 4C**) showed that luciferase activity of GSTP1 promoter co-transfected with GSTP1 gene was significantly lower than that of GSTP1 promoter transfected with GSTP1 gene only ($P < 0.05$). The luciferase activities of the GSTP1 promoter, GSTP1 gene, and lncRNA SNHG9 were significantly lower than that of GSTP1 promoter after co-transfection with GSTP1 gene ($P < 0.05$). Subsequently, FISH results showed that lncRNA SNHG9 was mainly located in the nucleus (**Figure 4D**). Besides, RIP analysis showed that lncRNA SNHG9 targeted and bound methylation-related proteins (DNMT1, DNMT3A, and DNMT3B) compared with the IgG group ($P < 0.05$)

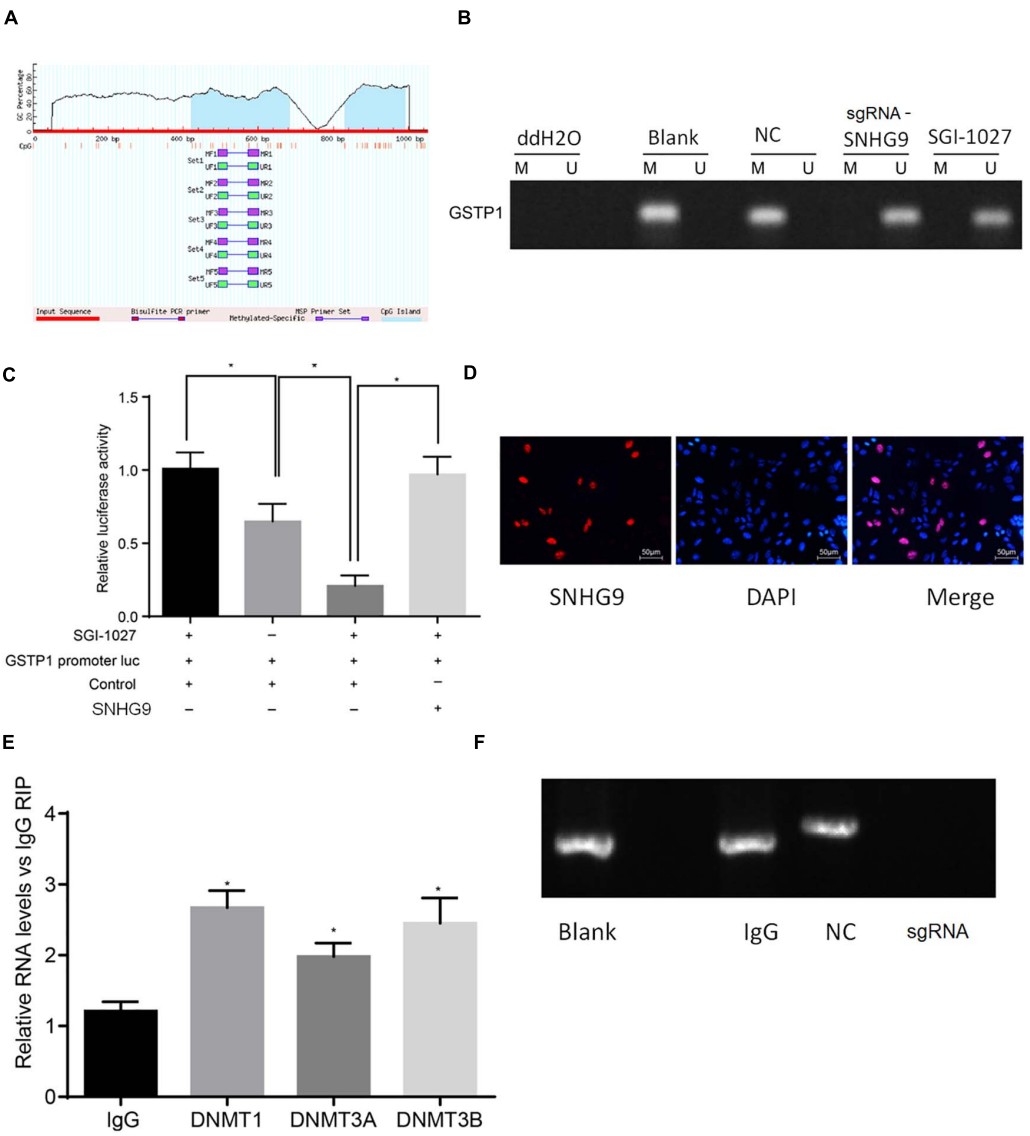

FIGURE 4 | SNHG9 promotes GSTP1 promoter methylation by recruiting methylated proteins. **(A)** localization of GSTP1 methylated SNHG9 and CpG Island predicted by bioinformatics; **(B)** Ms-PCR detected the methylation level of GSTP1 promoter after sgRNA-SNHG9 and SGI-1027 treatment. **(C)** Double luciferase reporter gene assay confirmed the binding of SNHG9 to GSTP1 promoter. **(D)** FISH analysis of lncRNA SNHG9; The RIP analysis of panel **(E)**, SNHG9 combined with DNMT1, DNMT3A, and DNMT3B; CHIP detection of GSTP1 promoter in panel **(F)**, IgG, and sgRNA-SNHG9.

(**Figure 4E**). CHIP analysis results revealed significantly higher enrichment of the blank group's GSTP1 promoter region than the sgRNA-SNHG9's group (**Figure 4F**). These findings provide evidence that lncRNA SNHG9 inhibits the expression of GSTPI by promoting the methylation of the GSTP1 promoter.

Downregulation of SNHG9 Inhibits Proliferation, Migration, and Invasion of HCC Cells by Upregulating GSTP1

The RT-qPCR was used to detect the expression of GSTP1 mRNA after treatment with sgRNA-SNHG9, sgRNA-GSTP1, PCDNA-GSTP1, PCDNA-SNHG9, and PCDNA-GSTP1 + SNHG9. The results are presented in **Figure 5A**. The GSTP1 mRNA's expression after treatment with PCDNA-GSTP1 and sgRNA-SNHG9 was significantly higher ($P < 0.05$). The expression of GSTP1 mRNA after PCDNA-GG9 +, sgRNA-GSTP1, and PCDNA-SNHG9 treatment was significantly decreased ($P < 0.05$) compared with that of the PCDNA-GSTP1 treatment. The expression of lncRNA SNHG9 after PCDNA-SNHG9 treatment was significantly increased ($P < 0.05$), while the expression of lncRNA SNHG9 after sgRNA-SNHG9 treatment was significantly low ($P < 0.05$). After treatment with sgRNA-GSTP1 and PCDNA-GSTP1, the expression of lncRNA SNHG9 showed no significant change ($P > 0.05$). Western blot analysis showed significantly higher GSTP1 protein level after PCDNA-GSTP1 and sgRNA-SNHG9 treatment ($P < 0.05$), while the GSTP1 protein level decreased significantly after treatment with sgRNA-GSTP1 and PCDNA-SNHG9 ($P < 0.05$). The GSTP1 protein level was significantly lower after PCDNA-GSTP1 + SNHG9 treatment than in PCDNA-GSTP1-treated group ($P < 0.05$; **Figure 5B**). CCK8 experimental results showed that the proliferation of the cells on the third and fourth day after the treatment of PCDNA-GSTP1 and sgRNA-SNHG9 was significantly low ($P < 0.05$), while the proliferation of the cells on the third and fourth day after the treatment of sgRNA-GSTP1 and PCDNA-SNHG9 was significantly high ($P < 0.05$). The cell proliferation after PCDNA-GSTP1 + SNHG9 treatment was significantly higher than that after PCDNA-GSTP1 treatment ($P < 0.05$) (**Figure 5C**). Besides, the scratch test revealed significantly reduced cell migration after PCDNA-GSTP1 and sgRNA-SNHG9 treatment ($P < 0.05$), while the cell migration was significantly enhanced after treatment with sgRNA-GSTP1 and PCDNA-SNHG9 ($P < 0.05$). PCDNA-GSTP1 + SNHG9 indicated significantly higher cell migration than PCDNA-GSTP1 ($P < 0.05$) (**Figures 5D,E**). Subsequently, Transwell assay results showed that pcDNA-GSTP1 and sgRNA-SNHG9 significantly reduced cell invasion ($P < 0.05$), while sgRNA-GSTP1 and PCDNA-SNHG9 significantly increased cell invasion ($P < 0.05$). The PCDNA-GSTP1 + SNHG9-triggered cells were significantly more aggressive than the PCDNA-GSTP1-triggered ones ($P < 0.05$; **Figures 5F,G**). In summary, lncRNA with low expression of SNHG9 and high expression of GSTP1 deters metastasis.

DISCUSSION

Elucidating the molecular mechanisms of hepatocellular carcinoma remains an urgent clinical challenge. Currently, the therapeutic efficacy of available drugs for advanced liver cancer is limited (Faivre et al., 2020; Pfister et al., 2020). In recent years, lncRNA has aroused extensive research interest in various countries in the world. There is increasing evidence that some lncRNAs are associated with the incidence and development of cancer. Multiple lncRNAs have been identified as playing a key role in HCC (Huang et al., 2020; Wei et al., 2020;

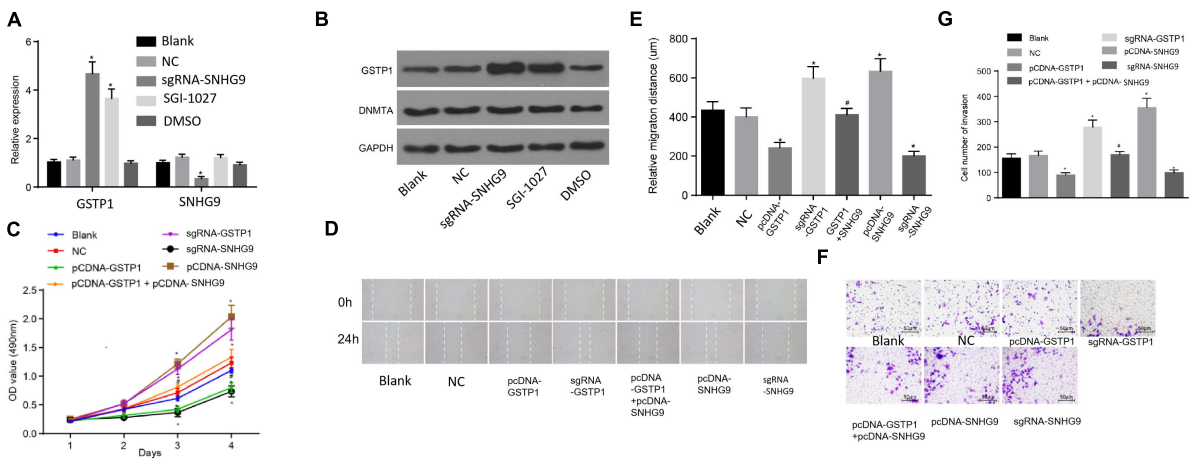

FIGURE 5 | Knockdown of SNHG9 can inhibit the proliferation, migration, and invasion of HCC cells by upregulating GSTP1. **(A)** The expression of SNHG9 and GSTP1 after sgRNA-SNHG9 and SGI-1027 treatment and detected by RT-qPCR; **(B)** Western blot analysis of GSTP1 and DNMT after treatment with sg-SNHG9 and SGI-1027; **(C)** The proliferation of hepatocellular carcinoma cells treated with sgRNA-SNHG9, sgRNA-GSTP1, PCDNA-GSTP1, PCDNA-SNHG9, and PCDNA-GSTP1 + SNHG9 as detected by the CCK-8 method. Panels **(D,E)** were used to detect the migration of hepatocellular carcinoma cells treated with sgRNA-SNHG9, sgRNA-GSTP1, PCDNA-GSTP1, PCDNA-SNHG9, and PCDNA-GSTP1 + SNHG9 by the scratch method. **(G)** Transwell assay was used to detect the invasive ability of sgRNA-SNHG9, sgRNA-GSTP1, PCDNA-GSTP1, PCDNA-SNHG9, and PCDNA-GSTP1 + SNHG9 to treat liver cancer cells.

Yang et al., 2020). LncRNAs may play an important role in predicting prognosis, treatment response, and cancer recurrence based on the patients' genetic profiles and can be used in a personalized treatment design. In addition to editing and modifying DNA sequences, the CRISPR system has also been proven to regulate gene transcription, which brings unprecedented convenience to the study of lncRNA functions. The dCas9 protein could inhibit lncRNA expression by blocking the binding of RNA polymerase and promoters through a roadblock effect (Zhou et al., 2018; Huynh et al., 2020).

SNHG9 has been identified as an oncogene in pancreatic cancer and glioblastoma (Zhang et al., 2018, 2019), but its function is unclear. This study attempted to explore the biological function of SNHG9 in HCC. We investigated the expression level of SNHG9 in HCC clinical specimens. Clinical data revealed overexpression of SNHG9 in HCC tissues than in normal counterparts, and high SNHG9 expression may indicate poor prognosis. Then, we investigated the biological function of SNHG9 using CRISPR-dCas9. Unlike other classical gene silencing methods, such as RNAi, which inhibit gene expression by degrading mRNA in the cytoplasm, the CRISPR-dcas9 system works as a transcriptional suppressor at the DNA level. The binding of dCas9 protein to the target can interfere with RNA polymerase binding in space and play a role in inhibiting the transcription of targeted genes, a process known as CRISPRi (or CRISPR interference). We found that reducing the expression of SNHG9 could inhibit HCC metastasis. Moreover, we investigated the molecular mechanism of SNHG9 in HCC. The binding of SNHG9 to DNA methyltransferase was observed, and the knockout of SNHG9 may cause GSTP1 promoter demethylation, depicting its role in gene expression and tumorigenesis.

In summary, these findings present new insights on the importance of SNHG9 in HCC progression and offer a theoretical basis for developing lncRNA-based targeted therapies for HCC.

DATA AVAILABILITY STATEMENT

The original contributions presented in the study are included in the article/supplementary material, further inquiries can be directed to the corresponding author/s.

ETHICS STATEMENT

The research was approved by the Ethics and Human Sciences Committee of Shenzhen University and conducted in accordance with the Helsinki Declaration. All patients received written informed consent.

AUTHOR CONTRIBUTIONS

SY: interpretation or analysis of the data, preparation of the manuscript, and revision for important intelectual content. YN: conception and supervision. Both authors contributed to the article and approved the submitted version.

FUNDING

This work was supported by Shenzhen Foundation of Science and Technology (JCYJ20170817172116272).

ACKNOWLEDGMENTS

We would like to acknowledge the reviewers for their helpful comments on this manuscript.

REFERENCES

Arun, G., Diermeier, S. D., and Spector, D. L. (2018). Therapeutic targeting of long non-coding RNAs in cancer. *Trends Mol. Med.* 24, 257–277. doi: 10.1016/j.molmed.2018.01.001

Beermann, J., Piccoli, M. T., Viereck, J., and Thum, T. (2016). Non-coding RNAs in development and disease: background, mechanisms, and therapeutic approaches. *Physiol. Rev.* 96, 1297–1325. doi: 10.1152/physrev.00041.2015

Chatterjee, A., and Gupta, S. (2018). The multifaceted role of glutathione S-transferases in cancer. *Cancer Lett.* 433, 33–42. doi: 10.1016/j.canlet.2018.06.028

Chen, J., Shishkin, A. A., Zhu, X., Kadri, S., Maza, I., Guttman, M., et al. (2016). Evolutionary analysis across mammals reveals distinct classes of long non-coding RNAs. *Genome Biol.* 17:19.

Chen, S., Cao, Q., Wen, W., and Wang, H. (2019). Targeted therapy for hepatocellular carcinoma: challenges and opportunities. *Cancer Lett.* 460, 1–9. doi: 10.1016/j.canlet.2019.114428

Chen, X., Yan, C. C., Zhang, X., and You, Z. H. (2017). Long non-coding RNAs and complex diseases: from experimental results to computational models. *Brief. Bioinform.* 18, 558–576.

Crawford, L. A., and Weerapana, E. (2016). A tyrosine-reactive irreversible inhibitor for glutathione S-transferase Pi (GSTP1). *Mol. Biosyst.* 12, 1768–1771. doi: 10.1039/c6mb00250a

Ding, F., Li, J. P., Zhang, Y., Qi, G. H., Song, Z. C., and Yu, Y. H. (2019). Comprehensive analysis of the association between the rs1138272 polymorphism of the GSTP1 gene and cancer susceptibility. *Front. Physiol.* 9:1897. doi: 10.3389/fphys.2018.01897

Faivre, S., Rimassa, L., and Finn, R. S. (2020). Molecular therapies for HCC: looking outside the box. *J. Hepatol.* 72, 342–352. doi: 10.1016/j.jhep.2019.09.010

Fang, Y., and Fullwood, M. J. (2016). Roles, functions, and mechanisms of long non-coding RNAs in cancer. *Genomics Proteomics Bioinformatics* 14, 42–54. doi: 10.1016/j.gpb.2015.09.006

Fu, J., and Wang, H. (2019). Precision diagnosis and treatment of liver cancer in China. *Cancer Lett.* 412, 283–288. doi: 10.1016/j.canlet.2017.10.008

Gurioli, G., Martignano, F., Salvi, S., Costantini, M., Gunelli, R., and Casadio, V. (2018). GSTP1 methylation in cancer: A liquid biopsy biomarker? *Clin. Chem. Lab. Med.* 56, 702–717. doi: 10.1515/cclm-2017-0703

Huang, W., Huang, F., Lei, Z., and Luo, H. (2020). LncRNA SNHG11 promotes proliferation, migration, apoptosis, and autophagy by regulating hsa-miR-184/AGO2 in HCC. *Onco Targets Ther.* 13, 413–421. doi: 10.2147/ott.s237161

Huynh, N. P., Gloss, C. C., Lorentz, J., Tang, R., Brunger, J. M., McAlinden, A., et al. (2020). Long non-coding RNA GRASLND enhances chondrogenesis via suppression of the interferon type II signaling pathway. *eLife* 9:e49558.

Kim, D. W., Talati, C., and Kim, R. (2017). Hepatocellular carcinoma (HCC): beyond sorafenib—chemotherapy. *J. Gastrointest. Oncol.* 8, 256–265. doi: 10.21037/jgo.2016.09.07

Mathy, N. W., and Chen, X. M. (2017). Long non-coding RNAs (lncRNAs) and their transcriptional control of inflammatory responses. *J. Biol. Chem.* 292, 12375–12382. doi: 10.1074/jbc.r116.760884

Pfister, D., Nunez, N., Sinha, A., Weiner, A., Deczkowska, A., Pinter, M., et al. (2020). Adverse effects of PD-1 targeted immunotherapy in NAFLD-triggered HCC. *Z. Gastroenterol.* 58:e71. doi: 10.1055/a-1143-8420

Shen, Y., Guo, H., Wu, T., Lu, Q., Nan, K. J., Lv, Y., et al. (2017). Lower education and household income contribute to advanced disease, less treatment received and poorer prognosis in patients with hepatocellular carcinoma. *J. Cancer* 8, 3070–3077. doi: 10.7150/jca.19922

Sophonnithiprasert, T., Saelee, P., and Pongtheerat, T. (2020). Glutathione S-Transferase P1 Polymorphism on Exon 6 and Risk of Hepatocellular Carcinoma in Thai male patients. *Oncology* 98, 243–247. doi: 10.1159/000505213

Tang, Y., Wang, J., Lian, Y., Fan, C., Zhang, P., Wu, Y., et al. (2017). Linking long non-coding RNAs and SWI/SNF complexes to chromatin remodeling in cancer. *Mol. Cancer* 16:42.

Umeda, S., Kanda, M., and Kodera, Y. (2019). Recent advances in molecular biomarkers for patients with hepatocellular carcinoma. *Expert Rev. Mol. Diagn.* 19, 725–738. doi: 10.1080/14737159.2019.1638254

Wang, M., Wang, Y., Feng, X., Wang, R., Wang, Y., Zeng, H., et al. (2017). Contribution of hepatitis B virus and hepatitis C virus to liver cancer in China north areas: experience of the Chinese National Cancer Center. *Int. J. Infect. Dis.* 65, 15–21. doi: 10.1016/j.ijid.2017.09.003

Wang, Z., Qu, K., Niu, W., Lin, T., Xu, X., Huang, Z., et al. (2016). Glutathione S-transferase P1 gene rs4147581 polymorphism predicts overall survival of patients with hepatocellular carcinoma: evidence from an enlarged study. *Tumor Biol.* 37, 943–952. doi: 10.1007/s13277-015-3871-7

Wei, Y., Wang, Z., Zong, Y., Deng, D., Chen, P., and Lu, J. (2020). LncRNA MFI2-AS1 promotes HCC progression and metastasis by acting as a competing endogenous RNA of miR-134 to upregulate FOXM1 expression. *Biomed. Pharmacother.* 125:109890. doi: 10.1016/j.biopha.2020.109890

Yang, Y., Chen, Q., Piao, H. Y., Wang, B., Zhu, G. Q., Chen, E. B., et al. (2020). HNRNPAB-regulated lncRNA-ELF209 inhibits the malignancy of hepatocellular carcinoma. *Int. J. Cancer* 146, 169–180. doi: 10.1002/ijc.32409

Zhang, B., Li, C., and Sun, Z. (2018). Long non-coding RNA LINC00346, LINC00578, LINC00673, LINC00671, LINC00261, and SNHG9 are novel prognostic markers for pancreatic cancer. *Am. J. Transl. Res.* 10, 2648–2658.

Zhang, H., Qin, D., Jiang, Z., and Zhang, J. (2019). SNHG9/miR-199a-5p/Wnt2 axis regulates cell growth and aerobic glycolysis in glioblastoma. *J. Neuropathol. Exp. Neurol.* 78, 939–948. doi: 10.1093/jnen/nlz078

Zhou, H., Liu, J., Zhou, C., Gao, N., Rao, Z., Li, H., et al. (2018). In vivo simultaneous transcriptional activation of multiple genes in the brain using CRISPR-dCas9-activator transgenic mice. *Nat. Neurosci.* 21, 440–446. doi: 10.1038/s41593-017-0060-6

Zhu, F., and Rhim, H. (2019). Thermal ablation for hepatocellular carcinoma: what's new in 2019. *Chin. Clin. Oncol.* 8:58. doi: 10.21037/cco.2019.11.03

Zhu, R. X., Seto, W. K., Lai, C. L., and Yuen, M. F. (2016). Epidemiology of hepatocellular carcinoma in the Asia-Pacific region. *Gut Liver* 10, 332–339.

Conflict of Interest: The authors declare that the research was conducted in the absence of any commercial or financial relationships that could be construed as a potential conflict of interest.

frontiers in Molecular Biosciences

ORIGINAL RESEARCH
published: 15 April 2021
doi: 10.3389/fmolb.2021.674632

CRISPR/dCas9-Mediated Parkin Inhibition Impairs Mitophagy and Aggravates Apoptosis of Rat Nucleus Pulposus Cells Under Oxidative Stress

Tao Lan[1†], Yu-chen Zheng[1†], Ning-dao Li[2†], Xiao-sheng Chen[1], Zhe Shen[1] and Bin Yan[1]**

[1] Department of Spine Surgery, Shenzhen Second People's Hospital, The First Affiliated Hospital of Shenzhen University, Shenzhen, China, [2] Department of Orthopedic Surgery, Shenzhen Luohu People's Hospital, The Third Affiliated Hospital of Shenzhen University, Shenzhen, China

OPEN ACCESS

Edited by:
Yonghao Zhan,
Zhengzhou University, China

Reviewed by:
Congcong Cao,
Peking University Shenzhen Hospital, China
Yuantao Zhang,
The Chinese University of Hong Kong, China

***Correspondence:**
Zhe Shen
doctorshenzhe@163.com
Bin Yan
08timmy@163.comand

† These authors have contributed equally to this work and share first authorship

Specialty section:
This article was submitted to Molecular Diagnostics and Therapeutics, a section of the journal Frontiers in Molecular Biosciences

Received: 01 March 2021
Accepted: 22 March 2021
Published: 15 April 2021

Citation:
Lan T, Zheng Y-c, Li N-d, Chen X-s, Shen Z and Yan B (2021) CRISPR/dCas9-Mediated Parkin Inhibition Impairs Mitophagy and Aggravates Apoptosis of Rat Nucleus Pulposus Cells Under Oxidative Stress. Front. Mol. Biosci. 8:674632. doi: 10.3389/fmolb.2021.674632

Objective: The aim of this study is to explore the role of Parkin in intervertebral disk degeneration (IDD) and its mitophagy regulation mechanism.

Study design and methods: Rat nucleus pulposus (NP) cells were stimulated with hydrogen peroxide (H_2O_2) to a mimic pathological condition. Apoptosis and mitophagy were assessed by Western blot, terminal deoxynucleotidyl transferase dUTP nick end labeling (TUNEL) assay, and immunofluorescence staining. The CRISPR–dCas9–KRAB system was used to silence the expression of Parkin.

Result: In this study, we found that Parkin was downregulated in rat NP cells under oxidative stress. In addition, treatment with H_2O_2 resulted in mitochondrial dysfunction, autophagy inhibition, and a significant increase in the rate of apoptosis of NP cells. Meanwhile, mitophagy inhibition enhanced H_2O_2-induced apoptosis. Furthermore, repression of Parkin significantly attenuated mitophagy and exacerbated apoptosis.

Conclusion: These results suggested that Parkin may play a protective role in alleviating the apoptosis of NP cells *via* mitophagy, and that targeting Parkin may provide a promising therapeutic strategy for the prevention of IDD.

Keywords: CRISPR/dCas9, IDD, mitophagy, apoptosis, Parkin

INTRODUCTION

Intervertebral disk degeneration (IDD) is widely known as a main contributor to low back pain (LBP), which has become a global public health problem associated with decline in quality of life and heavy socioeconomic burden (Hoy et al., 2010; Foster et al., 2018). It is estimated that approximately 80% of the population suffer from neck or back pain at some point in their lives (Côté et al., 2001). As the largest avascular structure in the human body, the intervertebral disk is a complex structure that consists of superior and inferior cartilage endplates (CEP), internal jelly-like nucleus pulposus (NP), and external annulus fibrosus (AF) (Kadow et al., 2015). NP cells are responsible for the synthesis of the extracellular matrix (ECM) and play an important role in

maintaining the biological function of the intervertebral disk. Emerging pieces of evidence reveal that excessive apoptosis of NP cells can trigger IDD (Liu et al., 2013; Chen et al., 2016, 2017). Hence, a better understanding of the apoptosis mechanism may provide a potential therapeutic target for the prevention and treatment of IDD.

Oxidative stress is a common pathological process that is characterized by overproduction of reactive oxygen species (ROS) (Feng et al., 2017). As a main intracellular ROS-generating organelle, mitochondria are also the primary target of ROS. ROS overproduction causes mitochondrial injury. Furthermore, mitochondrial dysfunction enhances ROS generation with a positive feedback loop. Accumulated research has indicated that ROS are a potent pro-apoptotic factor for NP cells (Xia et al., 2019; Xiang et al., 2020; Zhao et al., 2020). Additionally, mitochondria are responsible for the generation of ATP, which is essential for maintaining cell survival and physiological function. Considering that mitochondrial dysfunction is implicated in the senescence and apoptosis of NP cells, mitochondrial homeostasis is vital for the health of intervertebral disks.

Mitophagy is a special type of autophagy that selectively targets damaged or redundant mitochondria to the lysosome for elimination, which is a crucial step in mitochondrial quality control (Novak and Dikic, 2011; Sun et al., 2020). It is acknowledged that mitophagy impairment results in the accumulation of defective organelles and ROS overproduction, and subsequently increases the rate of apoptosis of NP cells (Chen et al., 2020; Kang et al., 2020a,b). Hence, balance between mitophagy and apoptosis determines the fate of NP cells. However, the relationship between mitophagy and apoptosis within disk cells in response to oxidative stress remains poorly understood. Parkin is a key player in the induction of mitophagy. It regulates ubiquitination of mitochondrial outer membrane proteins and promotes degradation of dysfunctional mitochondria. It is reported that Parkin is closely related to the crosstalk between mitophagy and apoptosis in NP cells (Zhang et al., 2018; Huang et al., 2020; Madhu et al., 2020).

In this study, we hypothesized that mitophagy plays a cytoprotective role in response to the oxidative stress of NP cells. To confirm this hypothesis, hydrogen peroxide (H_2O_2) was used to induce oxidative stress, which could mimic the pathological mechanisms of mitochondrial dysfunction and apoptosis in NP cells. Furthermore, we investigated the relationship between mitophagy and apoptosis, and the Parkin signaling pathways involved in their interactions. Finally, our study revealed that Parkin is involved in the pathogenesis of IDD and may serve as a therapeutic target for IDD.

MATERIALS AND METHODS

Cell Isolation and Culture

Nucleus pulposus cells were extracted from healthy NP of young Sprague-Dawley rats. NP tissues were isolated under a dissecting microscope and digested in 0.2% type II collagenase for approximately 4 h at 37°C. The isolated cells were cultured in Dulbecco's modified Eagle medium (DMEM) and 10% fetal bovine serum (FBS) supplemented with antibiotics (Gibco, Carlsbad, CA, United States). Second-generation NP cells were used throughout the experiments.

Cell Viability Assay and NP Cells Treatment

Cell Counting Kit-8 (CCK-8) assaying was performed to detect the viability of NP cells (CCK-8; Dojindo Co., Kumamoto, Japan) according to the protocol of the manufacturer. NP cells were seeded in 96-well plates and incubated in DMEM/F12 with 10% FBS and 1% antibiotics at 37°C for 24 h. NP cells were treated using H_2O_2 with different concentrations (0.1, 0.25, 0.5, and 1 mM) for 24 h or 1 mM for various times (0, 6, 12, and 24 h). The cells were then washed with phosphate-buffered saline (PBS), and a 10 μl CCK-8 solution was added to each well. The wells were incubated at 37°C for 1 h. Finally, the absorbance of the wells was then measured at 450 nm using a micro-plate reader (BioTek, Winooski, VT, United States).

Quantitative Real-Time PCR (RT-qPCR)

Total RNA was extracted from the cultured cells using a TRIzol reagent (Invitrogen, Carlsbad, CA, United States). Reverse transcription and gene amplification procedures were conducted according to the instructions of the kit manufacturer (TransGen Biotech, Beijing, China). Glyceraldehyde 3-phosphate dehydrogenase (GAPDH) was used to normalize the gene expression of other mRNAs. PCR primers were as follows.

Western Blotting

The cells were lysed using radioimmunoprecipitation assay (RIPA) buffer (Sigma, St. Louis, MO, United States). Total protein extracts from NP cells were obtained through whole-cell lysis assaying (KeyGen). Protein concentration was determined using the bicinchoninic acid (BCA) method. Protein samples were separated using sodium dodecyl sulfate–polyacrylamide gel electrophoresis (SDS–PAGE) and transferred to a polyvinylidene fluoride (PVDF) membrane. The membrane was incubated with primary antibodies against P62 (1:1,000, ab56416 Abcam, Cambridge, United Kingdom), Parkin (1:1,000, #4211; CST, Danvers, MA, United States), LC3 (1:1,000, #83506, CST, Danvers, MA, United States), Bcl-2 (1:1,000, #3498; CST, Danvers, MA, United States), Bax (1:1,000, #14796; CST, Danvers, MA, United States), GAPDH (1:10,000, #60004-1-Ig: Proteintech) overnight at 4°C; and target protein bands and internal reference bands were visualized and calculated using the ImageJ software (ImageJ 1.48v, United States).

Immunofluorescence

Nucleus pulposus cells were fixed with 4% paraformaldehyde for 15 min and permeabilized with 0.5% Triton X-100 for 30 min. After blocking with 5% bovine serum albumin (BSA) for 30 min, slides were incubated with primary antibodies against P62 (1:200) overnight at 4°C. Secondary antibody (1:100; Invitrogen,

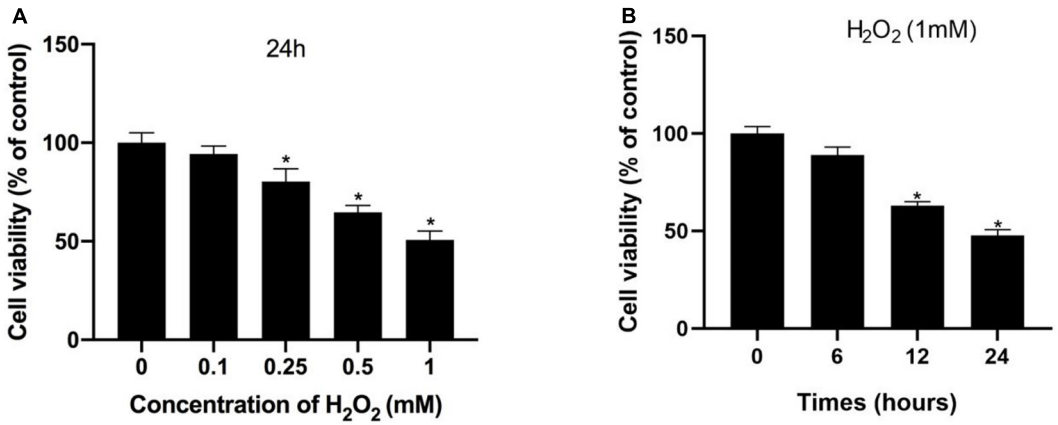

FIGURE 1 | Hydrogen peroxide inhibited cell viability in NP cells. **(A,B)** Effects of H_2O_2 on cell viability were detected using the Cell Counting Kit-8 (CCK-8). *$p <$ 0.05 vs. control group.

Carlsbad, CA, United States) was added the next day. The nuclei were stained with 4′,6-diamino-2-phenylindole (DAPI) for 1 min. The cells were observed using a fluorescence microscope (CTR4000B, Leica, Wetzlar, Germany).

Mitochondrial Membrane Potential Measurement, ATP, and Complex III

The mitochondrial membrane potential was determined by JC-1 staining (Beyotime, Shanghai, China) according to the protocol of the manufacturer. Intracellular ATP and complex III levels were determined using the ATP Assay and ROS Assay Kits according to the instructions of the manufacturer (Beyotime, Shanghai, China).

Flow Cytometry Assay of Apoptosis

The apoptosis rate of the NF cells was detected using the Annexin V-FITC/PI Double-Staining Kit (Fushen, Shanghai, China). NP cells were collected and washed with PBS and subsequently suspended in 100 μl binding buffer. The cells were then incubated with 5 μl Annexin V-FITC and 5 μl PI at 37°C for 30 min. The early (Annexin V+/PI−) and the late apoptotic (Annexin V+/PI−) cells were used to calculate apoptosis rate.

Transfection of Plasmids

Nucleus pulposus cells were plated using six-well plates overnight before transfection. When the cell density reached 70% confluence, the NP cells were co-transfected with sgRNA and dcas9-KRAB plasmids using Lipofectamine 2000 (Invitrogen, Carlsbad, CA, United States) according to the protocol of the manufacture.

Statistical Analysis

Results were presented as the mean ± SD and analyzed using SPSS 22 (IBM Corp., Armonk, NY, United States). Differences between groups were analyzed by Student's *t*-test or one-way analysis of variance (ANOVA) followed by Tukey's test. A *p* value of less than 0.05 was considered significant.

RESULTS

Hydrogen Peroxide Increases Rate of Apoptosis and Inhibits Mitophagy in Rat NP

Initially, H_2O_2 was used to mimic oxidative stress *in vitro*, and CCK-8 assaying was performed to investigate the cytotoxicity of H_2O_2 in NP cells. As shown in **Figures 1A,B**, H_2O_2 treatment was observed to reduce cell viability in a dose- and time-dependent manner. Exposure to H_2O_2 with a concentration exceeding 1 mmol/L for 24 h and treatment with H_2O_2 (1 mmol/L) for 24 h or longer showed a marked reduction in cell viability. Therefore, H_2O_2 with a concentration of 1 mmol/L was used in the subsequent experiments. Then, we assessed the apoptosis response of the NP cells to oxidative stress. The Western blot and qPCR results showed that H_2O_2-induced oxidative stress did significantly increase cleaved-caspase3 and Bax/bcl-2 (**Figures 2A–C**). Meanwhile, flow cytometry by Annexin V-FITC/PI staining showed that the percentage of apoptotic NP cells was higher in the H_2O_2-treated group than in the control group (**Figures 2D,E**). To investigate the effect of H_2O_2 on autophagy in the NP cells, we examined the expression of LC3-II/LC3-I and p62 by Western blot. As shown in **Figures 3A,B**, the ratio of LC3-II/LC3-I was decreased and the level of p62 was increased after H_2O_2 treatment for 24 h. The immunofluorescence analysis of NP cells revealed an accumulation of P62 protein in response to oxidative stress (**Figure 3C**). Taken together, these results indicated that oxidative stress induced by H_2O_2 could promote apoptosis and inhibit autophagy in NP cells.

Mitochondrial Dysfunction Is Involved in the H_2O_2-Induced Apoptosis of Rat NP

Mitophagy is responsible for quality control of mitochondria under oxidative stress. As expected, oxidative stress inhibits mitophagy but also causes mitochondrial dysfunction. After

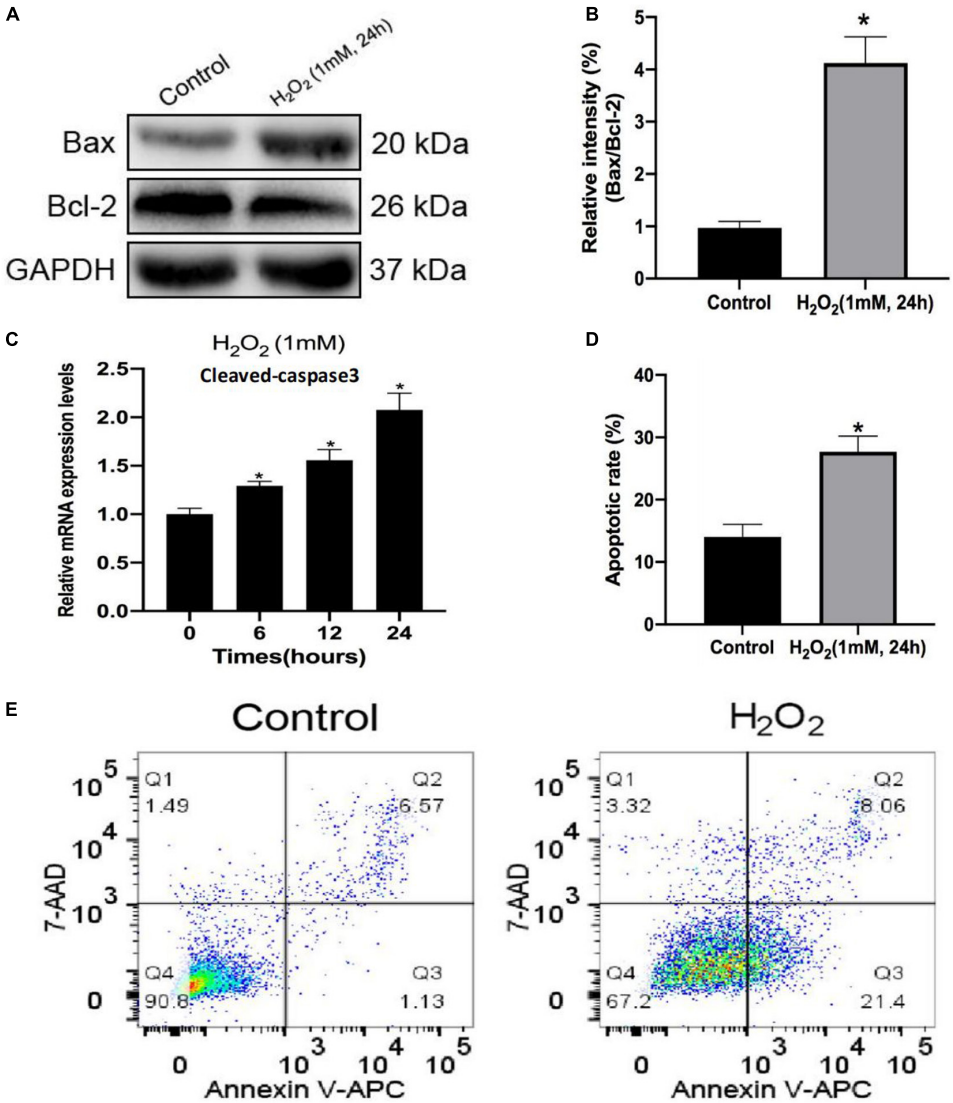

FIGURE 2 | Hydrogen peroxide promotes apoptosis in rat nucleus pulposus (NP) cells. **(A,B)** The protein levels of Bax and Bcl-2 in NP cells were measured by Western blotting. **(C)** Relative mRNA expression of cleaved caspase-3 by RT-qPCR. **(D,E)** Apoptosis of NP cells with or without H_2O_2 treatment was detected by flow cytometry. Data are represented as the mean ± SD. *$p < 0.05$ vs. control group.

treatment with H_2O_2, the green/red fluorescence ratio of NP cells significantly increased, indicating that mitochondrial membrane potential was reduced by the treatment of H_2O_2 (**Figure 4A**). Furthermore, the intracellular complex III level and ATP production were markedly decreased under oxidative stress (**Figures 4B,C**). Altogether, prolonged oxidative stress leads to mitochondrial damage.

Mitophagy Inhibition by 3-MA Enhances H_2O_2-Induced Apoptosis in Rat NP

To explore whether mitophagy was involved in the protective response against H_2O_2 induced apoptosis, we determined the expression of cleaved-caspase3, Bax, and Bcl-2. We found that NP cells pre-treated with mitophagy inhibitor 3-MA significantly increased pro-apoptotic protein expression (cleaved-caspase3 and Bax) and decreased anti-apoptotic protein (Bcl-2) expression (**Figures 5A,B**). Similarly, TUNEL assay results also showed that the mitophagy inhibitor dramatically exacerbated the apoptosis of NP cells (**Figure 5C,D**). Collectively, these findings showed that under oxidative stress mitophagy protected rat NP cells against apoptosis.

Inhibition of Parkin by dCas9-KRAB Significantly Attenuates H_2O_2-Induced Mitophagy

In order to investigate the relationship between Parkin and IDD in rat NP cells, we determined Parkin expression under oxidative stress by Western blotting, and we found that the Parkin expression decreased significantly in the H_2O_2 group compared with that in the control group (**Figure 6B**). To further verify

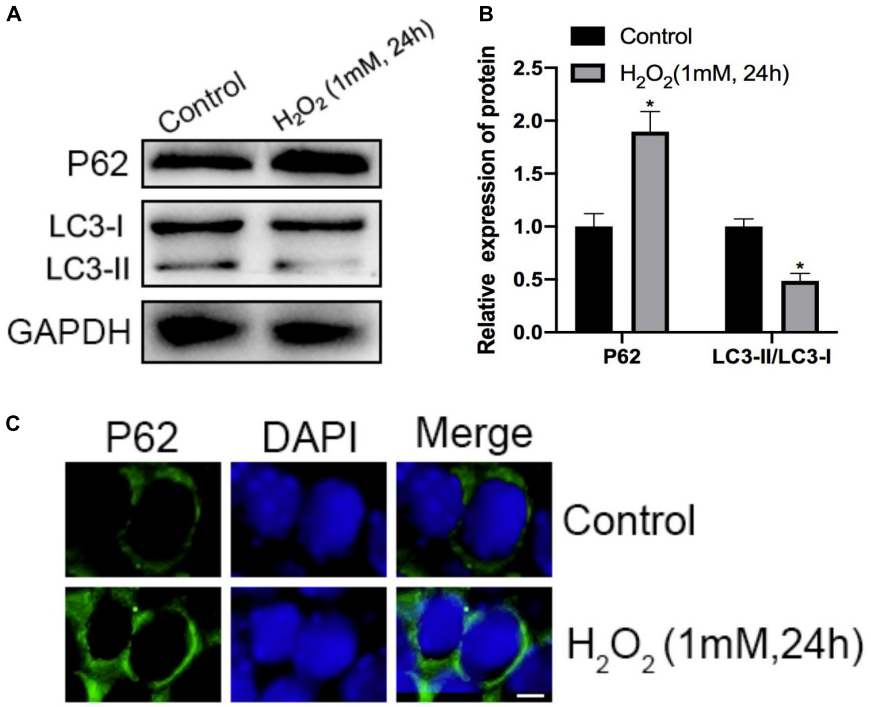

FIGURE 3 | Effects of H_2O_2 on mitophagy in NP cells. **(A,B)** The protein level of P62, LC3-I, and LC3-II in the NP cells was measured by Western blotting. **(C)** Immunofluorescence of the P62 protein in NP cells (Green signal represents P62, blue signal represents DAPI). *$p < 0.05$ vs. control group.

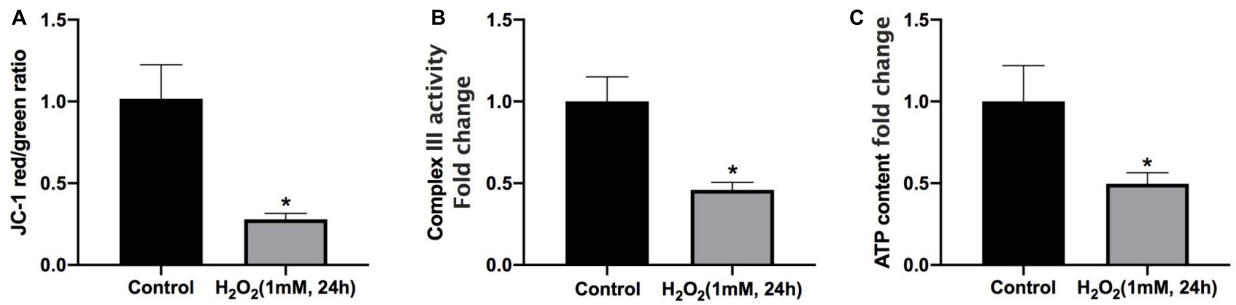

FIGURE 4 | Mitochondrial dysfunction is involved in H_2O_2-induced apoptosis of rat NP. **(A)** Effect of H_2O_2 on mitochondrial membrane potential. **(B)** Summary data for the effect of H_2O_2 on the relative content of complex III. **(C)** Intracellular ATP levels in NP cells. *$p < 0.05$ vs. control group.

the role of Parkin in mitophagy, we used the CRISPR/dCas9-KRAB system to repress the expression of Parkin (**Figure 6A**). We found that mitophagy decreased markedly (**Figures 6C,D**) while apoptosis of NP cells increased dramatically (**Figures 6E,F**) after repression of Parkin mediated with CRISPR/dCas9-KRAB. Overall, these results suggested that the activation of mitophagy against apoptosis was dependent on Parkin.

DISCUSSION

Intervertebral disk degeneration is a common reason for LBP, which is one of the leading causes of chronic disability. To date, conventional treatments including physical therapy, anti-inflammatory medications, and surgeries remain unsatisfactory (Legrand et al., 2007). Therefore, development of biological therapies to prevent IDD is an issue that needs to be solved urgently. Studies have shown that excessive apoptosis of NP cells plays a crucial role in the development of IDD (Guo et al., 2018; Yu et al., 2018). In addition, previous studies have shown that oxidative stress participates in the apoptosis process of NP cells (Nan et al., 2020). Nevertheless, the underlying mechanisms of apoptosis induced by oxidative stress have not been fully clarified.

In this study, we confirmed that both apoptosis and autophagy were involved in the pathogenesis of oxidative stress-induced IDD. In addition, we found that oxidative stress resulted in mitochondrial dysfunction, autophagy inhibition,

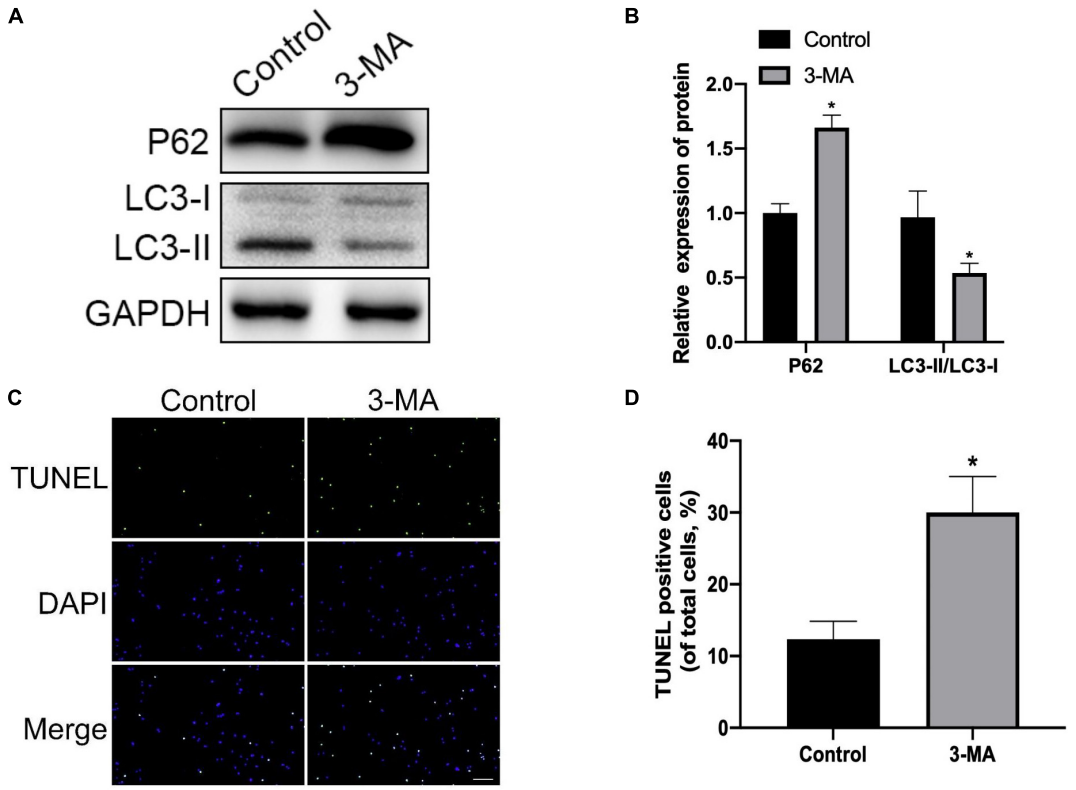

FIGURE 5 | Mitophagy inhibition enhances H_2O_2-induced apoptosis in rat NP. **(A,B)** Western blot of P62, LC3-I, and LC3-II expression in NP cells after treatment with 3-MA. **(C,D)** Representative images of TUNEL staining and quantitative analysis showing NP cells apoptosis after treatment with 3-MA. *$p < 0.05$ vs. control group.

and a significant increase in the rate of apoptosis of NP cells. Furthermore, we investigated the relationship between autophagy and apoptosis under oxidative stress by repressing autophagy and found that apoptosis of NP cells was dramatically enhanced, indicating that autophagy played a protective role against apoptosis in response to oxidative stress. Finally, mechanism study revealed that the expression of Parkin was suppressed after H_20_2 treatment, and downregulation of Parkin by dCas9-KRAB led to aggravation of NP cell apoptosis and autophagy inhibition. Hence, we propose that the activation of Parkin could prevent oxidative stress-induced apoptosis and mitochondrial dysfunction in rat NP cells *via* the promotion of mitophagy (**Figure 7**).

Apoptosis of NP cells is thought to play a critical role in the progression of IDD. In mammals, there are two main apoptotic pathways: the extrinsic (also called death receptor) and the intrinsic (also called mitochondrial) (Wajant, 2002). It is acknowledged that oxidative stress-induced mitochondrial dysfunction is one of the important mechanisms that trigger the intrinsic pathway of apoptosis in NP cells (Lin et al., 2020). An oxidative injury leads to decrease in mitochondrial membrane potential and ATP production, and increase in mitochondrial outer membrane permeability, followed by the release of cytochrome c and activation of caspase cascade, which eventually leads to apoptosis (Chen et al., 2003). Exposure to hydrogen peroxide (1 mmol/L for 24 h) elicited oxidative stress, and we confirmed that both mitochondria injury and apoptosis of NP cells increased markedly after H_2O_2 treatment. The results show that oxidative stress causes mitochondrial-mediated intrinsic apoptosis of NP cells. Therefore, maintenance of mitochondrial function and structural integrity is the key to prevent NP cell apoptosis and IDD development.

In recent years, mitophagy has attracted increasing research interest because of its important role in the clearance of damaged mitochondria. Numerous research studies have shown that proper activation of mitophagy plays a cytoprotective role against apoptosis while excessive mitophagy leads to apoptosis (Park and Park, 2013; Lan et al., 2021). A great effort has been made to clarify the relationship between mitophagy and apoptosis, however, the role of mitophagy in ROS-induced apoptosis of NP cells remains unclear. In this study, we used 3-MA to inhibit mitophagy and found that the apoptosis rate of NP cells increased significantly, indicating that mitophagy might be the cellular self-defense mechanism for oxidative stress damage. The results are consistent with those of some previous studies (Wang J. et al., 2018; Wang Y. et al., 2018). For example, the study conducted by Lin et al. (2020) showed that mitophagy suppressed NP cells apoptosis under oxidative stress and attenuated IDD. However, opposite conclusions have also been reported in other studies. For example, Zhan et al. (2020) found that autophagy

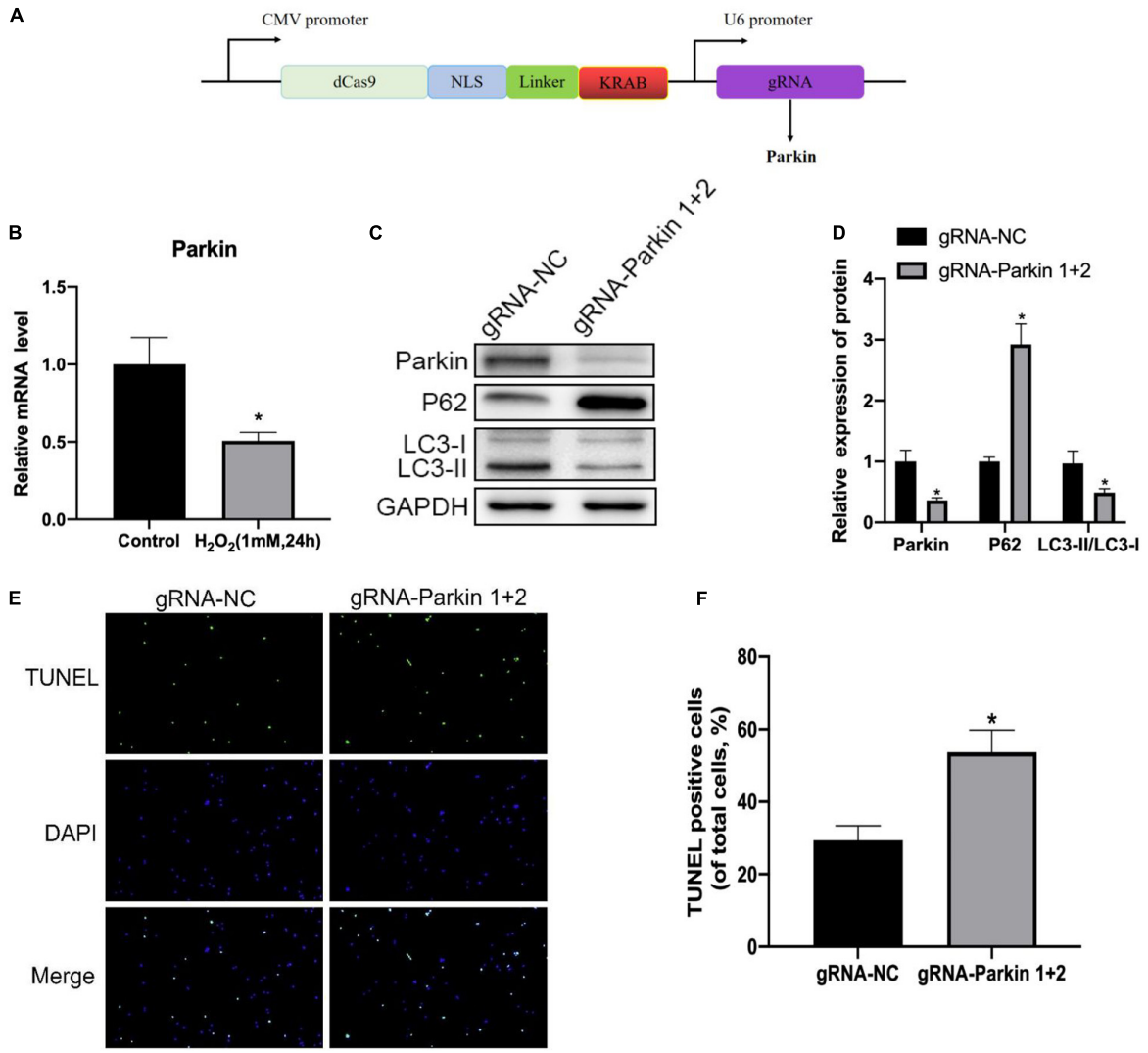

FIGURE 6 | Inhibition of Parkin by the dCas9-KRAB system significantly attenuates H_2O_2-induced mitophagy. **(A)** Vector map of clustered regularly interspaced palindromic repeat epigenome editing vectors targeting the Parkin gene promotor region. **(B)** Expression level of Parkin in NP cells. **(C,D)** Western blot of Parkin, P62, LC3-I, and LC3-II expression in NP cells after Parkin inhibition. **(E,F)** Representative images of TUNEL staining and quantitative analysis showing NP cells apoptosis after Parkin inhibition. *$p < 0.05$ vs. control group.

activation could promote NP cell apoptosis, senescence, and ECM catabolism. Nevertheless, more and more studies show that basal-level autophagy plays a housekeeping and cytoprotective role; while autophagy dysfunction, either inadequate or excessive autophagy, leads to the death of cells. In addition, the pro-survival or pro-death effect of autophagy is also attributed to cell types, time, and degree of stimulus.

Parkin-mediated mitochondrial autophagy is the most intensively investigated mitochondrial autophagy pathway. The autophagy mechanism is translocation of Parkin to defective mitochondria and recruitment of p62/SQSTM1, followed by engulfment of damaged mitochondria by autophagosomes, and degradation by lysosomes (Nguyen et al., 2016). Parkin, as a protective protein, plays many beneficial roles in preventing degenerative diseases, such as Parkinson's disease (Kamienieva et al., 2021), osteoarthritis (Ansari et al., 2018), and Alzheimer's disease (Zhao et al., 2021). However, studies regarding the relationship between Parkin and IDD are limited. Our results revealed that Parkin was downregulated in NP cells under oxidative stress. Moreover, the inhibition of Parkin aggravated NP cell apoptosis, exacerbated mitochondrial dysfunction, and suppressed mitophagy activity, indicating that Parkin was able to prevent NP cell apoptosis and protect mitochondrial function through upregulation of mitophagy. Therefore, Parkin is a promising therapeutic target for the treatment of IDD in the future. As mentioned, there are many conventional methods to repress Parkin gene expression. In this study, we innovatively used the dCas9-KRAB system to inhibit the Parkin gene expression in NP cells under oxidative stress. The CRISPR/Cas9 system, which is derived from *Streptococcus*

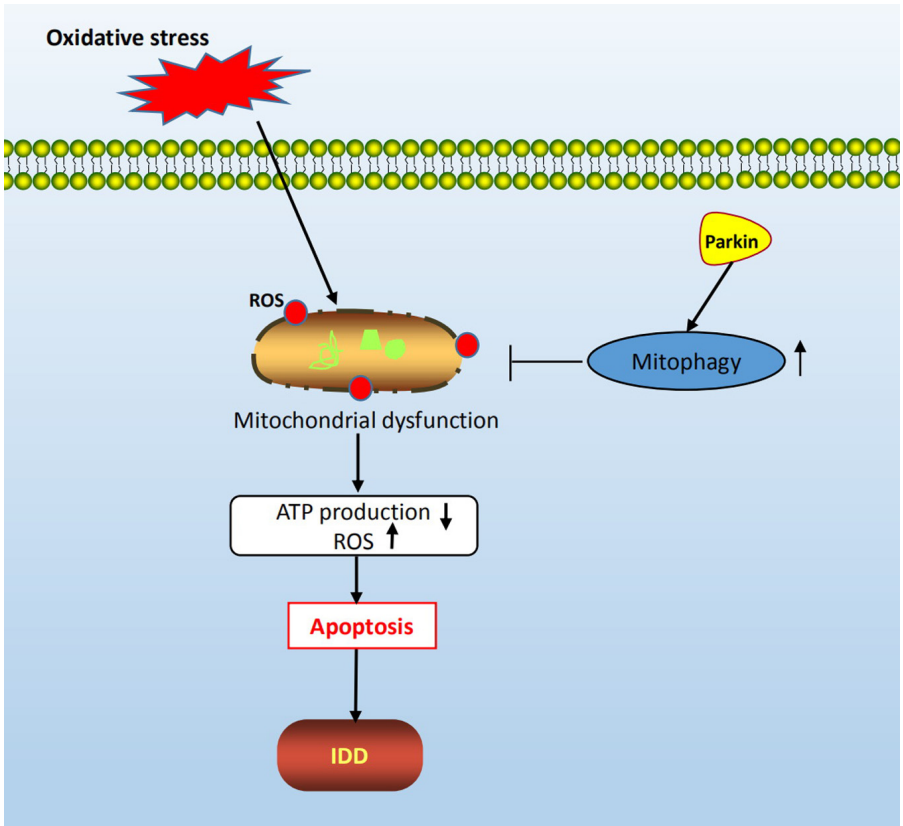

FIGURE 7 | Schematic diagram of mechanisms shows the protective role of mitophagy in rat NP cells under oxidative stress.

pyogenes, is a powerful genetic editing tool and is widely used in mammalian cells (Ran et al., 2013). CRISPR-dCas9-KRAB is a new tool to silence a target gene expression with high efficiency, low cost, and easy operation. However, the application of the CRISPR/Cas9 system in the intervertebral disk field is limited. A previous study by Stover et al. (2019) explored the potential application of CRISPR epigenome editing to target inflammatory receptors for pain modulation in degenerative intervertebral disk. Our study confirmed that the potential application of CRISPR/Cas9 as a novel gene therapy tool for IDD.

This study has several limitations. First, although our results suggest that Parkin could be a potential therapeutic target for IDD, this study is mainly *in vitro*; thus, further *in vivo* studies are needed to be carried out to provide more convincing evidence. Second, in this study we used NP cells from rats instead of NP cells from humans, and species may cause some differences. Third, since both AF cells and CEP chondrocytes also take part in the degeneration process, the response of AF cells and CEP cells to oxidative stress needs to be elucidated in the future.

CONCLUSION

In summary, this study has demonstrated that Parkin is involved in the pathogenesis of IDD and that it plays an important role in the clearance of damaged mitochondria *via* modulation of mitophagy. These findings suggest a potential therapeutic application of Parkin for the prevention and treatment of disk degeneration.

DATA AVAILABILITY STATEMENT

The raw data supporting the conclusions of this article will be made available by the authors, without undue reservation.

ETHICS STATEMENT

The animal study was reviewed and approved by The Animal Care and Use Committee of the Shenzhen Second People's Hospital.

AUTHOR CONTRIBUTIONS

ZS and BY conceived and designed the study. TL, YZ, and N-DL performed the experiments and data analysis. X-SC and TL wrote and revised the manuscript. All authors contributed to the article and approved the submitted version.

REFERENCES

Ansari, M. Y., Khan, N. M., Ahmad, I., and Haqqi, T. M. (2018). Parkin clearance of dysfunctional mitochondria regulates ROS levels and increases survival of human chondrocytes. *Osteoarthr. Cartil.* 26, 1087–1097. doi: 10.1016/j.joca.2017.07.020

Chen, D., Xia, D., Pan, Z., Xu, D., Zhou, Y., Wu, Y., et al. (2016). Metformin protects against apoptosis and senescence in nucleus pulposus cells and ameliorates disc degeneration in vivo. *Cell Death Dis.* 7:e2441. doi: 10.1038/cddis.2016.334

Chen, Q., Chai, Y. C., Mazumder, S., Jiang, C., Macklis, R. M., Chisolm, G. M., et al. (2003). The late increase in intracellular free radical oxygen species during apoptosis is associated with cytochrome c release, caspase activation, and mitochondrial dysfunction. *Cell Death Differ.* 10, 323–334.

Chen, S., Zhao, L., Deng, X., Shi, D., Wu, F., Liang, H., et al. (2017). Mesenchymal stem cells protect nucleus pulposus cells from compression-induced apoptosis by inhibiting the mitochondrial pathway. *Stem Cells Int.* 2017:9843120. doi: 10.1155/2017/9843120

Chen, Y., Lin, J., Chen, J., Huang, C., Zhang, Z., Wang, J., et al. (2020). Mfn2 is involved in intervertebral disc degeneration through autophagy modulation. *Osteoarthr. Carti.* 28, 363–374. doi: 10.1016/j.joca.2019.12.009

Côté, P., Cassidy, J. D., and Carroll, L. (2001). The treatment of neck and low back pain: who seeks care? who goes where? *Med. Care* 39, 956–967.

Feng, C., Yang, M., Lan, M., Liu, C., Zhang, Y., Huang, B., et al. (2017). ROS: crucial intermediators in the pathogenesis of intervertebral disc degeneration. *Oxid. Med. Cell Longev.* 2017:5601593. doi: 10.1155/2017/5601593

Foster, N. E., Anema, J. R., Cherkin, D., Chou, R., Cohen, S. P., Gross, D. P., et al. (2018). Prevention and treatment of low back pain: evidence, challenges, and promising directions. *Lancet* 391, 2368–2383. doi: 10.1016/s0140-6736(18)30489-6

Guo, W., Zhang, B., Mu, K., Feng, S. Q., Dong, Z. Y., Ning, G. Z., et al. (2018). Circular RNA GRB10 as a competitive endogenous RNA regulating nucleus pulposus cells death in degenerative intervertebral disk. *Cell Death Dis.* 9:319. doi: 10.1038/s41419-017-0232-z

Hoy, D., Brooks, P., Blyth, F., and Buchbinder, R. (2010). The epidemiology of low back pain. *Best Pract. Res. Clin. Rheumatol.* 24, 769–781. doi: 10.1016/j.berh.2010.10.002

Huang, D., Peng, Y., Li, Z., Chen, S., Deng, X., Shao, Z., et al. (2020). Compression-induced senescence of nucleus pulposus cells by promoting mitophagy activation via the PINK1/PARKIN pathway. *J. Cell Mol. Med.* 24, 5850–5864. doi: 10.1111/jcmm.15256

Kadow, T., Sowa, G., Vo, N., and Kang, J. D. (2015). Molecular basis of intervertebral disc degeneration and herniations: what are the important translational questions? *Clin. Orthop. Relat. Res.* 473, 1903–1912. doi: 10.1007/s11999-014-3774-8

Kamienieva, I., Duszyński, J., and Szczepanowska, J. (2021). Multitasking guardian of mitochondrial quality: parkin function and Parkinson's disease. *Transl. Neurodegener.* 10:5. doi: 10.1186/s40035-020-00229-8

Kang, L., Liu, S., Li, J., Tian, Y., Xue, Y., and Liu, X. (2020a). Parkin and Nrf2 prevent oxidative stress-induced apoptosis in intervertebral endplate chondrocytes via inducing mitophagy and anti-oxidant defenses. *Life Sci.* 243:117244. doi: 10.1016/j.lfs.2019.117244

Kang, L., Liu, S., Li, J., Tian, Y., Xue, Y., and Liu, X. (2020b). The mitochondria-targeted anti-oxidant MitoQ protects against intervertebral disc degeneration by ameliorating mitochondrial dysfunction and redox imbalance. *Cell Prolif.* 53:e12779. doi: 10.1111/cpr.12779

Lan, T., Shiyu, H., Shen, Z., Yan, B., and Chen, J. (2021). New insights into the interplay between miRNAs and autophagy in the aging of intervertebral discs. *Ageing Res. Rev.* 65:101227. doi: 10.1016/j.arr.2020.101227

Legrand, E., Bouvard, B., Audran, M., Fournier, D., and Valat, J. P. (2007). Sciatica from disk herniation: medical treatment or surgery? *Joint Bone Spine* 74, 530–535. doi: 10.1016/j.jbspin.2007.07.004

Lin, J., Zhuge, J., Zheng, X., Wu, Y., Zhang, Z., Xu, T., et al. (2020). Urolithin A-induced mitophagy suppresses apoptosis and attenuates intervertebral disc degeneration via the AMPK signaling pathway. *Free Radic. Biol. Med.* 150, 109–119. doi: 10.1016/j.freeradbiomed.2020.02.024

Liu, G., Cao, P., Chen, H., Yuan, W., Wang, J., and Tang, X. (2013). MiR-27a regulates apoptosis in nucleus pulposus cells by targeting PI3K. *PLoS One* 8:e75251. doi: 10.1371/journal.pone.0075251

Madhu, V., Boneski, P. K., Silagi, E., Qiu, Y., Kurland, I., Guntur, A. R., et al. (2020). Hypoxic regulation of mitochondrial metabolism and mitophagy in nucleus pulposus cells is dependent on HIF-1α-BNIP3 Axis. *J. Bone Miner Res.* 35, 1504–1524. doi: 10.1002/jbmr.4019

Nan, L. P., Wang, F., Liu, Y., Wu, Z., Feng, X. M., Liu, J. J., et al. (2020). 6-gingerol protects nucleus pulposus-derived mesenchymal stem cells from oxidative injury by activating autophagy. *World J. Stem Cells* 12, 1603–1622. doi: 10.4252/wjsc.v12.i12.1603

Nguyen, T. N., Padman, B. S., and Lazarou, M. (2016). Deciphering the molecular signals of PINK1/Parkin mitophagy. *Trends Cell Biol.* 26, 733–744.

Novak, I., and Dikic, I. (2011). Autophagy receptors in developmental clearance of mitochondria. *Autophagy* 7, 301–303. doi: 10.4161/auto.7.3.14509

Park, E. Y., and Park, J. B. (2013). High glucose-induced oxidative stress promotes autophagy through mitochondrial damage in rat notochordal cells. *Int. Orthop.* 37, 2507–2514. doi: 10.1007/s00264-013-2037-8

Ran, F. A., Hsu, P. D., Wright, J., Agarwala, V., Scott, D. A., and Zhang, F. (2013). Genome engineering using the CRISPR-Cas9 system. *Nat. Protoc.* 8, 2281–2308. doi: 10.1038/nprot.2013.143

Stover, J. D., Farhang, N., Lawrence, B., and Bowles, R. D. (2019). Multiplex epigenome editing of dorsal root ganglion neuron receptors abolishes redundant interleukin 6, tumor necrosis factor alpha, and interleukin 1β signaling by the degenerative intervertebral disc. *Hum. Gene Ther.* 30, 1147–1160. doi: 10.1089/hum.2019.032

Sun, K., Jing, X., Guo, J., Yao, X., and Guo, F. (2020). Mitophagy in degenerative joint diseases. *Autophagy*. doi: 10.1080/15548627.2020.1822097 [Epub ahead of print].

Wajant, H. (2002). The Fas signaling pathway: more than a paradigm. *Science* 296, 1635–1636. doi: 10.1126/science.1071553

Wang, J., Nisar, M., Huang, C., Pan, X., Lin, D., Zheng, G., et al. (2018). Small molecule natural compound agonist of SIRT3 as a therapeutic target for the treatment of intervertebral disc degeneration. *Exp. Mol. Med.* 50, 1–14.

Wang, Y., Shen, J., Chen, Y., Liu, H., Zhou, H., Bai, Z., et al. (2018). PINK1 protects against oxidative stress induced senescence of human nucleus pulposus cells via regulating mitophagy. *Biochem. Biophys. Res. Commun.* 504, 406–414. doi: 10.1016/j.bbrc.2018.06.031

Xia, C., Zeng, Z., Fang, B., Tao, M., Gu, C., Zheng, L., et al. (2019). Mesenchymal stem cell-derived exosomes ameliorate intervertebral disc degeneration via anti-oxidant and anti-inflammatory effects. *Free Radic. Biol. Med.* 143, 1–15.

Xiang, Q., Cheng, Z., Wang, J., Feng, X., Hua, W., Luo, R., et al. (2020). Allicin attenuated advanced oxidation protein product-induced oxidative stress and mitochondrial apoptosis in human nucleus pulposus cells. *Oxid. Med. Cell Longev.* 2020:6685043. doi: 10.1155/2020/6685043

Yu, Y., Zhang, X., Li, Z., Kong, L., and Huang, Y. (2018). LncRNA HOTAIR suppresses TNF-α induced apoptosis of nucleus pulposus cells by regulating miR-34a/Bcl-2 axis. *Biomed. Pharmacother.* 107, 729–737. doi: 10.1016/j.biopha.2018.08.033

Zhan, S., Wang, K., Xiang, Q., Song, Y., Li, S., Liang, H., et al. (2020). lncRNA HOTAIR upregulates autophagy to promote apoptosis and senescence of nucleus pulposus cells. *J. Cell Physiol.* 235, 2195–2208. doi: 10.1002/jcp.29129

Zhang, Z., Xu, T., Chen, J., Shao, Z., Wang, K., Yan, Y., et al. (2018). Parkin-mediated mitophagy as a potential therapeutic target for intervertebral

disc degeneration. *Cell Death Dis.* 9:980. doi: 10.1038/s41419-018-1024-9

Zhao, N., Xia, J., and Xu, B. (2021). Physical exercise may exert its therapeutic influence on Alzheimer's disease through the reversal of mitochondrial dysfunction via SIRT1-FOXO1/3-PINK1-Parkin-mediated mitophagy. *J. Sport Health Sci.* 10, 1–3. doi: 10.1016/j.jshs.2020.08.009

Zhao, Y., Qiu, C., Wang, W., Peng, J., Cheng, X., Shangguan, Y., et al. (2020). Cortistatin protects against intervertebral disc degeneration through targeting mitochondrial ROS-dependent NLRP3 inflammasome activation. *Theranostics* 10, 7015–7033. doi: 10.7150/thno.45359

Conflict of Interest: The authors declare that the research was conducted in the absence of any commercial or financial relationships that could be construed as a potential conflict of interest.

frontiers in Molecular Biosciences

ORIGINAL RESEARCH
published: 24 May 2021
doi: 10.3389/fmolb.2021.676021

Using CRISPRa and CRISPRi Technologies to Study the Biological Functions of ITGB5, TIMP1, and TMEM176B in Prostate Cancer Cells

Yi Yang[1]†, Qingxing Feng[2†], Kun Hu[1,3†] and Feng Cheng[2]*

[1]Department of Urology, Shenzhen Second People's Hospital, the First Affiliated Hospital of Shenzhen University, Shenzhen, China, [2]Deparment of Urology, Institute of Surgery Research, Daping Hospital, Third Military Medical University, Chongqing, China, [3]Anhui Medical University, Hefei, China

Although ITGB5, TIMP1, and TMEM176B are abnormally expressed in several cancers, their molecular biological mechanisms in prostate cancer cells are still to be investigated. The gene regulation technogies based on CRISPR transcription factors could be used to investigate the biological functions of genes in cancer. In this study, we used CRISPR interference (CRISPRi) and CRISPR activation (CRISPRa) technologies to regulate the transcription of ITGB5, TIMP1, and TMEM176B in prostate cancer cells. Through a series of cellualr experiments, we found that inhibition of ITGB5 or activation of TIMP1 and TMEM176B suppress prostate cancer. The three genes synergistically affect the proliferation, invasion and migration capabilities of cancer cells.

Keywords: prostate cancer, ITGB5, TIMP1, TMEM176B, CRISPR interference, CRISPR activation

OPEN ACCESS

Edited by:
Yonghao Zhan,
Zhengzhou University, China

Reviewed by:
Fan Lin,
Shantou University, China
Kai Yang,
Zhejiang University, China
Guo Xiao Qiang,
Hebei Normal University, China

****Correspondence:***
Yi Yang
516321223@qq.com

†These authors have contributed equally to this work

Specialty section:
This article was submitted to Molecular Diagnostics and Therapeutics, a section of the journal Frontiers in Molecular Biosciences

Received: *04 March 2021*
Accepted: *11 May 2021*
Published: *24 May 2021*

Citation:
Yang Y, Feng Q, Hu K and Cheng F (2021) Using CRISPRa and CRISPRi Technologies to Study the Biological Functions of ITGB5, TIMP1, and TMEM176B in Prostate Cancer Cells. Front. Mol. Biosci. 8:676021. doi: 10.3389/fmolb.2021.676021

INTRODUCTION

Prostate cancer is one of the most common malignant tumors in the genitourinary system. The incidence rate of prostate cancer ranks the second among all kinds of malignant tumors worldwide (Neupane et al., 2017). The incidence rate of prostate cancer is the highest in Europe and the United States, and its mortality rate is only less than lung cancer (Siegel et al., 2018). In China, with the acceleration of population aging, changes in diet structure and improvement of medical level, the incidence rate of prostate cancer has also increased rapidly (Zhang et al., 2009). Prostate cancer tends to occur in elderly men, but in recent years there is a trend of younger. For early diagnosis of prostate cancer, radical surgery or radiotherapy can achieve curative effect, and its 5-years survival rate is almost 100%. However, for advanced metastatic prostate cancer, the 5-years survival rate was only 34% (Preston, 2009). Therefore, early detection and diagnosis of prostate cancer is particularly important to improve the survival rate of patients after treatment.

The study on early diagnostic markers of prostate cancer has been a hot topic in recent years. At the same time, the clinical efficacy of advanced prostate cancer, especially castration resistant prostate cancer, is still very limited. New therapeutic methods still depend on the development and utilization of drug target molecules. The molecular biological mechanism of prostate cancer is also a hot issue in the research of urinary tumor.

ITGB5, TIMP1, and TMEM176B are abnormally expressed in several human cancers. Among them, ITGB5 is highly expressed cancers, TIMP1, and TMEM176B are lowly expressed in cancers. ITGB5 (Integrin β5, Integrin β5) is one of the integrin family members. As a type of transmembrane glycoprotein located on the cell surface, integrins are mainly dimers composed of α and β subunits

(Alavi et al., 2003; Hood et al., 2003). Recently, there is new evidence that ITGB5 can promote cell migration and invasion Bianchi et al. (2010), and may participate in the epithelial-mesenchymal transition. The epithelial-mesenchymal transition plays an extremely important role in tumor metastasis. It is found that ITGB5 promotes the lymph node metastasis of colorectal cancer (Denadai et al., 2013). Bianchi et al. found that over-expression of ITGB5 promotes the differentiation and mutation of breast cancer cells and makes breast cancer more aggressive (Bianchi et al., 2010). The protein encoded by TIMP1 is a natural inhibitor of matrix metalloproteinases which are a group of peptidases involved in the degradation of extracellular matrix. TIMP1 is thus closely related to tumor invasion and metastasis. TMEM176B is a transmembrane protein that regulates the immune response of the tumor microenvironment. Although these evidences suggest that ITGB5, TIMP1, and TMEM176B may work together to promote the invasion and metastasis of cancer cells, their molecular biological mechanisms in prostate cancer cells are still unclear and require further research.

In this work, we have used CRISPR interference (CRISPRi) and CRISPR activation (CRISPRa) technologies to study the biologocal functions of ITGB5, TIMP1, and TMEM176B in prostate cancer cells. We found that ITGB5 promotes cancer, while TIMP1 and TMEM176B suppress cancer. The three genes synergistically affect the proliferation, invasion, and migration capabilities of prostate cancer cells.

MATERIALS AND METHODS

Cell Culture

LNCap cells were obtained from The Cell Bank of Chinese Academy of Sciences (Shanghai, China). The cells were cultured in DMEM (HyClone, United States) added with 100 U/ml penicillin/streptomycin and 15% fetal bovine serum (FBS; Gibco, United States) under a moisturized atmosphere with a 5% CO_2 level.

CRISPR Interference and CRISPR Activation System

The CRISPR-dCas9-VPR and CRISPR-dCas9-KRAB plasmids were ordered from Addgene (Cambridge, MA, United States). The sgRNAs targeting ITGB5, TIMP1, and TMEM176B were designed by the online software CHOPCHOP, a CRISPR/Cas9, and TALEN web tool for genome editing.

Cell Transfection

LNCap cells were seeded in 6-well plates with a 3×10^6 cells per well density in the environment of DMEM. Followed the manufacturer's protocol of Lipofectamine 2000 Transfection Kit (Thermo Fisher Scientific, Waltham, MA, United States), transfection was conducted. After that, the cells were set for 48 h in order for future analysis.

Quantitative Real-Time Polymerase Chain Reaction

At 48 h after gene transfection, TRIzol (Invitrogen) was used as a separating reagent for total RNA to get the first-strand cDNA using a FastKing RT Kit (With gDNase) (Tiangen) following the official instructions. The qRT-PCR analysis was carried out by SYBR Green (Tiangen). GAPDH was taken as endogenous controllers for the three mRNAs.

Cell Proliferation Assay

LNCap cells were seeded in a 96-well plate at a 1×10^5/ml dose and incubated for 24 h. Subsequently, cells were starved for another 2 h. Culture medium was replaced with 20 μL of methyl thiazolyl tetrazolium (MTT) solution (5 g/L) (Sigma-Aldrich, St. Louis, MO, United States) and incubated at 37°C for 4 h. The supernatant was discarded and 100 μL of DMSO (dimethyl sulfoxide) (Sigma-Aldrich, St. Louis, MO, United States) was put on to each well. The absorbance value was tracked at the wavelength of 570 nm with a microplate reader.

Cell Apoptosis Assay

At 48 h after cell transfection, the apoptosis of LNCap cells was determined by the Caspase-3 Assay Kit (Fluorometric) (ab39383). Caspase-3 activity was detected by spectrophotometry and each assay was performed in triple.

Cell Migration Assay

LNCap cells were treated with 1.8 mmol/L hydroxyurea for 12 h to inhibit cell proliferation and then a 100 μL pipette tip was used to make cell scratches in a vertical well plate. Then the cell culture medium was discarded and washed three times with PBS. Then the cells were culture and taken pictures. The 0 and 24 h pictures were recorded, and the imageproplus 6.0 software was used to analyze and calculate the cell migration distance.

Cell Invasion Assay

After 48 h of transfection, cells from each group were taken, trypsinized, and then inoculated in a matrigel-Tran-swell chamber. The serum-free DMEM medium was used for culture in the chamber. 10% FBS culture medium was added to the lower chamber. After 24 h, the upper uninvaded cells was wipped with a cotton swab. After fixing with 4% polymethanol for 15 min, cells were stained with 1% crystal violet for 5 min. After washing with PBS for three times, five fields under the fluorescence microscope were randomly selected and observed, and the invaded cells were counted and recorded.

Statistical Analysis

The data were expressed as means ± standard deviations (SD). The SPSS version 19.0 software (IBM Corporation, United States) was used for statistical analysis. A p-value < 0.05 was considered statistically significant.

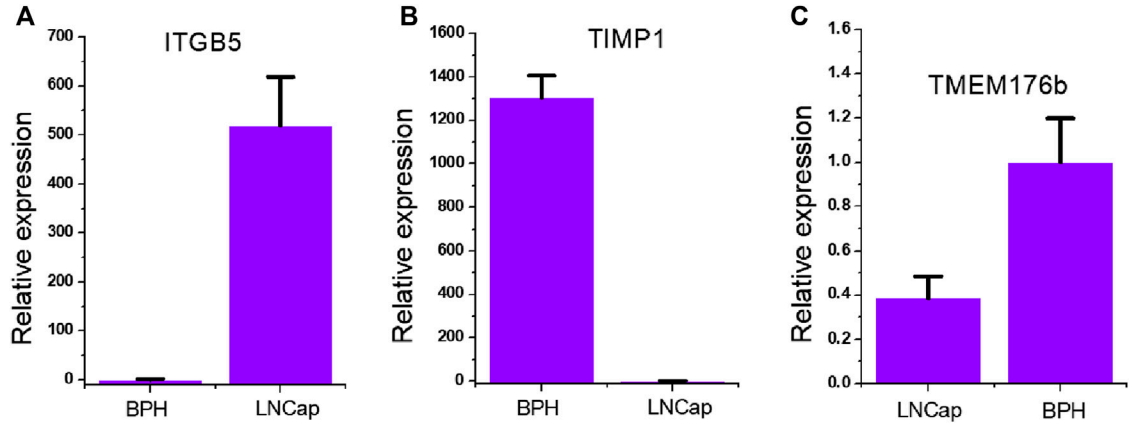

FIGURE 1 | Expression of ITGB5, TIMP1, TMEM176B in prostate cancer cells. **(A)** qRT-PCR analysis of ITGB5 expression in LNCap and BPH cell lines. **(B)** qRT-PCR analysis of TIMP1expression in LNCap and BPH cell lines. **(C)** qRT-PCR analysis of TMEM176Bexpression in LNCap and BPH cell lines.

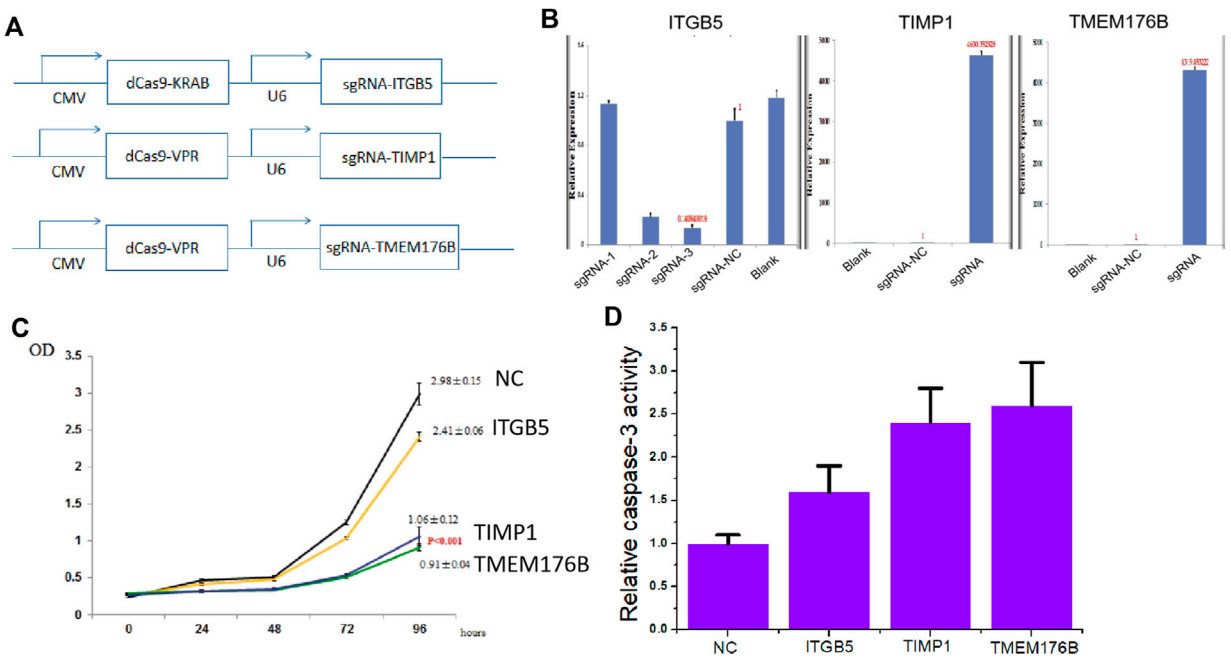

FIGURE 2 | The effects of knockdown of ITGB5 or activation of TIMP1 and TMEM176B expression on cell proliferation and apoptosis. **(A)** Vector maps of CRISPR-KRAB and CRISPR-VPR plasmids constructed in this work. **(B)** LNCap cells were transfected by CRISPRi or CRISPRa systems and gene expression was confirmed by real-time PCR. **(C)** MTT assays revealed that knockdown of ITGB5 or activation of TIMP1 and TMEM176B expression inhibited the growth rate of LNCap cells. **(D)** ELISA assays revealed that knockdown of ITGB5 or activation of TIMP1 and TMEM176B expression increased the apoptosis rate of LNCap cells.

RESULTS

Expression of ITGB5, TIMP1, TMEM176B in Prostate Cancer Cells

In order to clarify the overall expression patterns of the three genes in prostate cancer, we tested the expression of ITGB5 (**Figure 1A**), TIMP1 (**Figure 1B**), and TMEM176B (**Figure 1C**) in the prostate cancer LNCap cell line. We found that ITGB5 was significantly higher in prostate cancer compared with BPH cells, and that TMP1 and TMEM176B were significantly low expressed in prostate cancer. This suggests that ITGB5 is a potential proto-oncogene in the prostate cancer LNCap cell line, while TMP1 and TMEM176B are potential tumor suppressor genes.

The Effects of Knockdown of ITGB5 or Activation of TIMP1 and TMEM176B Expression on Cell Proliferation and Apoptosis

In order to further clarify whether ITGB5 is a proto-oncogene and whether TIMP1 and TMEM176B are tumor suppressor genes, we used dCas9-KRAB-mediated CRISPRi technology

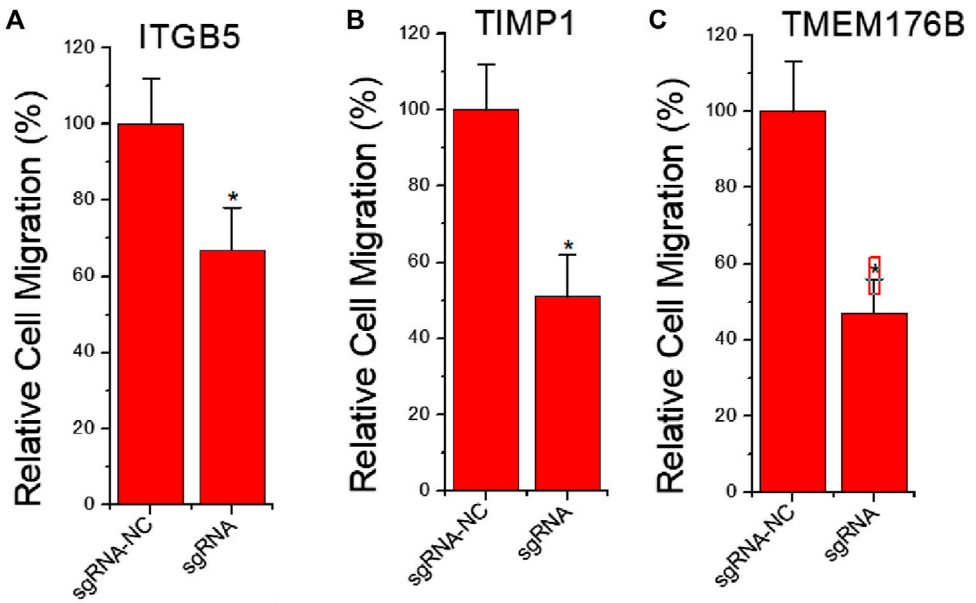

FIGURE 3 | The effects of knockdown of ITGB5 or activation of TIMP1 and TMEM176B expression on cell migration. LNCap cells were transfected by CRISPRi or CRISPRa systems and cell migration assay revealed that knockdown of ITGB5 **(A)** or activation of TIMP1 **(B)** and TMEM176B **(C)** expression inhibited the migration rate of LNCap cells.

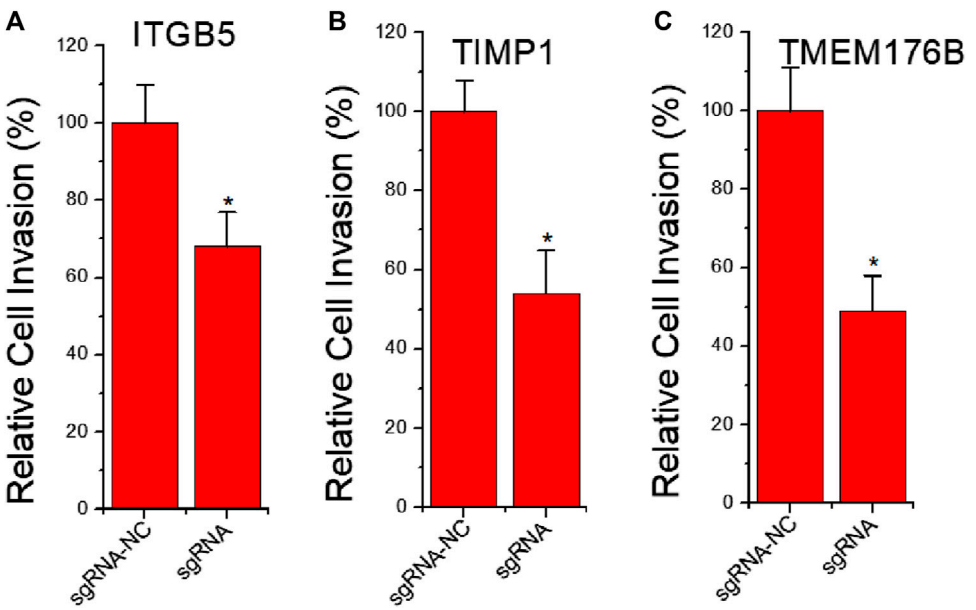

FIGURE 4 | The effects of knockdown of ITGB5 or activation of TIMP1 and TMEM176B expression on cell invasion. LNCap cells were transfected by CRISPRi or CRISPRa systems and cell migration assay revealed that knockdown of ITGB5 **(A)** or activation of TIMP1 **(B)** and TMEM176B **(C)** expression inhibited the invasion rate of LNCap cells.

(**Figure 2A**) to knock down the expression of ITGB5 (**Figure 2B**), and used dCas9-VPR-mediated CRISPRa technology (**Figure 2A**) to activate TIMP1 and TMEM176B expression (**Figure 2B**). The experimental results of MTT show that inhibiting the expression of ITGB5 can reduce cell proliferation, while activating the expression of TIMP1 and TMEM176B can achieve the same effect (**Figure 2C**). In addition, the results of Caspase-3 ELISA assay show that inhibiting the expression of ITGB5 can increase cell apoptosis, while activating the expression of TIMP1 and TMEM176B can observe the same effect (**Figure 2D**).

The Effects of Knockdown of ITGB5 or Activation of TIMP1 and TMEM176B Expression on Cell Migration

To further clarify whether inhibition of ITGB5 and activation of TIMP1 and TMEM176B affect tumor cell migration, we also used dCas9-KRAB-mediated CRISPRi technology to knock down ITGB5 expression, and used dCas9-VPR-mediated CRISPRa technology to induce TIMP1 and TMEM176B activation. The results of the cell scratch experiment showed that inhibiting the expression of ITGB5 can reduce cell migration viability, while activating the expression of TIMP1 and TMEM176B can achieve similar effects (**Figures 3A,B**).

The Effects of Knockdown of ITGB5 or Activation of TIMP1 and TMEM176B Expression on Cell Invasion

Cell migration is always directly related to invasion behavior. To further clarify whether knockdown of ITGB5 and activation of TIMP1 and TMEM176B expression affect tumor cell invasion, we used dCas9-KRAB-mediated CRISPRi to knock down ITGB5 expression, and used dCas9-VPR-mediated CRISPRa to activate TIMP1 and TMEM176B expression. The results of cell invasion experiments show that inhibiting the expression of ITGB5 can reduce the ability of cell invasion, while activating the expression of TIMP1 and TMEM176B can achieve similar effects (**Figures 4A,B**).

DISCUSSION

Previous studies on gene function have often focused on individual genes and lacked overall understanding of tumors. A convenience provided by the advancement of CRISPR technology is that by fusing dCas9 with different transcriptional regulators, we can easily activate and reduce the expression of different genes (Morgens et al., 2016). In this way, the research on the biological functions of genes can be quickly promoted. In the past, RNA interference technology represented by siRNA tends to have low gene knock-down efficiency and high off-target efficiency (Fakhr et al., 2016). The overexpression gene technology can only express genes with smaller coding fragments (Capriotti et al., 2020). So there is a rapid progress.

In this study, we found that compared with prostate hyperplasia cells BPH, ITGB5 is significantly higher expressed in prostate cancer cells, and TMP1 and TMEM176B are significantly lower expressed. We designed different CRISPR transcriptional regulatory systems to silence ITGB5 in prostate cancer cells and activate TIMP1 and TMEM176B at the same time. MTT experiments, cell invasion and migration experiments proved that knocking down ITGB5 or overexpressing TIMP1 and TMEM176B can significantly inhibit the proliferation, invasion and migration ability of LNCap cells. The three genes synergistically affect the proliferation, invasion and migration capabilities of cancer cells. ITGB5, TIMP1, and TMEM176B can be used as molecular diagnostic targets or therapeutic targets in the future, as their combination is useful for cancer treatment. Furthermore, we can also use AAV to deliver the CRISPR system to target and regulate these three genes for gene therapy of prostate cancer.

DATA AVAILABILITY STATEMENT

The original contributions presented in the study are included in the article/Supplementary Material, further inquiries can be directed to the corresponding author.

AUTHOR CONTRIBUTIONS

YY, QF, KH, and FC have done the cellular experiments and gene transfection. YY designed the study and wrote the paper.

FUNDING

This work was supported by the National Natural Science Foundation of China (81902557), National Key R&D Program of China (2019YFA0906000), and Shenzhen Key Medical Discipline Construction Fund (No.SZXK020).

REFERENCES

Alavi, A., Hood, J. D., Frausto, R., Stupack, D. G., and Cheresh, D. A. (2003). Role of Raf in Vascular protection from Distinct Apoptotic Stimuli. *Science* 301, 94–96. doi:10.1126/science.1082015

Bianchi, A., Gervasi, M. E., and Bakin, A. (2010). Role of β5-integrin in Epithelial-Mesenchymal Transition in Response to TGF-β. *Cell Cycle* 9, 1647–1659. doi:10.4161/cc.9.8.11517

Capriotti, L., Baraldi, E., Mezzetti, B., Limera, C., and Sabbadini, S. (2020). Biotechnological Approaches: Gene Overexpression, Gene Silencing, and Genome Editing to Control Fungal and Oomycete Diseases in Grapevine. *Int. J. Mol. Sci.* 21 (16), 5701. doi:10.3390/ijms21165701

Denadai, M. V., Viana, L. S., Affonso, R. J., Jr., Silva, S. R., Oliveira, I. D., Toledo, S. R., et al. (2013). Expression of Integrin Genes and Proteins in Progression and Dissemination of Colorectal Adenocarcinoma. *BMC Clin. Pathol.* 13, 16. doi:10.1186/1472-6890-13-16

Fakhr, E., Zare, F., and Teimoori-Toolabi, L. (2016). Precise and Efficient siRNA Design: a Key point in Competent Gene Silencing. *Cancer Gene Ther.* 23 (4), 73–82. doi:10.1038/cgt.2016.4

Hood, J. D., Frausto, R., Kiosses, W. B., Schwartz, M. A., and Cheresh, D. A. (2003). Differential αv Integrin-Mediated Ras-ERK Signaling during Two Pathways of Angiogenesis. *J. Cel Biol* 162, 933–943. doi:10.1083/jcb.200304105

Morgens, D. W., Deans, R. M., Li, A., and Bassik, M. C. (2016). Systematic Comparison of CRISPR/Cas9 and RNAi Screens for Essential Genes. *Nat. Biotechnol.* 34 (6), 634–636. doi:10.1038/nbt.3567

Neupane, S., Bray, F., and Auvinen, A. (2017). National Economic and Development Indicators and International Variation in Prostate Cancer Incidence and Mortality: an Ecological Analysis. *World J. Urol.* 35, 851–858. doi:10.1007/s00345-016-1953-9

Preston, S. H. (2009). Prostate-cancer Screening. *N. Engl. J. Med.* 361 (2), 202–206.

Siegel, R. L., Miller, K. D., and Jemal, A. (2018). Cancer Statistics, 2018. *CA: A Cancer J. Clinicians* 68, 7–30. doi:10.3322/caac.21442

Zhang, L., Wu, S., Guo, L.-R., and Zhao, X.-J. (2009). Diagnostic Strategies and the Incidence of Prostate Cancer: Reasons for the Low Reported Incidence of Prostate Cancer in China. *Asian J. Androl.* 11 (1), 9–13. doi:10.1038/aja.2008.21

Conflict of Interest: The authors declare that the research was conducted in the absence of any commercial or financial relationships that could be construed as a potential conflict of interest.

frontiers in Molecular Biosciences

ORIGINAL RESEARCH
published: 28 May 2021
doi: 10.3389/fmolb.2021.672040

CRISPReader System Sensing the Ets-1 Transcription Factor Can Effectively Identify Cancer Cells

Kang Yang[1]†, Yan Zhou[2]† and Hongcai Zhong[1]†*

[1] HuiZhou Municipal Central Hospital, Huizhou, China, [2] Logistics Management Office, HuiZhou University, Huizhou, China

By targeting key genes, the CRISPR system can effectively exert its anti-cancer activity. The latest research suggests that the CRISPReader system that regulates gene transcription can effectively target and inhibit bladder cancer cells by sensing transcription factors such as c-Myc and Get-1 in the cell. An interesting question is whether the CRISPReader system can exert its anti-cancer ability against a variety of tumors by sensing the broad-spectrum transcription factor Ets-1. In this work, a CRISPReader system that senses the Ets-1 transcription factor has been constructed. It can effectively identify a variety of cancer cell lines, and specifically induce apoptosis in cancer cells. This study fully confirmed the effectiveness of Ets-1 as a broad-spectrum cancer related signal and provided a new anti-cancer tool based on the CRISPReader system.

Keywords: Ets-1, CRISPReader, cancer, cancer related signal, gene therapy

OPEN ACCESS

Edited by:
Yonghao Zhan,
Zhengzhou University, China

Reviewed by:
Xiujuan Wu,
Shanghai Xuhui Central Hospital, China
Hongzhou Cui,
First Hospital of Shanxi Medical University, China

***Correspondence:**
Kang Yang
492552932@qq.com

†These authors have contributed equally to this work

Specialty section:
This article was submitted to Molecular Diagnostics and Therapeutics, a section of the journal Frontiers in Molecular Biosciences

Received: *25 February 2021*
Accepted: *16 April 2021*
Published: *28 May 2021*

Citation:
Yang K, Zhou Y and Zhong H (2021) CRISPReader System Sensing the Ets-1 Transcription Factor Can Effectively Identify Cancer Cells. Front. Mol. Biosci. 8:672040. doi: 10.3389/fmolb.2021.672040

INTRODUCTION

CRISPR has become a popular gene editing technology in recent years, which can be used to modify species and investigate gene functions (Lino et al., 2018). The CRISPR nuclease, such as Cas9 protein, can induce DNA double-strand breaks and DNA recombination repair mediated by homologous templates (Doudna and Charpentier, 2014). The mutated dead Cas9, dCas9, can bind to the gene promoter region to regulate gene transcription levels (Gjaltema and Schulz, 2018). By modifying the dCas9 protein or sgRNA, an inducible dCas9 system can be constructed (Dai et al., 2018). The regulation of target genes by dCas protein is activated by sensing exogenous inducers or endogenous proteins within cells (Liu Y. et al., 2016; Liu et al., 2017). This is significant because it successfully realizes the systematic sensation of the key signals of tumor cells. The regulation of downstream gene expression through inducible dCas9 is not only conducive to the specific recognition of cancer cells but also can effectively inhibit the malignant growth of tumors. This provides new strategies for basic research and the clinical treatment of tumors.

A key aspect of the research progress made for the CRISPR transcriptional regulation system is to use the dCas9 transcription activator to bind to its transcription initiation element to replace the promoter to perform gene expression functions. This is a very important technological advancement. The related technology is called "CRISPReader" (Zhan H. et al., 2019), which was originally used to reduce the gene expression cassette of CRISPR so that it can be loaded into AAV vectors with limited capacity. The gene circuit based on CRISPReader can sense transcription factors such as c-Myc and Get-1 in cancer cells (Liu et al., 2020). It can not only effectively identify

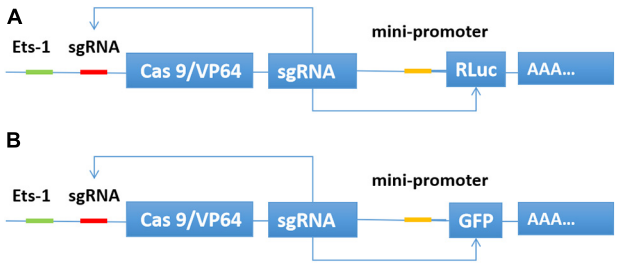

FIGURE 1 | Construction of CRISPReader sensing the Ets-1 transcription factor. When Ets-1 binds to the promoter region, weak expression of Cas9/VP64 can be initiated. After Cas9/VP64 is combined with sgRNA, it can further bind its promoter and drive its own expression. In this way, the expression level of Cas9/VP64 is continuously increased through positive feedback, and then the transcription of luciferase **(A)** or GFP **(B)** is activated.

bladder cancer cells from non-bladder cancer cells, but also effectively inhibit the growth and metastasis of cancer cells. However, this gene circuit is only suitable for the gene therapy of bladder cancer because of the tissue expression specificity of the Get-1 transcription factor.

Ets-1 is a transcription factor that is widely expressed in a variety of tumors (Hahne et al., 2008). Previous studies have found that the TERT promoter of many tumors has high frequency mutations, and the mutated sequence increases the binding site of Ets-1 (Li et al., 2015; Liu L. et al., 2016). TERT is also a broad-spectrum tumor marker, which is conducive to the excessive division of tumor cells.

A more interesting idea is to use CRISPReader to sense Ets-1 and to develop a broad-spectrum anti-cancer tool. In this study, based on the CRISPReader technology, we successfully constructed a gene circuit that senses the endogenous Ets-1 transcription factor in cells. It can identify a variety of cancer cells including bladder cancer and gastric cancer, and can specifically and effectively induce apoptosis of cancer cells.

MATERIALS AND METHODS

Cancer Cell Culture

The cancer cell lines used in this study were purchased from the Institute of Cell Research, Chinese Academy of Sciences (Shanghai, China). Cells were grown in a high-sugar DMEM medium (Qingdao Jieshikang Biotechnology Co., Ltd.) supplemented with 10% fetal bovine serum (Invitrogen) at 37°C in a 5% carbon dioxide atmosphere.

Construction of the CRISPReader System

The cDNA sequences for sgRNA binding regions were designed, synthesized, and inserted into the corresponding vector, which had been digested with restriction endonucleases. All vectors were transformed into One Shot TOP10 Chemically Competent *E. coli* cells, and the desired expression clones were identified using polymerase chain reaction (PCR) amplification and electrophoresis, and then confirmed with Sanger sequencing.

Gene Transfection

The above plasmids were transfected into various cancer cells using Lipofectamine 2000 kit according to the operation instructions when the cell density reached 60 ∼70%.

Luciferase Activity Detection

After transfection for 48 h, cells were obtained. Next, the activities of firefly and ranilla luciferase were analyzed by double luciferase reporting assay (Promega) in line with the manufacturer's specifications.

GFP Reporter Gene Assay

GFP reporter gene assay was also used for studying the regulation of gene expression. A specialized microscope was used to see

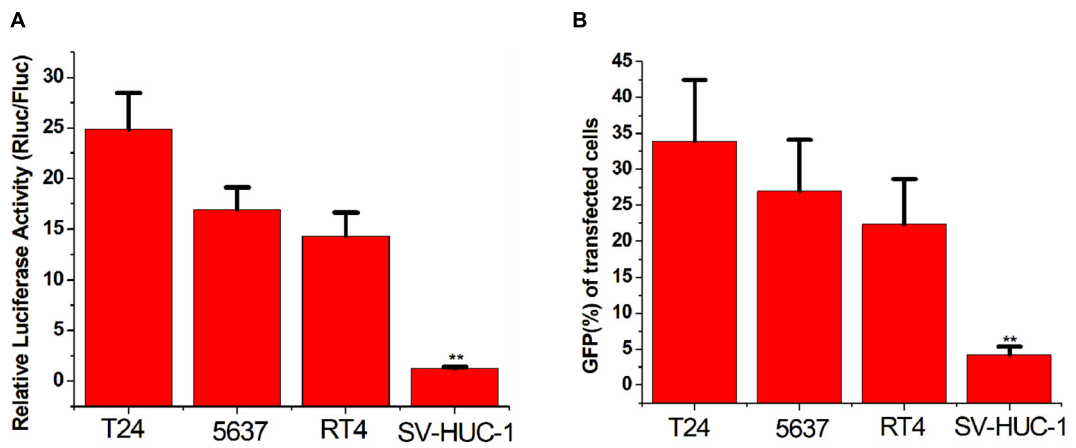

FIGURE 2 | Distinguishing between bladder cancer cells and normal cells. **(A)** Cell luciferase activity was determined using the dual luciferase reporting assay (**$p < 0.01$). Data were expressed as mean ± SD. **(B)** Cell GFP expression was determined using the GFP reporter assay (**$p < 0.01$). Data were expressed as mean ± SD.

GFP-expressing cells. The percentage of cells showing green fluorescence was quantified by the Image J software[1].

Cell Apoptosis Assay

Cancer cells were transiently transfected with plasmid vectors, and then a BD flow cytometer (Beijing Delica Biotechnology Co., Ltd.) was used to detect the cells that had been transfected for 48 h and stained by Annexin V and PI in a 6-hole plate, and the experiment was repeated three times.

CCK-8 Cell Proliferation Assay

Cancer cells were transiently transfected with plasmid vectors, and then cells were analyzed with CCK-8 assay after being cultured in DMEM medium for 24, 48, and 72 h. For the determination of cell proliferation, a Cell-Counting Kit 8 (Dojindo Laboratories) was used according to the instructions. Fluorescence (450 nm) was recorded using a microplate reader.

Statistical Analysis

SPSS 21.0 (SPSS, Inc., Chicago, IL, United States) was used to conduct statistical analysis. *T*-test was applied to express the measurement data, which was expressed by the mean number ± standard deviation ($x \pm SD$). $P < 0.05$ was considered statistically significant.

RESULTS

Construction of a CRISPReader That Senses the Ets-1 Transcription Factor

We inserted the binding sequence of transcription factor Ets-1 into the upstream of the transcription initiation element TATA box. Then, the sgRNA binding site was inserted between the two elements. The Cas9/VP64 and sgRNA expression framework were inserted downstream of the transcription start site. The sgRNA also targets the promoter region of luciferase or GFP. When the expression of the transcription factor Ets-1 in the cell is very low, neither Cas9/VP64 nor sgRNA is expressed. In cancer cells expressing Ets-1, Cas9/VP64 and sgRNA continue to drive their self-expression, and then transcriptionally activate luciferase (**Figure 1A**) or GFP (**Figure 1B**).

[1]https://imagej.nih.gov/ij/

Distinguishing Between Bladder Cancer Cells and Normal Cells

To verify whether the CRISPReader system can specifically recognize bladder cancer cells by sensing the expression of the transcription factor Ets-1, we transiently transferred the plasmid expressing the system into a series of cancer cells and corresponding normal cells. The luciferase test results suggest that the CRISPReader can significantly activate the expression

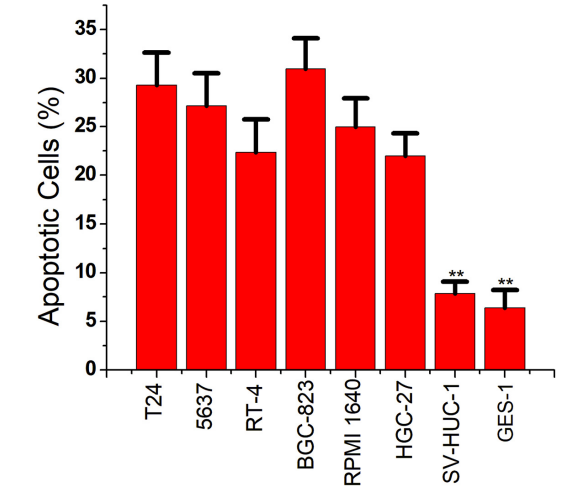

FIGURE 4 | Specifically induced cancer cell apoptosis. Cell apoptosis activity was determined using the flow cytometry assay (**$p < 0.01$). Data were expressed as mean ± SD.

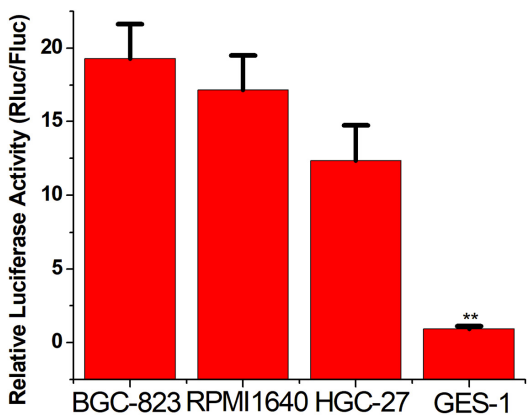

FIGURE 3 | Distinguishing between gastric cancer cells and normal cells. Cell luciferase activity was determined using the dual luciferase reporting assay (**$p < 0.01$). Data were expressed as mean ± SD.

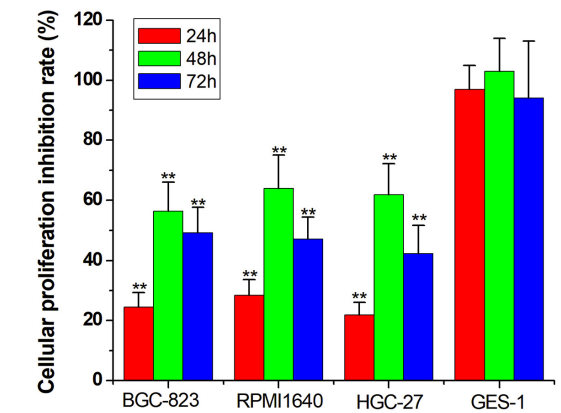

FIGURE 5 | Specifically inhibited cancer cell proliferation. Cell proliferation rate was determined using the CCK-8 assay (**$p < 0.01$). Data were expressed as mean ± SD.

of luciferase in T24, 5637, RT4 bladder cancer cell lines that highly express Ets-1, but cannot express luciferase in normal urothelial cells SV-HUC-1 (**Figure 2A**). The results were the same when the reporter gene was GFP (**Figure 2B**). The difference in the expression of reporter genes suggests that the CRISPReader system can effectively distinguish bladder tumor cells from normal bladder cells.

Distinguishing Between Gastric Cancer Cells and Normal Cells

To verify the broad spectrum of the CRISPReader system in recognizing tumor cells, we transiently transferred the plasmid expressing the system into a series of gastric cancer cells and corresponding normal cells. The luciferase test results suggest that the CRISPReader can significantly activate the expression of luciferase in BGC-823, RPMI 1640, and HGC-27 gastric cancer cell lines that highly express Ets-1, while it cannot express luciferase in normal gastric epithelial cells GES-1 (**Figure 3**). The expression difference of the reporter gene suggests that the CRISPReader system can effectively distinguish gastric tumor cells from normal gastric cells, indicating that the Ets-1-sensing CRISPReader system has potential broad-spectrum anti-tumor capabilities.

Inducing Cancer Cell Apoptosis

We then replaced the luciferase gene with the caspase-3 gene, which can induce apoptosis. The CRISPReader expression plasmid was transfected into bladder cancer and gastric cancer cell lines and the corresponding normal cell lines, respectively. The results of flow cytometry indicated that the apoptosis rate of tumor cell lines was significantly higher than that of normal cell lines (**Figure 4**), indicating that the Ets-1-sensitive CRISPReader system can effectively induce the apoptosis of different tumor cells and has broad-spectrum anti-tumor activity.

Inhibiting Cancer Cell Proliferation

For the final step, we replaced the luciferase gene with the PTEN gene, which can inhibit cell proliferation. The CRISPReader expression plasmid was transfected into bladder cancer and gastric cancer cell lines and the corresponding normal cell lines, respectively. The results of the CCK-8 assay indicate that the proliferation rate of tumor cell lines was significantly lower than that of normal cell lines (**Figure 5**), indicating that the Ets-1-sensitive CRISPReader system can effectively inhibit the proliferation of different tumor cells and has broad-spectrum anti-tumor activity.

DISCUSSION

The application of the CRISPR system to the basic and therapeutic research of tumors is a major trend in current academic circles. An effective anti-cancer strategy is to use the CRISPR system to target fusion genes to exert anti-cancer effects (Zhan T. et al., 2019). However, the CRISPR system can not only regulate its downstream target genes but also sense a series of upstream signals, thus playing the role of the signal transmitter (Liu et al., 2018). It has obvious advantages when applied to tumor biotherapy, which can effectively identify and kill cancer cells. The biggest problem is how to choose the carcinogenic signal to be sensed. Ets-1 is a transcription factor that is generally highly expressed in tumors, so it is an ideal signal molecule for the CRISPR system.

In this study, we successfully designed a CRISPReader system that senses the Ets-1 transcription factor. It can effectively identify a variety of tumor cell lines including bladder cancer and gastric cancer, and specifically induce apoptosis and inhibit the proliferation of cancer cells. This study fully confirmed the effectiveness of Ets-1 as a broad-spectrum tumor recognition signal and provided a new anti-cancer tool based on the CRISPR system.

The limitation of this study is that only in vitro cell experiments were performed, and animal experiments will be needed in the future to further prove the anti-cancer effect of this tool.

DATA AVAILABILITY STATEMENT

The original contributions presented in the study are included in the article/supplementary material, further inquiries can be directed to the corresponding author.

AUTHOR CONTRIBUTIONS

KY provided the idea and designed the study details. All authors finished the experiments and wrote the manuscript, contributed to the article, and approved the submitted version.

REFERENCES

Dai, X., Chen, X., Fang, Q., Li, J., and Bai, Z. (2018). Inducible CRISPR genome-editing tool: classifications and future trends. *Crit. Rev. Biotechnol.* 38, 573–586. doi: 10.1080/07388551.2017.1378999

Doudna, J. A., and Charpentier, E. (2014). Genome editing. The new frontier of genome engineering with CRISPR-Cas9. *Science* 346:1258096.

Gjaltema, R. A. F., and Schulz, E. G. (2018). CRISPR /dCas9 switch systems for temporal transcriptional control. *Methods Mol. Biol.* 1767, 167–185. doi: 10.1007/978-1-4939-7774-1_8

Hahne, J. C., Okuducu, A. F., Sahin, A., Fafeur, V., Kiriakidis, S., and Wernert, N. (2008). The transcription factor ETS-1: its role in tumour development and strategies for its inhibition. *Mini Rev. Med. Chem.* 8, 1095–1105. doi: 10.2174/138955708785909934

Li, C., Wu, S., Wang, H., Bi, X., Yang, Z., Du, Y., et al. (2015). The C228T mutation of TERT promoter frequently occurs in bladder cancer stem cells and contributes to tumorigenesis of bladder cancer. *Oncotarget* 6, 19542–19551. doi: 10.18632/oncotarget.4295

Lino, C. A., Harper, J. C., Carney, J. P., and Timlin, J. A. (2018). Delivering CRISPR: a review of the challenges and approaches. *Drug Deliv.* 25, 1234–1257. doi: 10.1080/10717544.2018.1474964

Liu, L., Liu, Y., Zhang, T., Wu, H., Lin, M., Wang, C., et al. (2016). Synthetic Bax-Anti Bcl2 combination module actuated by super artificial hTERT promoter selectively inhibits malignant phenotypes of bladder cancer. *J. Exp. Clin. Cancer Res.* 8:3.

Liu, Y., Han, J., Chen, Z., Wu, H., Dong, H., and Nie, G. (2017). Engineering cell signaling using tunable CRISPR-Cpf1-based transcription factors. *Nat. Commun.* 8:2095.

Liu, Y., Huang, W., and Cai, Z. (2020). Synthesizing AND gate minigene circuits based on CRISPReader for identification of bladder cancer cells. *Nat. Commun.* 11:5486.

Liu, Y., Li, J., Chen, Z., Huang, W., and Cai, Z. (2018). Synthesizing artificial devices that redirect cellular information at will. *Elife* 10:e31936.

Liu, Y., Zhan, Y., Chen, Z., He, A., Li, J., and Wu, H. (2016). Directing cellular information flow via CRISPR signal conductors. *Nat. Methods* 13, 938–944. doi: 10.1038/nmeth.3994

Zhan, H., Zhou, Q., Gao, Q., Li, J., Huang, W., and Liu, Y. (2019). Multiplexed promoterless gene expression with CRISPReader. *Genome Biol.* 20, 113.

Zhan, T., Rindtorff, N., Betge, J., Ebert, M. P., and Boutros, M. (2019). CRISPR. /Cas9 for cancer research and therapy. *Semin. Cancer Biol.* 55, 106–119.

Conflict of Interest: The authors declare that the research was conducted in the absence of any commercial or financial relationships that could be construed as a potential conflict of interest.

frontiers in Molecular Biosciences

ORIGINAL RESEARCH
published: 09 June 2021
doi: 10.3389/fmolb.2021.675683

Targeted Demethylation of the PLOD2 mRNA Inhibits the Proliferation and Migration of Renal Cell Carcinoma

Congcong Cao[1], Qian Ma[1], Xinbo Huang[1], Aolin Li[2], Jun Liu[2], Jing Ye[1] and Yaoting Gui[1]**

[1]Guangdong and Shenzhen Key Laboratory of Male Reproductive Medicine and Genetics, Institute of Urology, Peking University Shenzhen Hospital, Shenzhen-Peking University-The Hong Kong University of Science and Technology Medical Center, Shenzhen, China, [2]Department of Urology, Peking University First Hospital, Beijing, China

N6-methyladenosine (m^6A) RNA modification is the most common internal mRNA modification in mammals and has been reported to play a key role in gene expression regulation. In this study, we detected a high level of m^6A methylation of the PLOD2 3′-untranslated regions (3′UTR) in renal cell carcinoma (RCC). Furthermore, we found that the high expression level of PLOD2 was a prognostic indicator for patients with RCC. A dm^6ACRISPR demethylation system was performed to accurately and specifically demethylate 3′UTR of PLOD2 and caused an inactivation of PLOD2 expression. Furthermore, we also performed many *in vitro* experiments to confirm that PLOD2 exerted tumor promoter effects by promoting tumor proliferation and migration. In conclusion, PLOD2 mRNA demethylated by dCas13b-ALKBH5 might provide a new light on the treatment for RCC.

Keywords: CRISPR, dCas13b, (N6-methyladenosine), PLOD2, renal cell cancer

OPEN ACCESS

Edited by:
Yonghao Zhan,
Zhengzhou University, China

Reviewed by:
Mingde Cao,
The Chinese University of Hong Kong, China
Zhang Jin,
Huazhong University of Science and Technology, China
Soichiro Yamamura,
University of California, San Francisco, United States

****Correspondence:***
Jing Ye
ye2013j@163.com
Yaoting Gui
guiyaoting2007@aliyun.com

Specialty section:
This article was submitted to Molecular Diagnostics and Therapeutics, a section of the journal Frontiers in Molecular Biosciences

Received: *03 March 2021*
Accepted: *21 May 2021*
Published: *09 June 2021*

Citation:
Cao C, Ma Q, Huang X, Li A, Liu J, Ye J and Gui Y (2021) Targeted Demethylation of the PLOD2 mRNA Inhibits the Proliferation and Migration of Renal Cell Carcinoma. Front. Mol. Biosci. 8:675683. doi: 10.3389/fmolb.2021.675683

INTRODUCTION

Renal cell carcinoma (RCC) is one of the most common adult genitourinary cancers. According to the latest cancer statistics report, there are more than 65,000 newly diagnosed cases in the United States each year, and nearly 15,000 of them have renal cancer-related deaths, making it the sixth most common tumor site (Siegel, Miller, and Jemal 2019). Renal clear cell carcinoma (ccRCC) is the most common histologic subtype of renal cell carcinoma, accounting for 70% (Ronald and Bukowski. 1997). Although diagnostic techniques for renal cell carcinoma have improved in recent decades, ~30% of patients with RCC have metastatic or local progression at the time of diagnosis. Since ccRCC is resistant to chemoradiotherapy, surgery is still an effective method for the treatment of ccRCC. However, about one-third of patients with localized renal cancer develop local recurrence and metastasis after surgical treatment. Therefore, there is an urgent need to explore the molecular mechanism of renal cell carcinoma and find new effective targets for treatment and intervention of patients with renal cell carcinoma.

N6-methyladenosine (m^6A) RNA modification is an epigenetic modification that occurs at the transcriptome level, and is the most common post-transcriptional modification of mRNA in eukaryotes. It is widely involved in a series of RNA-related metabolic activities such as RNA stability regulation, splicing processing, transport and translation (Dominissini et al., 2012; Meyer et al., 2012; Bodi et al., 2015). About 1/3 of human gene transcripts are m^6A modified, with an average of 3–5 m^6A modifications per mRNA. M^6A modification is a dynamic and reversible process that is mainly regulated by three types of proteins: RNA methyltransferases (Writers), which promote the methylation of N6-adenylate in RNA, including Mettl3, Mettl14, and WATP; RNA

demethylases (erasers) were used to remove N6-adenosine methylation, and FTO and ALKBH5 were common (Jia et al., 2011; Liu et al., 2014; Ping et al., 2014; Schwartz et al., 2014). M^{6}A recognition proteins (readers) are responsible for binding to m^{6}A sites on RNA to affect splicing (Dominissini et al., 2012), processing (Wang et al., 2014), degradation and other processes of RNA, mainly including YTHDFs and YTHDCs subtypes (Deng et al., 2018; Huang, Weng, and Chen 2020).

PLOD2 is a member of the PLOD (Procollagen-Lysine, 2-oxoglutarate 5-dioxygenase) family, which selectively hydroxylates the lysine residues of collagen-terminal peptides to promote the picoline-hydroxyl cross-linking reaction of collagen, thereby enhancing the stability of collagen (Gilkes et al., 2013). Collagen is the most abundant protein in the extracellular matrix, which is known as the "highway" for tumor cell migration and invasion. Semenza et al.'s study showed that hypoxic inducible factor 1 (HIF-1) can induce the expression of collagen hydroxylase P4HA1, P4HA2, and PLOD2 under hypoxic conditions, change extracellular matrix fiber arrangement, and then affect cell morphology, adherent ability and directional migration ability (Eisinger-Mathason et al., 2013). PLOD2 expression was up-regulated in various malignant tumors and negatively correlated with prognosis. It has been reported that in sarcoma (Miyamoto et al., 2016), pancreatic cancer (Kurozumi et al., 2016) and breast cancer (Dong et al., 2005), HIF-1α can regulate the expression of PLOD2 and thus affect tumor migration and invasion ability (Rajkumar et al., 2011). PLOD2 up-regulates the expression of HK2 through the STAT3 signaling pathway, which is a key enzyme in glycolysis, thereby affecting the proliferation, migration and invasion of colorectal cancer cells (Reis et al., 2011). PLOD2 knockdown in glioma can inhibit the PI3K/Akt signaling pathway, and then inhibit the expression of downstream EMT-related molecules such as E-cadherin and Snailin (Blanco et al., 2012). Recent studies have shown that in head and neck squamous cell carcinoma (HNSCC), integrin β1 is more stable after Plod2-hydroxylated modification, and is subsequently recruited to the cell membrane to regulate tumor cell movement, thereby promoting tumor invasion and metastasis (Dong et al., 2005).

In this research, we found that the PLOD2 m^{6}A modification of mRNA and expression levels were significantly elevated in RCC. Then we wanted to clarify the effect of PLOD2 in the development of renal cancer and its molecular mechanism of m^{6}A methylation modification. Based on previous literature investigation and preliminary experimental results, we speculated that m^{6}A modification of PLOD2 could promote the translation of PLOD2 protein after YTHDF1 recognition, and then activate key molecules in the signaling pathway related to migration and invasion, thus promoting the occurrence and development of renal cancer.

In this study, we can achieve site-specific regulation of m^{6}A modification on PLOD2 mRNA by transfected with CRISPR/dCas13b-ALKBH5 and targeted PLOD2 sgRNAs (Li et al., 2020). At the cell level, the effects of PLOD2 m^{6}A modification on the proliferation, migration, invasion and apoptosis of renal carcinoma cells were analyzed to explore its molecular mechanism in the occurrence and development of renal carcinoma.

RESULTS

The Expression Level and N6-Methyladenosine Methylation Level of PLOD2 Were Significantly Increased in Renal Cell Carcinoma Tissues

To study the functional role of PLOD2 m^{6}A methylation in renal cell carcinoma (RCC), the PLOD2 m^{6}A methylation levels were measured in five tumor tissues relative to their normal control samples. A significant increase in m^{6}A modification in PLOD2 mRNA was observed in tumor samples (**Figure 1A**). Moreover, our previous results exhibited that m^{6}A methylation of PLOD2 in 3′′-untranslated regions increased remarkably in five tumor tissues compared to their paired adjacent normal tissues (**Figure 1D**). Then we checked the expression levels of PLOD2 in RCC tumor and adjacent tissues by RT-qPCR and IHC. We found the mRNA and protein levels of PLOD2 were significantly increased in RCC tumor tissues compared to adjacent tissues (**Figures 1B,C**). Besides, RCC patients with higher PLOD2 expression obtained shorter overall survival (OS) from TCGA database (**Figure 1E**). These results implied that dysregulation of PLOD2 mRNA and m6A methylation level might be involved in the progression of RCC.

The mRNA and N6-Methyladenosine Methylation Level of PLOD2 Was Significantly Upregulated in Renal Cell Carcinoma Cell Lines

To validate the expression pattern of PLOD2 *in vitro*, we firstly measured the mRNA and protein level of PLOD2 in RCC cell lines (786-O, 769-P, ACHN, OSRC, and CAKI-1) by RT-qPCR and western blotting. We found PLOD2 was highly expressed in 786-O and OSRC RCC cell lines compared to HK-2, a normal renal tubule epithelium cell (**Figures 2A,B**). Therefore, we then examined the m^{6}A methylation levels of PLOD2 in 786-O and OSRC cells which PLOD2 was highly expressed. The results showed that PLOD2 mRNA was highly methylated measured by MeRIP-qPCR in 786-O and OSRC cells (**Figure 2C**).

dm^{6}ACRISPR Induced Demethylation of PLOD2 mRNA

Then, PLOD2 mRNA was specifically demethylated by transfected with CRIPSR/dCas13b-ALKBH5 and PLOD2 sgRNAs in RCC cells lines. We designed two gRNAs targeted PLOD2 mRNA methylation region (**Figure 3A**). Firstly, dCas13b-ALKBH5 fusion protein was examined in cell by western blot (**Figure 3B**). Next, the demethylation effect of dm^{6}ACRISPR on PLOD2 mRNA was validated by MeRIP-qPCR. We found m^{6}A levels of PLOD2 mRNA were significantly inhibited after transfected with dCas13b-ALKBH5

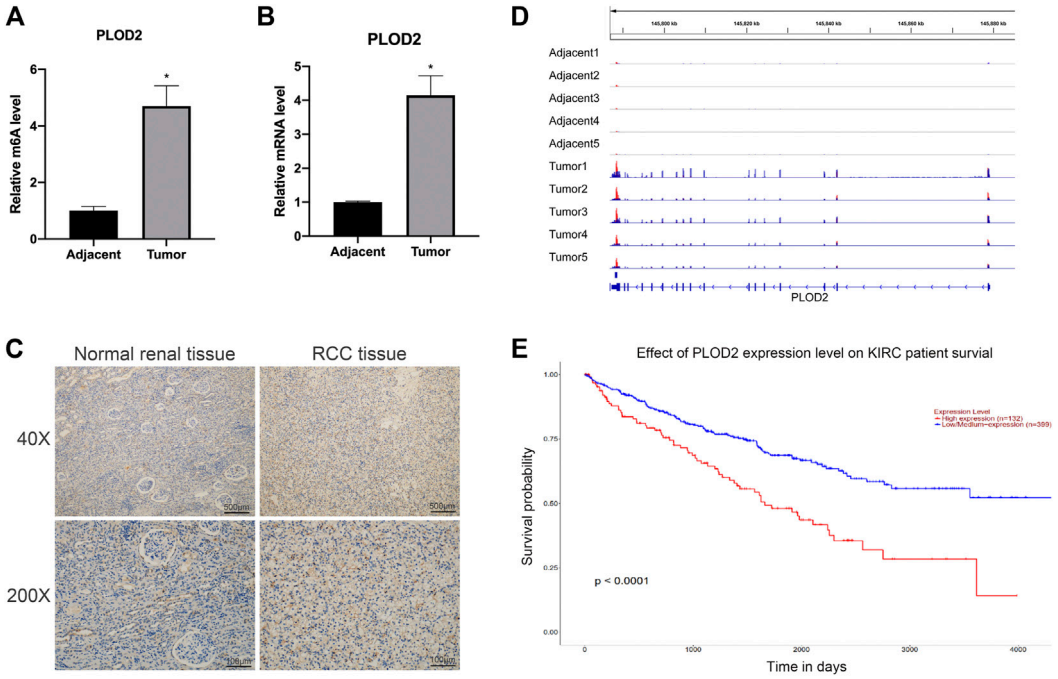

FIGURE 1 | The mRNA and m6A methylation levels of PLOD2 were significantly increased in RCC tissues compared to adjacent tissues. **(A)** M^{6}A enrichment of PLOD2 mRNA in five pairs of RCC tissues and matched adjacent tissues was measured by MeRIP-qPCR analysis. **(B)** PLOD2 mRNA expression levels in tumor and adjacent tissues were detected by RT-qPCR. **(C)** Representative IHC stains of PLOD2 in RCC tumor and adjacent tissues. **(D)** The m^{6}A abundances on PLOD2 mRNA transcripts in five pairs of tumor and adjacent tissues by m^{6}A-RIP-seq. **(E)** Survival analysis of PLOD2 expression in RCC patients. *p < 0.05.

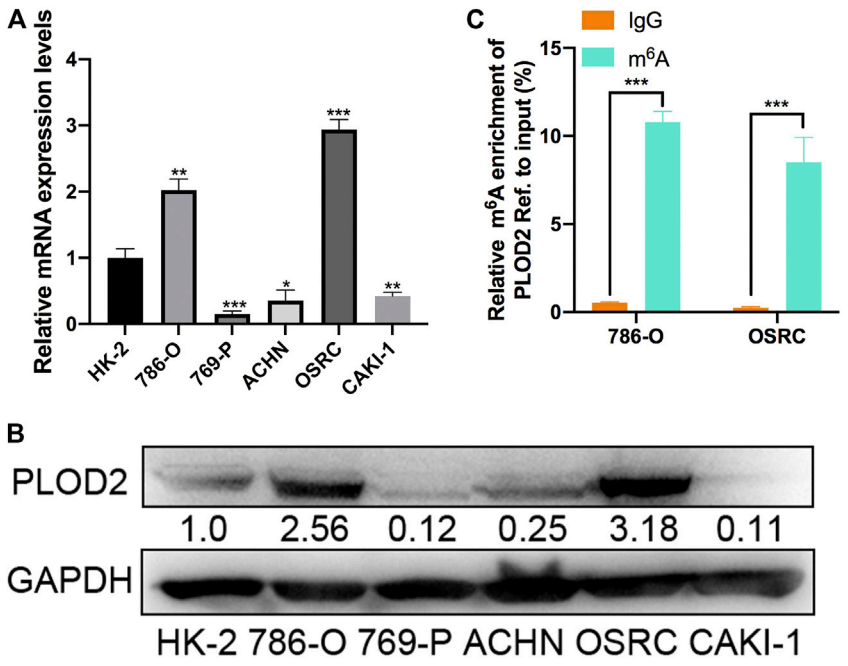

FIGURE 2 | The mRNA and m^{6}A methylation levels of PLOD2 were obviously increased in RCC cell lines. **(A,B)** PLOD2 mRNA and protein expressions in RCC cell lines (786-O, 769-P, ACHN, OSRC, and CAKI-1) and normal epithelium cells of renal tubule HK2 by RT-qPCR and western blot. **(C)** m^{6}A enrichment of PLOD2 in 786-O and OSRC RCC cells detected by MeRIP-qPCR. *p < 0.05, **p < 0.01, ***p < 0.005.

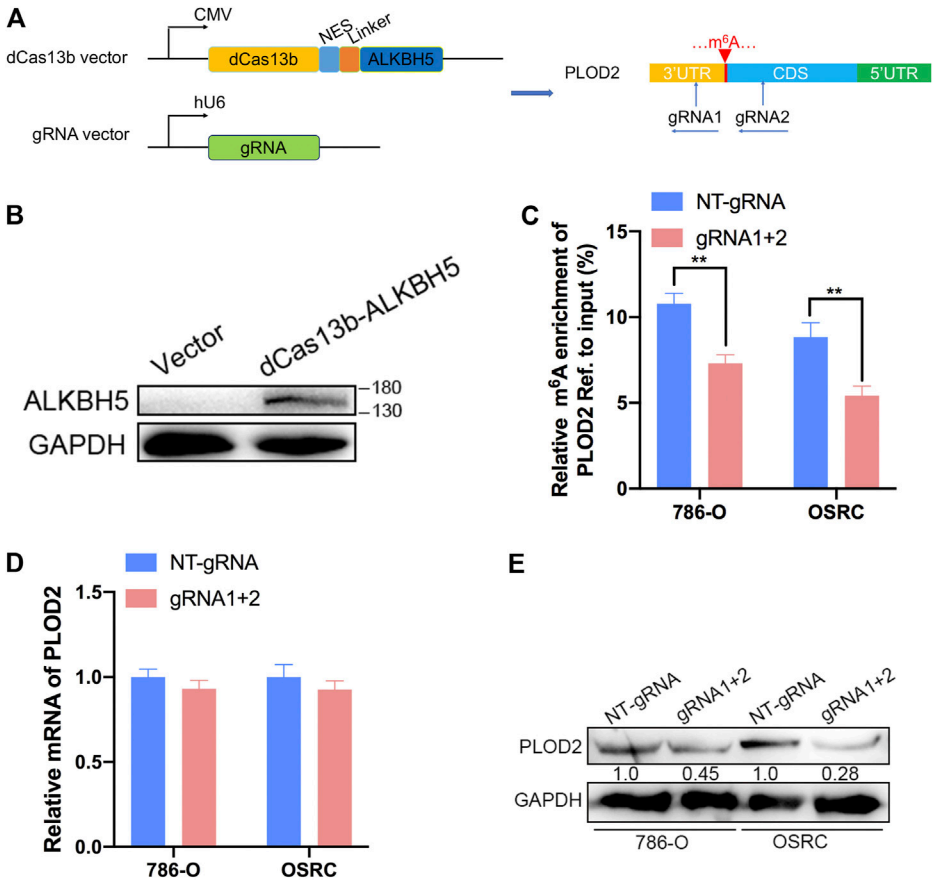

FIGURE 3 | dm^{6}ACRISPR induced demethylation of PLOD2 mRNA. **(A)** Construction of dCas13b-ALKBH5 with two gRNAs targeting methylation region of PLOD2 3'UTR. **(B)** dCas13b-ALKBH5 fusion protein was examined in cell by western blot. **(C)** MeRIP-qPCR analysis of PLOD2 mRNA in 786-O and OSRC RCC cells after transfected with dCas13b-ALKBH5 and sgRNAs for 24 h. **(D)** mRNA expression levels of PLOD2 in 786-O and OSRC RCC cells after transfected with dCas13b-ALKBH5 and sgRNAs for 24 h by RT-qPCR. **(E)** Protein levels of PLOD2 in 786-O and OSRC RCC cells after transfected with dCas13b-ALKBH5 and sgRNAs for 24 h by western blot. $^{**}p < 0.01$.

and PLOD2 sgRNAs in 786-O and OSRC cells (**Figure 3C**). However, there were no significant change of PLOD2 mRNA levels after transfected with dCas13b-ALKBH5 and PLOD2 sgRNAs (**Figure 3D**). But the protein levels of PLOD2 were decreased after transfected with dCas13b-ALKBH5 and PLOD2 sgRNAs in 786-O and OSRC cells (**Figure 3E**). In conclusion, our results exhibited that dCas13b-ALKBH5 could decrease protein level not mRNA level of PLOD2 after demethylating its mRNA.

Targeting Demethylation of PLOD2 Transcripts by dCas13b-ALKBH5 Inhibited Renal Cell Carcinoma Cells Proliferation

To further investigate that dm^{6}ACRISPR targeting PLOD2 whether can modulate RCC cells proliferation, we performed 5-ethynyl-20-deoxyuridine (EdU) and cell counting kit-8 (CCK-8) assays to evaluate the proliferative activity of RCC cells after dm^{6}ACRISPR targeting PLOD2 in 786-O and OSRC RCC cells. And the results showed that demethylation of PLOD2 mRNA induced by dm^{6}ACRISPR led to a decreased cell proliferation rate in the 786-O and OSRC RCC cells as compared with that of non-targeted gRNA combined with dCas13b-ALKBH5 (**Figures 4A–E**). These results confirmed that targeted demethylation of PLOD2 transcripts could inhibit RCC cells proliferation.

Targeting Demethylation of PLOD2 Transcripts by dCas13b-ALKBH5 Inhibited Renal Cell Carcinoma Cells Migration

To further explore the role of m^{6}A methylation of PLOD2 in RCC migration, we demethylated PLOD2 mRNA by dm^{6}ACRISPR in 786-O and OSRC RCC cells. Notably, an obvious delay in migration was observed in PLOD2-demethylating RCC cells in a scratch wound healing assay (**Figures 5A–C**). Furthermore, PLOD2 demethylation significantly suppressed the migration of RCC cells in transwell assay (**Figures 5D,E**). These results confirmed that targeted demethylation of PLOD2 transcripts in RCC cells inhibited wound closure and migration activity.

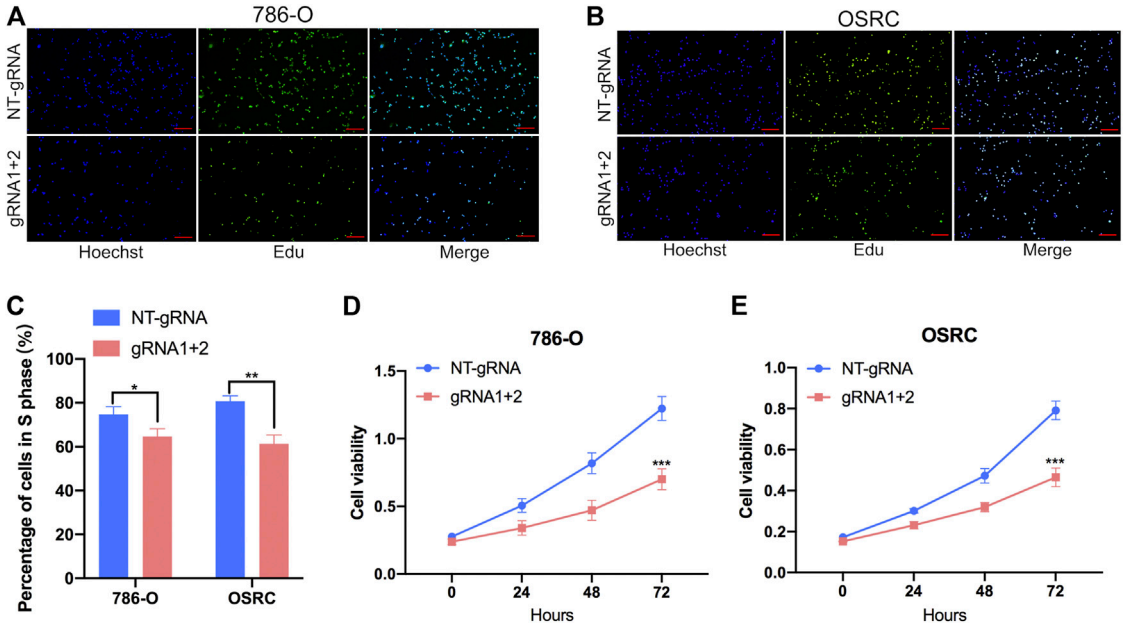

FIGURE 4 | Targeting demethylation of PLOD2 transcripts by dCas13b-ALKBH5 inhibited RCC cells proliferation. **(A–C)** EdU assays of 786-O and OSRC cells after transfected with dCas13b-ALKBH5 and sgRNAs. **(D,E)** CCK-8 assays of 786-O and OSRC cells after transfected with dCas13b-ALKBH5 and sgRNAs. $^{*}p < 0.05$, $^{**}p < 0.01$, $^{***}p < 0.005$.

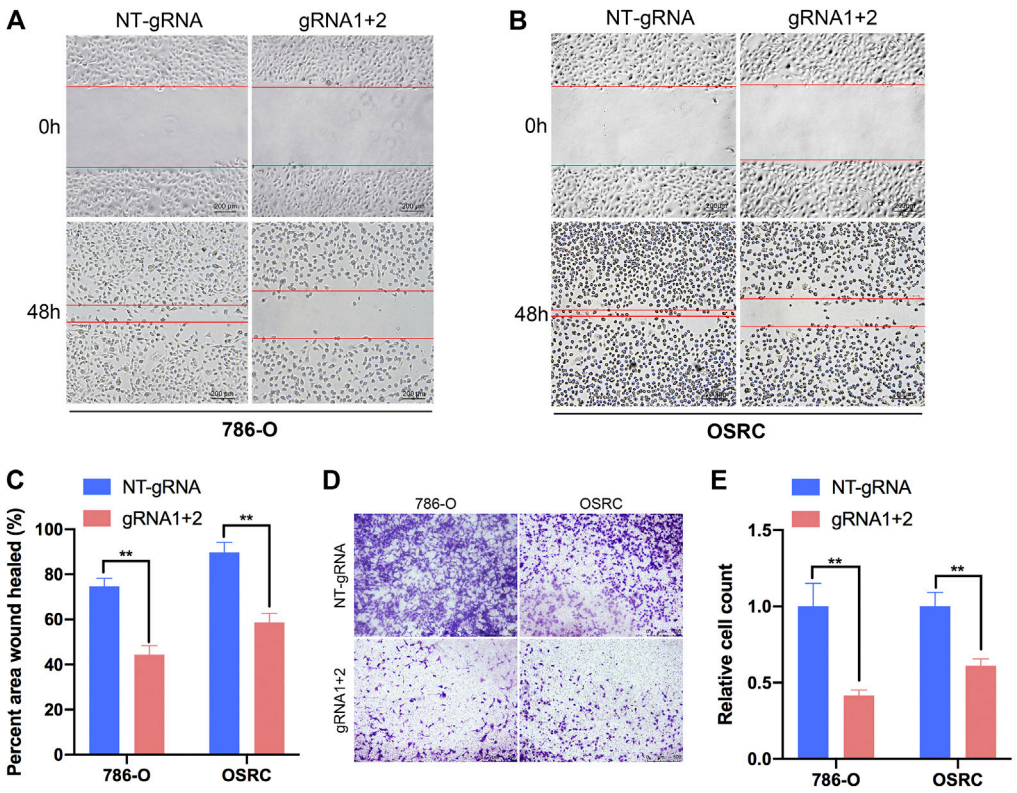

FIGURE 5 | Targeting m^6A of PLOD2 transcripts by $dm^6ACRISPR$ inhibited RCC cells migration. **(A–C)** Wound healing assays of 786-O and OSRC cells after transfected with dCas13b-ALKBH5 and sgRNAs. **(D,E)** Transwell migration assays of 786-O and OSRC cells after transfected with dCas13b-ALKBH5 and sgRNAs. $^{**}p < 0.01$.

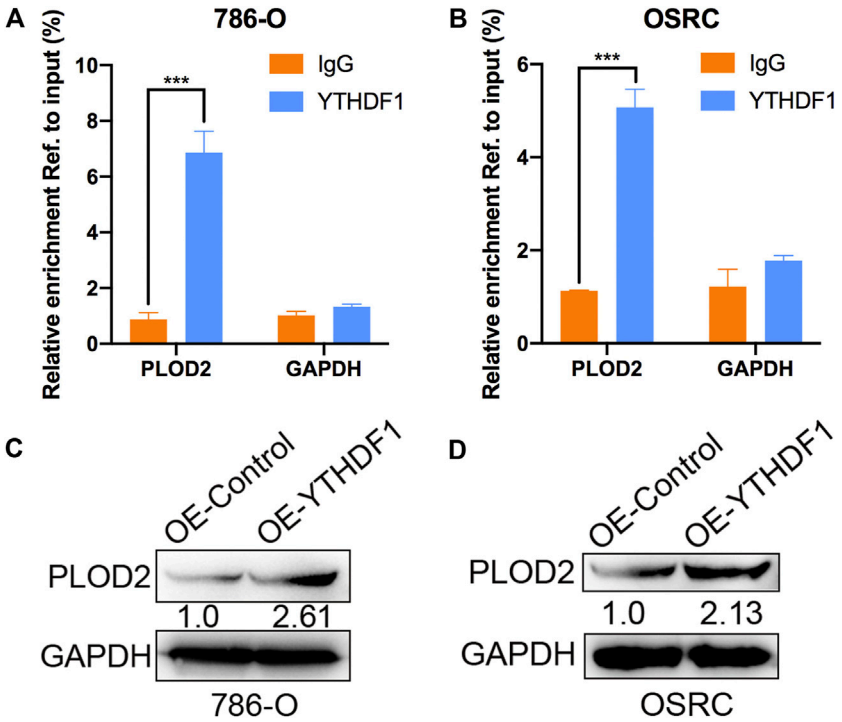

FIGURE 6 | YTHDF1 involved in m^{6}A regulated protein level of PLOD2. **(A,B)** YTHDF1 RIP-qPCR analysis of PLOD2 mRNA in 786-O and OSRC cells. GAPDH as a negative control. **(C,D)** Western blot analysis of PLOD2 protein levels in 786-O and OSRC cells transfected with control or YTHDF1 construct for 24 h. ***$p < 0.005$.

YTHDF1 Involved in N6-Methyladenosine Regulated Expression of PLOD2

Mechanism of targeting demethylation of PLOD2 transcripts by dCas13b-ALKBH5 inhibited its protein level need to be further investigated. YTHDF1 acted as "reader" can recognize m^{6}A methylated mRNA and regulate the methylated mRNA translation (Xiao et al., 2015). We then examined if there was relationship between YTHDF1 and methylated PLOD2 mRNA by RIP-qPCR. The results showed that PLOD2 mRNA could be interacted by YTHDF1 protein in 786-O and OSRC RCC cells (**Figures 6A,B**). In addition, after overexpressed YTHDF1 in 786-O and OSRC RCC cells, we found the protein levels of PLOD2 were increased which confirmed previous data (**Figures 6C,D**). These results validated that YTHDF1 could interact with methylated PLOD2 mRNA and regulate its protein level by m^{6}A modification.

Targeted Demethylation of PLOD2 mRNA Regulated Downstream Target Genes Expression

Finally, we examined the impact of PLOD2 mRNA demethylation on the transcriptome of 786-O and OSRC RCC cells by RNA-seq. We identified 308 and 269 differentially expressed genes in PLOD2 demethylated OSRC and 786-O cells compared to control cells (**Figures 7A,B,D**). By comparing differentially expressed genes in two cell lines, we identified 19 genes that might be regulated by PLOD2 (**Figure 7C**). These differentially expressed genes were further categorized based on the KEGG pathway, and we found they were associated with "Lysine degradation," "VEGF signaling pathway," "Transcriptional misregulation in cancer," "Renal cell carcinoma," "MAPK signaling pathway," "TNF signaling pathway," and "Metabolic pathways" in two RCC cell lines related with PLOD2 demethylation (**Figures 7E,F**). Finally, we demonstrated that demethylation of PLOD2 inhibited the activation of the MAPK signaling pathway in RCC cells (**Figures 7G–I**).

DISCUSSION

Renal cell carcinoma (RCC) is one of the most common malignancies of urinary system. In 2015, it was reported that there were 66,800 new cases and 23,400 deaths from renal cell carcinoma in China (Siegel, Miller, and Jemal 2019). Clear cell renal cell carcinoma (CCRCC) is the main pathological type of renal cell carcinoma, accounting for 70–80% of renal cell carcinoma (Ronald and Bukowski 1997). RCC has no specific clinical manifestations and features in its early stage, and 20–30% have metastasized at the time of initial diagnosis. Nephrectomy is the main treatment for renal cell carcinoma (RCC). The 5 years survival rate for patients with early stage surgery is more than 80%, while the prognosis for patients with advanced metastasis is very poor. Renal cell carcinoma is not sensitive to radiotherapy

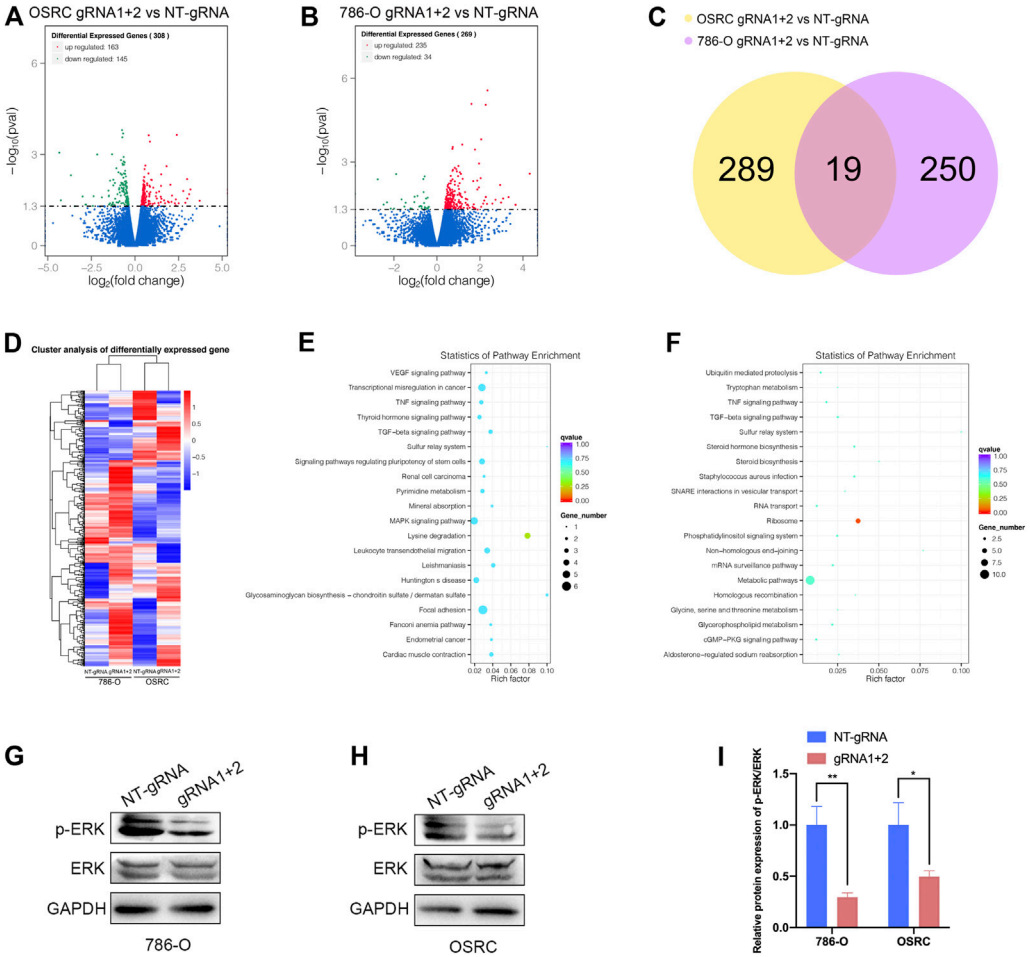

FIGURE 7 | Targeted demethylation of PLOD2 mRNA regulates downstream target genes expression. **(A,B)** The scatter diagram showed the differentially expressed genes (DEGs) in PLOD2 demethylated 786-O and OSRC cells. **(C)** The venn diagram summarized the overlap of PLOD2 regulated genes in both cells. **(D)** The heatmap showed the differentially expressed genes (DEGs) in PLOD2 demethylated 786-O and OSRC cells. **(E,F)** KEGG pathway analysis of DEGs in 786-O and OSRC cells. **(G–I)** The protein levels of MAPK pathway related proteins were measured in PLOD2 demethylated 786-O and OSRC cells by western blot.

and chemotherapy. Existing targeted drugs have uncertain efficacy, and most of them are still in clinical trials. Therefore, further study of the molecular mechanism of the occurrence and development of renal cell carcinoma and search for specific diagnostic markers and therapeutic targets are of great academic significance and application value for the early diagnosis and precise treatment of renal cell carcinoma.

N6-methyladenosine RNA modification on the sixth nitrogen atom of RNA molecule adenine has become one of the hot topics in the field of biomedical research in recent years (Dominissini et al., 2012; Meyer et al., 2012; Bodi et al., 2015). More and more studies have shown that abnormal m^{6}A modification is closely related to the occurrence and development of tumors (Jia et al., 2011; Liu et al., 2014; Ping et al., 2014; Schwartz et al., 2014). This project used MeRIP-seq to analyze the differences in m^{6}A methylation modification profiles of five pairs of RCC tumor tissues and adjacent tissues, and combined with RNA-seq to compare the differences in gene expression profiles of tumor tissues and adjacent tissues. Through joint analysis, a number of genes that might be caused by m^{6}A modification changes were found to change the expression levels. Among them, the modification and expression level of m^{6}A on PLOD2 mRNA were significantly increased in renal clear cell carcinoma tissues, which aroused our research interest.

Our preliminary experimental results showed that the incidence of tumor metastasis was significantly increased in RCC patients with elevated PLOD2 expression in cancer tissues, and overall survival rate was significantly reduced. And demethylation of PLOD2 significantly inhibited the proliferation and migration of RCC cells, suggesting that PLOD2 played an important role in the development and progression of RCC. Overexpression of YTHDF1 in RCC cells significantly up-regulated the protein levels of PLOD2, suggesting that modification of m^{6}A could regulate the protein level of PLOD2. Finally, the RNA-seq data showed that typical pathways involved in RCC development and progression such as “Lysine degradation,” “VEGF signaling pathway,”

"Transcriptional misregulation in cancer," "Renal cell carcinoma," "MAPK signaling pathway," "TNF signaling pathway," and "Metabolic pathways" were enriched by KEGG pathway analysis. These results demonstrate that PLOD2 is a transcriptional regulator associated with cancer development and progression.

This study explores the role and molecular mechanism of PLOD2 m^{6}A modification in the occurrence and development of RCC through targeted regulation of PLOD2 mRNA methylation by dm^{6}ACRISPR. The implementation of this study will have important academic value in further elucidating the molecular mechanism of the occurrence and development of renal cell carcinoma, and will also provide a new way for the early diagnosis and precise treatment of renal cell carcinoma.

METHODS

Patients and Tissue Specimen Collection

Five primary clear cell renal cell carcinoma (ccRCC) samples and five adjacent non-malignant renal tissues with patients' informed consent were obtained from the Urology Department of Peking University First Hospital (PKUFH), Beijing, China. This study followed the Helsinki declaration and was approved by the Institutional Ethical Review Board of PKUFH. The pathological diagnosis was made by professional urological pathologists. Samples were collected immediately in the operating room after surgical removal and were stored in liquid nitrogen after rapid freezing in liquid nitrogen for the following RNA isolation. We used these samples for the later mRNA and protein analysis.

RT-qPCR and MeRIP-qPCR

Total RNA of primary RCC tissues and cell lines were extracted using an RNA-easy Isolation Reagent (Vazyme Biotech, Nanjing, China) according to their instructions, respectively, as previously described. The fragmented RNA was incubated with anti-m^{6}A antibody-coupled beads. The m^{6}A-containing RNAs were then immunoprecipitated and eluted from the beads. Both input control and m^{6}A-IP samples were subjected to RT-qPCR with gene-specific primers. cDNA was synthesized using HiScript III RT SuperMix for qPCR (Vazyme Biotech, Nanjing, China). qRT-PCR was performed using spectrophotometry (ABI Prism 7500TM instrument, Applied Biosystems) with universal SYBR Green qPCR Master Mix (Vazyme Biotech, Nanjing, China). Glyceraldehyde 3-phosphate dehydrogenase (GAPDH) was used as reference gene. Primers were listed in **Supplementary Table S1**.

Vector Construction and Design of gRNAs

The CRISPR dCas13b plasmids and Cas13b-gRNA plasmids were purchased from Addgene. And All designed gRNAs and dCas13b-ALKBH5 vector were constructed by Synbio Technologies Company (Suzhou, China). The sequences of related plasmids were listed in **Supplementary Table S1**.

Cell Culture and Plasmid Transfection

RCC cell lines (786-O, 769-P, ACHN and OSRC) were used in this study. HK-2 human kidney proximal tubular epithelial cells were used as normal controls. These cell lines were purchased from the American Type Culture Collection (ATCC, Manassas, VA, United States) and National Infrastructure of Cell Line Resource, China. Cell lines were routinely cultured in RPMI 1640 or DMEM, which was supplemented with 10% fetal bovine serum (Invitrogen, Carlsbad, CA, United States) and incubated in a 5% CO_2 environment at 37°C. All plasmids were transfected with lipo3000 (Invitrogen) following manufacture's protocol and the number of plasmids used in the experiments were 1 μg.

Protein Isolation and Western Blot

Total protein of cells was extracted by KeyGEN Bio TECH protein extraction kit (KGP1100) and separated on 10% SDS-PAGE and transferred onto nitrocellulose membrane. After blocking, blots were immunostained with primary antibodies and secondary antibodies respectively as previously described. The antibodies were as follows: PLOD2 (1:1,000; Preteintech, United States); ALKBH5 (1:1,000; Sigma, United States); YTHDF1 (1:1,000; Preteintech, United States); ERK (1:1,000; Cell Signaling Technology, United States); *p*-ERK (1:1,000; Cell Signaling Technology, United States) and GAPDH (1:10,000; Preteintech, United States). Immunohistochemistry staining was performed using a primary antibody of PLOD2 at a 1:300 dilution following a protocol described previously. All photographs were taken randomly and measured using Image Pro Plus (Media Cybernetics, Rockville, MD, United States).

Wound-Healing Assay

The cell motility was assessed by scratch wound healing assay. 786-O and OSRC cells (2–3 × 106 per well) were plated in a six-well plate for 1 day and then transfected with vectors for 24 h. The cell layers were washed with PBS after carefully scratching by sterile tips. After incubation for 0 and 24 h, photos were taken. The assays were performed in triplicate.

Transwell Migration Assay

The 786-O and OSRC cells suspended in 150 ul serum-free medium (2 × 105 cells/ml) were placed on the upper layer of a cell permeable membrane. Following another 24–48 h incubation, the cells migrated through the membrane were stained with 1% Crystal Violet and counted.

RNA-Sequencing

Total RNA was prepared from RCC cells after transfected with the dCas13b-ALKBH5 and gRNAs using Rneasy kit (Qiagen) and was subjected to RNA-seq according the mRNA sequencing protocol provided by Illumina (TruSeq RNA Sample Preparation Kit). In brief, poly(A)-containing mRNA molecules were purified using poly(T)-oligo-attached magnetic beads, fragmented and applied to first-strand complementary DNA (cDNA) synthesis using reverse transcriptase and random

primers. Second-strand cDNA synthesis was performed using DNA polymerase I and RNase H. cDNAs were then end-repaired, A-tailed, ligated to adaptors and amplified to create the final cDNA library. Afterwards, adaptor-ligated cDNA was sequenced on a HiSeq2000 sequencer according to the manufacturer's instructions.

Statistical Analysis

When comparing two groups of measurement data, t test was used for data conforming to normal distribution, whereas a Wilcoxon test was used for data not conforming to normal distribution, and the measurement data were expressed as the mean ± standard deviation (SD). A Chi-square test was used to analyze comparisons between groups for enumeration data. The Kaplan-Meier method was used for survival analysis, and a log-rank test was applied for comparations between groups. R packages used in this study included "GDCRNATools," "clusterProfiler," "org.Hs.eg.db," "tidyr," "dplyr," "ggplot2," "ggsignif," "survival," and "survimier". Annotation gene sets used in GSEA were hallmark gene sets from the Molecular Signatures Database (MSigDB). All statistical analyses were performed and visualized using RStudio (Version1.2.1335, Boston, MA, United States), GSEA (Version4.0, UC San Diego and Broad Institute, United States) 23, Medcalc (Version16.8, Ostend, Belgium), and GraphPad Prism (Version 8.0, GraphPad, Inc., La Jolla, CA, United States). A two-tailed $p < 0.05$ was considered statistically significant.

DATA AVAILABILITY STATEMENT

The data presented in the study are deposited in the (NCBI SRA) repository, accession number (PRJNA718295).

ETHICS STATEMENT

The studies involving human participants were reviewed and approved by the Institutional Ethical Review Board of PKUFH. The patients/participants provided their written informed consent to participate in this study. Written informed consent was obtained from the individual(s) for the publication of any potentially identifiable images or data included in this article.

AUTHOR CONTRIBUTIONS

CC, QM, and AL performed the experiments and data analysis. XH and JL prepared diagrams and wrote the manuscript. CC and QM designed the project. YG and JY supervised the project and provided financial support. All authors contributed to the article and approved the submitted version.

FUNDING

This work was supported by grants from the National Key R&D Program of China (2019YFA0906003), National Natural Science Foundation of China (82073364) and Shenzhen High-level Hospital Construction Fund.

SUPPLEMENTARY MATERIAL

The Supplementary Material for this article can be found online at: https://www.frontiersin.org/articles/10.3389/fmolb.2021.675683/full#supplementary-material

REFERENCES

Blanco, M. A., LeRoy, G., Khan, Z., Alečković, M., Zee, B. M., Garcia, B. A., et al. (2012). Global Secretome Analysis Identifies Novel Mediators of Bone Metastasis. *Cell Res* 22 (9), 1339–1355. doi:10.1038/cr.2012.89

Bodi, Z., Bottley, A., Archer, N., May, S. T., and Frey, R. G. (2015). Yeast m6A Methylated mRNAs Are Enriched on Translating Ribosomes during Meiosis, and under Rapamycin Treatment. *Plos One*. 10 (7), e0132090. doi:10.1371/journal.pone.0132090

Deng, X., Su, R., Weng, H., Huang, H., Li, Z., and Chen, J. (2018). RNA N6-Methyladenosine Modification in Cancers: Current Status and Perspectives. *Cel Res* 28 (5), 507–517. doi:10.1038/s41422-018-0034-6

Dominissini, D., Moshitch-Moshkovitz, S., Schwartz, S., Salmon-Divon, M., Ungar, L., Osenberg, S., et al. (2012). Topology of the Human and Mouse m6A RNA Methylomes Revealed by m6A-Seq. *Nature* 485 (7397), 201–206. doi:10.1038/nature11112

Dong, S., Nutt, C. L., Betensky, R. A., Stemmer-Rachamimov, A. O., Denko, N. C., Ligon, K. L., et al. (2005). Histology-based Expression Profiling Yields Novel Prognostic Markers in Human Glioblastoma. *J. Neuropathol. Exp. Neurol.* 64 (11), 948–955. doi:10.1097/01.jnen.0000186940.14779.90

Eisinger-Mathason, T. S. K., Zhang, M., Qiu, Q., Skuli, N., Nakazawa, M. S., Karakasheva, T., et al. (2013). Hypoxia-dependent Modification of Collagen Networks Promotes Sarcoma Metastasis. *Cancer Discov.* 3 (10), 1190–1205. doi:10.1158/2159-8290.CD-13-0118

Gilkes, D. M., Bajpai, S., Chaturvedi, P., Wirtz, D., and Semenza, G. L. (2013). Hypoxia-inducible Factor 1 (HIF-1) Promotes Extracellular Matrix Remodeling under Hypoxic Conditions by Inducing P4HA1, P4HA2, and PLOD2 Expression in Fibroblasts*. *J. Biol. Chem.* 288 (15), 10819–10829. doi:10.1074/jbc.M112.442939

Huang, H., Weng, H., and Chen, J. (2020). m6A Modification in Coding and Non-coding RNAs: Roles and Therapeutic Implications in CancerA Modification in Coding and Non-coding RNAs: Roles and Therapeutic Implications in Cancer. *Cancer Cell* 37 (3), 270–288. doi:10.1016/j.ccell.2020.02.004

Jia, G., Fu, Y., Zhao, X., Dai, Q., Zheng, G., Yang, Y., et al. (2011). N6-methyladenosine in Nuclear RNA Is a Major Substrate of the Obesity-Associated FTO. *Nat. Chem. Biol.* 7 (12), 885–887. doi:10.1038/nchembio.687

Kurozumi, A., Kato, M., Goto, Y., Matsushita, R., Nishikawa, R., Okato, A., et al. (2016). Regulation of the Collagen Cross-Linking Enzymes LOXL2 and PLOD2 by Tumor-Suppressive microRNA-26a/b in Renal Cell Carcinoma. *Int. J. Oncol.* 48 (5), 1837–1846. doi:10.3892/ijo.2016.3440

Li, J., Chen, Z., Chen, Feng., Xie, Guoyou., and Wang, H. (2020). Targeted mRNA Demethylation Using an Engineered dCas13b-ALKBH5 Fusion Protein. *Nucleic Acids Res.* 48 (10). doi:10.1093/nar/gkaa269

Liu, J., Yue, Y., Han, D., Wang, X., Fu, Y., Zhang, L., et al. (2014). A METTL3-METTL14 Complex Mediates Mammalian Nuclear RNA N6-Adenosine Methylation. *Nat. Chem. Biol.* 10 (2), 93–95. doi:10.1038/nchembio.1432

Meyer, K. D., Saletore, Y., Zumbo, P., Elemento, O., Mason, C. E., and Jaffrey, S. R. (2012). Comprehensive Analysis of mRNA Methylation Reveals Enrichment in 3′ UTRs and Near Stop Codons. *Cell* 149 (7), 1635–1646. doi:10.1016/j.cell.2012.05.003

Miyamoto, K., Seki, N., Matsushita, R., Yonemori, M., Yoshino, H., Nakagawa, M., et al. (2016). Tumour-suppressive miRNA-26a-5p and miR-26b-5p Inhibit Cell Aggressiveness by Regulating PLOD2 in Bladder Cancer. *Br. J. Cancer* 115 (3), 354–363. doi:10.1038/bjc.2016.179

Ping, X.-L., Sun, B.-F., Wang, L., Xiao, W., Yang, X., Wang, W.-J., et al. (2014). Mammalian WTAP Is a Regulatory Subunit of the RNA N6-Methyladenosine Methyltransferase. *Cel Res* 24 (002), 177–189. doi:10.1038/cr.2014.3

Rajkumar, T., Sabitha, K., Vijayalakshmi, N., Shirley, S., Bose, M. V., Gopal, G., et al. (2011). Identification and Validation of Genes Involved in Cervical Tumourigenesis. *BMC Cancer* 11 (1), 80. doi:10.1186/1471-2407-11-80

Reis, P. P., Waldron, Levi., Goswami, R. S., Xu, W., and Kamel-Reid, S. (2011). mRNA Transcript Quantification in Archival Samples Using Multiplexed, Color-Coded Probes. *Bmc Biotechnol.* 11 (1), 1–10. doi:10.1186/1472-6750-11-46

Ronald, M., and Bukowski, D. M. (1997). Natural History and Therapy of Metastatic Renal Cell Carcinoma: the Role of Interleukin-2. *Cancer*. 80 (7), 1198–1220. doi:10.1002/(sici)1097-0142(19971001)80:7<1198::aid-cncr3>3.0.co;2-h

Schwartz, S., Mumbach, M. R., Jovanovic, M., Wang, T., Maciag, K., Bushkin, G. G., et al. (2014). Perturbation of m6A Writers Reveals Two Distinct Classes of mRNA Methylation at Internal and 5′ Sites. *Cel Rep.* 8 (1), 284–296. doi:10.1016/j.celrep.2014.05.048

Siegel, R. L., Miller, K. D., and Jemal, A. (2019). Cancer Statistics, 2019. *CA A. Cancer J. Clin.* 69 (1), 7–34. doi:10.3322/caac.21551

Wang, X., Lu, Z., Gomez, A., Hon, G. C., Yue, Y., Han, D., et al. (2014). N6-methyladenosine-dependent Regulation of Messenger RNA Stability. *Nature* 505 (7481), 117–120. doi:10.1038/nature12730

Xiao, W., Zhao, B. S., Roundtree, I. A., Lu, Z., Han, D., Ma, H., et al. (2015). N6-methyladenosine Modulates Messenger RNA Translation Efficiency. *Cell* 161 (6), 1388–99. doi:10.1016/j.cell.2015.05.014

Conflict of Interest: The authors declare that the research was conducted in the absence of any commercial or financial relationships that could be construed as a potential conflict of interest.

frontiers in Molecular Biosciences

ORIGINAL RESEARCH
published: 11 June 2021
doi: 10.3389/fmolb.2021.692941

Downregulation of CacyBP by CRISPR/dCas9-KRAB Prevents Bladder Cancer Progression

*Hanxiong Zheng and Chiheng Chen**

Department of Urology, The Eighth Affiliated Hospital, Sun Yat-sen University, Shenzhen, China

Bladder cancer (BCa) is a leading cause of cancer-related death in the world. CacyBP is initially described as a binding partner of calcyclin and has been shown to be involved in a wide range of cellular processes, including cell differentiation, proliferation, protein ubiquitination, cytoskeletal dynamics and tumorigenesis. In the present study, we found that CacyBP expression was significantly upregulated in BCa tissues compared with adjacent normal tissues. Moreover, its expression was negatively correlated with overall survival time. Secondly, CacyBP had higher expressions in BCa cell lines than normal urothelial cells which was consistent with the results of BCa tissues. Finally, knockdown of CacyBP by CRIPSR-dCas9-KRAB in T24 and 5,637 BCa cells inhibited cell proliferation and migration by CCK-8 assay and scratch assay, and promoted apoptosis by caspase-3/ELISA. These data elucidate that CacyBP is an important oncogene contributing to malignant behavior of BCa and provide a potentially molecular target for treatment of BCa.

Keywords: cacybp, bladder cacner, CRISPR, proliferation, migration

OPEN ACCESS

Edited by:
Tao Xu,
Anhui Medical University, China

Reviewed by:
Bin Zhao,
Shenzhen Peking University Hong Kong University of Science and Technology Medical Center, China
Yujiao Wen,
Huazhong University of Science and Technology, China

****Correspondence:***
Chiheng Chen
chenchh55@163.com

Specialty section:
This article was submitted to Molecular Diagnostics and Therapeutics, a section of the journal Frontiers in Molecular Biosciences

Received: *09 April 2021*
Accepted: *31 May 2021*
Published: *11 June 2021*

Citation:
Zheng H and Chen C (2021) Downregulation of CacyBP by CRISPR/dCas9-KRAB Prevents Bladder Cancer Progression. Front. Mol. Biosci. 8:692941. doi: 10.3389/fmolb.2021.692941

INTRODUCTION

Bladder cancer is the most common urinary tract tumor with a high degree of malignancy, most of which are urothelial carcinoma of the bladder, accounting for more than 90% (Pashos et al., 2002). Its incidence is high over the years, among all malignant tumors, it ranks the 10th in China (Chen et al., 2016). In 2012, the number of cases of bladder cancer in the world is expected to be as high as 430,000 (Feday et al., 2015). The morbidity and mortality of bladder cancer mainly occur in underdeveloped areas and developing countries, which will be significantly higher than that in developed areas (Antoni et al., 2017; Siegel et al., 2017). Bladder cancer is a heterogeneous disease with complex and varied clinical features and atypical early clinical symptoms. Most patients come to the hospital after hematuria occurs. As a result, when most patients are first diagnosed with bladder cancer, the tumor has already reached the middle and advanced stage, and most of the tumors have already undergone invasion and metastasis, leading to unsatisfactory treatment or recurrence of advanced bladder cancer (DeGeorge et al., 2017; Babjuk et al., 2017). Therefore, in order to explore the pathogenesis of bladder cancer, to analyze the molecular mechanism of its invasion and metastasis, and to find new screening biological indicators, diagnosis and treatment markers and molecular therapeutic targets for bladder cancer has always been a clinical difficulty and research hotspot. It is of great significance to improve the diagnosis and treatment effect of bladder cancer, reduce its recurrence rate and mortality rate, and improve the prognosis of patients.

CACYBP protein was first cloned from Eichenian ascites tumor cells by Filipek et al., with a molecular weight of about 30 kDa. It can bind to calcyclin, so it was first named as CACYCLIN

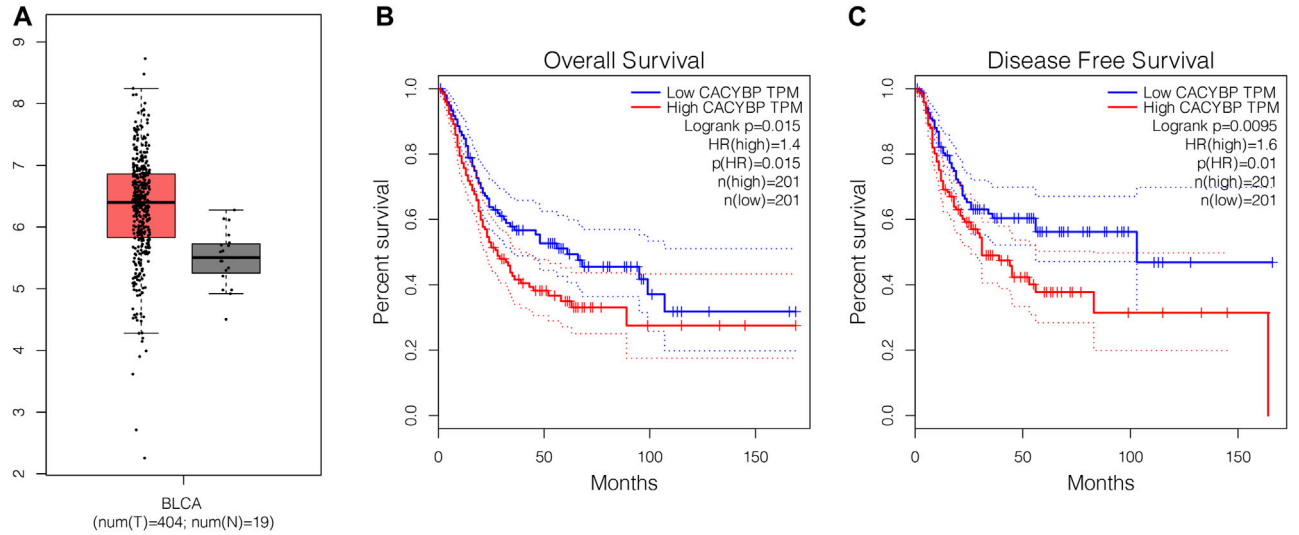

FIGURE 1 | The mRNA level of CacyBP was significantly increased in bladder cancer tissues **(A)** CacyBP expression levels in tumor and adjacent tissues from TCGA database **(B)** The Kaplan–Meier survival curves of CacyBP in bladder cancer tissues from TCGA database **(C)** The disease-free survival curves of CacyBP in bladder cancer tissues from TCGA database.

binding protein (CACYBP) (Filipek and Wojda, 1996; Filipek et al., 2002; Nowotny et al., 2000). In 2001, Matsuzawa et al. studied the process of β-catenin degradation induced by p53 activation in tumor cells, and found a new SAIH-1 binding protein (SIP), which can bind with SAIH-1, SKPL, EBI, etc., to form a complex, and eventually ubiquitinate to degrade β-catenin (Matsuzawa and Reed, 2001). After amino acid sequence alignment, it was found that human SIP was highly homologous to mouse CacyBP, thus the naming of CacyBP/SIP protein was formally established. Currently, it is known that CacyBP/SIP plays a variety of molecular biological functions. It is not only involved in protein ubiquitin and proteasome degradation pathway, but also involved in the regulation of cell cycle, mediating apoptosis signal transduction, and even affecting the occurrence and development of tumors (olska—Wo§ et al., 2016; Ning et al., 2016).

Taking gastric cancer as an example, CacyBP/SIP can inhibit the proliferation of tumor cells, reduce the invasion ability, and prolong the survival of tumor-bearing mice (Ning et al., 2007). Another team studied the expression profile of CacyBP/SIP in 181 cases of gastric cancer. Although the expression of CacyBP/SIP was highly expressed in gastric cancer tissues, it was not correlated with clinicopathological characteristics (Zhai et al., 2015). In addition, besides high expression in gastric cancer, CacyBP/SIP is also highly expressed in pancreatic cancer (Zhai et al., 2008; Chen et al., 2008), and plays a role in promoting cancer progression (Chen X. et al., 2011). However, in renal cancer and chronic lymphoblastic leukemia, the expression of CacyBP/SIP is decreased (Sun et al., 2007; Fu et al., 2016), which plays a role in tumor inhibition. Interestingly, in breast cancer and glioma, the CacyBP/SIP expression profiles reported by different teams were completely opposite (Nie et al., 2010; Wang et al., 2010; Zhao et al., 2011; Shi et al., 2014). These results suggest that CacyBP/SIP may be involved in different molecular mechanisms in different tumors and play a complex biological function.

In our present study, we found that CacyBP expression was significantly upregulated in bladder cancer tissues compared with adjacent normal tissues. And its expression level is negatively correlated with overall survival time. Moreover, knockdown of CacyBP by CRISPR-dCas9-KRAB inhibited BCa cell proliferation and migration but promoted cells apoptosis. Taken together, these results provide novel insight into how CacyBP regulate bladder cancer tumorigenesis and provide a potential therapeutic target for bladder cancer.

RESULTS

The Expression Level of CacyBP Was Significantly Upregulated in Bladder Cancer Tissues

To explore the expression patten of CacyBP in bladder cancer tissues, we firstly checked its expression level in TCGA database. The results showed that CacyBP was significantly upregulated in tumor tissues compared to normal tissues (**Figure 1A**). Furthermore, based on results of Kaplan–Meier survival curves, we found patients with high CacyBP expression level had a worse overall survival rate compared to those with low CacyBP expression (**Figure 1B**). In the disease-free survival analysis, we found the same results that patients with high CacyBP expression level had a worse survival rate compared to those with low CacyBP expression (**Figure 1C**). These results

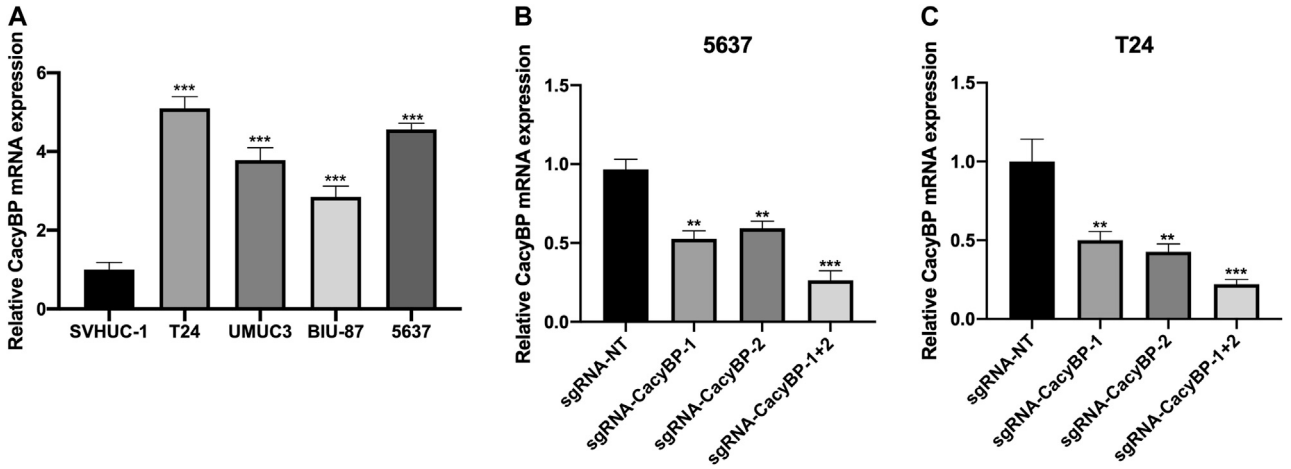

FIGURE 2 | CRIPSR/dCas9-KRAB decreased the expression level of CacyBP in bladder cancer cells **(A)** The expression level of CacyBP in bladder cancer cell lines (T24, UMUC3, BIU-87 and 5,637) and normal urothelial cells (SVHUC-1) by RT-qPCR **(B)** The expression level of CacyBP in 5,637 cells after transfected with dCas9-KRAB and sgRNAs for 24 h by RT-qPCR **(C)** The expression level of CacyBP in T24 cells after transfected with dCas9-KRAB and sgRNAs for 24 h by RT-qPCR. $^{**}p < 0.01$, $^{***}p < 0.001$.

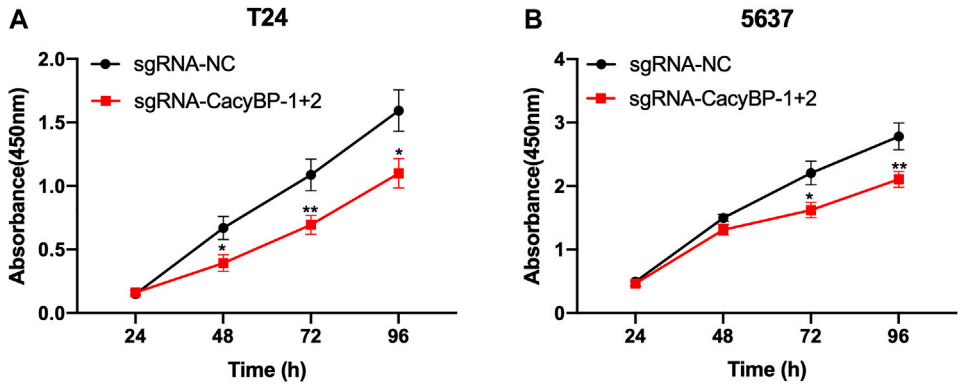

FIGURE 3 | Downregulation of CacyBP inhibited the proliferation of bladder cancer cells **(A, B)** CCK-8 assays of T24 and 5,637 cells after transfected with dCas9-KRAB and sgRNAs. $^{*}p < 0.05$, $^{**}p < 0.01$.

suggested that CacyBP was associated with the development and progression of bladder cancer.

CRIPSR/dCas9-KRAB Decreased the Expression Level of CacyBP in Bladder Cancer Cells

We measured the expression level of CacyBP in bladder cancer cell lines and found it was upregulated in bladder cancer cell lines (T24, UMUC3, BIU-87 and 5,637) compared to normal urothelial cells (SVHUC-1) (**Figure 2A**). Previous study had confirmed that CRIPSR/dCas9-KRAB could decrease the mRNA level of targeted genes (Chavez et al., 2015). Then we transfected with dCas9-KRAB fusion protein in T24 and 5,637 cells, the results showed that the expression level of CacyBP was decreased when transfected with sgRNAs targeted CacyBP compared to sgRNA-NT (**Figures 2B,C**).

Downregulation of CacyBP Inhibited the Proliferation of Bladder Cancer Cells

Next, we determined whether the downregulation of CacyBP inhibited bladder cancer cells proliferation. We found that the downregulation of CacyBP by dCas9-KRAB in T24 and 5,637 cells significantly inhibited cell proliferation detected by CCK-8 assay (**Figure 3A,B**).

Downregulation of CacyBP Inhibited the Migration of Bladder Cancer Cells

Besides, we further evaluated the migration ability after downregulated CacyBP in bladder cancer cell lines checked by wound healing and transwell migration assays. The wound-healing assays showed that CacyBP downregulated T24 and 5,637 cells closed the wound much slower than the

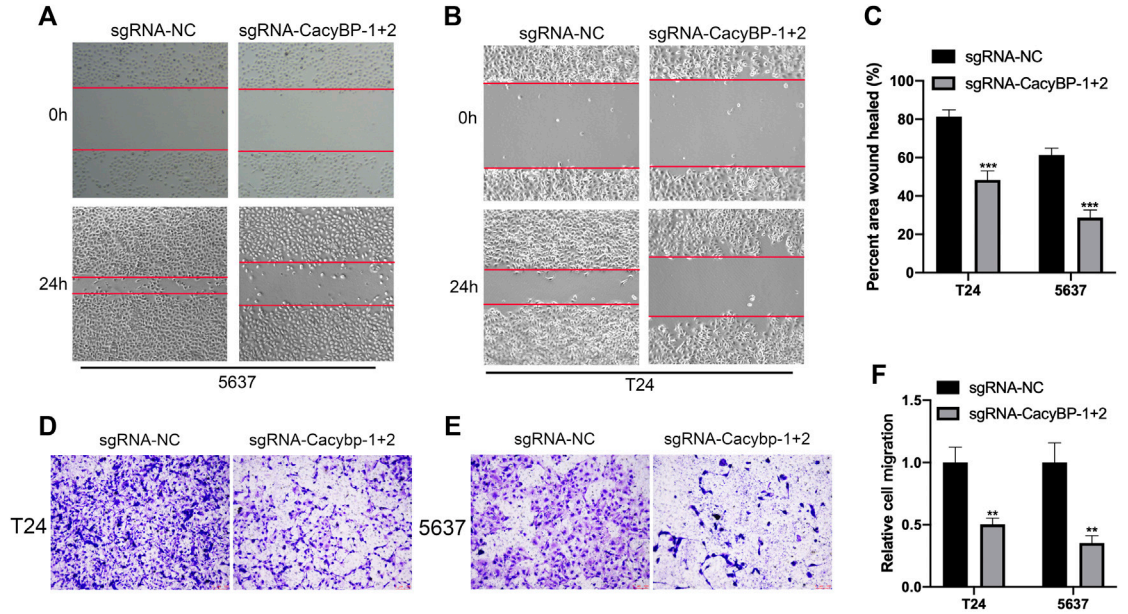

FIGURE 4 | Downregulation of CacyBP inhibited the migration of bladder cancer cells **(A–C)** Wound-healing assays for migration ability of T24 and 5,637 cells after transfected with dCas9-KRAB and sgRNAs **(D–F)** Transwell assays for migration ability of T24 and 5,637 cells after transfected with dCas9-KRAB and sgRNAs. $^{**}p < 0.01$, $^{***}p < 0.001$.

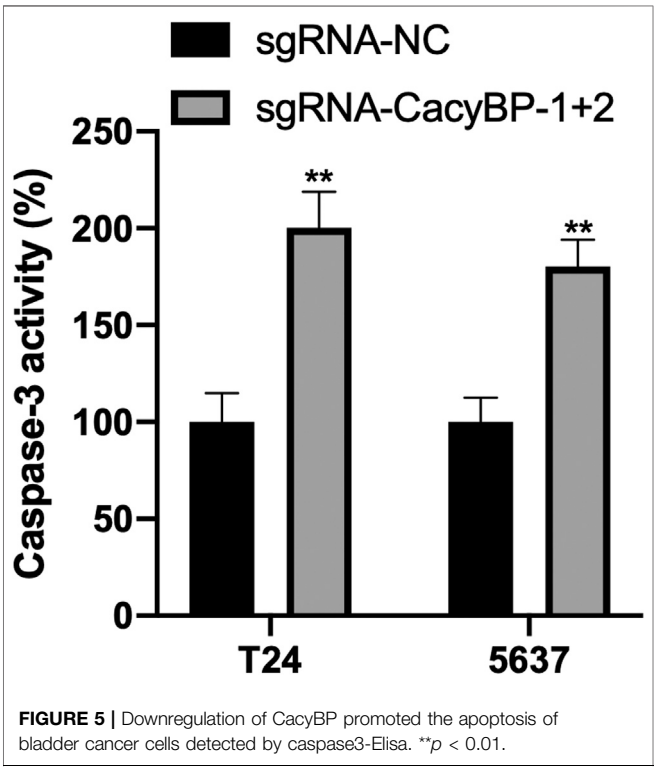

FIGURE 5 | Downregulation of CacyBP promoted the apoptosis of bladder cancer cells detected by caspase3-Elisa. $^{**}p < 0.01$.

controls after 24 h (**Figures 4A–C**). Transwell assays revealed that the migration ability of T24 and 5,637 cells was significantly decreased following the downregulation of CacyBP (**Figures 4D–F**). These results suggested that downregulated CacyBP by dCas9-KRAB inhibited the migration of bladder cancer cells.

Downregulation of CacyBP Promoted the Apoptosis of Bladder Cancer Cells

Finally, we performed the caspase3-Elisa assay and found the CacyBP downregulated T24 and 5,637 cells significantly promoted the cells apoptosis compared to the controls (**Figure 5**fig5).

DISCUSSION

Bladder cancer is a common malignancy in genitourinary diseases and one of the ten most common human tumors. Bladder cancer is the second most common cancer in western countries, after prostate cancer (Siegel et al., 2014). Bladder cancer is characterized by high malignancy, multi-centrality, easy recurrence and progression, and long treatment time, easy to develop drug resistance, which seriously threatens human health (Smith et al., 2014). Therefore, it is an urgent scientific problem to actively explore the pathogenesis and development of bladder cancer as well as new therapeutic targets.

More and more studies have shown that CACYBP/SIP protein plays an important role in the occurrence, development, invasion and metastasis of various tumors. Therefore, the role and mechanism of CACYBP/SIP protein in tumors have become a research hotspot. In the past 10 years, people have studied the role of CACYBP/SIP in the occurrence and development of a variety

of tumors. For instance, the high expression of CACYBP/SIP in pancreatic cancer cells is positively correlated with different stages and distant metastasis, suggesting that the high expression of CACYBP/SIP may be associated with the aggressiveness of pancreatic cancer (ZHAI et al., 2008; CHEN et al., 2008). Increased levels of CACYBP/SIP protein were also found in gastric, colon, nasopharyngeal, osteosarcoma, and melanoma (GHOSH et al., 2011; KILANCZYK et al., 2012; EVANS and CORFE, 2013; GHOSH et al., 2013; ZHU et al., 2014). Among them, some studies have found that the level of CACYBP/SIP in gastric cancer cells is positively correlated with cancer differentiation, and we have also found that the high expression of CACYBP/SIP can inhibit the proliferation and invasion ability of gastric cancer cells and inhibit the growth of tumor cells *in vitro* (NING et al., 2007). In colorectal cancer, a study found that the expression of CACYBP was increased in three different primary CRC cell lines and significantly decreased its adhesion and β-catenin levels, suggesting that CACYBP/SIP may be related to CRC metastasis (GHOSH et al., 2011). In renal cancer, the expression of CACYBP/SIP protein was significantly decreased in renal cancer tissues and renal cancer cell lines (GHOSH et al., 2013).

This study demonstrated that CacyBP expression was increased in bladder cancer tissues and cell lines, and CacyBP may be involved in the regulation of malignant biological behavior of bladder cancer. From our previous RNA-seq data of bladder cancer tissues, we found the mRNA levels of CacyBP were upregulated in bladder cancer tissues compared to normal tissues. Then we used CRIPSR/dCas9-KRAB to knock down CacyBP in T24 and 5,637 bladder cancer cells. We found the expression levels of CacyBP were downregulated after transfected with dCas9-KRAB in T24 and 5,637 bladder cancer cells. Then we examined the cell proliferation and migration ability after CacyBP downregulated through a serious of *in vitro* experiments in T24 and 5,637 bladder cancer cells. The results showed that the proliferation and migration ability of T24 and 5,637 bladder cancer cells was decreased after transfected with dCas9-KRAB and sgRNAs targeted CacyBP. Finally, we performed the caspase3-Elisa assay to examine the apoptosis in T24 and 5,637 bladder cancer cells, we found that downregulation of CacyBP promoted the apoptosis in bladder cancer cells.

Collectively, the expression level of CacyBP is frequently increased in bladder cancer. CRISPR/dCas9-KRAB targeting CacyBP inactivates its expression and suggested its potent oncogenous function in bladder cancer through a serious of *in vitro* experiments. It is hoped that these findings will contribute to a potential therapeutic strategy in bladder cancer.

METHOD

Cell Culture and Plasmid Transfection

Human normal urothelial cells SVHUC-1, bladder cancer cells T24, UMUC3, BIU-87 and 5,637 were cultured in DMEM medium with 10% fetal bovine serum, respectively. The fluid was changed once every 2 days, and the passage rate was 1:4 per week. After all cells were cultured for 48 h, the expression of CacyBP/SIP in cells was detected by RT-qPCR. Then T24 and 5,637 bladder cancer cells are used to transfected with dCas9-KRAB and sgRNA. Transfection was performed according to the instructions: T24 and 5,637 bladder cancer cells with a 1×10^6 density of/ mL were seeded into a 6-well plate. When 80% of the cells were fused, dCas9-KRAB and gRNAs were transfected into the cells. After 6 h of serum-free culture medium, 10% fetal bovine serum DMEM medium was replaced for further culture for 24 h.

Cell Scratch Assay

Cells were taken from each group and inoculated in a 6-well plate at a density of 1×10^6 cells/ mL. When the cells were completely filled, a vertical line was drawn with a 10 μL spear head, and the cells were rinsed with PBS for 3 times. Photographs were taken under an inverted microscope and marked as 0 h pictures. Then, 10% fetal bovine serum DMEM medium was added for further culture for 24 h. Photographs were taken under an inverted microscope and labeled as 24 h images. The Image of 0 h was used as reference, and the software ImageJ was used to analyze the relative migration area of cells. The relative cell migration rate is equal to the migration area of the experimental group divided by the migration area of the control group.

Transwell Migration Assay

The T24 and 5637 cells suspended in 150 μl serum-free medium (2×10^5 cells/ml) were placed on the upper layer of a cell permeable membrane. Following another 24–48 h incubation, the cells migrated through the membrane were stained with 1% Crystal Violet and counted.

Cell Counting Kit-8 Assay

Cells with good growth and in logarithmic phase were digested into cell suspension, and 3,000–5,000 cells were inoculated into 96-well plates after counting. Nine parallel wells were set in each group. Cell culture plates were taken out after 24, 48 and 72 h, respectively, and the medium in each well was drained. Then 100 μL of the reaction solution diluted 9:1 with normal medium and CCK-8 was added and put back to the cell incubator for incubation for 1 h. Finally, the absorbance of 450 nm wavelength was obtained by using BioTek microplate analyzer.

RT-qPCR Assay

48 h after transfection, the cells were collected, the total mRNA was extracted, and the target fragment was amplified after reverse transcription. The PCR reaction conditions were as follows: pre-denaturation at 95°C for 30°s, 95°C for 5°s, 60°C for 20°s, 40 cycles. The relative quantitative analysis was performed using 2-ΔΔCT with GAPDH as internal reference. The experiment was repeated for 3 times. CacyBP forward primer:5'-CTCCCATTACAACGGGCTATAC-3'; reverse primer:5'-GAACTGCCTTCCACAGAGATG-3'; GAPDH forward primer:5'-GGAGCGAGATCCCTCCAAAAT-3'; reverse primer:5'-GGCTGTTGTCATACTTCTCATGG-3'.

STATISTICAL ANALYSIS

All measurement results were expressed as (mean ± standard deviation). SPSS 19.0 was used for statistical analysis of all research data, and LSD-t test was used for pairwise comparison between measurement data groups. $p < 0.05$ indicated that the difference was statistically significant.

DATA AVAILABILITY STATEMENT

The original contributions presented in the study are included in the article/Supplementary Material, further inquiries can be directed to the corresponding author.

ETHICS STATEMENT

The studies involving human participants were reviewed and approved by the studies involving human participants were reviewed and approved by Institutional Ethical Review Board of Peking University First Hospital (PKUFH). The patients/participants provided their written informed consent to participate in this study.

AUTHOR CONTRIBUTIONS

HZ has done the experiments and statistical analysis. CC designed and supervised the project and provided financial support.

REFERENCES

Antoni, S., Ferlay, J., Soerjomataram, I., and Znaor, A. (2017). Bladder Cancer Incidence and Mortality: A Global Overview and Recent Trends[J]. *Eur. Urol.* 71 (1), 96–108. doi:10.1016/j.eururo.2016.06.010

Babjuk, M., Bohle, A., Burger, M., and Compérat, E. (2017). EAU Guidelines on Non-muscle-invasive Urothelial Carcinoma of the Bladder:update 2016[J]. *Eur. Urol.* 71 (6), 447–461. doi:10.1016/j.eururo.2016.11.029

Chavez, A., Scheiman, J., Vora, S., Pruitt, B. W., Tuttle, M., and Pri, E.(2015). Highly Efficient Cas9-Mediated Transcriptional Programming. *Nat. Methods* 12 (4), 326–328. doi:10.1038/nmeth.3312Epub 2015/03/03PubMed PMID: 25730490; PubMed Central PMCID: PMCPMC4393883

Chen, W., Zheng, R., Baade, P. D., and Zhang, S. (2016). Cancer Statistics in China, 2015[J]. *CA Cancer J. Clin.* 66 (2), 115–132. doi:10.3322/caac.21338

Chen, X., Han, G., Zhai, H., and Zhang, F. (2008). Expression and Clinical Significance of CacyBP/SIP in Pancreatic Cancer [J]. *Pancreatology* 8 (4-5), 470–477. doi:10.1159/000151774

Chen, X., Han, G., Zhai, H., Zhang, F., Wang, J., Li, X., et al. (2008). Expression and Clinical Significance of CacyBP/SIP in Pancreatic Cancer. *Panereatology* 8 (4—5), P. 470–477. doi:10.1159/000151774

Chen, X., Mo, P., Li, X., Zheng, P., Zhao, L., Xue, Z., et al. (2011). CacyBP/SIP Protein Promotes Proliferation and G1/S Transition of Human Pancreatic Cancer Cells. *Mol. Carcinogenesis* 50 (10), P. 804–810. doi:10.1002/mc.20737

DeGeorge, K. C., Holt, H. R., and Hodges, S. C. (2017). Bladder Cancer: Diagnosis and Treatment[J]. *Am. Fam. Physician* 96 (8), 507–514.

Evans, C., and Corfe, B. (2013). Promotion of Cancer Metastasis: Candidate Validation Using an iTRAQ-Based Approach [J]. *Expert Rev. Proteomics* 10 (4), 321. doi:10.1586/14789450.2013.820538

Feday, J., Soerjomataram, I., Dikshit, R., and Eser, S. (2015). Cancer Incidence and Mortality Worldwide:sources, Methods and Major Patterns in GLOBOCAN 2012[J]. *Int. J. Cancer* 136 (5), E359–E386.

Filipek, A., Jastrzebska, B., Nowotny, M., and Kuznicki, J. (2002). CacyBP/SIP, a Calcyclin and Siah—1-Interacting Protein, Binds EF-Hand Proteins of the S I 00 Family. *J. Biol. Chem.* 277 (32), P. 28848–28852. doi:10.1074/jbc.M203602200

Filipek, A., and Wojda, U. (1996). p30, a Novel Protein Target of Mouse Calcyclin (S100A6). *Bioehem J.* 320 (Pt 2), P. 585–587. doi:10.1042/bj3200585

Fu, C., Wan, Y., Shi, H., Gong, Y., Wu, Q., Yao, Y., et al. (2016). Expression and Regulation of CacyBP/SIP in Chronic Lymphocytic Leukemia Cell Balances of Cell Proliferation with Apoptosis. *J. Cancer Res. Clin. Oncol.* 142 (4), P. 741–748. doi:10.1007/s00432-015-2077-0

Ghosh, D., Li, Z., Tan, X., and Lim, T. K. (2013). iTRAQ Based Quantitative Proteomics Approach Validated the Role of Calcyclin Binding Protein (CacyBP) in Promoting Colorectal Cancer Metastasis [J]. *Mol. Cel Proteomics* 12 (7), 1865–1880. doi:10.1074/mcp.m112.023085

Ghosh, D., Yu, H., Tan, X. F., Lim, T. K, Zubaidh, R. M, Tan, H. T, et al. (2011). Identification of Key Players for Colorectal Cancer Metastasis by iTRAQ Quantitative Proteomics Profiling of Isogenic SW480 and SW620 Cell Lines [J]. *J. proteome Res.* 10 (10), 4373–4387. doi:10.1021/pr2005617

Ghosh, D., Yu, H., Tan, X. F., and Lim, T. K. (2011). Identification of Key Players for Colorectal Cancer Metastasis by iTRAQ Quantitative Proteomics Profiling of Isogenic SW480 and SW620 Cell Lines [J]. *J. proteome Res.* 10 (10), 4373–4387. doi:10.1021/pr2005617

Kilanczyk, E., Wasik, U., and Filipek, A. (2012). CacyBP/SIP Phosphatase Activity in Neuroblastoma NB2a and colon Cancer HCT116 Cells [J]. *Biochem. Cel Biol* 90 (4), 558–564. doi:10.1139/o2012-011

Matsuzawa, S. I., and Reed, J. C. (2001). Siah—1, SIP, and Ebi Collaborate in a Novel Pathway Forbeta-Catenin Degradation Linked to P53 Responses. *Mol. Cel.*7(5), 915–926. doi:10.1016/s1097-2765(01)00242-8

Nie, F., Yu, X. L., Wang, X. G., Tang, Y. F., Wang, L. L., and Ma, L. (2010). Down. Regulation of CacyBP Is Associated with Poor Prognosis and the Effects on COX—2 Expression in Breast Cancer. *Int. J. Oncol.* 37 (5), P. 1261–1269. doi:10.3892/ijo_00000777

Ning, X., Sun, S., Hong, L., and Liang, J. (2007). Calcyclin-binding Protein Inhibits Proliferation, Tumorigenicity, and Invasion of Gastric Cancer [J]. *Mol. Cancer Res. : MCR* 5 (12), 1254–1262. doi:10.1158/1541-7786.mcr-06-0426

Ning, X., Chen, Y., Wang, X., Li, Q., and Sun, S. (2016). The Potential Role of CacyBP/SIP in Tumorigenesis. *Tumor Biol.* 37 (8), 10785–91. doi:10.1007/s13277-016-4871-y

Ning, X., Sun, S., Hong, L., Liang, J., Liu, L., Han, S., et al. (2007). Calcyclin-Binding Protein Inhibits Proliferation, Tumorigenicity, and Invasion of Gastric Cancer. *Mol. Cancer Res.* 5 (12), P. 1254–1262. doi:10.1158/1541-7786.MCR-06-0426

Nowotny, M., Bhattacharya, S., Filipek, A., Krezel, A. M., Chazin, W., and Kuznicki, J. (2000). Characterization of the Interaction of Calcyclin($1 00A6)and Calcyclin—Binding Protein. *J. Biol. Chem.* 275 (40), P. 3 1 178–182. doi:10.1074/jbc.M001622200

olska—Wo§, A. M., Chazin, W. J., and Filipek, A. (2016). CacyBP/SIP—Structure and Variety of Fmactions. *Biochim. Biophys. Acta(BBA)—General Subjects* 1860 (1), P. 79–85.

Pashos, C. L., Botteman, M. F., Laskin, B. L., and Redaelli, A. (2002). Bladder Cancer: Epidemiology, Diagnosis, and Management[J]. *Cancer Pract.* 10 (6), 311–322. doi:10.1046/j.1523-5394.2002.106011.x

Shi, H., Oao, Y., Tang, Y., Wu, Y., Gong, H., Du, J., et al. (2014). CacyBP/SIP Protein Is Important for the Proliferation of Human Glioma Ceils. *IUBMB Life* 66 (4), P. 286–291. doi:10.1002/iub.1263

Siegel, R. L., Miller, K. D., and Jemal, A. (2017). Cancer Statistics, 2017[J]. *CA Cancer J. Clin.* 67 (1), 7–30. doi:10.3322/caac.21387

Siegel, R., Ma, J., Zou, Z., and Jemal, A. (2014). Cancer Statistics, 2014[J]. *CA Cancer J. Clin.* 64 (1), 9–29. doi:10.3322/caac.21208

Smith, R. A., Manassaram-Baptiste, D., Brooks, D., and Cokkinides, V. (2014). Cancer Screening in the United States, 2014: a Review of Current American Cancer Society Guidelines and Current Issues in Cancer Screening[J]. *CA Cancer J. Clin.* 65 (1), 30–51. doi:10.3322/caac.21212

Sun, S., Ning, X., Liu, J., Liu, L., Chen, Y., Han, S., et al. (2007). Overexpressed CacyBP/SIP Leads to the Suppression of Growth in Renal Cell Carcinoma. *Biochem. Biophysical Res. Commun.* 356 (4), P. 864–871. doi:10.1016/j.bbrc.2007.03.080

Wang, N., Ma, e., Wang, Y., Ma, G., and Zhai, H. (2010). CacyBP/SIP Expression Is Involved in the Clinical Progression of Breast Cancer. *World J. Surg.* 34 (1 1), P. 2545–2552. doi:10.1007/s00268-010-0690-2

Zhai, H., Shi, Y., Jin, H., and Li, Y. (2008). Expression of Calcyclin-Binding protein/Siah-1 Interacting Protein in normal and Malignant Human Tissues: an Immunohistochemical Survey [J]. *J. Histochem. Cytochem.* 56 (8), 765–772. doi:10.1369/jhc.2008.950519

Zhai, H., Meng, J., Jin, H., Li, Y., and Wang, J. (2015). Role of the CacyBP/SIP Protein in Gas⁴Tic Cancer. *Oncol. Lett.* 9 (5). doi:10.3892/ol.2015.3059

Zhai, H., Shi, Y., Jin, H., Li, Y., Lu, Y., Chen, X., et al. (2008). Expression of Calcyclin—Binding protein/Siah-1 Interacting Protein in normal and Malignant Human Tissues: an Immunohistochemical Survey. *J. Histochem. Cytochem.* 56 (8), P. 765–772. doi:10.1369/jhc.2008.950519

Zhao, W., Wang, C., Wang, J., Ge, A., Li, Y., Li, W., et al. (2011). Relationship between CacyBP/SIP Expression and Prognosis in Astrocytoma. *J. Cl⫛neurosci* 18 (91), P. 1240–1244. doi:10.1016/j.jocn.2011.01.024

Zhu, L., Miake, S., Ijichi, A., and Kawahara, S. (2014). Upregulated Expression of Calcyclin-Binding Protein/siah-1 Interacting Protein in Malignant Melanoma [J]. *Ann. Dermatol.* 26 (5), 670–673. doi:10.5021/ad.2014.26.5.670

Conflict of Interest: The authors declare that the research was conducted in the absence of any commercial or financial relationships that could be construed as a potential conflict of interest.

frontiers in Molecular Biosciences

ORIGINAL RESEARCH
published: 05 July 2021
doi: 10.3389/fmolb.2021.697962

LncRNA LINC00944 Promotes Tumorigenesis but Suppresses Akt Phosphorylation in Renal Cell Carcinoma

*Chiheng Chen and Hanxiong Zheng**

Department of Urology, The Eighth Affiliated Hospital, Sun Yat-sen University, Shenzhen, China

Long non-coding RNA (lncRNA) is a kind of RNA that possesses longer than 200 nucleotides and lacks protein coding function. It was recognized as a junk sequence for a long time. Recent studies have found that lncRNAs are actively functioning in almost every aspect of cell biology and involved in a variety of biological functions. LncRNAs are closely related to a variety of human diseases, especially tumors. Recently, lncRNAs are being increasingly reported in renal cancer. In our study, we identified the expression of lncRNA LINC00944 is significantly elevated in renal cell carcinoma (RCC) tissues and cell lines and high LINC00944 expression is significantly correlated with the tumor stage and prognosis of RCC. The knockdown of LINC00944 by CRISPR/dCas9-KRAB in higher expressing 786-O and 769-P RCC cells could significantly decrease proliferation and migration and also promote phosphorylation of Akt compared with the control group. Our study is the first to report the function of lncRNA LINC00944 in RCC. And we provide clinicopathological and experimental evidence that lncRNA LINC00944 acts as an oncogene in RCC, suggesting that targeting lncRNA LINC00944 expression might be a promising therapeutic strategy for the treatment of RCC.

Keywords: LINC00944, tumorigenesis, Akt, phosphorylation, RCC

OPEN ACCESS

Edited by:
Tao Xu,
Anhui Medical University, China

Reviewed by:
Xixiang Ma,
Huazhong University of Science and Technology, China
Wencun Li,
Zhejiang University, China

****Correspondence:***
Hanxiong Zheng
zhenghx28@163.com

Specialty section:
This article was submitted to Molecular Diagnostics and Therapeutics, a section of the journal Frontiers in Molecular Biosciences

Received: *20 April 2021*
Accepted: *25 May 2021*
Published: *05 July 2021*

Citation:
Chen C and Zheng H (2021) LncRNA LINC00944 Promotes Tumorigenesis but Suppresses Akt Phosphorylation in Renal Cell Carcinoma. Front. Mol. Biosci. 8:697962. doi: 10.3389/fmolb.2021.697962

INTRODUCTION

Renal cell carcinoma (RCC), referred to as renal cancer for short, accounts for about 85% of primary renal malignancies, ranking the third among urinary system tumors, and accounts for about 2–3% of all adult malignancies (Lopez-Beltran et al., 2006; Siegel et al., 2019). In recent years, the global incidence of RCC has been gradually increasing, with about 209,000 new cases and 102,000 deaths per year (GUPTA et al., 2008). Although diagnostic techniques continue to improve, renal cancer treatment has not progressed. The main reason for this is that, in addition to early resection, renal cancer is not sensitive to other types of treatments, such as radiotherapy, chemotherapy, and endocrine therapy, so the treatment effect is not obvious. Postoperative treatment cannot reduce the metastasis rate of renal cancer, and immunotherapy is only effective for 15–20% of patients (Bukowski, 2000; Negrier et al., 2000). However, about 50% of patients with renal cancer were already in the advanced stage when they first visited the doctor, almost 40% of patients showed recurrence or metastasis after surgery, and the three-year survival rate of patients without any treatment was less than 5% (Mulders et al., 1997). At present, researchers are concerned about finding out some new therapeutic methods to improve the therapeutic effect of renal cancer, reduce

postoperative recurrence and metastasis, and improve the quality of life of patients while conducting surgical treatment as early as possible.

In the past decade, many new types of non-coding RNAs have been discovered, and the important roles of some non-coding RNAs in gene regulatory networks have been revealed (Qi and Du, 2013). The results of a large number of clinical observations and experimental evidence show that there is a close relationship between the occurrence of renal clear cell carcinoma development and the long chain of non-coding RNAs (lncRNAs). LncRNA is considered important in epigenetics research, especially in life science research (Tang et al., 2013), and is also one of the most popular areas of current research. LncRNA is non-coding RNA with a length of more than 200 nucleotides, including non-coding small RNA, interfering small RNA, PIWI-interacting RNA, nucleolar small RNA, and nuclear small RNA. One of the clear characteristics of lncRNA is the acquisition of secondary and tertiary three-dimensional structures, which are mainly dependent on Watson–Crick base pairing (Geisler and Coller, 2013; Mercer and Mattick, 2013; Novikova et al., 2013). This structure enables it to perform both RNA-related functions based on nucleic acid complementarity and protein-like functions based on spatial conformations (Ørom et al., 2010; Long et al., 2017).

Approximately 2,000 lncRNAs are abnormally expressed in renal cell carcinoma (Malouf et al., 2015). These lncRNAs are characteristic in RCC and are considered to play an important role in the activation of the HIF pathway and are involved in a variety of carcinogenic mechanisms. Zhang et al. (2015) verified this in renal cancer tissues and cell lines and found that compared with paratumoral tissues and normal renal tubular epithelial cell lines, MALAT-1 was highly expressed in renal cancer tissues and renal cancer cell lines and the high expression was correlated with prognosis. Subsequently, Hirata et al. (2015) also reported that MALAT-1 was highly expressed in renal cancer tissues and the high expression of MALAT-1 could promote the expression of EZH2, thus promoting tumor epithelial-to-mesenchymal transition (EMT) and further promoting the progression of renal cancer. Pei et al. (2014) found that HOTAIR was closely related to the metastatic ability of renal cancer cell lines and curcumin may inhibit HOTAIR, thereby inhibiting renal cancer metastasis. Chiyomaru et al. (2014) found that, in renal cancer tissues and cell lines, the expression of miR-141 was negatively correlated with the expression of HOTAIR. Further studies showed that miR-141 could regulate the expression of HOTAIR by interacting with the immune complex A902.

In this study, through the screening and analysis of multiple databases, we screened the lncRNA LINC00944 with obvious differential expression in renal cancer tissues and paracancerous tissues and verified the high expression of LINC00944 in renal cancer tissues. Then, we knocked down LINC00944 by CRISPR/dCas9-KRAB in 786-O and 769-P RCC cell lines. Cell function experiments have shown that downregulation of LINC00944 can reduce the proliferation and metastasis of renal cancer cells. Moreover, we found there was a relationship between the expression pattern of LINC00944 and TYMP in RCC tissues; this indicated that LINC00944 might regulate TYMP expression in RCC. Finally, we detected the activity of the PI3K/Akt pathway by western blot and found LINC00944 knockdown promoted phosphorylation of Akt in RCC cell lines. Therefore, LINC00944 may be closely related to the proliferation and metastasis of renal cancer and play a role in promoting tumor progression. LINC00944 may become one of the effective therapeutic targets for renal cancer.

RESULTS

Long Non-Coding RNA LINC00944 Is Highly Expressed in Renal Cell Carcinoma Tissues and Is Associated With Patient Prognosis

To explore the role of lncRNA LINC00944 in the development of RCC, we firstly checked its expression level in RCC tissues and normal tissues from the TCGA database. We found the expression of LINC00944 was significantly increased in RCC tissues compared to normal tissues (**Figure 1A**). Then, we examined its expression levels in ten RCC patients by qRT-PCR and found it was increased in tumors (**Figure 1B**). Moreover, Kaplan–Meier survival analysis from the TCGA database showed that the low-expression group of LINC00944 had a longer postoperative survival than the high-expression group (**Figure 1C**). Furthermore, the disease-free survival analysis showed the same results with the overall survival (**Figure 1D**).

Long Non-Coding RNA LINC00944 Is Highly Expressed in Renal Cell Carcinoma Cells and Can Be Knocked Down by dCas9-KRAB

We have confirmed that LINC00944 was highly expressed in RCC tissues, so we used qRT-PCR to detect the expression of LINC00944 in six human renal carcinoma cell lines with different malignant potentials (ACHN, Caki-2, Caki-1, 769-P, 786-O, and OSRC) and one human normal renal tubular epithelial cell line HK-2. The results showed that LINC00944 was highly expressed in OSRC, Caki-1, 786-O, and 769-P RCC cells (**Figures 2A**,**B**). To investigate the function of LINC00944 in RCC, we knocked down LINC00944 in 786-O and 769-P RCC cells by dCas9-KRAB, and the expression levels of LINC00944 were decreased (**Figures 2C**,**D**).

Long Non-Coding RNA LINC00944 Promotes the Proliferation in 786-O and 769-P Renal Cell Carcinoma Cells

The CCK-8 assay was performed on 786-O and 769-P cells transfected with sgRNAs, respectively. The cell proliferation of 786-O and 769-P groups transfected with sgRNA-LINC00944 was significantly reduced, and the difference gradually increased after the second day compared with the 786-O and 769-P control groups transfected with sgRNA-NT (**Figures 3A**,**B**). In order to further verify the effect of LINC00944 on the proliferation ability of RCC cells, the colony formation assay was performed on the cells treated with the above method. The results showed that the

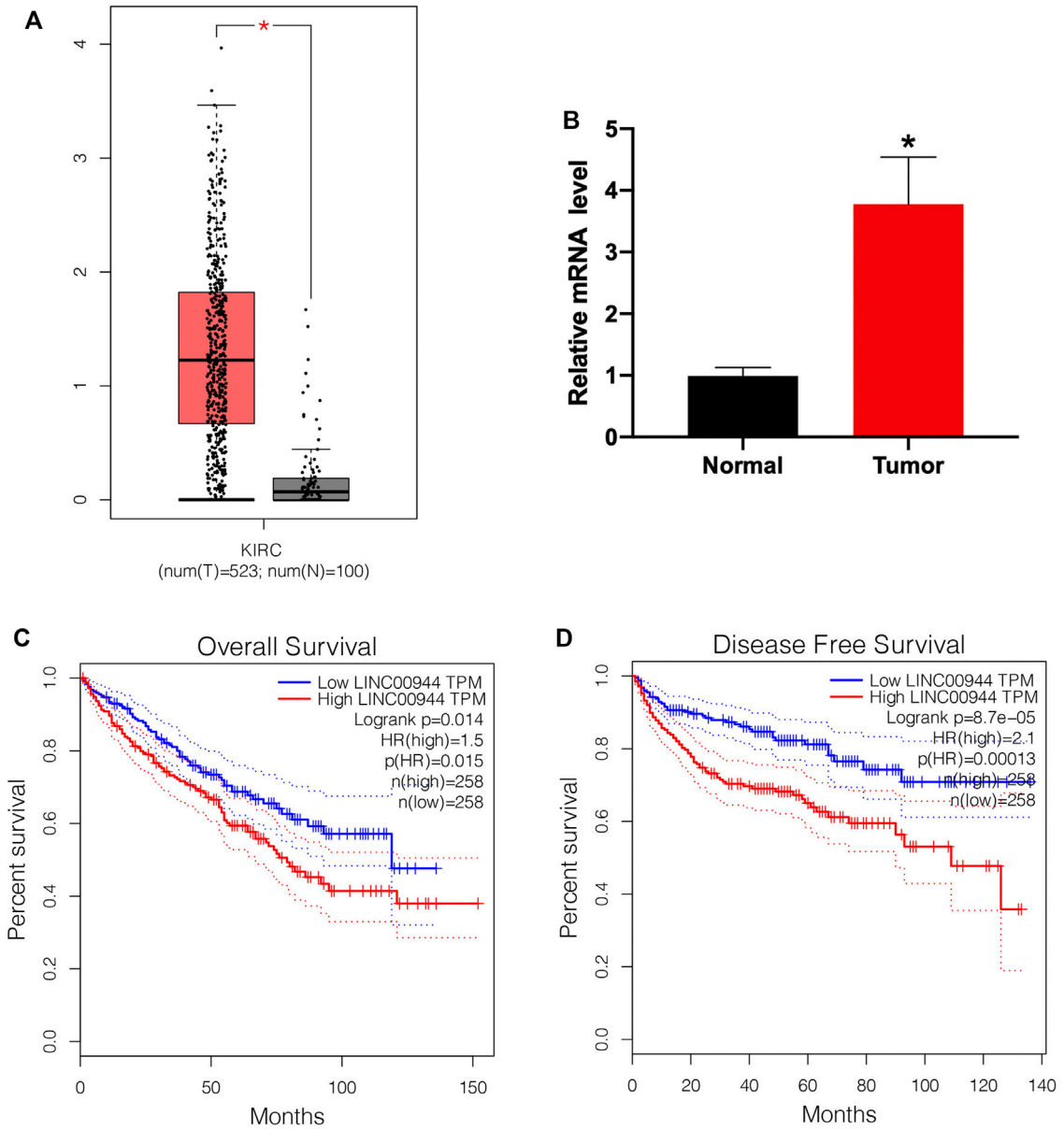

FIGURE 1 | The expression level of lncRNA LINC00944 was significantly increased in RCC patients. **(A)** LINC00944 expression levels in tumor and adjacent tissues from the TCGA database. **(B)** Expression levels of LINC00944 in ten RCC patients detected by qRT-PCR. **(C)** Kaplan–Meier survival curves of LINC00944 in RCC tissues from the TCGA database. **(D)** Disease-free survival curves of LINC00944 in RCC tissues from the TCGA database. *$p < 0.05$.

number of cell colonies in the 786-O and 769-P groups transfected with sgRNA-LINC00944 was significantly less than that in the 786-O and 769-P control groups transfected with sgRNA-NT (**Figures 3C,D**).

Long Non-Coding RNA LINC00944 Promotes the Migration of 786-O and 769-P Renal Cell Carcinoma Cells

The migration ability of tumor cells is an important aspect of tumor progression. Therefore, in order to further explore the effect of LINC00944 on the migration ability of 786-O and 769-P RCC cells, we conducted the scratch assay and transwell assay. The ability of scratch healing in the scratch experiment reflects the ability of cell migration. The scratch test results showed that the scratch healing rate of 786-O and 769-P groups transfected with sgRNA-LINC00944 was less than that of 786-O and 769-P control groups transfected with sgRNA-NT after transfection for 24 h (**Figures 4A–C**). Transwell results showed that compared with the 786-O and 769-P control groups transfected with sgRNA-NT, the 786-O and 769-P groups transfected with sgRNA-LINC00944

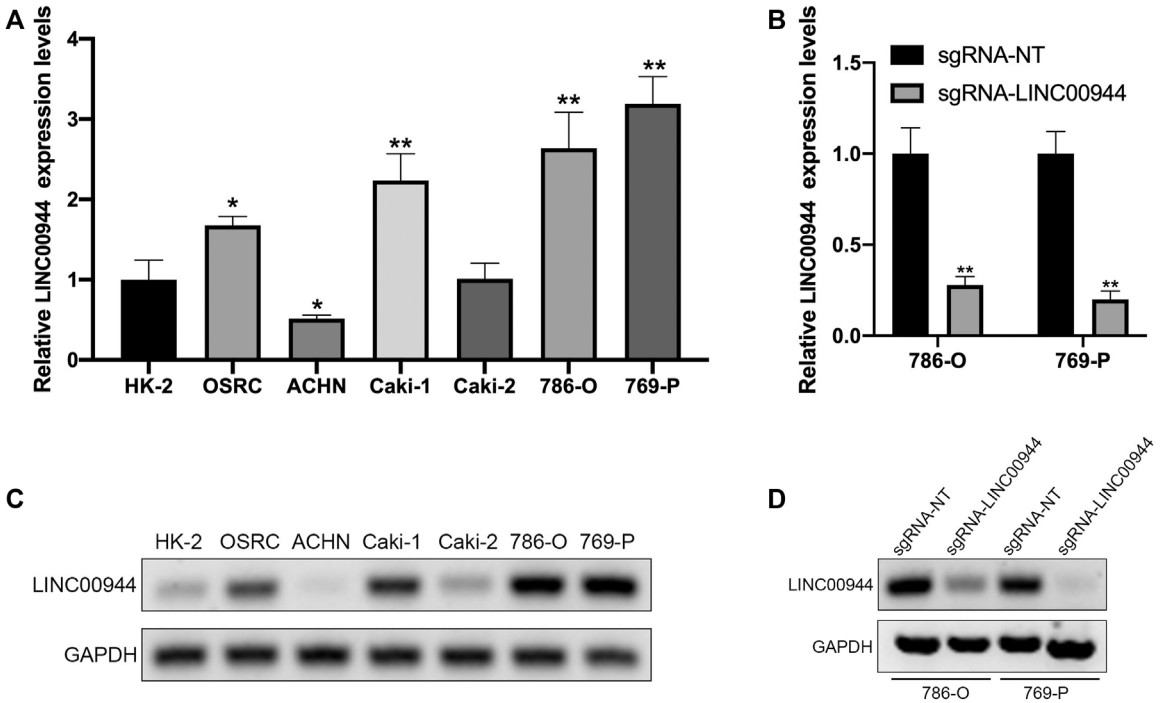

FIGURE 2 | CRISPR/dCas9-KRAB decreased the expression level of LINC00944 in RCC cells. **(A,C)** Expression levels of LINC00944 in RCC cell lines (OSRC, ACHN, Caki-1, Caki-2, 786-O, and 769-P) and normal renal tubular epithelial cell line (HK-2) by qRT-PCR and semi-quantitative RT-PCR. **(B,D)** Expression levels of LINC00944 in 786-O and 769-P RCC cells transfected with dCas9-KRAB and sgRNA-NT or sgRNA-LINC00944 for 24 h by qRT-PCR and semi-quantitative RT-PCR. $^{*}p < 0.05$; $^{**}p < 0.01$.

inhibited the migration of 786-O and 769-P cells (**Figures 4D–F**). These results suggest that LINC00944 can promote the migration ability of RCC cells.

Long Non-Coding RNA LINC00944 Regulates TYMP Expression and Suppresses Akt Phosphorylation

From the TCGA database, we investigated the association of LINC00944 expression with the expression of TYMP in a large number of RCC tissues. Expectedly, there was a significantly positive relationship between LINC00944 expression and the expression of TYMP in RCC tissues (**Figure 5A**). Then, we found the expression level of TYMP was also upregulated in RCC tissues compared to normal tissues (**Figure 5B**). And Kaplan–Meier survival analysis from the TCGA database showed that the low-expression group of TYMP had a longer postoperative survival than the high-expression group (**Figure 5C**), which was the same with the expression pattern of LINC00944. Finally, we detected the protein levels of TYMP in 786-O and 769-P RCC cells after knocking down LINC00944. The results showed that the expression levels of TYMP were also decreased after downregulating LINC00944 in RCC cells. Furthermore, the knockdown of LINC00944 significantly promoted Akt phosphorylation in RCC cells (**Figure 5D**).

DISCUSSION

Renal cancer is one of the most common malignancies of the urinary system. For early or locally advanced renal cancer, surgical resection is still the most effective treatment, but there are still 20–30% patients with tumor recurrence or metastasis after surgery. Advanced renal cancer is not sensitive to radiation and chemotherapy, and the efficacy of immunotherapy is very limited (Murai and Oya, 2004; Chen et al., 2015). Therefore, it is particularly important and urgent to explore the mechanism of renal cancer development and metastasis and to find a reliable therapeutic target. It is of great significance to clarify the mechanism of renal cancer development and metastasis and to find suitable therapeutic targets for the treatment of the disease. Designing drugs for key targets can reduce drug development effort, and related drugs tend to be more effective and have lower adverse reaction rates. A good example is targeted therapy for renal cancer, where researchers have developed drugs that target the mechanisms involved in angiogenesis in renal cancer such as vascular endothelial growth factor tyrosine kinase inhibitors (TKIs) sunitinib, axitinib, pazopanib, and so on.

Recent studies have found that long non-coding RNAs play important roles in a variety of biological processes, such as cell growth, apoptosis, differentiation, and metastasis. Similarly, long non-coding RNAs are thought to be involved in tumor progression and metastasis. In fact, long non-coding RNAs

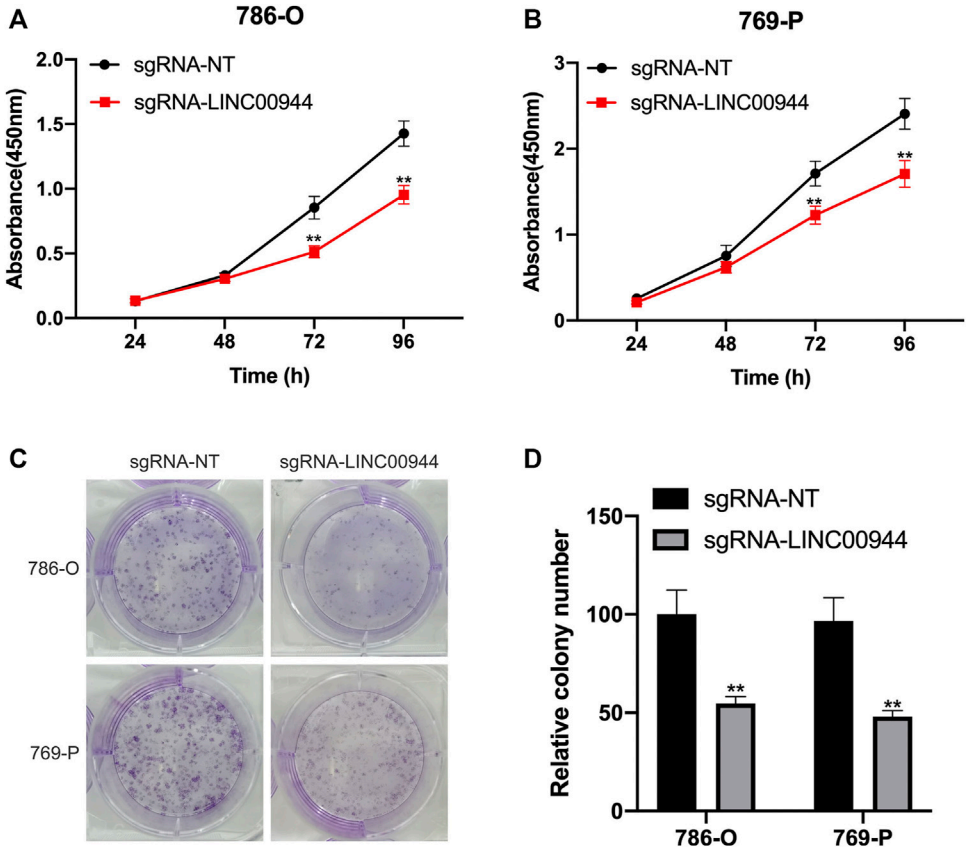

FIGURE 3 | Downregulation of LINC00944 inhibited the proliferation of RCC cells. **(A,B)** CCK-8 assays of 786-O and 769-P RCC cells transfected with dCas9-KRAB and sgRNAs. **(C,D)** Colony formation assays of 786-O and 769-P RCC cells transfected with dCas9-KRAB and sgRNAs. $^{**}p < 0.01$.

can affect the transcription and translation of coding genes through a variety of pathways, such as chromosome remodeling, transcriptional activation or inhibition, protein inhibition, and post-transcriptional modification. Fachel et al. (2013) found that a series of intergene lncRNAs can affect gene expression through cis and trans effects, thereby regulating the occurrence and development of tumors. For example, HOTAIR can recruit PRC2 and LSDL complexes to specific sites through trans-regulation, resulting in methylation or demethylation of specific genes, thereby mediating tumor genesis and metastasis (Wu et al., 2014). LncRNA can also play a role by acting as a competitive binding miRNA between ceRNA and mRNA (Zhou et al., 2014). For example, Yuan et al. (2014) found that, in the occurrence of liver cancer, lncRNA-ATB could competitively bind to miRNA-200 with ZEBL and ZEB2, thereby upregulating the expression of ZEBL and ZEB2, promoting the process of tumor EMT, and thus promoting the metastasis of liver cancer. However, the mechanism of action of long non-coding RNA in renal cancer is still unclear, which needs further exploration and research.

In this study, we searched renal cancer–related datasets through the TCGA database and screened lncRNAs, and we found that lncRNA LINC00944 was significantly upregulated in renal cancer tissues. The expression level and clinical characteristics of lncRNA LINC00944 were analyzed, and it was found that the high expression of lncRNA LINC00944 was related to the tumor stage. The results of survival analysis showed that compared with the low-expression group, the high-expression group had shorter postoperative survival time. In order to further investigate the biological function of lncRNA LINC00944 in RCC, we constructed 786-O and 769-P cell lines capable of knocking down lncRNA LINC00944 by using CRISPR/dCas9-KRAB plasmid transfection. The results showed that compared with the control group transfected with sgRNA-NT, the proliferation and migration abilities of 786-O and 769-P cells transfected with sgRNA-LINC00944 were significantly decreased, suggesting that knockdown of lncRNA LINC00944 expression could inhibit the proliferation and metastasis of RCC. Furthermore, we found lncRNA LINC00944 could regulate TYMP expression and suppress Akt phosphorylation in RCC cells.

In summary, this study is the first to report the function of lncRNA LINC00944 in RCC. Through clinicopathological data and *in vitro* cell experiments, it is confirmed that lncRNA LINC00944 plays an oncogenic role in RCC. Knocking down the expression of lncRNA LINC00944 could inhibit cell proliferation and migration. These experiments suggested that

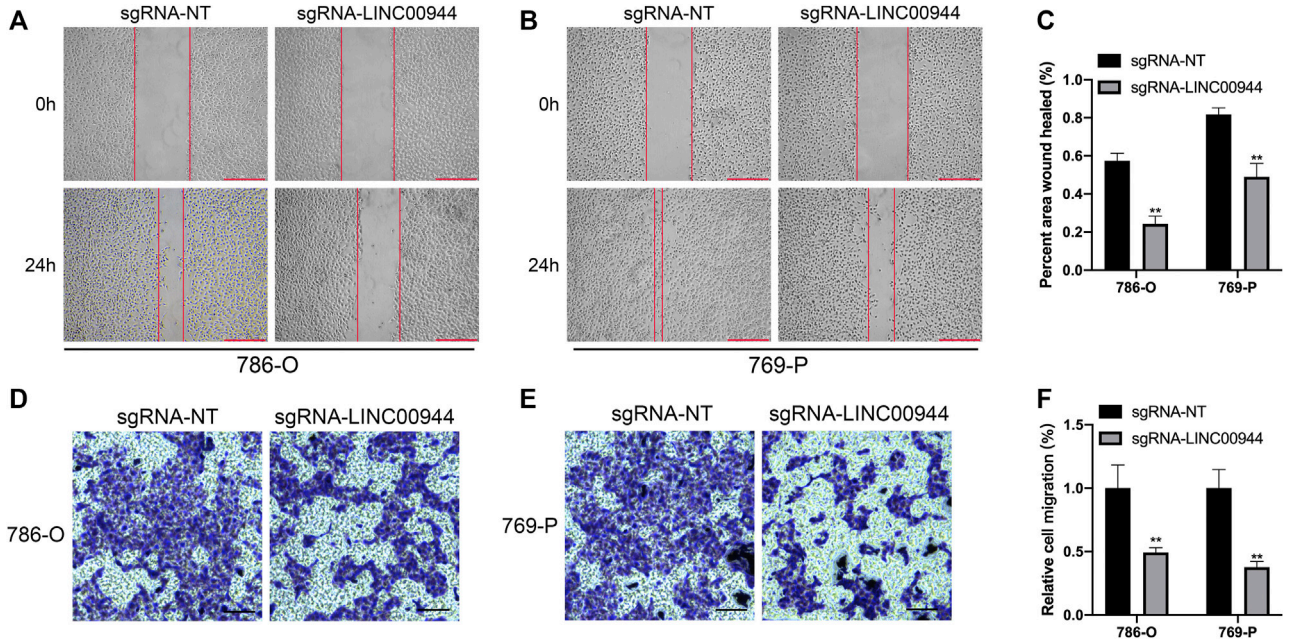

FIGURE 4 | Downregulation of LINC00944 inhibited the migration of RCC cells. **(A–C)** Wound-healing assays for migration ability of 786-O and 769-P RCC cells transfected with dCas9-KRAB and sgRNAs. **(D–F)** Transwell assays for migration ability of 786-O and 769-P RCC cells transfected with dCas9-KRAB and sgRNAs. $^{**}p < 0.01$.

lncRNA LINC00944 could serve as a new therapeutic target for RCC therapy.

METHODS

Cell Culture

The human RCC cell lines 786-O, 769-P, ACHN, OSRC, Caki-1, and Caki-2 and human renal tubular epithelial cell line HK-2 used in this study were all preserved by the Eighth Affiliated Hospital of Sun Yat-sen University. In *in vitro* cell culture and experiment, 786-O, ACHN, and OSRC cell lines were cultured in RPMI-1640 medium (Hyclone), Caki-1 cells were cultured in high-glucose medium (Hyclone), and Caki-2 cells were cultured in McCoy 5A medium (Hyclone). All the above media were supplemented with 10% fetal bovine serum (FBS; Gibco); all cells were incubated in a 37°C chamber containing 95% air and 5% carbon dioxide. In addition, trypsin used in cell culture came from Beijing Solarbio Biological Technology Co., Ltd., and pipette heads, centrifuge tubes, petri dishes, and cryopreserved tubes were all from Coming Company. The other main instruments are used continuously in the laboratory all year round with good performance.

Plasmid Transfection

The plasmids used in this study were synthesized and provided by Beijing Yingmaoxiang Technology Co., Ltd. According to the instructions, dCas9-KRAB and sgRNA-NT or sgRNA-LINC00944 were transfected into 786-O and 769-P cell lines using Lipofectamine 2000 (Invitrogen, United States), and the cells after transfection for 24–48 h were used for the next experiment. After treatment, 786-O and 769-P cell lines were divided into two groups: the experimental group (transfected with sgRNA-LINC00944) and the control group (transfected with sgRNA-NT).

Cell Proliferation Assay

The CCK-8 assay is used to reflect cell proliferation. The untreated cells (about 1×10^5 786-O cells and 2×10^5 769-P cells) were spread into a 60 mm plate and cultured for 24 h; then, the plasmid was transfected into the cells according to the above method. 24 h after transfection, 1,000 cells were spread into 96-well plates, and 100 μL of 10% serum was added to each well, followed by incubation in a 37°C incubator. The 96-well plates to be measured were removed at 0, 24, 48, 72, and 96 h after plate placement, and 20 μL buffer was added to each well (Promega, United States). After further incubation for 2 h, the absorbance values of each well at 490 nm were read using a 96-well plate enzyme-linked immunoreader (BioTek Instruments, United States). The abscissa of absorbance value of cells treated in each period was time, and the ordinate was the absorbance value to draw the cell proliferation curve. The experiment was repeated three times with three replicates each time.

Colony Formation Assay

786-O or 769-P cells were inoculated into six-well plates and transfected with plasmids, respectively. After 36 h of transfection, cells in each group were collected and counted by suspension. Cells in each group were inoculated into six-well plates containing 5 ml medium with 10% fetal bovine serum, with 500 cells in each plate. After 14 days, they were taken out (the

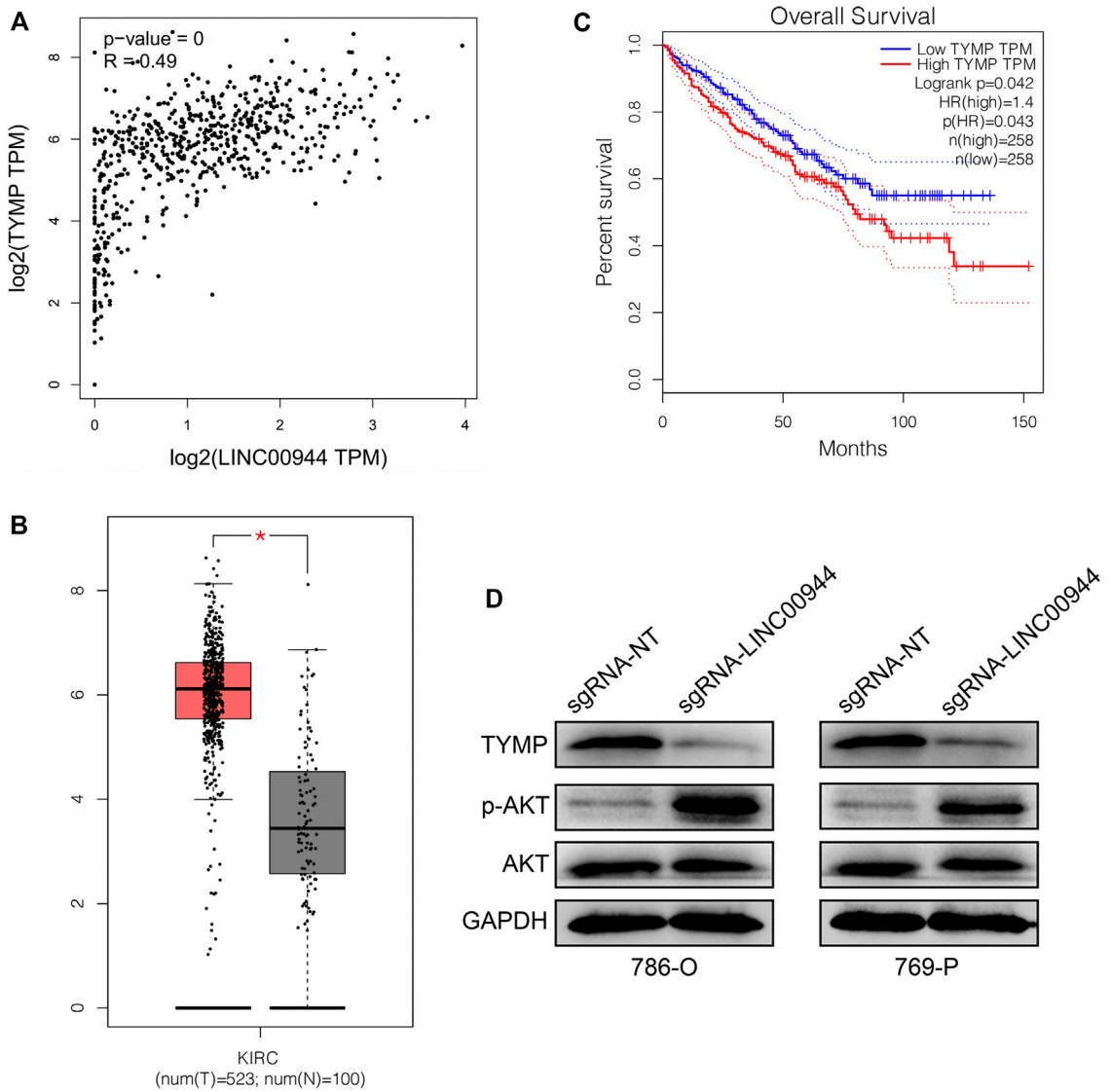

FIGURE 5 | LncRNA LINC00944 regulates TYMP expression and suppresses Akt phosphorylation. **(A)** LINC00944 expression was significantly positively correlated with the expression of TYMP in RCC tissues (data from the TCGA database). **(B)** TYMP expression levels in tumor and adjacent tissues from the TCGA database. **(C)** Kaplan–Meier survival curves of TYMP in RCC tissues from the TCGA database. **(D)** Protein levels of TYMP and Akt phosphorylation in 786-O and 769-P RCC cells transfected with dCas9-KRAB and sgRNAs. *$p < 0.05$.

solution could be changed 1–2 times), fixed with formaldehyde for half an hour, and stained with crystal violet. The number of clones was counted under high magnification (the number of cells per clone should be greater than 50). Each experiment was repeated three times, and three replicates were set for each sample.

Cell Scratch Assay

The scratch test was used to detect cell migration. 2×10^5 786-O or 769-P cells were inoculated into a six-well plate, and 3 ml medium containing 10% serum was added. After the cells were fused into a layer of monolayer cells and covered the bottom of the dish, a 200 μL sterile yellow spear head was used to draw a straight line at the diameter of the dish at a constant speed. The fresh serum-free medium was changed and incubated in a warm box. Photographs were taken at the same location in the same dish 0 and 24 h after scratches. The scratch experiment was repeated three times, and three points were selected from the same dish for measurement each time.

Transwell Assay

After 48 h of cell transfection, the supernatant was discarded and suspended to 10,000 cells/mL, and 200 μL of suspension was added into the upper chamber of the 24-well plate. 500 μL culture medium containing 5% fetal bovine serum was added in the lower chamber, followed by incubation in a warm box for 8–12 h. The

upper chamber and the medium were removed, the upper cells and matrix were wiped out with a clean cotton swab, and the migratory cells were retained on the lower surface of the upper chamber. The cells were fixed with formaldehyde for half an hour, stained with crystal violet for 1 h, rinsed with water for a few seconds, and placed in an oven at 80°C for 30 min, and the number of cells that migrated to or invaded the lower surface was counted under a microscope. Each experiment was repeated three times.

RNA Isolation and Quantitative Real-Time PCR

Total RNA of the cell lines was extracted using Trizol reagent (Invitrogen, CA) and reverse transcribed into cDNA using the One-Step RT-PCR Kit (Beijing Transgen Biotechnology Co., Ltd.) according to the instructions. The expression level of lncRNA was quantitatively detected using a 7500 detection system (Applied Biosystems, Foster City, CA), and the SYBR reagent was purchased from Beijing Transgen Biotechnology Co., Ltd. The reaction system of qRT-PCR was as follows: a 20 μL system consisting of 0.5 μL cDNA, 0.8 μL upstream and downstream mixed primers, 10 μL mix containing SYBR Green, 0.4 μL ROX mixture, and 8.3 μL deionized water. The cycle parameters were as follows: one cycle at 95°C for 60 s and then 40 cycles at 95°C for 5 s and 60°C for 34 s.

Western Blotting

Proteins in cells were extracted according to the instructions of the cell protein extraction kit. According to the instructions of the Western Blot Kit, 80 μg protein was added to each well for SDS-PAGE electrophoresis. After cell electrophoresis, the protein was transferred to the PVDF membrane. The PVDF membrane was sealed with 5% skimmed milk powder, and the primary antibody was incubated in a shaker at room temperature for 2 h. The films were washed with TBST for 3 × 5 min, incubated with a corresponding dilution ratio of secondary antibody for 60 min, and washed with TBST for 3 × 10 min. Enhanced chemiluminescence was performed with GAPDH as the internal reference, and the gray optical density of the relative bands was analyzed with ImageJ software.

Statistical Analysis

Each experiment was repeated three times, and the data were expressed in terms of mean ± standard deviation. All data were analyzed using SPSS 16.0 (SPSS, Chicago, United States), and graphs were drawn using GraphPad Prism 6 (GraphPad Software, San Diego, CA, United States) and Adobe Illustrator (Adobe, United States). *t*-test, ANOVA, Fisher's exact test, chi-square test, and Wilcoxon test were used to determine whether the differences between groups were statistically significant. $p < 0.05$ was considered statistically significant.

DATA AVAILABILITY STATEMENT

The original contributions presented in the study are included in the article/**Supplementary Material**, and further inquiries can be directed to the corresponding author.

AUTHOR CONTRIBUTIONS

CC and HZ were responsible for research design and performing the whole experiment. CC analyzed the data and wrote the manuscript. HZ revised the paper.

SUPPLEMENTARY MATERIAL

The Supplementary Material for this article can be found online at: https://www.frontiersin.org/articles/10.3389/fmolb.2021.697962/full#supplementary-material

REFERENCES

Bukowski, R. M. (2000). Cytokine Combinations: Therapeutic Use in Patients with Advanced Renal Cell Carcinoma. *Semin. Oncol.* 27 (2), 204–212.

Chen, W., Zheng, R., Baade, R. D., Zhang, S., Zeng, H., Bray, F., et al. (2015). Cancer Statistics in China[J]. *CA: a Cancer J. clinicians* 66, 115-32. doi:10.3322/caac.21338

Chiyomaru, T., Fulcuhara, S., Saini, S., Majid, S., Deng, G., Shahryari, V., et al. (2014). Long Non-coding Rna Hotair Is Targeted and Regulated by Mir-141 in Human Cancer Cells. *J. Biol. Chem.* 289 (1 8), 12550–12565. doi:10.1074/jbc.m113.488593

Fachel, A. A., Tahira, A. C., V'tlella-Arias, S. A., Maracaja-Coutinho, V., Gimba, E. P. R., and Vignal, G. M., et al. (2013). Expression Analysis and In Silico Characterization of Intronic Long Noncoding RNAs in Renal Eell Carcinoma: Emerging Functional Associations. *Mol. Cancer*. 2013 Nov 15; 12(1):140. doi:10.1186/1476-4598-12-140

Geisler, S., and Coller, J. (2013). RNA in Unexpected Places: Long Non-coding RNA Functions in Diverse Cellular Contexts. *Nat. Rev. Mol. Cel Biol* 14 (11), 699–712. doi:10.1038/nrm3679

Gupta, K., Miller, J. D., Li, J. Z., Russell, M. W., and Charbonneau, C. (2008). Epidemiologic and Socioeconomic burden of Metastatic Renal Cell Carcinoma (mRCC): A Literature Review. *Cancer Treat. Rev.* 34 (3), 193–205. doi:10.1016/j.ctrv.2007.12.001

Hirata, H., Hinoda, Y, Shahryari, V., Deng, G., Nakajima, K., Tabatabai, Z. L., et al. (2015). Long Noncoding Ma Malatl Promotes Aggressive Renal Cell Carcinoma through Ezh2 and Interacts with Mir-205. *Cancer Res.* 75 (7), 1322–1331. doi:10.1158/0008-5472.can-14-2931

Long, Y., Wang, X., Youmans, D. T., and Cech, T. R. (2017). How Do lncRNAs Regulate Transcription? *Sci. Adv.* 3 (9), eaao2110. doi:10.1126/sciadv.aao2110

Lopez-Beltran, A., Scarpelli, M., Montironi, R., and Kirkali, Z. (2006). 2004 WHO Classification of the Renal Tumors of the Adults. *Eur. Urol.* 49 (5), 798–805. doi:10.1016/j.eururo.2005.11.035

Malouf, G. G., Zhang, J., Yuan, Y., Compérat, E., Rouprêt, M., Cussenot, O., et al. (2015). Characterization of Long Non-coding RNA Transcriptome in clear-cell Renal Cell Carcinoma by Next-Generation Deep Sequencing. *Mol. Oncol.* 9 (1), 32–43. doi:10.1016/j.molonc.2014.07.007

Mercer, T. R., and Mattick, J. S. (2013). Structure and Function of Long Noncoding RNAs in Epigenetic Regulation. *Nat. Struct. Mol. Biol.* 20 (3), 300–307. doi:10.1038/nsmb.2480

Mulders, P., Figlin, R., deKernion, J. B., Wiltrout, R., Linehan, M., Parkinson, D., et al. (1997). Renal Cell Carcinoma: Recent Progress and Future Directions. *Cancer Res.* 57 (22), 5189–5195.

Murai, M., and Oya, M. (2004). Renal Cell Carcinoma: Etiology,incidence and Epidemiology [J]. *Curr. Opin. Urol.* 14 (4), 229–233. doi:10.1097/01.mou.0000135078.04721.f5

Negrier, S., Maral, J., Drevon, M., Vinke, J., Escudier, B., and Philip, T. (2000). Long-term Follow-Up of Patients with Metastatic Renal Cell Carcinoma Treated with Intravenous Recombinant Interleukin-2 in Europe. *Cancer J. Sci. Am.* 6 (Suppl. l), S93–S98.

Novikova, I., Hennelly, S., and Sanbonmatsu, K. (2013). Tackling Structures of Long Noncoding RNAs. *Ijms* 14 (12), 23672–23684. doi:10.3390/ijms141223672

Ørom, U. A., Derrien, T., Beringer, M., Gumireddy, K., Gardini, A., Bussotti, G., et al. (2010). Long Noncoding RNAs with Enhancer-like Function in Human Cells. *Cell* 143 (1), 46–58. doi:10.1016/j.cell.2010.09.001

Pei, C. S., Wu, H. Y., Fan, F. T., Wu, Y., Shen, S.-C., and Pan, Q.-L. (2014). Influence of Curcumin on Hotair-Mediated Migration of Human Renal Cell Carcinoma Cells. *Asian Pac. J. Cancer prevention:APJCP* 15 (10), 4239–4243. doi:10.7314/apjcp.2014.15.10.4239

Qi, P., and Du, X. (2013). The Long Non-coding RNAs, a New Cancer Diagnostic and Therapeutic Gold Mine. *Mod. Pathol.* 26 (2), 155–165. doi:10.1038/modpathol.2012.160

Siegel, R. L., Miller, K. D., and Jemal, A. (2019). Cancer Statistics. *CA Cancer J. Clin.* 69 (1), 7–34. doi:10.3322/caac.21551

Tang, J. Y., Lee, J. C., Chang, Y. T., Hou, M. F., Huang, H. W., Liaw, C. C., et al. (2013). Long Noncoding RNAs-Related Diseases, Cancers, and Drugs. *ScientificWorldJournal* 2013, 943539. doi:10.1155/2013/943539

Wu, Y., Liu, J., Zheng, Y., You, L., Kuang, D., and Liu, T. (2014). Suppressed Expression of Long Non-coding RNA HOTAIR Inhibits Proliferation and Tumourigenicity of Renal Carcinoma Cells. *Tumour Biol. J. Int. Soc. Oncodevelopmental Biol. Med.* 35 (12), 11887–11894. doi:10.1007/s13277-014-2453-4

Yuan, J. H., Yang, F., Wang, F., Ma, Z. J., Guo, J.-Y., Tao, F.-Q., et al. (2014). A Long Noncoding RNAactivated by TGF-Beta Promotes the Invasion-Metastasis cascade in Hepatocellular Carcinoma. *Cancer cell* 25 (5), 666–681. doi:10.1016/j.ccr.2014.03.010

Zhang, H.-M., Yang, F.-Q., and Chen, S.-J. (2015). Upregulation of Long Non-coding Rna Malatl Correlates with Tumor Progression and Poor Prognosis in clear Cell Renal Cell Carcinoma. *Tumour biology:the J. Int. Soc. Oncodevelopmental Biol. Med.* 36 (4), 2947–2955. doi:10.1007/s13277-014-2925-6

Zhou, S., Wang, J., and Zhang, Z. (2014). An Emerging Understanding of Long Noncoding RNAsin Cancer. *J. Cancer Res. Clin. Oncol.* 140 (12), 1989–1995. doi:10.1007/s00432-014-1699-y

Conflict of Interest: The authors declare that the research was conducted in the absence of any commercial or financial relationships that could be construed as a potential conflict of interest.

frontiers in Molecular Biosciences

ORIGINAL RESEARCH
published: 17 August 2021
doi: 10.3389/fmolb.2021.676957

Pacbio Sequencing of PLC/PRF/5 Cell Line and Clearance of HBV Integration Through CRISPR/Cas-9 System

Chia-Chen Chen[1†], Guiwen Guan[1†], Xuewei Qi[1], Abudurexiti Abulaiti[1], Ting Zhang[1], Jia Liu[1], Fengmin Lu[1,2] and Xiangmei Chen[1]**

[1]*Department of Microbiology and Infectious Disease Center, School of Basic Medical Sciences, Peking University Health Science Center, Beijing, China,* [2]*Peking University People's Hospital, Peking University Hepatology Institute, Beijing Key Laboratory of Hepatitis C and Immunotherapy for Liver Diseases, Beijing, China*

OPEN ACCESS

Edited by:
Yonghao Zhan,
Zhengzhou University, China

Reviewed by:
Yun-Tao Zhao,
Aerospace Center Hospital, China
Shaomin Xiao,
Johns Hopkins University, United States
Lanyuan Zhang,
University of Maryland, United States

***Correspondence:**
Xiangmei Chen
xm_chen6176@bjmu.edu.cn
Fengmin Lu
lu.fengmin@hsc.pku.edu.cn

†These authors have contributed equally to this work

Specialty section:
This article was submitted to Molecular Diagnostics and Therapeutics, a section of the journal Frontiers in Molecular Biosciences

Received: *06 March 2021*
Accepted: *01 June 2021*
Published: *17 August 2021*

Citation:
Chen C-C, Guan G, Qi X, Abulaiti A, Zhang T, Liu J, Lu F and Chen X (2021) Pacbio Sequencing of PLC/PRF/5 Cell Line and Clearance of HBV Integration Through CRISPR/Cas-9 System. Front. Mol. Biosci. 8:676957. doi: 10.3389/fmolb.2021.676957

The integration of HBV DNA is one of the carcinogenic mechanisms of HBV. The clearance of HBV integration in hepatocyte is of great significance to cure chronic HBV infection and thereby prevent the occurrence of HBV-related hepatocellular carcinoma (HCC). However, the low throughput of traditional methods, such as Alu-PCR, results in low detecting sensitivity of HBV integration. Although the second-generation sequencing can obtain a large amount of sequencing data, but the sequencing fragments are extremely short, so it cannot fully explore the characteristics of HBV integration. In this study, we used the third-generation sequencing technology owning advantages both in sequencing length and in sequencing depth to analyze the HBV integration characteristics in PLC/PRF/5 cells comprehensively. A total of 4,142,311 cleaning reads was obtained, with an average length of 18,775.6 bp, of which 84 reads were fusion fragments of the HBV DNA and human genome. These 84 fragments located in seven chromosomes, including chr3, chr4, chr8, chr12, chr13, chr16, and chr17. We observed lots of DNA rearrangement both in the human genome and in HBV DNA fragments surrounding the HBV integration site, indicating the genome instability causing by HBV integration. By analyzing HBV integrated fragments of PLC/PRF/5 cells that can potentially express HBsAg, we selected three combinations of sgRNAs targeting the integrated fragments to knock them out with CRISPR/Cas9 system. We found that the sgRNA combinations could significantly decrease the level of HBsAg in the supernatant of PLC/PRF/5 cells, while accelerated cell proliferation. This study proved the effectiveness of third-generation sequencing to detect HBV integration, and provide a potential strategy to reach HBsAg clearance for chronic HBV infection patients, but the knock-out of HBV integration from human genome by CRISPR/Cas9 system may have a potential of carcinogenic risk.

Keywords: HBV integration, PLC/PRF/5, third-generation sequencing, pacbio, HBsAg clearance, CRISPR/Cas9

INTRODUCTION

Hepatocellular carcinoma (HCC) is one of the most aggressive human cancers which currently ranks the fourth leading cause of cancer-related deaths worldwide (Petrick et al., 2020). The major risk factors for HCC include infection with hepatitis B virus (HBV) and hepatitis C virus (HCV), exposure to aflatoxins, alcohol abuse, and non-alcoholic steatohepatitis (Baecker et al., 2018). The integration of HBV in the human genome is considered to be one of the key mechanisms of HBV carcinogenesis (D'Souza et al., 2020). However, the characteristics of integration, its functions, and the clinical implications are still not fully understood.

The detection of HBV integration is the basis of all HBV integration research. In the early 1980s, HBV DNA integration was firstly found in the human chromosome of PLC/PRF/5 cell line (Edman et al., 1980). Subsequently, a series of studies confirmed HBV DNA is randomly inserted into the human genome in HBV-infected liver tissues, including acute hepatitis B, chronic hepatitis B, cirrhosis and especially HCC (Jiang et al., 2012; Li et al., 2014). Previously, Southern blot, FISH (fluorescence *in situ* hybridization) and Alu-PCR have been used to detect HBV integration, but due to the low throughput, these methods are less sensitive. With the development of next-generation sequencing (NGS), many studies have achieved genome-wide surveys of HBV integration in HCC, and a great deal of data on the HBV pathogen in HCC has been obtained. However, NGS-based integration discovery is limited by the reads length, especially for long complex structural variations (Zhao et al., 2016a). The third-generation sequencing (TGS) technology developed in recent years not only has extremely high sequencing throughput, but also generate reads up to 60 kbp long (Rhoads and Au, 2015), showing a good potential for detecting HBV integration.

Studies have shown that the integrated HBV genome can express viral proteins, such as HBsAg and HBx (Natoli et al., 1992; Tu et al., 2001). Among them, HBsAg is not only a serological marker of HBV infection, but also associated with the occurrence of HCC. Because existing antiviral therapy does not target HBV integration, the integration of HBV sequence expression of HBsAg is also one of the reasons why CHB patients are difficult to achieve clinical cure (Moucari et al., 2009). Although studies have shown that siRNA can effectively knock down the HBsAg level in PLC/PRC/5 cell lines, this technology cannot eliminate the integrated HBV genome (Li et al., 2004). CRISPR/Cas (clustered regularly interspaced short palindromic repeat/CRISPR associated Cas) is considered a breakthrough technology of genome editing, mainly because of its high effectiveness and technical simplicity (Lin et al., 2014). The earlier results in our laboratory have confirmed that CRISPR/Cas9 technology can eliminate HBV cccDNA effectively, and we have designed a series of sgRNA targeting HBV genome (Wang et al., 2015; Wang et al., 2017), but whether it can effectively knock out HBV integration is yet to be revealed.

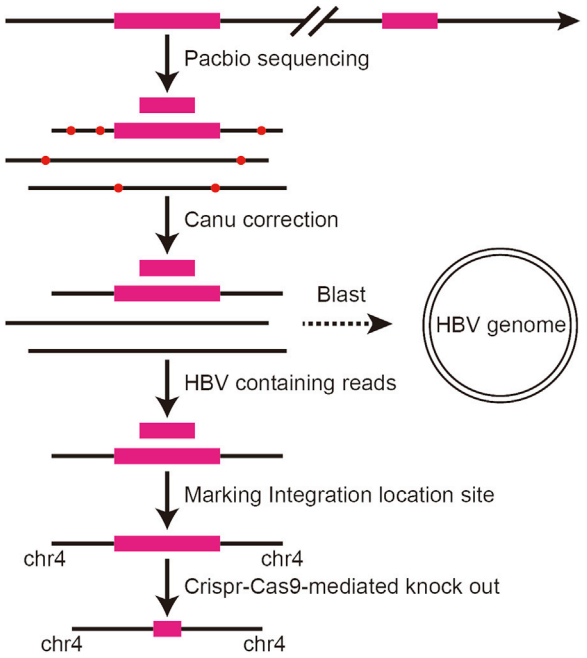

FIGURE 1 | Analysis flow chart of HBV integration in PLC/PRF/5 cells.

To gain a comprehensive panorama of HBV DNA integration of PLC/PRF/5 cell line in a more unbiased way, this study directly sequenced the DNA of PLC/PRF/5 cells using the whole genome TGS technology. In addition, the CRISPR/Cas9 technology was used to knock out the S genes in the HBV DNA integrated fragments, so as to inhibit HBsAg expression in PLC/PRF/5 cells. This study provides a more accurate and comprehensive information of HBV integration in PLC/PRF/5 cells and a new idea for the HBsAg clearance from HBV integration genome.

RESULTS

Detection of Hepatitis B Virus Integration in PLC/PRF/5 Cell Line Using Third-Generation Sequencing Technology

We applied the third-generation sequencing technology to scan the HBV integration site at the whole genome level in PLC/PRF/5 cells, and the analysis flow chart is shown in **Figure 1**. In brief, the DNA extracted from PLC/PRF/5 is sequenced by the Pacbio platform, and then the correction module of the Canu software was used for row reads correction. Next, the reads were mapped to the HBV genome and the HBV containing reads were extracted by using of BLAST. Finally, the TSD software was used to analyze the HBV integration sites.

The PLC/PRF/5 pacbio raw sequencing data contained 5,770,093 reads, totaling 99.3 billion bases, and the average sequencing depth was about 33.1 times. By the correction of Canu, we finally obtained 4,142,311 reads, totaling 77.7 billion bases, and the average sequencing depth was about 25.9 times.

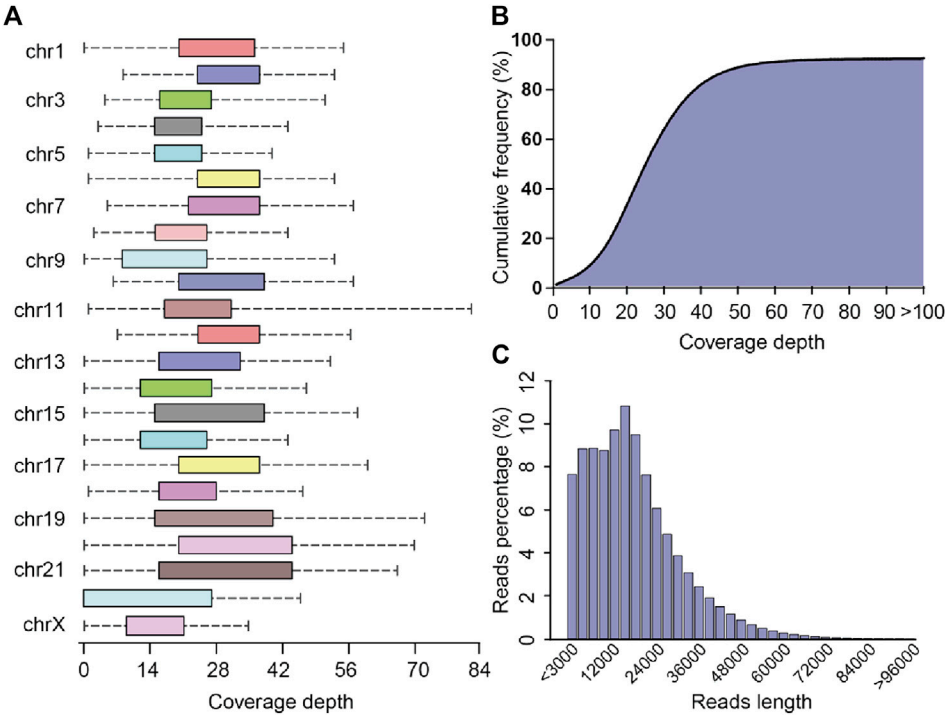

FIGURE 2 | Sequencing coverage and reads length distribution plots **(A)** Box plot of sequencing coverage of each chromosome. **(B)** Cumulative percentage plots of coverage depth for the whole genome, the *x*-axis represents the coverage depth, and the *y*-axis represents the percentage of bases that reach this coverage depth level. **(C)** Distribution diagram of reads length.

After mapping with the human reference genome, the coverage of cleaning reads in chr2, chr3, chr4, chr7, chr8, chr10, and chr12 reached 100%, while the coverage of chr22 was the lowest, about 71.7% (**Figure 2A**). Overall, the coverage of the whole genome by sequencing data reached 91.7%. (**Figure 2B**). The maximum length of the reads is 120445 bp, and the average reads length is 18,775.6 bp (**Figure 2C**). The above result shows that the quality and coverage of this sequencing reached the downstream analysis requirements.

Hepatitis B Virus Integration Profiles in PLC/PRF/5 Cells

After mapping with HBV and the human genome, we obtained 84 HBV-human genome fusion reads in PLC/PRF/5 cell line, with reads length range 5,067–119,485 bp (**SupplementaryTable S1**). These reads are located on 7 chromosomes including chr3, chr4, chr8, chr12, chr13, chr16 and chr17 (**Figure 3**). The reads located at chr4, chr8, chr16 and chr17 contain at least one read that both the 3 end and 5 end are human genome thereby we called it complete sequence. For the reads located on chr3, although we did not find the complete sequence, we found two types of reads, one is HBV fragment at the 3 end and the other is HBV fragment at the 5 end. Therefore, for the above five chromosomes, we confirmed both the upstream and downstream integration sites of HBV DNA. As for chr12 and chr13, we can only confirm the downstream site of HBV integration.

The integration of HBV often causes genome instability. Previous studies could not fully explore this problem due to the limitation of sequencing length. Based on the advantages of the third-generation sequencing length, we comprehensively analyzed the instability of HBV integration fragment and the nearby human genome. In chr3 and chr16, we observed about 1400 and 12 bp human genome fragment deletions near the HBV integration site, respectively (**Figure 3**; **Supplementary Figure S1**). In chr4, a large-scale genome amplification was observed, and the amplified fragments of each reads are not the same. It is worth noting that in chr4, the insertion direction of the copy number amplified fragment is opposite to the original direction of the genome (**Figure 3**; **Supplementary Figure S1**). In chr17, we found two types of reads, one of which contained about 1800 bp human genome deletion near the insertion site, and another type contained about 14600 bp human genome amplification (**Figure 3**; **Supplementary Figure S2**). In chr8, the sequence upstream of the HBV insertion site cannot be mapped to the human genome. The sequence similarity comparison shows that the homology of this fragment with chr8 is 72%, and the homology with chr1 is 79% (**Figure 3**). In addition, viral genome rearrangements including deletions, inversions and duplications were also observed. For example, the end of the integration fragment in chr12 is located at positions 814 nt–816 nt of the HBV genome, with a difference of 3 bp, and the end of the integration fragment in chr13 is located at 1673 nt–1799 nt of the HBV genomes, with a difference of more

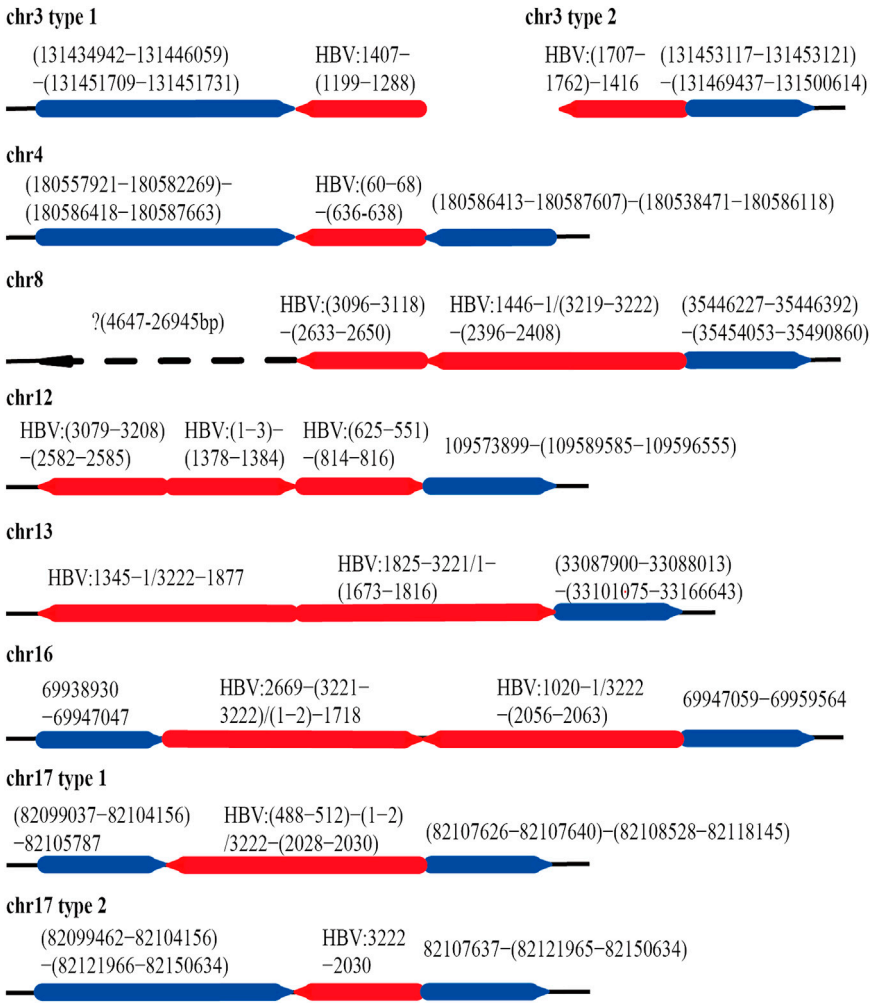

FIGURE 3 | HBV integration pattern plots of PLC/PRF/5 cell line. The red line represents the HBV genome, the blue line represents the human genome, the direction of the arrow represents the direction of the sequence, and the dashed line represents the sequence not mapping to the human reference genome.

than 100 bp. In chr17, there is a big difference in the length of the HBV integration fragment, the shortest one is 1192 bp, and the longest one is 1706 bp (**Figure 3**; **Supplementary Figure S2**). The above results indicate that the human genome and HBV genome nearby the integration site contain many structural variations, suggesting that HBV integration increases the genome instabilities in both the HBV integrated fragment and the nearby human genome.

Distribution of Hepatitis B Virus Integration Fragment Breakpoints and Its Homology With Human Chromosomes

Previous study shows that HBV breaks mainly at the DR1 and DR2 regions and integrates into human genome (Li et al., 2014). We also analyzed the distribution of the HBV integration breakpoints of the 84 HBV containing reads in PLC/PRF/5 cells. A total of 116 HBV breakpoints were identified and the distribution of these breakpoints is shown in **Figure 4A**. We found that rather than concentrated in the DR1 and DR2 regions, the HBV breakpoints of PLC/PRF/5 distributed randomly throughout the HBV genome.

Next, we explored the homology of the HBV genome and sequencing of the host cell genome close to the viral-host junction revealed 52 (44.8%) microhomology connections among 116 HBV breakpoints between the HBV fragment and the human genome in chr3, chr4, chr8, chr13, and chr17. Among them, the micro homologous sequences in chr3 are AGAA and GGAC, in chr4 are GTAATT and ACCAG, in chr8 are ATTT, in chr13 are CGACAT, in chr16 are TACAGC and GCTGTA, and in chr17 are CCT and AGG (**Figure 4B**).

Host Genes Around the Hepatitis B Virus Integration Sites

Previous studies by us and other teams have confirmed that HBV integration can affect the expression of genes near the integration site through a variety of mechanisms, which is one of the

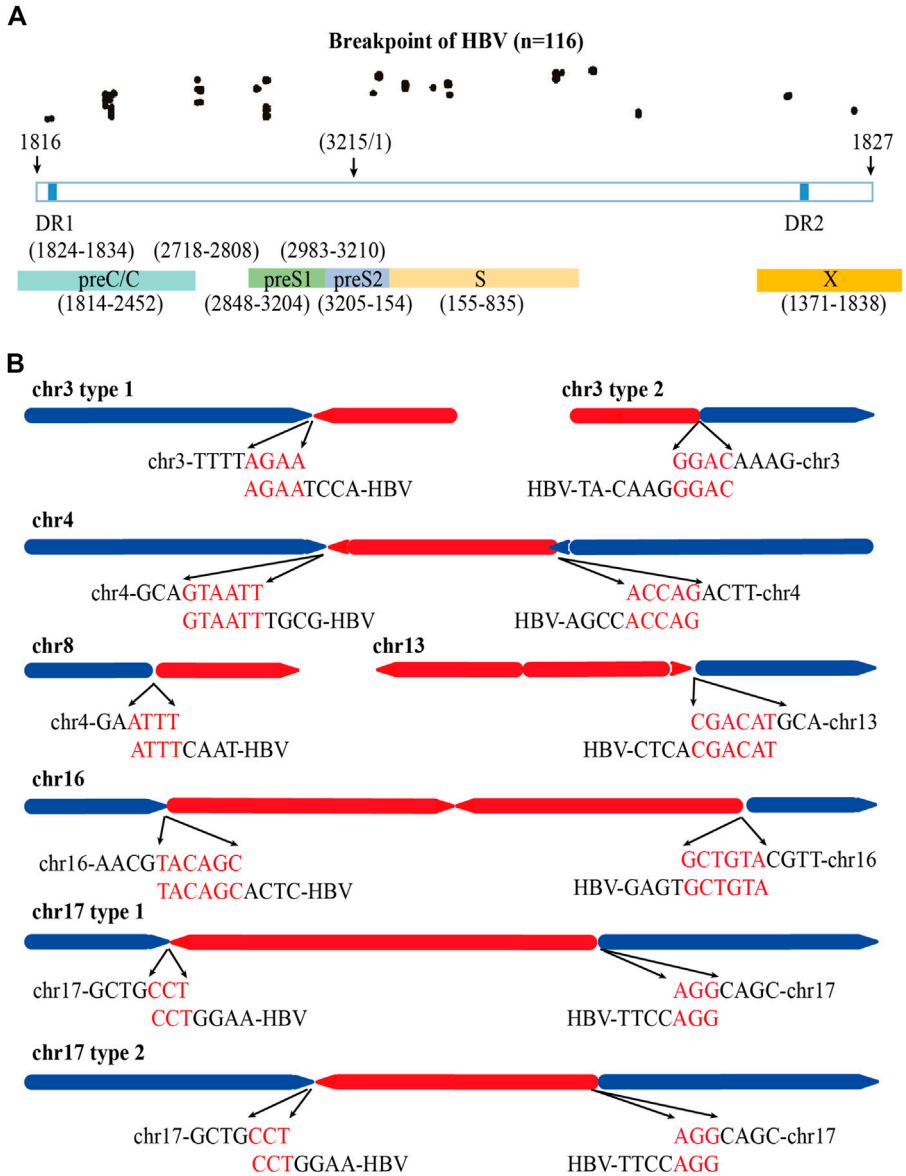

FIGURE 4 | Distribution of HBV integration fragment breakpoints and its homology with human chromosomes. **(A)** Distribution of HBV integration fragment breakpoints in HBV genome. **(B)** Homology analysis of virus-host junction sequences in HBV integration events. The red line represents the HBV genome, the blue line represents the human genome, the direction of the arrow represents the direction of the sequence, and the red words represents microhomology connections of HBV DNA and human genome.

carcinogenic mechanisms of HBV integration (D'Souza et al., 2020). We analyzed the genes within 100 kb upstream and downstream of the HBV integration sites in PLC/PRF/5 cells. There are 27 genes in the upstream of HBV integration sites and 13 genes in the downstream of HBV integration sites, with a total of 43 potential target genes. Among the 43 genes, 23 genes were protein coding genes, 9 genes were non-coding RNA, 3 genes were miRNA and 8 genes were pseudogenes (**SupplementaryTable S2**). This result suggested that there were a large number of host functional genes around HBV integration sites that might be affected by HBV integration.

Expression Potential of Viral Proteins by the Integrated Hepatitis B Virus Fragment

The integrated HBV fragments have the potential to express HBV proteins or HBV-human fusion proteins (Edman et al., 1980; D'Souza et al., 2020;). According to the sequencing results, we analyzed the possible viral proteins expressed by the integrated fragments in PLC/PRF/5 cells. The analysis results showed that the integrated fragments located in chr12, chr13, chr16, and chr17 have the potential to express HBsAg. Moreover, the integrated fragments located in chr13 and chr16 also have the potential to express truncated HBx (**Figure 5**). In consistent with

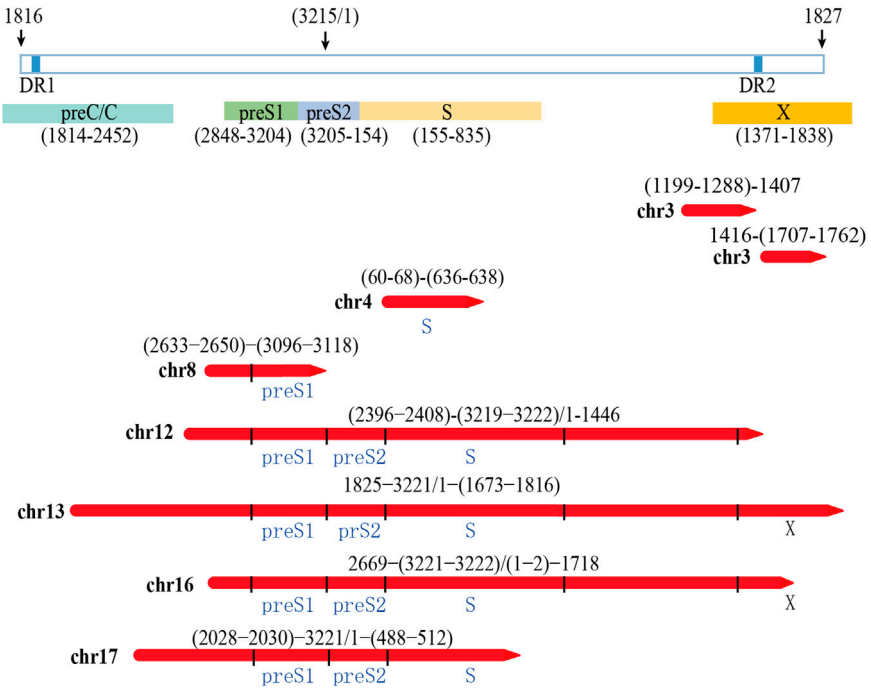

FIGURE 5 | Analysis of the possibility of integrating HBV fragment sequences expressing HBV viral proteins

these analyses, we can detect the expression of HBsAg in the supernatant of PLC/PRF/5 cells, which reached 1.796 IU/mL.

Knock-Out of Integrated Hepatitis B Virus Genes by CRISPR/Cas9 System in PLC/PRF-5 Cells

Our previous studies have designed 15 gRNAs against HBV genome and demonstrated these gRNAs could specifically destroy HBV expressing template, thereby inhibited HBV replication (Wang et al., 2015). To eliminate HBsAg in PLC/PRF/5 cell lines, we selected sgRNA2, sgRNA3 and sgRNA7 from our previous studies and the targeting sites of these sgRNA in integrated HBV fragments are shown in **Supplementary Figure S3**. For better knocking out the integrated preS/S gene fragments in the PLC/PRF/5 cell genome, the HBV specific gRNA/Cas9 plasmids containing sgRNA2, sgRNA3 and sgRNA7 were combined in pairs for transient transfection. To determine whether the paired gRNA can successfully knock out the target HBV integration fragments, two pairs of PCR primers were designed respectively in the upstream and downstream of sgRNA, and the target sites of the primer are shown in the **Supplementary Figure S3**.

In PLC/PRF/5 cells, after transfection of HBV specific gRNA/Cas9 plasmids expressing sgRNA2+3, sgRNA3+7 and sgRNA2+3 + 7, the expected small bands were observed by using PCR assay (**Figure 6A**). No obvious off-target effects were observed in the predicted off-target sites corresponding to the three sgRNAs by using the T7 endonuclease I assay (**Figure 6B**). The sequencing of these small bands showed that the integrated HBV fragments were indeed cut at the expected sites and the integrated HBV fragments were knocked out (**Figures 6C,D**). Most importantly, the HBsAg level in the supernatant was significantly decreased in these PLC/PRF/5 cells with integrated S genes knocked-out (**Figure 6E**). Unexpectedly, we noticed that no matter which sgRNA combination, after sgRNAs transfection, the proliferation rate of PLC/PRF/5 cells was significantly faster than that of the control group (**Figure 6F**). We also performed the same knock-out assays with same sgRNA combination together with 1.2 mer HBV plasmid in Huh7 cells. We found that the sgRNA combination could significantly knocked out HBV S gene and downregulated HBsAg level in Huh7 cells, demonstrating that the combined HBV specific gRNA/Cas9 plasmids could efficiently decline HBV expressing templates (**Supplementary Figure S4**). Taken together, these results suggested that CRISPR/Cas9 system could effectively knock out the S gene from the integrated genome, but it might accelerate cell proliferation of hepatocytes.

DISCUSSION

HBV integration is regarded as a pivotal process of HBV infection to induce liver cancer. In this study, we detected the HBV integration profiles at the whole genome level in PLC/PRF/5 cells by using the whole genome TGS technology. This method is a novel technique that overcomes the low-throughput shortcomings of sanger sequencing and also overcomes the

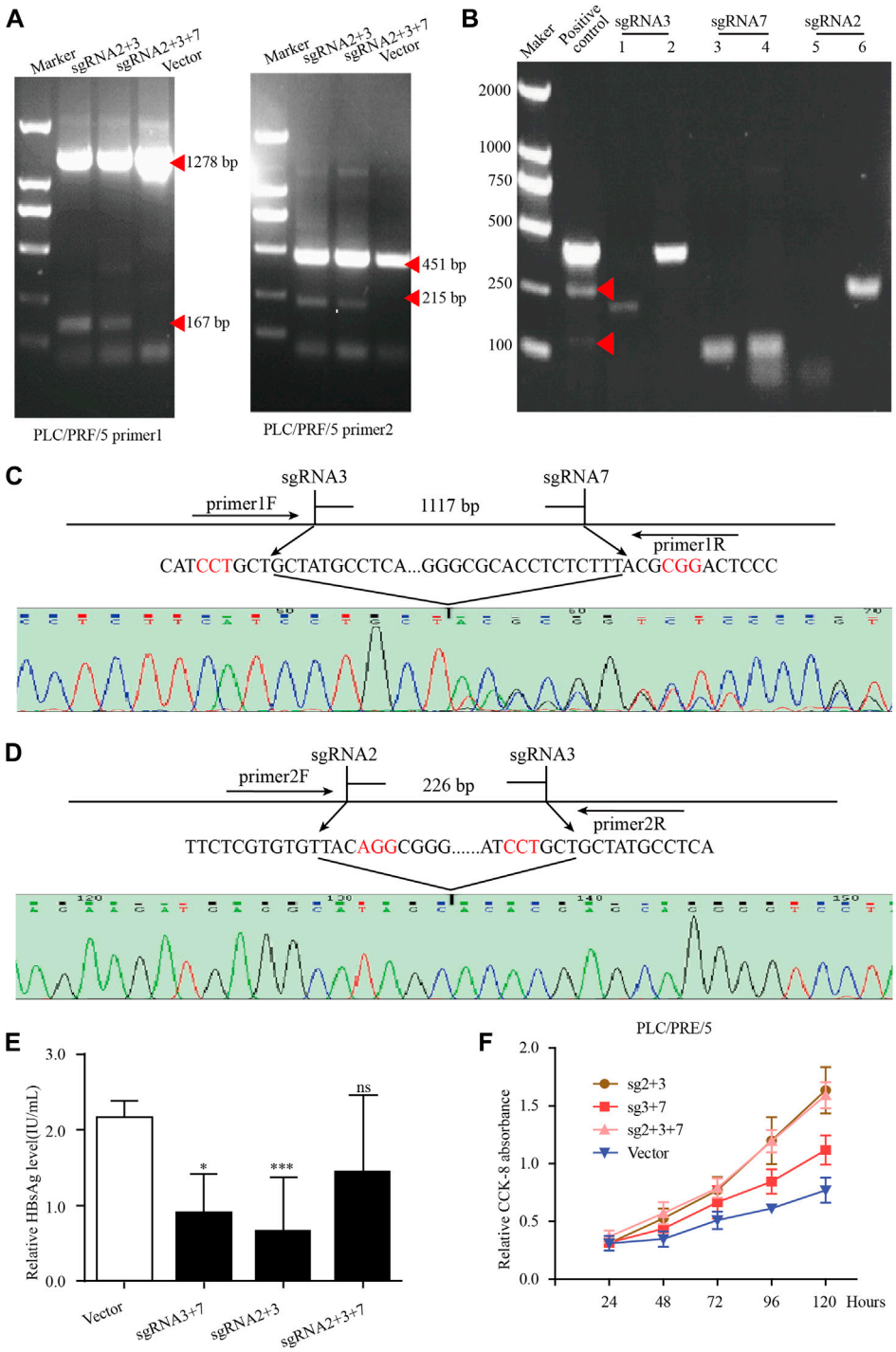

FIGURE 6 | The knockout of integrated HBV S gene by CRISPR/Cas9 system in PLC/PRF/5 cells. **(A)** The plasmid pBB4.5-HBV1.2 (0.5 μg) was co-transfected with gRNA2+3, gRNA3+7 and gRNA2+3+7 expression vectors (each 0.75 μg) to PLC/PRF/5 cells. Cellular DNA was extracted at 72 h post transfection, and PCR amplifications were performed using the primers beyond the cleavage sites of each dual gRNAs. **(B)** The off-target effect of sgRNA was detected by T7 endonuclease I assay. Each sgRNA detected the two most likely off-target sites. **(C–D)** Sequencing analysis of the smaller fragment formed by sgRNA3+7 and sgRNA2+3. **(E)**. HBsAg level in culture supernatant was measured by using an enzyme-linked immune sorbent assay. Data are shown as mean ± SE of 3 independent samples. Statistical method: *t* test (two-side), * means $p < 0.05$, ** means $p < 0.01$,*** means $p < 0.001$. **(F)** The cell proliferation of PLC/PRF/5 cells after transfecting different sgRNA plasmids. Cells transfected with empty PX458 plasmid were used as control group. Data are shown as mean ± SE of 3 independent samples. Statistical method: *t* test (two-side).

short reads shortcomings of the NGS. Our sequencing data will help researchers to have a more comprehensive understanding of the genome characteristics of PLC/PRF/5, the most classic cell model for studying HBV integration. In addition, using CRISPR/Cas9 system, we knocked out the integrated HBV S fragment and decreased HBsAg level in PLC/PRF/5 cells, suggested the potential use of CRISPR/Cas9 genome editing technique to cut integrated HBV DNA, as well as for function cure of chronic hepatitis B patients.

As early as the 1980, researchers have found that PLC/PRF/5 cell line genome contains HBV genome integration (Edman et al., 1980). Since then, the HBV integration of PLC/PRF/5 cell line had been successively detected by Northern blot, FISH, Alu-PCR and NGS technology (Jiang et al., 2012; Li et al., 2013; Watanabe et al., 2015; Ishii et al., 2020). Although researchers used the HBV-specific probe capture technology to improve the sensitivity of HBV DNA detection and found that PLC/PRF/5 has HBV integration on chromosomes 3, 4, 5, 8, 10, 11, 12, 13, 16, 17, 19 (Li et al., 2013; Watanabe et al., 2015; Ishii et al., 2020), there were selective bias in this technology so that it is impossible to have a comprehensive analysis of the characteristics of PLC/PRF/5 HBV integration. Meanwhile, it is hard to analyze the complex variation of the genome sequence surrounding the HBV integration sites through NGS because the length of the sequencing fragment was only 100 bp. In this study, we directly sequenced the DNA of PLC/PRF/5 cell which made the maximum length of the sequencing segment reach 150 kbp. The longest HBV integrated fragment detected in this study was as long as 40 kbp. Therefore, the results of this study can not only detect HBV integration in PLC/PRF/5 cell lines without bias but also made an in-depth analysis of the structural variation of the upper and lower host genome. We successfully detected HBV integration on chromosomes 3, 4, 8, 12, 13, 16, and 17 in PLC/PRF/5 cell line through the whole genome TGS technology. From the perspective of detection sensitivity, our method is much higher than Northern blot, FISH, Alu-PCR, and even has the same sensitivity as the targeted captured NGS technology, proving that the whole genome TGS technology is a powerful method for detecting the HBV integration.

Studies have shown that HBV integration affects the genetic stability near the integration site, which is one of the reasons for HBV integration to cause cancer (Sung et al., 2012). Since the whole genome TGS technology can obtain longer integration fragments, it is more suitable for the analysis of rearrangement of integrated HBV sequence and the local host genome sequence surrounding integration sites. In this study, we found that there are many viral DNA rearrangements in the integrant including deletions, inversions and duplications of HBV sequence. In addition, sequences of host genome near the viral-host junction also has also undergone structural changes. Additionally, despite the fact that previous studies have showed the breakpoint of HBV integration concentrated between DR1 and DR2 (Li et al., 2014) due to the features of dslDNA which is the major source of the HBV integration (Tu et al., 2017), in this study, we observed that the breakpoints of HBV integration in PLC/PRF/5 cell lines are randomly distributed. All these results indicate that HBV integration will lead to the instability of the genome near the integration site which was contributed to the pathogenesis of HCC, while the long-term host DNA repair during tumor cell proliferation exacerbate the genetic instability in host cells. Besides genetic instability, we also observed that about 45% of the viral-host junctions sites in PLC/PRF/5 cell connect to the human genome were microhomology connections contained a short homologous region between HBV integration fragments and the human genome sequences. It is consisted with the previous studies that proposed homologous end joining is the major source for HBV to integrate into the human genome (Zhao et al., 2016b) (Zhao et al., 2016b) (Zhao et al., 2016b) (Zhao et al., 2016b).

In recent years, quantitated serum HBsAg has been becoming an important viral marker for evaluating the response to antiviral therapy, and the seroclearance of HBsAg is regarded as the most reliable indicator for functional cure by several major guidelines (Sarin et al., 2016). A large number of studies have confirmed that the HBV sequence integrated into the genome has the potential to express HBV protein (Sung et al., 2012). Therefore, serum HBsAg can be produced from both HBV cccDNA and the integrated HBV S gene in patients with HBV integration. Especially in the HBeAg-negative group, the main source of serum HBsAg was mainly derived from integrated HBV fragments (Wooddell et al., 2017). Because the current antiviral drugs could not eliminate HBsAg production originated from the integrated HBV S gene, it is very difficult to obtain serum HBsAg loss even if prolonging nucleos(t)ide analogue (NUC) therapy. It has been demonstrated that CHB patients who achieve HBsAg seroclearance have reduced risks of HCC development (Liu et al., 2016). Therefore, effective strategies to eliminate integrated HBV DNA fragment-derived HBsAg should be developed. In PLC/PRF/5 cells, we found that the integration of HBV located in chr13, chr16, and chr17 in lines has the potential to express HBsAg. Based on the sequences of these integrated HBV DNA fragments, we selected three CRISPR/Cas9-sgRNA combinations to target HBV S gene in PLC/PRF/5 cells. The results showed that all our CRISPR/Cas9-sgRNA combinations could effectively reduce the HBsAg level in the PLC/PRF/5 cell supernatant, proving that CRISPR/Cas9 system could effectively eliminate HBV integration. The previous results in our laboratory have confirmed that the transfection of these CRISPR/Cas9-sgRNA plasmid did not affect the proliferation rate of Huh-7 cells when co-transfecting HBV plasmids (Wang et al., 2017). Surprisingly, in this study we found that the proliferation rate of PLC/PRF/5 cells increased significantly after transfection of the three CRISPR/Cas9-sgRNA combinations, suggested that the potential dangers of CRISPR/Cas9 need to be carefully considered.

We speculate that the cleavage of chromosomally integrated HBV DNA may trigger unpredictable consequences of chromosomal DNA recombination which induce cell proliferation. In addition, there are a large number of host

functional genes located within 100 kb upstream and downstream of the HBV integration sites in PLC/PRF/5 cells. Whether these genes could be affected by the cut of integrated HBV DNA and thereby accelerate PLC/PRF/5 cell proliferation need be further explored.

In summary, our study provided a comprehensive panorama of HBV DNA integration profile of PLC/PRF/5 cell line, which is of great significance for us to fully understand the characteristics and mechanisms of HBV integration. In addition, under the guidance of the sequencing results, we successfully reduced the HBsAg level of PLC/PRF/5 through the CRISPR/Cas9 system, suggested that the cleavage of chromosomally integrated HBV DNA might be a new therapeutic approach for the clearance of HBsAg for CHB patients. However, the potential dangers of this approach must be further explored.

MATERIALS AND METHODS

The Third-Generation Sequencing and Data Analysis

DNA was extracted from PLC/PRF/5 cell line using DNeasy Plant Mini Kit (Qiagen, Dusseldorf, Germany) according to the manufacturer's instructions and the quality of the extracted DNA was evaluated by agarose gel electrophoresis. Then DNA was commissioned to conduct subsequent DNA quality assessment, library construction, and third-generation sequencing by Annoroad Inc (Beijing, China). The sequencing platform was PacBio Sequel II. Through SMRTLink (v4.0) we converted the BAM format files into fastq format files. Next, the Canu (v2.0, default parameter) software (Koren et al., 2017) was used to clean and correct the fastq files. The coverage statistics of the sequencing were completed using the stats module of samtools (v1.9, default parameter) (Li et al., 2009). The cleaned and corrected reads were mapped with HBV A genotype by BLAST to obtain HBV containing reads. TSD software (Meng et al., 2019) was used to analysis the HBV integration site and hg19 was used as the reference genome. The genes around 100 kb upstream and downstream of the HBV integration site were searched on the NCBI website (https://www.ncbi.nlm.nih.gov/).

Plasmids and Transfection

The 1.2xHBV plasmid was constructed using a 1.2-fold length HBV genome and pBB4.5 plasmid. The gRNA/Cas9 dual expression vector pSpCas9(BB)-2A-GFP (PX458) was obtained from Addgene (Cambridge, MA). The oligonucleotide sequences for the construction of HBV-specific gRNA/Cas9 expression vectors are listed in **SupplementaryTable S3**. The construction method was described in the previous research of our lab (Wang et al., 2015).

PLC/PRF/5 and Huh-7 cells were maintained in Dulbecco's Modified Eagle Medium (DMEM) supplemented with 10% fetal bovine serum (Gibco, Maryland, United States). Before transfection, cells were seeded into a 12-well plate at 1.5×10^5 cells/well. 24 h later, Huh-7 cells were co-transfected with HBV expression plasmid and HBV-specific gRNA/Cas9 dual expression plasmids with Lipofectamine 2000 (Invitrogen, New York, United States) for 72 h. PLC/PRF/5 cells were transfected with HBV specific gRNA/Cas9 dual expression plasmids with Lipofectamine 2000 for 72 h.

Testing the Deletion of the Integrated Hepatitis B Virus S Gene Induced by CRISPR/Cas9

After the CRISPR/Cas9 plasmid transfecting, genomic DNA from PLC/PRF/5 or Huh7 cells were amplified by PCR using unique primers designed to span the expected knockout positions and the primers are listed in **SupplementaryTable S4**. The PCR products were gel purified and then sequenced by conventional Sanger sequencing. Off-target sites were predicted using website http://crispr.mit.edu/ and identified with T7E1 assay system as described in our previous studies (Liang et al., 2015). Primers for amplifying three sgRNAs off-target sites were shown in **SupplementaryTable S5**.

Detection of HBsAg

Cell culture supernatants were collected for detection of HBsAg by a time-resolved fluoroimmunoassay according to manufacturer's instructions (PerkinElmer, Waltham, MA). In brief, culture supernatant (100 μl) was added into a microtiter plate coated with anti-HBsAg and shook for 40 min at room temperature, then washed for four times. Europium-labeled anti-HBsAg was diluted 1:50 with HBsAg or HBeAg dilution buffer and added at 100 μl per well, shook for 40 min in room temperature, then washed six times. At last, after incubation with enhancement solution (100 μl) for 5 min, the plates were read using Anytest reader (SYM-BIO, Washington, United States), and the concentrations of HBsAg were calculated according to the standard curve. The relative HBsAg level was calculated as the ratio of HBsAg concentration in the cell culture supernatant of gRNA treated and vector control cells.

Cell Counting Kit-8 Cell Proliferation Assay

Cell viability was evaluated using the Cell Counting Kit-8 (CCK8) assay (Dojindo, Japan) according to the manufacturer instruction. Cells were plated at a density of 1×10^3 cells per well in 96-well plates for culturing 1, 2, 3, 4 and 5 days. At the indicated times, 10 μl CCK8 solution was added to each well and incubated at 37°C temperature. The absorbance was assessed at a 450 nm wavelength under a plate reader (Bio-Rad Laboratories, California, United States) after 2 h. All experiments were performed in triplicate.

Statistical Analysis

The difference comparison of quantitative data is done by *t*-test using GraphPad Prism 5 software. *p*-value that less than 0.05 was considered statistically significant.

DATA AVAILABILITY STATEMENT

The data presented in the study are deposited in the SRA (www.ncbi.nlm.nih.gov) repository, accession number (PRJNA717995).

AUTHOR CONTRIBUTIONS

XC and FL designed the study. C-CC, GG, XQ, AA, TZ, and JL carried out the experiments. C-CC and GG analyzed the data. C-CC, GG, XQ, XC, and FL wrote the manuscript.

FUNDING

This work was supported by the Natural Science Foundation of China (No. 81572366), and the National S&T Major Project for Infectious Diseases of China (No. 2017ZX10202203).

ACKNOWLEDGMENTS

We thank Professor Ence Yang from Peking University for his supporting on third-generation sequencing analysis.

SUPPLEMENTARY MATERIAL

The Supplementary Material for this article can be found online at: https://www.frontiersin.org/articles/10.3389/fmolb.2021.676957/full#supplementary-material

REFERENCES

Baecker, A., Liu, X., La Vecchia, C., and Zhang, Z.-F. (2018). Worldwide Incidence of Hepatocellular Carcinoma Cases Attributable to Major Risk Factors. *Eur. J. Cancer Prev.* 27 (3), 205–212. doi:10.1097/cej.0000000000000428

D'Souza, S., Lau, K. C., Coffin, C. S., and Patel, T. R. (2020). Molecular Mechanisms of Viral Hepatitis Induced Hepatocellular Carcinoma. *World. J. Gastroentrol.* 26 (38), 5759–5783. doi:10.3748/wjg.v26.i38.5759

Edman, J. C., Gray, P., Valenzuela, P., Rall, L. B., and Rutter, W. J. (1980). Integration of Hepatitis B Virus Sequences and Their Expression in a Human Hepatoma Cell. *Nature* 286 (5772), 535–538. doi:10.1038/286535a0

Ishii, T., Tamura, A., Shibata, T., and Kuroda, K., Kanda, T., Sugiyama, M., et al. (2020). Analysis of HBV Genomes Integrated into the Genomes of Human Hepatoma PLC/PRF/5 Cells by HBV Sequence Capture-Based Next-Generation Sequencing. *Genes (Basel)* 11 (6), 661. doi:10.3390/genes11060661

Jiang, S., Yang, Z., Li, W., Li, X., Wang, Y., Zhang, J., et al. (2012). Re-evaluation of the Carcinogenic Significance of Hepatitis B Virus Integration in Hepatocarcinogenesis. *PLoS One* 7 (9), e40363. doi:10.1371/journal.pone.0040363

Koren, S., Walenz, B. P., Berlin, K., Miller, J. R., Bergman, N. H., and Phillippy, A. M. (2017). Canu: Scalable and Accurate Long-Read Assembly via Adaptivek-Mer Weighting and Repeat Separation. *Genome Res.* 27 (5), 722–736. doi:10.1101/gr.215087.116

Li, H., Handsaker, B., Wysoker, A., Fennell, T., Ruan, J., Homer, N., et al. (2009). The Sequence Alignment/Map Format and SAMtools. *Bioinformatics* 25 (16), 2078–2079. doi:10.1093/bioinformatics/btp352

Li, W., Zeng, X., Lee, N. P., Liu, X., Chen, S., Guo, B., et al. (2013). HIVID: an Efficient Method to Detect HBV Integration Using Low Coverage Sequencing. *Genomics* 102 (4), 338–344. doi:10.1016/j.ygeno.2013.07.002

Li, X., Zhang, J., Yang, Z., Kang, J., Jiang, S., Zhang, T., et al. (2014). The Function of Targeted Host Genes Determines the Oncogenicity of HBV Integration in Hepatocellular Carcinoma. *J. Hepatol.* 60 (5), 975–984. doi:10.1016/j.jhep.2013.12.014

Li, Y., Wasser, S., Lim, S. G., and Tan, T. M. C. (2004). Genome-wide Expression Profiling of RNA Interference of Hepatitis B Virus Gene Expression and Replication. *Cell Mol Life Sci.* 61 (16), 2113–2124. doi:10.1007/s00018-004-4111-2

Liang, P., Xu, Y., Zhang, X., Ding, C., Huang, R., Zhang, Z., et al. (2015). CRISPR/Cas9-mediated Gene Editing in Human Tripronuclear Zygotes. *Protein Cell* 6 (5), 363–372. doi:10.1007/s13238-015-0153-5

Lin, S.-R., Yang, H.-C., Kuo, Y.-T., Liu, C.-J., Yang, T.-Y., Sung, K.-C., et al. (2014). The CRISPR/Cas9 System Facilitates Clearance of the Intrahepatic HBV Templates *In Vivo*. *Mol. Ther. - Nucleic Acids* 3, e186. doi:10.1038/mtna.2014.38

Liu, F., Wang, X.-W., Chen, L., Hu, P., Ren, H., and Hu, H.-D. (2016). Systematic Review with Meta-Analysis: Development of Hepatocellular Carcinoma in Chronic Hepatitis B Patients with Hepatitis B Surface Antigen Seroclearance. *Aliment. Pharmacol. Ther.* 43 (12), 1253–1261. doi:10.1111/apt.13634

Meng, G., Tan, Y., Fan, Y., Wang, Y., Yang, G., Fanning, G., et al. (2019). TSD: A Computational Tool to Study the Complex Structural Variants Using PacBio Targeted Sequencing Data. *G3 (Bethesda)* 9 (5), 1371–1376. doi:10.1534/g3.118.200900

Moucari, R., Korevaar, A., Lada, O., Martinot-Peignoux, M., Boyer, N., Mackiewicz, V., et al. (2009). High Rates of HBsAg Seroconversion in HBeAg-Positive Chronic Hepatitis B Patients Responding to Interferon: a Long-Term Follow-Up Study. *J. Hepatol.* 50 (6), 1084–1092. doi:10.1016/j.jhep.2009.01.016

Natoli, G., Avantaggiati, M. L., Balsano, C., De Marzio, E., Collepardo, D., Elfassi, E., et al. (1992). Characterization of the Hepatitis B Virus preS/S Region Encoded Transcriptional Transactivator. *Virology* 187 (2), 663–670. doi:10.1016/0042-6822(92)90469-6

Petrick, J. L., Florio, A. A., Znaor, A., Ruggieri, D., Laversanne, M., Alvarez, C. S., et al. (2020). International Trends in Hepatocellular Carcinoma Incidence, 1978-2012. *Int. J. Cancer* 147 (2), 317–330. doi:10.1002/ijc.32723

Rhoads, A., and Au, K. F. (2015). PacBio Sequencing and its Applications. *Genomics, Proteomics & Bioinformatics* 13 (5), 278–289. doi:10.1016/j.gpb.2015.08.002

Sarin, S. K., Kumar, M., Lau, G. K., Abbas, Z., Chan, H. L., Chen, C. J., et al. (2016). Asian-Pacific Clinical Practice Guidelines on the Management of Hepatitis B: a 2015 Update. *Hepatol. Int.* 10 (1), 1–98. doi:10.1007/s12072-015-9675-4

Sung, W.-K., Zheng, H., Li, S., Chen, R., Liu, X., Li, Y., et al. (2012). Genome-wide Survey of Recurrent HBV Integration in Hepatocellular Carcinoma. *Nat. Genet.* 44 (7), 765–769. doi:10.1038/ng.2295

Tu, H., Bonura, C., Giannini, C., Mouly, H., Soussan, P., Kew, M., et al. (2001). Biological Impact of Natural COOH-Terminal Deletions of Hepatitis B Virus X Protein in Hepatocellular Carcinoma Tissues. *Cancer Res.* 61 (21), 7803–7810. doi:10.3390/v9040075

Tu, T., Budzinska, M. A., Shackel, N. A., and Urban, S. (2017). HBV DNA Integration: Molecular Mechanisms and Clinical Implications. *Viruses* 9 (4). 75. doi:10.3390/v9040075

Wang, J., Chen, R., Zhang, R., Ding, S., Zhang, T., Yuan, Q., et al. (2017). The gRNA-miRNA-gRNA Ternary Cassette Combining CRISPR/Cas9 with RNAi Approach Strongly Inhibits Hepatitis B Virus Replication. *Theranostics* 7 (12), 3090–3105. doi:10.7150/thno.18114

Wang, J., Xu, Z. W., Liu, S., Zhang, R. Y., Ding, S. L., Xie, X. M., et al. (2015). Dual gRNAs Guided CRISPR/Cas9 System Inhibits Hepatitis B Virus Replication. *World. J. Gastroenterol.* 21 (32), 9554–9565. doi:10.3748/wjg.v21.i32.9554

Watanabe, Y., Yamamoto, H., Oikawa, R., Toyota, M., Yamamoto, M., Kokudo, N., et al. (2015). DNA Methylation at Hepatitis B Viral Integrants Is Associated with Methylation at Flanking Human Genomic Sequences. *Genome Res.* 25 (3), 328–337. doi:10.1101/gr.175240.114

Wooddell, C. I., Yuen, M. F., Chan, H. L Y., Gish, R. G., Locarnini, S. A., Chavez, D., et al. (2017). RNAi-based Treatment of Chronically Infected Patients and Chimpanzees Reveals that Integrated Hepatitis B Virus DNA Is a Source of HBsAg. *Sci. Transl Med.* 9 (409), eaan0241. doi:10.1126/scitranslmed.aan0241

Zhao, L. H., Liu, X., Yan, H. X., Li, W. Y., Zeng, X., Yang, Y., et al. (2016). Genomic and Oncogenic Preference of HBV Integration in Hepatocellular Carcinoma. *Nat. Commun.* 7, 12992. doi:10.1038/ncomms13591

Zhao, X., Emery, S. B., Myers, B., Kidd, J. M., Mills, R. E., et al. (2016). Resolving Complex Structural Genomic Rearrangements Using a Randomized Approach. *Genome Biol.* 17 (1), 126. doi:10.1186/s13059-016-0993-1

Conflict of Interest: The authors declare that the research was conducted in the absence of any commercial or financial relationships that could be construed as a potential conflict of interest.

Advantages of publishing in Frontiers

OPEN ACCESS
Articles are free to read for greatest visibility and readership

FAST PUBLICATION
Around 90 days from submission to decision

HIGH QUALITY PEER-REVIEW
Rigorous, collaborative, and constructive peer-review

TRANSPARENT PEER-REVIEW
Editors and reviewers acknowledged by name on published articles

Frontiers
Avenue du Tribunal-Fédéral 34
1005 Lausanne | Switzerland

Visit us: www.frontiersin.org
Contact us: frontiersin.org/about/contact

REPRODUCIBILITY OF RESEARCH
Support open data and methods to enhance research reproducibility

DIGITAL PUBLISHING
Articles designed for optimal readership across devices

FOLLOW US
@frontiersin

IMPACT METRICS
Advanced article metrics track visibility across digital media

EXTENSIVE PROMOTION
Marketing and promotion of impactful research

LOOP RESEARCH NETWORK
Our network increases your article's readership